SHORT TITLE

2-D SYMMETRIC AND ASYMMETRIC

TURBULENT SHEAR FLOWS

Mechanical Engineering Department Rajni P. Patel
Ph. D. Thesis

A STUDY OF TWO-DIMENSIONAL SYMMETRIC AND ASYMMETRIC TURBULENT SHEAR FLOWS

The two-dimensional, incompressible, symmetric and asymmetric, self-preserving and non-self-preserving turbulent shear flows are investigated both theoretically and experimentally.

The theoretical analysis involves an integral method and an auxiliary equation which avoids the use of an eddy viscosity or the mixing length concept. For a jet in uniform streaming flow, the integrated momentum equation and the auxiliary equation are solved. For the asymmetric jet, the additional information required to close the system of equations, is obtained from experimental results.

Experimental results are presented for a plane jet in still air, a plane mixing layer and the asymmetric jet. Collected results for a wall jet in uniform streaming flow and a plane jet in uniform streaming flow are used for comparison with theoretical predictions.

As a subsidiary experimental investigation, attention is given to the effects of free stream turbulence on free turbulent shear flows.

A STUDY OF TWO-DIMENSIONAL SYMMETRIC AND ASYMMETRIC TURBULENT SHEAR FLOWS

by

Rajni P. Patel

A thesis submitted to the Faculty of
Graduate Studies and Research in
partial fulfilment of the requirement for
the degree of Doctor of Philosophy

Department of Mechanical Engineering
McGill University
Montreal, P.Q.
July, 1970

Summary

The two-dimensional, incompressible, symmetric and asymmetric, self-preserving and non-self-preserving turbulent shear flows are investigated both theoretically and experimentally.

The theoretical analysis involves an integral method and an auxiliary equation which avoids the use of an eddy viscosity or the mixing length concept. For a jet in uniform streaming flow, the integrated momentum equation and the auxiliary equation are solved. For the asymmetric jet, the additional information required to close the system of equations, is obtained from experimental results.

Experimental results are presented for a plane jet in still air, a plane mixing layer and the asymmetric jet. Collected results for a wall jet in uniform streaming flow and a plane jet in uniform streaming flow are used for comparison with theoretical predictions.

As a subsidiary experimental investigation attention is given to the effects of free stream turbulence on free turbulent shear flows.

To

MIREILLE and PASCALE

Acknowledgements

The author is very much indebted to Dr. B. G. Newman for his guidance, advice, criticisms and help throughout the investigation of these projects. In fact, the problem of the asymmetric jet was identified originally by him.

The wind tunnel and the experimental apparatus were mainly constructed by Mr. Alex Gustavsen and the late Mr. E. Hansen and their help and technical advice are gratefully acknowledged. The help of Mr. O. Muehling with the construction of the traversing gear is very much appreciated. Messrs. L. Vroomen and J. Kelly are also thanked for their help in connection with instrumentation problems.

Discussions with the members of the "low-speed Aerodynamics Group" were very useful, in particular, I owe a special debt to Peter Smith for reading the manuscript and his criticisms. I also wish to thank Dan Guitton for his assistance in connection with the measurements of triple correlations.

To Teresa Miller for typing the manuscript I am most thankful. My thanks are also due to Misses B. Lowles, D. F. McKeown and Mrs. D. Fekete for typing figures and references.

Thanks are due to the University College, Nairobi, for granting the author leave of absence during the course of this work.

The work was undertaken with the financial assistance of the Defence Research Board of Canada under DRB Grant, No. 9551-12.

Preface

The subject matter of this thesis is a collection of related investigations carried out by the author under Dr. B. G. Newman's direction.

The aim was to originate a simple method to predict the development of the flow for an asymmetric jet. To do this it was realized that there was no satisfactory method to predict the affiliated flow (i.e. a plane jet in uniform streaming flow) on which the analysis could be based. Therefore, the study of a plane jet in uniform streaming flow became the centre of attention in section 2. The prediction of this flow by the present method being satisfactory, it was decided to try the same approach on a well known experimentally investigated asymmetric flow, i.e. a wall jet in uniform streaming flow. The success of the prediction on these flows stimulated the author to extend the analysis to the asymmetric jet.

I am aware of the frequent repetition of certain equations in this thesis but it simply reflects the way my thoughts evolved. It would be helpful to the reader to note the recurrence of the following equations:

The mean velocity profile: $U = U_1 + u_o f(\eta)$

The similarity form for the turbulence kinetic energy: $\overline{q^2} = \overline{q_1^2}\, g(\eta)$

The turbulence structure parameter (SP): $\left[\overline{q^2}/\overline{uv}\right]_\eta = 1$

The auxiliary equation for the rate of growth: $\left[\dfrac{dl_o}{dx}\right] = C\left[\dfrac{u_o}{U_1 + u_o}\right]$

Full momentum equation.

Half momentum equation.

Total kinetic energy equation.

Also the free shear flows investigated in this thesis are:

a plane jet in uniform streaming flow.

a plane wall jet in uniform streaming flow.

a plane jet in still air.

a plane mixing layer.

an asymmetric jet which is formed when a plane jet is blown underneath a uniform stream in zero pressure gradient.

Regarding the format of the thesis, I have presented introduction and review of theoretical methods in section 1 and the present major theoretical analysis in section 2. I have given priority to the results (i.e. for plane jets and wall jets in uniform streaming flow) of other investigators in comparing their results (section 3) with the analyses of section 2. This is then followed by my own experimental investigations (section 4) of a plane jet in still air (section 5), a plane mixing layer (section 6) and the asymmetric jet (sections 7, 8, and 9). Section (10) gives the summary and conclusions drawn from the present study. Two Appendices are included and they give respectively details of experimental arrangement and checks on flow, and the effects of stream turbulence on free shear flows.

All figures are given at the end and consecutive numbers, as they appear in the text, are assigned to them. Sketches and figures are given for on-the-spot comparison in the main body of this thesis.

CONTENTS

Notation

A	A constant in equation (6.2.8)
A_1	A constant
B	A constant in equation (6.2.10)
b	Width of slot opening (= 0.265 in.)
C	A constant in a particular flow and usually varies from flow to flow, e.g. a constant defining the rate of growth for a plane jet in quiescent surroundings; or the rate of growth for a plane wall jet in still air;(see equation (18))
C_1	= (1/2)C, see equation (17). Same as β in Townsend's (1970) paper.
d	Diameter of hot-wire
E	Rate of entrainment defined by equation (8.1), or bridge D.C. voltage in Appendix I
$E(\underset{\sim}{K})$	Three dimensional energy spectrum function
E_s	Rate of entrainment on the streaming side of an asymmetric jet
E_z	Rate of entrainment on the zero velocity side of an asymmetric jet
e	Instantaneous bridge voltage fluctuation
f	Function of non-dimensional cross stream co-ordinate for the variation of mean velocity, or frequency in section (7.2.7)
g	Function of non-dimensional cross stream co-ordinate for the variation of turbulence energy
g_n	(n = 1,2,3) function of η (see equations (6.2.1 and 5.3.5.2))
g_{12}	Function of η (see equations (6.2.1 and 5.3.5.2))
I_n	(n = 1,2,3) = $\int_0^\infty f^n(\eta)\, d\eta$
K	A non-dimensional factor (see equation (73))
$\underset{\sim}{K}$	Wavenumber vector
K'	The Kolmogoroff constant

k	$= \ln 2$, or a constant (see equation (6.2.13))
k_1	One dimensional wave number $(= 2\pi f/U)$
L_ϵ	Average dissipation length scale of turbulent motion
l	Mixing length, or length of hot-wire
l_o	$(= y_{m/2})$ length scale defined as that value of y at which $U = (1/2)u_o$
l_1	Length scale for the streaming side of an asymmetric jet
l_2	Length scale for the zero velocity side of an asymmetric jet
M	Excess kinematic momentum $(= Me_1(x) + Me_2(x) = bU_j(U_j - \frac{1}{2} U_1))$
Me	Excess kinematic momentum (see equation (16))
$Me_1(x)$	Kinematic momentum defined by equation (70)
$Me_2(x)$	Kinematic momentum defined by equation (71)
$\overline{q^2}$	$= (\overline{u^2} + \overline{v^2} + \overline{w^2})$
$\overline{q_1^2}$	Turbulence energy scale (see section (2))
R_T	Eddy viscosity Reynolds number $(= u_o l_o/\nu_T)$
R_λ	Turbulence Reynolds number $(= \sqrt{\overline{u^2}} \, . \, \lambda/\nu)$
R_{T_j}	Eddy viscosity Reynolds number for a jet in still air
R_{T_w}	Eddy viscosity Reynolds number for a small perturbation jet or wake
Re_x	Reynolds number $(= U_1 x/\nu)$
(SP)	Turbulence structure parameter $(= \left[\overline{q^2}/\overline{uv}\right]_{\eta=1})$
s	Spacing between two wires in an x-wire probe
U	Mean velocity in the x-direction

U_j	Jet velocity at slot exit
U_m	(or $U_{max.}$) maximum mean velocity in the x-direction (= U_1 for a plane mixing layer)
U_1	Free stream velocity in the x-direction and independent of x
u	(Longitudinal) turbulent fluctuation component of velocity in the x-direction
u_o	Velocity scale (= U_m for a jet and wall jet in still air, = U_1 for a plane mixing layer, otherwise = $(U_m - U_1)$)
V	Mean velocity in the y-direction
V_m	Mean lateral velocity at the point of maximum velocity (see Fig.(4))
v	(Lateral) turbulent fluctuating component of velocity in the y-direction
w	(Transverse) turbulent fluctuating component of velocity in the x-direction
x	Downstream distance from slot exit, or tunnel exit
x_o	Distance of hypothetical origin from slot exit
$Y_{\gamma=0.5}$	Edge of an asymmetric jet on the streaming side defined by the value of y at which $\gamma = 0.5$
y	Lateral co-ordinate
y_e	Edge of turbulent shear flow
y_m	Value of y at which $U = U_m$
$y_{m/2}$	Value of y at which $U = \frac{1}{2} u_o$
Z	A constant defined by equation (6.2.18)
z	Co-ordinate orthogonal to x and y, or transverse co-ordinate

Greek Alphabet

α_m	Maximum effective strain (see equation (9.2))
γ	Intermittency
δ	Edge of an asymmetric jet on the streaming side defined by the value of y at which $U=0.01u_o$
ϵ	The rate of energy dissipation per unit volume
η	Non-dimensional cross stream co-ordinate (y/l_o or y/x)
η_o	A constant (see equation (6.2.14)
η_1	Non-dimensional cross stream co-ordinate $(y - y_m)/l_1$
η_2	Non dimensional cross stream co-ordinate $(=(y_m - y)/l_2)$
η_∞	(= 2.0) approximately the edge of non-dimensional mean velocity profile (see equation 9)
θ	Momentum thickness defined by equation (21)
λ	The Taylor lateral microscale, or a mixing length
ν	Kinematic viscosity
ν_T	Eddy viscosity
ρ	Density
τ	Shear stress
$\Phi(k_1)$	One dimensional energy spectrum function for u

1. INTRODUCTION

1.1 General

It is natural that the simplest flow situations should draw the attention of investigators first, and their investigations fall in a sequence going from the least to the more complex flow configurations. In the process, considerable knowledge in both theoretical methods and experimental results has been accumulated. For turbulent flows in general, however, the task is formidable and many difficulties and uncertainties in theoretical analysis and experimental techniques exist. A brief review of theoretical approaches adopted to analyse turbulent flows is given in section (1.2); and a modest effort is made in this investigation to examine some of the experimental uncertainties.

It is interesting to note that useful solutions of the boundary layer equations have been obtained by examining those particular flows for which the profiles of mean velocity are similar or self-preserving as the flow proceeds downstream. For such flows the partial differential equation of motion is replaced by a total differential equation which can be solved either analytically or numerically. Such solutions have been obtained in the past for both laminar and turbulent flows with success. This type of approach is followed in this investigation and because no generalized theory is available for turbulent shear flows, it is felt that experiments are very useful for physical understanding and may provide a direction for analytical approach in the future.

As mentioned before most investigations connected with free turbulent shear flows have been associated with simple geometries, i.e. flows with a line of symmetry or a wall. There are many practical flow situations in which neither a symmetry line nor a wall boundary exist. These are the flow situations of interest for this investigation, and in particular an asymmetric free jet flow is investigated in detail experimentally. Boundary layer control by blowing often produces asymmetric flow configurations and when intensive blowing is used a jet flap results. Indeed, these flows are extremely difficult to investigate analytically.

Incompressible asymmetric jet flows may be classified into two groups:

(a) flows influenced by a solid boundary; e.g. wall jets, and step flows;

(b) free asymmetric jet flows; e.g. plane mixing layers and jet flaps.

A characteristic feature of the asymmetric jets is that the maximum shearing stress does not occur at the wall or at the maximum velocity point whereas in ordinary boundary layer flow with zero pressure gradient it occurs near the wall where viscosity has the greatest influence. Figure (1) shows typical asymmetric jet flows. Some of these flows such as wall jets and plane mixing layers have been investigated in the past but for others even experimental results are lacking.

A slightly simpler case of the asymmetric turbulent jet is the one in which the flow produced by a two-dimensional jet is bounded on one side by a uniform streaming flow and on the other by quiescent surroundings. This simple case is of special interest because it lies in between two asymptotic self-preserving cases, i.e. when jet velocity or maximum velocity in the shear layer is much greater than the free stream velocity the flow resembles, at least geometrically, a jet in still surroundings and when the maximum velocity decays to the free stream velocity it becomes a plane mixing layer. From now on, unless specified otherwise, throughout this investigation the term "asymmetric turbulent jet" will imply the flow configuration shown below.

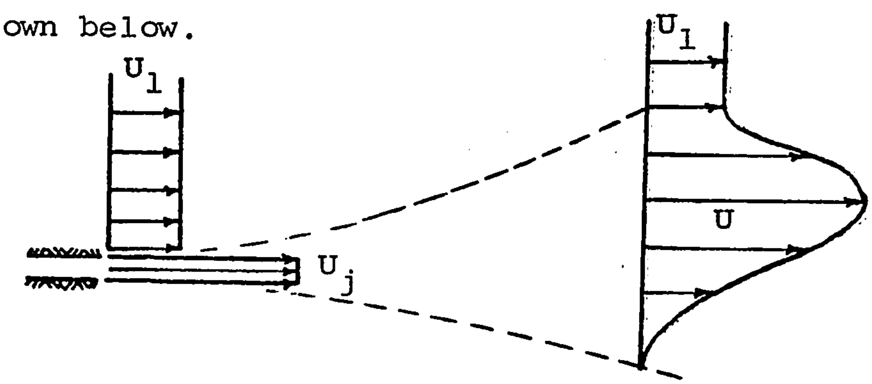

The purpose of this investigation is to obtain experimentally variation of width and decay of the maximum velocity for the asymmetric jets. Because the two halves of the asymmetric jet are apparently quite different it is interesting to evaluate entrainment rates on either side.

It is well known that in self-preserving flows, such as a jet in quiescent surroundings, a plane mixing layer, and jets and wakes in equilibrium pressure gradients, turbulence quantities scale with local mean velocity scale but for non-self-preserving flows they may or may not correlate with the local mean velocity scale and thus may have some upstream history effects. It is, therefore, hoped that measurements and correlations of turbulence quantities may provide an insight of the structure of the asymmetric turbulent jets. Finally, an additional purpose of this investigation is to present experimental results to permit detailed testing of prediction procedures in future.

The general outline of the present investigation is as follows:

In view of the geometric similarity of the asymmetric jet to the combination of a half jet in quiescent surroundings and a half jet in uniform streaming flow, the background of theoretical and experimental work on these flows is given in section (2). This is then followed by an analysis of a jet in uniform streaming flow. Also in this section a simple analysis is presented for the asymmetric jet.

In section (3), applicability of the analysis of section (2) is demonstrated by comparing existing experimental results for the two-dimensional jet in uniform streaming flow and wall jets in uniform streaming flow.

In section (4), the experimental arrangement is briefly described, and the details of the experimental set up together with instrumentation and checks on the apparatus are given in Appendix (1). Because some of the free shear flows are associated with a free stream, it is probable that the stream turbulence may have some effect on the development of these flows. Hence the effects of free stream turbulence on free shear flows are given in Appendix (2).

Examination of existing literature is revealing in that although many investigations have been carried out for the asymptotic states (i.e. a jet in still air and a plane mixing layer) of the asymmetric jet, only one or two present turbulence measurements. It was, therefore, decided to investigate these flows and compare measurements with the few existing results. Investigation of a two-dimensional jet in still air is described in section (5) whereas that of a plane mixing layer is given in section (6).

Section (7) deals with measurements of the asymmetric jets. To cover the entire range, i.e. from a very strong to a very weak jet, three values of the ratio (U_j/U_1) were selected. Note that U_j is the mean velocity at the nozzle exit and U_1 is the free stream velocity which is independent of x. For one case (i.e. $U_j/U_1 \simeq 5.0$) measurements were made in detail and they include mean velocities, turbulence intensities, shear stresses, intermittency, triple correlations and one dimensional $\overline{u^2}$-spectra. For other cases measurements of mean velocity and turbulence quantities are presented.

Section (8) describes methods of evaluating entrainment rates and gives results for the two-dimensional jet in still air, the plane mixing layer and the asymmetric turbulent jets. Finally in section (9) it is shown that for practical purposes the simple analysis (presented in section 2.4.2) for the asymmetric jet is in good agreement with experimental results for all cases as far as length scales and velocity scales are concerned.

In section (10) general conclusions drawn from this investigation are presented.

1.2 A Brief Review of Theoretical Methods for Turbulent Shear Flows

Although this investigation is highly biased to experimental approach it is interesting to glance at some of the recent developments in theoretical methods for turbulent shear flows. These methods have centered around two approaches. In spite of the sophistication and analytical satisfaction of the statistical methods it is extremely difficult to solve exactly the equations of motion. In statistical analysis one studies the equations of motion in terms of time average quantities. It is well known that in doing so considerable information of the flow field is lost and resulting equations contain more unknowns and higher order correlations than there were originally. Analytical studies following this approach are bedevilled with many simplifying assumptions and experimental verification for them is hard to obtain. However, some solutions have been obtained which are restricted to isotropic and homogeneous turbulent flow. Because free turbulent shear flows are neither isotropic nor homogeneous the complications in the above method are compounded further. In obtaining practical results another approach has been very useful. This method is generally referred to as phenomenological approach. In this approach, in order to determine the velocity distribution, one establishes an expression for shear stress in terms of some empirical exchange coefficient.

Well known names associated with phenomenological approach are Taylor (1915), Prandtl (1925), von Karman (1930) and many others who have recently reverted to this method. In view of its simplicity, practical usefulness and the fact that the physics of turbulent motion is built in (primarily from experimental results) a short review of the evolution of the phenomenological theories is in order at this stage.

It should be recalled that the Navier-Stokes equations of motion when time averaged according to the method of Reynolds contain turbulent momentum transport terms which are referred to as Reynolds (or apparent, or turbulent) shear stresses. The existence of these terms in the momentum equation requires that every phenomenological theory of turbulence must provide some means of calculating them. The obvious and most tempting approach in the old theories has been to relate the Reynolds shear stress to the mean local velocity gradient. Thus in terms of the eddy-viscosity concept of Boussinesq (1877), the Reynolds shear stress $\overline{uv}$ is given by $\nu_T(\partial U/\partial y)$ where ν_T is defined as the eddy-viscosity. In doing this, however, one difficulty has been replaced by another and unlike laminar kinematic viscosity the eddy-viscosity is not the property of a fluid, so a definite number cannot be assigned to it. In fact ν_T depends on Reynolds number, the position of the point where it is evaluated and the boundary conditions of a problem under investigation. The problem is, therefore, not simplified but other means have to be found to relate ν_T to the flow parameters.

Prandtl (1925) proposed two mixing length hypotheses in his paper but the one widely known and used is the one in which ν_T is given by $l^2\left|\partial U/\partial y\right|$ and the mixing length, l, in turn is assumed to be proportional to the typical width of a shear layer; in other words $\tau = \rho l^2\left|\frac{\partial U}{\partial y}\right|\frac{\partial U}{\partial y}$. As Batchelor (1950) has pointed out, this hypothesis is equivalent to the assumption that transfer of momentum is carried out by fluctuating motions that are small in length compared with representative lengths associated with mean motion. This implies that small eddies are responsible for the transfer mechanism. Furthermore, the mixing length hypothesis of Prandtl implies a balance between turbulent production and dissipation, e.g. see Batchelor (1950), Townsend (1961), Bradshaw et al. (1967), Nee and Kovsznay (1969), and Rodi and Spalding (1969). Because the convection and diffusion of turbulence energy are ignored the mixing length approach is said to be too local, in other words, this model ignores the upstream history effects. In spite of these objections the mixing length approach has produced surprisingly good results for many boundary layer type flows.

For free jet flows Prandtl (1942) suggested that the eddy-viscosity is proportional to the product of a typical width, l_o, and velocity scale, $u_o = (U_{max.} - U_{min.})$, of a shear layer. The suggestion is a consequence of Reynolds number similarity when ν_T is assumed constant across the flow. This implies that big eddies are now responsible for the transfer mechanism, but note that this is inconsistent with the concept of Boussinesq and his original suggestion. Also another restriction has been imposed; this is that ν_T is assumed to be a constant across the shear layer.

To overcome some of the objections of the mixing length model Kolmogorov (1942), Prandtl (1945) and Emmons (1954) have proposed a model which relates the eddy-viscosity to turbulence kinetic energy and a length scale, i.e. $\tau = \rho l(\overline{q^2})^{1/2}\ \partial U/\partial y$. This suggestion has been used to predict various boundary layer flows by Wieghardt (1942), Glushko (1965), and Beckwith and Bushnell (1968). For separated flows the model has been used by Spalding (1967). The applicability of this model to self-preserving turbulent jets and wakes is demonstrated by Newman (1968). For interest it is noted that Beckwith and Bushnell use differential method whereas both Spalding and Newman use integral method. Newman has also pointed out that any eddy-viscosity model is incorrect in some specific instances where the Reynolds shear stress is not zero even though the mean velocity gradient is zero (e.g. at the point of maximum velocity in a wall jet in still surroundings).

Townsend (1956) has given considerable impetus to the phenomenological approach by providing a framework for future work. The essence of his approach, unlike others, is to accept the fact that for many turbulent shear flows, mean velocity profiles are similar and merely appropriate velocity scales and length scales are required to specify the mean velocity profiles. He then postulates a transfer mechanism and attempts to predict variations of the velocity and length scales. In some of the earlier methods Townsend (1965, 1966) assumes that the turbulence is geometrically similar, i.e. the ratio of $\overline{uv}$ to $\overline{q^2}$ might be a universal constant. For free shear flows, collected experimental results (see Fig. (96)) indicate that this is not a bad assumption. It should be realized that to make use of these models, the turbulence energy equation has to be introduced in the analysis and in doing so additional complications are brought in the problem. Following Townsend (1965) Bradshaw et al. (1967) transformed the turbulent energy equation into an equation for the Reynolds shear stress and using this equation together with the continuity and the momentum equation they have successfully predicted several incompressible turbulent boundary layer flows both with and without pressure gradient. Using a similar approach Nash (1969) has recently demonstrated the feasibility of predicting three dimensional turbulent boundary layers. In many flow situations, however, this method is bound to fail; for often the Reynolds shear stress vanishes where $\overline{q^2}$ remains finite, as for example, near the line of symmetry in free shear flows.

Recently another approach has been suggested by Harlow and Nakayama (1967). They have based their transport equation for the eddy-viscosity on the turbulent energy equation. The process involves a large number of equations and a large number of empirical constants. Following Phillips (1967) Nee and Kovasznay (1969) have also proposed a rate equation to govern the variation of the eddy viscosity. Instead of the turbulent energy equation they use this rate equation in conjunction with the momentum and continuity equations to form a closed system of equations for turbulent shear flows. They have obtained satisfactory agreement with experimental results for a turbulent boundary layer with zero pressure gradient. The degree of empiricism is, however, rather high.

It should now be pointed out that all the phenomenological models proposed so far contained a length scale which had to be related empirically to the width of shear flow in one way or another. To obtain improvement and universality of a prediction method for various shear flows it is believed that an independent differential equation for turbulent length scale is necessary, contrary to "the rules for the game" due to Bradshaw (1969). Originally a suggestion of this kind was made by Kolmogorov (1942) who introduced a differential equation for the "frequency". From Navier-Stokes equations, Rotta (1951) has derived the differential equation for the turbulent length scale (which is a measure of energy containing eddies). Spalding (1967) and his associates have produced a hybrid approach by retaining Kolmogorov-Prandtl-Emmons model and incorporating it into the turbulent energy equation and Rotta's equation for ($\overline{q^2}$ x turbulent length scale). After certain assumptions they have managed to reduce the number of constants to seven which are then obtained by procuring the best agreement with experimental results for the plane mixing layer, the plane jet and the radial jet. It is noted by them that no set of constants produces exact agreement in respect of all the main experimental data. The resulting differential equations are solved simultaneously by the finite difference method of Spalding and Patankar (1967). Other advanced turbulence models are given by Launder (1970). Further comments on this field or micro integral or differential method are presented later together with the present experimental results for a two-dimensional jet in still air, a plane mixing layer and a two-dimensional jet in a uniform streaming flow.

In view of the difficulties in obtaining universal constants for all boundary layer type turbulent shear flows there is still some value in those methods which are semi universal in nature. Even though integral methods are losing popularity, McDonald (1968) has shown that predictions made from them are in no way inferior to those made from field methods. It is important to bear in mind that for either integral or differential method to possess a long lasting value in real practice requires that it should be easier, quicker and cheaper to use. Indeed in this respect Townsend's approaches for free shear flows have been very rewarding. As an example his "large eddy equilibrium hypothesis", although at variance with experimental observations as noted by Bradbury (1963), Newman (1969) and many others, has stimulated some investigators to formulate a method of finding a relation for the eddy-viscosity in terms of mean flow parameters (Bradbury (1963), Gartshore (1965)). Gartshore and Newman (1969) have demonstrated the success of this approach for turbulent wall jet in an arbitrary pressure gradient although it must be recognized that the wall constraints are important in this flow.

For a limited class of turbulent shear flows, as for example jets and wall jets, an admirable review of prediction methods is given by Newman (1969). Application of the phenomenological theories to other shear flows can be found in text books by Schlichting (1968), Hinze (1959) and a review paper by Halleen (1964). Phillips (1969), in an interesting paper, reviews various approaches in search of establishing a relation for the Reynolds shear stress in turbulent shear flows.

For turbulent shear flows Batchelor (1950) has pointed out that neither the large eddies nor the small eddies alone are responsible for the momentum transfer hence in these flows some other kind of transfer mechanism must be present. In a recent paper Townsend (1970) discusses the "nature and origin of the "universal" structure of fully sheared turbulence" and he postulates the flow development in variety of shear flows by using an analysis based on total strain rather than the usual rate of strain concept. In this approach the eddy-viscosity is related to the total strain and mean flow parameters.

2. THEORETICAL ANALYSIS

2.1 General Outline of the Analysis

The analytical investigation of an asymmetric turbulent jet is a highly complex problem. For example, Wygnanski and Hawaleshka (1966) attempted to analyse an asymmetric jet (see the sketch below) created by the mixing of a wall jet with quiescent surroundings downstream of a trailing edge.

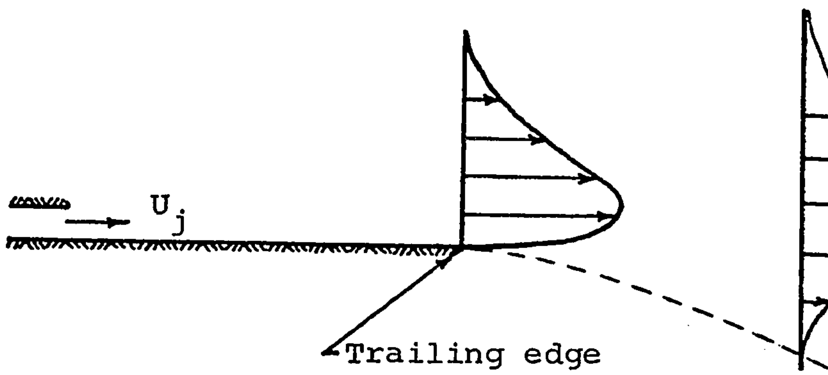

Their approach was essentially a coordinate perturbation type and therefore its accuracy was limited to the immediate neighbourhood of the trailing edge. It is interesting to observe that their solution for the mean velocity distribution breaks down within one inch downstream of the trailing edge and thus the range of value of their analysis is very limited.

On the other hand for the present asymmetric turbulent jet (see the sketch below) considerable simplification would result if it were possible to divide the jet at the maximum velocity and then analyse the two parts in a manner similar to a half jet in uniform streaming flow or a half jet in still surroundings.

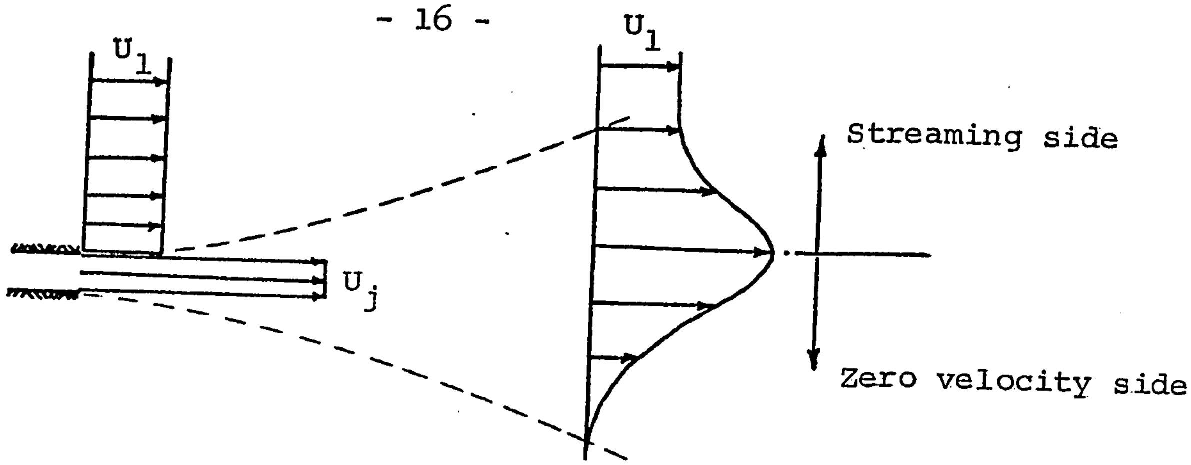

It should be emphasized, however, that the locus of the maximum velocity points is not a streamline and this will become clear as the analysis evolves.

Following the approach of Patel and Newman (1961) for jets in streaming flow, Gartshore (1965) attempted to analyse the asymmetric jet by using a multi-integral technique. He divided the asymmetric jet in a manner similar to the one described above ignoring the interactions between the two parts, and was able to predict the width of the jet on the zero velocity side with fair accuracy whereas on the streaming side his predictions for the width were very poor. It is of interest to note that in methods similar to Gartshore's one requires, a priori, at least some or all of the variables at one station to predict the flow development downstream of that station. Such methods imply that each prediction is restricted to only one case of U_j/U_1. In addition use of the multi-integral technique requires some information regarding the variation of the Reynolds shear stress. For the asymmetric jets Gartshore (1965) confined his experimental investigation to only the mean velocity measurements* and these are compared with the present results later. Because analyses of a free jet in still air and a jet in uniform streaming flow are anticipated to be applicable these are examined before extending the analyses to the asymmetric jet. The present analysis (section (2.4.2)) for the asymmetric jet involves application of an integrated x-momentum equation for each half of the flow. The analysis does not impose restrictions on the interactions between the two halves. The interactions are represented by the ratio of mean flow length scales l_1 and l_2. The variation of (l_2/l_1) is obtained from experimental results. An auxiliary equation which is the same for a jet in uniform streaming flow is used. With this information it is possible to evaluate explicitly the variations of l_1, l_2 and u_o for the asymmetric jet.

2.2 A Plane Jet in Quiescent Surroundings

For a plane jet in quiescent surroundings, from dimensional analysis, Newman (1961) has shown that the distributions of the mean velocity and the mean turbulence parameters are similar at all downstream stations. The similar profiles differ only in scales of length and velocity. The growth of the length scale is linear with the downstream distance, x, and the velocity scale varies as $x^{-1/2}$. The shape of the non-dimensional mean velocity

---

* It should be noted that Dr. Gartshore's measurements of this flow were exploratory and ancillary to the main work of his thesis, which was 'The streamwise development of two-dimensional wall jets and other two-dimensional shear flows'.

profile is predicted by Tollmien (1926), Görtler (1942) and Townsend (1970) by using phenomenological approaches. These observations are well substantiated by many experiments (for mean velocity only), however, some disagreement between experimental results exist and these will be discussed in section (5).

In many investigations (for example, see Newman (1968), Townsend (1970)) information derived from a plane jet in quiescent surroundings is used to extend analyses to more complex free shear flows. In particular when the turbulence energy equation is incorporated in an analysis some assumption regarding the dissipation length scale is required and often the ratio of mean flow length scale to the dissipation length scale is assumed to be the same as that for the plane jet. The purpose of the following analysis is to show that for a plane jet in still air the ratio of the mean flow length scale to the dissipation length scale is related to the rate of growth, a parameter representing the structure of turbulence, and shape factors.

Consider a two-dimensional jet in quiescent surroundings for which the time averaged equation of motion in downstream direction x (for constant density ρ, and incorporating the approximate form of the y-directional momentum equation) is (see Fig. (2a)):

$$U\frac{\partial U}{\partial x} + V\frac{\partial U}{\partial y} + \frac{\partial}{\partial x}(\overline{u^2}-\overline{v^2}) = \frac{1}{\rho}\frac{\partial \tau}{\partial y} \qquad (1)$$

where:

U and V are mean velocities in directions x and y respectively; u and v are the associated turbulent fluctuations about the mean,

and $\tau/\rho = -\overline{uv} + \nu \dfrac{\partial U}{\partial y}$

The time averaged continuity equation is:

$$\frac{\partial U}{\partial x} + \frac{\partial V}{\partial y} = 0 \qquad (2)$$

Combining equations (1) and (2) and integrating between limits y = 0 and y = ∞, (i.e. the full integrated momentum equation),

$$\frac{d}{dx} \int_0^\infty \left[U^2 + (\overline{u^2} - \overline{v^2}) \right] dy = 0 \qquad (3)$$

The difference between the normal Reynolds stresses is often neglected (Townsend (1956)) and similarity profiles are assumed as follows:

$$U = u_o\, f(\eta)$$
$$\overline{q^2} = \overline{q_1^2}\, g(\eta) \qquad (4)$$

where $\eta = y/l_o$,

u_o = the mean velocity scale and is equal to U_m,

$\overline{q^2} = (\overline{u^2} + \overline{v^2} + \overline{w^2})$,

$\overline{q_1^2}$ = turbulence energy scale and is found to be proportional to u_o^2 for self-preserving flows,

l_o = length scale defined as that value of y at which $U = \frac{1}{2} u_o$

and U_m is the maximum velocity at $y = 0$.

Combining equations (4) with equation (3) one obtains,

$$u_o^2 \, l_o \, I_2 = \text{constant} \tag{5}$$

where $I_2 = \int_0^\infty f^2 \, d\eta$

Similarly the integrated half-momentum equation is obtained by combining equations (1) and (2) and integrating between limits $y = 0$ and $y = l_o$,

i.e. $$\frac{(\overline{uv})_{\eta=1}}{u_o^2} = \frac{1}{2} \frac{dl_o}{dx} f(1) \int_0^1 f d\eta \tag{6}$$

where $-\rho\overline{uv}$ is the Reynolds shear stress and the viscous shear stress is neglected.

For a plane jet in still air the non-dimensional mean velocity distribution is represented well by an exponential function (Hinze (1959), Newman (1967), etc.) (e.g. $f = e^{-k\eta^2}$ where $k = \ln 2$ because of the definition of l_o) so equation (6) reduces to:

$$\frac{(\overline{uv})_{\eta=1}}{u_o^2} = 0.2 \frac{dl_o}{dx} \tag{7}$$

The integrated total energy equation is:

$$\frac{1}{2} \int_0^\infty \frac{\partial}{\partial x} \left[U \left(U^2 + \overline{q^2} \right) \right] dy = - \int_0^\infty \epsilon \, dy \tag{8}$$

where ϵ is the rate of energy dissipation per unit volume.

If the momentum condition and equations (4) are used in equation (8) then one gets,

$$\int_0^\infty f^3 \, d\eta + \frac{\overline{q_1^2}}{u_o^2} \left[3 \int_0^\infty fg \, d\eta - 2g(0) \right]$$

$$= 4\eta_\infty \frac{(\overline{q_1^2})^{3/2}}{u_o^3} \frac{l_o}{L_\epsilon} \cdot \frac{1}{dl_o/dx} \tag{9}$$

where $\int_0^\infty \epsilon \, dy = \eta_\infty \frac{l_o}{L_\epsilon} (\overline{q_1^2})^{3/2}$

L_ϵ = the average dissipation length scale of the turbulent motion

and η_∞ = the non-dimensional position of the approximate edge of the non-dimensional mean velocity profile, i.e. $\eta_\infty \simeq 2.0$. (The traditional definition of η_∞ is the non-dimensional mean position of the super layer.)

Equation (7) when substituted into equation (9) gives,

$$\int_0^\infty f^3 \, d\eta + \frac{\overline{q_1^2}}{(\overline{uv})_{\eta=1}} \, 0.2 \, \frac{dl_o}{dx} \left[3 \int_0^\infty fg \, d\eta - 2g(0) \right]$$

$$= \frac{4\eta_\infty}{11.2} \left[\frac{\overline{q_1^2}}{(\overline{uv})_{\eta=1}} \right]^{3/2} \left[\frac{dl_o}{dx} \right]^{1/2} \frac{l_o}{L_\epsilon} \qquad (10)$$

It should be mentioned that until now $\overline{q_1^2}$ was not specified except that it is a characteristic scale for the turbulence energy in the shear layer. $\overline{q_1^2}$ is now defined as the value of $\overline{q^2}$ at $\eta = 1$ corresponding to the position where U is equal to a half centre line value. In the investigations of Townsend and Newman it is assumed to be the value of $\overline{q^2}$ at $\eta = 0$. Present measurements (to be described later see section (5)) for a plane jet in still air show that:

$$g(0) \approx 1.12; \quad \left[\frac{\overline{q^2}}{\overline{uv}} \right]_{\eta=1} \approx 5.9; \quad \int_0^\infty fg \, d\eta \approx 1.10$$

$$\frac{dl_o}{dx} = c = 0.103 \qquad (11)$$

and for the exponential profile $\int_0^\infty f^3 \, d\eta = 0.62$.

Hence with the numerical values of equations (11) and defining the turbulence structure parameter, $(SP) = \left[\frac{\overline{q^2}}{\overline{uv}} \right]_{\eta=1}$ (Townsend (1970) uses $\overline{uv}/\overline{q^2}$ to specify the turbulence structure), equation (10) becomes,

$$0.62 + 0.2 \, c \, (SP) = 0.715 \, c^{1/2} \, (SP)^{3/2} \, \frac{l_o}{L_\epsilon} \qquad (12)$$

Equation (12) shows that the ratio of the mean flow length scale, l_o, to the dissipation length scale, L_ϵ, depends on the rate of growth and the structure parameter. The experimental values for C and (SP) when substituted into equation (12) give, $l_o/L_\epsilon = 0.23$.

It is interesting to compare the present value of l_o/L_ϵ to the one ($l_o/L_\epsilon = 0.254$) obtained by Newman (1968) (although he does not explicitly quote the value of l_o/L_ϵ it was calculated from his equation (3) using his suggested values for the parameters appearing in this equation). It should be emphasized that the close agreement between the two values is noteworthy since they were obtained by using different assumptions. For instance Newman's equation (3) is derived with the assumption that $\overline{q^2}$ at y = 0 is a representative value within the fully turbulent part of the flow whereas the analysis presented here is comparatively more exact. An important conclusion is that the value of l_o/L_ϵ is insensitive to plausible assumptions regarding the distribution of the turbulent energy in the shear layer.

2.3 A Plane Jet in a Uniform Streaming Flow

2.3.1 General

Although many investigations in the past have been undertaken for a plane jet in a uniform streaming flow none of the methods proposed has been satisfactory in correlating the existing experimental results. Essentially most of the methods except the one proposed by Wygnanski (1969) are integral methods. Wygnanski's approach is based on a coordinate-type perturbation expansion and a series truncation together with the assumption of constant eddy viscosity across the flow (i.e. ν_T a function of x only). His method requires two experimental constants which are obtained from the limiting self-preserving cases.

All the integral methods although different in concept assume geometrical similarity of mean velocity profiles. Squire and Trouncer (1944) use a "double integral" technique and introduce Prandtl's mixing length hypothesis, ($\tau = \rho l^2 \frac{\partial U}{\partial y} \left|\frac{\partial U}{\partial y}\right|$), to specify shear stress at the "half-velocity" point in the shear layer. The mixing length, l, in turn is assumed to be a constant proportion of the width of the shear layer (i.e. in effect $\nu_T \propto u_o l_o$ and the eddy viscosity Reynolds number, $u_o l_o/\nu_T$, equals a constant throughout the flow field). Hill (1965) uses integral momentum and moment of momentum equations. The latter has an integral, involving shear stress, which is evaluated from the experimental results of jets in still surroundings. Abramovich (1963) uses the integral momentum equation together with an auxiliary equation (see section 2.3.2) which involves one experimental constant. These integral methods have one serious objection in that they do not exhibit the expected asymptotic behaviour, i.e. a strong jet in a uniform streaming flow degenerates to a small-perturbation jet and both these extreme cases are self-preserving with quite different values for the eddy viscosity Reynolds number.

Integral methods known as variable eddy viscosity Reynolds number methods have been developed to incorporate the expected asymptotic behaviour. This group of methods endeavours to allow for changes in the eddy viscosity Reynolds number by applying Townsend's (1956) large eddy equilibrium hypothesis using local values of strain-rate ratio to compute local values of the eddy viscosity Reynolds number. Methods of Bradbury (1963) and Gartshore (1965) fall into this category. Indeed they must exhibit the expected asymptotic behaviour because Townsend used his large eddy equilibrium hypothesis originally to explain differences in the eddy viscosity Reynolds numbers for the two extreme cases.

In Gartshore's method the eddy viscosity Reynolds number is related to scale of the largest eddies, and this scale is assumed to be proportional to the standard deviation of the position of the laminar super-layer. The standard deviation in turn is obtained from measured intermittency distributions. The double integral technique similar to the one of Squire and Trouncer is used and the resulting equations are solved numerically by a four-point Runge Kutta technique. It should be noted that in his method, apart from initial conditions to start numerical calculations, two experimental constants are required. In spite of the sophistication and extra assumptions introduced by Gartshore, his predictions for turbulent jets in uniform streaming flow are not in good agreement with the experimental results of Bradbury.

Bradbury and Riley (1967) have also concluded that simple integral theories using Townsend's large eddy equilibrium hypothesis do not predict this flow accurately. They have, in fact, shown that the application of the large eddy equilibrium hypothesis leads to errors in the predictions of flow development, opposite in sense but equal in order of magnitude to the errors obtained with the constant eddy viscosity Reynolds number theories. Thus there is as yet no simple method for predicting jets in uniform streaming flow.

For interest it is noted that Naudascher (1967) has proposed a method which incorporates a new form of similarity for such flows but his similarity form introduces an inconsistency into the analysis and also has limited experimental verification.

An attempt is therefore made to analyse the development of mean flow characteristics for the plane jet in a uniform streaming flow that is valid over the entire range of flow rather than over asymptotic regions only. The integral momentum equation is used together with an auxiliary equation to provide solutions for both u_o and l_o. Only one well established experimental constant is required. Even though the investigation is limited to incompressible and isothermal conditions it can be extended to studies of other main characteristics of the flow, e.g. temperature, density and concentration profiles (see for example Abramovich (1963)).

2.3.2 Simple Analysis for Plane Turbulent Jet in Uniform Streaming Flow

Although the analysis presented here specifically applies to two-dimensional flows it can be extended to axi-symmetric flows (see Newman (1967) for the general equations). Since the approach is to use the integral momentum equation some assumption must be made for the mean velocity profile. Following Townsend (1956) the velocity profile in both jets and wakes to a good degree of accuracy may be written as (see Fig. (2b)):

$$U = U_1 + u_o f(\eta) \tag{13}$$

where $f(\eta)$ is a universal function of $\eta = y/l_o$

U_1 is the velocity of the external irrotational flow and is independent of x,

u_o is a mean velocity scale ($= U_m - U_1$) and l_o is a characteristic length scale for this layer. Both u_o and l_o are functions of x only.

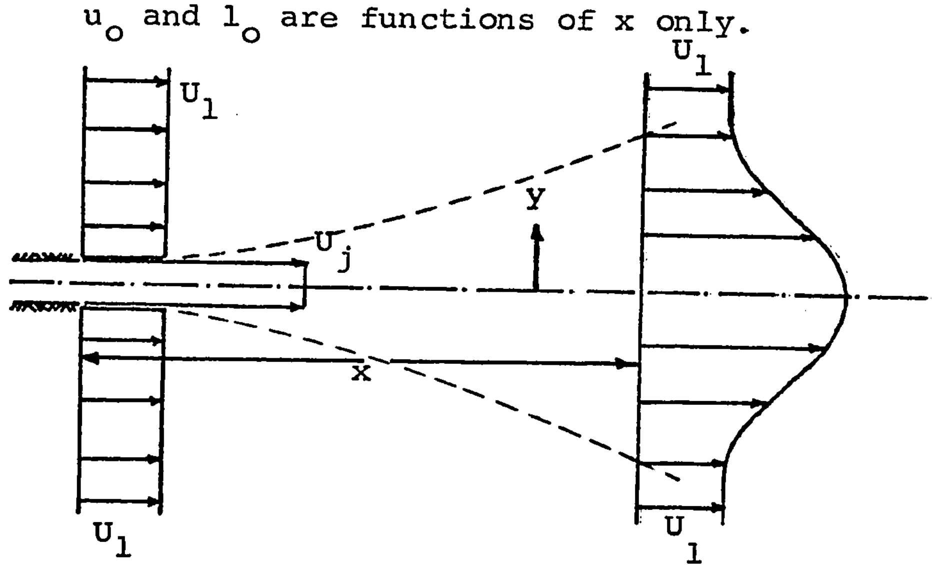

Because the shear flow under investigation is in a constant pressure field, the time-averaged boundary layer equation in downstream direction x (for constant density ρ, and using the approximate equation in the y-direction) applicable to this flow is:

$$U\frac{\partial U}{\partial x} + V\frac{\partial U}{\partial y} + \frac{\partial(\overline{u^2} - \overline{v^2})}{\partial x} = \frac{1}{\rho}\frac{\partial \tau}{\partial y}$$

which is the same as equation (1) with the same notation but different boundary conditions.

The time-averaged continuity equation (2) also remains the same. Hence combining the continuity equation and the momentum equation and integrating the resulting equation between limits $y = 0$ and $y = \infty$ (note that at both limits $\tau = 0$), one gets;

$$\frac{d}{dx}\int_0^\infty \left[(U^2 - UU_1) + (\overline{u^2} - \overline{v^2})\right] dy = 0 \qquad (14)$$

Once more if the difference between the normal Reynolds stresses (which is quite small compared to the excess momentum flux, except possibly near the edges where the intermittency fouls up the integral analysis anyway) can be neglected then equation (14) reduces to:

$$\int_0^\infty (U^2 - UU_1)\, dy = \text{constant} \qquad (15)$$

Equation (15) simply implies that the excess momentum in the x-direction is constant. Substituting the velocity profile equation (13) into the integrated momentum equation (15) one obtains:

$$l_o \left(u_o^2 I_2 + u_o U_1 I_1\right) = \text{constant } (= Me \text{ say}) \qquad (16)$$

where

$$I_1 = \int_o^\infty f(\eta)\, d\eta$$

and

$$I_2 = \int_o^\infty f^2(\eta)\, d\eta$$

There are two unknowns in equation (16), u_o and l_o, and hence another equation giving a connection between u_o and l_o is necessary before any prediction regarding their individual variations in the x-direction can be made.

Choice of an Auxiliary Equation

The choice of a second equation varies from one method to another but whatever the choice may be, a necessary requirement is that the method must exhibit proper variation of the eddy viscosity Reynolds number, $u_o l_o/\nu_T$. It should be mentioned that this requirement is not sufficient, as can be seen from the methods based on Townsend's hypothesis of "large eddy equilibrium" (e.g. Bradbury (1963) and Gartshore (1965)). Hence an additional requirement is that there must be agreement between predictions and experimental results. The author (1969) has recently shown that use of a simple auxiliary equation satisfies both the requirements mentioned above. In that paper the auxiliary equation was based on Abramovich's (1958, 1963) approach. The same equation can also be derived using a relativistic approach (Kruka and Eskinazi (1964); Newman (1969)). It will be shown in the next section that the auxiliary equation suggested by the author is approximately related to the structure parameter, (SP).

For reference, the auxiliary equations used by Abramovich (1958) and Patel (1969) are given below.

Abramovich, following Prandtl, suggested the following equation:

$$\frac{dl_o}{dx} = C_1 \left[\frac{u_o}{U_1 + \frac{u_o}{2}} \right] \tag{17}$$

Newman (1967) has derived equation (17) from consideration of a mixing layer in constant pressure. Equation (17) can be derived by using Prandtl's mixing length hypothesis, (i.e. $\tau = \rho l (\overline{q^2})^{1/2} \frac{\partial U}{\partial y}$), and "the restricted form of the energy-length model" of Spalding (1968). For self-preserving flows Townsend (1970), (see his equation (7.3)), obtains equation (17) by considering equations for the overall balance of momentum and total energy. It will be shown later that Abramovich's equation (17) is not in agreement with experimental results (Patel (1969)).

The auxiliary equation proposed by the author* is:

$$\frac{dl_o}{dx} = C \left[\frac{u_o}{U_1 + u_o} \right] \tag{18}$$

where C is the rate of growth of a plane jet in still surroundings.

The constant C depends on the definition of l_o. Usually l_o is defined as that value of y at which $(U-U_1) = \frac{1}{2} u_o$ and then the value of C can be obtained experimentally by analyzing data of a jet in still surroundings. The auxiliary equation (18) for a jet in still surroundings becomes $\frac{dl_o}{dx} = C$. Newman (1967) has collected values of C from various experimental investigations on jet in still air and suggests an average value of C = 0.104. The author's measured value, C = 0.103, is in agreement with Newman's suggestion. With the same definition of l_o as above the value of C_1 in Abramovich's equation (17) is 0.052 (i.e. $C_1 = C/2$).

Moreover, comparison of Abramovich's equation (17) and the auxiliary equation (18) indicates that there is hardly any qualitative difference between the two equations except for the change in constants. In effect, as will be shown later,

---

* The author proposed this auxiliary equation independently but later discovered that it was used to transform the longitudinal coordinate by Kruka and Eskinazi (1964) for wall jets in uniform streaming flow.

one is an approximately constant eddy viscosity Reynolds number hypothesis and the other is a variable eddy viscosity Reynolds number hypothesis with correct asymptotic values.

Solutions for l_o and u_o

The auxiliary equation (18) together with the integrated momentum equation (16) gives:

$$\frac{du_o}{dx} = -\left(\frac{C}{2Me}\right)\left[\frac{u_o^3\left(I_2 + I_1\frac{U_1}{u_o}\right)^2}{\left(1+\frac{U_1}{u_o}\right)\left(I_2 + \frac{1}{2}I_1\frac{U_1}{u_o}\right)}\right] \tag{19}$$

Equation (19) can now be integrated after some manipulations and the solution is:

$$\frac{1}{2}\left(\frac{U_1}{u_o}\right)^2 + \left(\frac{U_1}{u_o}\right) + \left(\frac{I_2}{I_1}\right)^2 \ln\left[\frac{I_2/I_1}{(I_2/I_1 + U_1/u_o)}\right]$$

$$+ \frac{(I_2/I_1)^2\,(1 - I_2/I_1)}{(I_2/I_1 + U_1/u_o)} - \left(\frac{I_2}{I_1}\right)\left(1 - \frac{I_2}{I_1}\right) = \frac{CI_1U_I^2}{Me}(x-x_o)$$

(20)

where x_o is introduced as the constant of integration and is such that when $x = x_o$, $u_o \to \infty$ and the hypothetical origin of the jet is identified.

Define $$\theta = \frac{Me}{U_1^2} = \int_o^\infty \frac{U}{U_1}\left(\frac{U}{U_1} - 1\right) dy \tag{21}$$

Equations (20) and (16) now reduce to:

$$\frac{1}{2}\left(\frac{U_1}{u_o}\right)^2 + \left(\frac{U_1}{u_o}\right) + \left(\frac{I_2}{I_1}\right)^2 \ln\left[\frac{I_2/I_1}{(I_2/I_1 + U_1/u_o)}\right]$$

$$+ \frac{(I_2/I_1)^2 (1 - I_2/I_1)}{(I_2/I_1 + U_1/u_o)} - \left(\frac{I_2}{I_1}\right)\left(1 - \frac{I_2}{I_1}\right) = CI_1 \left(\frac{x-x_o}{\theta}\right) \tag{22}$$

and $$\frac{l_o}{\theta} = \frac{1}{I_1}\left[\frac{(U_1/u_o)^2}{(I_2/I_1 + U_1/u_o)}\right] \tag{23}$$

These are most convenient expressions and give implicitly the variation of l_o with $(x-x_o)$.

From equations (22) and (23) for a strong jet,

$$u_o \propto (x-x_o)^{-1/2} \quad \text{and} \quad l_o \propto (x-x_o)$$

For a small-perturbation jet equation (22) reduces to

$$\left(\frac{U_1}{u_o}\right)^2 \propto (x-x_o) \tag{24}$$

and equation (23) then gives:

$$l_o \propto (x-x_o)^{1/2} \tag{25}$$

Hence it is noted that equations (22) and (23) do predict the expected behaviour of the jet development. Furthermore, note that there is only one experimental constant, C, in these equations.

The corresponding results are now obtained using Abramovich's equation (17). With equations (17) and (16) the solutions for u_o and l_o are:

$$\frac{1}{2}\left(\frac{U_1}{u_o}\right)^2 + \frac{1}{2}\left(\frac{U_1}{u_o}\right) + \left(\frac{I_2}{I_1}\right)^2 \ln\left[\frac{I_2/I_1}{(I_2/I_1 + U_1/u_o)}\right]$$

$$+ \frac{(I_2/I_1)^2(\frac{1}{2} - I_2/I_1)}{(I_2/I_1 + U_1/u_o)} - \left(\frac{I_2}{I_1}\right)\left(\frac{1}{2} - \frac{I_2}{I_1}\right) = C_1 I_1 \left(\frac{x-x_o}{\theta}\right) \tag{26}$$

and $$\frac{l_o}{\theta} = \frac{1}{I_1}\left[\frac{(U_1/u_o)^2}{(I_2/I_1 + U_1/u_o)}\right] \tag{27}$$

Equation (27) is identical to equation (23) as would be expected, however comparison of equations (26) and (22) indicates that equation (26) for a small-perturbation jet will give a value of $(U_1/u_o)^2$ at a particular downstream station half that obtained from equation (22), e.g. equation (26) for a small-perturbation jet becomes:

$$\left(\frac{U_1}{u_o}\right)^2 \approx CI_1 \left(\frac{x-x_o}{\theta}\right) \tag{28}$$

compared to the one obtained from equation (22),

$$\left(\frac{U_1}{u_o}\right)^2 \approx 2CI_1 \left(\frac{x-x_o}{\theta}\right) \tag{29}$$

2.3.3 An Approximate Relation Between the Auxiliary Equation (18) and the Structure Parameter (SP)

The merit of the auxiliary equation (18) for jets in uniform streaming flow has been demonstrated by Patel (1969), however, to agument confidence in its use, the following analysis is presented. The method is similar to that of Townsend (1970) but the objective is different. It is known that a plane jet in uniform streaming flow (i.e. U_1 = constant) is not a self-preserving flow (Patel and Newman (1961)) but the experimental evidence (Bradbury (1965)) suggests otherwise, and therefore, it is anticipated that an extension of Townsend's approach may prove useful as far as the turbulent structure of this flow is concerned.

Townsend obtains an equation for C_1 (see equation (17) for the definition of C_1 which is the entrainment constant) and relates it to the maximum effective strain. From this equation he then postulates whether or not a self-preserving development of a flow is possible. Although many assumptions must have been involved in deriving his equations, the specific equation for C_1 applicable to the plane jet in uniform streaming flow is not given. Thus the author has borrowed the spirit of his unifying and approximating approach for self-preserving turbulent shear flows in the present analysis. The purpose of the present investigation is to show that the auxiliary equation (18) for $\frac{dl_o}{dx}$ is related to the structure parameter, (SP), as defined in section 2.2. Because many assumptions are involved in the derivation, the analysis is presented in detail and each assumption is clearly stated.

Neglecting terms involving the viscous and normal Reynolds stresses, the integrated equation for the mean-flow kinetic energy for the flow under investigation is:

$$\frac{1}{2}\frac{d}{dx}\int_0^\infty U\,(U^2-U_1^2)\;dy = -\int_0^\infty \frac{\tau}{\rho}\frac{\partial U}{\partial y}\;dy \qquad (30)$$

Equation (30) can also be written as:

$$\frac{1}{2}\frac{d}{dx}\int_0^\infty U(U-U_1)^2\,dy = -\int_0^\infty \frac{\tau}{\rho}\frac{\partial U}{\partial y}\;dy \qquad (31)$$

It should be noted that in deriving equation (31) both the integral momentum equation (15) and the fact that U_1 is a constant are used.

To the same approximation as equation (30), the integrated turbulence energy equation is:

$$\frac{1}{2}\frac{d}{dx}\int_0^\infty U\,\overline{q^2}\;dy - \int_0^\infty \frac{\tau}{\rho}\frac{\partial U}{\partial y}\;dy = -\int_0^\infty \epsilon\;dy \qquad (32)$$

Adding equations (31) and (32), the integrated total energy equation becomes:

$$\frac{1}{2}\int_0^\infty \frac{\partial}{\partial x}\left[U\left\{(U-U_1)^2 + \overline{q^2}\right\}\right]dy = -\int_0^\infty \epsilon\;dy \qquad (33)$$

Equation (33) is in agreement with those given by Townsend (1970) and Newman (1968). (Note that adding equations (30) and (32) one obtains the integrated total energy equation given by Newman.)

Now following the approach similar to the one used for the plane jet in section 2.2 it is necessary to evaluate the integrated half momentum equation. For this purpose the velocity profile equation (13) is substituted in the momentum and continuity equations (1) and (2) respectively, and to the same approximation as the integrated momentum equation (15), the resulting equation is then integrated between limits $y = 0$ and $y = l_o$.

i.e.
$$\frac{(\overline{uv})_{\eta=1}}{u_o^2} = \frac{dl_o}{dx}\left[\frac{U_1}{u_o}\left(\frac{1}{2} - \int_0^1 f d\eta\right) + \frac{1}{2}\int_0^1 f d\eta - \int_0^1 f^2 d\eta\right]$$
$$- \frac{l_o}{u_o}\frac{du_o}{dx}\left[\frac{U_1}{u_o}\int_0^1 f d\eta + 2\int_0^1 f^2 d\eta - \frac{1}{2}\int_0^1 f d\eta\right] \tag{34}$$

Measurements of Bradbury (1963) show that the non-dimensional mean velocity distribution as represented by the velocity profile equation (13) may be given by an exponential function, $f = e^{-k\eta^2}$ where $k = \ln 2$ thus defining l_o, and the mean velocity scale, u_o, is given by $(U_m - U_1)$, where U_m is the maximum velocity at $y = 0$. Hence with the exponential velocity distribution one gets:

$$\left.\begin{aligned} \int_0^1 f d\eta = 0.81 \; ; \; I_1 &= \int_0^\infty f\, d\eta = 1.065 \\ \int_0^1 f^2 d\eta = 0.68 \; ; \; I_2 &= \int_0^\infty f^2 d\eta = 0.755 \\ I_3 &= \int_0^\infty f^3 d\eta = 0.62 \end{aligned}\right\} \tag{35}$$

In equation (35) one could use the values given by Bradbury (1963) based on experimental results.

From the momentum condition (i.e. equation (16)) it can be shown that:

$$\frac{l_o}{u_o}\frac{du_o}{dx} = -\frac{dl_o}{dx}\left[\frac{I_2/I_1 + U_1/u_o}{2(I_2/I_1) + U_1/u_o}\right] \tag{36}$$

Substituting equations (35) and (36) into equation (34) one obtains:

$$\frac{(\overline{uv})_{\eta=1}}{u_o^2} = 0.81\frac{dl_o}{dx}\left[\frac{(0.705 + U_1/u_o)}{(1.41 + U_1/u_o)}\right]\left(1.18 + \frac{U_1}{u_o}\right) - 0.31\frac{dl_o}{dx}(0.886 + U_1/u_o) \tag{37}$$

As expected equation (37) reduces to equation (7) when $U_1 \to 0$, but because of the subsequent simplifying assumptions in the following analysis the final equations do not display exact agreement with corresponding equations of section 2.2.

To simplify the algebra later, and following Townsendian spirit, equation (37) may be approximated to (see figure below):

$$\frac{(\overline{uv})_{\eta=1}}{u_o^2} \simeq 0.5\frac{dl_o}{dx}\left(1 + \frac{U_1}{u_o}\right) \tag{38}$$

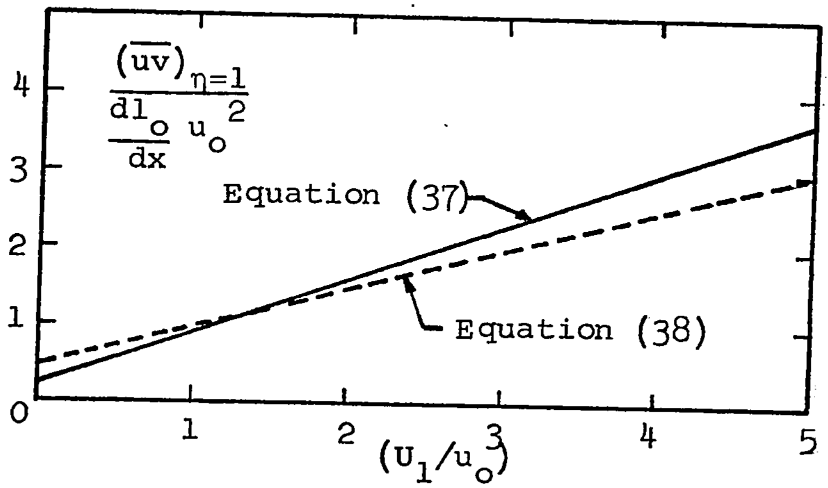

Comparison of the exact (equation (37)) and the approximated (equation (38)) half momentum equations

Reverting to the integrated total energy equation (33) which on substitution of the velocity profile equation (13) becomes:

$$\frac{1}{2} \int_o^\infty \frac{\partial}{\partial x} \left[u_o^2 \, f^2 \, (U_1 + u_o f) \right] dy + \frac{1}{2} \int_o^\infty \frac{\partial}{\partial x} \left[(U_1 + u_o f) \overline{q^2} \right] dy$$

$$= - \int_o^\infty \epsilon \, dy \qquad (39)$$

Equation (39) with $\overline{q^2} = \overline{q_1^2}\, g(\eta)$ becomes:

$$\frac{1}{2} U_1 \, u_o^2 \left[\frac{dl_o}{dx} + \frac{2l_o}{u_o} \frac{du_o}{dx} \right] \int_o^\infty f^2 d\eta + \frac{1}{2} u_o^3 \left[\frac{dl_o}{dx} + \frac{3l_o}{u_o} \frac{du_o}{dx} \right] \int_o^\infty f^3 d\eta$$

$$+ \frac{1}{2} U_1 \, \overline{q_1^2} \left[\frac{dl_o}{dx} + \frac{2l_o}{u_o} \frac{du_o}{dx} \right] \int_o^\infty g \, d\eta + \frac{1}{2} u_o \overline{q_1^2} \left[\frac{dl_o}{dx} + \frac{3l_o}{u_o} \frac{du_o}{dx} \right]$$

$$\int_o^\infty fg \, d\eta = - \int_o^\infty \epsilon \, dy \qquad (40)$$

In deriving equation (40) it is assumed that

$$\overline{q^2} = \overline{q_1^2}\, g(\eta) \quad \text{and} \quad \frac{\overline{q_1^2}}{u_o^2} = \text{constant.}$$

Combining equations (36) and (40) one gets:

$$\frac{1}{2}\left[\frac{(\frac{U_1}{u_o})^2}{2+ U_1/u_o}\right]\int_o^\infty f^2\, d\eta + \frac{1}{2}\left[\frac{(1+2\, U_1/u_o)}{2 + U_1/u_o}\right]\int_o^\infty f^3 d\eta$$

$$+ \frac{1}{2}\,\frac{\overline{q_1^2}}{u_o^2}\,\eta_\infty \left[\frac{(\frac{U_1}{u_o})^2}{2 + U_1/u_o}\right] + \frac{1}{2}\,\frac{\overline{q_1^2}}{u_o^2}\left[\frac{(1+2\, U_1/u_o)}{2 + U_1/u_o}\right]\int_o^\infty fg\, d\eta$$

$$= \eta_\infty\,\frac{l_o}{L_\epsilon}\,\frac{\overline{q_1^3}}{u_o^3}\,\frac{1}{dl_o/dx} \tag{41}$$

where equation (36) is approximated to:

$$\frac{l_o}{u_o}\,\frac{du_o}{dx} = -\,\frac{dl_o}{dx}\left[\frac{1 + U_1/u_o}{2 + U_1/u_o}\right]$$

and $\displaystyle\int_o^\infty \epsilon\, dy = \eta_\infty\, \overline{q_1^3}\, \frac{l_o}{L_\epsilon}$

$\displaystyle\int_o^\infty g\, d\eta = \eta_\infty$; η_∞ is taken, generally, as mean position of the super layer, i.e. a value of η at which intermittency is $\frac{1}{2}$. (See equation (9) for the present definition.) To reduce equation (41) further, the following assumptions are made:

$$\int_o^\infty fg \simeq 1.0 \quad ; \quad \eta_\infty = 2.0 \text{ and because } \int_o^\infty f^2\, d\eta = 0.755;$$

and $\int_0^\infty f^3\, d\eta = 0.62$, these two integrals are assumed to be the same. With these values equation (41) becomes:

$$\frac{1}{2}\left[\frac{(1 + U_1/u_o)^2}{2 + U_1/u_o}\right]\int_0^\infty f^2 d\eta + \frac{1}{2}\,\frac{\overline{q_1^2}}{u_o^2}\left[\frac{2\,(U_1/u_o)^2 + 2\,(U_1/u_o) + 1}{2 + U_1/u_o}\right]$$

$$= 2\;\frac{l_o}{L_\epsilon}\;\frac{\overline{q_1^3}}{u_o^3}\;\frac{1}{dl_o/dx} \tag{42}$$

The half momentum equation (38) and the total energy equation (42) give:

$$\frac{1}{2}\left[\frac{(1+ U_1/u_o)^2}{2 + U_1/u_o}\right]\int_0^\infty f^2 d\eta + \frac{1}{2}\,\frac{\overline{q_1^2}}{(\overline{uv})_{\eta=1}}\left\{\frac{1}{2}\,\frac{dl_o}{dx}\,(1 + U_1/u_o)\right.$$

$$\left.\left[\frac{2\,(U_1/u_o)^2 + 2\,(U_1/u_o) + 1}{2 + U_1/u_o}\right]\right\}$$

$$= 2\left[\frac{\overline{q_1^2}}{(\overline{uv})_{\eta=1}}\right]^{3/2}\frac{l_o}{L_\epsilon}\left(\frac{dl_o}{dx}\right)^{1/2}\left[\frac{1}{2}\left(1+\frac{U_1}{u_o}\right)\right]^{3/2} \tag{43}$$

Equation (43) is further approximated to:

$$\frac{1}{2}\left[1 + \frac{U_1}{u_o}\right]\int_0^\infty f^2 d\eta + \frac{1}{2}\,\frac{\overline{q_1^2}}{(\overline{uv})_{\eta=1}}\,\frac{dl_o}{dx}\left[\left(1 + \frac{U_1}{u_o}\right)^2\right]$$

$$= \frac{1}{\sqrt{2}}\;\frac{l_o}{L_\epsilon}\left[\frac{\overline{q_1^2}}{(\overline{uv})_{\eta=1}}\right]^{3/2}\left(\frac{dl_o}{dx}\right)^{1/2}\left[1 + \frac{U_1}{u_o}\right]^{3/2} \tag{44}$$

which becomes:

$$\int_o^\infty f^2 d\eta + \frac{\overline{q_1^2}}{(\overline{uv})_{\eta=1}} \frac{dl_o}{dx} (1 + \frac{U_1}{u_o}) = \sqrt{2} \frac{l_o}{L_\epsilon} \left\{ \left[\frac{\overline{q_1^2}}{(\overline{uv})_{\eta=1}} \right]^{3/2} \right.$$

$$\left. \left[\frac{dl_o}{dx} (1 + \frac{U_1}{u_o}) \right]^{1/2} \right\} \qquad (45)$$

As mentioned in section (2.2) $\overline{q_1^2}$ is defined as the value of $\overline{q^2}$ at $\eta = 1$ and with this definition it is clear from equation (45) that equation (18) (i.e. the auxiliary equation suggested by the author) is at least related to the structure parameter (SP). This relation is now established.

Rewriting equation (45) together with the auxiliary equation (18),

$$\int_o^\infty f^2 d\eta + C \left[\frac{\overline{q^2}}{\overline{uv}} \right]_{\eta=1} = \sqrt{2} \frac{l_o}{L_\epsilon} C^{1/2} \left[\frac{\overline{q^2}}{\overline{uv}} \right]^{3/2}_{\eta=1} \qquad (46)$$

It is interesting to note that in equation (46) the velocity ratio, $\frac{U_1}{u_o}$, does not appear explicitly and thus it appears that at least within the range of the approximations the turbulence structure parameter is not directly dependent on the velocity ratio ($C = C$ (velocity ratio)). It is interesting to note that for self-preserving flows Newman (1968) has predicted $(\overline{uv}/u_o^2)_{\eta=1}$ to be more or less constant (see his figure 2.2). In making this statement it is implied that the ratio (l_o/L_ϵ) is also independent of U_1/u_o. It will be shown later that Bradbury's (1963) measurements are in agreement with this general conclusion (see Fig. (7)).

It has been noted that as a consequence of the numerous simplifying assumptions equation (46) does not reduce to the equivalent equation for the plane jet in still air (i.e. compare equation (12)). However, some estimate of the error can be obtained by comparing measured values of the structure parameter to the one obtained from equation (46). To obtain the structure parameter from equation (46) it is required that some assumption regarding (l_o/L_ϵ) be made and following Townsend (1970) and Newman (1968) it is assumed that the ratio l_o/L_ϵ has the same value as that in the plane jet in still air i.e. $l_o/L_\epsilon = 0.230$. Note that $C = 0.103$. Hence, with these values equation (46) predicts the structure parameter to be about 5.5. The measured value of this parameter deduced from Bradbury's (he quotes a value of $\overline{uv}/\overline{q^2} = 0.2$) measurements is about 5.9 (see Fig. (7)). Considering the nature of the assumptions and the uncertainties in the measurements, the predicted value for the structure parameter is not unreasonable. Furthermore, it is noted that the nature of the total energy equation (46) is such that the structure parameter is weakly dependent on the value of C normally encountered in plane free shear flows. In other words it is anticipated that the structure parameter does not vary a great deal from one flow to another, e.g. in jets and wall jets in uniform streaming flow, jets and wall jets in still air, etc. Collected experimental results for these flows to be described later confirm this conclusion (see Fig. (96)).

2.3.4 Variation of the Eddy Viscosity Reynolds Number*

Patel (1969) has shown that the auxiliary equation (18) gives the correct asymptotic value of the eddy viscosity Reynolds number, $R_{T_w} = u_o l_o/\nu_T$, for a small perturbation jet or wake. In this section the details of R_T variation from one asymptotic value (i.e. corresponding to a jet in still air) to another (i.e. corresponding to a small increment jet or to a small deficit wake) are given. For this purpose it should be noted that either the half momentum integral equation or the mean energy equation may be used. The former will provide R_T values at $y = l_o$ (see at the end of this section) whereas the latter provides an average value of R_T at a particular downstream station. The mean energy integral equation is (see equation (30)):

$$\frac{1}{2}\frac{d}{dx}\int_0^\infty U\,(U^2-U_1{}^2)\,dy = -\int_0^\infty \frac{\tau}{\rho}\frac{\partial U}{\partial y}\,dy$$

The turbulent shear stress may be represented by

$$\frac{\tau}{\rho} = -\overline{uv} = \nu_T\ \frac{\partial U}{\partial y} \tag{47}$$

where ν_T is eddy viscosity.

It is assumed that ν_T is a function of x only (Townsend (1956)). It is noted that this assumption is not necessary if

*Note that R_T is directly related to (SP) by definition, i.e. $R_T \propto (u_o^2/\overline{q_1^2})(SP)$ and is a constant for a particular self-preserving flow.

the half momentum integral equation is used. Substituting the velocity profile equation (13) and (47) into the mean energy equation gives:

$$\left(I_3 + I_2 \frac{U_1}{u_o}\right) \frac{dl_o}{dx} + \left(3I_3 + 2I_2 \frac{U_1}{u_o}\right) \frac{l_o}{u_o} \frac{du_o}{dx} = - \frac{2I'}{R_T} \qquad (48)$$

where $I_3 = \int_o^\infty f^3(\eta)d\eta$

and $I' = \int_o^\infty \left(\frac{df}{d\eta}\right)^2 d\eta$

Now with equations (16), (18) and (19) equation (48) can be reduced to:

$$\frac{C}{(1 + U_1/u_o)} \left[\frac{\left(I_2 + I_1 \frac{U_1}{u_o}\right)\left(3I_3 + 2I_2 \frac{U_1}{u_o}\right)}{2\left(I_2 + \frac{1}{2} I_1 \frac{U_1}{u_o}\right)} - \left(I_3 + I_2 \frac{U_1}{u_o}\right) \right]$$

$$= \frac{2I'}{R_T} \qquad (49)$$

For a jet in still air equation (49) becomes:

$$R_{T_j} = \frac{4I'}{CI_3} \qquad (50)$$

For a small perturbation jet equation (49) reduces to:

$$R_{T_w} = \frac{2I'}{CI_2} \qquad (51)$$

It can be seen from equations (50) and (51) that both R_{T_j} and R_{T_w} are absolute constants throughout the respective flow fields and that their values are indeed different. With $C = 0.104$ and using Bradbury's (1963) integral values (i.e. $I'/I_3 = 0.9125$ and $I'/I_2 = 0.745$) $R_{T_j} = 35.1$ compared to Bradbury's value of $R_{T_j} = 36.5$, the difference being entirely due to the value of C used to calculate R_{T_j}. Bradbury used $C = 0.10$. Similarly $R_{T_w} = 14.35$ compared to 14.7 which Townsend obtained from measurements of the rate of spread of the wake. Note that $R_{T_j} = 32.6$ and $R_{T_w} = 13.3$ if the velocity profile is assumed to be Gaussian. Newman (1967) has obtained $R_{T_w} = 13.3$ for both round and two-dimensional wakes from the measurements of Townsend.

It is easy to show that the corresponding results using Abramovich's equation (17) are:

$$\frac{C_1}{\left(\frac{1}{2} + \frac{U_1}{u_o}\right)} \left[\frac{\left(I_2 + I_1 \frac{U_1}{u_o}\right)\left(3I_3 + 2I_2 \frac{U_1}{u_o}\right)}{2\left(I_2 + \frac{1}{2} I_1 \frac{U_1}{u_o}\right)} - \left(I_3 + I_2 \frac{U_1}{u_o}\right) \right]$$

$$= \frac{2I'}{R_T} \qquad (52)$$

For a jet in still air equation (52) reduces to:

$$R_{T_j} = \frac{2I'}{C_1 I_3} = \frac{4I'}{CI_3} \qquad (53)$$

For a small perturbation jet equation (52) reduces to:

$$R_{T_w} = \frac{2I'}{C_1 I_2} = \frac{4I'}{CI_2} \tag{54}$$

It is now obvious that as a consequence of the assumption (i.e. the characteristic velocity is replaced by the mean, $\frac{1}{2}(U_1 + U_m)$) which Abramovich made, his method fails to give the correct value of R_{T_w}.

It was mentioned at the beginning of this section that the variation of R_T can be obtained without imposing the restriction on ν_T (i.e. $\nu_T(x)$ is taken as an average value at a cross section) if the half-momentum equation were used. In fact it can be seen from equation (37) which is the integrated half-momentum equation and substituting equation (47) into equation (37) and taking the limit as $U_1 \to 0$ one gets:

$$R_{T_j} = -4.9 \frac{(f')_{\eta=1}}{dl_o/dx} \tag{55}$$

where $(f')_{\eta=1} = \frac{df}{d\eta}$ at $\eta = 1$.

For the exponential profile and $C = 0.103$, equation (55) gives $R_{T_j} = 32.6$ which is the same as derived from equation (49).

Similarly equation (37), for a small perturbation jet (i.e. $u_o \to 0$), gives:

$$R_{T_w} = \frac{-(f')_{\eta=1}}{0.5 \frac{U_1}{u_o} \frac{dl_o}{dx}} \tag{56}$$

From equation (18) it can be shown that for a small perturbation jet:

$$\frac{U_1}{u_o} \frac{dl_o}{dx} = C \tag{57}$$

Hence equation (56) with equation (57) and the exponential velocity distribution gives $R_{T_w} = 13.3$ which is, once more, in agreement with the value derived from equation (49). Note that Abramovich's equation (17) together with equation (56) will give $R_{T_w} = 26.6$ which is not in agreement with the measured value.

Finally, as mentioned before, the validity of equation (18) may be confirmed by comparing experimental results with predictions from equations (22) and (23).

2.4 Extended Analysis for Wall Jets and the Asymmetric Jet

2.4.1 Wall Jets in Uniform Streaming Flow

As stated in the introduction, plane wall jets in streaming flow form a special group of flow configurations in the general class of asymmetric flows. Therefore, before extending the analysis of section (2.3) to the turbulent asymmetric jet it is of interest to see whether or not the analysis is capable of predicting the flow development for a plane wall jet in uniform streaming flow (see the sketch below).

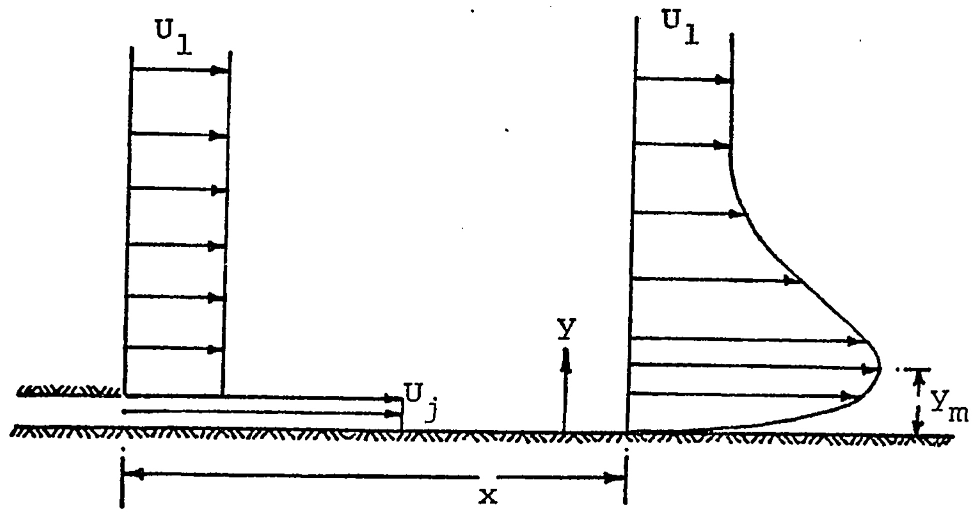

It should be noted that the wall jets in uniform streaming flow offer an excellent opportunity to evaluate the merit of the analysis and possibly some direction for its extension because in many investigations of wall jets (e.g. Patel (1962); Kruka and Eskinazi (1964); Gartshore (1965), etc.) it is found experimentally that the mean velocity profiles are approximately similar to half the profile for a jet in uniform streaming flow. If the analysis of section (2.3) is applied to the outer part of the wall jets additional assumptions have to be made. The assumptions are:

(a) Reynolds shear stress at $y = y_m$ is zero, where y_m is the value of y at which $U = U_m$, and

(b) changes in y_m with respect to x are small.

Strictly speaking both assumptions are invalid, nevertheless, it is observed that the measured shear stress at the point of maximum velocity is small compared to some characteristic shear stress, say at $y = l_o$ (for example see the results of Bradshaw and Gee (1960); Kruka and Eskinazi (1964)), and the variation of y_m with respect to x is of second order. As a matter of interest it is noted that changes in y_m with respect to x have compensating effects (Patel (1969)). Hence one may expect the previous analysis (section 2.3) to apply, at least approximately, to the outer part of the wall jets in uniform streaming flow. Figure (3) defines the notation and with these definitions variations in u_o and l_o are given by equations (22) and (23). The values of I_n (n = 1, 2, 3, etc.) are kept the same as before because the non-dimensional mean velocity profiles are practically the same. It is reasonable to assume that the wall on one side affects the growth of the outer part, presumably by suppressing transverse fluctuations, and hence the constant C would be different. On the basis of linear growth Bradshaw and Gee (1960) have concluded that the influence of a wall is fairly small. This is contrary to experimental results because the experimental rate of growth for a wall jet in still air is about half that for a free jet in still air. Indeed this suggests that the distribution of $(\overline{v^2}/u_o^2)$ across a free jet would be about twice that for the wall jet provided the above assumption is valid. Guitton (1970) has compared his measurements of $(\overline{v^2}/u_o^2)$ for a plane wall jet in still air with the author's free jet results and his comparison confirms the above conclusion. Furthermore, for free shear flows (outer part of wall jets included) it is observed that mean flow energy is transferred first to u-component of turbulence, then to v-component and finally to w-component, therefore, any reduction in $\overline{v^2}$

would reflect as an increase in $\overline{w^2}$ provided the transfer mechanism follows the above sequence. Guitton's turbulence measurements for the plane wall jet show that the reduction in $(\overline{v^2}/u_o^2)$ is reflected as an increase in $(\overline{w^2}/u_o^2)$. His measurements also show that both $(\overline{u^2}/u_o^2)$ and $(\overline{w^2}/u_o^2)$ are of the same order of magnitude whereas $(\overline{v^2}/u_o^2)$ is about half of $(\overline{u^2}/u_o^2)$ or $(\overline{w^2}/u_o^2)$. On the other hand, for a free jet in still air the measurements (to be described later) show that $(\overline{v^2}/u_o^2)$ and $(\overline{w^2}/u_o^2)$ are of the same order of magnitude and slightly smaller than $(\overline{u^2}/u_o^2)$. For a free jet in still air and a wall jet in still air the distributions of $(\overline{u^2}/u_o^2)$ are approximately the same. Thus, even though loss of momentum to a wall is small, the streamwise variation of the outer part of a wall jet is strongly influenced by the wall.

For wall jets in still air the values of C collected from various investigations are given below:

INVESTIGATORS	VALUE OF C
Sigalla (1958)	0.0664
Bradshaw and Gee (1960)	0.0695
Schwarz and Cosart (1961)	0.0678
Patel (1962)	0.0650
Kruka and Eskinazi (1964)	0.0737
Gartshore and Hawaleshka (1964)	0.0650
Guitton (1968)	0.0710

Finally, equations (22) and (23) together with the appropriate value for C will be used to predict the development of wall jets in uniform streaming flow.

2.4.2 The Asymmetric Turbulent Jet

It should be recalled that the ultimate aim of the analysis presented in sections (2.2) and (2.3) was to describe the asymmetric jet. As mentioned before the geometric division of the asymmetric jet is assumed. Application of the analysis of previous sections to the asymmetric jet implies that any interaction from one part to other is ignored. This is not a serious restriction for wall jets because of the presence of the wall. However, for the asymmetric jet there is no apparent restriction on fluid parcels making excursions from one side to the other. Thus there is some degree of interaction which may depend on the shear stress at the point of maximum velocity and on the history of fluid crossing the maximum velocity layer with velocity V_m where V_m is the transverse velocity at the point of maximum velocity. The analyses of previous sections, therefore, cannot be applied directly to the asymmetric jet. It is of interest to note that the shear stress at the point of maximum velocity is expected to be small compared to some characteristic shear stress in the layers, say at inflection points. The influence of a finite V_m is difficult to estimate and, therefore, two approaches are presented. The first one is slightly more exact than the second but the second one is more useful from a practical point of view.

(a) The First Approach

Figure (4) shows a sketch of the asymmetric jet which is divided into a half jet in uniform streaming flow (sometimes referred to as the streaming side) and a half jet in still air (sometimes referred to as the zero velocity side).

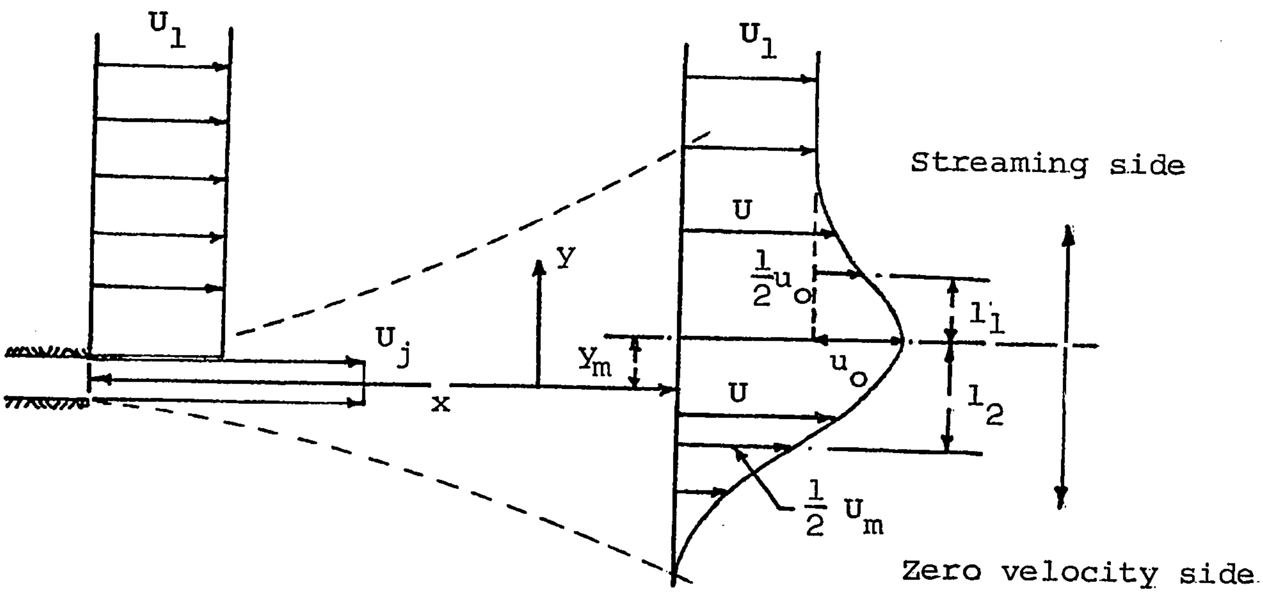

The velocity profiles on the two sides of the asymmetric jet are assumed to be,

Streaming Side:

$$U = U_1 + u_o f(\eta_1) \tag{58}$$

where $\eta_1 = \frac{y-y_m}{l_1}$

Zero velocity side:

$$U = U_m f(\eta_2) \tag{59}$$

where $\eta_2 = \frac{y_m - y}{l_2}$ and $U_m = U_1 + u_o$

Note that because of asymmetry two length scales (l_1 and l_2) are now required to specify the velocity distributions. Moreover, the locus of the maximum velocity points is also unspecified although experiments indicate linear variation of y_m with the downstream distance, x. Furthermore, it is reasonable to assume the transverse velocity $V_1 = 0$, in the uniform stream far away from the vortical zone. In actual experimental investigation this condition was satisfied by providing a top wall in a working section. With these preliminaries the equations of motion can be formulated as follows.

For the streaming side, the continuity equation when combined with the velocity profile equation (58) and integrated between limits η_1 and $\eta_1 = 0$, gives:

$$\frac{V}{u_o} = f(\eta_1)\frac{dy_m}{dx} + \left(\frac{dl_1}{dx} + \frac{l_1}{u_o}\frac{du_o}{dx}\right)\left[I_1 - \int_o^{\eta} f(\eta_1)d\eta_1\right] + \eta_1 f(\eta_1)\frac{dl_1}{dx} \qquad (60)$$

where $I_1 = \int_o^{\infty} f(\eta)d\eta$

Similarly, substituting equations (58) and (60) into the momentum equation (1) and integrating between limits η_1 and $\eta_1 = 0$ (the normal Reynolds stress terms are neglected) one gets:

$$\left[\frac{(\overline{uv})}{u_o^2}\right]_{\eta_1=0} - \frac{(\overline{uv})}{u_o^2} = \frac{U_1}{u_o}\frac{l_1}{u_o}\frac{du_o}{dx}\int_0^{\eta_1} f(\eta_1)d\eta - \frac{U_1}{u_o}(f(\eta_1)-1)\frac{dy_m}{dx}$$

$$- \frac{U_1}{u_o}\frac{dl_1}{dx}\left[\eta_1 f(\eta_1) - \int_0^{\eta_1} f(\eta_1)d\eta_1\right] + \frac{l_1}{u_o}\frac{du_o}{dx}\int_0^{\eta_1} f^2(\eta_1)d\eta_1$$

$$+ \left(\frac{dl_1}{dx} + \frac{l_1}{u_o}\frac{du_o}{dx}\right)\left[I_1\,(f(\eta_1)-1) - f(\eta_1)\int_0^{\eta_1} f(\eta_1)d\eta_1\right.$$

$$\left. + \int_0^{\eta_1} f^2(\eta_1)d\eta_1\right] \tag{61}$$

From equation (61) it is clear that (i.e. when $\eta_1 \to \infty$, $(\overline{uv}) \to 0$ and $f(\infty) \to 0$),

$$\frac{(\overline{uv})}{u_o^2}\eta_1{=}0 = \left(\frac{dl_1}{dx} + \frac{2l_1}{u_o}\frac{du_o}{dx}\right) I_2 + \left(\frac{dl_1}{dx} + \frac{l_1}{u_o}\frac{du_o}{dx}\right)\left(\frac{U_1}{u_o} - 1\right) I_1$$

$$+ \frac{U_1}{u_o}\frac{dy_m}{dx} \tag{62}$$

where $I_2 = \int_0^{\infty} f^2 d\eta$

For the zero velocity side the continuity equation when combined with the velocity profile equation (59) and integrated between limits η_2 and $\eta_2 = 0$ gives:

$$\frac{V}{U_m} = \left(\frac{dl_2}{dx} + \frac{l_2}{U_m}\frac{du_o}{dx}\right)\int_o^{\eta_2} f(\eta_2)d\eta_2 + \left(\frac{dl_1}{dx} + \frac{l_1}{u_o}\frac{du_o}{dx}\right)\frac{u_o}{U_m} I_1$$

$$+ \left(\frac{u_o}{U_m} + f(\eta_2) - 1\right)\frac{dy_m}{dx} - \frac{dl_2}{dx}\eta_2 f(\eta_2) \qquad (63)$$

where $U_m = (U_1 + u_o)$

The integrated momentum equation for the zero velocity side is:

$$\frac{(uv)_{\eta_2=0}}{U_m^2} - \frac{(\overline{uv})}{U_m^2} = \left(\frac{dl_2}{dx} + \frac{l_2}{U_m}\frac{du_o}{dx}\right)f(\eta_2)\int_o^{\eta_2} f(\eta_2)d\eta_2$$

$$- \left(\frac{dl_2}{dx} + \frac{2l_2}{U_m}\frac{du_o}{dx}\right)\int_o^{\eta_2} f^2(\eta_2)d\eta_2$$

$$+ (f(\eta_2) - 1)\left[I_1\frac{u_o}{U_m}\left(\frac{dl_1}{dx} + \frac{l_1}{u_o}\frac{du_o}{dx}\right) + \left(\frac{u_o}{U_m} - 1\right)\frac{dy_m}{dx}\right]$$

$$(64)$$

The boundary condition on the zero velocity side (i.e. at $y=-\infty$ $\eta_2 = \infty$; $\overline{uv} = 0$ and $f(\infty) = 0$) reduces equation (64) to:

$$-\left(\frac{\overline{uv}}{U_m^2}\right)_{\eta_2=0} = I_2\left(\frac{dl_2}{dx} + \frac{2l_2}{U_m}\frac{du_o}{dx}\right) + I_1\frac{u_o}{U_m}\left(\frac{dl_1}{dx} + \frac{l_1}{u_o}\frac{du_o}{dx}\right)$$

$$+ \left(\frac{u_o}{U_m} - 1\right)\frac{dy_m}{dx} \qquad (65)$$

It should be pointed out that because of the different length scales on either side of the maximum velocity point, (i.e. at $\eta_1 = \eta_2 = 0$), the gradient of the non-dimensional Reynolds stress distribution will not be continuous but the magnitude of the Reynolds stress at the maximum velocity point must be the same. Hence it can be shown from the momentum equations (62) and (65) that the locus of maximum velocity points must satisfy the following equation:

$$\frac{dy_m}{dx} = I_2 \frac{u_o^2}{U_1^2} \left(\frac{dl_1}{dx} + \frac{2l_1}{u_o}\frac{du_o}{dx}\right) + I_2 \frac{U_m^2}{U_1^2} \left(\frac{dl_2}{dx} + \frac{2l_2}{U_m}\frac{du_o}{dx}\right)$$

$$+ \; 2I_1 \frac{u_o}{U_1} \left(\frac{dl_1}{dx} + \frac{l_1}{u_o}\frac{du_o}{dx}\right) \qquad (66)$$

In equation (66) the second term on the right hand side is positive and usually much greater than the other combined terms, therefore (dy_m/dx) is generally positive, i.e. the locus of the points of maximum velocity moves towards the streaming side as the flow develops downstream. This is in agreement with measurements and would be expected physically.

In the set of equations (62), (65) and (66) there are five unknowns, namely, l_1, l_2, u_o, y_m and $(\overline{uv})_m$. In order to solve these unknowns, of course, five equations are required. It should be realized that there is no additional independent equation which can be formulated for the problem without introducing further unknowns. Hence at this stage some assumptions are required. Because of the assumed similarity between a half jet in uniform streaming flow and the streaming side of the asymmetric jet, it may be possible to use the auxiliary equation (18) and assume $(\overline{uv})_m$ to be negligible. Now the number of equations is equal to the number of unknowns with only one constant (i.e. C) which can be established from experimental results for a jet in still air. In principle, therefore, these equations can be solved by using starting conditions (i.e. solutions are now restricted to only a particular case of the asymmetric jet unless some technique has been developed to calculate the initial conditions) and the Runge Kutta technique. However, to obtain equations (i.e. for l_1, l_2 and u_o) of wider practical use and since some assumptions are, in any case, necessary the above analysis is reformulated below.

(b) Simple Analysis for the Asymmetric Jet

The following analysis, although simple, seems to work very well. It uses the same momentum equations derived above but they are remodelled for the present purpose. For the rate of growth on the streaming side the auxiliary equation (18) is used. The only additional information required is obtained from experimental variation of the ratio (l_2/l_1). With this information it is possible to calculate explicitly the variations of l_1, l_2 and u_o for the asymmetric jet.

For the streaming side equation (62) can be rewritten as:

$$\frac{d}{dx}\left[l_1(I_1U_1u_o + I_2u_o^2)\right] = (\overline{uv})_{\eta_1=0} + u_o\frac{d}{dx}\left[I_1u_ol_1 - U_1y_m\right] \tag{67}$$

Similarly for the zero velocity side equation (65) can be re-written as:

$$\frac{d}{dx}\left[I_2\ l_2\ U_m^2 \right] = -\ (\overline{uv})_{\eta_2=0} - U_m \frac{d}{dx}\left[I_1\ u_o\ l_1 - U_1\ y_m \right] \qquad (68)$$

Adding equations (67) and (68) one obtains:

$$\frac{d}{dx}\left[l_1 (I_1 U_1 u_o + I_2 u_o^2) \right] + \frac{d}{dx}\left[I_2 l_2 U_m^2 \left(1 + \frac{I_1}{I_2}\frac{l_1}{l_2}\frac{U_1 u_o}{U_m^2} - \frac{1}{I_2}\frac{y_m}{l_2}\frac{U_1^2}{U_m^2}\right) \right] = 0 \qquad (69)$$

Let

$$l_1\ (I_1 U_1 u_o + I_2 u_o^2) = Me_1(x) \qquad (70)$$

and

$$I_2 l_2 U_m^2\ \left(1 + \frac{I_1}{I_2}\frac{l_1}{l_2}\frac{U_1 u_o}{U_m^2} - \frac{1}{I_2}\frac{y_m}{l_2}\frac{U_1^2}{U_m^2}\right) = Me_2(x) \qquad (71)$$

Hence from equation (69) it is clear that:

$$Me_1(x) + Me_2(x) = \text{constant, say } M \qquad (72)$$

From equations (67) and (68) it can be seen that if the interaction between the two parts were absent then Me_1 and Me_2 would be constants and analysis of sections (2.2) and (2.3) would apply. However, because Me_1 and Me_2 are functions of x this implies some interaction between the two parts. The degree of interaction depends on asymmetry which in turn may be expressed by the ratio (l_2/l_1). It is difficult to estimate explicitly the exact division of momentum M between the streaming side and the zero velocity side, but for simplicity the x-wise dependence of both Me_1 and Me_2 is isolated by introducing a non-dimensional factor K such that

$$\left.\begin{aligned} Me_1(x) &= KM \\ \text{and} \qquad Me_2(x) &= (1-K)M \end{aligned}\right\} \tag{73}$$

where K is a function of x only and M is defined as follows:

$$M = bU_j \left(U_j - \frac{1}{2} U_1\right) \tag{74}$$

Now from equations (70), (71) and (73) it can be shown that

$$\frac{(1-K)}{K} = \frac{l_2}{l_1} \left[\frac{\left(1 + \frac{U_1}{u_o}\right)^2}{\left(1 + \frac{I_1}{I_2} \frac{U_1}{u_o}\right)} \right] \left\{ 1 + \frac{I_1}{I_2} \frac{l_1}{l_2} \frac{U_1 u_o}{U_m^2} - \frac{I}{I_2} \frac{y_m}{l_2} \frac{U_1^2}{U_m^2} \right\} \tag{75}$$

Examination of equation (75) indicates that over the whole range of the asymmetric jet (i.e. from $U_m \gg U_1$ to $u_o \rightarrow 0$) the last two terms in the curly bracket are much smaller than one and hence they may be neglected. Experimental results to be described later substantiate this assumption. Therefore equations (75) and (71) can be approximated to

$$\frac{l_2}{l_1} \simeq \frac{(1-K)}{K} \left[\frac{1 + \frac{I_1}{I_2} \frac{U_1}{u_o}}{\left(1 + \frac{U_1}{u_o}\right)^2} \right] \tag{76}$$

and $\quad I_2\, l_2\, U_m^2 \approx Me_2(x) = (1 - K)M \qquad (77)$

It is clear from equation (76) that when U_1 tends to zero (i.e. for a jet in still air) K must tend to $\frac{1}{2}$. On the other hand the limiting value of K for a small increment jet (i.e. $u_o \to 0$) cannot be estimated from equation (76) because K may depend on the ratio (U_1/u_o) in some unknown fashion. Note that equation (76) is not an independent equation but it does provide a guide to the estimation of K.

The two independent equations (70) and (77) contain four unknowns (i.e. l_1, l_2, u_o and K) and equation (76) suggests how the variation in K can be obtained from experimental results, but this is not sufficient to calculate the four unknowns. It should be recalled that in the previous analysis three more independent equations are required. Hence to close the system of equations for the simple analysis it is proposed to use the auxiliary equation (18) for the rate of growth on the streaming side and an equation for K obtained from experimental results.

The following equation fits the present experimental results fairly well when (l_2/l_1) is plotted against $\dfrac{(1+(I_1/I_2)\,U_1/u_o)}{(1+U_1/u_o)^2}$ (see figure (91)):

$$\frac{l_2}{l_1} = 1 - 2\log_{10}\left[\frac{(1+[I_1/I_2]\,U_1/u_o)}{(1+U_1/u_o)^2}\right] \qquad (78)$$

Hence from equations (76) and (78) one gets,

$$K = \frac{1}{1 + \dfrac{(1 + U_1/u_o)^2}{1+(I_1/I_2)(U_1/u_o)} \left\{ 1 - 2\log_{10} \left[\dfrac{1+(I_1/I_2)(U_1/u_o)}{(1+U_1/u_o)^2} \right]\right\}} \tag{79}$$

From equations (70) and (79) it can be shown that

$$\frac{l_1}{b\frac{U_i}{U_1}(\frac{U_i}{U_1} - \frac{1}{2})} = \frac{\frac{1}{I_1}\left[(U_1/u_o)^2/(I_2/I_1 + U_1/u_o)\right]}{1 + \left[\dfrac{(1 + \frac{U_1}{u_o})^2}{1 + \frac{I_1}{I_2}\frac{U_1}{u_o}}\right]\left\{ 1 - 2\log_{10}\left[\dfrac{1 + \frac{I_1}{I_2}\frac{U_1}{u_o}}{(1+ \frac{U_1}{u_o})^2}\right]\right\}} \tag{80}$$

and from equations (77) and (79),

$$\frac{l_2}{b\frac{U_i}{U_1}(\frac{U_i}{U_1} - \frac{1}{2})} = \frac{\frac{1}{I_1}\left[\dfrac{(\frac{U_1}{u_o})^2}{I_2/I_1 + U_1/u_o}\right]\left\{ 1 - 2\log_{10}\left[\dfrac{1 + \frac{I_1}{I_2}\frac{U_1}{u_o}}{(1+U_1/u_o)^2}\right]\right\}}{1 + \dfrac{(1 + \frac{U_1}{u_o})^2}{1 + \frac{I_1}{I_2}\frac{U_1}{u_o}}\left\{ 1 - 2\log_{10}\left[\dfrac{1 + \frac{I_1}{I_2}\frac{U_1}{u_o}}{(1+ \frac{U_1}{u_o})^2}\right]\right\}} \tag{81}$$

Equations (80) and (81) give the variations of l_1 and l_2 in terms of the ratio (U_1/u_o). Then the variation of the ratio (U_1/u_o) with downstream distance, x, is obtained as follows:

Combining equation (70) and the auxiliary equation (18) one gets:

$$\frac{du_o}{dx} = \frac{u_o \left(1 + \frac{I_1}{I_2}\frac{U_1}{u_o}\right)}{2\left(1 + \frac{1}{2}\frac{I_1}{I_2}\frac{U_1}{u_o}\right)} \quad \frac{1}{K}\frac{dK}{dx} - \frac{CI_2}{2MK} \frac{u_o^3 \left(I + \frac{I_1}{I_2}\frac{U_1}{u_o}\right)^2}{\left(1+ \frac{U_1}{u_o}\right)\left(1 + \frac{1}{2}\frac{I_1}{I_2}\frac{U_1}{u_o}\right)}$$

(82)

It can be seen that to solve equation (82) explicitly with the variation of K given by equation (79) is quite a complex problem. The complexity may be reduced by approximating the variation of K by the simple expression given below (see figure (93) for variation of K versus U_1/u_o):

$$K = \frac{1}{2\left(1 + \frac{1}{2}\frac{I_1}{I_2}\frac{U_1}{u_o}\right)} \qquad (83)$$

Substituting equation (83) into equation (82) gives,

$$\frac{du_o}{dx}\left[1 - \frac{\frac{I_1}{I_2}\left(\frac{U_1}{u_o}\right)\left(1 + \frac{I_1}{I_2}\frac{U_1}{u_o}\right)}{\left(2 + \frac{I_1}{I_2}\frac{U_1}{u_o}\right)^2}\right] = - \frac{CI_2 u_o^3}{M} \frac{\left(1 + \frac{I_1}{I_2}\frac{U_1}{u_o}\right)^2}{\left(1 + U_1/u_o\right)}$$

(84)

The solution of equation (84) is:

$$\frac{(I_2/I_1)^3}{CI_2}\left[3\ln\left(1+\frac{I_1}{I_2}\frac{U_1}{u_o}\right) - 4\ln\left\{\frac{2+2\frac{I_1}{I_2}\frac{U_1}{u_o}}{2+\frac{I_1}{I_2}\frac{U_1}{u_o}}\right\} + \frac{(I_1/I_2-1)}{(1+\frac{I_1}{I_2}\frac{U_1}{u_o})}\right.$$

$$\left. + \frac{(8-4\frac{I_1}{I_2})}{(2+\frac{I_1}{I_2}\frac{U_1}{u_o})} - (3-\frac{I_1}{I_2})\right] = \frac{(x-x_o)}{b\frac{U_j}{U_1}(\frac{U_j}{U_1}-\frac{1}{2})} \tag{85}$$

where x_o is introduced as the constant of integration and is such that when $x = x_o$, $u_o \rightarrow \infty$ and the hypothetical origin of the jet is identified.

In summary, the assumptions involved in the simple analysis are enumerated below:

(1) The usual boundary layer approximations are assumed to be applicable.

(2) The mean velocity profiles on the two sides of the asymmetric jet are assumed to be geometrically similar with the length scales l_1 and l_2 and the velocity scales u_o and U_m (see equations (58) and (59)).

(3) The gradient of the difference of normal Reynolds stresses (i.e. $\overline{u^2} - \overline{v^2}$) in the momentum equation for the downstream direction is neglected.

(4) The excess momentum on the streaming side is assumed to be a fraction, (K), of the total excess momentum, M, at a slot exit where M is given by equation (74) (see sketch below).

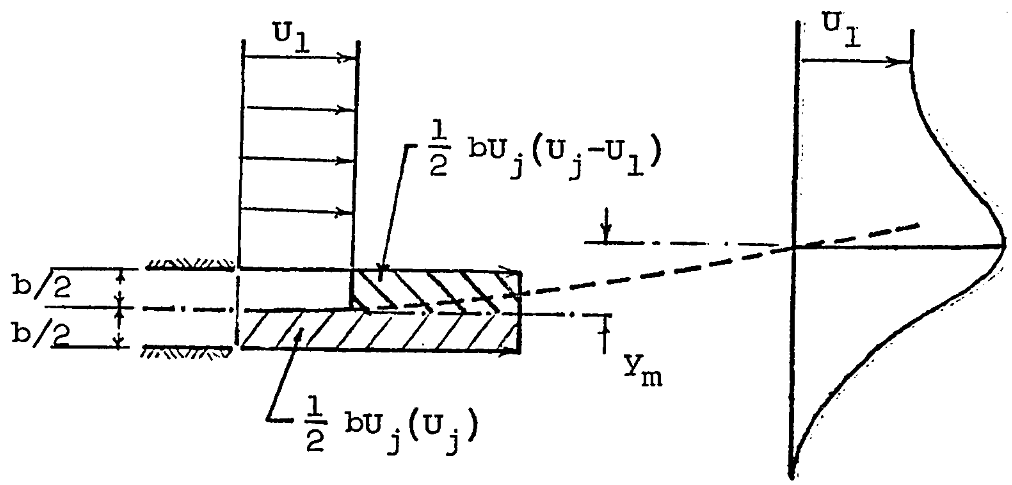

$$M = \frac{1}{2}\, bU_j(U_j-U_1) + \frac{1}{2}\, bU_j(U_j)$$

(5) The empirical expression (equation (79)) describing the variation of K obtained from the experimental results (Fig. (91)) is simplified (see equation (83) and Fig. (93)) so that the variation of the velocity scale u_o can be given explicitly.

(6) The auxiliary equation (18) is assumed to be applicable to the streaming side of the asymmetric jet.

The experimental investigation of the asymmetric jets (to be described later in sections (7 and 9)) justifies the above set of assumptions.

3. DEMONSTRATIONS OF APPLICABILITY OF THE SIMPLE ANALYSIS (SECTION 2.3)

3.1 Plane Turbulent Jets in Uniform Streaming Flow

To check equations (22) and (23) the experimental results of Bradbury and Riley (1967) for plane, symmetrical turbulent jets in uniform streaming flow are selected. Furthermore, for the purpose of demonstrating the conclusion regarding the structure parameter being independent of the velocity ratio, U_1/u_o, the results of Bradbury (1963) will be used.

The reason for using the results of Bradbury and Riley is that they have given their results in tabulated form and, moreover, their results are considered to be of fairly good quality. One of the serious objections to their tabulated results is that they have been obtained by arbitrarily shifting the curves to correlate the results for all the (U_1/U_j) ratios they investigated. The details are not given except that the shifts are attributed to changes in the hypothetical origin, x_o, but these are not listed. Fortunately, they have presented some of their raw data in graphical form and these are used for the comparisons in Fig. (6).

Fig. (5) gives the variation in growth of the jet, l_o, in accordance with equation (23). The tabulated results of Bradbury and Riley are compared with the prediction from equation (23) which is represented by a solid line. Use of their tabulated results is possible here because this presentation does not involve x_o. The agreement between experimental results and equation (23) is excellent as would be expected because equation (23) is simply a statement of conservation of excess momentum.

Fig. (6) shows the variation of velocity scale u_o with x. In this figure both tabulated and raw data (obtained from their $((\frac{U_1}{u_o})^2$ vs x/θ curves) are given, the former being represented by a broken line. Also included in the figure is a curve representing equation (22) with $2CI_1 = 0.2025$. In replotting the data of Bradbury and Riley for all the cases of (U_1/U_j) shown in Fig. (6) it was noted that $(x_o/2\theta)$ was small and hence it was neglected. The effect of arbitrary adjustments of the curves by them clearly shows in the disagreement between the predicted curve (equation (22)) and the dotted line and it also shows that such adjustments are indeed not justified because the raw data and prediction from equation (22) are in agreement.

Since the publication (Patel (1969)) of the present results other investigators have attempted to predict the development of this flow. For instance, Newman (1969) selected Bradbury's results for $U_1/U_j = 0.162$ as a test case to compare the predictions using Abramovich's (equation (17)) and the author's (equation (18)) auxiliary equations. He obtained the variations in l_o and u_o using the Runge Kutta technique to solve the equations. To show the range over which this comparison was made, the results of Bradbury for $U_1/U_j = 0.162$ are included in Figs.

(5) and (6), and also the curve representing equation (26) (this equation is obtained by using Abramovich's auxiliary equation (17)) is given in Fig. (6). Note that over this narrow range all methods shown in Fig. (6) may be considered equally good.

Another example is the recent investigation of Rodi (1970) who adopted the field method (or differential method) of Spalding (1968) and his associates to predict the development of jets in uniform streaming flow. (For details of this method the reader is requested to refer to many reports by Professor Spalding and his associates at Imperial College, London.) His predictions are also included for comparison in Fig. (6). He employed two methods to evaluate the variations in U_1/u_o; the first is described by Rodi and Spalding (1969) (the results are shown as line $C_R = \infty$), and the second one employs an empirical relation for the proportionality constant in the Prandtl-Kolmogorov-Emmons model for turbulence (i.e. $-\overline{uv} = A_1\, l \sqrt{\overline{q^2}}\, \frac{\partial U}{\partial y}$, and A_1 is given by $\dfrac{C_R}{C_R + (\frac{P}{\epsilon} - 1)}$ where P is the production of kinetic energy whereas ϵ is the dissipation of kinetic energy). For the latter case the predictions are indicated by a line representing $C_R = 2.5$.

From Figs. (5) and (6) it is clear that the method proposed in section (2.3) does predict satisfactorily the variations in l_o and u_o for jets in uniform streaming flow. It should be noted that the present method is simple, and unlike Newman's or Rodi's methods it is quite cheap because it does not require computer calculations.

Finally, in Fig. (7) the turbulence results of Bradbury (1963) are replotted to show that the structure parameter, $(SP) = \left[\overline{q^2}/\overline{uv} \right]_{\eta=1}$ is independent of the velocity ratio U_1/u_o. This was the conclusion reached from the analysis of section (2.3.3). Note that the value of the structure parameter is about 5.9 for the range $0.5 \leqslant U_1/u_o \leqslant 5.0$. Here it is reemphasized that one may use the analysis of section (2.3.3) either to predict the structure parameter having obtained C or to predict C having measured the structure parameter. In any case it is worth noting that in the present method only one constant is required to be evaluated from experimental results for a jet in still air. Furthermore, an important remark may be made for the present method, that is, it avoids the main shortcomings of the eddy viscosity and mixing length theories, (see Batchelor (1950)), and at the same time it is not contrary to them for it is capable of predicting the correct asymptotic values of the eddy viscosity Reynolds numbers (see section 2.3.4).

3.2 Plane Turbulent Wall Jets in Uniform Streaming Flow

As mentioned in section (2.4.1), wall jets in uniform streaming flow offer an excellent opportunity to evaluate the merit of the present method. The analysis of section (2.3) is assumed to be applicable to wall jets in uniform streaming flow. For comparison measurements of Patel (1962); Kruka and

Eskinazi (1964) and Gartshore (1965) are selected. These investigations incorporate sufficient experimental variations between them for the present purpose, for example the measurements of Gartshore and the author were made in the same apparatus but Gartshore used a modified slot construction (see Gartshore and Hawaleshka (1964)).

Fig. (8) shows experimental results of Kruka and Eskinazi, Gartshore, and Patel plotted in accordance with equation (23). A line representing equation (23) with I_1 = 1.0125 (note that this is the same value of I_1 as used in Figs. (5) and (6)) is drawn. It can be seen from this figure that the collected experimental results for various ratios of (U_1/U_j) are in agreement with equation (23).

Fig. (9) shows the variation of velocity scale u_o with x. It should be noted that for all the wall jet cases considered here the hypothetical origin x_o is found to be 20 slot widths upstream of the slot (see Fig. (10)). Equation (22) can now be fitted to the experimental results in Fig. (9) by selecting various values of C. Two such curves with values of CI_1 = 0.062 and 0.0653 are represented by solid lines. From this figure it may be concluded that the constant C for wall jets is about 0.065. It is interesting to compare this value of C with that obtained from growth of wall jets in still air, e.g. Schwarz and Cosart (1961) give C = 0.0678; Sigalla (1958) gives C = 0.0664; Patel (1962) gives C = 0.065; Kruka and Eskinazi (1964) give C = 0.0737 and Gartshore and Hawaleshka

(1964) give $C = 0.065$. Note that the value of C obtained from Fig. (9) is not inconsistent with the values of C obtained from wall jets in still air. It is therefore concluded that the simple method presented in section (2.4.1) is capable of predicting reasonably well the development of main characteristics of wall jets in uniform streaming flow.

4. GENERAL DETAILS OF THE EXPERIMENTAL INVESTIGATION

A detailed description of the experimental apparatus is given in Appendix 1. The aim was to produce a plane two-dimensional jet, a plane mixing layer and the asymmetric jet without unnecessary modifications and/or complications in the experimental apparatus. This was achieved by using the McGill 17 in. x 30 in. blower cascade wind tunnel and a two-dimensional slot 0.265 in. x 30 in. Although the slot arrangement appears to be similar to that of Patel (1962), and Gartshore and Hawaleshka (1964) it differs in detail . These details are given in Appendix 1.

To produce the two-dimensional jet alone the slot was supplied with air from an auxiliary centrifugal compressor, driven by a 10 H.P. constant speed three phase motor, situated in a compressor room underneath the Aerodynamics Laboratory. The supply pipe from the compressor room to a service point in the laboratory is permanently installed. Other details and connections to the slot are given in Appendix 1. For the investigation of a two-dimensional jet in still air the top wall from the working section (see Fig. (28)) was removed. For a plane mixing layer the blower tunnel was operated and the slot was carefully taped off. For the asymmetric jets both the tunnel and the jet were used.

The air supplied by the auxiliary centrifugal compressor was maintained at the same temperature as the tunnel air by incorporating a watercooled heat exchanger in the supply line and care was taken to stabilize the air temperature in the laboratory before any measurements were taken. The maximum variation in air temperature was thus maintained within 1°F and it is known (see Patel (1968)) that this change in temperature has very small influence on hot-wire output.

To avoid the contamination of hot-wires by dust particles both the tunnel and the centrifugal compressor inlets were provided with air filters (DRI-Pak No. 2100 with prefilters, manufactured by American Air Filter Company, which is claimed to filter dust down to about 0.5 microns diameter). This was found to be extremely effective and practically no accumulated dust was observed on the wires even after considerable running time.

The blower tunnel is driven by a single stage centrifugal fan with backward curved blades (Buffalo 980 B.L.), and powered by a three phase, 550 volts, constant speed, 25 H.P. electric motor. An alternative 5 H.P., variable speed D.C. motor was used to run the tunnel at low speeds (i.e. less than 60 ft/s.). Appendix 2 gives the reasons for providing this alternative.

The working section for the plane jet and the mixing layer investigations was the same as that of Fekete (1970) except that a screen and louvres (at top and bottom) used in his investigation were removed. For the asymmetric jets this working section was replaced by a similar one with a top wall. (This was done so as not to disturb the louvre settings in Fekete's experiment.) Both working sections were mounted on roller castors to facilitate easy removal and attachment of the working section to the tunnel exit.

A special traversing gear, (similar to that used by Fekete (1970) except that the one used in the present investigation had an approximately 42 in. long lead screw) was used for all traverses. The details of the traversing gear together with its drive mechanism are given by Fekete (1970).

The hot-wire anemometer used in this investigation was a commercial unit manufactured by DISA, (55A01 anemometer modified to accept a 55D10 linearizer); it is a constant temperature anemometer. The hot-wire probes were also manufactured by DISA. (The author welded hot-wires whenever the probes were found unsatisfactory.) Other details of the hot-wire probes used in this investigation are given in Appendix I. All the hot-wire calibrations were obtained by using a pitot tube made from 0.030 in. O.D. hypodermic stainless steel tubing with internally sharpened lips. The calibration procedure is described in detail by Patel (1968) and for the present investigation this was accomplished in the free stream produced by the tunnel. The linearized hot-wire output was measured by two RMS-meters (DISA 55D35 and Hewlett-Packard 3400A), a Hewlett-Packard (2212A) voltage to frequency converter, a Hewlett-Packard (5216A) digital counter, a Heathkit Audio Generator (Model AG-8) for external time control to vary the time for averaging the signal and a Hewlett-Packard (562A) printer.

For the measurements of energy spectra a Brüel and Kjoer audio frequency spectrometer type 2112 was used and frequency analysis was made by using $\frac{1}{3}$ octave filters. For triple and quadruple correlations DISA random signal indicators, (Correlator Type 55A06), together with a precision full wave rectifier circuit (see Guitton (1968) for details) were used. The intermittency measurements were made by using a differentiating circuit and 'Ultra Violet' Recorder Type 1050 (New Electronic Products Ltd.) incorporating a galvanometer type BB 3000. The galvanometer response was limited to fluctuations below 3000 c/s.

The conventional two-dimensionality checks for a plane jet in still air and the asymmetric jet were made at $x/b = 53.4$ and 217.0 downstream of the slot exit by pitot and hot-wire traverses. All pressure readings were taken with a single tube precision manometer (Lambrecht) which was calibrated against the Askanian Werke filled with distilled water. The results of these checks are reported in Appendix 1.

Although the experimental results reported here do not include two complementary investigations on the technique of hot-wire anemometry it is important to mention them briefly.

(a) The analysis of slanting wire readings involves knowledge of the longitudinal cooling of a hot-wire. Investigations of Champagne and others (1965, 1967) have confirmed the directional sensitivity of an inclined hot-wire but in their investigations the conclusion regarding the effect of longitudinal cooling was reached through measurements obtained statically. A dynamic test of their conclusion is given by Patel (1968).

(b) The measurement of triple and/or quadruple correlations and cross-component spectra involves the use of matched X-wires rather than single slanting wire. An investigation of X-wire probes was therefore undertaken. The detailed results of this investigation are reported by Guitton and Patel (1969) (see also Jerome, Guitton and Patel (1970); DISA special information C.T.A. Note No. 14). The summary of this investigation is:

"In constructing an X-type hot-wire probe it has been the policy of a number of experimenters and manufacturers to place the two wires forming the X close to each other to assure that they are both measuring in effectively the same plane. A number of important experiments have been made using such a probe design.

Recent experiments at the University of British Columbia and McGill University have shown that a X-wire probe which has two wires almost in the same plane is quite sensitive to movements of the velocity vector out of that plane (defined as pitching motion). This has been attributed to the influence on one wire of the hot wake produced by the other. In this note a DISA X-type probe (type 55A32), with the wires 0.006" apart, is tested and found to have a static sensitivity to small angles of pitch, which is very significant for low wire Reynolds numbers (< 5) but becomes small for Reynolds numbers greater than 10. A modified probe, having the wires one wire length apart, is suggested and when tested found to have no pitch sensitivity."

Since the above investigation the author has collected typical investigations as examples in which X-wire probes are either built by the investigator, or use DISA probes, or completely ignore the details of their X-wire probes. Because the effect due to thermal wake interference is a function of both the wire separation to diameter ratio (s/d) and the wire separation to wire length ratio (s/l), these values are also reported in the following table. Note that the smaller these parameters are the more severe will be the interference. Recommended values of these ratios are: $s/d \approx 200$ and $s/l \approx 1.0$.

Investigators	Built X-wire probes	Used DISA X-wire probes	Ignored details of X-wire probes	s/d	s/l
Grant, H.L. (1958)	*			30.0	0.075-0.15
Kruka, V. and Eskinazi, S. (1964)	*			53.3	0.20
Guitton, D.E. and Patel, R.P. (1969)		All DISA* X-wire probes built before this investigation had separation of approx. 0.2 mm (DISA factory specification)		32	0.16
Mobbs, F.R. (1968)		*		?	?
Wygnanski, I. and Fiedler, H.E. (1969, 1970)		*		?	?
Champagne, F.H. Harris, V.G. and Corrsin, S. (1970)		*		?	?
Chao, J.L., and Sandborn, V.A. (1966)			*		
Rose, W.G. (1966)			*	?	?
Bradshaw, P. (1967)			*	?	?

5. TWO-DIMENSIONAL JET IN STILL AIR

5.1 General

Although the number of experiments on jets in quiescent surroundings has been considerable, the detailed information on a plane jet as opposed to an axisymmetric jet is very limited. For instance, Miller and Comings (1957), van der Hegge Zijnen (1958) and Heskestad (1963) have reported the measurements of Reynolds stresses in a plane jet. van der Hegge Zijnen and Miller and Comings made their measurements within the range $0 < x/b < 40$ and there is some doubt that the flow within this range may not be strictly self-preserving (Heskestad (1963); for axisymmetric jet in still air, Wygnanski and Fiedler (1969) suggest $x/d > 70$ for self-preservation). It is also of interest to recall that their turbulence measurements are in disagreement which may be due in part to different techniques used. van der Hegge Zijnen used a non-linearized constant current hot-wire anemometer and diffusion technique whereas Miller and Comings deduced $\overline{v^2}$ from static pressure measurements.

On the other hand Heskestad made his measurements far downstream from the nozzle where the flow is expected to be self-preserving but restricted his measurements of Reynolds stresses to only one station ($x/b \approx 102$). He used a linearized constant temperature hot-wire anemometer to measure Reynolds stresses, and hot-wires of aspect ratio (i.e. length to diameter ratio) of about 400. He found disagreement between the measured and the calculated shear stress distribution and attributed the discrepancy to shortcomings of hot-wires in high intensity flows.

It appears from the existing measurements of a plane turbulent jet in still air that experimental confirmation of self-preserving nature of the jet is not yet demonstrated. Furthermore, it is shown by Bradbury (1963) and Newman (1967) that the flows in the previous investigations may not be two-dimensional. In addition there is no mention regarding variation in temperature between jet air and the still surroundings and, therefore, one presumes that in these investigations (except Heskestad's) there may be some effect on hot-wire measurements due to the possible temperature gradient across the flow.

The present investigation was, therefore, undertaken to reinvestigate a plane turbulent jet in still air experimentally and at the same time check the usefulness of hot-wire technique and confirm the two-dimensionality of the jet flow before embarking on the asymmetric jet investigation.

The measurements reported here are for a jet Reynolds number, $U_j b/\nu$, of 3.51×10^4 and include mean velocities and the Reynolds stresses. All measurements were made with a linearized constant temperature (DISA) hot-wire anemometer and only single wires were used. Apart from the longitudinal cooling corrections (Champagne (1965), Patel (1968)) to the results of inclined wires no other corrections have been applied unless specified. It should be mentioned that the temperature of the jet air was maintained at room temperature by a heat exchanger to within 1°F. For other details on the experimental technique, care and precautions taken during this investigation the reader is referred to Patel (1968) and Appendix 1.

5.2 Experimental Arrangement

Two-dimensional turbulent jet was produced by a slot the details of which are given in Appendix 1. The design of the slot is essentially the same as suggested by Gartshore and Hawaleshka (1964), however, the slot opening is now of fixed width and some modifications have been made between the 6° diffuser and the slot. The slot was 30 in. x 0.265 in. thus having an aspect ratio of approximately 113. The slot was mounted in the tunnel floor as shown in Fig. (A.2).

The filtered air was supplied to the slot from a 10 H.P. centrifugal compressor (see section 4). The air supply was controlled by a butterfly valve in the supply line upstream of a heat exchanger which controlled the air temperature.

The two-dimensionality checks on the flow emerging from the slot are given in Appendix 1.

5.3 Results and Discussions

5.3.1 Mean Velocity

The mean velocity measurements were made with a linearized hot-wire anemometer at five stations within the range $12.275 \leqslant x/b \leqslant 152.0$. Fig. (11) shows the mean velocity distribution across the jet at various stations. The results shown in this figure are non-dimensionalized by the velocity scale U_m and the length scale x, the distance from the slot exit. The use of x as the length scale enables one to detect deviations from similarity quite easily and also shows changes in the location of hypothetical origin of the flow. From Fig. (11) it can be seen that the mean velocity profiles are similar beyond $x/b = 27.35$ and the hypothetical origin does not change with the downstream distance.

For comparison results of Heskestad (1963) are shown by a solid line (mean line drawn through his data) in Fig. (11). Also included in the figure is an exponential profile given by $U/U_m = e^{-(8.03\ y/x)^2}$. The exponential profile fits the experimental results fairly well and it will be used later (see Figure (18)) to calculate shear stress distribution across the jet. The slight disagreement between the present results and those of Heskestad may be due to the difference in geometry of the experimental apparatus. Heskestad used solid boundaries in (y-z) plane at x = 0 and the existence of these boundaries is likely to impose adverse pressure gradient on the jet flow thus giving slightly broader velocity distribution. Associated with this is the higher rate of growth for a jet in still air.

5.3.2 <u>Growth of the Plane Jet</u>

It is well known that the growth of a plane jet in still air is linear but there exists some doubt regarding the value of the rate of growth. Newman (1967) has collected values of rates of growth from various investigations and concludes that the variations in this rate are mainly due to end effects (i.e. earlier investigations were made with slots having aspect ratio, (slot length/b), less than 100). Newman gives an average value for the rate of growth as 0.104 ± 2%. Fig. (12) shows the variation of ($y_{m/2} = l_o/b$) versus (x/b) for the present investigation. The results of Heskestad are also included in this figure for comparison. From the figure it can be seen that the rate of growth for the present investigation is 0.103 and it is thus in agreement with the value suggested by Newman. Heskestad's measurements show rate of growth of 0.11 (Heskestad (1965)).

As mentioned in section 1.2, considerable progress has been made in finite difference (differential) methods since the investigation of Spalding* and Patankar (1967). They have developed a simple and fast computational method for solving partial differential equations. It is beyond the scope of this investigation to give here all the details involved in their method but as a test their programme (GENMIX - see Spalding (1968)) was used to predict the growth and decay of the centre line velocity, U_m, for the simple case of a jet in still air. Fig. (12) also shows the variation of ($y_{m/2}/b$) obtained from their method. Note that the differential method requires some

---

* The author wishes to take this opportunity to sincerely thank Professor D.B. Spalding for providing him with his papers, GENMIX programme and valuable suggestions on the use of his computer programme.

starting conditions and in this case the starting condition was provided by the velocity profile at $x/b = 12.275$. The velocity profile was represented by 16 points and it was necessary to use finite values of the velocity at the edge (about 10% of the centre line value). Any attempt to specify the edge velocity near zero involved either excessive computer time or erroneous results. It can be seen from figure (12) that the predicted rate of growth is not in agreement with experimental results. However, the discrepancy can be removed by varying the mixing length constant, λ, in their method (Spalding (1969)).

5.3.3 Decay of Centre-line Velocity

It is easy to show that the centre line velocity for a jet in still air varies as $x^{-1/2}$ provided the jet momentum is conserved. Fig. (13) shows $(U_j/U_m)^2$ versus (x/b) where U_j is the slot exit velocity. From the figure it can be concluded that the centre line velocity, U_m, varies as $x^{-1/2}$. Fig. (14) shows a comparison between the present results and those obtained using Spalding's (1968) method. Once more it is possible to reduce the discrepancy by varying the mixing length as noted above. It was observed that the same value of λ does not remove discrepancy for both U_m and $y_{m/2}$. It should be noted that the hypothetical origin of the jet is at $x = 0$ (see Figs. (12) and (13)).

5.3.4 Distributions of the Normal Reynolds Stresses

The normal Reynolds stresses were measured with single normal and slanted linearized hot-wires and the direction of the mean flow was assumed to be parallel to the axis of the jet. The non-dimensional distributions of the normal Reynolds stresses are shown in Figs. (15, 16 and 17). Fig. (15) shows $(\sqrt{\overline{u^2}}/U_m)$ versus (y/x) distributions for various downstream stations. It can be seen from this figure that all measurements except at x/b = 12.275 collapse on a single curve. It is interesting to note that for the plane jet the longitudinal fluctuations become self similar beyond about 30 slot widths downstream of the slot. As Wygnanski and Fiedler (1968) have noted it appears that mean velocity distributions become self similar first and then $(\sqrt{\overline{u^2}}/U_m)$ distributions attain self similar state. This is to be expected because for plane turbulent flows the transport equation for $\overline{u^2}$ contains a production term whereas the transport equations for $\overline{v^2}$ and $\overline{w^2}$ do not contain the production term thus the energy is transferred from the mean motion directly to $\overline{u^2}$ and only pressure-velocity-gradient correlations transfer the energy to $\overline{v^2}$ and $\overline{w^2}$. For this reason measurements of $\overline{v^2}$, $\overline{w^2}$ and $\overline{uv}$ were made beyond x/b = 70.

In Fig. (15) measurements of Heskestad are represented by a dashed line which is a mean line through his data. It can be observed that Heskestad's measurements are generally higher by about 10% than the present measurements but the shapes of $(\sqrt{\overline{u^2}}/U_m)$ distributions are very similar. On an average there is ± 5% scatter in his measurements of $\sqrt{\overline{u^2}}/U_m$ and since his experimental investigation he has reported an error in his calbrations of the vacuum thermocouple circuit (see footnote on page 733, Heskestad (1965)). In the same figure measurements of Bradbury (1963) are shown by a solid line. His measurements are for a jet in a small axial flow ($U_1/U_j = 0.07$; and far downstream where the data was obtained the streaming velocity, U_1, is about 20% of the centre line velocity). It can be seen that his measurements are lower than those of Heskestad and in reasonable agreement with the present results.

Fig. (16) shows distributions of $(\sqrt{\overline{v^2}}/U_m)$ at $x/b = 74.0$ and 152.0. For comparison measurements of Heskestad are also included in this figure. It should be mentioned that although Heskestad's result is represented by a mean line through his data there is much bigger scatter in his data than the present results. It is surprising, in spite of care and precautions taken in the present investigation, that scatter of such a magnitude exists in these results. Furthermore, it cannot be blamed on lack of sufficient averaging time (e.g. Heskestad used two minutes as typical integration time and the present measurements were made with one minute integration time). Further investigation is indeed required to explain the large scatter observed in $\overline{v^2}$ and $\overline{w^2}$ measurements. For the present purpose it can be concluded that the measurements of $\overline{v^2}$ in this investigation are in agreement with those of Heskestad and that $(\sqrt{\overline{v^2}}/U_m)$ distributions attain similarity beyond $x/b \simeq 70$.

Fig. (17) shows the comparison of $(\sqrt{\overline{w^2}}/U_m)$ between the present results and those of Heskestad. As mentioned above these results are also in agreement with each other.

Comparison of Figs. (15, 16 and 17) shows that at the centre line of the jet all components of turbulent intensities are nearly equal thus it appears that the flow is nearly isotropic on the centre line of the jet. Everywhere else $(\sqrt{\overline{u^2}}/U_m$ is bigger than both $(\sqrt{\overline{v^2}}/U_m)$ and $(\sqrt{\overline{w^2}}/U_m)$, the latter two components of turbulent intensities are of the same order of magnitude across the jet. Although large scatter appears in experimental results it may be concluded that the plane jet flow attains similarity beyond $x/b = 70$.

5.3.5 Distributions of the Reynolds Shear Stress

As mentioned in section (5.1), Heskestad found considerable disagreement between his measured and calculated Reynolds shear stress and indicated that the hot-wire technique of measuring various Reynolds stresses in high intensity flow may be suspect. In this connection it is worthwhile to note that one may doubt his calculated shear stresses because details of his calculation method are not reported (i.e. whether he used a graphical integration technique or represented the non-dimensional mean velocity profile by an empirical function). In the following investigation details of the Reynolds shear stress calculations are given and it is shown that the measured values are in agreement with the calculated shear distribution.

The equations of motion for a plane, incompressible, turbulent jet are:

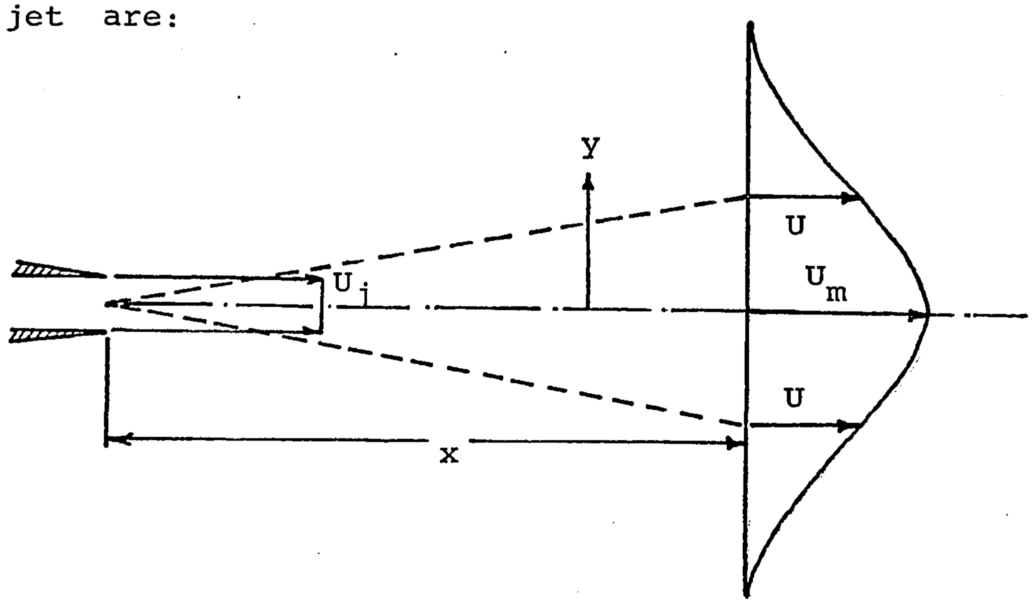

$$\text{Continuity:} \quad \frac{\partial U}{\partial x} + \frac{\partial V}{\partial y} = 0$$

$$\text{Momentum:} \quad U\frac{\partial U}{\partial x} + V\frac{\partial U}{\partial y} + \frac{\partial(\overline{u^2} - \overline{v^2})}{\partial x} = \frac{\partial \tau/\rho}{\partial y} \tag{5.3.5.1}$$

The well known similarity forms for this flow are:

$$\begin{aligned} U &= U_m f(y/x) \\ \overline{u^2} &= U_m^2\, g_1\,(y/x) \\ \overline{v^2} &= U_m^2\, g_2\,(y/x) \\ \overline{w^2} &= U_m^2\, g_3\,(y/x) \\ \text{and } \overline{uv} &= U_m^2\, g_{12}\,(y/x) \end{aligned} \tag{5.3.5.2}$$

where U_m is the maximum velocity at the centre line and x is taken as a length scale. (Note that the hypothetical origin of the jet was found to be at the slot exit.)

Substituting the similarity forms in the momentum and continuity equations and combining the two, one obtains:

$$\frac{1}{2}f^2 + \frac{1}{2}f' \int_0^\eta f d\eta + (g_1-g_2) + \eta(g_1'-g_2') = g_{12}' \qquad (5.3.5.3)$$

where a dash refers to differentiation with respect to η.

It is a common practice to ignore the normal Reynolds stress terms in the momentum equation, but for the present investigation these terms are retained in the above equation.

The above equation on integration gives:

$$\frac{\overline{uv}}{U_m^2} = \frac{1}{2}f \int_0^\eta f d\eta + \eta\,(g_1-g_2) \qquad (5.3.5.4)$$

This equation will be used to evaluate the shear stress distribution across the jet. It should be noted that to calculate $(\overline{uv}/U_m^2)$ one needs to know the forms of the functions f, g_1 and g_2. It is possible to obtain (of course with the approximation that the term $\eta(g_1-g_2)$ may be neglected) the functional form for f adopting the eddy viscosity concept (see Heskestad (1963)), but g_1 and g_2 have to be obtained from measurements. To be consistent it is proposed to use experimental results for f, g_1 and g_2. Furthermore, the equation for $(\overline{uv}/U_m^2)$ contains a term involving $\int_0^\eta f d\eta$ which can be evaluated best by fitting an empirical expression to the experimental data. As mentioned in section (5.3.1) the following expression fits the experimental results fairly well (see Fig. (11)).

$$f = e^{-(8.03\ y/x)^2} \qquad (5.3.5.5)$$

It is mentioned in passing that this expression is consistent with the rate of growth found in the present investigation.

In Fig. (18) a comparison is made between the measured and calculated shear stress distributions. The shear stress measurements were made at $x/b = 74.0$ and 152.0. The measured values are corrected for both the longitudinal cooling (Patel (1968)) and the high intensity effects. For the latter Guitton's (1970) correction factor was used. From the figure it can be seen that the measured shear stress distribution is in reasonable agreement (e.g. the agreement is no worse than that reported by Wygnanski and Fiedler for axi-symmetric jet) with that calculated from the momentum equation. Moreover, the results show that similarity of shear stress distribution is attained beyond $x/b = 70$. The comparison of calculated and measured shear stress also serves as a test for the two-dimensionality of the jet flow. Other two-dimensionality checks are given in Appendix 1 and considering overall results (see Figs. 12, 13 and 18) it can be concluded that the flow emerging from the slot was satisfactorily two-dimensional.

It should be mentioned that measurements show $\overline{uw} = 0$ across the jet.

5.3.6 Turbulent Energy Distribution Across the Jet

In section (2.2), (see equations (11)), it was reported that to obtain the dissipation length scale, L_ϵ, of the turbulent motion it is required that the distribution of the turbulent energy across the jet be known. Fig. (19) shows the distributions of the turbulent energy and other functional relations required for this purpose. Note that in this figure the length scale, l_o ($= y_{m/2}$), is the value of y at which $U = \frac{1}{2} U_m$ and the function g is defined as follows:

$$g(\eta) = \frac{\overline{q^2}\ (\equiv \overline{u^2} + \overline{v^2} + \overline{w^2})}{(q_1^2)_{\eta=1}}$$

The values of $\overline{q^2}$ were obtained from Figs. (15, 16 and 17). From Fig. (19) it can be found that:

$$g(0) \approx 1.2 \quad \text{and} \quad \int_0^\infty fg d\eta \approx 1.10$$

The above values are used for the calculation of L_ϵ in section (2.2).

5.3.7 General Conclusions

(i) The measurements reported in this section confirm the self-preserving nature of the two-dimensional jet in still air. It was noted that similarity of various distributions is attained in steps i.e. first the mean velocity distributions become similar at $x/b \geqslant 28.0$, then $\overline{u^2}$ distributions become similar beyond $x/b = 30.0$ and finally $\overline{v^2}$, $\overline{w^2}$ and $\overline{uv}$ distributions become similar beyond $x/b = 70.0$.

(ii) On the whole the present measurements are generally in agreement with those of Heskestad (1963). The experimental scatter in the present results is much smaller compared to Heskestad's results. Although constant temperature, linearized, hot-wire anemometers (of different design) were used in both investigations the techniques of extracting turbulence components from hot-wire results were different and thus the general agreement between Heskestad's and the present results is encouraging.

(iii) Comparison of mean velocity profiles at various z-positions (Appendix 1), the expected variations of $l_o (= y_{m/2})$ and U_m (Figs. (12) and (13)) and comparison of the measured and calculated distributions of the Reynolds shear stresses (Fig. (18)) enhance the conclusion that the flow emerging from the slot was two-dimensional.

6. A PLANE MIXING LAYER

6.1 General

Recently considerable effort has been directed towards the study of free shear flows. In this group of shear flows a plane, turbulent, incompressible mixing layer between a uniform stream and quiescent surroundings is a comparatively simple flow to investigate because of its complete self-preserving nature. However, except for a few investigations (Gartshore (1965); Hackett and Cox (1967)) dealing with mean velocity measurements not much renewed attention appears to have been given to the plane turbulent mixing layer since the appearance of the work of Liepmann and Laufer (1947). It should be recalled that Liepmann and Laufer did not measure $\overline{w^2}$ and $\overline{uw}$ presumably because $\overline{w^2}$ is expected to be of the same order as $\overline{v^2}$ and $\overline{uw}$ is expected to be zero. Furthermore, techniques of hot-wire anemometry have developed considerably since their investigation therefore it is of interest to reinvestigate the plane mixing layer.

This investigation, although far from being complete, was undertaken with a hope that a certain duplication of the measurements would be desirable. Since the completion of the present investigation Wygnanski and Fiedler (1970) have reported extensive and sophisticated turbulence measurements in this type of flow. Unfortunately, they overlooked (see footnote on page 333 of their paper) the importance of the geometry of their experimental apparatus (i.e. they used a trip wire and a solid surface in the plane $x = 0$) and the parasitic effects on their hot-wire probes (i.e. they used conventional DISA X-wire probes); also the range, $(15 < x < 23)$, over which their measurements were taken is quite small. Thus their measurements are suspect. Nevertheless, their measurements are compared with the present results later.

It is worthwhile to note that Hackett and Cox (1967) have indicated that there is need for a unified approach to calculate shear stress distribution from mean velocity profiles in this flow. The difficulty arises from the non-existence of well defined boundaries. An approach to the calculation of $\overline{uv}$ is presented which agrees with shear stress measurements.

Experimental results presented here are for $U_1/\nu = 54.8 \times 10^4$ per foot which is higher than most other investigations and the free stream turbulent intensity of 0.5% (see Appendix 2). The results include mean velocities and the Reynolds stresses at three stations. These were obtained by using linearized constant temperature hot-wire anemometer (only single wires were used) and include the longitudinal cooling corrections where appropriate (Patel (1968)). The mixing layer was formed at the exit of the McGill 17 in. x 30 in. blower cascade wind tunnel. An investigation regarding the two-dimensionality of the flow emerging from this tunnel is given by Patel (1964). Other details of instruments, experimental techniques, etc. are given in section (4) and Appendix 1.

6.2 A Method for Calculating the Reynolds Shear Stress

It is well known that the plane turbulent mixing layer is completely self-preserving and the lateral width of the flow is proportional to the distance from a suitably chosen origin.

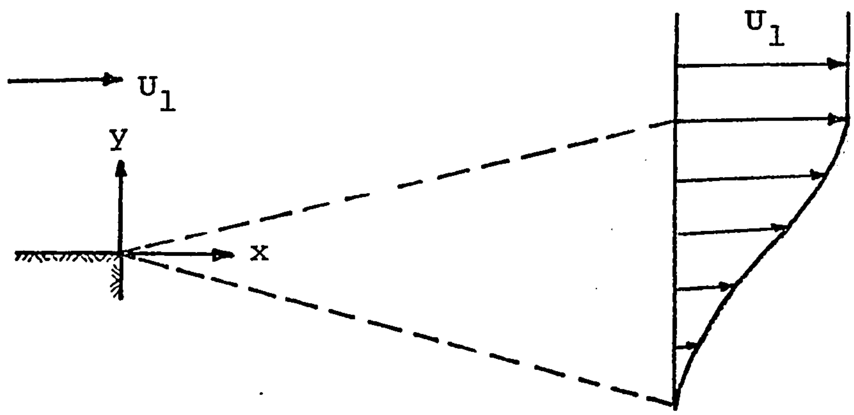

The self-preservation is represented by

$$\begin{aligned} U &= U_1\ f(\eta) \\ \overline{u^2} &= U_1^2\ g_1(\eta) \\ \overline{v^2} &= U_1^2\ g_2(\eta) \\ \overline{w^2} &= U_1^2\ g_3(\eta) \\ \text{and}\quad \overline{uv} &= U_1^2\ g_{12}(\eta) \end{aligned} \tag{6.2.1}$$

where $\eta = y/x$ and f and gs' are universal functions of η.

The equation of mean motion in the x-direction with boundary layer approximations is given by

$$U\frac{\partial U}{\partial x} + V\frac{\partial U}{\partial y} + \frac{\partial}{\partial x}(\overline{u^2}-\overline{v^2}) + \frac{\partial}{\partial y}(\overline{uv}) = \nu\ \frac{\partial^2 U}{\partial y^2} \tag{6.2.2}$$

and the continuity equation is

$$\frac{\partial U}{\partial x} + \frac{\partial V}{\partial y} = 0 \tag{6.2.3}$$

Substituting the similarity forms from equation (6.2.1) into equations (6.2.2) and (6.2.3), and then combining the momentum equation (6.2.2) and the continuity equation (6.2.3) one gets:

$$-\eta ff' + f' \int_1 \eta df - \eta(g_1' - g_2') + g_{12}' = \frac{\nu}{U_1 x} f'' \tag{6.2.4}$$

where dashes denote differentiation with respect to η, and it is assumed that $V = 0$ at $\eta = 0$ or where $f(0) = 1$. For high Reynolds numbers the right hand side of equation (6.2.4) can be neglected, and also neglecting the difference between the normal Reynolds stresses, equation (6.2.4) after integration reduces to:

$$g_{12} = \int_1 \eta df^2 - f \int_1 \eta df \tag{6.2.5}$$

This equation is identical to the one given by Townsend (1956; see equation 8.3.5) except for the term involving normal Reynolds stresses. For the condition that shear stress is zero at $y = \pm\infty$, Townsend gives

$$\int_0^1 \eta df^2 + \int_{-\infty}^{+\infty} \eta(g_1' - g_2')d\eta = 0 \tag{6.2.6}$$

Equation (6.2.5) can also be written as

$$g_{12} = f \int_0 f d\eta - \int_0 f^2 d\eta \tag{6.2.7}$$

Equation (6.2.7) has been used by Hackett and Cox (1967) to evaluate the shear stress distribution from a measured mean velocity profile. They had to determine the constant of integration by trial and error such that at the edges of the mixing layer the shear stresses were zero. In this connection it is of interest to note that Liepmann and Laufer (1947) have also assumed that $V = 0$ at $\eta = 0$ and must have determined the constant of integration on this basis. Although Wygnanski and Fiedler (1970) do not give details of their calculation for the shear stress distribution they too have made the same assumption as Liepmann and Laufer (see their figure (41)). Furthermore, they had to impose a condition that the calculations for the shear stress distribution proceed from high velocity side and far away from the mixing zone. The logical question here seems to be: what happens if one starts the calculations from the zero velocity side?

In practice it is difficult to locate exactly where the edge $\eta = 0$ should be and, moreover, the assumption $V = 0$ at this point can be questioned because there is no reason to believe that it is so, for instance, $\eta = 0$ is not a symmetry line or a solid boundary. Therefore it appears that the difficulty in calculating the shear stress distribution from a mean velocity profile using equations (6.2.5) or (6.2.7) arises from both the difficulty in locating $\eta = 0$ and the assumption that $V = 0$ at $\eta = 0$. Since it is not necessary to impose this restrictive assumption following analysis is presented and used to calculate the shear stress distribution for a plane mixing layer.

The continuity equation (6.2.3) after substitution from equation (6.2.1) and integration reduces to:

$$V = U_1 \left[\eta f - \int f d\eta + A \right] \tag{6.2.8}$$

where A is a constant of integration which gives the inflow velocity from the high velocity side. Substituting equations (6.2.1) and (6.2.8) into equation (6.2.2), and as before neglecting terms containing the normal Reynolds stresses and viscosity, gives

$$g_{12}' = f' \int f d\eta - Af' \tag{6.2.9}$$

Equation (6.2.9) on integration gives

$$g_{12} = f \int f d\eta - \int f^2 d\eta - fA + B \tag{6.2.10}$$

where B is another constant of integration.

Now examination of equation (6.2.10) indicates that two boundary conditions are required to evaluate the constants A and B. These boundary conditions are:

$$\begin{aligned} \text{at } \eta = 0 \;;\quad \overline{uv} = 0 \\ \text{and at } \eta = \infty \;;\quad \overline{uv} = 0 \end{aligned} \tag{6.2.11}$$

Equation (6.2.10) with these boundary conditions becomes

$$g_{12} = f \int_0^\eta f d\eta - \int_0^\eta f^2 d\eta + (1-f) \int_0^\infty f^2 d\eta \tag{6.2.12}$$

Note that in equation (6.2.12), as a consequence of V being not zero at $\eta = 0$, an extra term, which is <u>not a constant</u>, appears compared to equation (6.2.7). Equation (6.2.12) can be used to calculate the shear stress distribution from a mean velocity profile, but the second boundary condition (i.e. at $\eta = \infty$, $\overline{uv} = 0$) is not satisfactory. The reason for this is that the equation of motion without the terms containing the normal Reynolds stresses is not applicable in the outer region (i.e. edge towards which $U \to 0$). In any case, even measurements in this region would be contaminated. Hence to establish the boundary conditions with some confidence and to avoid using graphical integration techniques the following approach is preferred.

The non-dimensional mean velocity distribution to a good degree of accuracy may be expressed analytically by (see Fig. (21))

$$\frac{U}{U_1} = f(\eta) = e^{-(k\eta)^2} \qquad (6.2.13)$$

where $\eta = \eta_o - \left(\frac{y_{m/2} - y}{x}\right)$

k is a constant, $y_{m/2}$ is the value of y at which $U = \frac{1}{2}U_1$

and $$e^{-(k\eta_o)^2} = 0.50 \qquad (6.2.14)$$

Note that the edge of the mixing layer on the high velocity side is now established by the value of η_o and once this value has been assigned the constant k can be obtained from equation (6.2.14). The analytical expression for the non-dimensional mean velocity profile (i.e. equation (6.2.13)) can then be compared with a measured profile and adjustment in η_o may be made if necessary. Thus the first boundary condition in equation (6.2.11) can be assigned with some confidence and justification. The second boundary condition is specified from the measured $(\overline{uv}/U_1^2)$ distribution. It should be recalled that Liepmann and Laufer have also discarded the second boundary condition of equation (6.2.11) and replaced it by the condition that the distribution of $(\overline{uv})$ has a maximum where $\partial^2U/\partial y^2 = 0$. It will be shown later that the present approach is not inconsistent with the condition of Liepmann and Laufer.

The revised boundary conditions, therefore, are:

$$\text{at } \eta = 0 \text{ (i.e. } \frac{y_{m/2}-y}{x} = \eta_o) \; ; \; \overline{uv}/U_1^2 = 0 \text{ and } f(0) = 1$$

$$\text{at } \eta = \eta_o \text{ (i.e. } \frac{y_{m/2}-y}{x} = 0) \; ; \; \overline{uv}/U_1^2 = 0.0096 \text{ (measured data)}$$

$$\text{and } f(\eta_o) = 0.50 \qquad (6.2.15)$$

With these boundary conditions the integrated momentum equation (6.2.10) reduces to

$$g_{12} = \frac{\overline{uv}}{U_1^2} = f\int_0^\eta f d\eta - \int_0^\eta f^2 d\eta + (1-f)\left[0.0192 + 2\int_0^{\eta_o} f^2 d\eta - \int_0^{\eta_o} f d\eta\right] \qquad (6.2.16)$$

Substituting the velocity profile equation (6.2.13) into equation

(6.2.16) gives

$$\frac{\overline{uv}}{U_1^2} = \frac{\sqrt{\pi}}{2}\left[\frac{1}{k}\, e^{-(k\eta)^2}\,\mathrm{erf}(k\eta) - \frac{1}{k\sqrt{2}}\,\mathrm{erf}(\sqrt{2}k\eta) + Z\,\left(1-e^{-(k\eta)^2}\right)\right] \tag{6.2.17}$$

where Z is a constant and depends on η_o as follows:

$$Z = 0.0216 + \frac{\sqrt{2}}{k}\,\mathrm{erf}\,(\sqrt{2}k\eta_o) - \frac{1}{k}\,\mathrm{erf}\,(k\eta_o) \tag{6.2.18}$$

In this investigation equations (6.2.17) and (6.2.18) are used to calculate the shear stress distribution. It is pointed out that the non-dimensional mean velocity profiles given by equation (6.2.13) where η_o = 0.125 and 0.118 equally fit the collected experimental results (see Fig. (21)), so the following constants corresponding to these values of η_o will be used to calculate $(\overline{uv}/U_1^2)$ from equation (6.2.17)

η_o	k	Z
0.125	6.67	0.0994
0.118	7.07	0.0948

6.3 Results and Discussion

6.3.1 Mean Velocity

Initially a test was performed to evaluate the effect of a top wall in the working section on velocity distribution in the mixing layer (also see Fig. (B.12) for $\sqrt{\overline{u^2}}/U_1$ distributions). This was undertaken because Liepmann and Laufer (1947) recommended that it is especially important, for the two-dimensional character of a mixing layer and for reducing effects of any draft in a room, to close the boundary opposite to the mixing zone. Fig. (20) shows mean velocity distribution at x = 27.75 in. both with and without the top wall in the working section for a test condition $U_1/\nu = 16.1 \times 10^4$ per foot and $\left(\sqrt{\overline{u^2}}/U_1\right)_{x=0} = 0.56\%$. From this figure it can be seen that there is hardly any influence on the mixing layer by the absence of the top wall. This may be due to a bigger depth of free stream (i.e. $\frac{x}{H} < 1.63$ where H is the depth of free stream at $x = 0$) in the present investigation compared to that (i.e. $\frac{x}{H} < 4.7$) for the experiments of Liepmann and Laufer. A more appropriate parameter in this connection would be the ratio of the width of a mixing layer to the width of a free stream, and the smaller this ratio the better chance there is for a mixing layer to be not affected by the other boundary (Townsend (1956)).

The subsequent experimental results reported here are for $U_1/\nu = 54.8 \times 10^4$ per foot and without the top wall in the working section.

Fig. (21) shows the non-dimensional mean velocity distributions measured at three downstream stations (i.e. x = 11.0 in. 25.75 in. and 40.25 in.). In this and subsequent figures y is measured from the centre line of the tunnel and $y_{m/2}$ is the value of y at which $U = \frac{1}{2}U_1$. Included in this figure are the measurements of Liepmann and Laufer (1947), Gartshore (1965) and Wygnanski and Fiedler (1970). Except near the zero velocity region the present measurements are in good agreement with those of Liepmann and Laufer, and Gartshore. Also from this figure it can be concluded that the mean velocity profiles are self-preserving as anticipated. The measurements of Wygnanski and Fiedler are not in agreement with other results reported in this figure. It is interesting to note that recently Rodi and Spalding (1969) used a field (or differential) method to predict the velocity distribution in a plane mixing layer. They used the results of Wygnanski and Fiedler together with other free shear flows (i.e. a plane jet and a radial jet) to obtain constants (seven in all) in their calculation method. With this set of constants they predicted velocity distribution in the plane mixing layer and showed good agreement between their prediction and the results of Wygnanski and Fiedler. Their conclusion is acceptable if the non-dimensional mean velocity profiles are plotted as U/U_1 versus $(\frac{y_{m/2}-y}{y_{0.9}-y_{0.1}})$ where $(y_{0.9}-y_{0.1})$ is the distance between the points at which the velocity is $0.9U_1$ and $0.1U_1$. However, when their predictions are replotted in Fig. (21) they are in agreement with other results but not Wygnanski and Fiedler's. It should be mentioned that the present way of plotting the results is preferred because deviations from similarity are easy to discern in such a plot.

6.3.2 Growth of the Mixing Layer

Fig. (22) shows the growth of the characteristic layers in the plane mixing layer where, for example, $y_{0.95}$ refers to the locus of points at which $U = 0.95U_1$. For comparison, measurements of Gartshore, Liepmann and Laufer, and Wygnanski and Fiedler are included. From this figure it can be seen that the characteristic layers in the mixing layer grow linearly with the downstream distance x as expected and the hypothetical origin of the mixing layer is at approximately $x = \frac{3}{4}$ in. Note that for $y_{0.95}$, $y_{0.50}$ and $y_{0.10}$ the present measurements are in agreement with the measurements of Liepmann and Laufer. However, considerable disagreement is apparent between the present results and those of Gartshore for $y_{0.10}$. It is worth noting that in this region measurements with both a pitot tube and a hot-wire become unreliable and therefore comparisons of results are not meaningful.

6.3.3 Distributions of the Normal Reynolds Stresses

Measurements of the normal Reynolds stresses in the plane mixing layer are presented in Figs. (23), (24) and (25). For comparison measurements of Liepmann and Laufer, and Wygnanski and Fiedler are also included. From these figures it can be concluded that the present measurements confirm the self-preserving nature of the turbulence quantities as postulated by equation (6.2.1). It should be mentioned that the range (11.0 in. $\leqslant x \leqslant 40.25$ in.) over which these measurements were taken is bigger than that of Liepmann and Laufer (11.8 in. $\leqslant x \leqslant 29.5$ in.) or that of Wygnanski and Fiedler (15.275 in. $\leqslant x \leqslant 23.1$ in.). Considering the measurements of Wygnanski and Fiedler note that their results for $(\sqrt{\overline{u^2}}/U_1)$ are in agreement with the present results on the high velocity side. However, their results for $(\sqrt{\overline{v^2}}/U_1)$ and $(\sqrt{\overline{w^2}}/U_1)$ are considerably higher than the author's. As noted in section (6.1) this was anticipated because of the geometry of their experimental arrangement and the contamination of their X-wire by thermal wake interference (Guitton and Patel (1969)).

On the other hand the results of Liepmann and Laufer are slightly lower than the present measurements. The difference may be attributed to the old electronic networks, non-linear hot-wire anemometer and the omission of the longitudinal cooling effects on slanted hot-wires in their investigation.

On the whole the general shapes for the distributions of the normal Reynolds stresses are very similar for all the investigations reported in these figures. It is noted that contrary to the conclusion of Wygnanski and Fiedler the points of maxima in these distributions occur approximately where the Reynolds shear stress distribution attains a maximum. This is not unreasonable because one would expect maximum turbulence intensities where turbulence production is maximum. Also contrary to their conclusion is the observation that both $(\sqrt{\overline{v^2}}/U_1)$ and $(\sqrt{\overline{w^2}}/U_1)$ are of the same order of magnitude over the range $-0.06 \leqslant (y_{m/2}-y)/x \leqslant 0.06$.

6.3.4 Distributions of the Reynolds Shear Stresses

Fig. (26) shows the measured Reynolds shear stresses at three downstream stations, i.e. $x = 11.0$ in., 25.75 in. and 40.25 in. For comparison the calculated shear stress distributions (using equation (6.2.17)) are also given in this figure. The two calculated curves refer to two values of η_o selected to represent the measured non-dimensional mean velocity distribution (see section (6.2)). The results of Wygnanski and Fiedler are compared in Fig. (26).

From Fig. (26) it can be seen that contrary to the conclusion of Hackett and Cox (1967), and in spite of a large change in η_o compared to that given by them (i.e. 0.003), both calculated curves are in satisfactory agreement with the measurements. Thus it may be concluded that the method presented in section (6.2) (i.e. equations (6.2.17) and (6.2.18)) provides a satisfactory approach for calculating the Reynolds shear stress distribution from a measured non-dimensional mean velocity profile. Note that the shear stress measurements are in accord with the self-preserving nature of a plane mixing layer.

Comparison between the present results and those of Wygnanski and Fiedler indicate that the agreement between the two is not satisfactory. As mentioned before their measurements are suspect. It should be noted that their measured and calculated (see the author's comments in section (6.2)) shear stress distributions "agree quite well" and this was attributed to the small scatter in their non-dimensional mean velocity profile. It is recalled here that Liepmann and Laufer have also obtained close agreement between their measured and calculated results. In view of the methods used by these investigators to calculate the shear stress distributions such claims for close agreement between measured and calculated results are rather premature as will be shown below.

Fig. (27) is presented for interest because it clearly shows that a variety of shear stress distributions have been calculated from practically the same non-dimensional mean velocity profile. Because of a lack of definite boundary conditions various investigators have used different methods. Common among their methods is the assumption or implication that at the high velocity edge $V = 0$. Presumably V could be worked out by a suitable sink distribution placed along the edge of the streaming side to represent constant entrainment. As mentioned before Hackett and Cox used trial and error methods to establish a constant such that the shear stresses at both edges of the mixing layer become zero. They used both theirs and Liepmann and Laufer's non-dimensional mean velocity profiles (these velocity profiles are in good agreement with each other). Rodi and Spalding (1969) used their differential method to calculate the shear stress distribution. They observed discrepancy between their shear stress profile and the profile given by Wygnanski and Fiedler. They were unable to explain this discrepancy and concluded that some clarification was needed.

For the present investigation two profiles are given in Fig. (27), they refer to the sets of boundary conditions of equations (6.2.11) and (6.2.15). The set of boundary conditions in equation (6.2.11) does not procure agreement between the measured and the calculated profiles. It should be noted also that the calculated as well as the measured shear stress profiles attain maxima at $\eta \approx 0.10$ (i.e. at $(y_{m/2}-y)/x \approx 0.025$) and this is in agreement with the second boundary condition suggested by Liepmann and Laufer (i.e. the shear stress is maximum where $\partial^2U/\partial y^2 = 0$. It is easy to show that for the present velocity profiles $\partial^2U/\partial y^2 = 0$ at $\eta \approx 0.10$.)

From Fig. (27) it can be seen that the discrepancy between various methods is enormous and unbelievable. This stems primarily from the difficulty in assigning proper boundary conditions in the plane mixing layer. The present method therefore seems at least consistent and removes arbitrariness from the investigation.

It should be mentioned that $(\overline{uw})$ was found to be zero across the mixing layer in this investigation.

6.3.5 General Conclusions

Following conclusions are drawn from this investigation:

(i) the measurements of mean velocity and the Reynolds stresses confirm the self-preserving nature of the plane turbulent mixing layer. The range of Reynolds numbers, $5.02 \times 10^5 \leqslant (Re_x = \frac{U_I x}{\nu}) \leqslant 1.84 \times 10^6$, for this investigation is quite large compared to other similar investigations reported in the literature.

(ii) the assumption $V = 0$ at $\eta = 0$ commonly adopted in previous investigations on a plane mixing layer is not made in the present investigation. Its use in an analysis leads to erroneous distributions of shear stress calculated from the non-dimensional mean velocity measurements. A method which does not impose restriction on V but involves a further empirical input as a boundary condition is presented and it gives satisfactory agreement between the measured and the calculated shear stress profiles.

(iii) the discrepancy between the present turbulence measurements and those of other investigators (i.e. Liepmann and Laufer (1947); Wygnanski and Fiedler (1970)) are attributed to either the differences in the experimental arrangements, or omission of the longitudinal cooling corrections to inclined hot-wires results, or the thermal wake interference between the closely spaced wires of an X-wire probe.

7. THE ASYMMETRIC JET

7.1 General

In applications of technological interest jet and wake flows are frequently asymmetric; examples are the flows in the wakes of slotted aerofoils or behind jet-flapped aerofoils. A simple case of an asymmetric jet is being investigated here and consists of a two-dimensional turbulent jet in zero pressure gradient with uniform streaming flow on one side and quiescent conditions on the other. Fig. (28) shows a sketch of the experimental set up to produce this simple case.

The streaming flow is provided by the 17 in. x 30 in McGill blower wind tunnel. The various ratios of jet-to-free stream velocity, (U_j/U_1), are obtained by varying either the tunnel speed or the jet velocity. To obtain high values of (U_j/U_1), however, it was necessary to reduce the tunnel speed by a large factor. This introduced a complication because the turbulence intensity in the uniform stream was not constant (see Fig. (B.1)) over the whole operating range of the wind tunnel (the tunnel was driven by a 25 H.P., constant r.p.m. (720), A.C. motor and the free stream velocity was changed by adjusting the inlet guide vanes). For example, at 115 ft/s. the turbulence intensity in the free stream (on centre line) was about 0.4% whereas at 25 ft/s. it was about 1.3%. It was thought that such a variation of turbulence level might significantly affect the growth of the jet. To the knowledge of the author the effects of free stream turbulence on free shear flows have not been investigated.

To determine the sensitivity of jet flows to free stream turbulence a subsidiary investigation was therefore undertaken. Measurements were made in both plane mixing layers and the asymmetric jets with free stream turbulence ranging from 0.5% to 1.1% (see Appendix (2)). It was concluded that the turbulence intensity must be reduced below 0.7% of the free stream for the effect to be negligible. To achieve this level at low tunnel speeds, an additional 5 H.P. D.C. motor drive was therefore installed. This was found satisfactory for speeds less than 60 ft/s. and the turbulence level remained constant at about 0.5%.

The results of experiments on the asymmetric jets for values of U_j/U_1 = 2.275, 5.08 and 9.0 are given in this section. The above ratios of (U_j/U_1) were selected to cover the entire range (i.e. from a strong jet case to a weak jet case) of the asymmetric jet flow. The measurements include pitot and hot-wire traverses for mean velocity, Reynolds stresses, intermittency and spectra of the longitudinal fluctuations. Certain local double and triple correlations have also been obtained. The conventional (i.e. by velocity profiles) two-dimensionality checks on the flow are given in Appendix 1. In section (8) evaluation of entrainment velocities for the various free shear flows investigated here is given. This is then followed in section (9) by comparison of experimental results of the asymmetric jets with the simple analysis presented in section

(2.4.2).

It should be noted that unless specified otherwise all hot-wire measurements for the asymmetric jets are not corrected for the longitudinal cooling and the high intensity effects. The longitudinal cooling correction factor for $\overline{uv}$ is 1.08 and for both $\overline{v^2}$ and $\overline{w^2}$ it is 1.16.

For convenience the three cases of the asymmetric jet are identified as follows:

$U_j/U_1 = 2.275$ (a weak asymmetric jet)

$U_j/U_1 = 5.08$ (a mild asymmetric jet)

$U_j/U_1 = 9.0$ (a strong asymmetric jet)

7.2 Results and Discussions for the Asymmetric Jet with $U_j/U_1 = 5.08$

7.2.1 Mean Velocity Profiles

The mean velocity profiles at various downstream positions were measured by both a pitot tube and linearized hot-wires. For the pitot traverses the static pressure across the asymmetric jet was assumed to be a constant and equal to the atmospheric pressure. For comparison Figs. (29) and (30) show typical results for the case $U_j/U_1 = 5.08$ at two downstream stations, x = 26.75 in. and 33.75 in. It can be seen from these figures that apart from the edge of the zero velocity side the results from the pitot tube and the hot-wires are in good agreement with each other. Towards the edge of the zero velocity side measurements made by the pitot tube probably give velocities lower than the actual whereas the hot-wire results probably over-estimate the velocities in this region. On these figures positions of the half velocity scales (see Fig. (4)) are also indicated to show that within this range ($l_1 < y < l_2$) the agreement between the pitot tube and hot-wire results is very good. The reason for this is that the turbulence intensity within this range is less than 15%, and therefore one would expect the agreement to be fairly good. Moreover, these hot-wire and pitot tube results give independent checks on the velocity measurements.

Figs. (31) and (32) show non-dimensional mean velocity profiles on the two sides of the asymmetric jet. The measurements were made with a linearized hot-wire at seven downstream stations within the range 3.125 in. $< x <$ 40.75 in. For the streaming side the velocity scale u_o and the length scale l_1 (see figure (4)) are used whereas for the zero velocity side the scales are U_m and l_2 respectively. A comparison is made by including in these figures the tabulated profile of Bradbury (1963) which is shown by a solid line. Also an exponential profile is shown in Fig. (32). The discrepancy between the experimental results and the exponential profile is not large and thus an approximate method, incorporating a similarity hypothesis, for predicting the growth of the asymmetric jet is not likely to be seriously in error. The figures (31) and (32) substantiate the assumptions of section (2.4.2) (see equations (58) and (59)) in that the velocity distribution in the asymmetric jet can be divided into two parts: (a) the streaming side resembling a half jet in uniform stream and (b) the zero velocity side resembling a half jet in still air. It is also observed that the present velocity measurements are in general agreement with Bradbury's results on the streaming side although some disagreement exists in the region of very low velocities. As mentioned before in this region the hot-wire overestimates the velocities.

7.2.2 Variations of Main Characteristics of the Asymmetric Jet; $U_j/U_1 = 5.08$

The variations of main characteristics such as the lengths and velocity scales and the locus of the points of maximum velocity for the asymmetric jet ($U_j/U_1 = 5.08$) are given in Fig. (33). These measurements are reported because they display some characteristics of the asymmetric jet and furthermore the knowledge of their distributions is required to evaluate distributions of $\overline{uv}$ from mean velocity measurements (see equations (61) and (64) in section (2.4.2)).

Considering the growth of the asymmetric jet it can be seen from Fig. (33) that the zero velocity side (i.e. l_2) grows linearly with downstream distance and the streaming side growth (i.e. l_1) exhibits non-linearity very clearly. Note that the shear layer on the streaming side grows less rapidly than the one on the zero velocity side, as expected. Another feature worth noting is that the locus of (y_m) is a straight line over the range 10 in. $\leqslant x \leqslant$ 40 in. but with a different origin.

This is in agreement with the observation of Gartshore (1965). In section (2.4.2) it was noted (equation (66)) that the locus of the points of maximum velocity moves towards the streaming side as the flow develops downstream. The variation of (y_m) in Fig. (33) clearly substantiates this observation. Similar conclusions may be drawn from the results of other cases of the asymmetric jet reported later.

The variation of velocity scales (i.e. u_o and U_m) is represented by the distribution of (u_o/U_1) because ($U_m = U_1 + u_o$) and U_1 is a constant. It is interesting to note that most of the variation (or decay) in (u_o/U_1) for this case takes place within a short distance from the slot exit, and beyond about $x = 20$ in. (i.e. $x/b = 75.5$) (u_o/U_1) decays very nearly linearly with downstream distance x.

7.2.3 Distributions of Reynolds Stresses

The Reynolds stresses in the asymmetric jet (case $U_j/U_1 = 5.08$) were measured at six downstream stations. It is instructive to note that for non-self-preserving flows (e.g. Bradbury's jet in a uniform streaming flow) one is tempted to use a velocity scale which is the same for both mean velocity distributions and Reynolds stresses. On the other hand Kruka and Eskinazi (1964) following Förthmann's suggestion recommend the maximum shear as the characteristic quantity for expressing Reynolds stresses in similarity forms. It transpires that for non-self-preserving flows the mean velocity and Reynolds stresses are not both reduced to similarity forms by the same velocity scale.

Therefore in the present investigation it is proposed to use the local maximum velocity as the scaling velocity for turbulence quantities on the streaming side of the asymmetric jet. For comparison Reynolds stresses are also non-dimensionalized by the velocity scale u_o.

Figs. (34) to (37) show the distributions of Reynolds stresses on the streaming side of the asymmetric jet. The distributions of the turbulence energy, $(\overline{q^2})$, is shown in Fig. (38). Note again, that these results are not corrected for the longitudinal cooling effects but if the reader wishes to correct them, the correction factors are as follows:

no correction for $\overline{u^2}$,

correction factor for $\overline{v^2}$ and $\overline{w^2}$ is 1.16,

and correction factor for $\overline{uv}$ is 1.08.

In these figures the turbulence quantites are non-dimensionalized with the velocity scale u_o. The measurements were made over a wide range of values of x (i.e. from very close to the slot to far away from it) and they clearly show that as the flow develops downstream the values of $(\overline{u^2}/u_o^2)$, $(\overline{v^2}/u_o^2)$, $(\overline{w^2}/u_o^2)$, $(\overline{uv}/u_o^2)$ and $(\overline{q^2}/u_o^2)$ increase, and it can be concluded that the use of u_o as the velocity scale does not reduce the experimental results to the usual similarity forms. For interest it should be mentioned that although Bradbury's (1963) tabulated results for a jet in uniform streaming flow are not compared in these figures they lie very close to the results of station x = 3.125 in. The variations in these figures are mainly due to the decay of u_o because the turbulence is expected to be maintained by some transfer from the zero velocity side.

It was proposed at the beginning of this section that the local maximum velocity will be used to non-dimensionalize the turbulence quantities. Figs. (39) to (43) show the distributions of turbulence parameters across the asymmetric jet. The results on the streaming side (i.e. Figs. (34) to (38)) are replotted with U_m as the velocity scale. Also note that the length scales on the streaming side and the zero velocity side are not the same thus the gradients of these distributions at $\eta_1 = \eta_2 = 0$ will be discontinuous. For comparison uncorrected results of the plane jet in still air (see section (5)) are shown by solid lines on the zero velocity side.

From Figs. (39) to (43) it can be seen that for the streaming side the results collapse better when U_m (instead of u_o) is used for the velocity scale. This is particularly true for measurements beyond x = 20.50 in. On the zero velocity side the measurements show similar trends as do the results of the plane jet in still air, but the asymmetric jet turbulence intensities are slightly lower than those of the plane jet. However, within the experimental scatter and beyond x = 20.50 in. the present results show that the zero velocity side of the asymmetric jet behaves very much like a plane jet in still air. It is of interest to note that the shear stress at the maximum velocity points (see Figs. (37) and (42)) is nearly zero. This is not inconsistent if one observes the results of other asymmetric flows associated with a uniform stream, for instance, a wall jet in uniform streaming flow (see measurements of Bradshaw and Gee (1962), and Kruka and Eskinazi (1964)).

Fig. (44) shows the distributions of $(\overline{uv}/\overline{q^2})$ across the asymmetric jet. From the figure it can be seen that although $(\overline{uv}/\overline{q^2})$-distributions on the streaming and zero velocity sides do not display exact similarity of shapes, their magnitudes at $\eta_1 = \eta_2 = 1.0$ are about the same.

Figs. (45) and (46) show the shear stress correlation coefficients, $R_{\overline{uv}} = (\overline{uv}/\sqrt{\overline{u^2}}\sqrt{\overline{v^2}})$, in the asymmetric jet and these are compared on the streaming side with the measurements for a plane jet in uniform stream made by Bradbury (1963). It should be mentioned that Bradbury has compared his measurements of $R_{\overline{uv}}$ with those of Eskinazi and Kruka (1962) for a plane turbulent wall jet in a uniform stream and also with the measurements of Gibson (1963) for a turbulent axisymmetric jet in quiescent surroundings. His measurements were in good agreement with those of Eskinazi and Kruka, and Gibson. From Fig. (45) it can be seen that the present measurements of $R_{\overline{uv}}$ on the streaming side are in agreement with Bradbury's results.

For the zero velocity side the distribution of the shear stress correlation coefficient, $R_{\overline{uv}}$, is compared in Fig. (46) with the author's results for the plane jet in still air (section (5)). The agreement is again quite good. It should be mentioned that the measurements of $R_{\overline{uv}}$ are effectively independent of both intermittency factor and the longitudinal cooling effects. A comparison between Figs. (45) and (46) (i.e. the streaming side and zero velocity side) shows that apart from the position of maximum $R_{\overline{uv}}$ the results are in general agreement with each other. Thus it appears that there is a tendency to a universally similar structure for all turbulent shear flows.

7.2.4 Measurements of Triple Correlations

It was mentioned in section (4) that the analysis of slanting hot-wire readings involves knowledge of both the longitudinal cooling effects and high intensity effects. The dynamic test for the former effect is given by Patel (1968) and the latter is investigated by Guitton (1970). It should be noted that all shear flows associated with quiescent surroundings encounter high turbulence intensities in regions close to the still surroundings. Hot-wire measurements in this region, therefore, have to be corrected for high intensity effects. The correction factors for various turbulence components, however, involve triple and quadruple correlations (see Heskestad (1963) and Guitton (1968)) and these have to be measured by a matched X-wire probe. In this investigation DISA equipment was used in conjunction with a precision full wave rectifier (details of this and a full description of how the correlation coefficients were obtained, are given by Guitton (1968)).

In section (4) it was stated that the standard DISA X-wire probes were prone to thermal cross talk because of the close proximity of the two slanted wires (Guitton and Patel (1969)). For the present purpose a modified X-wire probe was used (the modification is given by Guitton and Patel). To verify the dynamic response of the modified X-wire probe and to check the repeatability of the turbulence measurement, the shear stress correlation coefficients across the asymmetric jet were measured at x = 26.75 in. A comparison between the results obtained by a single slanted hot-wire and the modified X-wire probe is shown in Fig. (47). In this figure the full line represents the results obtained by the single slanted wire and the points are for the modified X-wire probe results. The agreement between the two sets of results is very good and enhances confidence in both the modified X-wire probe and the electronic equipment. Note also that $R_{\overline{uw}}$ is nearly zero across the flow.

The triple and quadruple correlations for the asymmetric jet were measured at x = 26.75 in. only. However, because Guitton's (1968) correction factors for Reynolds stresses involve only triple correlations these are presented in Fig. (48). The triple correlations shown in the figure are as follows:

$$R_{\overline{uw^2}} = \frac{\overline{uw^2}}{\sqrt{\overline{u^2}} \cdot \overline{w^2}}$$

$$R_{\overline{uv^2}} = \frac{\overline{uv^2}}{\sqrt{\overline{u^2}} \cdot \overline{v^2}}$$

$$R_{\overline{v}3} = \frac{\overline{v^3}}{\overline{v^2}.\sqrt{\overline{v^2}}}$$

$$\text{and } R_{\overline{w}3} = \frac{\overline{w^3}}{\overline{w^2}.\sqrt{\overline{w^2}}}$$

Fig. (48) shows that across the asymmetric jet $R_{\overline{uw}2}$ and $R_{\overline{uv}2}$ are of the same order and the shapes of their distributions are very similar. On the other hand note that $R_{\overline{v}3}$ is much bigger than $R_{\overline{w}3}$, the latter being approximately zero across the flow. It is also noted that on the streaming side $R_{\overline{v}3}$ is practically of the same order of magnitude as $R_{\overline{uv}}$. For interest it is mentioned here that $R_{\overline{uw}}$ was approximately zero (negligibly small compared to $R_{\overline{uv}}$) across the asymmetric jet. Not only at this station (i.e. x = 26.75 in.) but at various streamwise stations single slanted wire results also indicated that $(\overline{uw})$ was approximately zero.

The results shown in Fig. (48) were used to work out Guitton's (1968) high intensity correction factor for the Reynolds shear stress. Fig. (49) shows the combined correction due to the longitudinal cooling effects and the high intensity at x = 26.75 in. Note that between the half velocity points on either side of the maximum velocity point, the correction due to the high intensity, on the average, is small and this is attributed to low turbulence intensity (< 20%) encountered within this region. In the following section the measured Reynolds shear stress distribution is corrected by using the correction factor shown in Fig. (49).

7.2.5 Check on the Momentum Balance

Coles (1968) has pointed out that a severe test for the two-dimensionality of a plane turbulent shear flow is to demonstrate the momentum balance by measuring various terms in the momentum equation. For the asymmetric jet under investigation the momentum equations on the streaming and zero velocity sides are given by equations (61) and (64) respectively (see section (2.4.2)). It is mentioned that in these equations the term containing the difference between normal Reynolds stresses (i.e. $\frac{\partial}{\partial x}(\overline{u^2}-\overline{v^2})$) is neglected because it was found that its contribution is quite small. Various terms appearing in equations (61) and (64) were measured (see Fig. (33)) and the Reynolds shear stress distribution at $x = 26.75$ in. for the asymmetric jet was computed. The result is shown in Fig. (50). At this station the Reynolds shear stress distribution was measured by using a single slanted, linearized hot-wire. As mentioned above the hot-wire results are corrected for the longitudinal cooling effects and high intensity effects (for correction factor see Fig. (49)). From Fig. (50) it can be seen that although a perfect agreement between the results shown therein is not achieved, the agreement is indeed satisfactory. The disagreement at the point of maximum shear on the zero velocity side is about 8%. A general observation can be made from many published measurements of Reynolds shear stress distributions in various turbulent shear flows and that is that the measured shear stresses in the regions of maximum velocity gradient are usually smaller than those calculated using the momentum equation. This indicates that some complicated interference mechanism may be in operation for a hot-wire in these regions. No attempt is made here to investigate effects of velocity gradients on hot-wire measurements. Therefore, it may be concluded that for the asymmetric jet the momentum balance is satisfactory and the flow is effectively two-dimensional.

7.2.6 Intermittency

The intermittency was measured using a differential signal from a linearized normal wire and recording the signal on an 'Ultra-Violet' recorder. The technique of analyzing the recorded signal was similar to the one used by Gartshore (1965) and Guitton (1970).

The intermittency measurements were made at five downstream stations. The results are shown in Fig. (51). For comparison measurements of Bradbury (1963) (for a jet in uniform streaming flow) are shown by a dotted line on the streaming side and those of Gartshore (1965), and Heskestad (1963), (for a jet in still air), are shown on the zero velocity side. From the figure it can be seen that for the zero velocity side, apart from the results at x = 6.125 in., the present results fall on a single curve and, furthermore, they are in agreement with the results of both Heskestad and Gartshore. For the streaming side, however, the results show systematic change in the intermittency distributions. The intermittent zone becomes bigger and bigger as the flow develops downstream and at x = 40.75 in. there is hardly any fully turbulent zone on the streaming side. This is not surprising because as the asymmetric jet tends to its asymptotic state (i.e. a plane mixing layer) the whole flow becomes intermittent (Wygnanski and Fiedler (1970) have shown that there is no fully turbulent zone in a plane mixing layer). It is interesting to note that over the streamwise range of the intermittency measurements the half intermittency point on the zero velocity side is at $\eta_2 \approxeq 1.65$ whereas on the streaming side it lies between 1.42 and 1.88. Finally, from Fig. (51) it may be concluded that the zero velocity side of the asymmetric jet behaves very much like a jet in still air as far as the intermittency distribution is concerned.

7.2.7 One-Dimensional $\overline{u^2}$-spectra

In theoretical discussions of isotropic turbulence, it is a general practice to define a mathematical quantity which has the closest analogy to the physical notion of the energy associated with a particular scale of motion. This quantity is the three dimensional spectral density function $E(\underset{\sim}{K})$. However, the way in which $E(\underset{\sim}{K})$ can be measured directly is unknown and therefore measurements are usually made of the one dimensional spectrum function $\phi(k_1)$ where $\phi(k_1)$ is defined by

$$\int_0^\infty \phi(k_1)dk_1 = \overline{u^2}$$

The one dimensional spectrum function is related to the three dimensional spectrum function by (Batchelor (1953), Hinze (1959)):

$$2E(\underset{\sim}{K}) = k_1^2 \frac{\partial^2 \phi(k_1)}{\partial k_1{}^2} - k_1 \frac{\partial \phi(k_1)}{\partial k_1} \quad \text{for isotropic turbulence}$$

where $\int_0^\infty E(\underset{\sim}{K})\, dk_1 = \frac{1}{2}\overline{q^2} = \frac{1}{2}(\overline{u^2} + \overline{v^2} + \overline{w^2})$

It is well known that in small scales of motion the important parameter of turbulence is the energy dissipation, ϵ, (Hinze (1959)) which is defined as follows:

$$\epsilon = 2\nu \int_0^\infty k_1^2\, E(\underset{\sim}{K})\, dk_1$$

where ν is the kinematic viscosity

It can be shown that the energy dissipation density, ϵ, is related to the one dimensional spectrum function, e.g.

$$\epsilon = \nu \int_0^\infty k_1^2 \left[k_1^2 \frac{\partial^2 \phi}{\partial k_1^2} - k_1 \frac{\partial \phi}{\partial k_1} \right] dk_1$$

$$= -5\nu \int_0^\infty k_1^3 \frac{\partial \phi}{\partial k_1}\, dk_1$$

$$\text{or} \quad \epsilon = 15\nu \int_0^\infty k_1^2\, \phi(k_1)\, dk_1$$

The integrand, $k_1^2\phi(k_1)$, is known as the dissipation spectrum and describes the distribution in wave number of the rate of decay of turbulent energy to heat.

In the inertial subrange viscosity has little direct effect and hence from dimensional arguments it can be shown that

$$\phi(k_1) \propto \epsilon^{2/3} k_1^{-5/3}$$

The constant of proportionality in the above equation is an absolute constant and is often referred to as Kolmogoroff's constant. The existence of an inertial subrange depends on the magnitude of turbulence Reynolds number, $R_\lambda = (\lambda\sqrt{\overline{u^2}})/\nu$, where λ is Taylor lateral microscale (Gibson (1963)). λ is also referred to as the dissipation length (Naudascher (1965)). Gibson, following Corrsin, suggests $R_\lambda > 500$ for the existence of the inertial subrange. The microscale λ is evaluated from the following relation:

$$\frac{\frac{1}{3}\overline{q^2}}{\lambda^2} = \int_0^\infty k_1^2 \, \phi \, (k_1) \, dk_1 = \frac{\overline{u^2}}{\lambda^2} \quad \text{(for isotropic turbulence)}$$

Following Gibson (1963) and Grant et al. (1962) values of λ at various lateral and streamwise positions were obtained. The technique involves a plot of $k_1^2 \, \phi \, (k_1)$ versus k_1 and the area under the curve then provides ϵ and λ. It should be mentioned that λ can be considered roughly a measure of the eddies responsible for the energy dissipation in the final stages only thus it differs from the dissipation length L_ϵ used by Townsend (1956) and Newman (1968). Townsend (see equation (5.6.4) on page 95 of his book) defines the dissipation length in isotropic turbulence as follows:

$$\epsilon = \frac{3}{2} \frac{(\overline{u^2})^{3/2}}{L_\epsilon}$$

where ϵ is not the rate of turbulent energy dissipation by viscosity as above but it is the rate of turbulent energy dissipation which is determined by the rate of energy transfer from the large scale motions.

The purpose of the present measurements was to check whether or not the inertial subrange with -5/3 power exists, to obtain variations of λ and to obtain the Kolmogoroff constant.

Figs. (52) and (53) show typical results of one dimensional $\overline{u^2}$ -spectra measured by a B and K audio frequency spectrometer using 1/3 octave filters. The wave number k_1 was assumed to be equal to $(2\pi f/U)$ and by definition $\int_0^\infty \phi(k_1)\, dk_1 = \overline{u^2}$. These measurements were made at typical lateral positions which are indicated on a sketch included in the figures. Also included in these figures is a line with -5/3 slope. From both figures (52) and (53) it can be concluded that the spectra exhibit a range with -5/3 power. The range of turbulence Reynolds numbers for measurements shown in these figures was $326 \leqslant R_\lambda \leqslant 715$.

In Figs. (54) and (55) $(k_1^2\ \phi\ (k_1)/\overline{u^2})$ is plotted against k_1. The shapes of these curves are very similar to those given by Grant et al. (1962). All the curves exhibit a peak around $k_1 = 300\ \text{ft}^{-1}$. As mentioned before from plots similar to Figs. (52) and (54) the energy dissipation, ϵ, and λ were calculated.

It was found that values of λ were approximately independent of the lateral position. In Figs. (56) to (58) the value of λ

is the mean value at a particular streamwise station. Fig. (56) shows variation of λ with downstream distance x. From the figure it can be seen that beyond x = 20 in. (i.e. in the region where the flow is not affected by conditions at the slot) λ does not vary a great deal. For interest variation of λ with the mean flow length scales l_1 and l_2 is shown in Fig. (57), and Fig. (58) shows variations of (I_1/λ) and (l_2/λ) with downstream distance x. It may be concluded from these figures that λ is not directly proportional to the mean flow length scales l_1 and l_2.

Fig. (59) shows values of the Kolmogoroff constant, K', obtained in the present investigation plotted against dissipation ϵ. For comparison values of K' obtained by Grant et al. (1962) in a tidal channel and by Gibson (1963) in an axisymmetric jet in still air are included. The value of K' for grid turbulence is the one quoted by Gibson from measurements of Kistler and Vrebalovich in California Institute of Technology Co-op Tunnel. It should be recalled that K' is expected to be an absolute constant, however the present measurements show a definite trend i.e. it increases as ϵ increases. Similar behaviour can be seen in the results of Grant et al as well. It is possible that the measurements near the slot are contaminated by the conditions at the slot and values of K' are much larger than those of other investigators. Far away from the slot, however, values of K' are in agreement with those reported by Gibson and Grant et al. An interesting observation from other measurements not reported here is that the extent of the inertial subrange for measurements near the slot was quite small even though the turbulence Reynolds numbers were quite large (i.e. $R_\lambda > 750$). On the other hand far from the slot the turbulence Reynolds numbers were small ($326 \leqslant R_\lambda \leqslant 715$) but the inertial subrange extended over much wider wave number space (see Figs. (52) and (53)). The turbulence Reynolds number for the experiment of Grant et al. was 3600 and for the experiment of Gibson it was about 780. It is difficult to draw any definite conclusion without further measurements of the $\overline{v^2}$, $\overline{w^2}$ and $\overline{uv}$ spectra.

7.3 Results and Discussion for the Asymmetric Jet with $U_j/U_1=9.0$

It was noted before that as the ratio of jet to free stream velocity increases the asymmetric jet approaches the jet in still air. Measurements were, therefore, made with $(U_j/U_1) = 9.0$. These measurements include mean velocity traverses and Reynolds stresses at a number of streamwise stations.

7.3.1 Mean Velocity Profiles

As shown in Figs. (60) and (61), the non-dimensional mean velocity profiles are again geometrically similar and in agreement with those obtained with $(U_j/U_1) = 5.08$. For comparison the tabulated results of Bradbury (1963) are shown by a solid line. Once more the agreement is satisfactory.

7.3.2 Variations of Main Characteristics of the Asymmetric Jet $U_j/U_1 = 9.0$

Fig. (62) shows the variations of the main characteristics of the asymmetric jet with $(U_j/U_1) = 9.0$. Compared to the results for the case $(U_j/U_1) = 5.08$ (Fig. (33)), both l_1 and l_2 grow approximately in a linear fashion with downstream distance and they are roughly equal in magnitude. However, deviations from linearity are apparent as the ratio (u_o/U_1) decreases. It is also worth noting that the locus of (y_m) beyond x = 13.5 in. is again a straight line and moves towards the streaming side as postulated by equation (66) in section (2.4.2).

7.3.3 Distributions of Reynolds Stresses

It was mentioned in section (7.2.3) that for the streaming side of the asymmetric jet a better collapse of Reynolds stresses is obtained when they are non-dimensionalized with the local maximum velocity U_m instead of the excess velocity u_o. Hence the Reynolds stresses for the present case are first scaled with the excess velocity u_o (Figs. (63) to (67)) and then in Figs. (70) to (74) they are non-dimensionalized with U_m. A comparison is made with Bradbury's (1963) tabulated results in Figs. (63), (64), (65) and (67). From these figures it can be seen that the results do not collapse on a single curve and that the disagreement between Bradbury's and the present results is quite pronounced. However, if one ignores the measurements below x = 26.75 in. on the ground that the flow may not be fully developed then the results in Figs. (63) to (67) may be considered to lie close to a single curve.

Fig. (68) shows the distributions of $(\overline{uv}/\overline{q^2})$ across the streaming side of the asymmetric jet. Over the streamwise range (i.e. 6.125 in. < x < 40.75 in.) these measurements display a similarity form as before (compare Fig. (44)) but there is some difference in the shapes of these profiles. In particular, for the strong asymmetric jet, (i.e. with U_j/U_1 = 9.0), the shape of $(\overline{uv}/\overline{q^2})$ distribution on the streaming side is approximately symmetrical about $\eta_1 = 1$, and similar to that for a jet in still air. Note that for the asymmetric jet with $(U_j/U_1) = 5.08$ (see Fig. (44)) the maximum value of $(\overline{uv}/\overline{q^2})$ occurs at about $\eta_1 = 1.6$ and the shape of the $(\overline{uv}/\overline{q^2})$ distribution is no longer symmetrical. It appears that this is a characteristic feature of small perturbation $(u_o/U_1 < 0.5)$ jets (in uniform streaming flow) or wake flows.

The distribution of shear stress correlation coefficient, $(\overline{uv}/\sqrt{\overline{u^2}}\cdot\sqrt{\overline{v^2}})$ for the streaming side of the asymmetric jet with $U_j/U_1 = 9.0$ is shown in Fig. (69). In this figure results of Bradbury are given for comparison. As noted above Bradbury's results show a maximum around $\eta_1 = 1.6$ and his $R_{\overline{uv}}$ distribution is not symmetrical whereas the mean line drawn through the present results indicate a maximum value around $\eta_1 = 1.0$ and the $R_{\overline{uv}}$-distribution is approximately symmetrical. It is also noted that $\overline{uv}$ at the point of maximum velocity is quite small.

The Reynolds stresses on the streaming side of the jet were non-dimensionalized with the local maximum velocity U_m in a manner similar to that for the case of $U_j/U_1 = 5.08$.

These results are shown in Figs. (70) to (74). Comparison of these figures with corresponding results in Figs. (63) to (67) indicates that over the whole range of measurements the velocity scale U_m produces better collapse of results on single curves. In Fig. (70) $(\overline{u^2}/U_m^2)$ distribution for a jet in still air is shown by a solid line. Figs. (70), (74) and (75) also contain results for the zero velocity side. From these figures it may be concluded that the zero velocity side of the asymmetric jet behaves in a manner similar to a plane jet in still air. However, it would be amiss not to point out that apart from $(\overline{u^2}/U_m^2)$-distributions the other distributions of Reynolds stresses are lower than the corresponding ones for a jet in still air. On the other hand the two sides of the strong asymmetric jet display similar profiles for Reynolds stresses (e.g. see Figs. (70), (73), (74) and (75)).

Fig. (76) gives distributions of $(\overline{uv}/\overline{q^2})$ across the zero velocity side of the strong asymmetric jet. From the figure similar conclusion as that for the streaming side may be drawn once more.

The distributions of shear stress correlation coefficient, $R_{\overline{uv}}$, for the zero velocity side is shown in Fig. (77). In this figure a mean line representing $R_{\overline{uv}}$-distribution on the streaming side is shown by a solid line and $R_{\overline{uv}}$-distribution for a jet in still air is shown by a dotted line. From the figure it can be observed that $R_{\overline{uv}}$-distributions on both sides of the strong asymmetric jet are of the same order of magnitude. It should be pointed out that measurements reported in this thesis indicate that the shear stress correlation coefficient, $R_{\overline{uv}}$, is not a constant over the major portion of shear flows investigated here.

7.4 Results and Discussion for the Asymmetric Jet with $U_j/U_1=2.275$

In sections (7.2) and (7.3) results were presented for a mild and a strong asymmetric jet respectively. This section deals with a weak asymmetric jet in which the ratio of jet to free stream velocity is small. As this ratio decreases the asymmetric jet tends to its other asymptotic state, i.e. a plane mixing layer. For the weak asymmetric jet measurements of mean velocity and Reynolds stresses are presented. Because the asymmetric jet with $(U_j/U_1)=$ 2.275 very quickly (within approximately 70 slot widths downstream) becomes a plane mixing layer, as far as the mean velocity distribution is concerned, it was found difficult to identify accurately the length scale, l_1, and velocity scale, u_o, on the streaming side and therefore turbulence measurements on the zero velocity side only are presented.

7.4.1 Mean Velocity Profiles

The non-dimensional mean velocity profiles are shown in Fig. (78). In the figure, for the streaming side a tabulated profile of Bradbury (1963) is shown for comparison, and on the zero velocity side the exponential profile is shown by a solid line. Also for comparison, on the zero velocity side measurements of a plane mixing layer are included. The plane mixing layer results were obtained for $U_1/\nu = 3.58 \times 10^5$ ft^{-1} at x = 27.75 in. and they are in agreement with other mixing layer results reported in Fig. (21). From Fig. (78) it can be concluded as before that even for the weak asymmetric jet the mean velocity profiles are similar. Also note that the results on the zero velocity side are in very good agreement with the results for the plane mixing layer.

7.4.2 Distributions of Reynolds Stresses

As mentioned above distributions of Reynolds stresses are presented for the zero velocity side only. The distributions of $(\overline{u^2}/U_m^2)$ are shown in Fig. (79). In this figure the author's measurements for a plane mixing layer (see section (6)) and a plane jet in still air (see section (5)) are given for comparison. It can be observed from the figure that the measurements for the zero velocity side of the weak asymmetric jet display a trend similar to the plane mixing layer results. There are indications that if the measurements were extended further downstream, where the zero velocity side of the weak asymmetric jet truly becomes a plane mixing layer, they would be in agreement with the results for a plane mixing layer.

Figs. (80) and (81) show the distributions of $(\overline{v^2}/U_m^2)$ and $(\overline{w^2}/U_m^2)$ respectively. In these figures the plane mixing layer results are also included. It can be seen from Figs. (80) and (81) that the results for the weak asymmetric jet are considerably higher than those for the plane mixing layer. On the other hand the results for the weak asymmetric jet lie below those for the plane jet in still air. It is also noticeable that although the measurements of $(\overline{u^2}/U_m^2)$ collapse on a single curve (it is emphasized here that these measurements were made over a narrow range of downstream distance, e.g. 12.625 in. $\leqslant$ x $\leqslant$ 21.625 in., and therefore it is possible that variations in $(\overline{u^2}/U_m^2)$ are not distinguishable.) the distributions of $(\overline{v^2}/U_m^2)$ and $(\overline{w^2}/U_m^2)$ do not collapse on single curves. This indicates that the structure of the flow represented by turbulence components is continuously changing. On the other hand, as shown in Fig. (82), it appears that turbulence energy distributions (i.e. $(\overline{q^2}/U_m^2)$) exhibit a self similar structure (note that these results are also for a narrow range of x) but it is difficult to draw a definite conclusion from Fig. (82).

Fig. (83) shows the distributions of $(\overline{uv}/U_m^2)$ on the zero velocity side of the weak asymmetric jet. In the figure these are compared with the results for the plane mixing layer. The shapes of the shear distributions in both cases are very similar and the results for the weak asymmetric jet seem to collapse on a single curve.

Finally, a comparison is made, in Fig. (84), of the shear stress correlation coefficients for the weak asymmetric jet, the plane mixing layer and the plane jet in still air. It is encouraging to note from Fig. (84) that for all these flows the distributions of $R_{\overline{uv}}$ are roughly the same. Following table gives the maximum values of $R_{\overline{uv}}$ in other turbulent shear flows for comparison

Investigator	Flow	$(R_{\overline{uv}})_{max.}$
Gibson (1963)	Axisymmetric jet in still air	0.53
Kruka and Eskinazi (1964)	Wall jet in uniform streaming flow	0.50
Bradbury (1963)	Plane jet in uniform streaming flow	0.575
Klebanoff (1954)	Boundary layer in zero pressure gradient	0.5
Present investigation	Plane mixing layer	0.55
	Plane jet in still air	0.475
	The asymmetric jet:	
	Strong jet case $U_j/U_1=9.0$	0.65
	Mild jet case $U_j/U_1=5.08$	0.40-0.50
	Weak jet case $U_j/U_1=2.275$	0.42-0.47

8. EVALUATION OF ENTRAINMENT

The basic process in the spread of turbulent flows such as jets, wakes and boundary layers is the entrainment of non-turbulent fluid by the turbulent fluid within the shear flow. The process takes place at the free edges which are neither plane nor well defined. Although the vorticity transfer at the edges is controlled by the action of viscous forces, the entrainment is essentially independent of viscosity and is probably controlled by the large scale turbulent motion. Townsend (1970) suggests that the structure of the whole flow establishes both the level of turbulent motion and the entrainment rate. Using the information of the structure parameter (Townsend uses the ratio of mean turbulence energy, $\overline{q_o^2}$, to the maximum shear stress to represent the structure of a particular flow). Townsend then predicts the entrainment rates in wakes, jets, mixing layers and boundary layers.

The purpose of this section is to present methods to evaluate the entrainment from experimental results of the various shear flows reported here.

The rate of entrainment by definition is given by:

$$E = \frac{d}{dx} \int_{y_{low}}^{y_e} U \, dy \qquad (8.1)$$

where E is the rate of entrainment and y_e represents the free edge of the turbulent shear flow and y_{low} is zero for flows with a solid boundary or a symmetry line.

Following Spalding it can be shown that the rate of entrainment is given by

$$E = - \left[\frac{\partial \tau/\rho}{\partial U}\right]_{y_e} \quad \text{at a constant } x \qquad (8.2)$$

The above equation was derived using von Mises' form of the equation of motion, however it can also be derived by applying the momentum equation at the edge, for example, see Michel et al. (1968) and Newman (1966). It is noted that although the edge of a plane turbulent shear flow is not very well defined in τ-y plane, it is sharply defined in τ-U plane (Escudier (1968)). Thus a plot of τ versus U not only gives the entrainment rate but also provides the dissipation integral: $\int_0^{y_e} \tau/\rho \, \frac{\partial U}{\partial y} \, dy$.

Another method for evaluating the rate of entrainment is to integrate mean velocity profiles and use equation (8.1).

For the asymmetric jets the entrainment takes place on both sides. The entrainment on the zero velocity side, E_z, is obtained by integrating complete velocity profiles and on the streaming side it is obtained by evaluating the rate of decrease of volume flow in the uniform stream. However, to evaluate the entrainment rate on the streaming side, E_s, one has to identify the edge of the uniform stream at each station. In the present investigation two criteria were used to identify this edge; (a) it was assumed that the edge on the streaming side is located at a value of y where $U = 0.01\, u_o$; and, (b) it was located at a value of y where the intermittency $\gamma = 0.5$. It should be noted that these criteria allow sufficient flexibility in the definition of the edge on the streaming side. The rate of entrainment, E_s, is then given by

$$E_s = U_1 \frac{d\delta}{dx} \quad \text{where } \delta \text{ is the value of } y \text{ at which } U = 0.01\, u_o$$

$$E_s = U_1 \frac{dY_{\gamma=0.5}}{dx} \quad \text{where } Y_{\gamma=0.5} \text{ is the value of } y \text{ at which } \gamma = 0.5. \tag{8.3}$$

To establish confidence in the evaluation of the rate of entrainment by equation (8.2) it was proposed to test the method in a flow field where the rate of entrainment can be obtained by some other means. Such a flow field is a plane jet in still air for which it is easy to show that the rate of entrainment is given by

$$\frac{E}{U_m} = \frac{1}{2} \frac{dl_o}{dx} \cdot I_1 \tag{8.4}$$

where $\frac{dl_o}{dx}$ is the rate of growth for the plane jet in still air and $I_1 = \int_0^\infty f(y/l_o)d(y/l_o) = 1.065$ (with the exponential profile). Measurements for the plane jet in still air reported in Fig. (12) give $dl_o/dx = 0.103$, hence the non-dimensional entrainment rate from equation (8.4) is $E/U_m = 0.055$.

In Fig. (85) the measured values of the Reynolds shear stress are plotted against the mean velocity for the jet in still air. The measurements for two downstream stations, $x/b \simeq 129$ and 152, are included. In the figure lines are drawn to indicate the slope at the edge and according to equation (8.2) the slope of these lines gives the rate of entrainment. The lines shown in the figure have a slope of 0.05, i.e. $E/U_m = \dfrac{\partial(\overline{uv}/U_m^2)}{\partial(U/U_m)} = 0.05$ compared to 0.055 obtained from equation (8.4). It is, therefore, concluded that equation (8.2) provides a fairly satisfactory (within 10%) means of evaluating the rate of entrainment in plane turbulent shear flows. In passing it should be mentioned that the edges of the plane jet are clearly defined but they do not coincide with $U = 0$. The edges seem to be located where $U/U_m \simeq 0.15$ or very nearly where the intermittency $\gamma = 0.5$. Furthermore, the results shown in Fig. (85) are corrected for the effects of the longitudinal cooling only. With the uncertainty in the high intensity corrections at the edges (Heskestad (1963) extrapolates his correction factors beyond $\eta = 1.0$ (approximately 1 or 2% correction), whereas Guitton (1968) gives roughly 5% correction due to the high intensity within the range $0.8 \leqslant \eta \leqslant 1.6$.) the rate of entrainment obtained from Fig. (85) is thus indeed satisfactory.

Fig. (86) shows the results for the plane mixing layer (section (6)) replotted to obtain entrainment rates according to equation (8.2). The results are for three downstream stations and they collapse on a single curve as would be expected. In the case of a plane mixing layer the irrotational fluid is entrained on both the streaming and zero velocity sides. The slopes at the edges of the plane mixing layer are indicated in

Fig. (86) and they give the rates of entrainment as follows:

zero velocity side: $E_z/U_1 = 0.035$

Streaming side: $E_s/U_1 = 0.06$

It is interesting to compare the value of E_z/U_1 with the results of Begg etal. (1967) who measured the rate of entrainment directly using a technique developed by Spalding and Ricou (1961). They measured the rate of entrainment, ($E_z/U_1 \approx 0.037$), in the core region of a symmetrical two-dimensional jet which is a mixing layer. The agreement between the results of Begg et al. and the present is very good and once again augments confidence in the use of equation (8.2). Note that the rate of entrainment on the streaming side of the plane mixing layer is nearly twice that on the zero velocity side. This may be due to the higher intermittency on the streaming side compared to that on the still air side (see intermittency results of Wygnanski and Fiedler (1970)).

Fig. (87) shows a typical plot of ($\overline{uv}/U_1^2$) versus (U/U_1) for the asymmetric jet. The shear and mean velocity measurements, for all the asymmetric jets investigated here, were replotted in this manner to obtain the rates of entrainment on both sides. Figs. (88) and (89) show (E_s/U_1) and (E_z/U_1) plotted against (u_o/U_m). Also included in these figures are the values of the rate of entrainment obtained using equations (8.3). From these figures it may be concluded that both methods (equations (8.2) and (8.3)) give satisfactory results and they do not depend critically on the criteria specifying the free edges. It should be mentioned that since the rate of entrainment depends on the structure of the whole flow the appropriate scaling velocity for it would be U_m (see sections (7.2), (7.3) and (7.4)) but to show the variations of E_s and E_z with downstream distance they are scaled with U_1 in Figs. (88) and (89). These figures also show that the results for the asymmetric jets follow a particular trend, however, because of large scatter in Fig. (89) it would be difficult to extract a particular distribution curve. In Fig. (90) the ratio (E_s/E_z) is plotted against (u_o/U_m) and for this figure the entrainment rates obtained by equation (8.2) are used. From the figure it can be seen that the ratio (E_s/E_z) remains very roughly constant (about 1.7) over the range $0 \leqslant u_o/U_m \leqslant 0.6$. For large values of (u_o/U_m) it appears that (E_s/E_z) tends to one as would be expected for an ideal jet in still air. It is interesting to note here that although the rate of growth on the streaming side decreases with increasing (U_1/u_o) the rate of entrainment on that side is always greater than that on the zero velocity side.

9. COMPARISON BETWEEN EXPERIMENTAL RESULTS AND THEORETICAL PREDICTION FOR THE ASYMMETRIC JETS

It was mentioned in the Introduction that the primary purpose of the present investigation was to predict the development of the asymmetric jet. To this end a simple analysis was presented in section (2.4.2). In this section a comparison is made between the experimental results of section (7) and the theoretical predictions for the variations of l_1, l_2 and u_o (see equations (80), (81) and (85) in section (2.4.2)). The only other experimental results (i.e. of mean velocity profiles) for the asymmetric jets are those due to Gartshore (1965) and these are included also for comparison.

In deriving equations (80) and (81) it is noted that some experimental information was needed in order to predict variations of both l_1 and l_2 (see figure (4) for the definitions of l_1, l_2 and u_o). Equation (76) provides this information. Hence in Fig. (91) the ratio of (l_2/l_1) is plotted against $(1 + [U_1/u_o] I_1/I_2)/(1+ U_1/u_o)^2$. It should be noted that in Fig. (91) all experimental results seem to correlate very well according to equation (76). A curve which fits the present results is included in the figure (see equation (78)).

Fig. (92) shows a comparison between measured and predicted (equations (80) and (81)) variations of l_1 and l_2. From this figure it can be concluded that equations (80) and (81) adequately describe the variations in l_1 and l_2 respectively.

It should be recalled that to reduce the complexity of the analysis presented in section (2.4.2) the variation of K (see equation (79)) was proposed to be represented by a simple expression given in equation (83). Fig. (93) is presented to show the comparison between equation (79) and the simple expression given in equation (83). For all practical purposes, as can be seen from the figure, the disagreement between the two is small. Indeed the discrepancy for the range of (U_1/u_o) shown in Fig. (93) increases as (U_1/u_o) increases.

Fig. (94) shows the variation of u_o with the downstream distance x. It should be noted that for all the cases of asymmetric jets investigated so far the hypothetical origin x_o is found to be 20 slot widths upstream of the slot (see Fig. (95)). In the figure equation (85) is represented by a solid line. In equation (85) the values of $I_1/I_2 = 1.411$ and C=0.103 were used. From Fig. (94) it can be concluded that the agreement between the measured and predicted variation of u_o is very good. Thus the simple analysis presented in section (2.4.2) not only provides means of correlating experimental results for the main characteristics of the asymmetric jets but also predicts them satisfactorily. Also it is restated here that the method of analysis in section (2.4.2) avoids the usual objections associated with the eddy viscosity and mixing length theories (Batchelor (1950)).

It was noted in section (2.3.3.) that the structure parameter $(SP) = \left[\overline{q^2}/\overline{uv}\right]_{\eta=1}$, does not vary a great deal in many plane, free turbulent shear flows. Collected results of both self-preserving and non-self-preserving shear flows are, therefore, shown in Fig. (96). Note that apart from the results on the streaming side for the asymmetric jet, $U_j/U_1 = 9.0$, all other results collapse reasonably on a single curve. This substantiates the observation of Townsend (1970) that in all free shear flows the ratio of mean turbulence energy to the maximum shear stress, $(\overline{q_o^2}/\overline{uv}_m)$, is roughly a constant. However, it should be pointed out that no systematic change in this ratio from one flow to another is observable in Fig. (96).

It can be observed from Fig. (96) that there is no substantial region across the flow over which the ratio $(\overline{uv}/\overline{q^2})$ remains constant. However, note that in most of the free shear flows the non-dimensional mean velocity profiles are similar (usually the exponential profile fits experimental results reasonably well), and Fig. (96) indicates that $(\overline{uv}/\overline{q^2})$ distributions are also similar, therefore, one would expect (see figures below) the ratio $f'/(-\overline{uv}/\overline{q^2})$ to remain constant over the major portion of a turbulent shear flow.

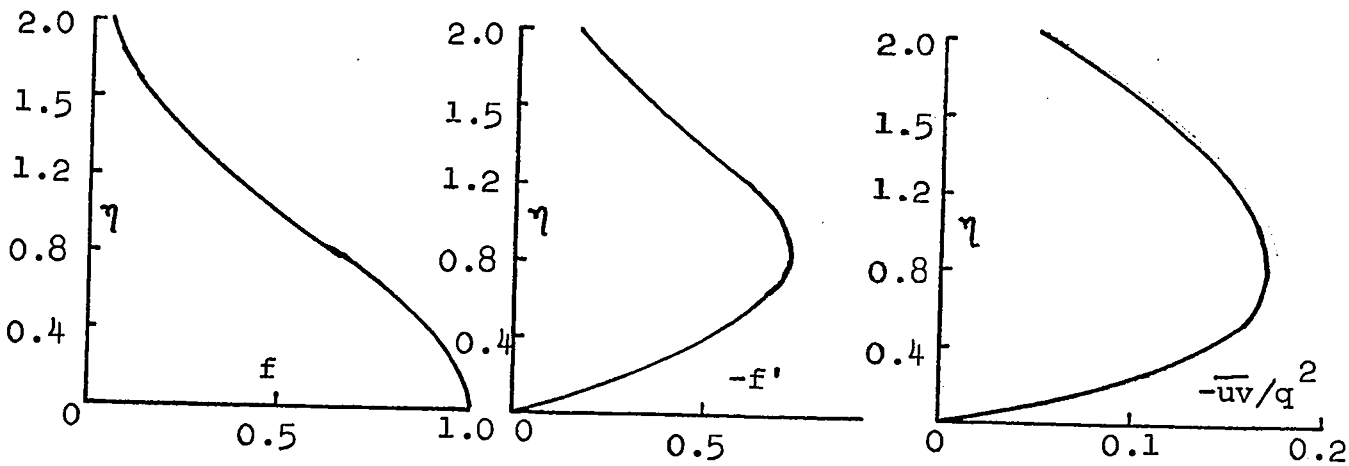

It can be shown that the above ratio can be rewritten as:

$$\frac{f'}{(-\overline{uv}/q^2)} = \left(\frac{\overline{q^2}}{u_o^2}\right)\left(\frac{u_o l_o}{\nu_T}\right) \tag{9.1}$$

where u_o is an appropriate velocity scale (i.e. for jets and wall jets in still air it is equal to U_m and for jets in streaming flow it is $(U_m - U_1)$) and l_o is the length scale defined as the value of y where $U = \frac{1}{2} u_o$.

It is interesting to note that $\left(\frac{\overline{q^2}}{u_o^2}\right)\left(\frac{u_o l_o}{\nu_T}\right)$ is proportional to the effective strain in a turbulent shear flow. It is shown by Townsend (1970) that the maximum effective strain is roughly the same in all flows and it is given by

$$\text{maximum effective strain, } \alpha_m \propto \frac{\overline{q_o^2}}{\tau_m} \tag{9.2}$$

$$\text{i.e. } \alpha_m = \text{constant x } \left(\frac{\overline{q_o^2}}{u_o^2}\right)\left(\frac{u_o l_o}{\nu_{T_m}}\right) \tag{9.3}$$

In equation (9.3) $\overline{q_o^2}$ is the average value across a turbulent shear layer. In this respect equation (9.1) is more general because, there, both $\overline{q^2}$ and ν_T are local values.

To test the hypothesis that $\left(\frac{\overline{q^2}}{u_o^2}\right)\left(\frac{u_o l_o}{\nu_T}\right)$ may be an absolute constant (over the major portion of the flow) in most free turbulent shear flows, Fig. (97) is presented. In this figure results for both self-preserving and non-self-preserving flows are included. It can be seen from the figure that $\left[(\overline{q^2}/u_o^2)(u_o l_o/\nu_T)\right]$ is roughly a constant and has a value of about 4.0

over the range $0.2 \leqslant \eta \leqslant 1.2$ for the fully developed part of the flow and the the following flows:

(a) Plane jet in still air,

(b) Plane jet in uniform streaming flow,

(c) Plane wall jet in still air,

(d) Plane wall jet in uniform streaming flow,

(e) Plane mixing layer,

(f) Plane jet in equilibrium pressure gradient, and

(g) The asymmetric jet; the streaming side and the zero velocity side.

10. SUMMARY AND CONCLUSIONS

The primary object of the investigations presented in this thesis was to originate a method capable of predicting the development of the flow in the simple case of the asymmetric jets. In the Introduction some of the commonly encountered asymmetric jets are named and the simple asymmetric jet is defined. The general outline of the present investigation is given there. The same section also gives a brief review of theoretical methods to analyse turbulent shear flows.

The theoretical method for predicting the flow development in the asymmetric jet is based on the observation that it may be possible to divide the asymmetric jet into two parts: (a) the part on the streaming side resembling a half jet in uniform streaming flow, and (b) the part on the zero velocity side resembling a half jet in still air. The locus of points of maximum velocity divides the asymmetric jet. Attention is therefore focussed first on analysing these basic flows. By introducing an auxiliary equation (18) (which avoids the use of an eddy viscosity or the mixing length concept) it is possible to predict the development of a plane jet in uniform streaming flow (section (2.3)). In this section, following Townsend (1970), an approximate analysis which uses the integrated total energy equation is given and it is shown that the auxiliary equation (i.e. equation (18)) depends on the turbulence structure parameter, (SP) = $\left[\overline{q^2}/\overline{uv}\right]_{\eta=1}$.

The analysis for a jet in still air is well known. In section (2.2) it is shown that the ratio of length scale to average dissipation length, (l_o/L_ϵ), is insensitive to plausible assumptions regarding the distribution of the turbulent energy in the shear layer. Moreover, the rate of growth (dl_o/dx) is related to the turbulence structure parameter, (SP), and the ratio (l_o/L_ϵ) (see equation (12)).

The analysis for the asymmetric jet is given in section (2.4.2). It uses an integral method and solutions are obtained for the variations of l_1, l_2 and u_o, where l_1 and l_2 are length scales on the streaming side and zero velocity side respectively. For this purpose the same auxiliary equation (i.e. the one used in the analysis for a jet in uniform streaming flow, equation (18)) is retained and the additional information required is obtained from the experimental variation of the ratio (l_1/l_2).

To demonstrate the applicability of the analyses presented in section (2) some experimental results of other investigators were used.

For plane jets in uniform streaming flow the results of Bradbury and Riley (1967) are used. It is shown in section (3.1) that the present method predicts their results satisfactorily. For comparison predictions obtained by Rodi (1970) using a differential method (Spalding (1968)) are also included. It is concluded that the predictions by the present method are valid over the entire range of the flow rather than for asymptotic regions only and also for various free stream to jet exit velocity ratios. The turbulence results of Bradbury (1963) confirm that the structure parameter (SP) is independent of the velocity ratio as indicated by equation (46). It is worth noting that in the present method only two parameters, (i.e. C and l_o/L_ϵ) are required to be evaluated from experimental results for a plane jet in still air.

For plane wall jets in uniform streaming flow measurements of Patel (1962), Kruka and Eskinazi (1964) and Gartshore (1965) are selected. These investigations incorporated sufficient experimental variations between them to assess the present method. The comparisons of experimental results and predictions (i.e. for l_o and u_o) using the present method show that the analysis of section (2.3) is applicable to wall jets in uniform streaming flow.

A survey of literature indicates that not many investigations have been made for both a plane turbulent jet in still air and a plane mixing layer. In particular the experimental confirmation of the self-preserving nature of a plane jet in still air was not demonstrated heretofore. Also it has been found (Bradbury (1963)), Newman (1967)) that previous investigations suffered from problems of two-dimensionality. Therefore experimental investigation was undertaken to obtain results for a plane jet in still air. The results are presented in section (5). From the experimental results it was concluded that similarity of various distributions (e.g. mean velocity and turbulence components) is attained in steps. First the mean velocity distributions become similar at $x/b > 28.0$, then

$\overline{u^2}$-distributions become similar beyond $x/b = 30$ and finally $\overline{v^2}$, $\overline{w^2}$ and $\overline{uv}$ distributions become similar beyond $x/b = 70.0$. On the whole the present measurements are generally in agreement with those of Heskestad (1963).

A plane mixing layer was also investigated experimentally (see section (6)). It is shown that one of the commonly adopted assumptions (i.e. $V = 0$ at the edge of a plane mixing layer) leads to erroneous distribution of shear stress calculated from the non-dimensional mean velocity measurements. A method which does not impose restriction on V is presented and its use gives satisfactory agreement between the measured and the calculated shear stress profiles. The discrepancy between the present turbulence measurements and those of other investigators (i.e. Liepmann and Laufer (1947); Wygnanski and Fiedler (1970)) are attributed to either the differences in the experimental arrangements, or omission of the longitudinal cooling corrections to inclined hot-wires results, or the thermal wake interference between the closely spaced wires of a X-wire probe (Guitton and Patel (1969)).

Having obtained the measurements for the two asymptotic states of the asymmetric jet, experimental investigation for three asymmetric jets was commenced. The results are presented in sections (7, 8 and 9). The experimental results show that it is possible to divide the asymmetric jet into two parts. The locus of maximum velocity points divides the asymmetric jet. The shapes of the non-dimensional mean velocity profiles on the streaming side are in agreement with Bradbury's (1963) results for a plane jet in uniform streaming flow. On the zero velocity side they are in agreement with the author's results for a plane jet in still air. It is noted that for non-self-preserving flows the mean velocity and Reynolds stresses are not both reduced to similarity forms by the same velocity scale. The main characteristics (i.e. l_1, l_2 and u_o) of the asymmetric jet can be predicted satisfactorily by the simple analysis of section (2.4.2) (see section (9)).

Collected experimental results of both self-preserving and non-self-preserving shear flows indicate that the structure parameter, (SP), does not vary a great deal from one flow to another. Therefore an analysis based on its invariance would appear to be attractive and would be even simpler than the analysis presented here. Finally, experimental confirmation of Townsend's (1970) suggestion, that maximum effective strain in most of the turbulent shear flows remains roughly constant, is obtained.

It is required by the regulations of the Faculty of Graduate Studies and Research that a clear statement of the claim of original work be made in the thesis, therefore, following is claimed by the author as contribution to knowledge:

(a) Measurements presented in this thesis are claimed to be more accurate than those previously made for a plane jet in still air and a plane mixing layer. Detailed mean velocity and turbulence measurements for the asymmetric jet are original.

(b) On the theoretical side an auxiliary equation is suggested as a replacement for Abramovich's equation (17). The justification of the author's auxiliary equation (18) by various means is also original.

APPENDIX I

Apparatus

A schematic diagram of the experimental apparatus is shown in Fig. (A.1). The McGill blower tunnel which was used for the experiments has an exit section 30 in. wide and 17 in. high. It is driven by either a 25 H.P., fixed r.p.m., A.C. motor or a 5 H.P., variable speed, D.C. motor (see Appendix 2). Downstream of the fan is a 5° diffuser, a settling chamber with deep cell honey-comb and three removable screens, followed by a 6:1 two-dimensional contraction. Since the investigation of Patel (1964) the screens in the settling chamber have been replaced to produce effectively two-dimensional flow in the working section. The test section (or working section) (see Fig. (28)) for the present investigation is attached to the tunnel exit. The general description and calibration of the tunnel is given by Wygnanski and Gartshore (1963). For the present investigation the inlet of the tunnel was provided with a DRI-PAK filter box to remove dust. The top wall of the working section was removed for the investigation of the plane jet in still air. A jet slot, 30 in. wide and 0.265 in. high, was incorporated at the bottom of the tunnel exit as shown in Fig. (A.2). The jet was emitted parallel to and below the uniform flow from the tunnel. The jet air supply was provided by an auxiliary 10 H.P. centrifugal compressor. A DRI-PAK filter box was used also at the inlet of the compressor. An 8 in. diameter flexible pipe followed by a 6° diffuser (Fig. (A.2)) connected the compressor supply to the slot. The mass flow to the jet was controlled by a bleed valve far upstream of the slot. In between the bleed valve and the diffuser was provided a water cooled heat exchanger to control the air temperature. The contraction ratio for the slot was approximately 16. Other details of the slot design are given in Fig. (A.2). The slot arrangement is very similar to that used by Patel (1962), Gartshore and Hawaleshka (1964), and Gartshore (1965).

The hot-wire anemometer used in this investigation was a commercial unit manufactured by DISA (see section (4)). It was mentioned in section (4) that DISA probes were used for all the hot-wire results reported here. For mean velocity and longitudinal turbulence intensity measurements DISA miniature hot-wire probes (55A25) were used. The active section of the hot-wire on these probes is 1 mm. long and 0.005 mm. in diameter. The hot-wire is made of platinum plated tungsten, and has resistance at 20°C of $3.5 \pm {}^{0.7}_{0.5}$ ohm. The temperature coefficient of resistance is about $4 \times 10^{-3}/°C$. All hot-wires were operated at approximately 1.8 times their cold resistance.

For Reynolds stresses $\overline{v^2}$, $\overline{w^2}$ and $\overline{uv}$, only single slanted wires (DISA probes 55A29) were used. These wires have length to diameter ratio of approximately 200.

The angle of yaw was measured with an optical comparator (for other details of care and calibrations see Patel (1968)).

For measurements of triple correlations a DISA (55A32) X-wire probe was modified as suggested by Guitton and Patel (1969). The modification requires that the separation distance between the two wires be approximately one wire length. For this probe the wire separation to diameter ratio was nearly 200 and the wire separation to wire length ratio was almost 1.

Checks on Two-Dimensionality

It was noted in section (5) that the flow issuing from the slot (Fig. (A.2)) was effectively two-dimensional. This conclusion was reached through observing the expected behaviour of l_o, U_m and $\overline{uv}$ for a plane jet in still air. The conventional check on the two-dimensionality by measuring the mean velocity profiles is given in Figs. (A.3 to A.7).

Fig. (A.3) shows the linearized normal hot-wire D.C. and r.m.s. voltage output for a plane jet in still air. These measurements were obtained at $x/b = 53.4$ and they are proportional to the mean velocity and $\sqrt{\overline{u^2}}$ respectively. The measurements were made at 3 in. and 9 in. on either side of the centre line. From the figure it can be seen that the flow issuing from the slot is effectively two-dimensional. For the range $0 < y < l_o$ measurements indicate nearly perfect agreement, however, beyond $y > l_o$, i.e. in the region of low velocities, there seems to be some scatter in $\sqrt{\overline{e^2}}$-measurements. Note also the tail appearing in the distribution of D.C. voltage, E, which is an inherent characteristic of a hot-wire because the wire cannot distinguish between positive and negative flow directions and it simply transfers the heat loss into a positive voltage E. In other words, at the zero velocity edge of the flow where the fluctuations are large and the flow direction is uncertain, the wire acts merely as a rectifier. Thus the average voltage differs from the voltage which would have been generated by the true mean velocity.

The two-dimensionality checks for the asymmetric jet were made by pitot tube and linearized hot-wire traverses. The measurements were made at two downstream stations, namely $x/b = 53.4$ and 217. These results are shown in Figs. (A.4 to A.7). From these figures it can be concluded that within 6 in. on either side of the centre line the flow is effectively two-dimensional.

APPENDIX 2

EFFECTS OF STREAM TURBULENCE ON FREE SHEAR FLOWS

Introduction

Considerable work has been done on the effects of free stream turbulence on boundary layer transition, separation and on drag of models and plates (Schubauer and Dryden (1935), Dryden et al. (1937), Liepmann and Fila (1947) and Dryden and Keuthe (1929)). The effect of free stream turbulence on the characteristics of the turbulent boundary layer on a flat plate has been experimentally investigated by Kline et al. (1960). Recently, Junkhan and Serovy (1967) have reported an experimental investigation dealing with effects of free stream turbulence on heat transfer from various boundary layers. It should be noted that all of the above investigations were concerned primarily with gross effects on flows associated with solid boundaries. It was observed by Kline et al. that the boundary layer thickness increases with increase in free stream turbulence. A similar conclusion was obtained also by Junkhan and Serovy.

No experimental investigation on free shear flows specifically aimed at the study of effects of stream turbulence has been reported before. It is, therefore, the purpose of this investigation to appraise whether or not free shear flows are sensitive to the effects of stream turbulence. The types of free shear flows referred to in this context are necessarily coupled with free streams, e.g. plane mixing layers, turbulent jets in streaming flows, asymmetric jets, etc.

Attention is focussed on the asymmetric jet and a plane mixing layer in this investigation. For the asymmetric jet the results reported here are for two values of free stream turbulence intensity and for two downstream stations, one near the slot and another away from it. The reason for this choice is that in one case the effects of both the slot and free stream turbulence are present whereas in the other only free stream turbulence effects predominate. The results include measurements of mean velocity and distributions of turbulent intensities.

Experimental Arrangements

The experimental apparatus used in this investigation is already described in Appendix 1 and section (4). The McGill blower tunnel had been used for investigations of jets and wall jets in the past (Patel and Newman (1961), Patel (1962), Gartshore and Hawaleshka (1964) and Gartshore (1965)). The tunnel was driven by an A.C. constant speed motor and the air speed was controlled previously by variable inlet vanes.

Variation of the Tunnel Turbulence Intensity

The longitudinal turbulence intensity measurements in the McGill blower tunnel were originally carried out by Patel (1962) using turbulence spheres and it was found that at high tunnel velocity the turbulence intensity at the centre of the exit plane was less than 0.5%. Later, Wygnanski and Gartshore (1963) confirmed this by using a non-linearized hot-wire anemometer. They found that the turbulence intensity in this tunnel increases as the velocity decreases. They attributed this behaviour to flow separation from the variable inlet vanes which are upstream of the centrifugal fan.

In view of the various modifications, reported earlier, to the tunnel it was decided to measure turbulence intensity at the centre of the tunnel exit. At the same time a test was performed to show whether or not the inlet vanes are the sole cause of increase in turbulence intensity. This test consisted of simply throttling the flow by a perforated plate at the fan exit to get the low velocity range, leaving the inlet vanes open.

Fig. (B.1) shows the variation of turbulence intensity at the centre of the tunnel exit. In this figure results of tests with and without the perforated plate, and those of Wygnanski and Gartshore (1963) are included for comparison. Note that with the perforated plate the turbulence intensity reduces a little but not a great deal. This suggests, contrary to the proposition of Wygnanski and Gartshore, that the constant speed fan may be the cause of the increase in turbulence intensity at low tunnel speeds. Indeed, a detailed investigation would be required to establish whether or not any specific relation between the fan speed and turbulence intensity exists. For the purpose of the present investigation, the main objective was to establish a limit of free stream turbulence intensity below which the effects are negligible. It was also desirable to maintain the free stream turbulence at a constant value over the whole operating range of the tunnel. From Fig. (B.1) it can be seen that the present results are in agreement with those of Wygnanski and Gartshore thus indicating that the modifications to the tunnel have not affected the turbulent intensity distribution. The figure also indicates that the existing test facility, fortunately, provides an excellent opportunity (without introducing external turbulence generating bodies in the working section) for investigating effects of stream turbulence on free shear flows. The perforated plate was removed from the tunnel in subsequent investigations.

To maintain the turbulence intensity at a constant value a variable speed D.C. motor drive was installed. Only a 5 H.P. D.C. motor was available at the time and this restricted the range of the tunnel speed between zero and about 60 ft/s. maximum. Fig. (B.2) shows a comparison of turbulence intensity distributions obtained with the constant speed A.C. motor drive and the variable speed D.C. motor drive. With D.C. motor drive two tests were performed; one with the inlet vanes completely open and another one with the inlet vanes about half open. From the figure it can be seen that the turbulence intensity level has considerably reduced in the range 1.0×10^5 ft^{-1} $< U_1/\nu$ 4.0×10^5 ft^{-1} and it remains roughly at a constant value of 0.55% with the D.C. motor drive. Also the positions of inlet vanes do not have any significant effect on the level of turbulence intensity. For $U_1/\nu > 4 \times 10^{+5}\ ft^{-1}$ the A.C. motor drive gives a level of turbulence intensity of about 0.5% and, therefore, it was decided to retain the A.C. motor drive for high speeds only.

Effects of Stream Turbulence on the Asymmetric Jet

The effects of stream turbulence were investigated for the asymmetric jet with $(U_j/U_1) = 2.275$. Because the speed in the tunnel can be varied from about 30 ft/s. to 120 ft/s/ with A.C. motor drive and the maximum jet velocity obtainable was about 265 ft/s., the ratio $(U_j/U_1) = 2.275$ was selected. For this purpose the free stream velocities were 34 ft/s. and 112.2 ft/s/ with corresponding turbulence intensities of 1.1% and 0.4% respectively.

Figs. (B.3) and (B.4) show mean velocity distributions at two downstream stations, namely x/b = 16.5 and 81.7. From these figures it can be seen that the asymmetric jet with high stream turbulence grows or spreads faster than the one with low stream turbulence, as would be expected.

Figs. (B.5) and (B.6) show distributions of longitudinal turbulence intensity across the asymmetric jet at x/b = 16.5 and 81.7 respectively. It is interesting to observe from Fig. (B.5) that the distribution of $(\sqrt{\overline{u^2}}/U_1)$ for the asymmetric jet with 1.1% turbulence intensity is greater at all values of y than the one with 0.4% turbulence intensity. This is rather unexpected and this behaviour may be due to the combined influences of the slot and the stream turbulence. It would be difficult to uncouple the individual influences of the slot and the stream turbulence at this station. However, far from the slot the flow is expected to be independent of the slot effects and there it is possible to assess effects of the stream turbulence alone.

Fig. (B.6) shows $(\sqrt{\overline{u^2}}/U_1)$ distributions at $x/b = 81.7$ and it can be seen that the stream turbulence has significant effect on the streaming side only of the asymmetric jets. Repeated measurements are also in agreement with this conclusion.

Figs. (B.7), (B.8) and (B.9) represent distributions of $(\sqrt{\overline{v^2}}/U_1)$, $(\sqrt{\overline{w^2}}/U_1)$ and $(\overline{uv}/U_1^2)$ respectively at $x/b = 81.7$. These measurements also suggest that the distributions of turbulence components are dependent on the stream turbulence.

To decide the level of free stream turbulence intensity below which free shear flows may not be affected seriously, the following measurements on a plane mixing layer were made.

Effects of Stream Turbulence on Plane Mixing Layers

For plane mixing layers mean velocities were measured at various downstream stations with different free stream turbulence intensities. From the measurements of velocities the rate of growth of a mixing layer with a particular free stream turbulence intensity was evaluated. The rate of growth is defined as $\frac{d}{dx}\left[y_{0.95} - y_{0.5}\right]$ where $y_{0.95}$ and $y_{0.5}$ represent y-co-ordinates at which $U/U_1 = 0.95$ and 0.50 respectively.

Fig. (B.10) shows the rate of growth plotted against the free stream turbulence intensity at $x = 0$. For comparison, results of Gartshore (1965) and Liepmann and Laufer (1947) are included also. Because Liepmann and Laufer do not specify the free stream turbulence intensity in their investigation, their results are indicated by a dotted line. Similarly, for the results of Gartshore, the level of free stream turbulence was estimated from Fig. (B.1) because he investigated his mixing layer in the same tunnel. Since the flow characteristics of a fully developed turbulent mixing layer are expected to be independent of Reynolds number, the variation in growth rate in Fig. (B.10) is due to the variation of stream turbulence. It is interesting to note that the rate of growth is not affected significantly for values of free stream turbulence intensity below 0.6%.

Fig. (B.11) shows distributions of longitudinal turbulent intensity across plane mixing layers at $x = 27.75$ in. for various values of free stream turbulence. For this test the intensity was varied from 0.76% to 1.4%. It is interesting to see from the figure that the distributions of $(\sqrt{\overline{u^2}}/U_1)$ depend considerably on the free stream turbulence intensity.

Fig. (B.12) shows distributions of $(\sqrt{\overline{u^2}}/U_1)$ for the same Reynolds number, $(U_1/\nu) = 1.61 \times 10^5$ ft^{-1}, and various values of stream turbulence. For comparison, in the figure, results of tests with $U_1/\nu = 3.58 \times 10^5$ ft^{-1}, and with $U_1/\nu = 1.61 \times 10^5$ ft^{-1} and the top wall in the working section, are included.

From the figure it can be seen that both Reynolds number and the top wall do not have an appreciable effect on the $(\sqrt{\overline{u^2}}/U_1)$ distribution but the free stream turbulence intensity of 1.4% significantly changes the distribution of $(\sqrt{\overline{u^2}}/U_1)$. It is, therefore, concluded that the flow characteristics of a plane mixing layer are independent of Reynolds number and free stream turbulence provided the value of the stream turbulence is less than about 0.7%.

Conclusions

The results of tests carried out in this investigation show that even though the stream turbulence was much smaller than the self generated turbulence in the shear layers, its effects on the main characteristics of the flows associated with free streams cannot be neglected. In the case of plane mixing layers it was found that the rate of growth was altered by about 30% when the turbulence intensity in the free stream was changed from 0.5% to 1.4%. On the whole, judging from the results of plane mixing layers, it may be concluded that for free stream turbulence intensities of less than 0.6% the characteristics of free shear flows will be independent of the effects of stream turbulence. Measurements reported in the main text of this thesis were, therefore, made with free stream turbulence intensities less than 0.6%.

REFERENCES

Abramovich, G.N., (1958) The Turbulent Jet in a Moving Fluid R.A.E. Library Translation No. 778

Abramovich, G.N., (1963) The Theory of Turbulent Jets M.I.T. Press, Cambridge, Mass.

Batchelor, G.K., (1950) Note on Free Turbulent Flows, with Special Reference to the Two-dimensional wake J. Aero Science, Vol.17, pp. 441-445

Batchelor, G.K., (1953) The Theory of Homogeneous Turbulence Cambridge Monographs on Mechanics and Applied Mathematics, Cambridge University Press

Boussinesq, J., (1877) Essai sur la Théorie des Eaux Courantes Mém. présentés par div. Sav. XXlll, à L'Acad. des Sci., Paris

Beckwith, I.E. and Bushnell, D.M., (1968) Detailed Description and Results of a Method for Computing Mean and Fluctuating Quantities in Turbulent Boundary Layers NASA TN D-4815

Begg, R.D., Carter, J.H.T. and Maclellan, G.D.S., (1967) Some Incompressible Jet Flow and Reattachment Effects in Fluid Control Elements Glasgow Univ., Dept. of Mech. Eng.

Bradbury, L.J.S., (1963) An Investigation into the Structure of a Turbulent Plane Jet Ph.D. Thesis, University of London

Bradbury, L.J.S., (1965) The Structure of a Self-Preserving Turbulent Plane Jet J.F.M., Vol. 23, part 1, pp. 31-34

Bradbury, L.J.S. and Riley, J., (1967) The Spread of a Turbulent Plane Jet Issuing into a Parallel Moving Stream J.F.M., Vol. 27, pp. 381-397

Bradshaw, P., (1967) The Turbulence Structure of Equilibrium Boundary Layers J.F.M., Vol. 29, part 4, pp. 625-646

Bradshaw, P., (1969) — Transport Equations for Turbulent Shear Stress
(Abstract of Papers)
Symposium on Turbulence, Seattle, B.S.R.L. Document No. D1-82-0853

Bradshaw, P. and Gee, M.T., (1960) — Turbulent Wall Jets with and without an External Stream
A.R.C. R. and M. No. 3252 - 1962
A.R.C. 22,008, F.M. 2971 - 1960

Bradshaw, P., Ferriss, D.H. and Atwell, N.P., (1967) — Calculation of Boundary Layer Development using the Turbulent Energy Equation
J.F.M., Vol. 28, part 3, pp. 593-616

Champagne, F.H., (1965) — Turbulence Measurements with Inclined Hot Wires
B.S.R.L., Seattle, Document No. D1-82-0491.
Flight Sciences Laboratory Report No. 103

Champagne, F.H. and Sleicher, C.A., (1967) — Turbulence Measurements with Inclined Hot-Wires: Part 2, Hot-Wire Response Equations
J.F.M., Vol. 28, pp. 177-182

Champagne, F.H., Sleicher, C.A. and Wehrmann, O.H., (1967) — Turbulence Measurements with Inclined Hot-Wires: Part I, Heat Transfer Experiments with Inclined Hot-Wires
J.F.M., Vol. 28, pp. 153-175

Chao, J.L. and Sandborn, V.A., (1966) — Evaluation of Momentum Equation for a Turbulent Wall Jet
J.F.M., Vol. 26, part 4, pp. 819-828

Coles, D.E., (1968) — The Young Person's Guide to the Data
A survey lecture prepared for the 1968 AFOSR-IFP-Stanford Conference on Computation of Turbulent Boundary Layers
Proceedings, Vol. II, Ed. Coles, D.E. and Hirst, E.A.

DISA (Special Information), (1970) — DISA X-probes
Thermal Wake Interference between the Wires of X-type Hot-Wire Probes
CTA-Note No. 14, Denmark

Dryden, H.L. and Kuethe, A.M., (1929) — Effect of Turbulence in Wind Tunnel Measurements
NACA Report No. 342

Dryden, H.L., Schubauer, G.B., Mock, W.C., Jr. and Skramstad, H.K., (1937) — Measurements of Intensity and Scale of Wind Tunnel Turbulence and their Relation to the Critical Reynolds Numbers of Spheres. NACA Report No. 581

Emmons, H.W., (1954) — Shear Flow Turbulence. Proc. 2nd. National Congress of Applied Mechanics, ASME

Escudier, M., (1968) — See: Discussion on Integral Entrainment Methods. Proc. Computation of Turbulent Boundary Layers - 1968, AFOSR-IFP Stanford Conference, Vol. 1, pp. 255-256

Eskinazi, S. and Kruka, V., (1962) — Turbulence Measurements in a Two-Dimensional Rectangular Wall Jet with Longitudinal Free-Stream. Syracuse Univ. Research Institute Report No. ME 937-6205 P

Fekete, G.I., (1970) — Self-Preserving, Two-Dimensional Jets in Streaming Flow. Ph.D. Thesis, Department of Mech. Eng., McGill University

Gartshore, I.S., (1965) — The Streamwise Development of Two-Dimensional Wall Jets and Other Two-Dimensional Turbulent Shear Flows. Ph.D. Thesis, Department of Mech. Eng., McGill University

Gartshore, I.S. and Hawaleshka, O., (1964) — The Design of a Two-Dimensional Blowing Slot and its Application to a Turbulent Wall Jet in Still Air. Mech. Eng. Res. Lab., Tech. Note 64-5 McGill University

Gartshore, I.S. and Newman, B.G., (1969) — The Turbulent Wall Jet in an Arbitrary Pressure Gradient. The Aero. Quarterly, Vol.XX, p. 25

Gibson, M.M., (1963) — Spectra of Turbulence in a Round Jet. J.F.M., Vol. 15, part 2

Glushko, G.S., (1965) — Turbulent Boundary Layer on a Flat Plate in an Incompressible Fluid. NASA TT F-10,080, translation from: Izv. Akad. Nauk SSSR, Mekh. No. 4, pp. 13-23

Görtler, H., (1942) — see: Schlichting, H. (1968) Boundary Layer Theory, McGraw Hill, 6th. Ed., p.696

Grant, H.L., (1958) — Large Eddies of Turbulent Motion J.F.M., Vol. 4, part 2, p. 143

Grant, H.L., Stewart, R.W. and Moilliet, A., (1962) — Turbulence Spectra from a Tidal Channel J.F.M., Vol. 12, pp. 241-268

Guitton, D.E., (1968) — Correction of Hot Wire Data for High Intensity Turbulence, Longitudinal Cooling and Probe Interference Mech. Eng. Res. Lab., Report No.68-6 McGill University

Guitton, D.E., (1970) — Some Contributions to the Study of Equilibrium and Non-Equilibrium Turbulent Wall Jets over Curved Surfaces Ph.D. Thesis, Department of Mech. Eng., McGill University

Guitton, D.E. and Patel, R.P., (1969) — An Experimental Study of the Thermal Wake Interference Between Closely Spaced Wires of a X-type Hot-Wire Probe Mech. Eng. Res. Lab. Report No. 69-7 McGill University

Hackett and Cox (1967)*

Halleen, R.M., (1964) — Literature Review on Subsonic Free Turbulent Shear Flow Dept. of Mech. Eng., Stanford University, Report No. MD-11

Harlow, F.H. and Nakayama, P.I., (1967) — Turbulent Transport Equations The Phys. of Fluids, Vol. 10, No. 11, p. 2323

Heskestad, G., (1963) — Two Turbulent Shear Flows (A Plane Jet and a Radial Jet) Department of Mechanics, Johns Hopkins University

Heskestad, G., (1965) — Hot-Wire Measurements in a Plane Turbulent Jet J.App.Mech., Trans. A.S.M.E. Vol. 87, Series E, pp. 721-734

Hill, P.G., (1965) — Turbulent Jets in Ducted Streams J.F.M., Vol. 22, pp. 161-186

* See at the end of references.

Hinze, J.O., (1959) | Turbulence
An Introduction to its Mechanism and Theory
McGraw-Hill Book Co., Inc.

Jerome, F.E., Guitton, D.E. and Patel, R.P., (1970) | Experimental Study of the Thermal Wake Interference Between Closely Spaced Wires of a X-type Hot-Wire Probe
(To be published in Aero. Quart.)

Junkhan, G.H. and Serovy, G.K., (1967) | Effects of Free Stream Turbulence and Pressure Gradient on Flat Plate Boundary Layer Velocity Profiles and on Heat Transfer
ASME, Series C, Vol. 89, pp.169-176

Klebanoff, P.S., (1954) | Characteristics of Turbulence in a Boundary Layer with Zero Pressure Gradient
NACA TN 3178

Kolmogorov, A.N., (1942) | Equations of Turbulent Motion of an Incompressible Fluid
Itv. Akad. Nauk SSR, Seria Zizicheska VI 1942, No. 1-2, pp.56-58

Kruka, V. and Eskinazi, S., (1964) | The Wall Jet in a Moving Stream
J.F.M., Vol. 27, pp. 381-397

Launder, B.E., (1970) | Some Notes on the Simulation of Turbulence Transport Equations
A lecture on advanced turbulence models given at The Sir George Williams University, Montreal, July 11, 1970

Liepmann, H.W. and Fila, G.H., (1947) | Investigation of Effects of Surface Temperature and Single Roughness Elements on Boundary Layer Transition
NACA Rep. No. 890

Liepman, H.W. and Laufer, J., (1947) | Investigation of Free Turbulent Mixing
NACA TN 1257

McDonald, H., (1968) | The Departure from Equilibrium of Turbulent Boundary Layers
Aero. Quart., Vol. 19, p. 1

Michel, R., Quémard, C. and Durant, R., (1968) | Hypotheses on the Mixing Length and Application to the Calculation of the Turbulent Boundary Layers
Proc. Computation of Turbulent Boundary Layers - 1968 AFOSR-IFP-Stanford Conference, Vol. 1, pp. 195-212

Miller, D.R. and Comings, E.W. (1957-8) — Static Pressure Distribution in the Free Turbulent Jet. J.F.M., Vol. 3, pp. 1-16

Mobbs, F.R. (1968) — Spreading and Contraction at the Boundaries of Free Turbulent Flows. J.F.M. Vol. 33, pp. 227-239

Nash, J.F. (1969) — The Calculation of Three-Dimensional Turbulent Boundary Layers in Incompressible Flow. J.F.M. Vol. 37, part 4, pp. 625-642

Naudascher, E. (1965) — Flow in the Wake of Self-Propelled Bodies and Related Sources of Turbulence. J.F.M., Vol. 22, part 4, pp. 625-656

Naudascher, E. (1967) — On the General Similarity Analysis for Turbulent Jet and Wake Flows. Iowa Inst. of Hydraulic Research, Report No. 106, University of Iowa

Nee, V.W. and Kovasznay, L.S.G. (1969) — Simple Phenomenological Theory of Turbulent Shear Flow. The Phys. of Fluids, Vol. 12, 3 p. 473

Newman, B.G. (1961) — The Deflexion of Plane Jets by Adjacent Boundaries - Coanda Effect. Boundary Layer and Flow Control, Vol. 1, p. 232, Pergamon Press

Newman, B.G. (1966) — Private Communications

Newman, B.G. (1967) — Turbulent Jets and Wakes in a Pressure Gradient. Fluid Mechanics of Internal Flow, ed. Gino Sovran, pp. 170-209, Elsevier Publishing Company

Newman, B.G. (1968) — The Growth of Self-Preserving Turbulent Jets and Wakes. Mech, Eng. Res. Lab., Report No. 68-10, McGill University

Newman, B.G. (1969) — The Prediction of Turbulent Jets and Wall Jets. Canadian Aeronautics and Space Journal, Vol. 15, No. 8, pp. 288-305

Patel, R.P. (1962) Self-Preserving, Two-Dimensional Turbulent Jets and Wall Jets in a Moving Stream
M. Eng. Thesis, Mech. Eng. Dept. McGill University

Patel, R.P. (1964) The Effects of Wind Tunnel Screens and Honeycombs on the Spanwise Variation of Skin Friction in "Two-Dimensional" Turbulent Boundary Layers
Mech. Eng. Res. Lab., Tech. Note 64-7 McGill University
Proceedings of the Second Australasian Conference on Hydraulics and Fluid Mechanics, pp. B65-B82 (1965)
Auckland University, Newzealand

Patel, R.P. (1968) Reynolds Stresses in Fully Developed Turbulent Flow Down a Circular Pipe
Mech. Eng. Res. Lab., Report No. 68-7
McGill University

Patel, R.P. (1969) Turbulent Jets and Wall Jets in Uniform Streaming Flow
Mech. Eng. Res. Lab., Report No. 70-3
McGill University

Patel, R.P. and Newman, B.G. (1961) Self-Preserving, Two-Dimensional Turbulent Jets and Wall Jets in a Moving Stream
Mech. Eng. Res. Lab., Ae. Sec, Report No. Ae 5, McGill University

Phillips, O.M. (1967) The Maintenance of Reynolds Stress in Turbulent Shear Flow
J.F.M., Vol. 27, part 1, pp. 131-144

Phillips, O.M. (1969) Shear Flow Turbulence
Annual Review of Fluid Mechanics
Vol. 1, pp. 245-263

Prandtl, L. (1925) Bericht über Untersuchungen zur ausgebildeten Turbulenz
Z. Angew. Math. Mech. 5, 136 (also see: Ludwig Prandtl - Gesammelte Abhandlungen, Vol. 2, pp. 714-718 (1961))

Prandtl, L. (1942) Bemerkungen zur Theorie der Freien Turbulenz
Z. Angew. Math. Mech. Vol. 22 s. 241-243 (also see: Ludwig Prandtl, Gesammelte Abhandlungen, Vol. 2, p.869 (1961)

Prandtl, L. and Wiegkardt, K. (1945) — Über ein neues Formelsystem für die ausgebildete Turbulenz
Nachr. Akad. Wiss., Göttingen Math-phys., kl 1945,6 (also see: Ludwig Prandtl, Gesammelte Abhandlungen, Vol. 2, p. 874 (1961))

Rodi, W. (1970) — Private Communication
May, 1970

Rodi, W. and Spalding, D.B. (1969) — A Two-Parameter Model of Turbulence, and its Application to Free Jets
Imperial College of Science and Technology, Dept. of Mech. Eng., BL/TN/B/12

Rose, W.G. (1966) — Results of an Attempt to Generate a Homogeneous Turbulent Shear Flow
J.F.M., Vol. 25, part 1, pp. 97-120

Rotta, J. (1951) — Statistical Theory of Non-Homogeneous Turbulence (Translated by Rodi, W.)
Imperial College of Science and Technology, TWF/TN/39, (March, 1968)

Schlichting, H. (1968) — Boundary Layer Theory (6th edition)
McGraw-Hill Book Co.

Schubauer, G.B. and Dryden, H.L. (1935) — The Effect of Turbulence on the Drag of Flat Plates
NACA Report No. 546

Schwarz, W.H. and Cosart, W.P. (1961) — The Two-Dimensional Turbulent Wall-Jet
J.F.M., Vol. 10, part 4

Sigalla, A. (1958) — Experimental Data on Turbulent Wall Jets
Aircraft Engineering, May 1958

Spalding, D.B. (1967) — Heat Transfer from Turbulent Separated Flows
J.F.M., Vol. 27, part 1, pp. 97-109

Spalding, D.B. (1967) — The Calculation of the Length Scale of Turbulence in Some Boundary Layers Remote from Walls
Imperial College, Mech. Eng. Dept. TWF/TN/31

Spalding, D.B. (1968) — GENMIX: A Computer Programme for Calculating the Turbulent Mixing and Chemical Reaction of Three Co-axial Gas Streams Confined in a Duct of Uniform Cross Sectional Area
Imperial College, London, Dept. of Mech. Eng., BL/TN/5

Spalding, D.B. (1969) — Private Communication
27th May, 1969

Spalding, D.B. and Patankar, S.V. (1967) — Heat and Mass Transfer in Boundary Layers
Morgan-Grampian, London

Spalding, D.B. and Ricou, F.P. (1961) — Measurement of the Entrainment of Axisymmetric Jets
J.F.M., Vol. 11, p. 21

Squire, H.B. and Trouncer, J. (1944) — Round Jets in a General Stream
A.R.C., Tech. Report, R. and M. No. 1974

Taylor, G.I. (1915) — Eddy Motion in the Atmosphere
Phil. Trans. Roy. Soc. London
A 215; pp. 1-26

Tollmien, W. (1926) — Berechnung Turbulenter Ausbreitungsvorgänge
ZAMM 6, pp. 468-478 (1926)
see also: NACA TM 1085 (1945)

Townsend, A.A. (1956) — The Structure of Turbulent Shear Flow
Cambridge Monographs on Mechanics and Applied Mathematics
Cambridge University Press

Townsend, A.A. (1961) — Equilibrium Layers and Wall Turbulence
J.F.M., Vol. 11, p. 97

Townsend, A.A. (1965) — Self-Preserving Flow Inside a Turbulent Boundary-Layer
J.F.M., Vol. 22, p. 773

Townsend, A.A. (1966) — The Mechanism of Entrainment in Free Turbulent Flows
J.F.M., Vol. 26, p. 689

Townsend, A.A. (1970) — Entrainment and the Structure of Turbulent Flow
J.F.M., Vol. 41, (1970)

van der Hegge Zijnen, B.G. (1958) — Measurements of the Velocity Distribution in a Plane Turbulent Jet of Air
App. Sci. Res., Sec. A., Vol. 7, pp. 256-276, (1958)

van der Hegge Zijnen, B.G. (1958) — Measurements of Turbulence in a Plane Jet of Air by the Diffusion Method and by the Hot-Wire Method App. Sci, Res. Sec. A., Vol. 7, p. 293

von Karman, T. (1930) — Mechanische Ähnlichkeit Und Turbulenz paper No. 53, in Collected Works of Theodore von Karman Vol. 2., Butterworths Scientific Publications

Wieghardt, K. (1942) — See: Prandtl, L. (1942)

Wygnanski, I. (1969) — Two-Dimensional Turbulent Jet in a Uniform, Parallel Stream A.I.A.A. Journal, Vol. 7, p. 86

Wygnanski, I. and Fiedler, H.E. (1969) — Some Measurements in the Self-Preserving Jet J.F.M. Vol. 38, pp. 577-612; also see: Boeing Sci. Res. Lab., Document D1-82-0712, April 1968

Wygnanski, I. and Fiedler, H.E. (1970) — The Two-Dimensional Mixing Layer J.F.M., Vol. 41, part 2, pp. 327-361

Wygnanski, I. and Gartshore, I.S. (1963) — General Description and Calibration of the McGill 17in.x30in. Blower Cascade Wind Tunnel Mech. Eng. Res. Lab., T.N. 63-7, McGill University

Wygnanski, I. and Hawaleshka, O. (1966) — The Effect of Upstream Velocity Profile on the Free Mixing of Jets With Ambient Fluid B.S.R.L., Flight Sciences Laboratory, Document No. D1-82-0528

Hackett, J.E. and Cox, D.K. (Miss) (1967) — Measurements in a 3-Dimensional Mixing Layer Between Two Grazing Perpendicular Streams N.P.L., Aerodynamics Division N.P.L., Aero Report 1248, A.R.C. 29544

Fig. 1

TYPICAL EXAMPLES OF ASYMMETRIC JETS

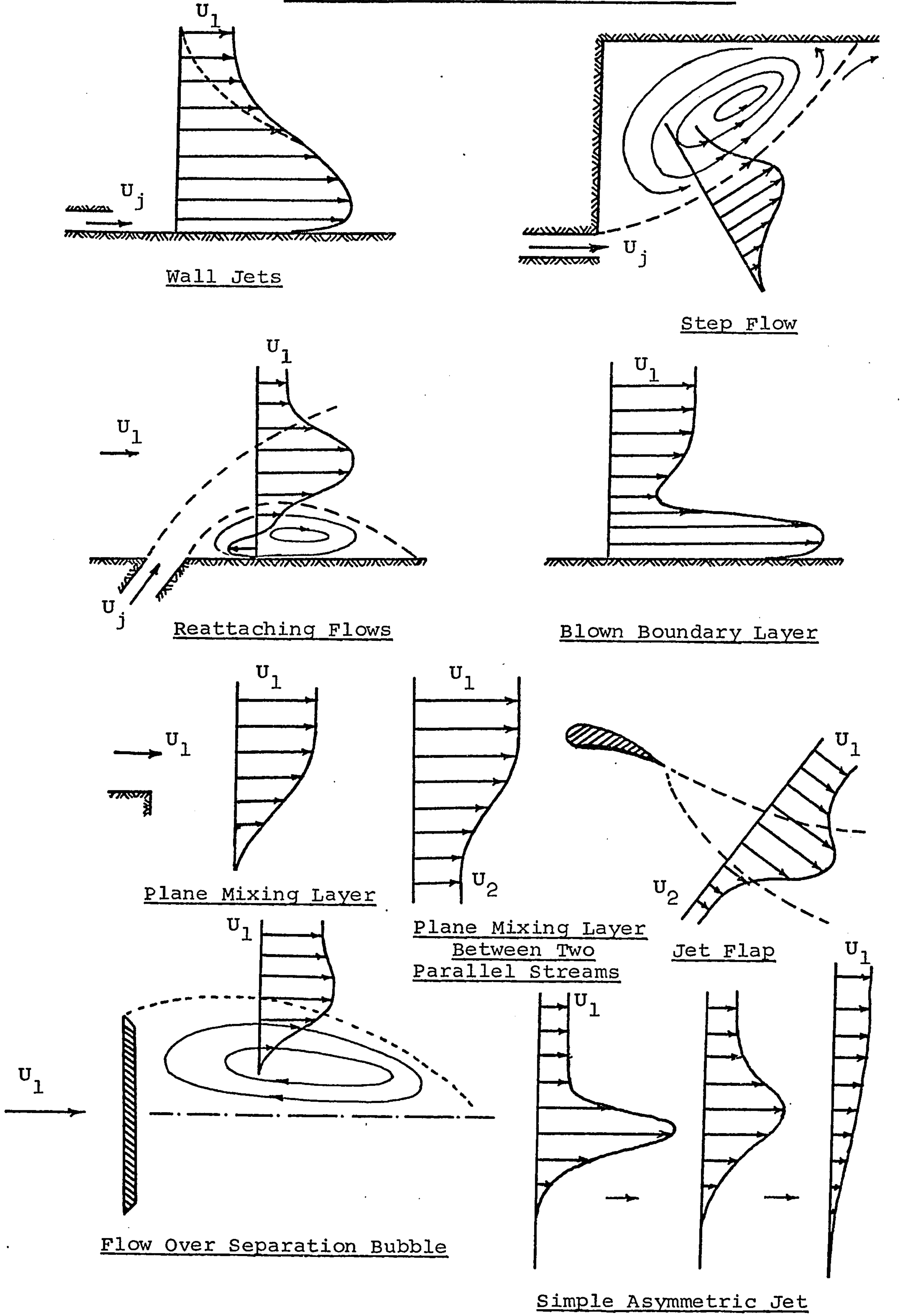

SKETCHES OF PLANE, SYMMETRIC F

Sketch of a 2-d Jet in Still Air

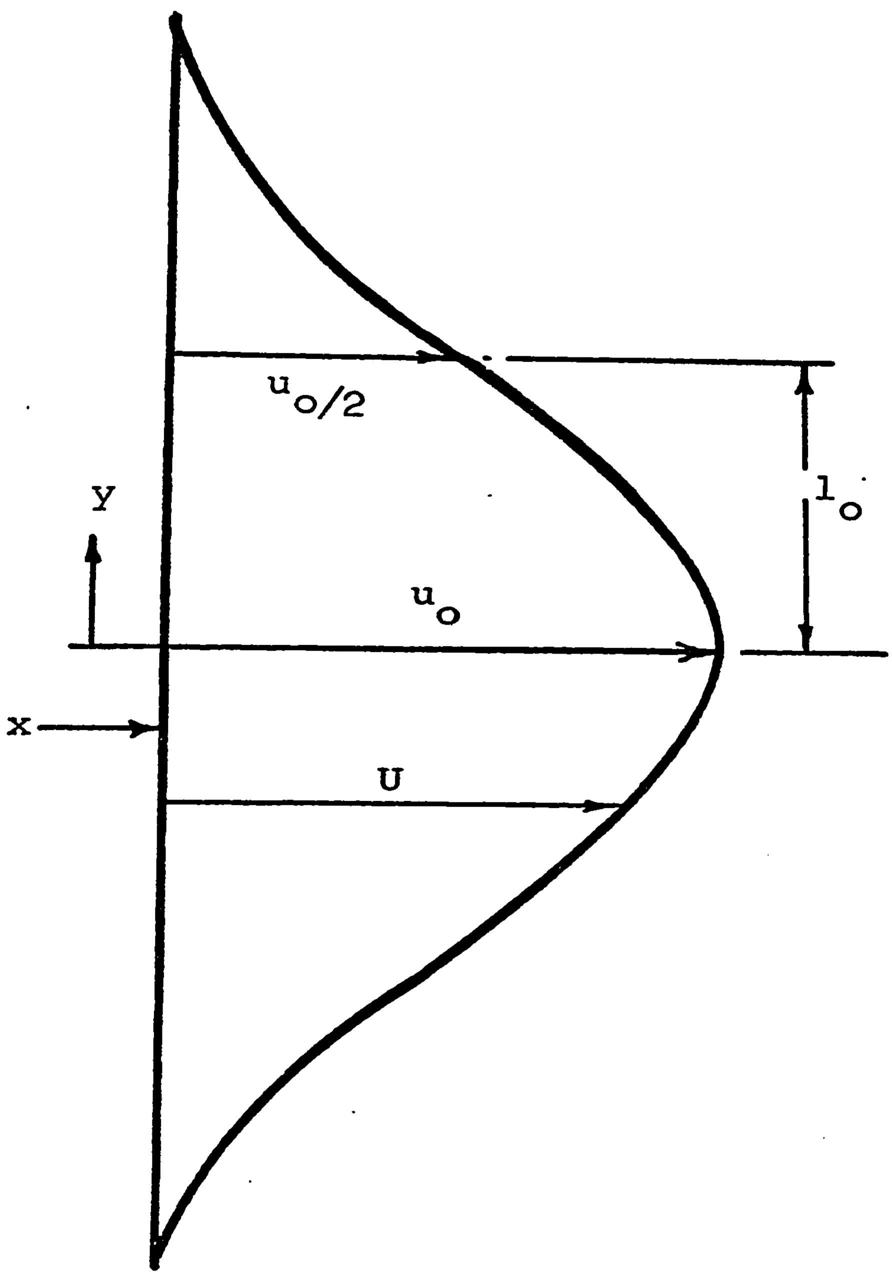

Fig. (2a)

Sketch of a P

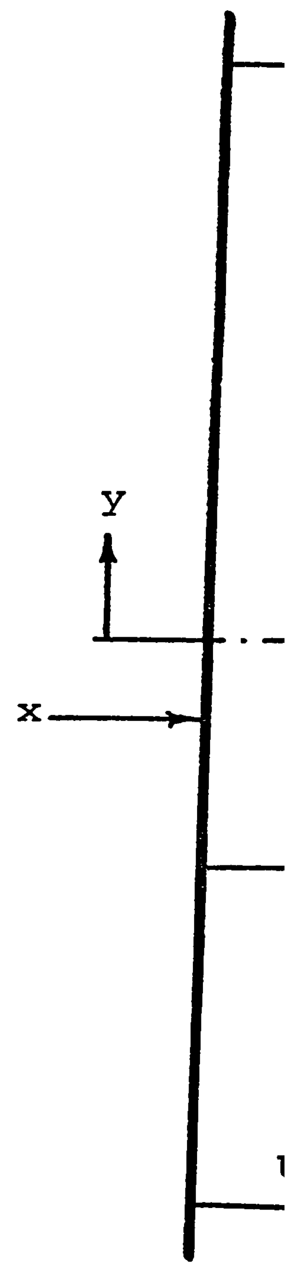

?LANE, SYMMETRIC FREE JETS

Sketch of a Plane Jet in Uniform Streaming Flow

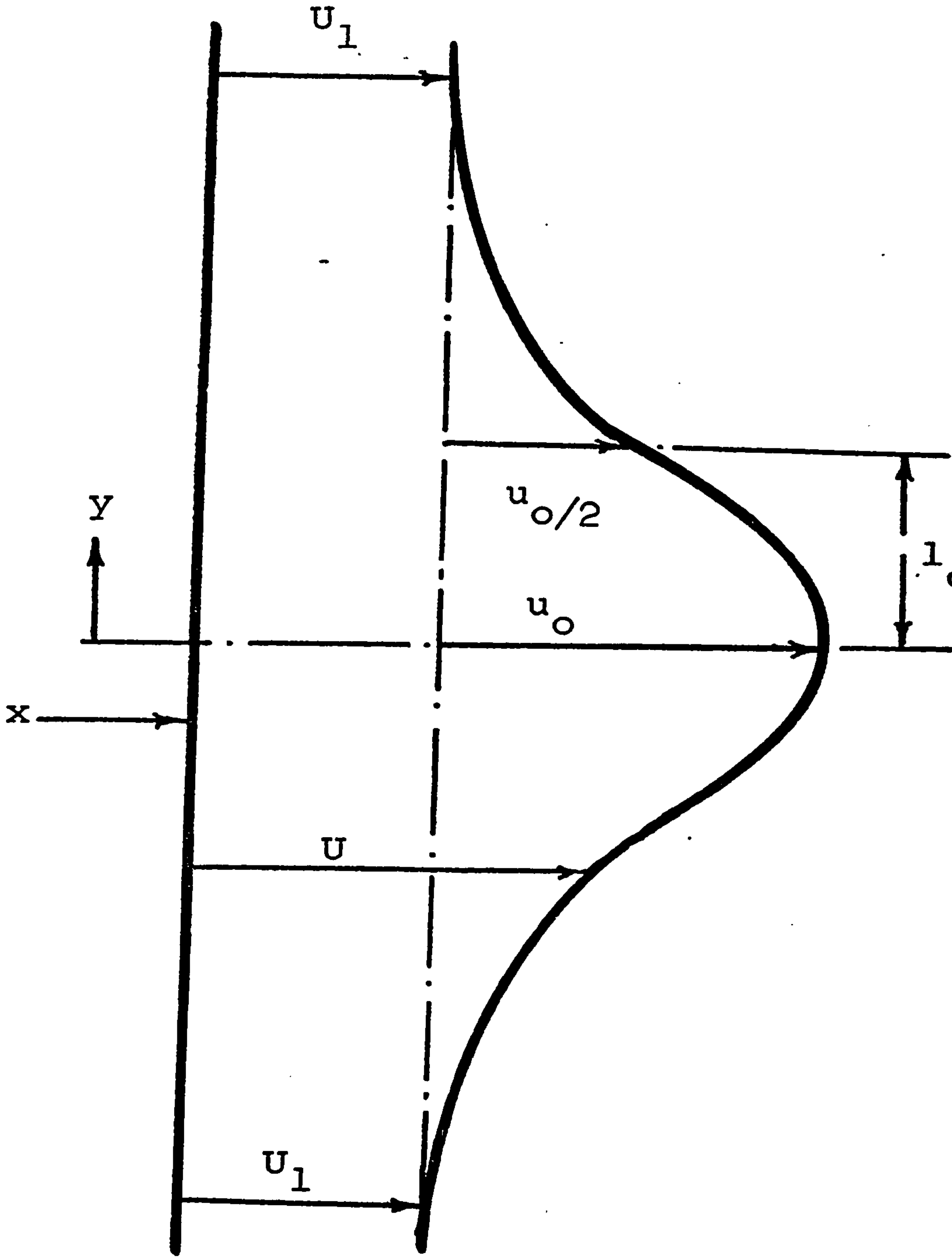

Fig. (2b)

Fig. 2

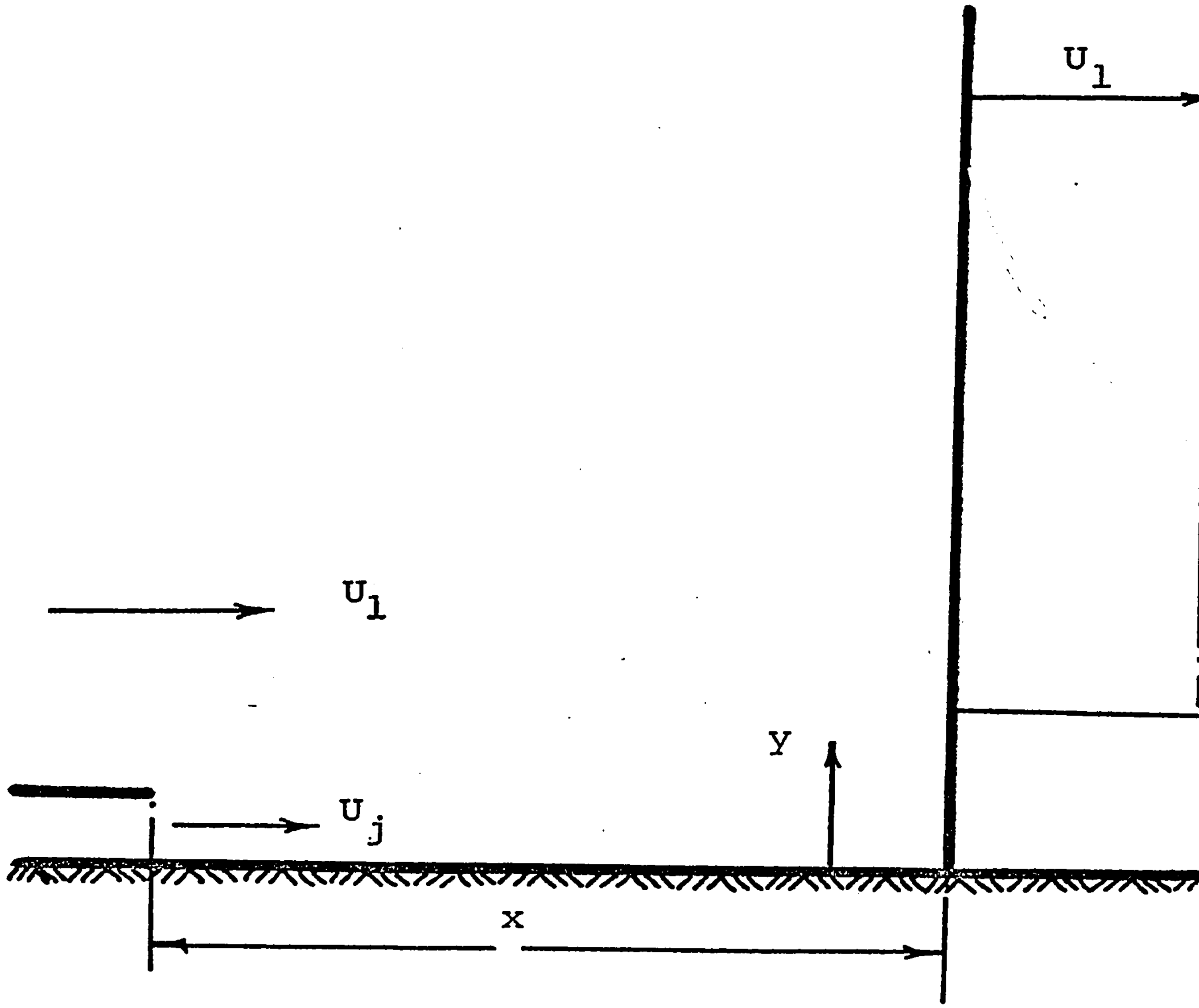

SKETCH OF A WALL JET IN UNIFORM ST

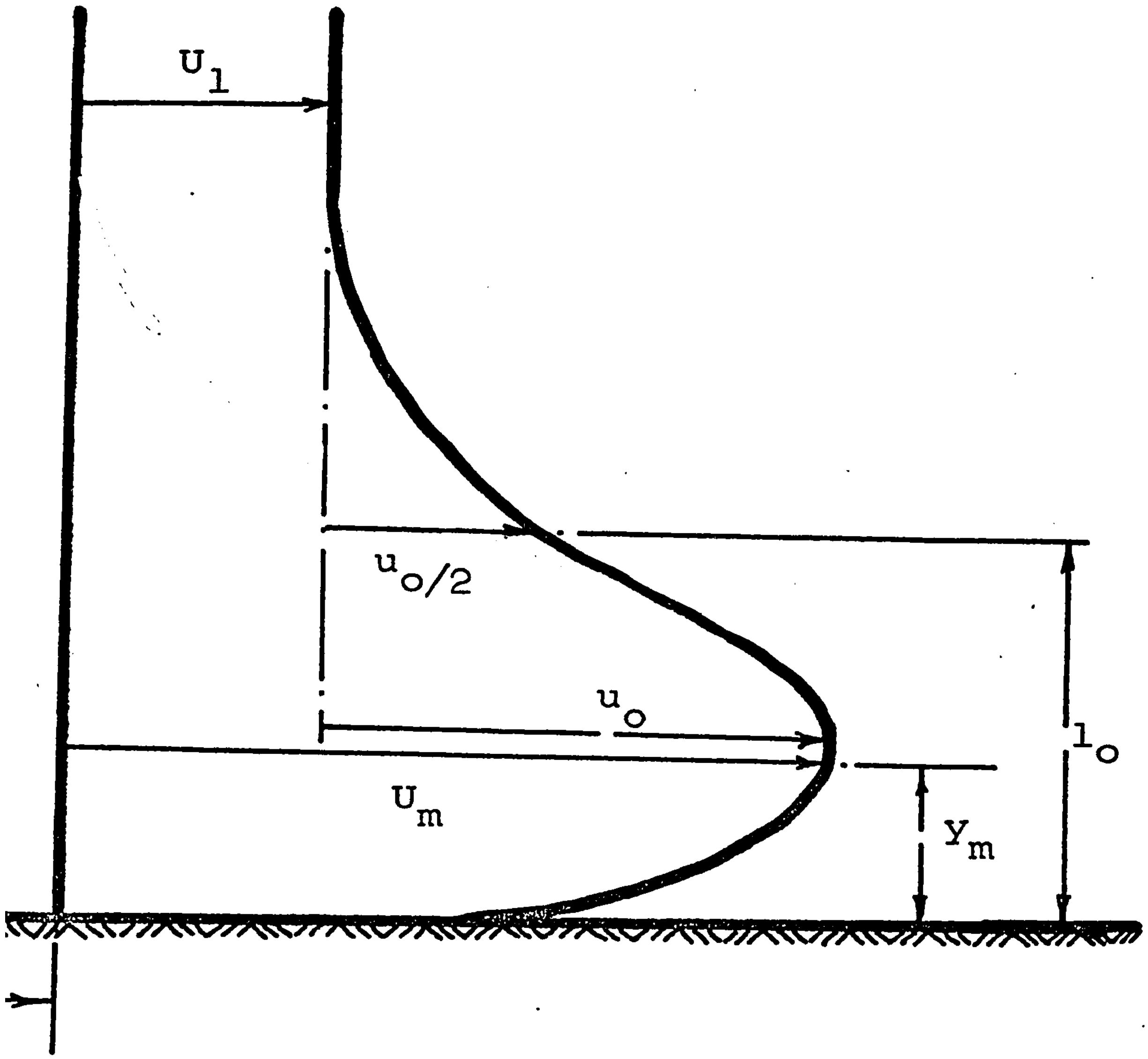

IN UNIFORM STREAMING FLOW

Fig. 3

SKETCH OF THE ASYMMETRIC JET

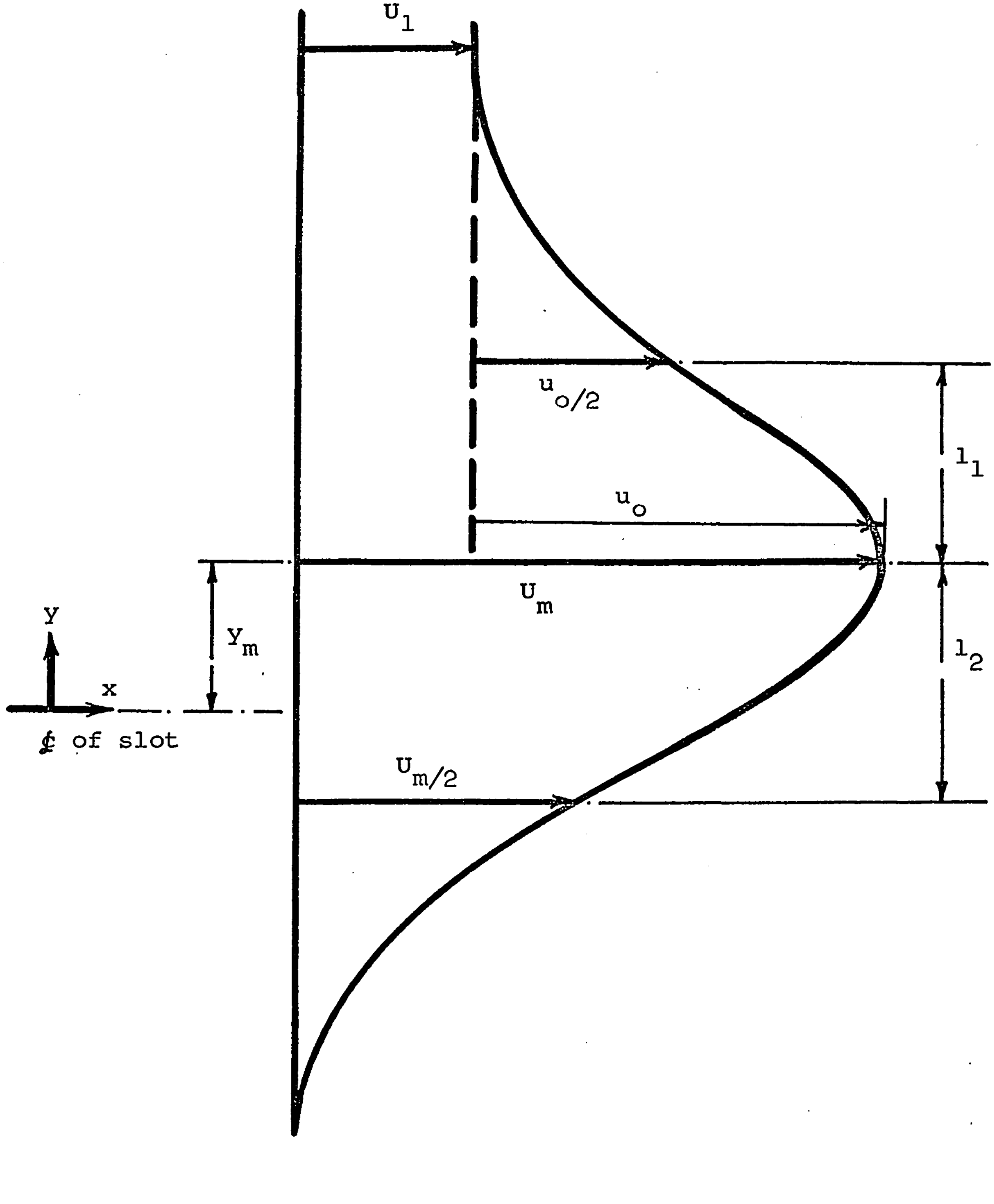

Fig. 5

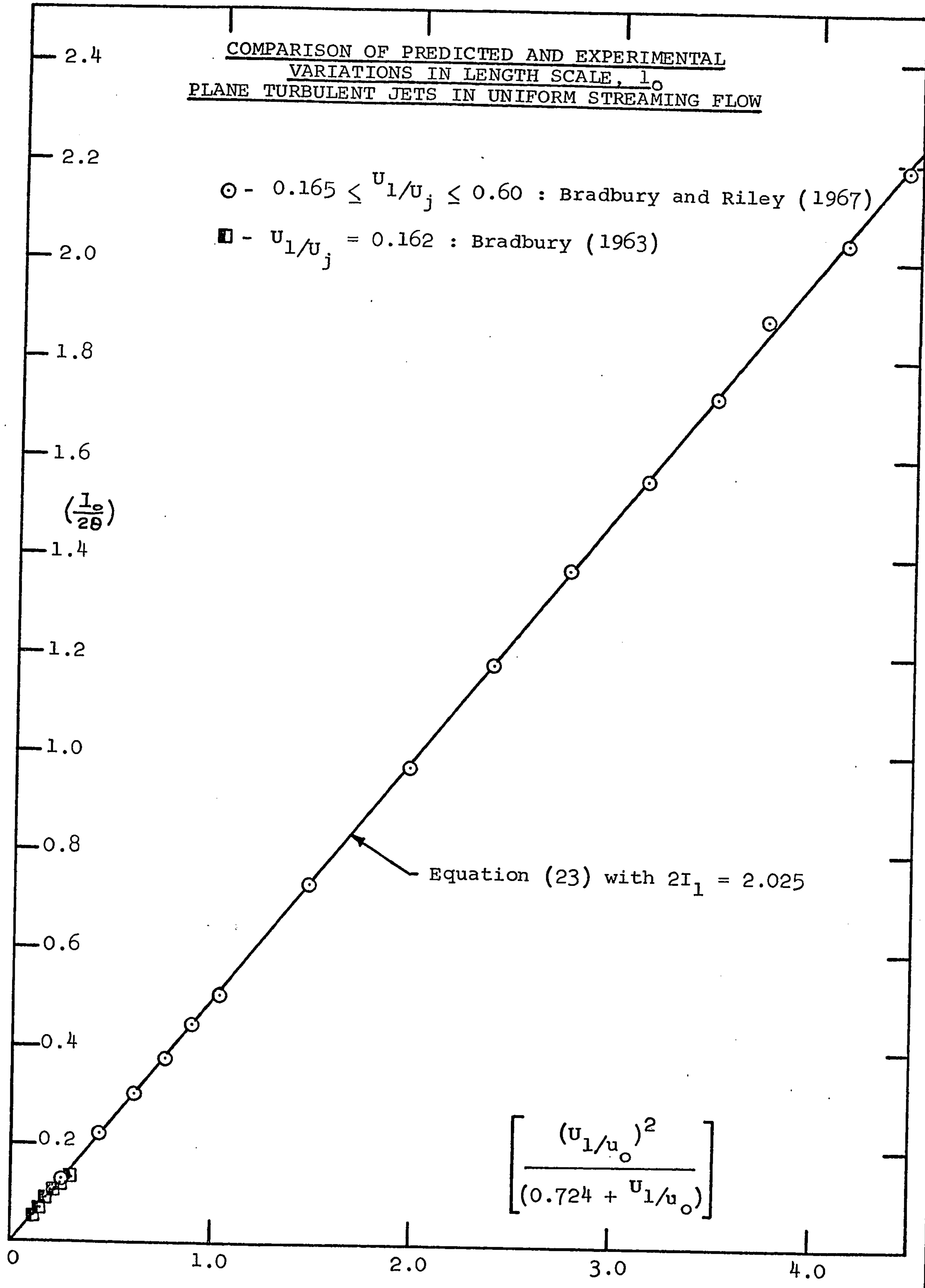

COMPARISON OF PREDICTED AND EXPERIMENTAL
VARIATIONS IN LENGTH SCALE, l_o
PLANE TURBULENT JETS IN UNIFORM STREAMING FLOW
⊙ - $0.165 \leq U_1/U_j \leq 0.60$: Bradbury and Riley (1967)
◨ - $U_1/U_j = 0.162$: Bradbury (1963)
Equation (23) with $2I_1 = 2.025$
$\left(\frac{l_o}{2\theta}\right)$
$\left[\frac{(U_1/u_o)^2}{(0.724 + U_1/u_o)}\right]$
2.4
2.2
2.0
1.8
1.6
1.4
1.2
1.0
0.8
0.6
0.4
0.2
0
1.0
2.0
3.0
4.0

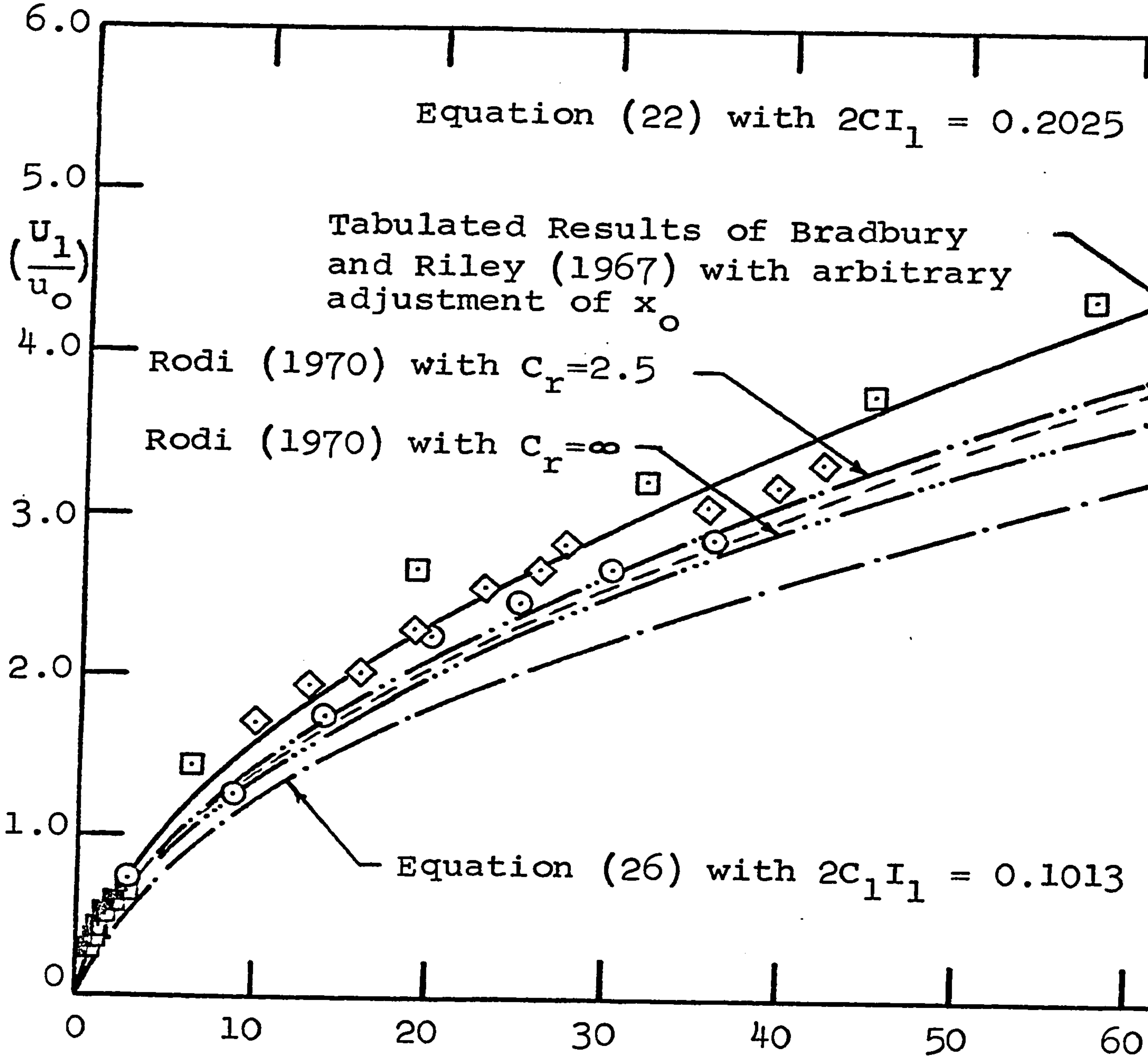

COMPARISON OF PREDICTED AND EXPERIMENTAL VARIATIONS

PLANE TURBULENT JETS IN UNIFORM S

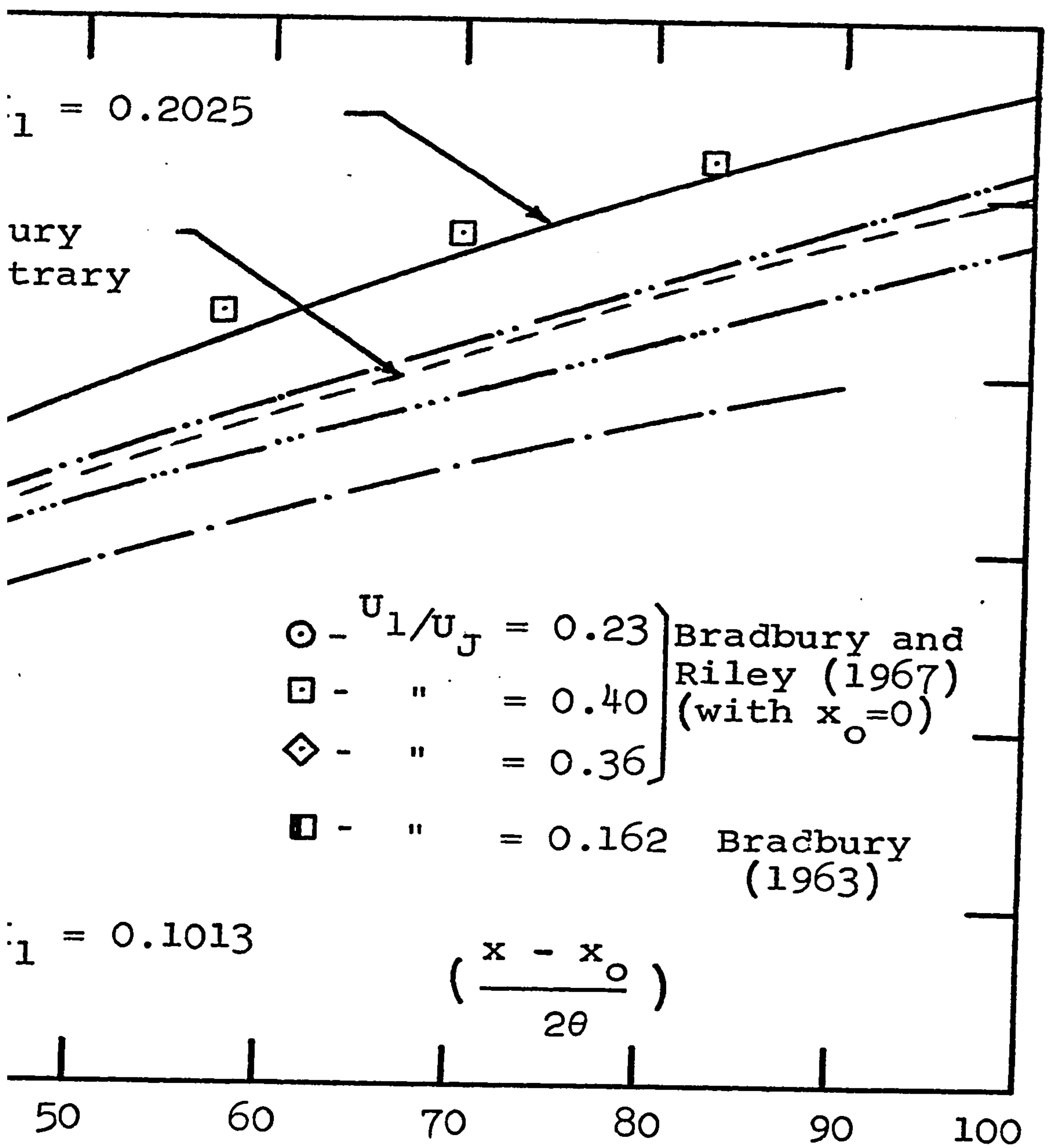

VARIATIONS IN PERTURBATION VELOCITY SCALE, u_o

:N UNIFORM STREAMING FLOW

Fig. 6

VARIATION OF $\overline{uv}/\overline{q^2}$ ACROSS PLANE TURBULENT JETS IN UNIFORM STREAMING FLOW

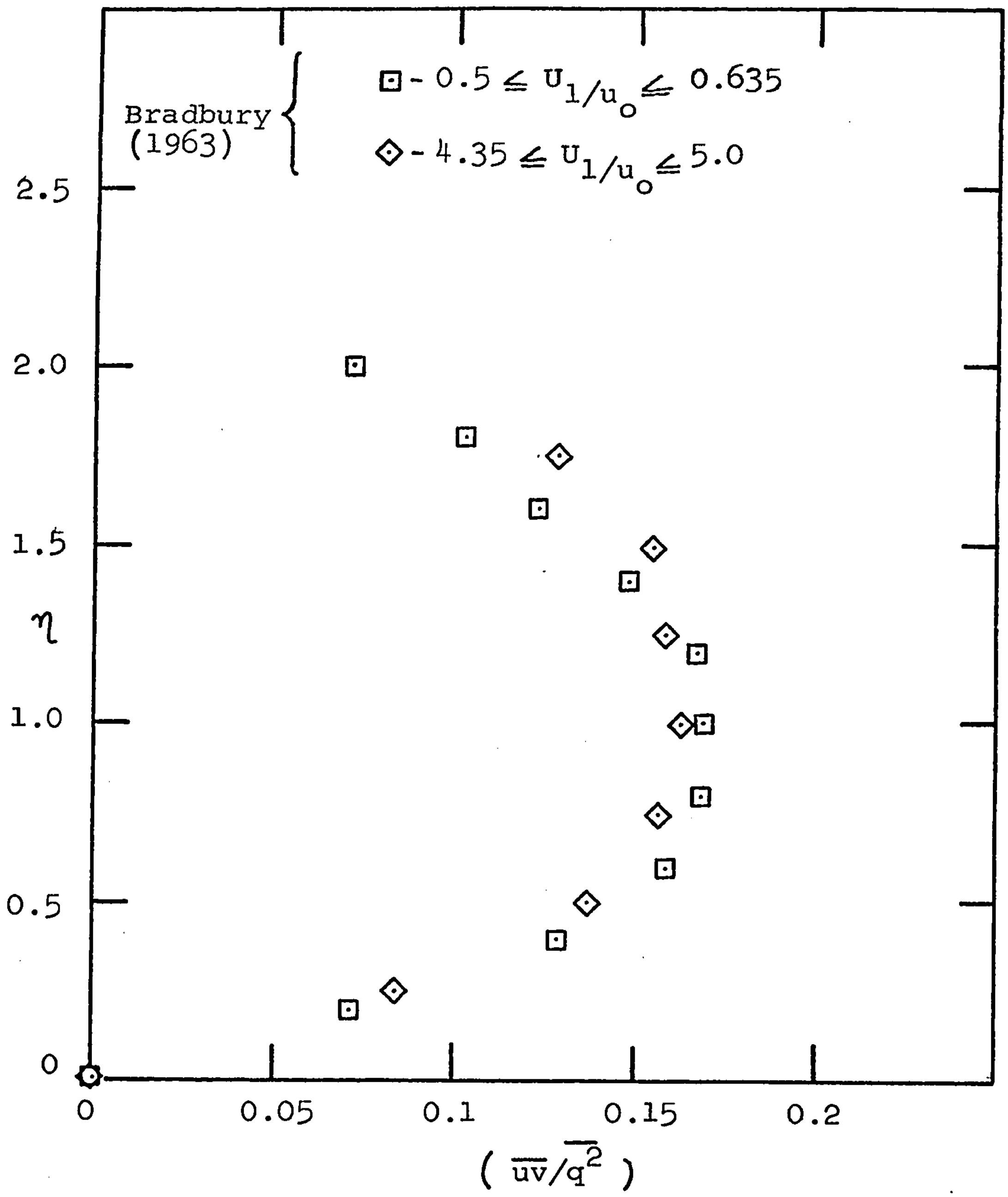

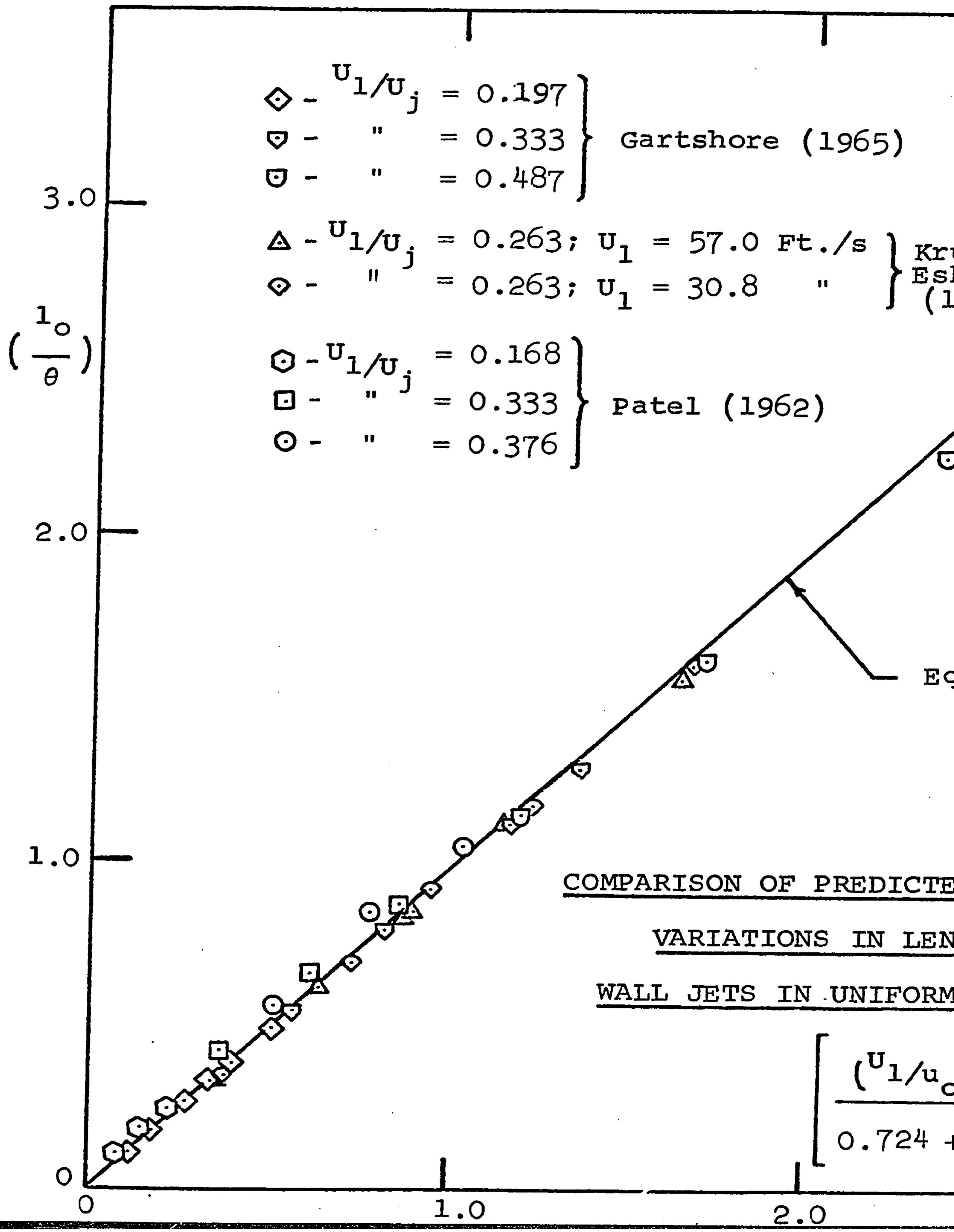

COMPARISON OF PREDICTE

VARIATIONS IN LEN

WALL JETS IN UNIFORM

$$\left[\frac{(U_1/u_c}{0.724 +}\right.$$

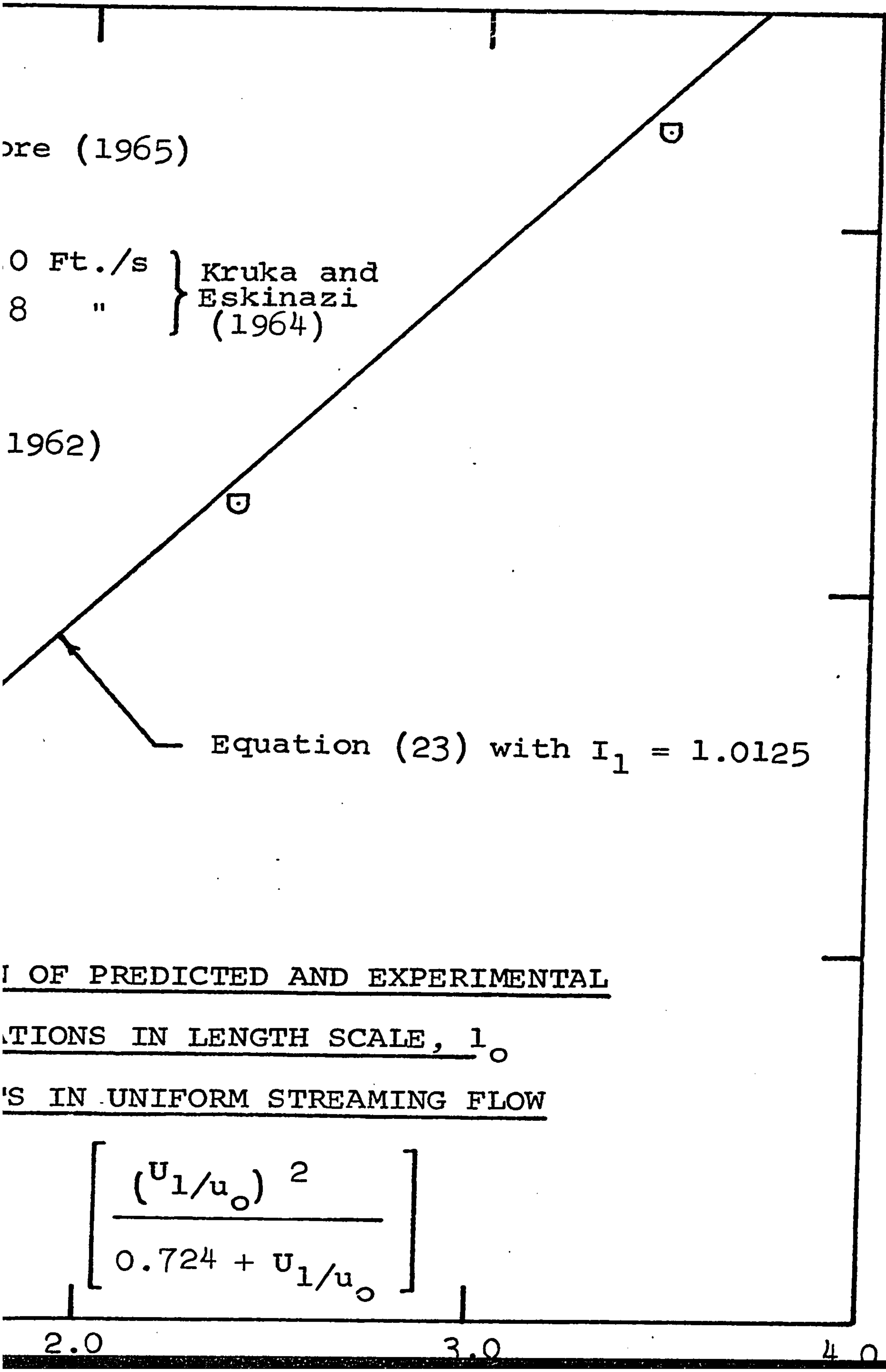

N OF PREDICTED AND EXPERIMENTAL
ATIONS IN LENGTH SCALE, l_o
'S IN UNIFORM STREAMING FLOW

Fig. 8

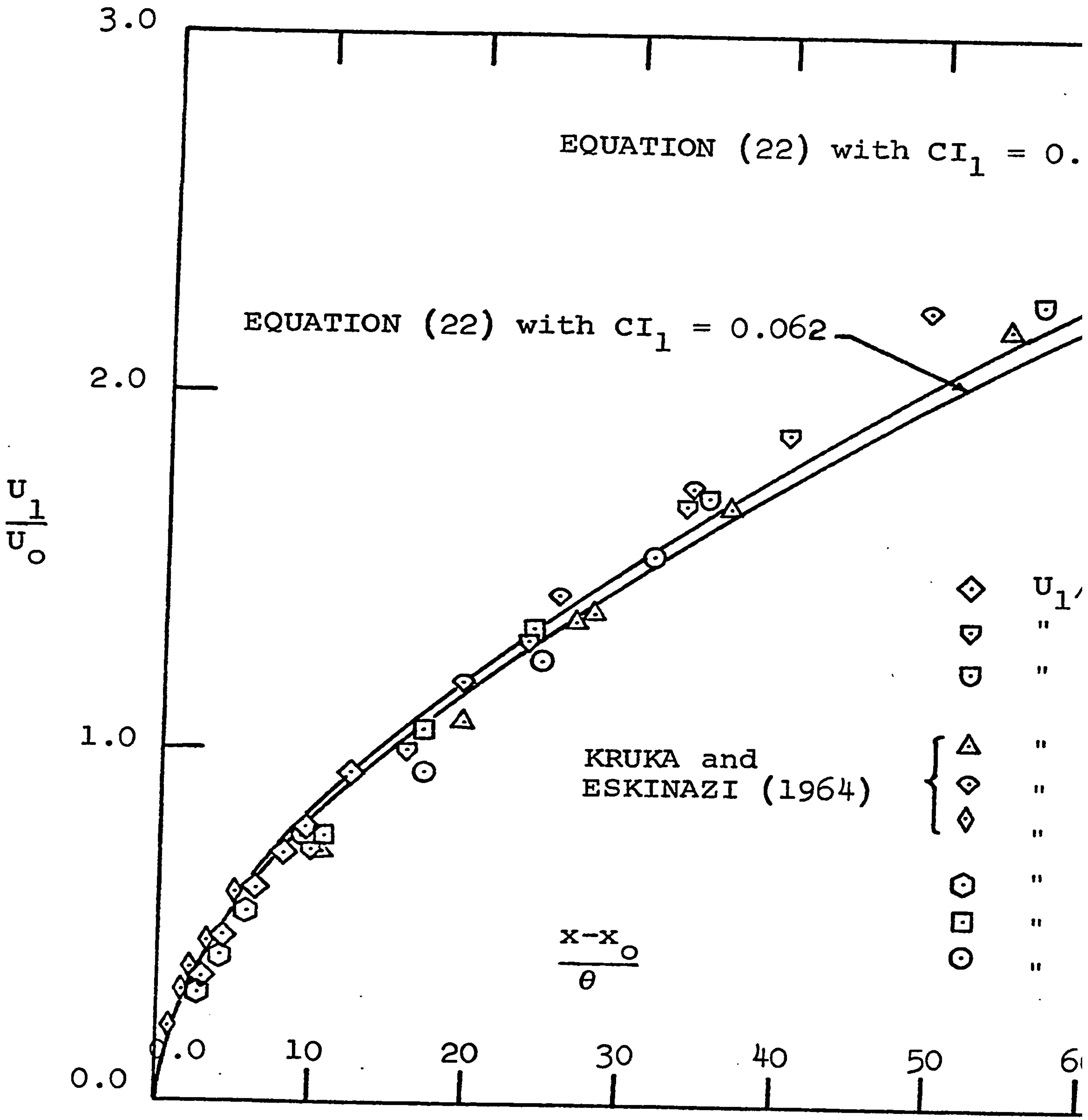

COMPARISON OF PREDICTED AND EXPERIMENTAL VARIATI
SCALE, u_o:

WALL JETS IN UNIFORM STREAMING FLOW.

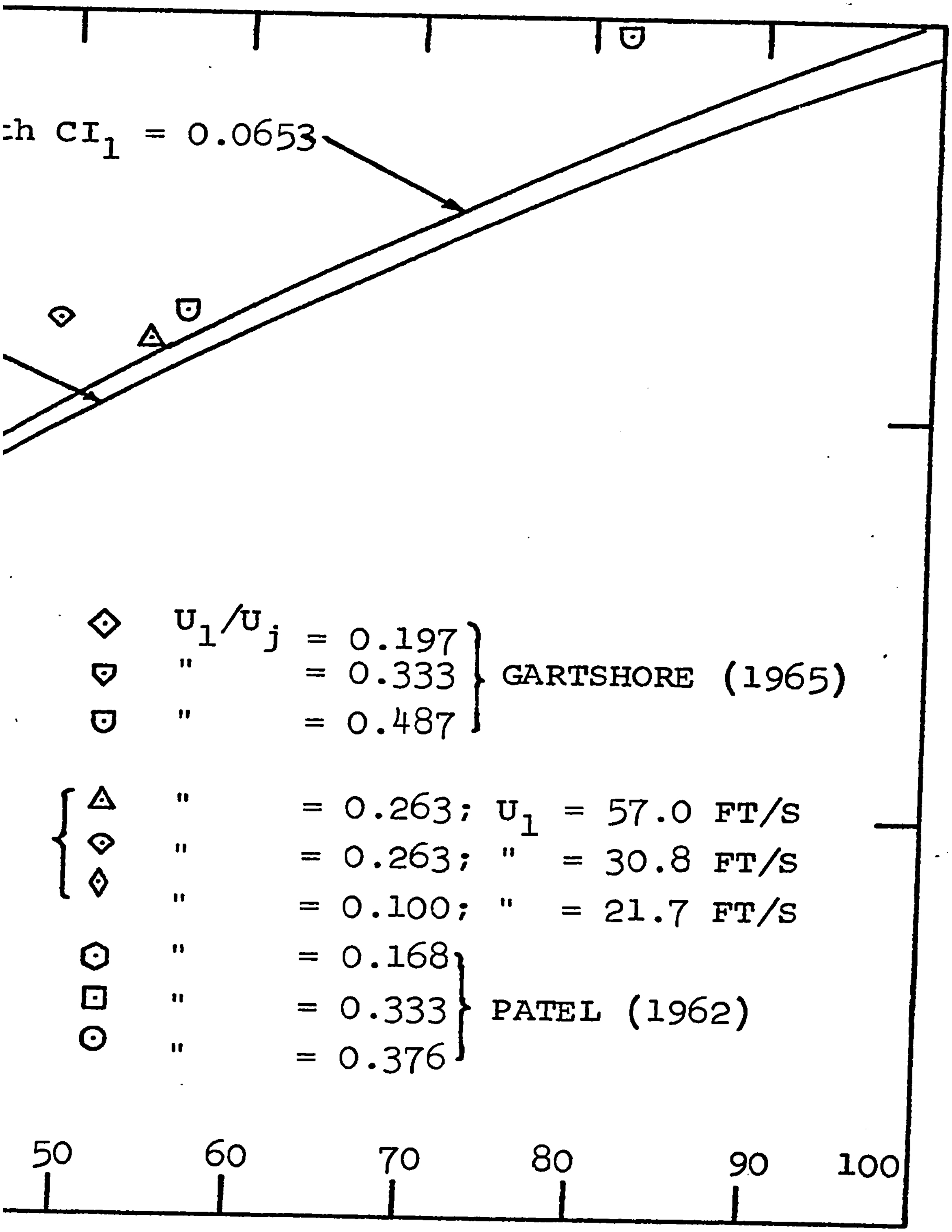

'AL VARIATIONS IN PERTURBATION VELOCITY

Fig. 9

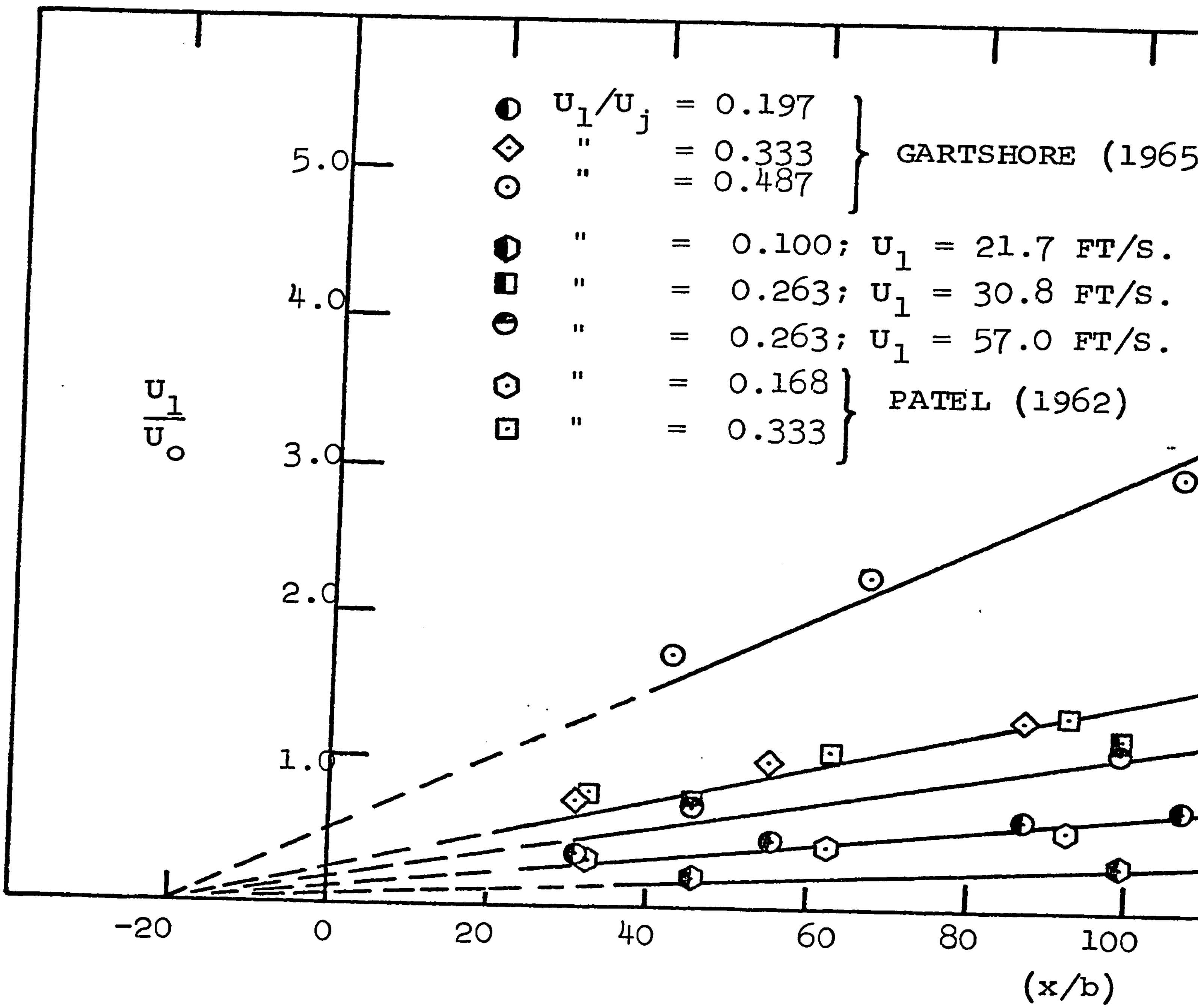

HYPOTHETICAL ORIGIN, x_o, FOR WALL JETS

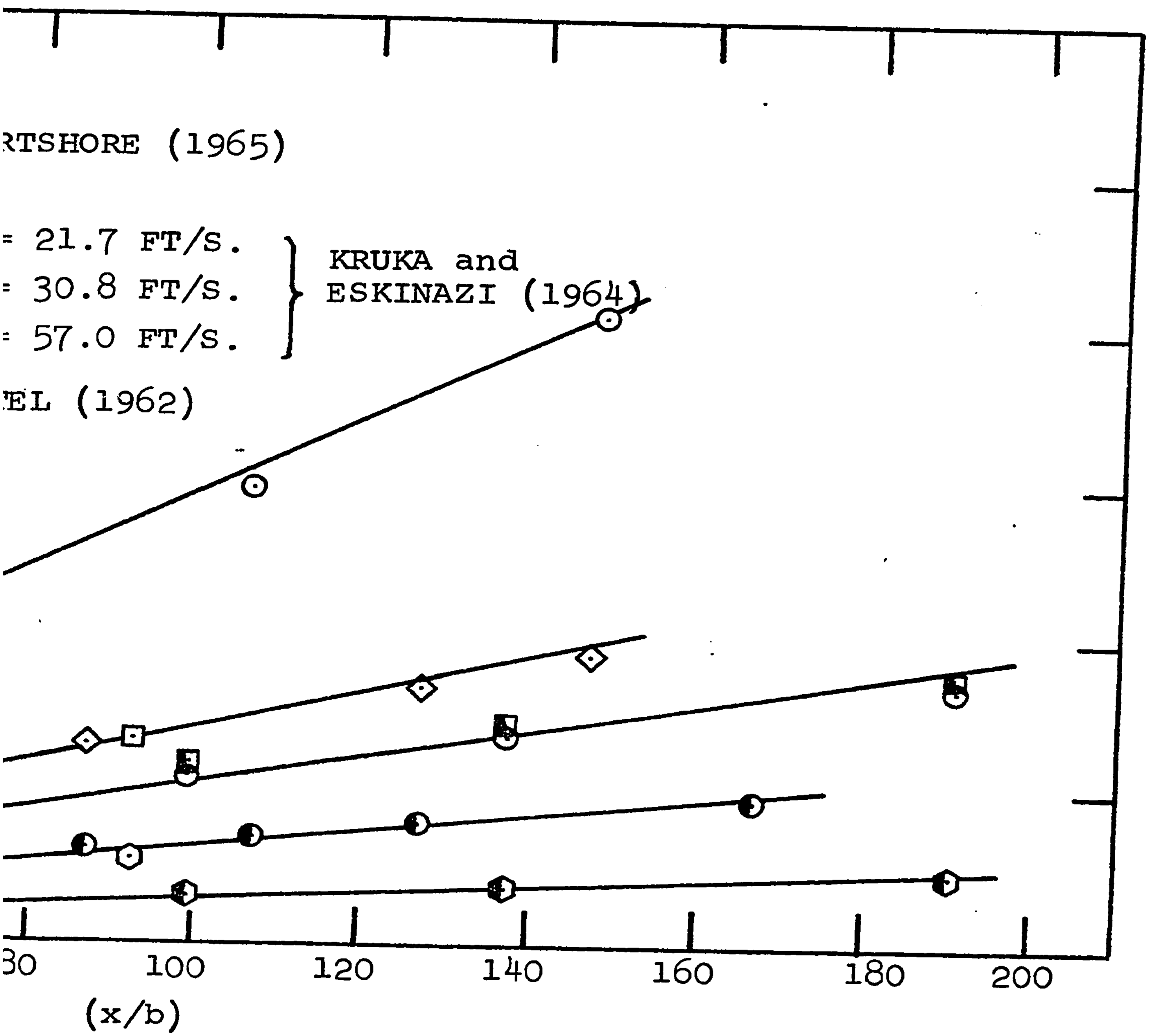

FOR WALL JETS IN UNIFORM STREAMING FLOW

Fig. 10

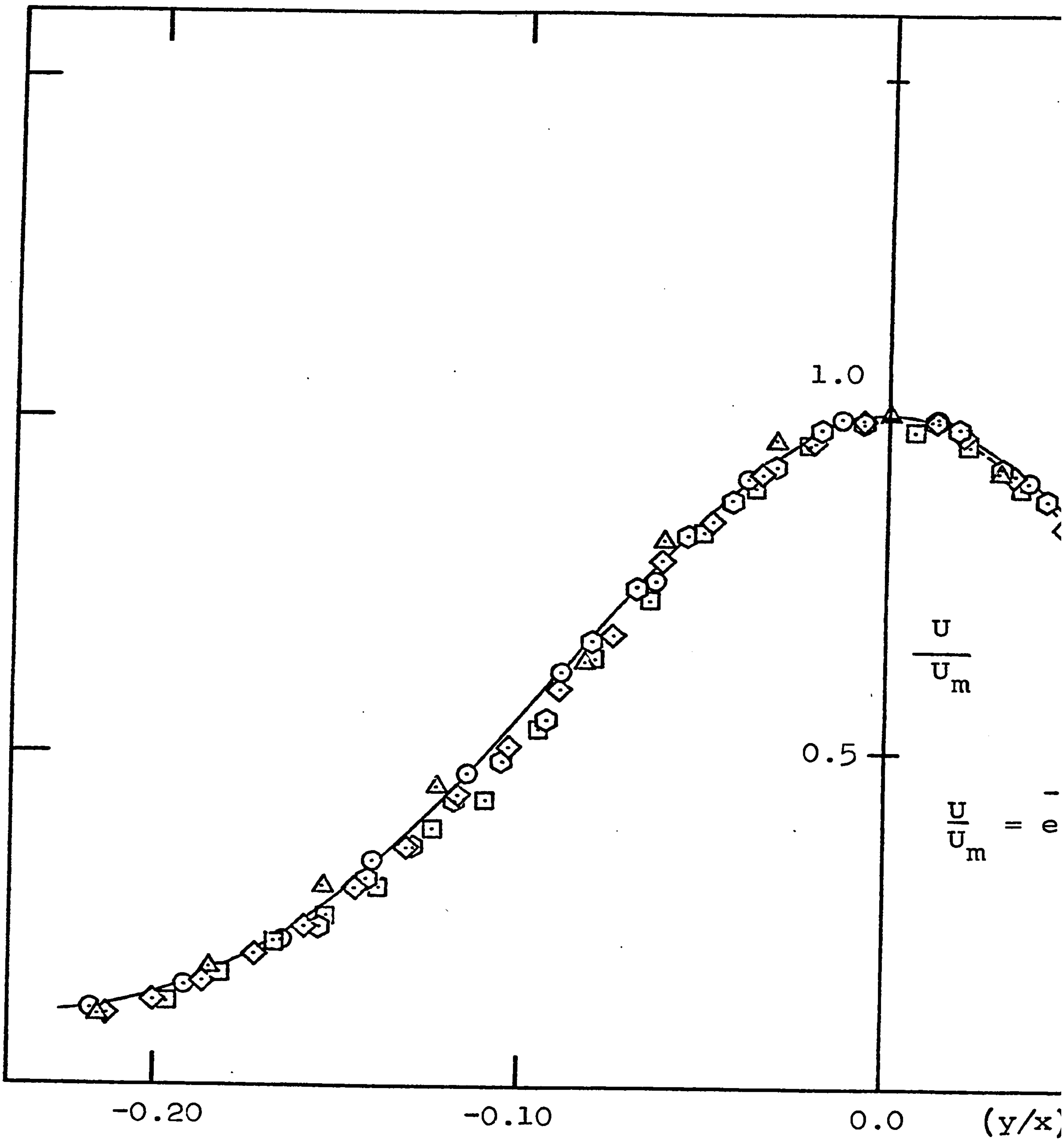

NON-DIMENSIONAL MEAN VELOCITY DISTRIBUTIONS ACROS

$(U_j b)/\nu = 3.51 \times 10^4$

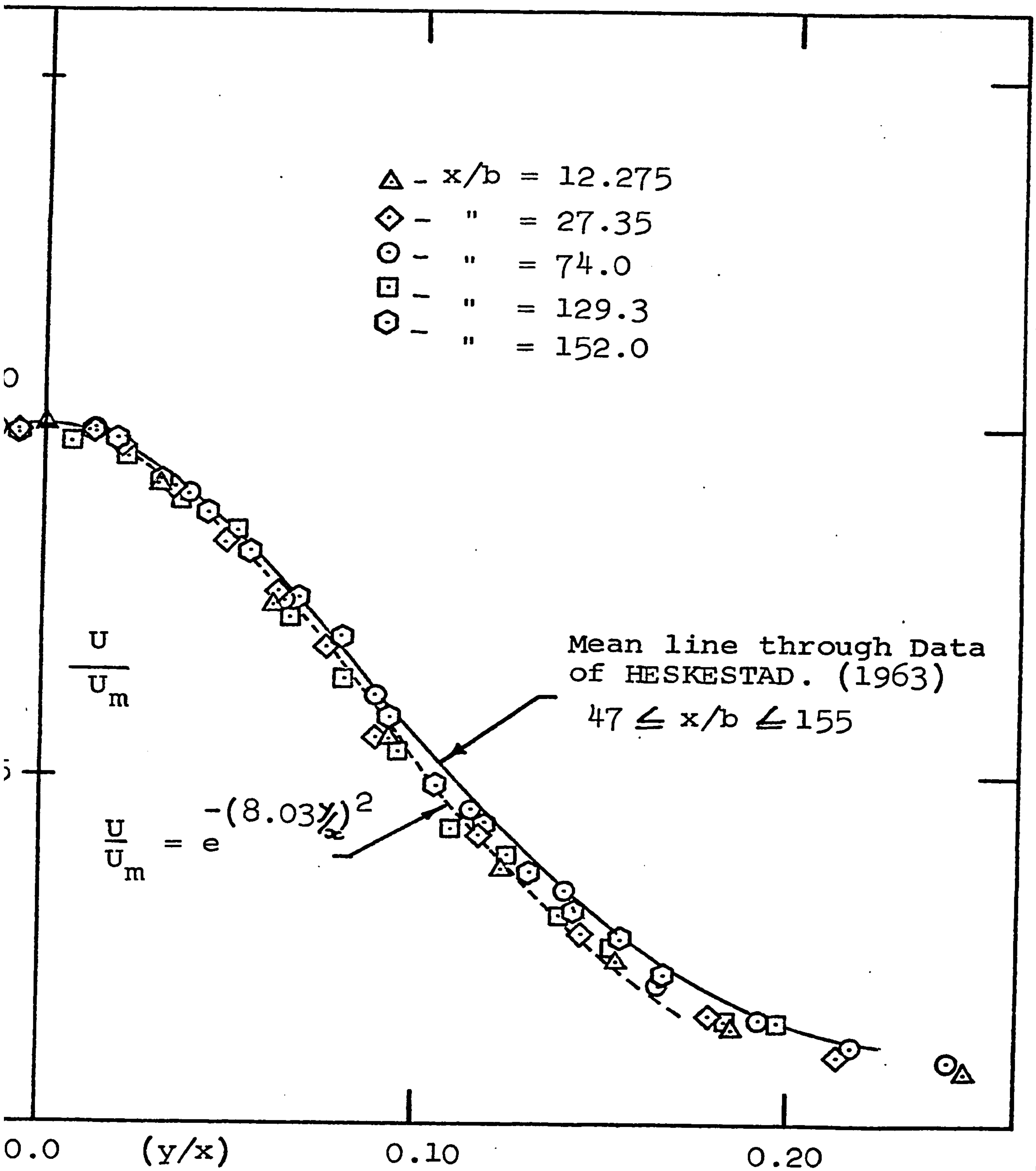

UTIONS ACROSS THE PLANE JET IN STILL AIR.

Fig. 11

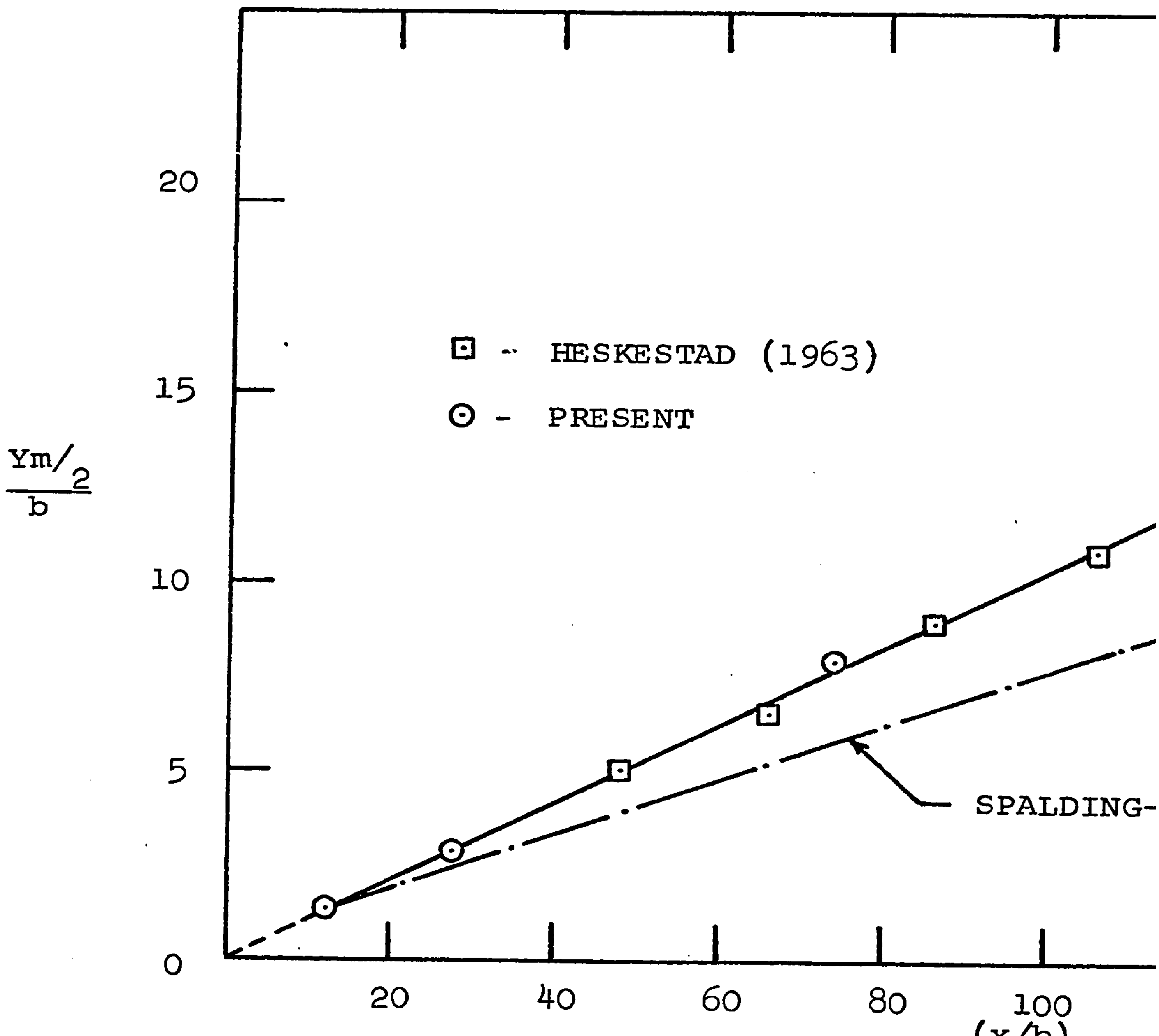

THE GROWTH OF THE PLANE JET IN STILL AIR (U

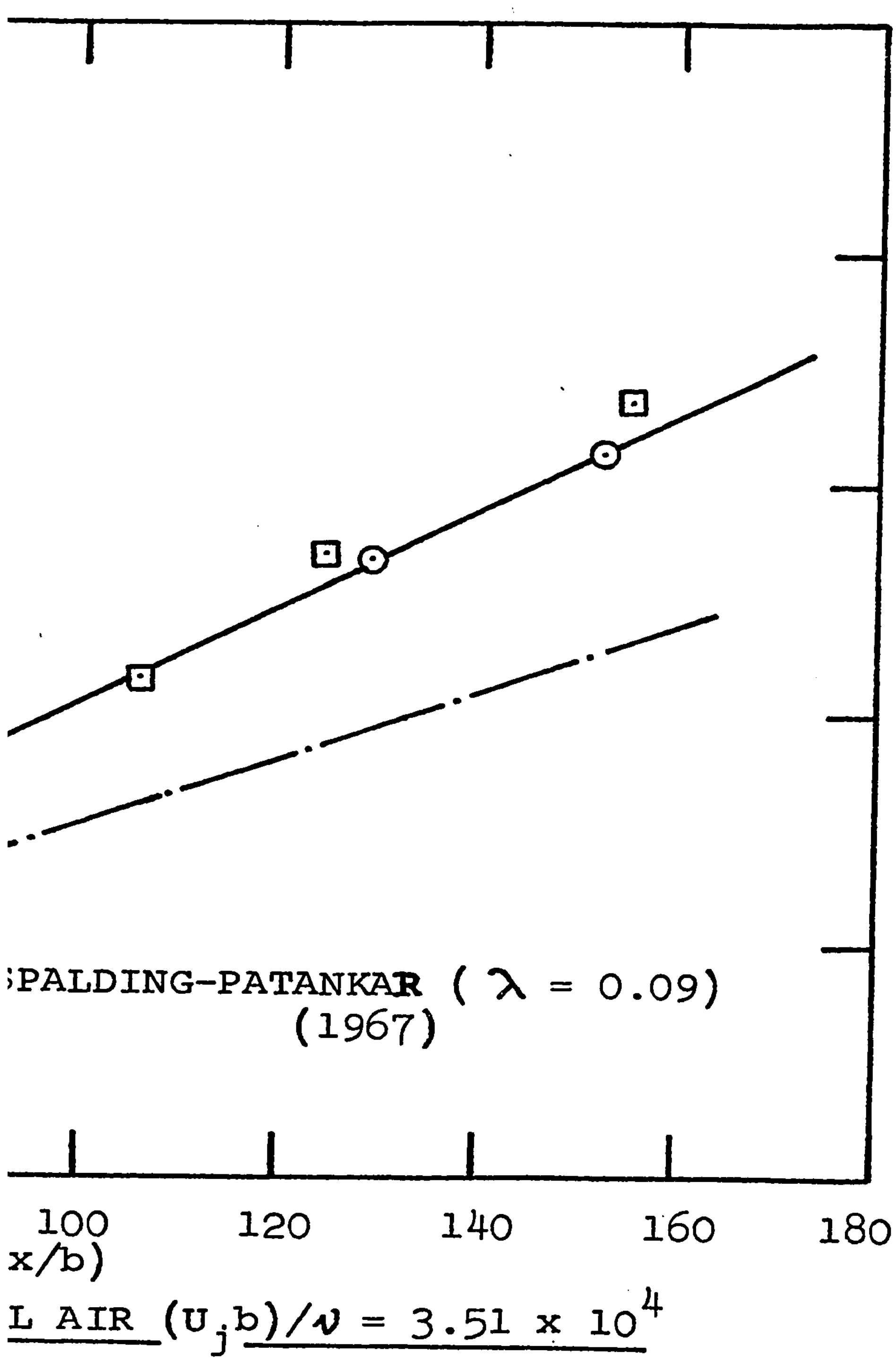

SPALDING-PATANKAR (λ = 0.09)
(1967)
100
120
140
160
180
x/b)
L AIR (Uj b)/ν = 3.51 x 10^4

Fig. 12

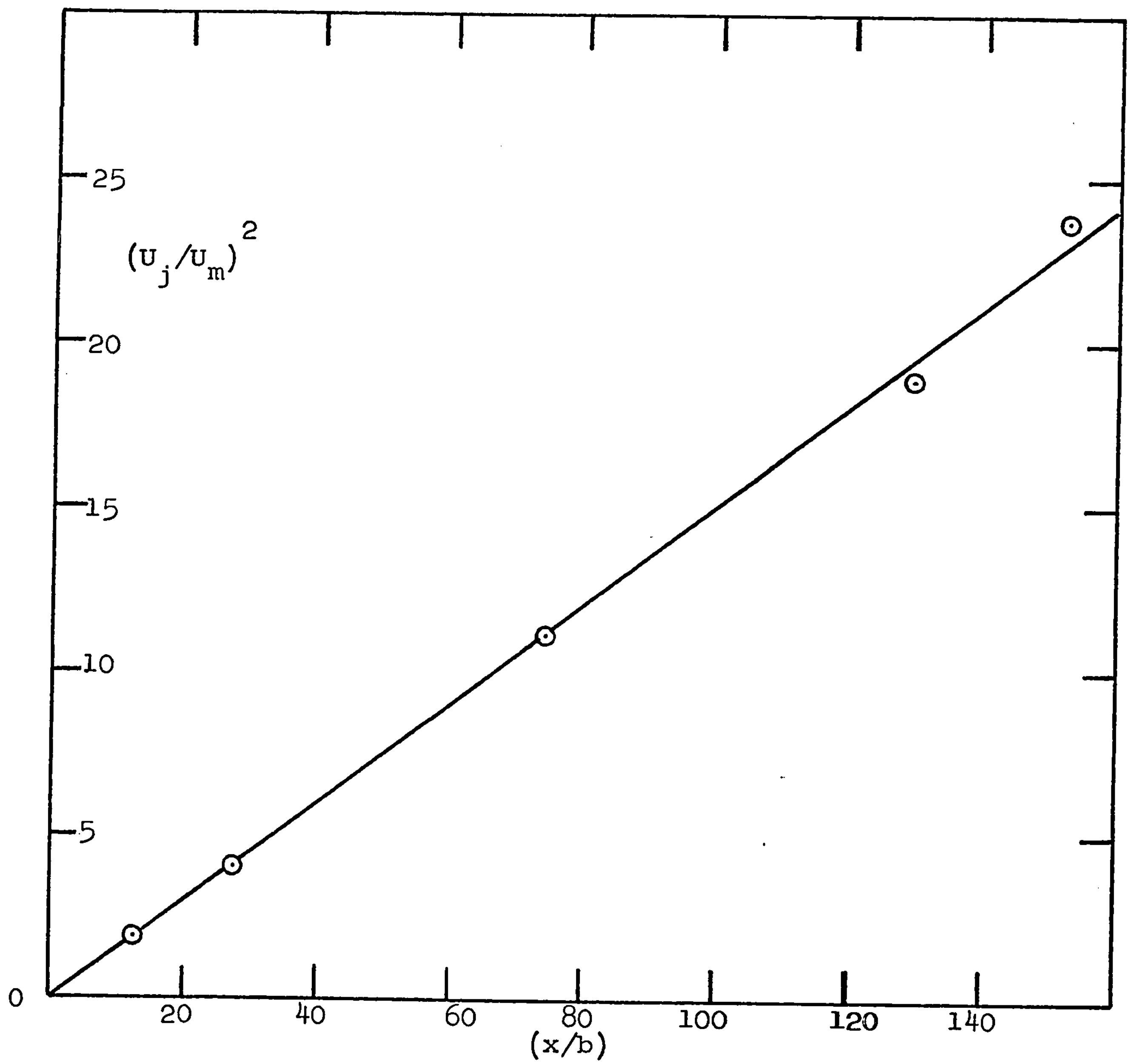

VARIATION OF CENTRE LINE VELOCITY WITH DOWNSTREAM DISTANCE.
THE PLANE JET IN STILL AIR $(U_j b)/\nu = 3.5 \times 10^4$

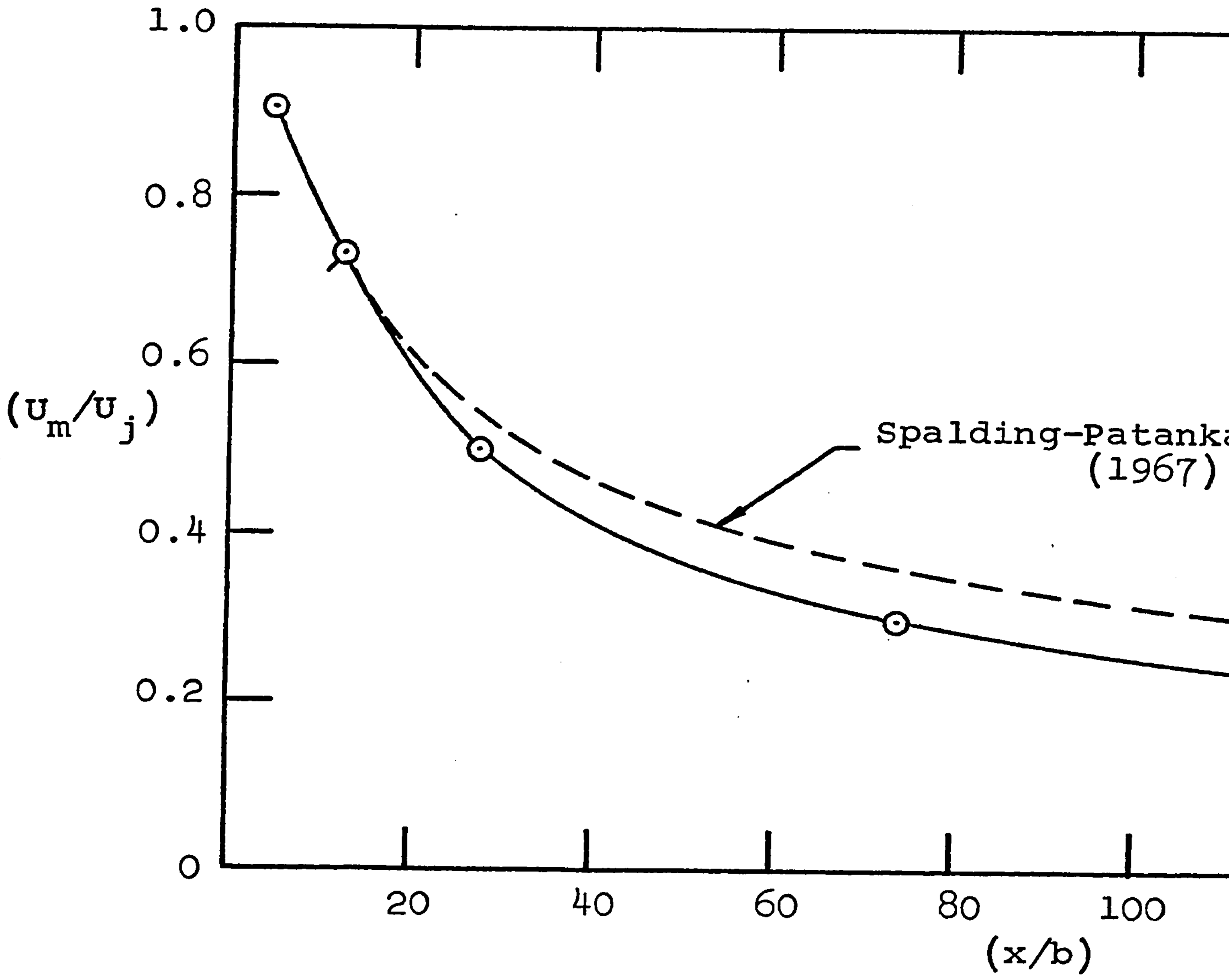

VARIATION OF CENTRE LINE VELOCITY WITH DOWNS

THE PLANE JET IN STILL AIR $(U_j b)/\nu = 3.51$

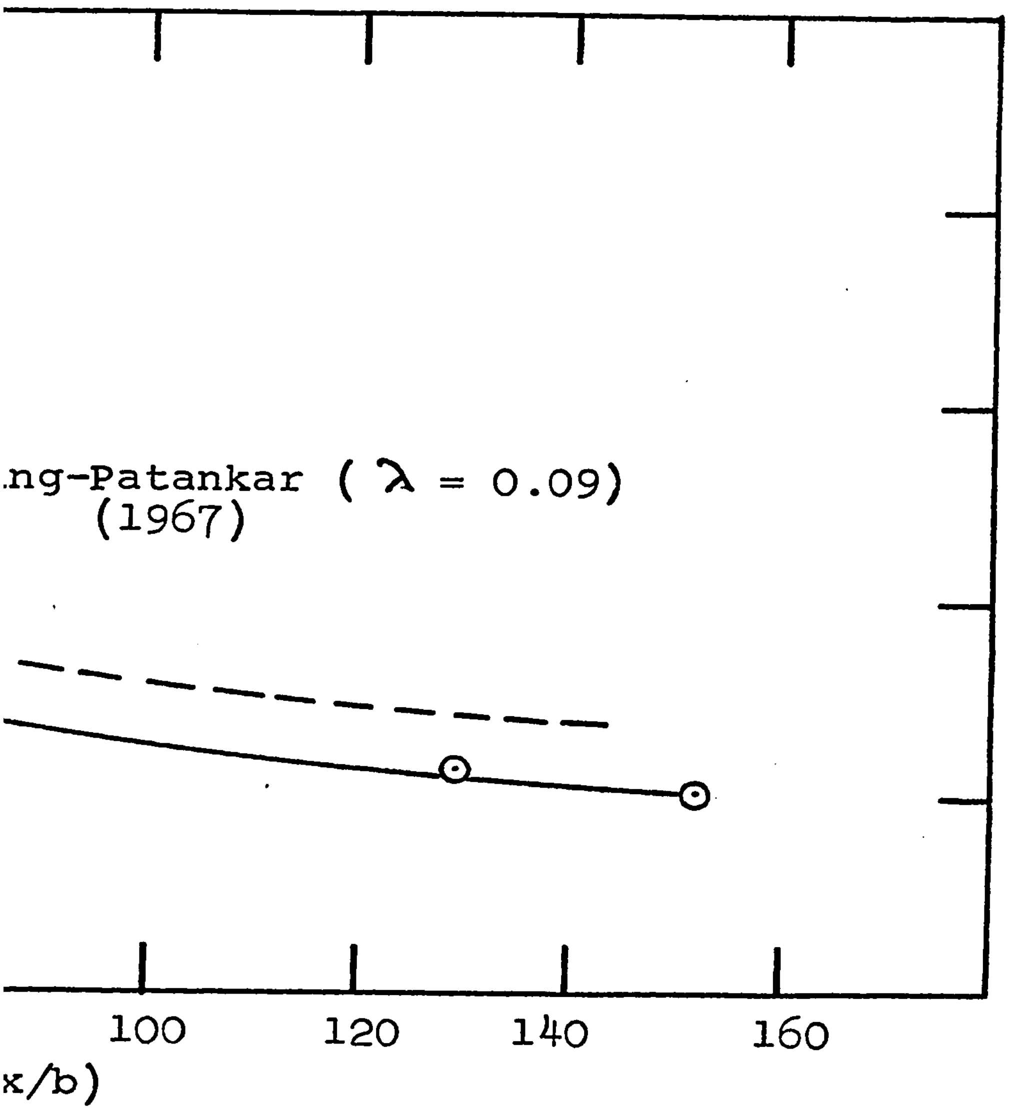

WITH DOWNSTREAM DISTANCE.

ν = 3.51×10^4

Fig. 14

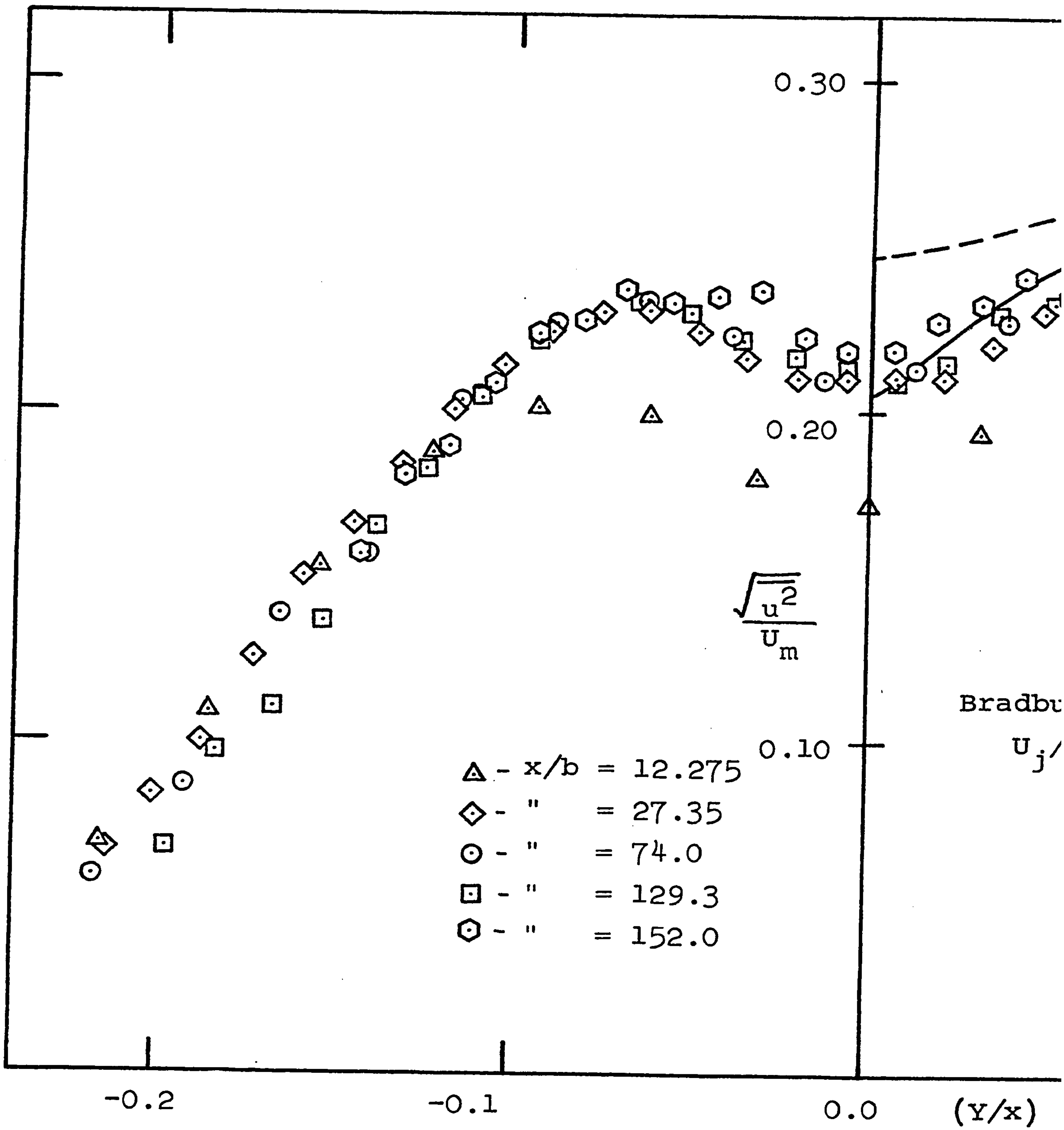

DISTRIBUTIONS OF LONGITUDINAL TURBULENT INTENSITY
THE PLANE JET IN STILL AIR $(U_j b)/\nu = 3.51 \times 10^4$

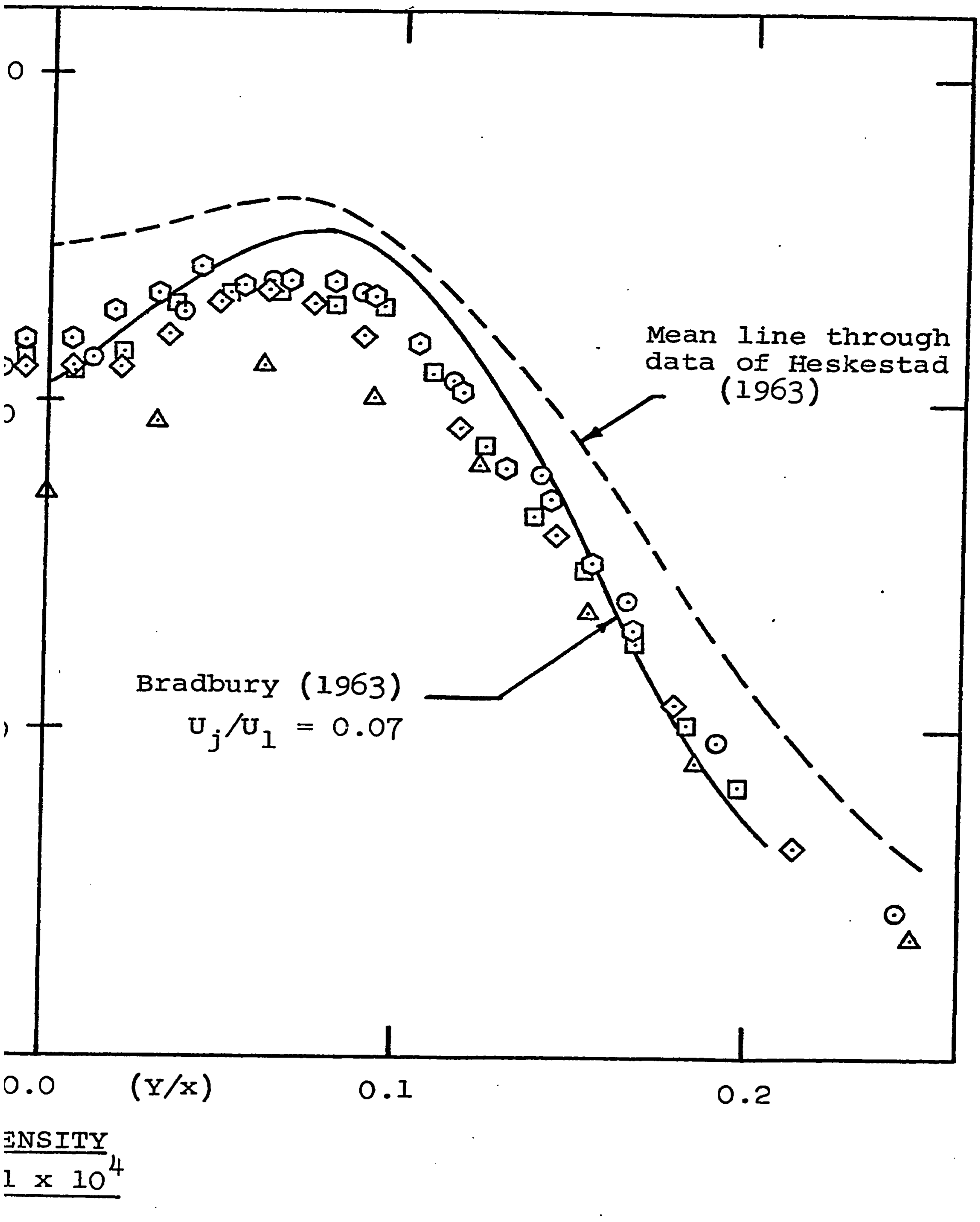
Mean line through data of Heskestad (1963)
Bradbury (1963) $U_j/U_1 = 0.07$
0.0
(Y/x)
0.1
0.2
ENSITY
l x 10^4

Fig. 15

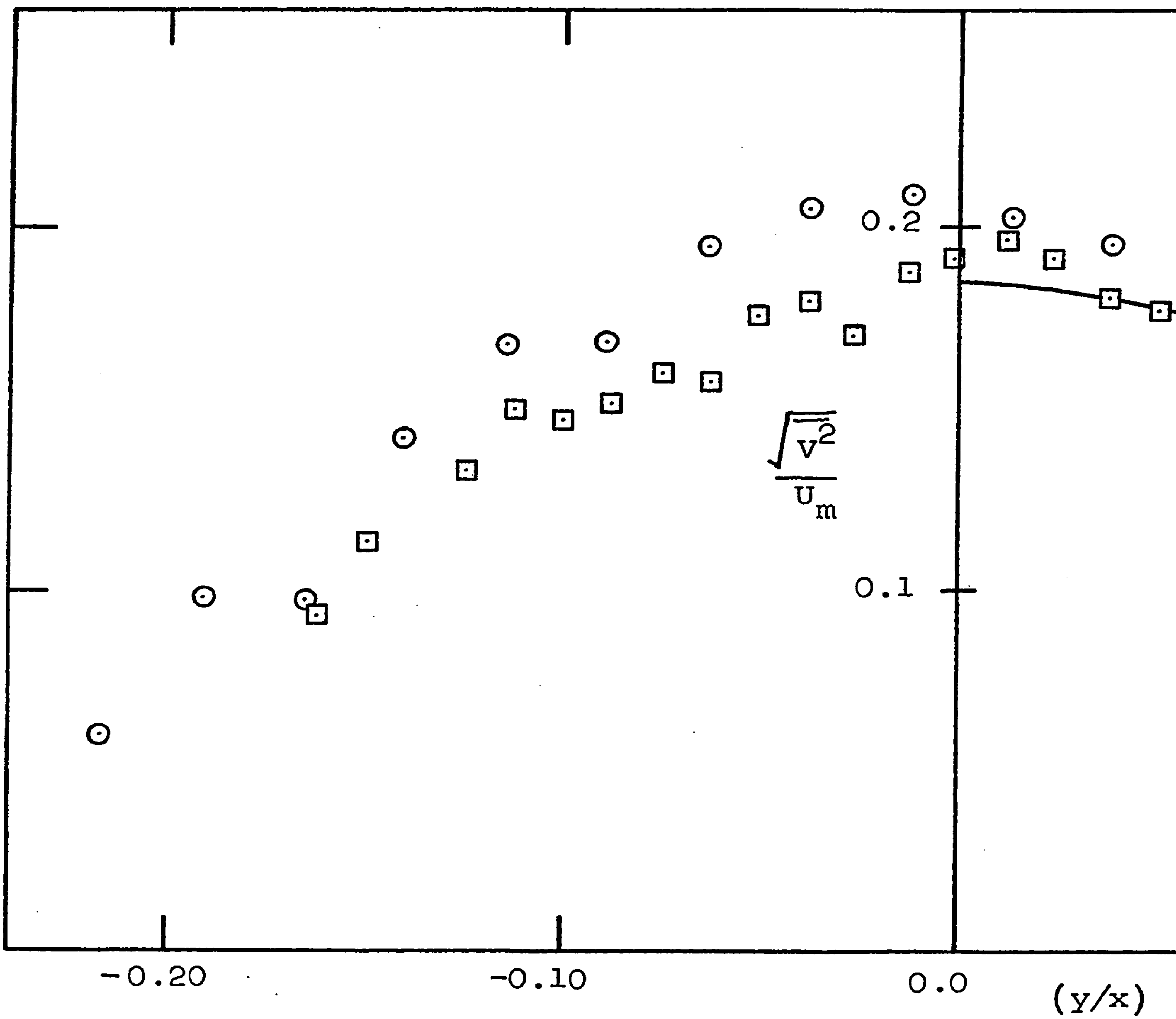

DISTRIBUTIONS OF LATERAL TURBULENT INTENSITY
THE PLANE JET IN STILL AIR $(U_j b)/\nu = 3.51 \times 10^4$

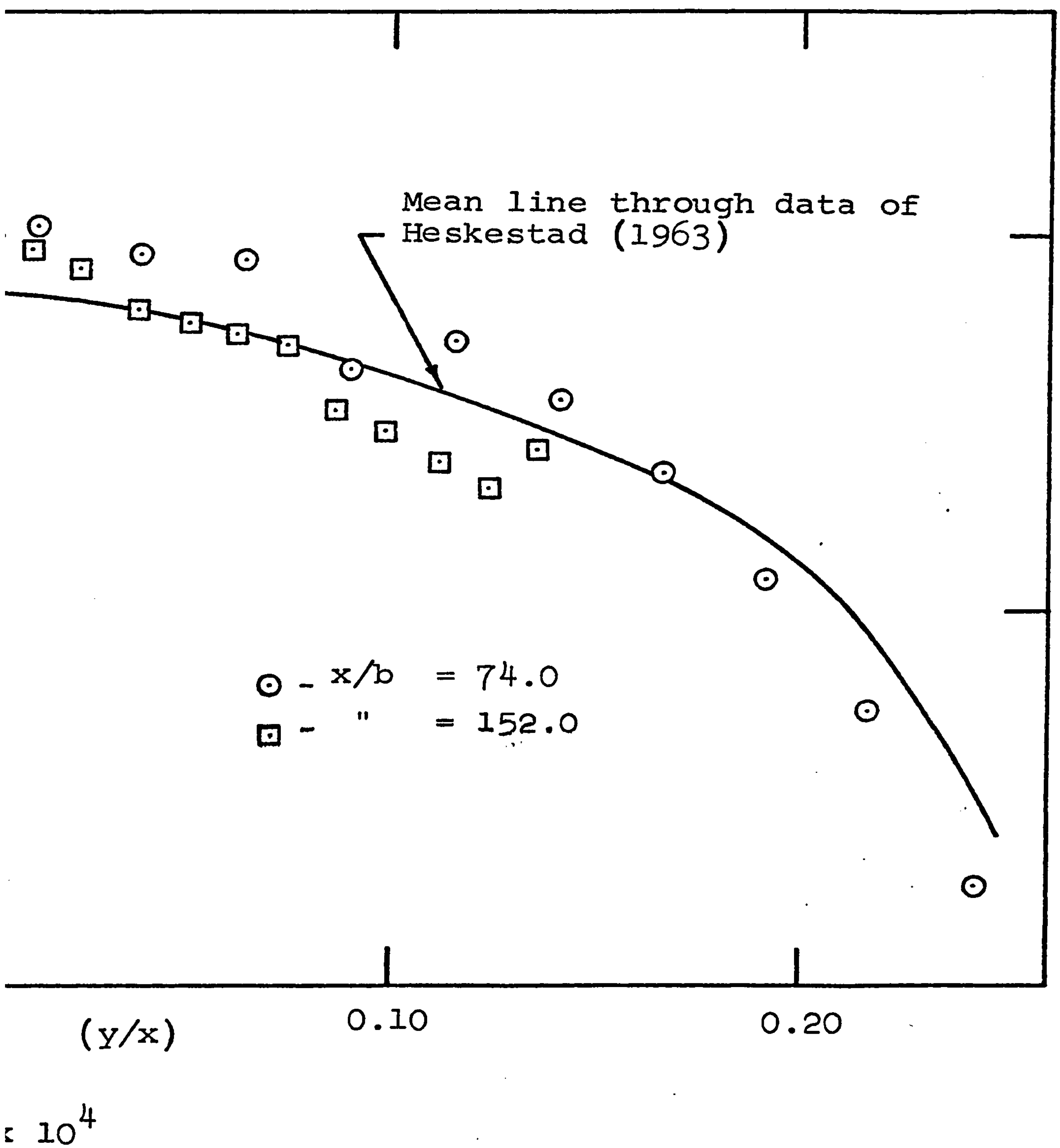
Mean line through data of Heskestad (1963)
⊙ - x/b = 74.0
⊡ - " = 152.0
(y/x)
0.10
0.20
x 10⁴

Fig. 16

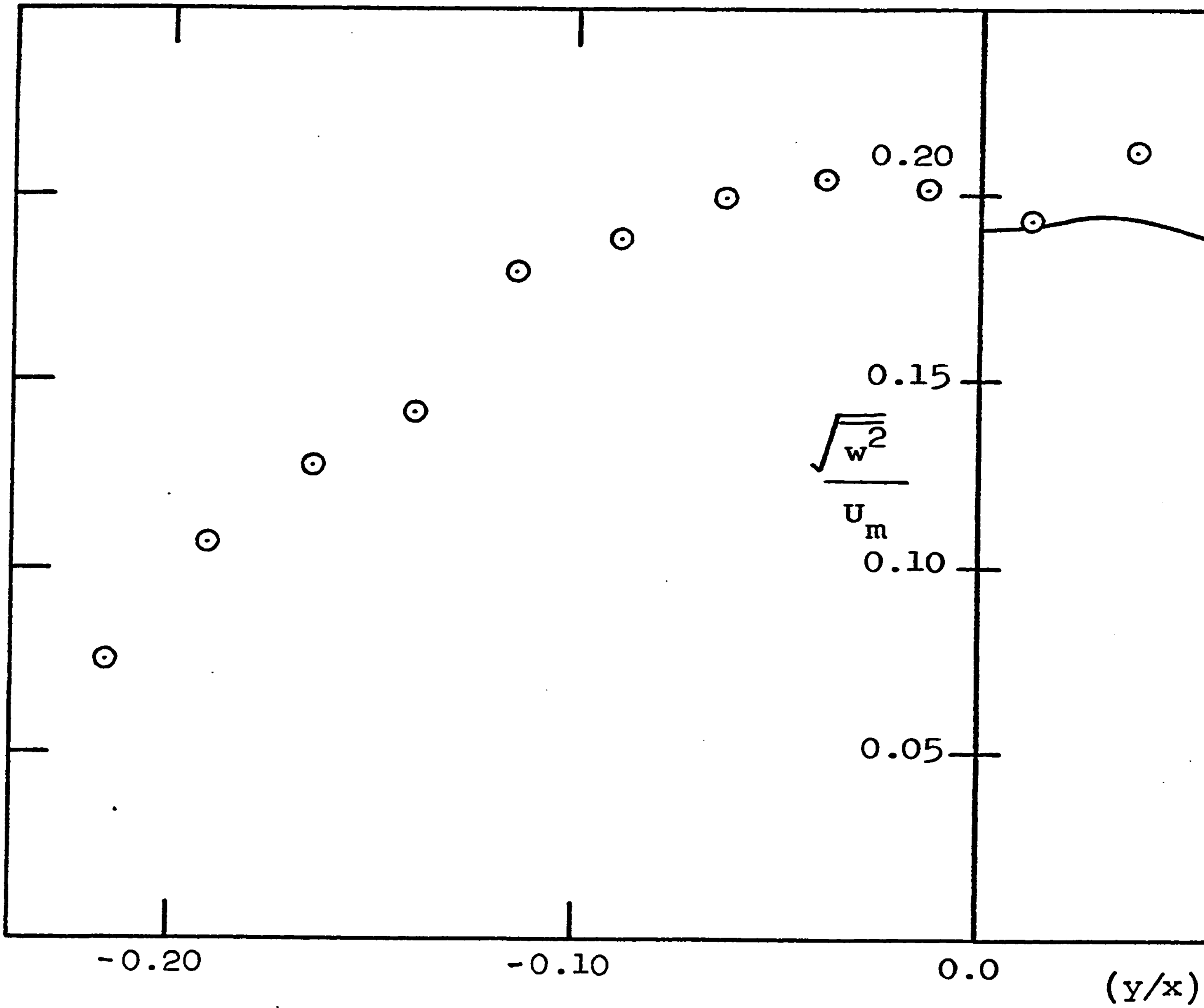

DISTRIBUTIONS OF TRANSVERSE TURBULENT INTENSITY THE PLANE JET IN STILL AIR $(U_j b)/\nu = 3.51 \times 10^4$

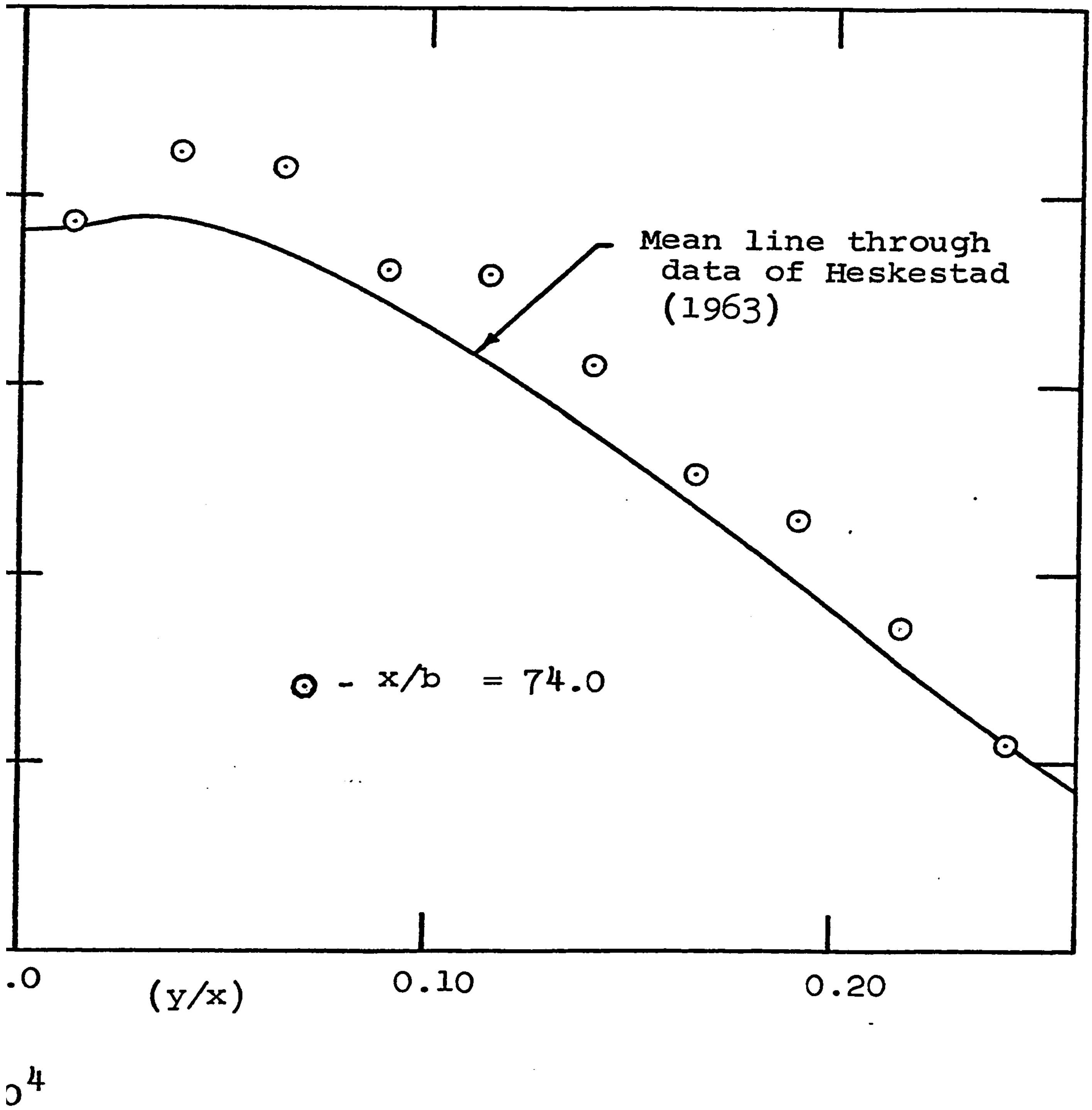

Fig. 17

COMPARISON OF THE MEASURED AND CALCULATED SHEAR STRESS DISTRIBUTIONS.

THE PLANE JET IN STILL AIR $(U_j b)/\nu = 3.51 \times 10^4$

(corrected for longitudinal cooling and high intensity effects)

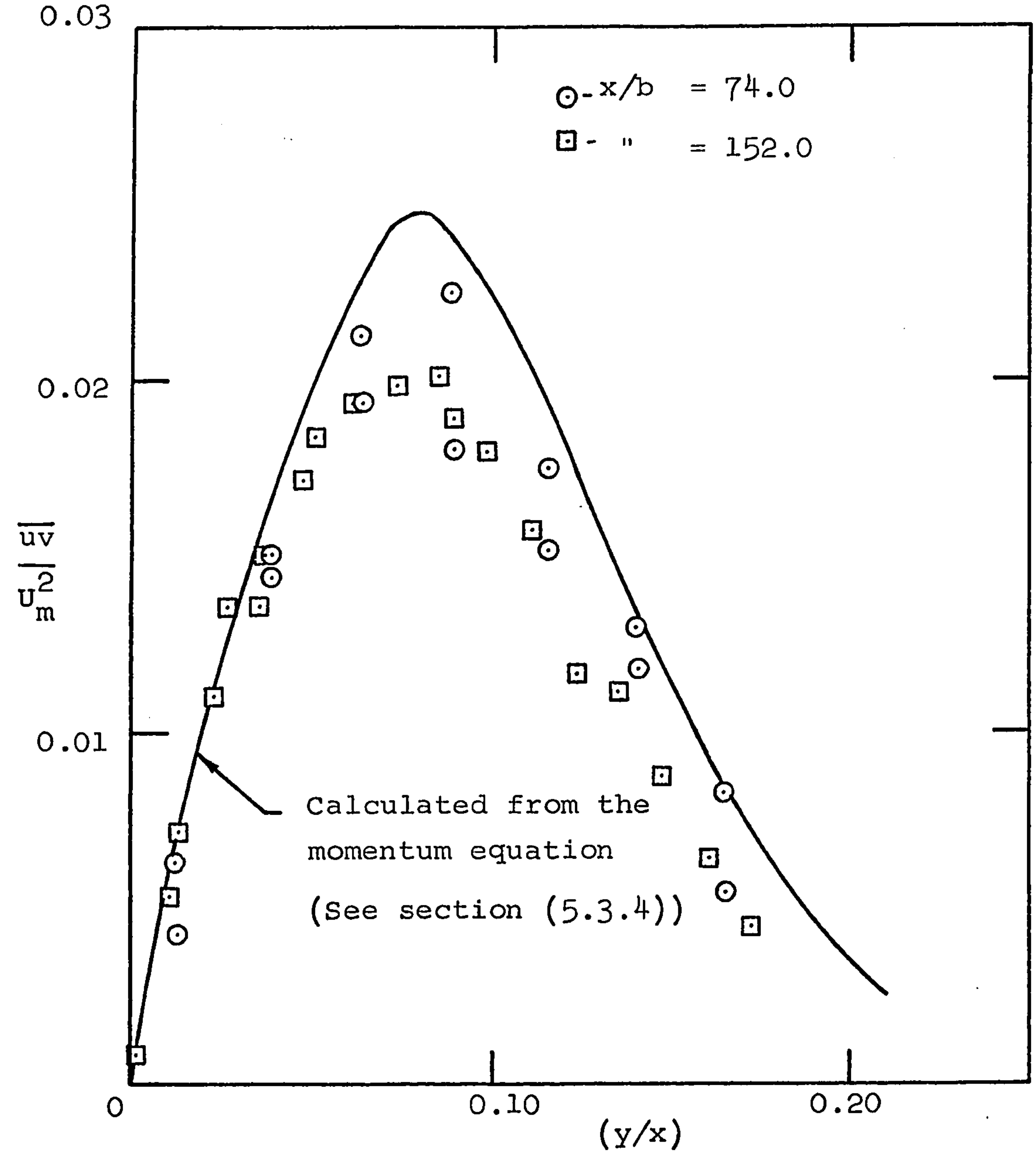

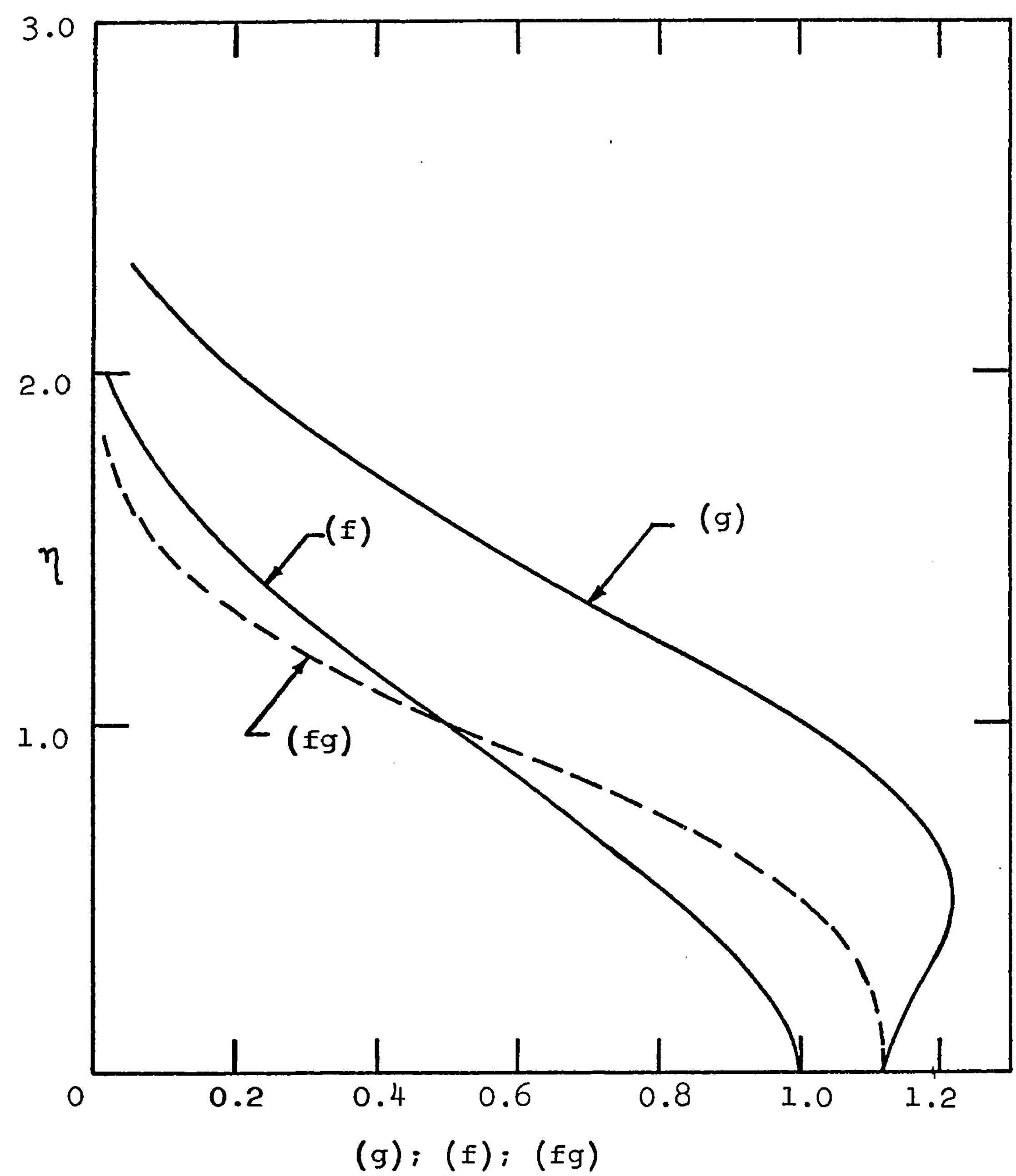

DISTRIBUTION FUNCTIONS FOR MEAN VELOCITY AND TURBULENCE ENERGY

THE PLANE JET IN STILL AIR (see section(2.2))

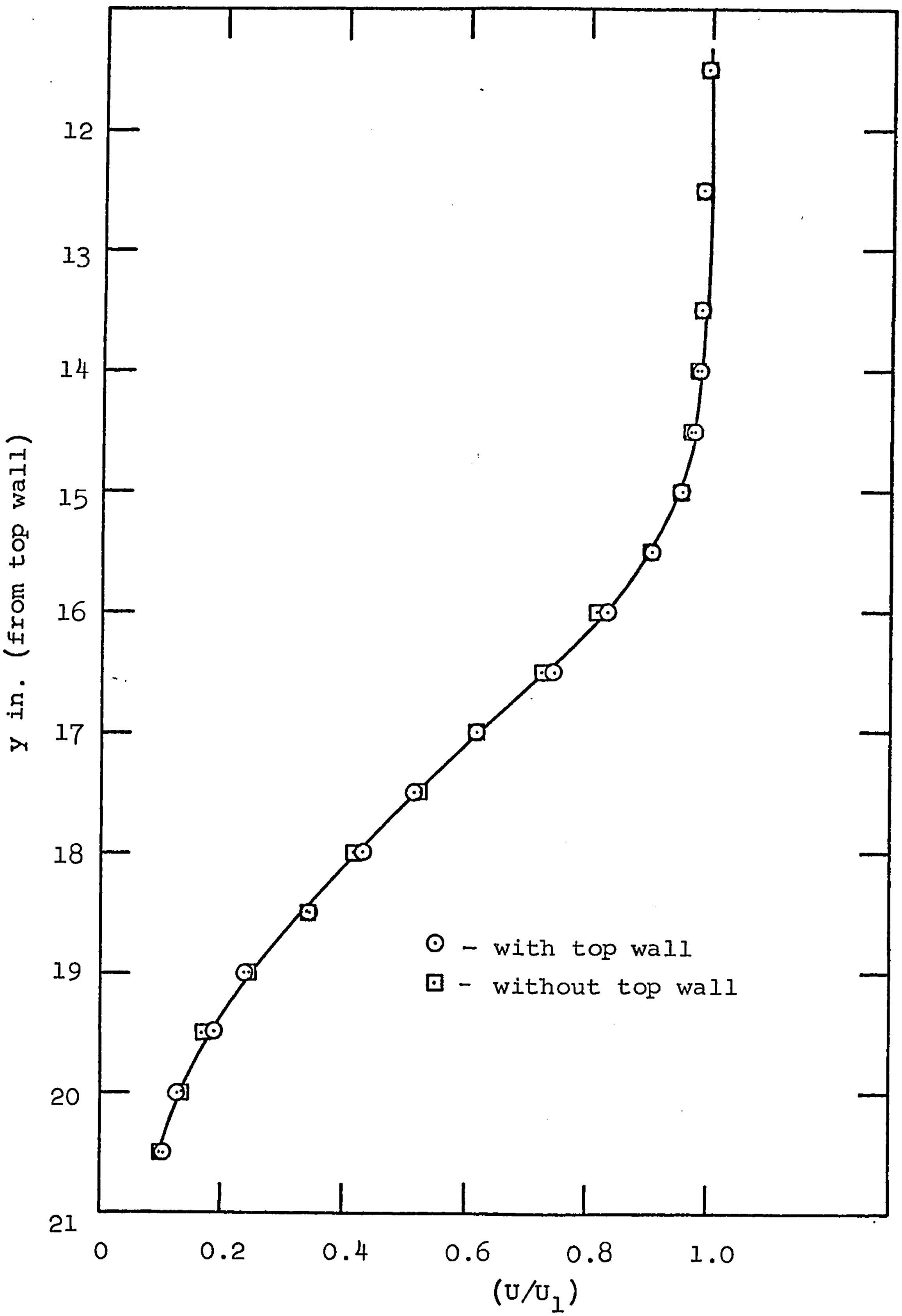

COMPARISON OF PLANE MIXING LAYERS WITH AND WITHOUT TOP WALL IN WORKING SECTION.

$x = 27.75$ in.; $U_1/\nu = 1.61 \times 10^5\ \mathrm{FT}^{-1}$; Free stream turbulence, $\left[\sqrt{\overline{u^2}}/U_1\right]_{x=0} = 0.56\%$

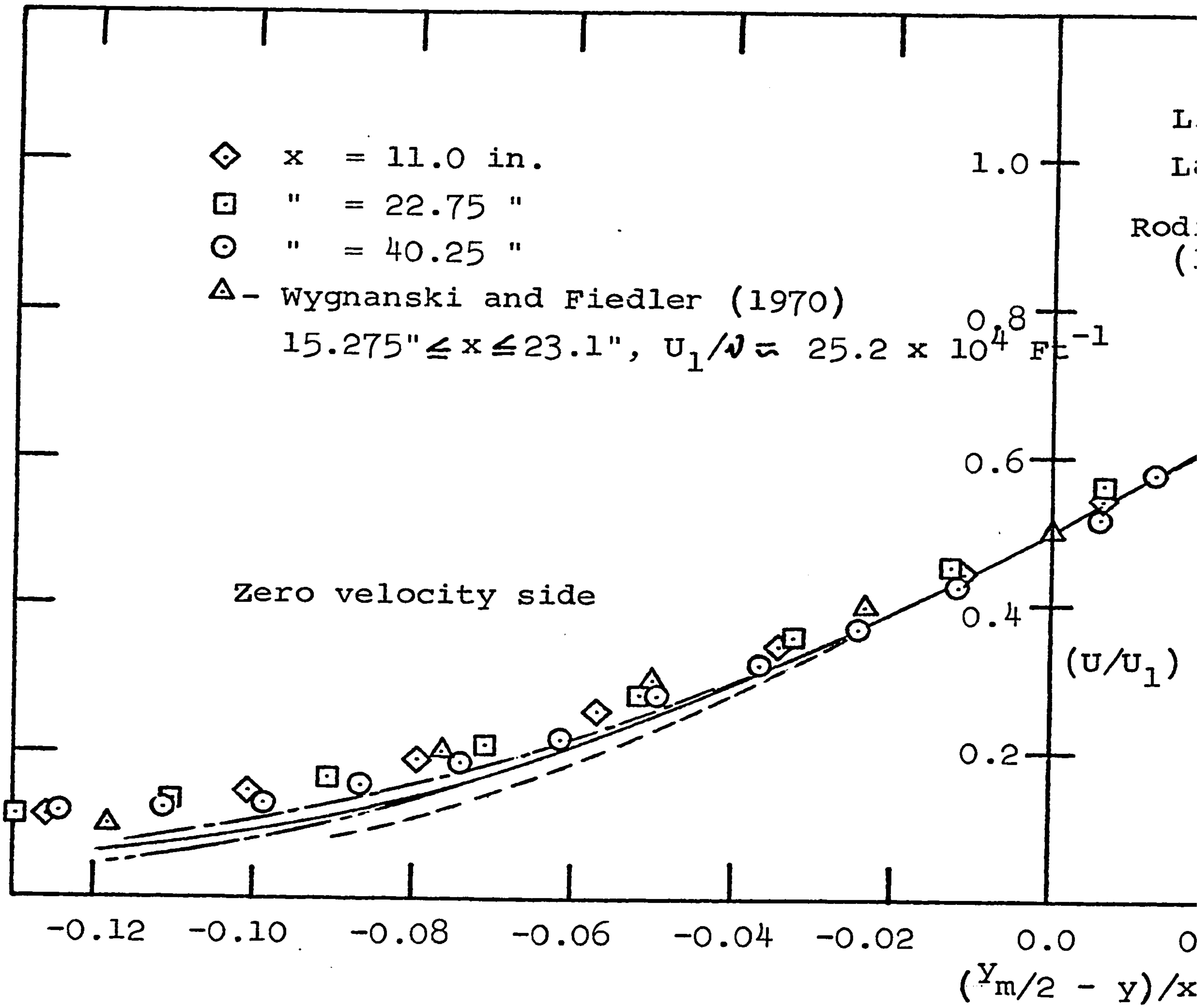

NON-DIMENSIONAL MEAN VELOCITY DISTRIBUTIONS ACROSS THE P

$U_1/\nu = 54.8 \times 10^4 \ Ft.^{-1}$

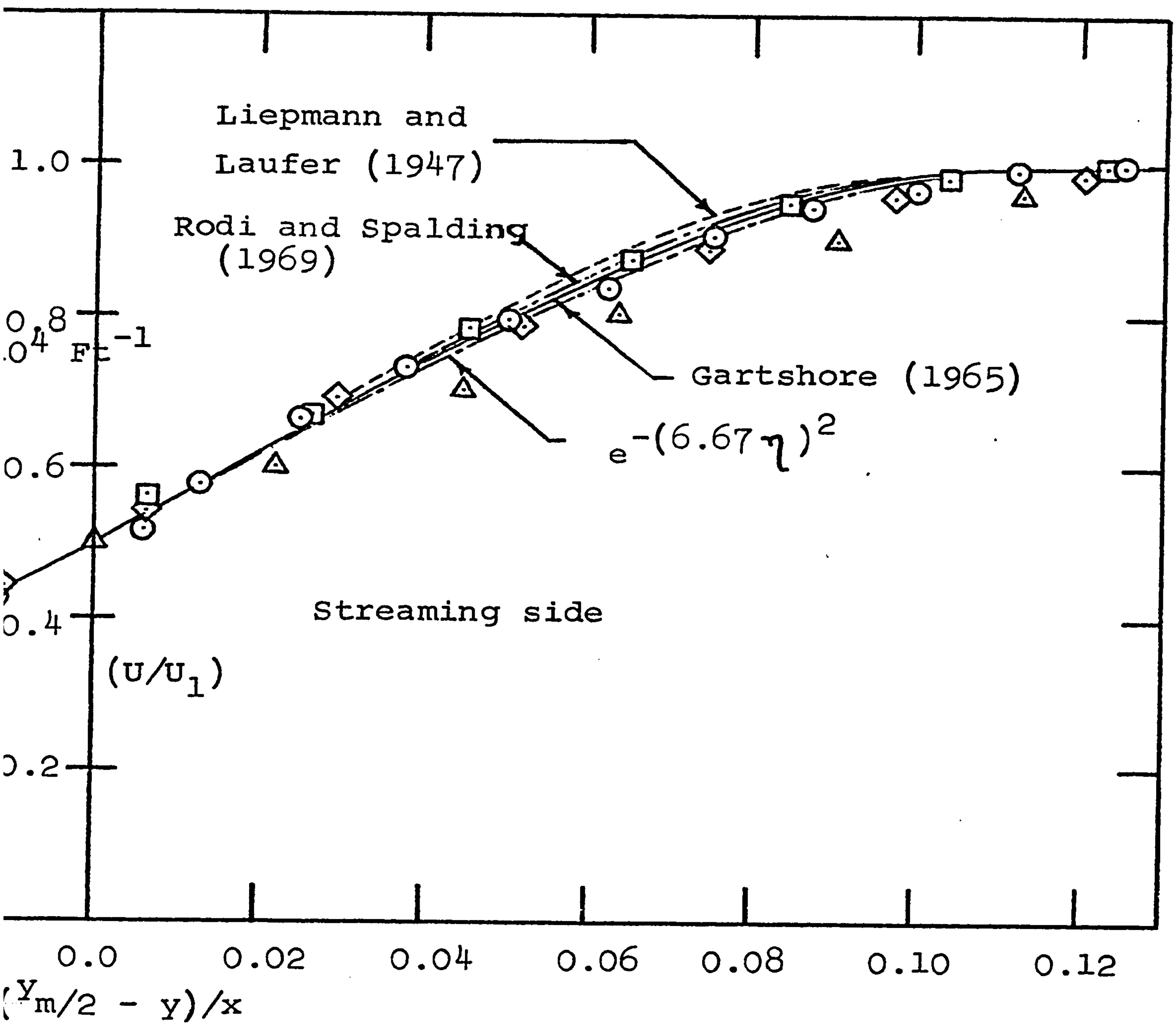

ACROSS THE PLANE MIXING LAYER

Fig. 21

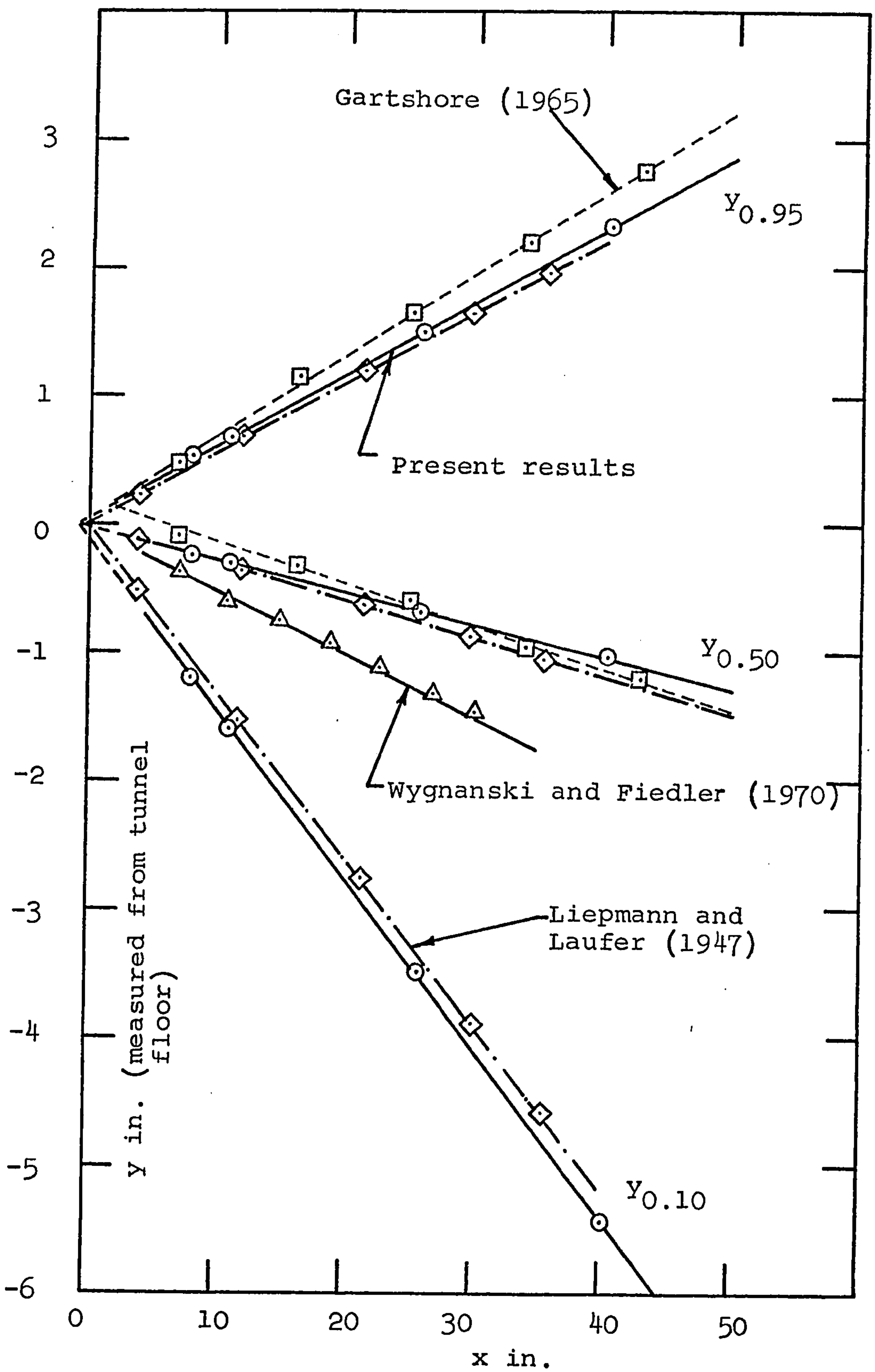

COMPARISON OF GROWTH FOR PLANE MIXING LAYERS

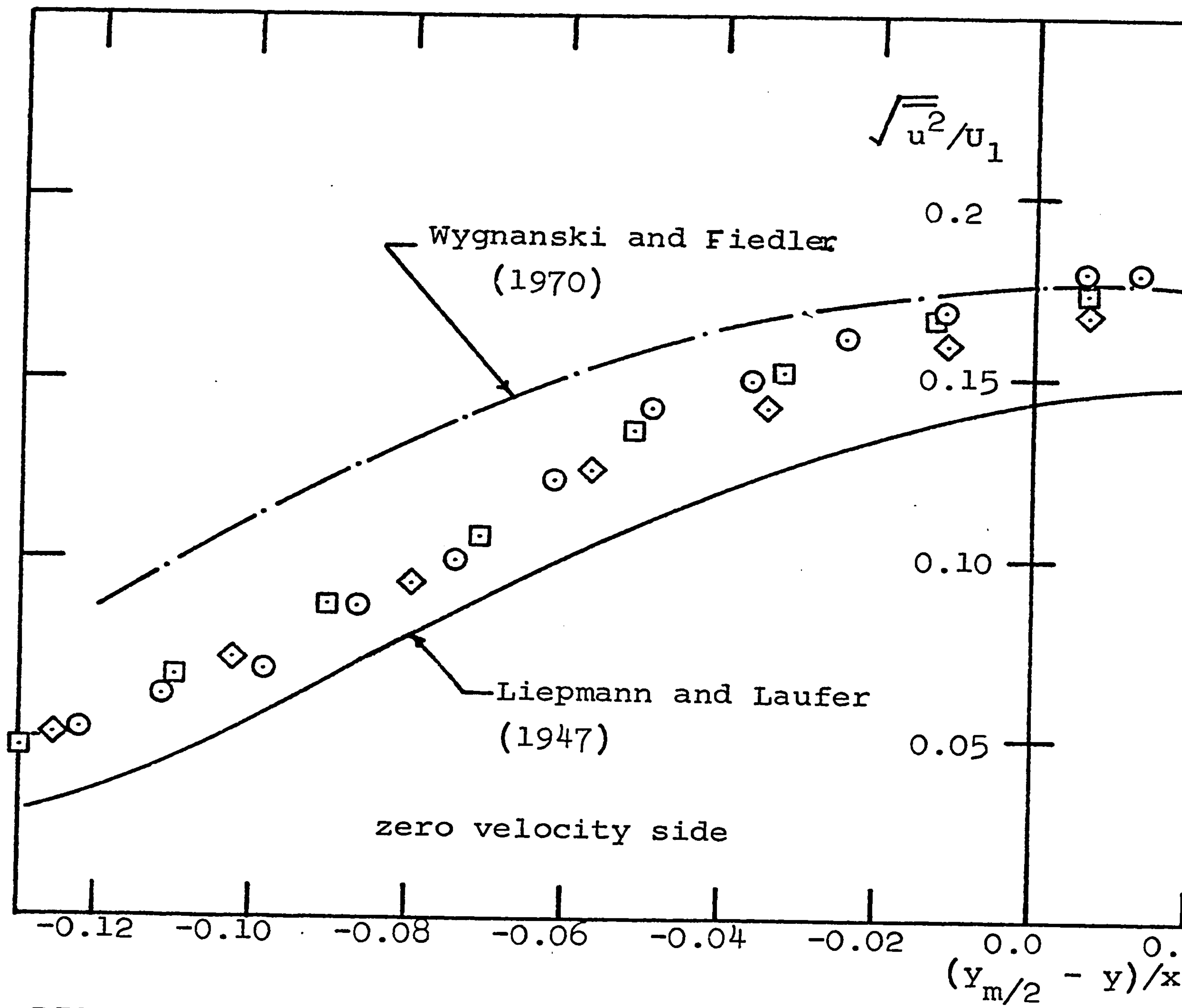

DISTRIBUTIONS OF LONGITUDINAL TURBULENT INTENSITY
THE PLANE MIXING LAYER $U_1/\nu = 54.8 \times 10^4$ Ft.$^{-1}$

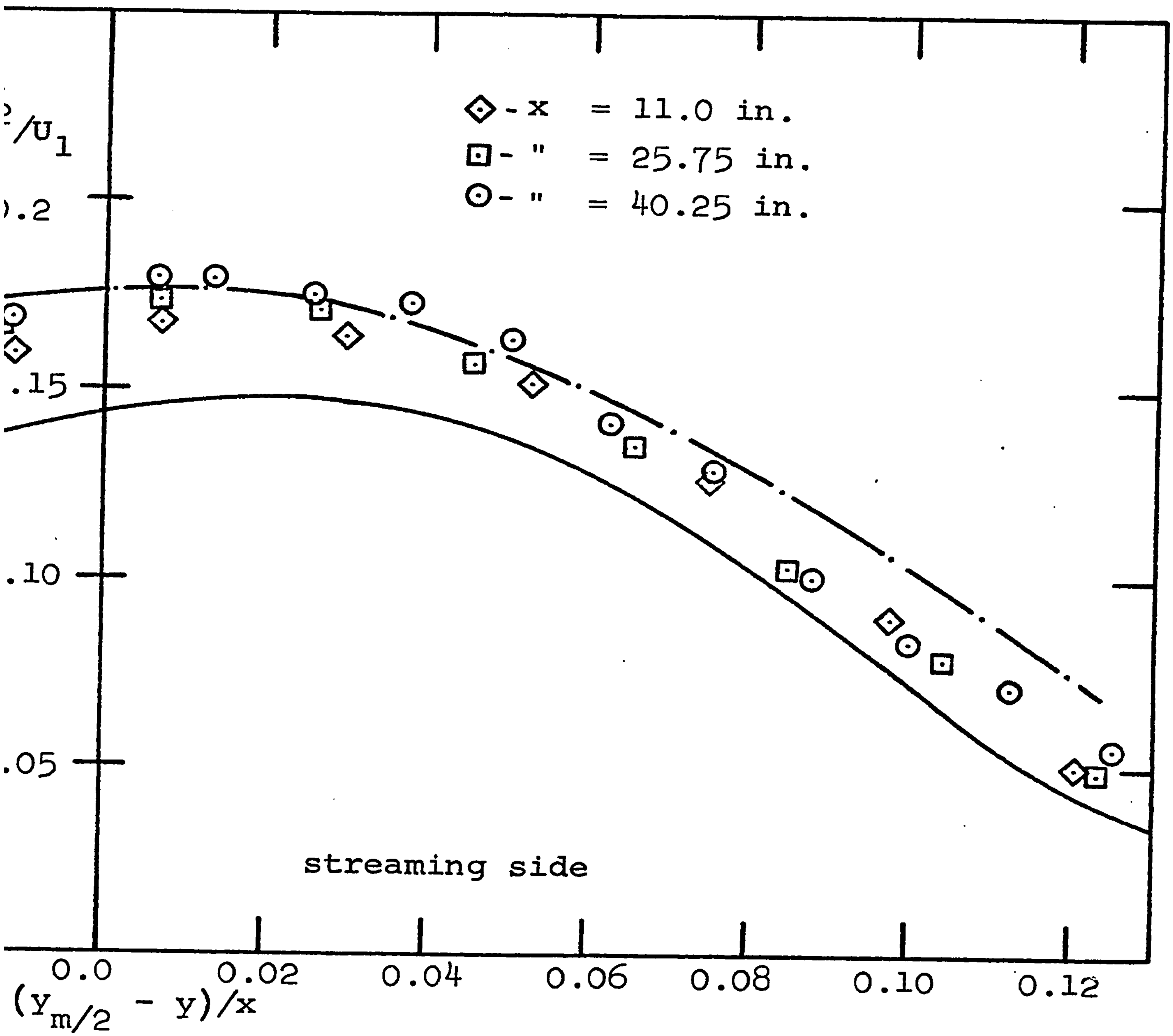

²/U₁
).2
.15
.10
.05
◇ - x = 11.0 in.
□ - " = 25.75 in.
⊙ - " = 40.25 in.
streaming side
0.0
0.02
0.04
0.06
0.08
0.10
0.12
(y_{m/2} - y)/x

ITY
-1

Fig.23

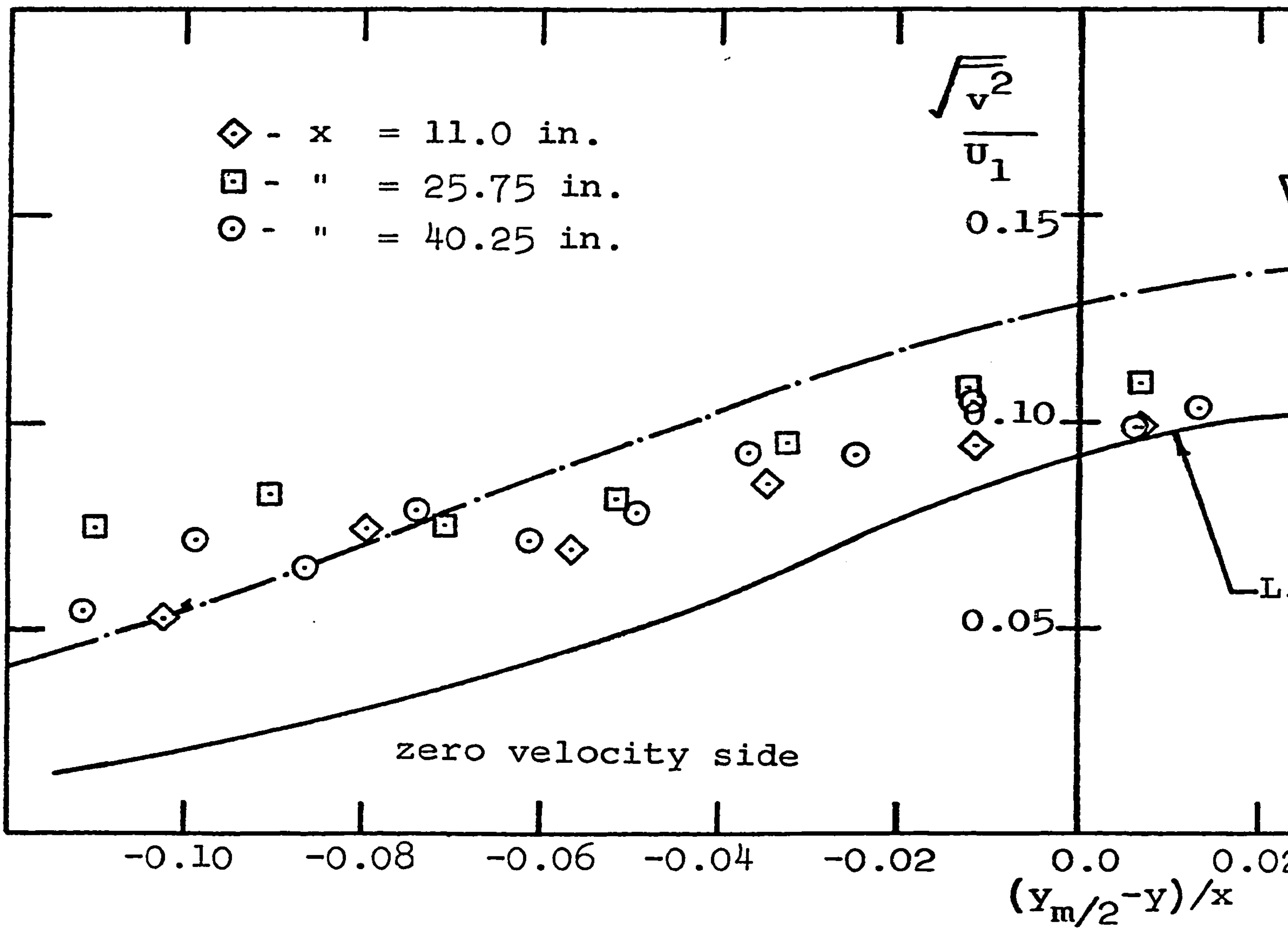

DISTRIBUTIONS OF LATERAL TURBULENT INTENSITY
THE PLANE MIXING LAYER

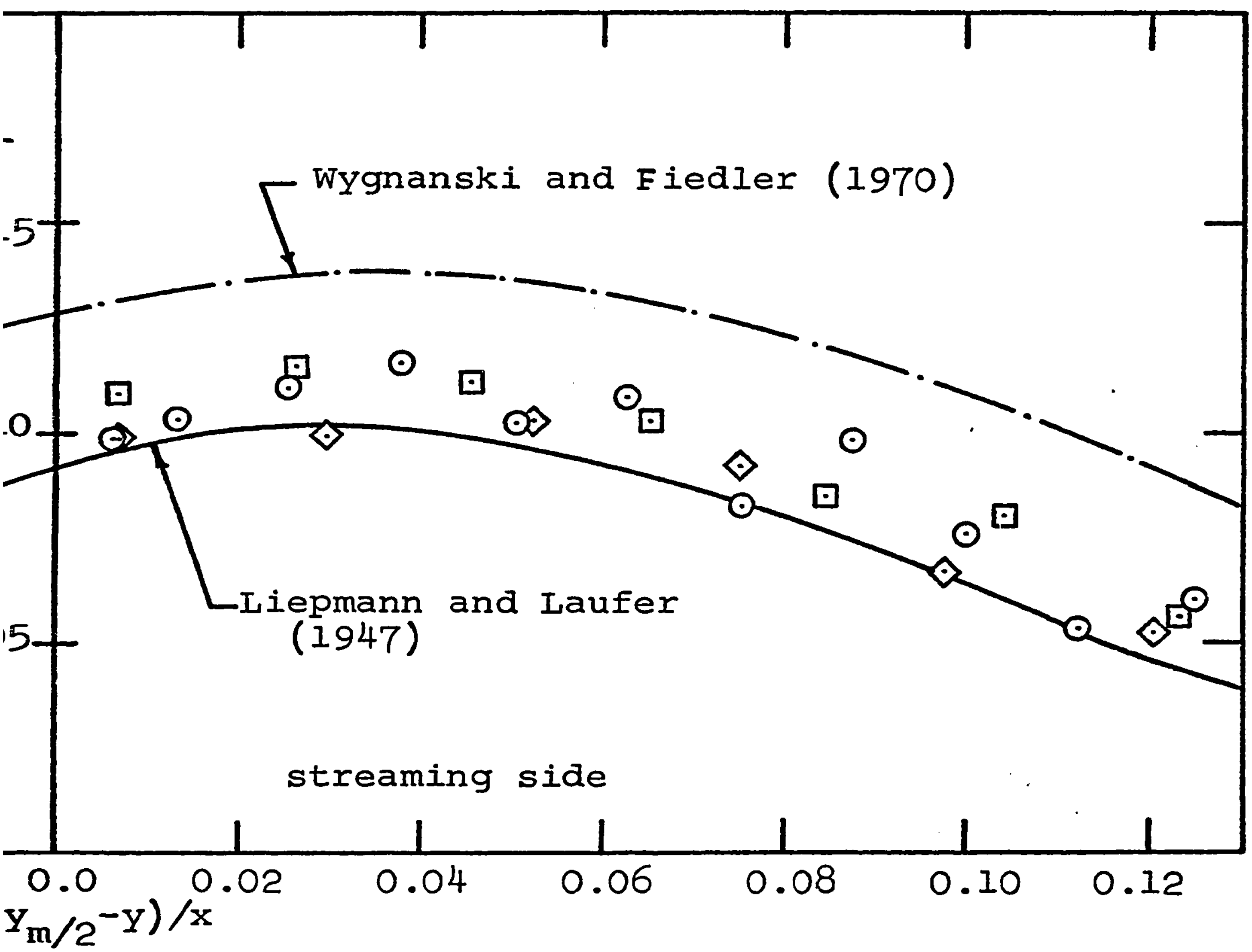

Wygnanski and Fiedler (1970)
Liepmann and Laufer (1947)
streaming side
.5
.0
5
0.0
0.02
0.04
0.06
0.08
0.10
0.12
Ym/2-Y)/x

TY

Fig. 24

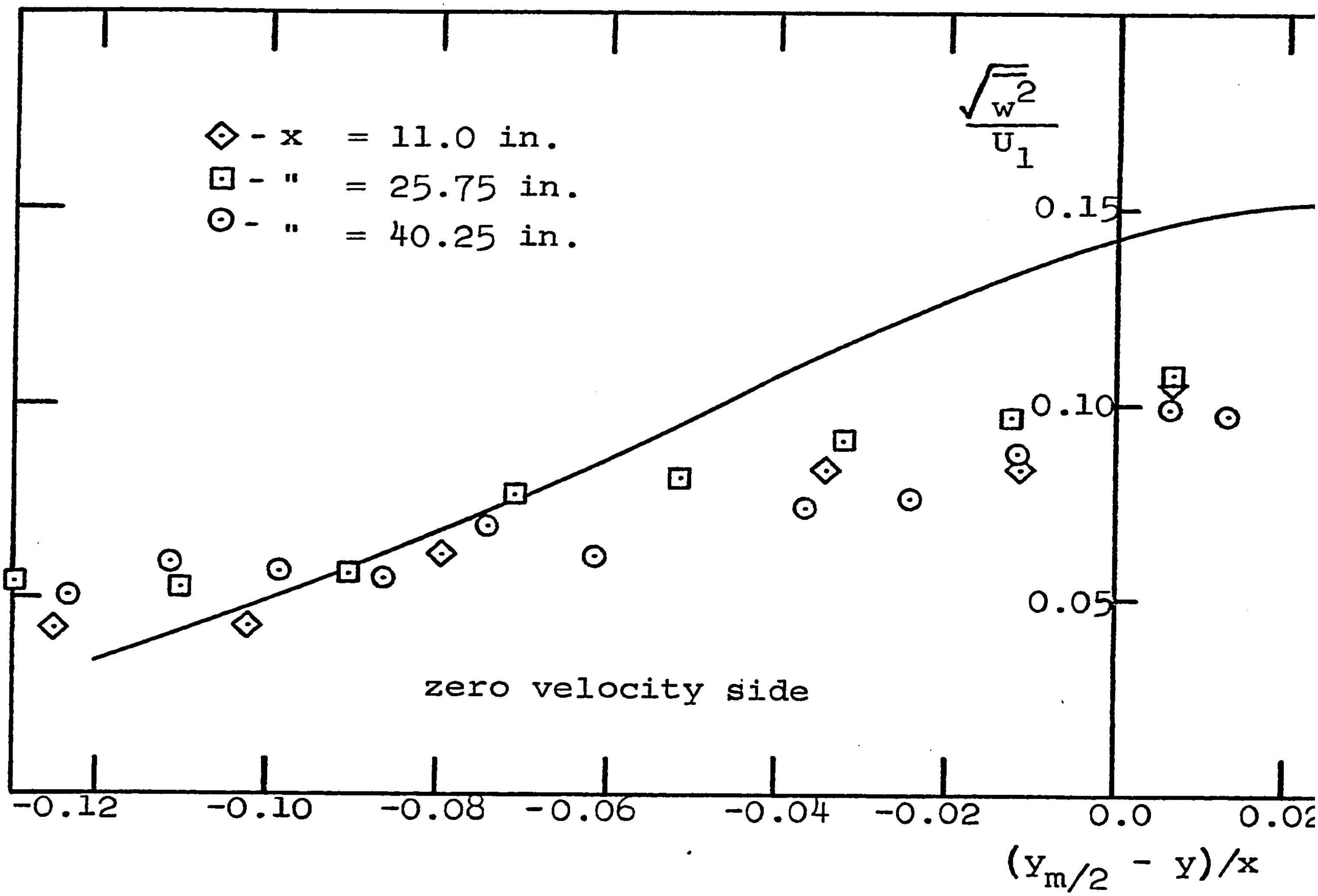

<u>DISTRIBUTIONS OF TRANSVERSE TURBULENT INTENSITY</u>
<u>THE PLANE MIXING LAYER $U_1/\nu = 54.8 \times 10^4$ Ft.$^{-1}$</u>

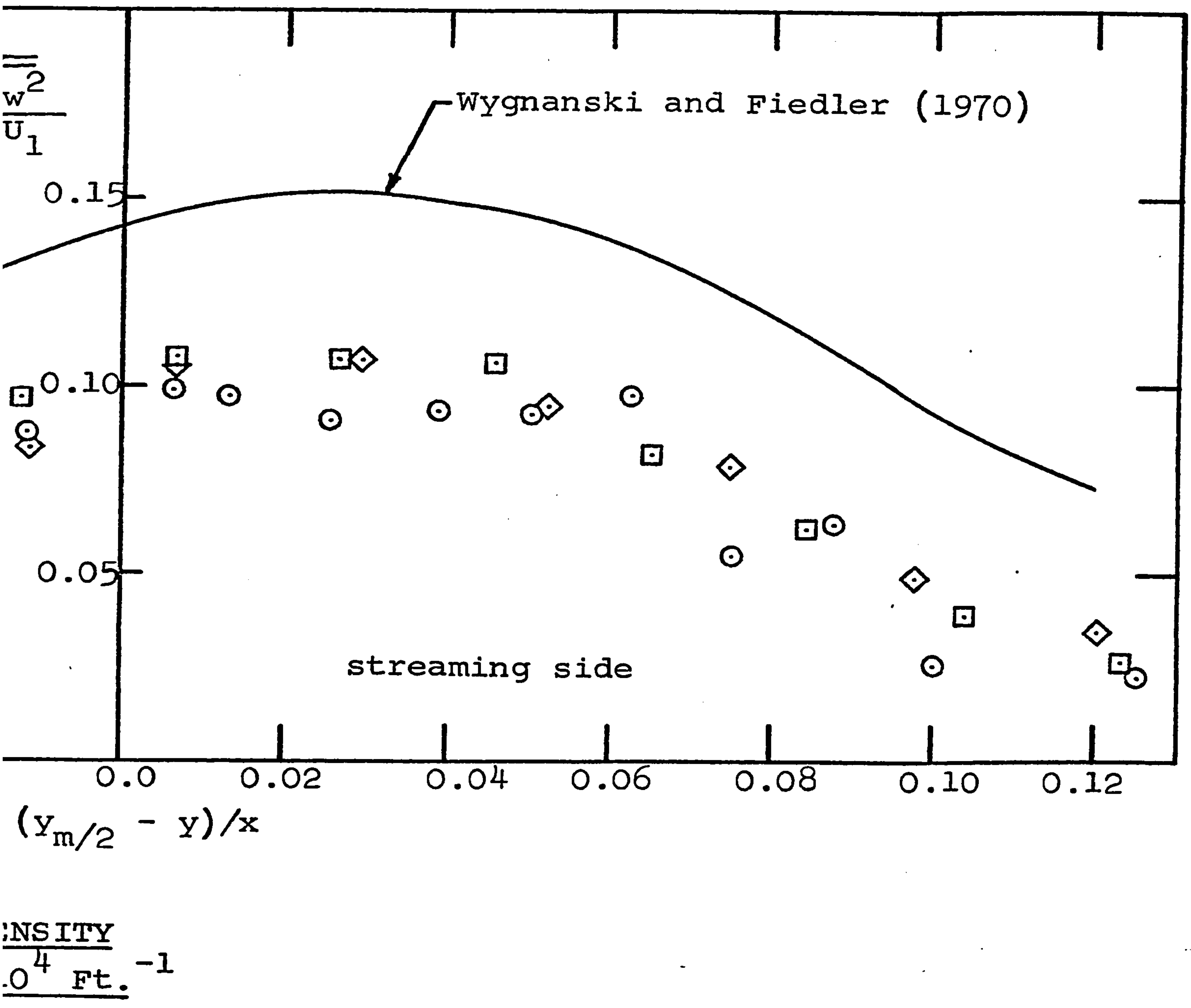

$\overline{w^2}$ / U_1
Wygnanski and Fiedler (1970)
0.15
0.10
0.05
streaming side
0.0
0.02
0.04
0.06
0.08
0.10
0.12
$(y_{m/2} - y)/x$
:NSITY
.0^4 Ft.$^{-1}$

Fig. 25

COMPARISON OF THE MEASURED AND CALCULATED SHEAR STRES
THE PLANE MIXING LAYER $U_1/\nu = 54.8 \times 10^4$ Ft.$^{-1}$

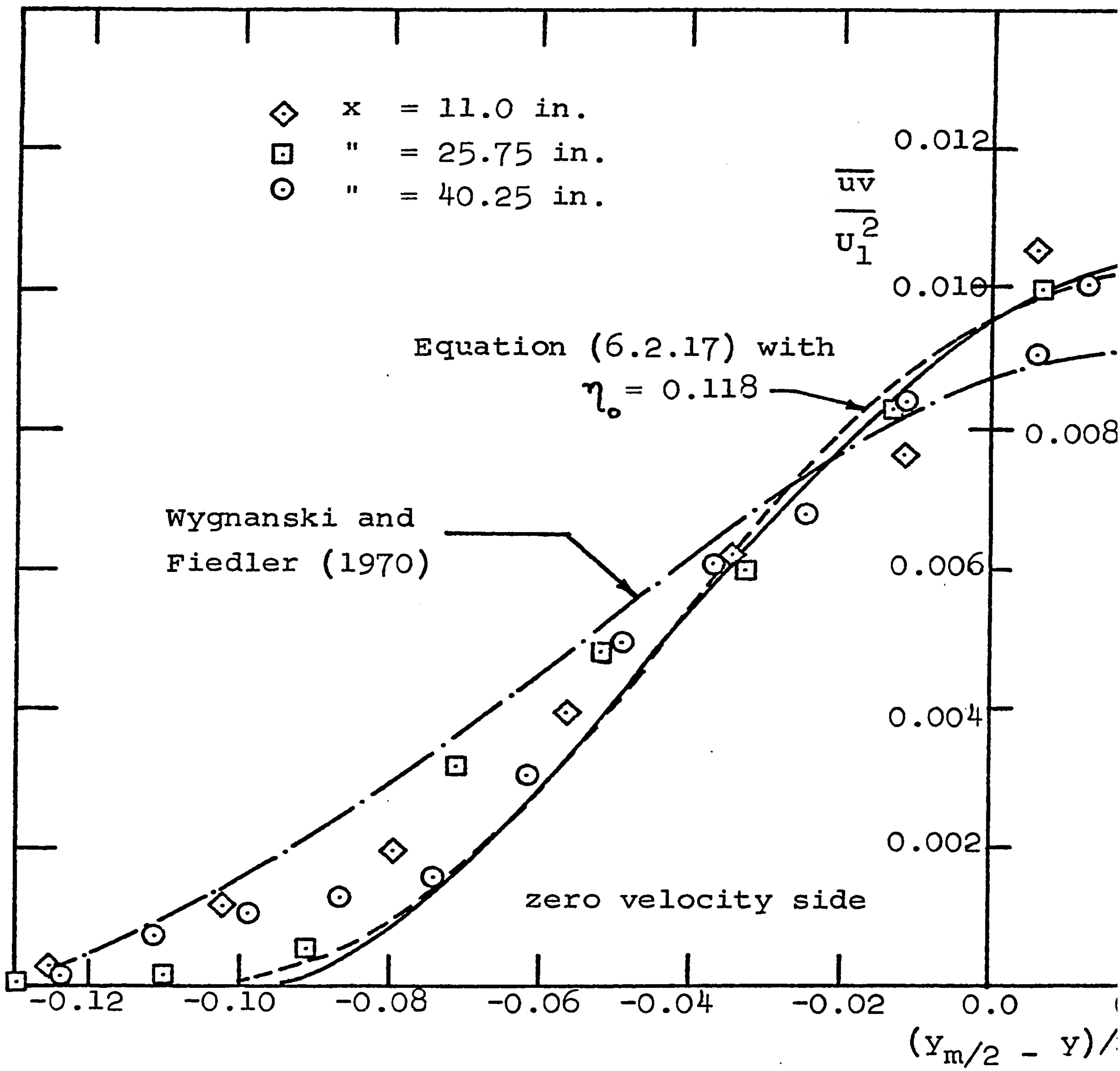

SHEAR STRESS DISTRIBUTIONS

10^{4} Ft.$^{-1}$

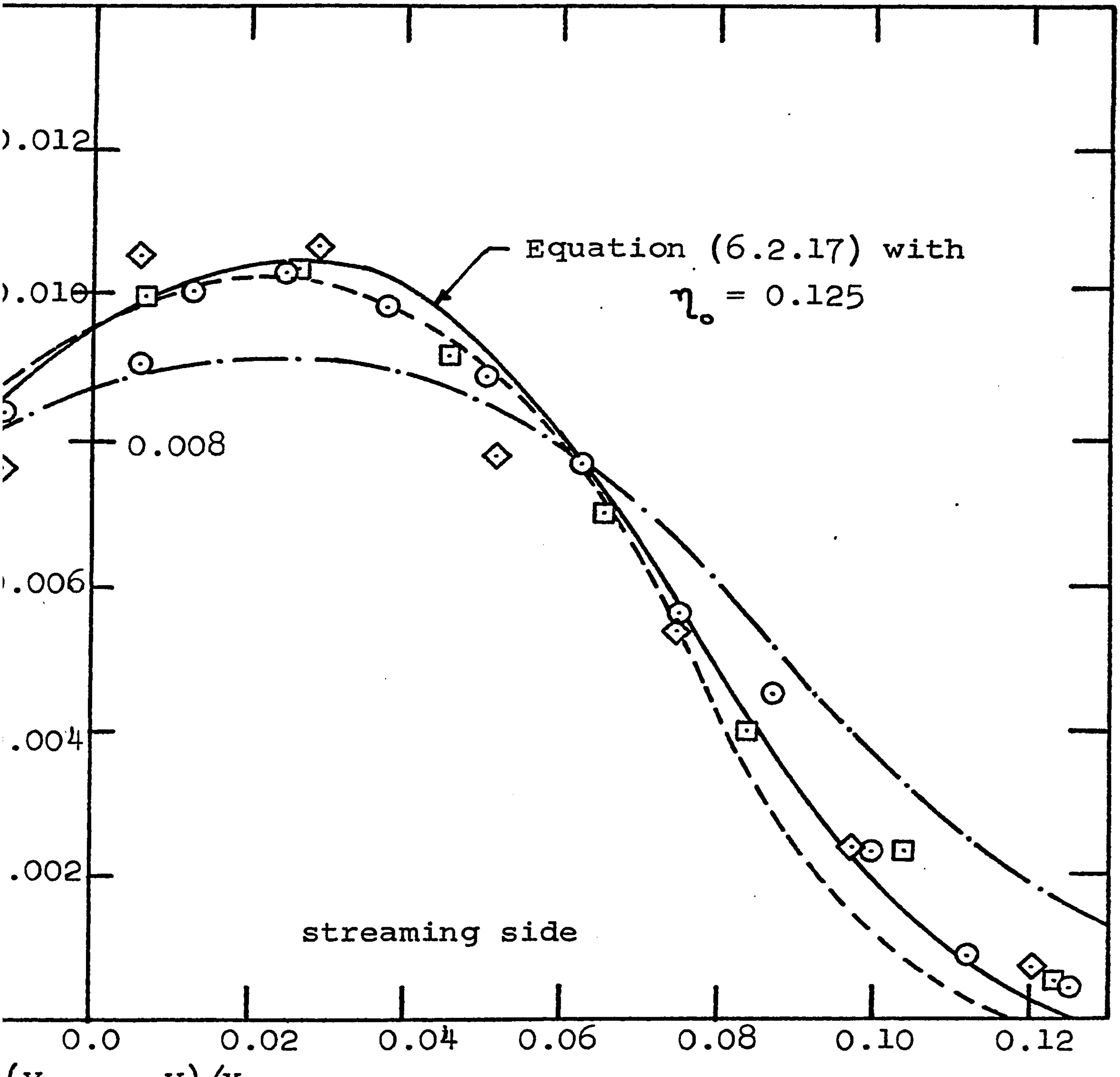

Fig. 26

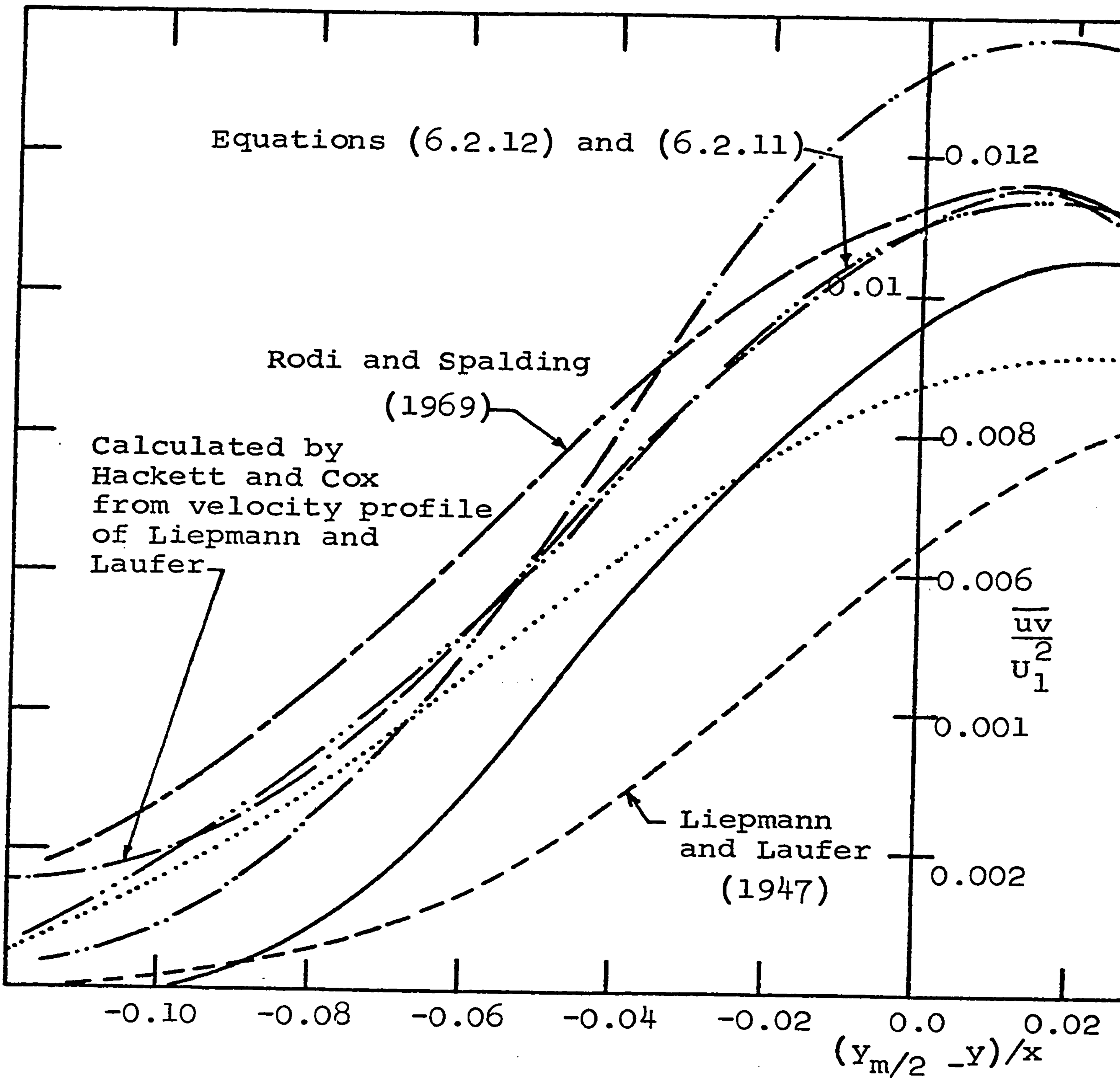

COMPARISON OF CALCULATED $\overline{uv}/U_1^2$ FROM NON-DIMENSIONAL MEA
THE PLANE MIXING LAYER

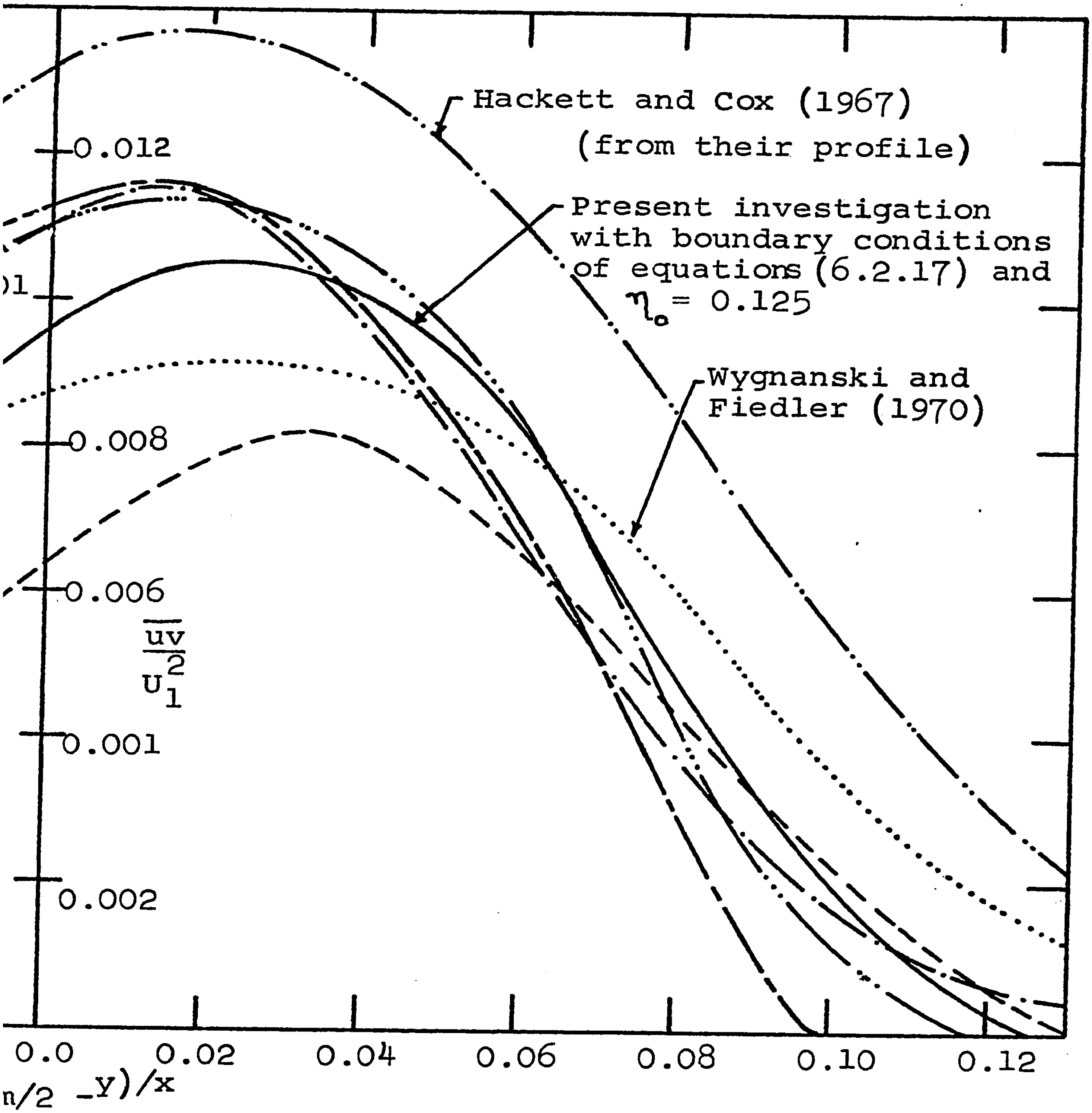

ÆNSIONAL MEAN VELOCITY PROFILES

Fig. 27

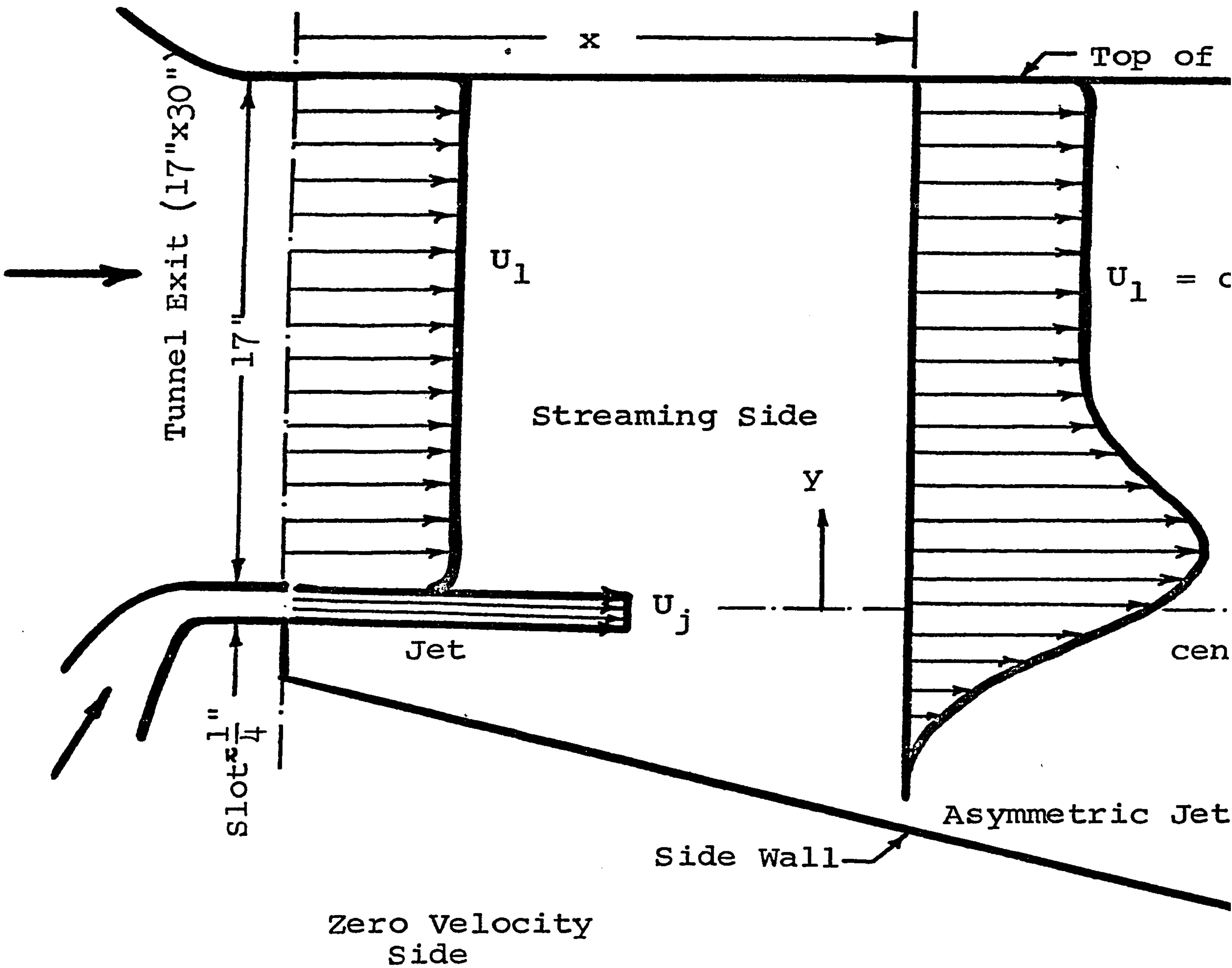

DEFINITION SKETCH OF THE A

(see also Fig.

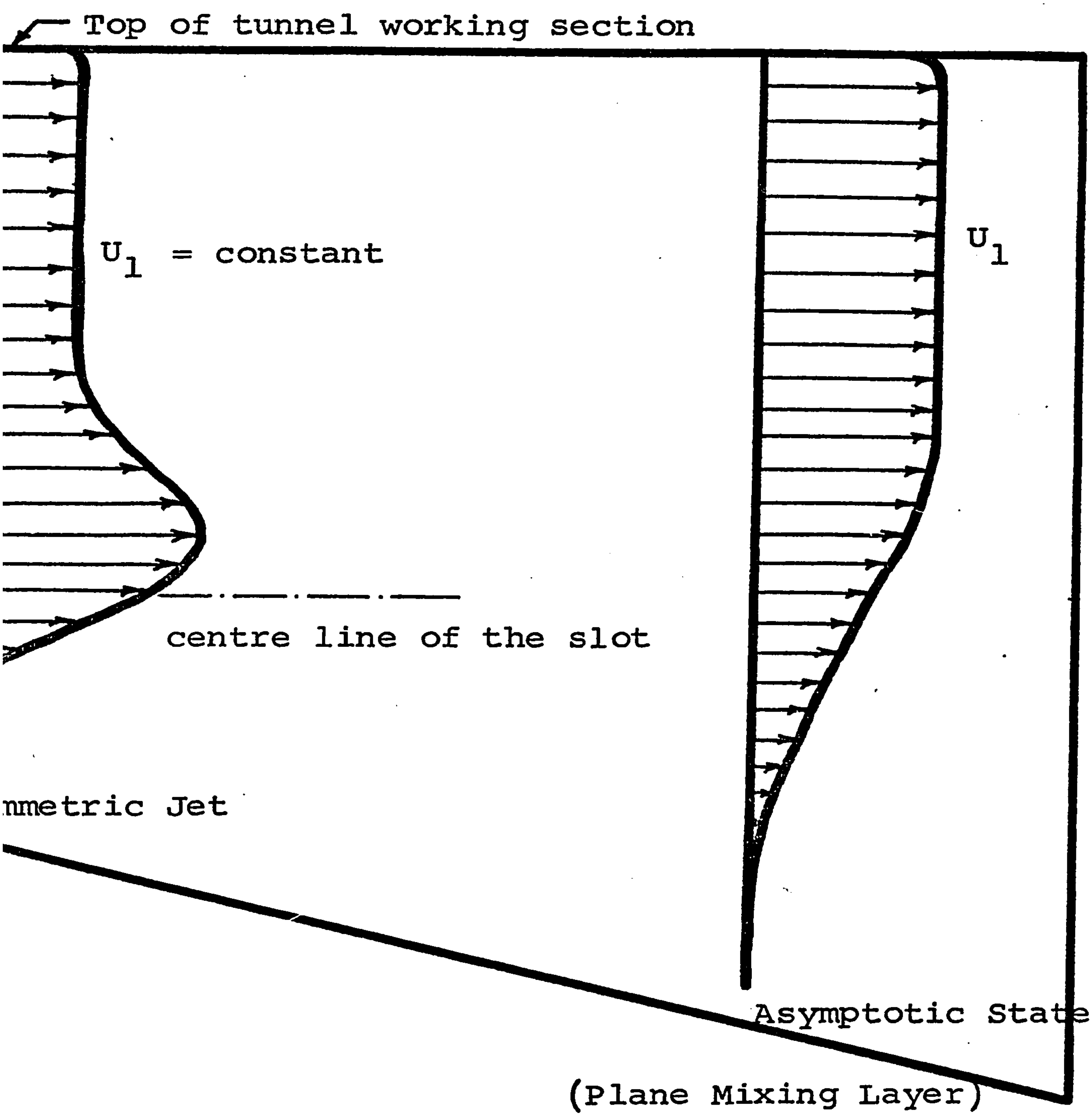

Fig. 28

:H OF THE ASYMMETRIC JET

also Fig. 4)

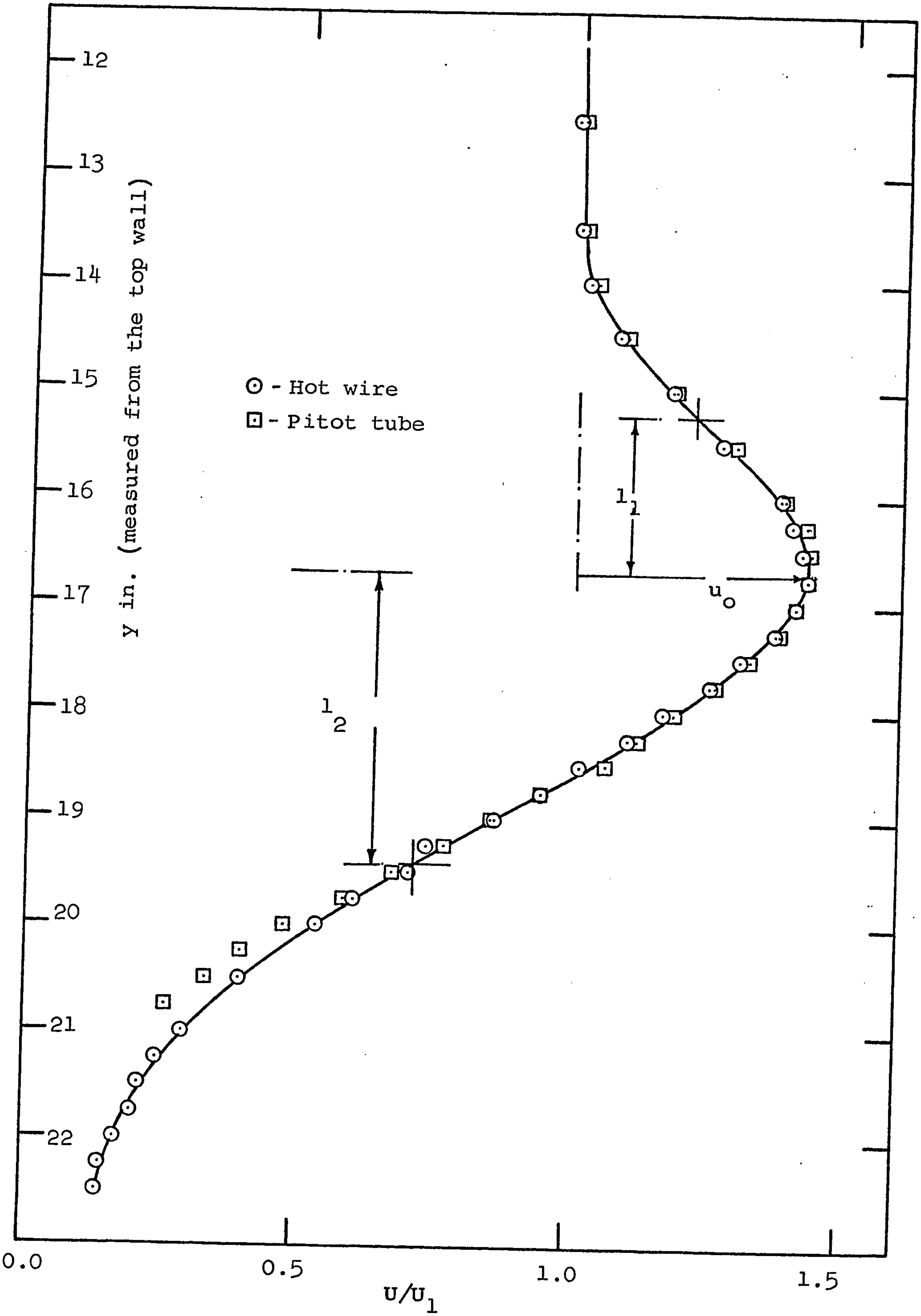

COMPARISON OF PITOT AND LINEARIZED NORMAL HOT-WIRE TRAVERSES. THE ASYMMETRIC JET. $x = 26.75$ in.; $U_j/U_1 = 5.08$

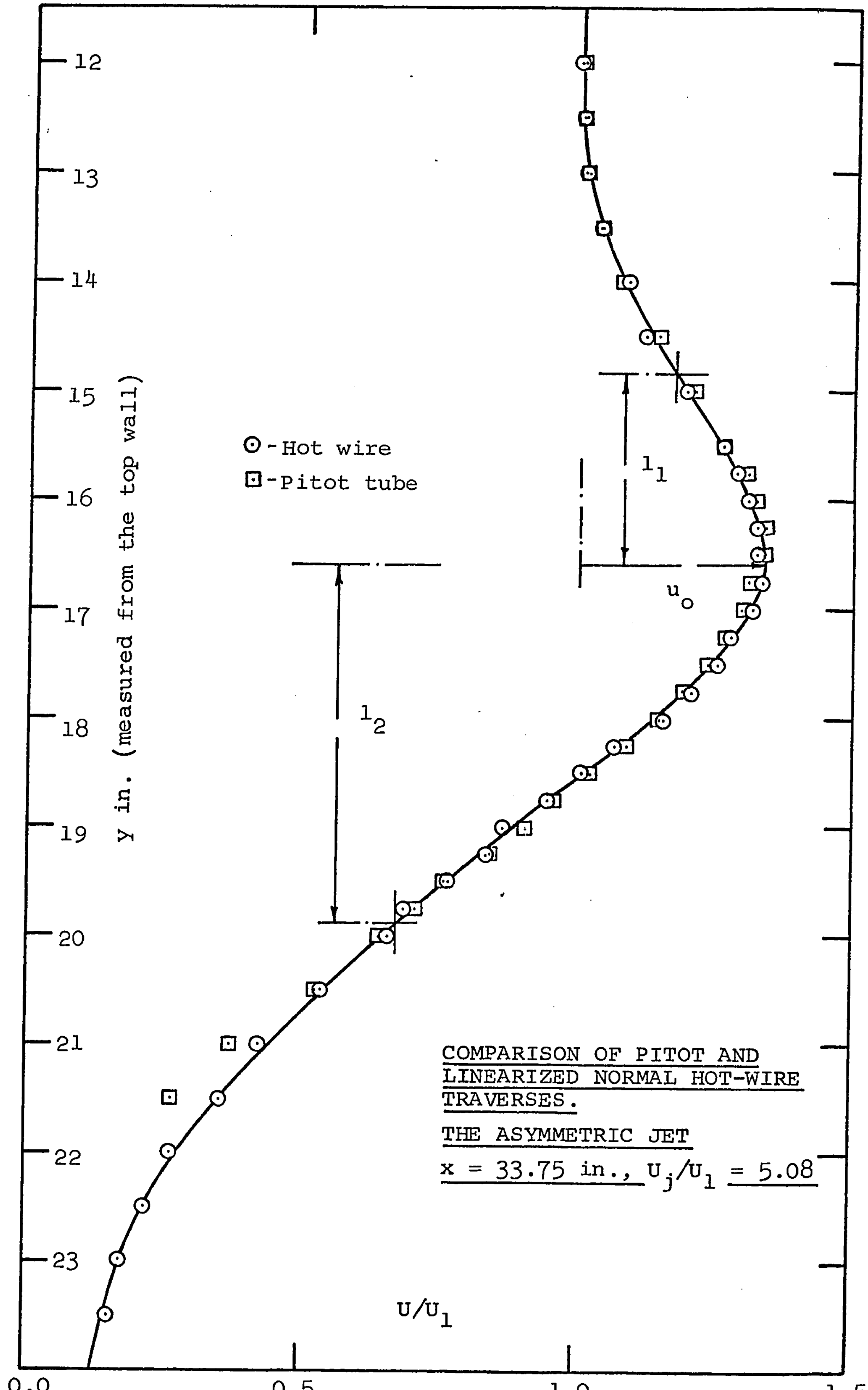

COMPARISON OF PITOT AND LINEARIZED NORMAL HOT-WIRE TRAVERSES.

THE ASYMMETRIC JET

$x = 33.75$ in., $U_j/U_1 = 5.08$

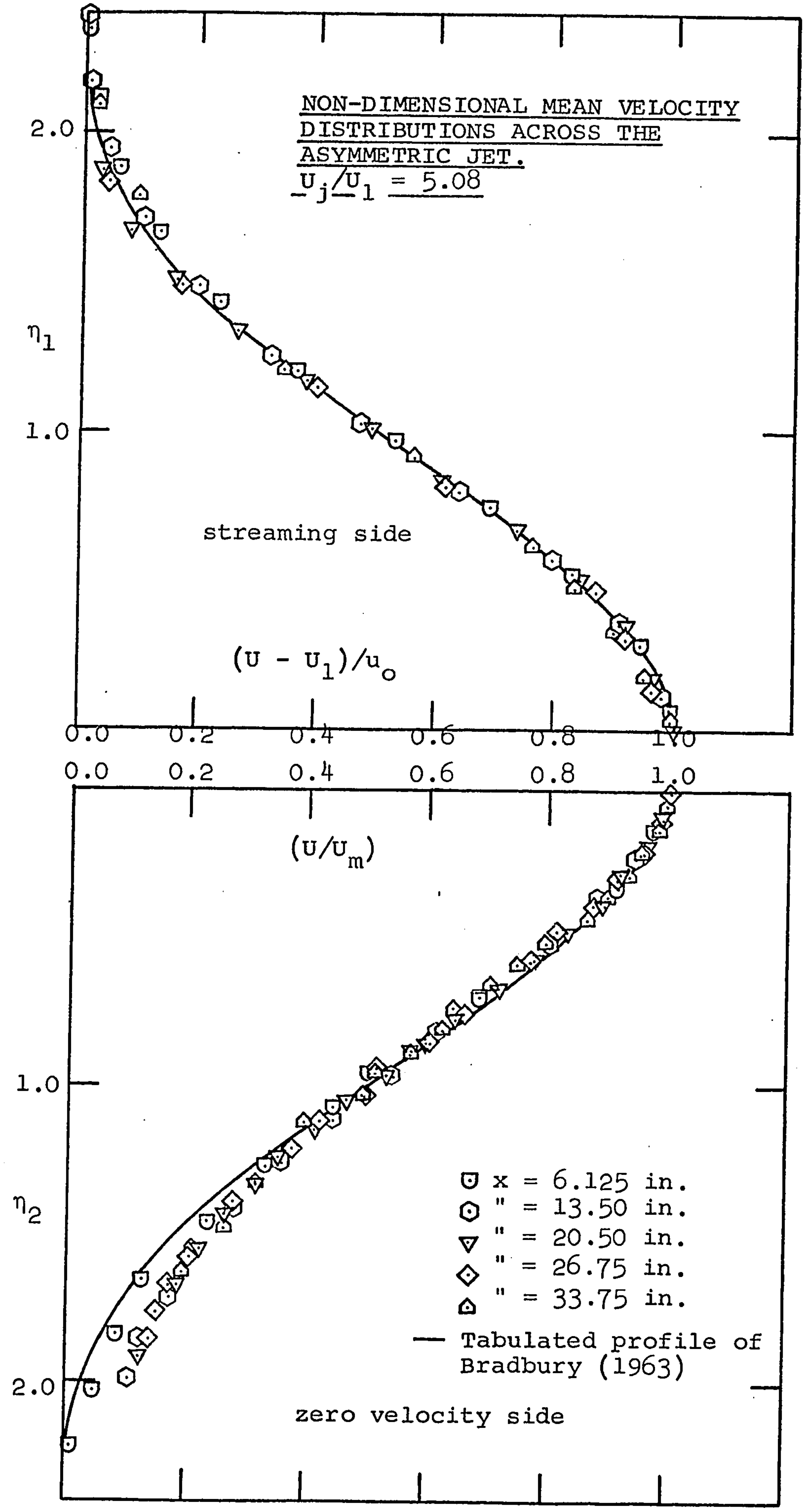
NON-DIMENSIONAL MEAN VELOCITY DISTRIBUTIONS ACROSS THE ASYMMETRIC JET.
$U_j/U_1 = 5.08$
streaming side
η_1
$(U - U_1)/u_o$
2.0
1.0
0.0
0.2
0.4
0.6
0.8
1.0
(U/U_m)
η_2
zero velocity side
x = 6.125 in.
" = 13.50 in.
" = 20.50 in.
" = 26.75 in.
" = 33.75 in.
Tabulated profile of Bradbury (1963)

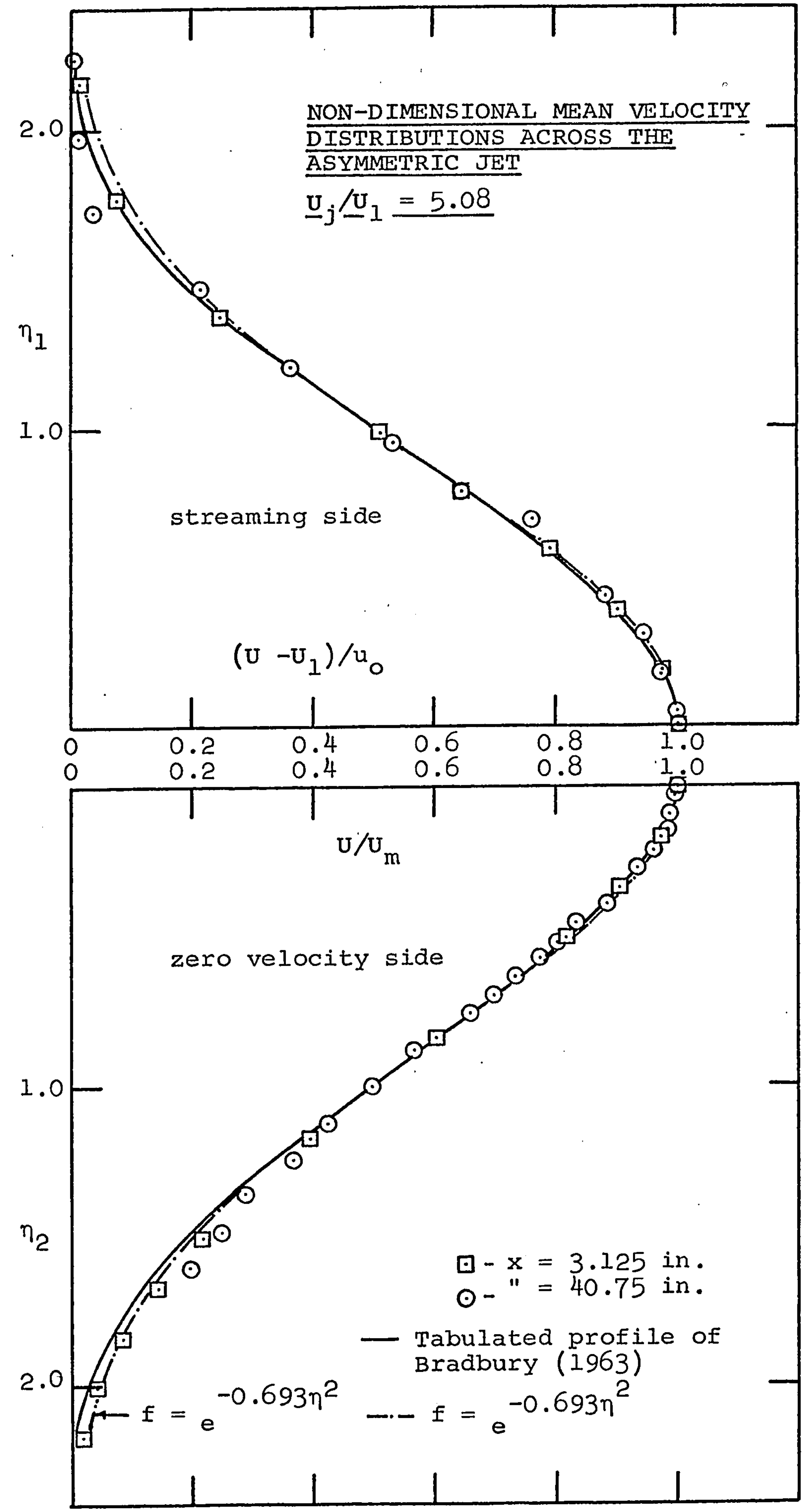
NON-DIMENSIONAL MEAN VELOCITY DISTRIBUTIONS ACROSS THE ASYMMETRIC JET
$U_j/U_1 = 5.08$
η_1
2.0
1.0
streaming side
$(U - U_1)/u_o$
0 0.2 0.4 0.6 0.8 1.0
0 0.2 0.4 0.6 0.8 1.0
U/U_m
zero velocity side
η_2
1.0
2.0
⊡ - x = 3.125 in.
⊙ - " = 40.75 in.
— Tabulated profile of Bradbury (1963)
$f = e^{-0.693\eta^2}$
—·— $f = e^{-0.693\eta^2}$

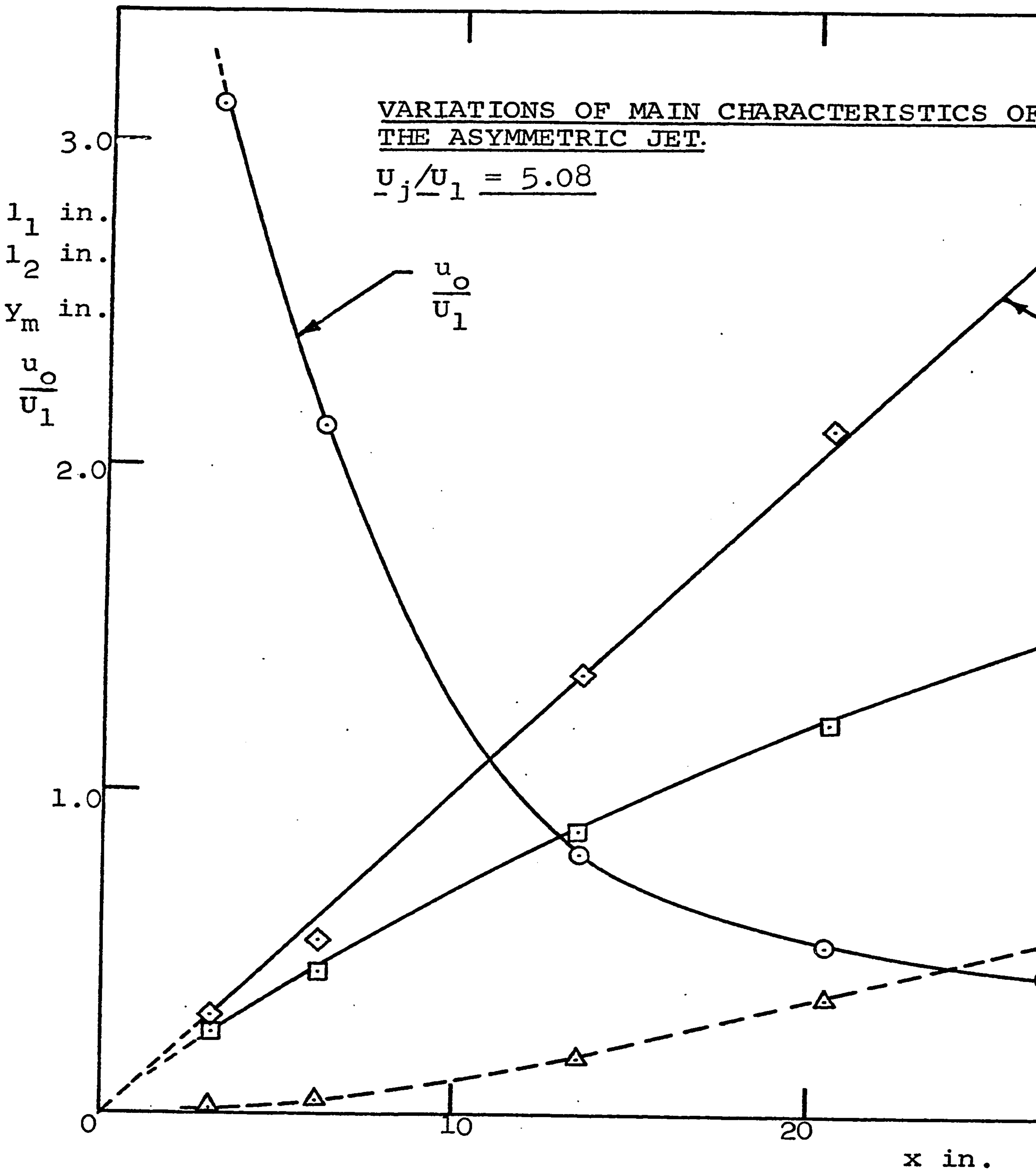

VARIATIONS OF MAIN CHARACTERISTICS OF
THE ASYMMETRIC JET.
$U_j/U_1 = 5.08$
l_1 in.
l_2 in.
y_m in.
$\frac{u_o}{U_1}$
3.0
2.0
1.0
0
10
20
x in.

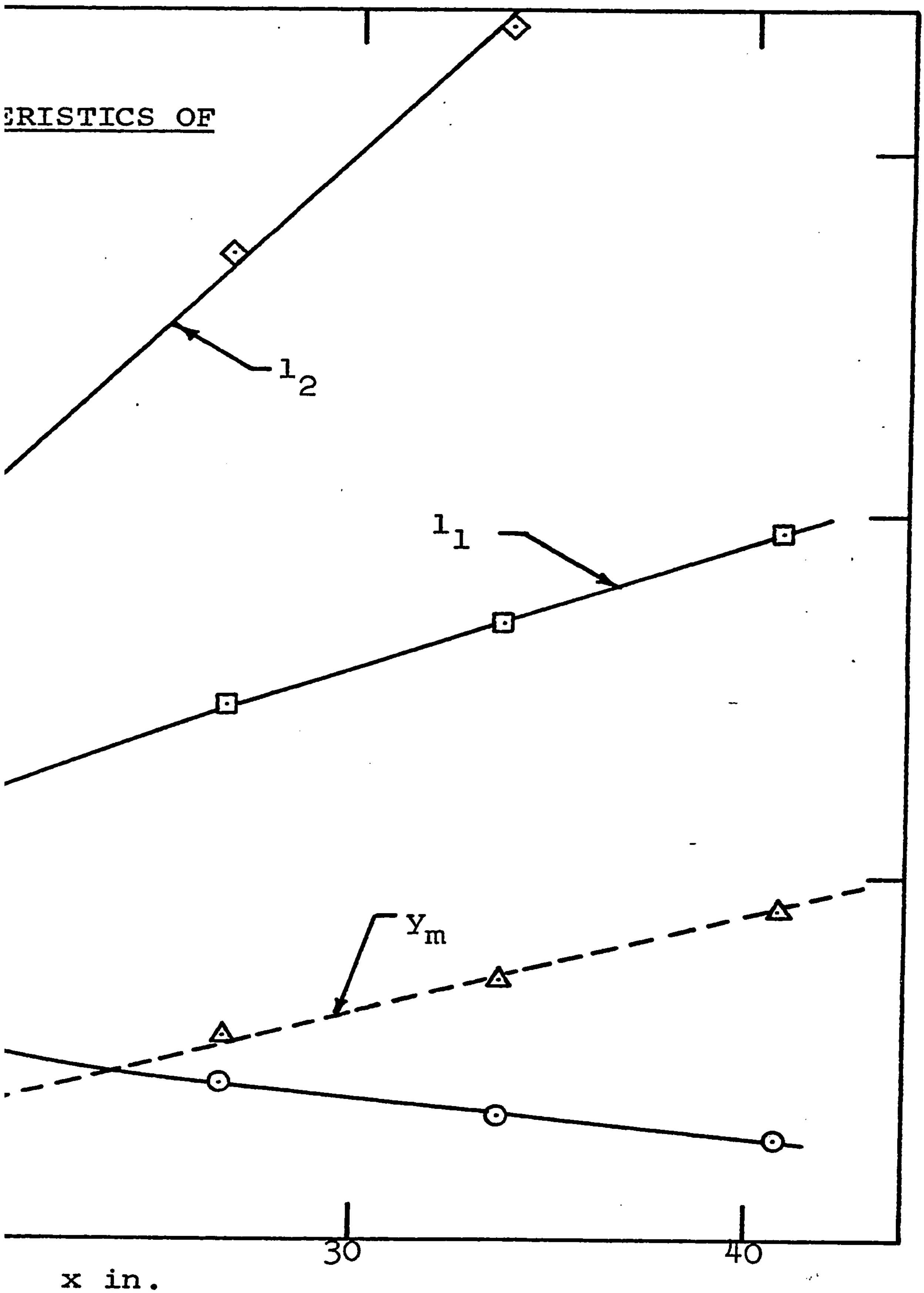

Fig. 33

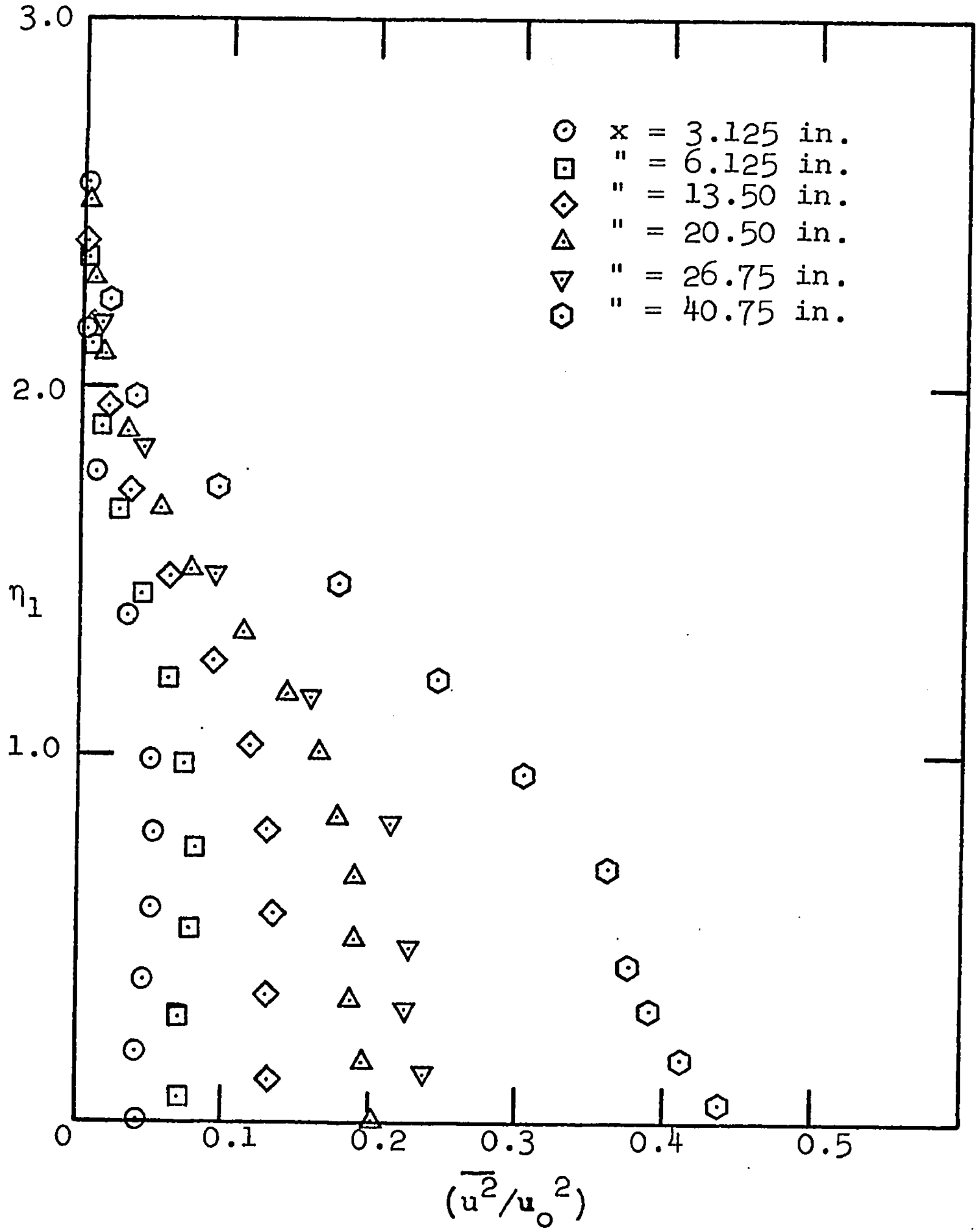

$\overline{u^2}/u_o^2$ - DISTRIBUTIONS ON THE STREAMING SIDE OF THE ASYMMETRIC JET. $U_j/U_1 = 5.08$

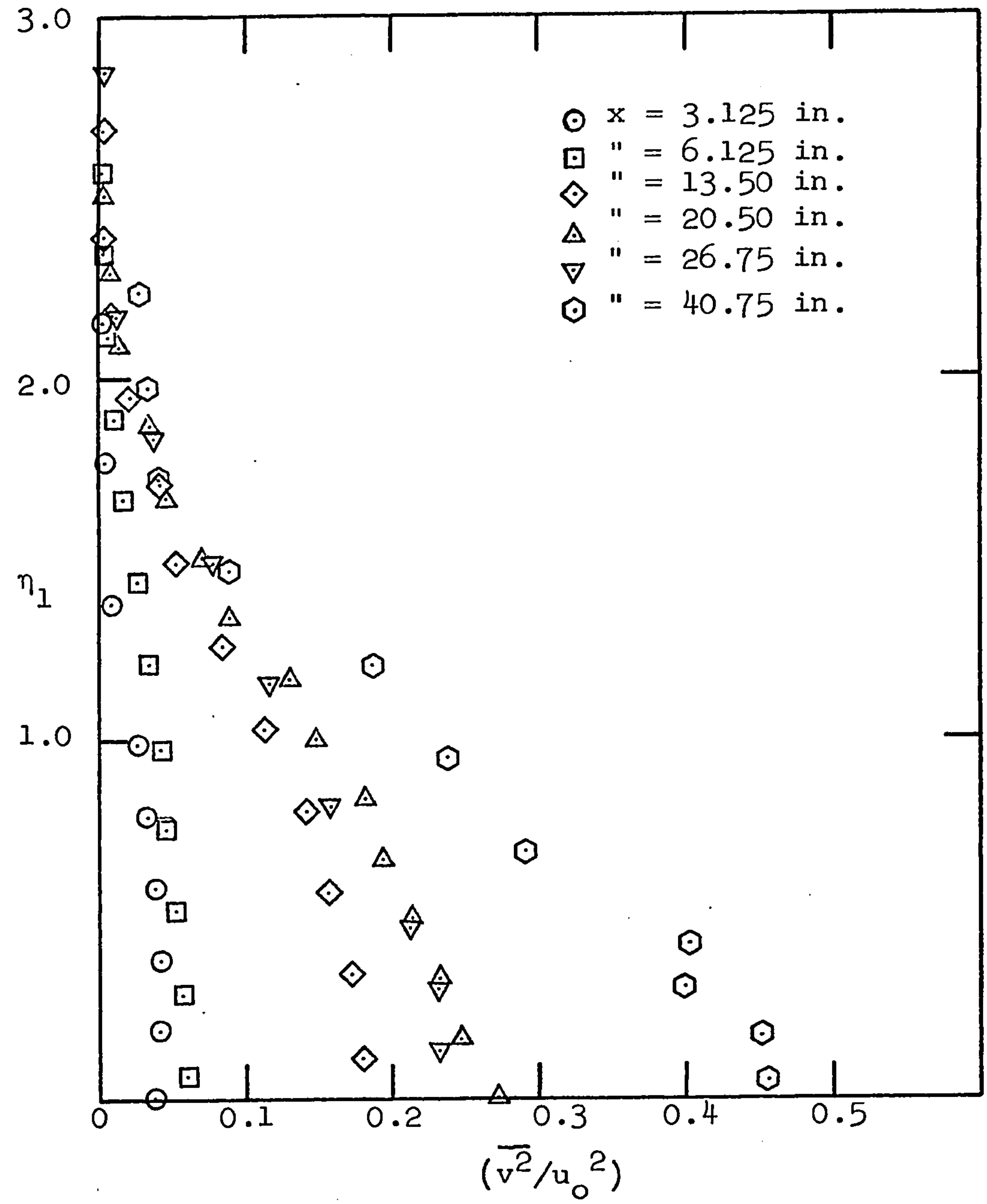

$\overline{v^2}/u_o^2$ - DISTRIBUTIONS ON THE STREAMING SIDE OF THE ASYMMETRIC JET. $U_j/U_1 = 5.08$

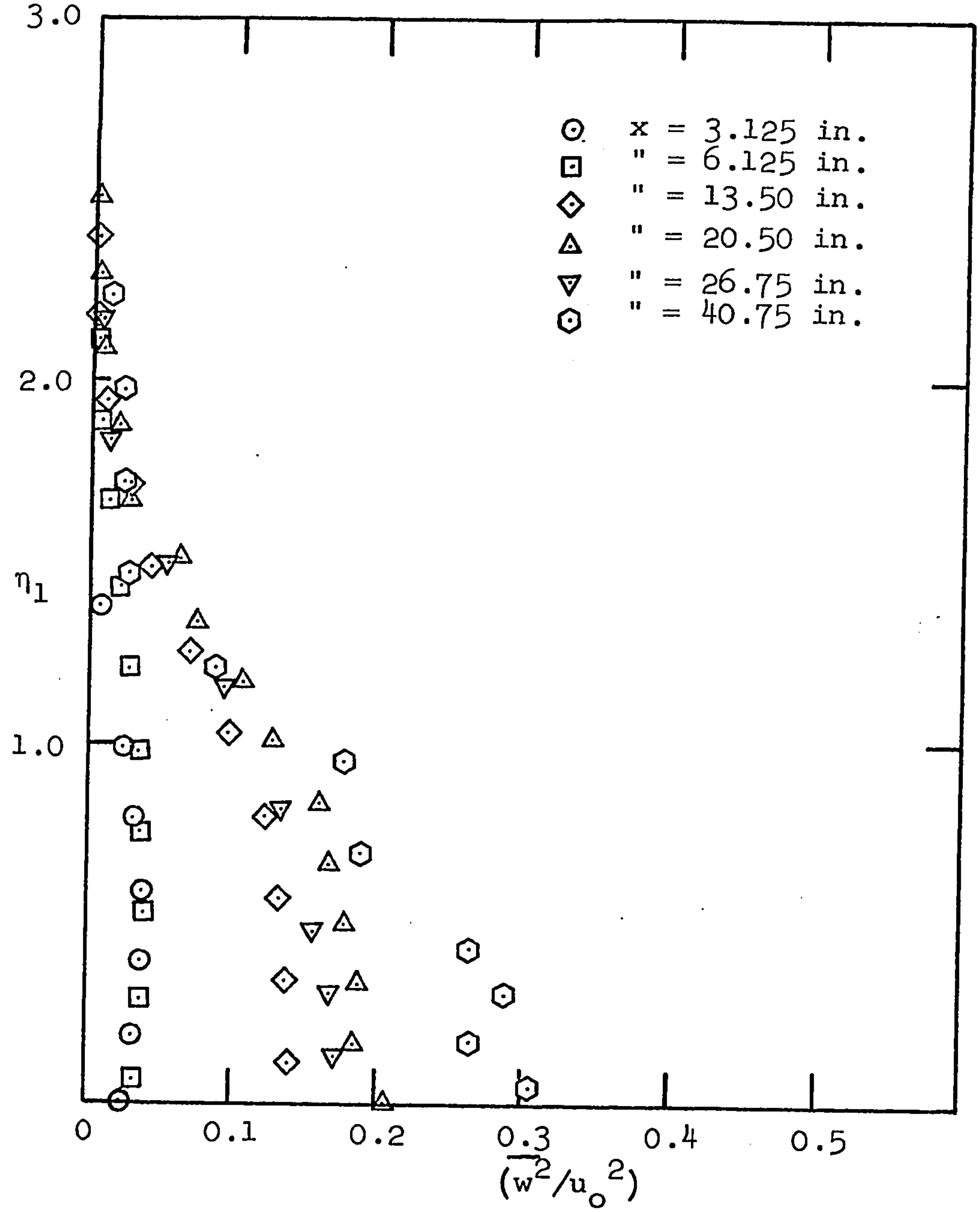

$\overline{w^2}/u_o^2$ - DISTRIBUTIONS ON THE STREAMING SIDE OF THE ASYMMETRIC JET. $U_j/U_1 = 5.08$

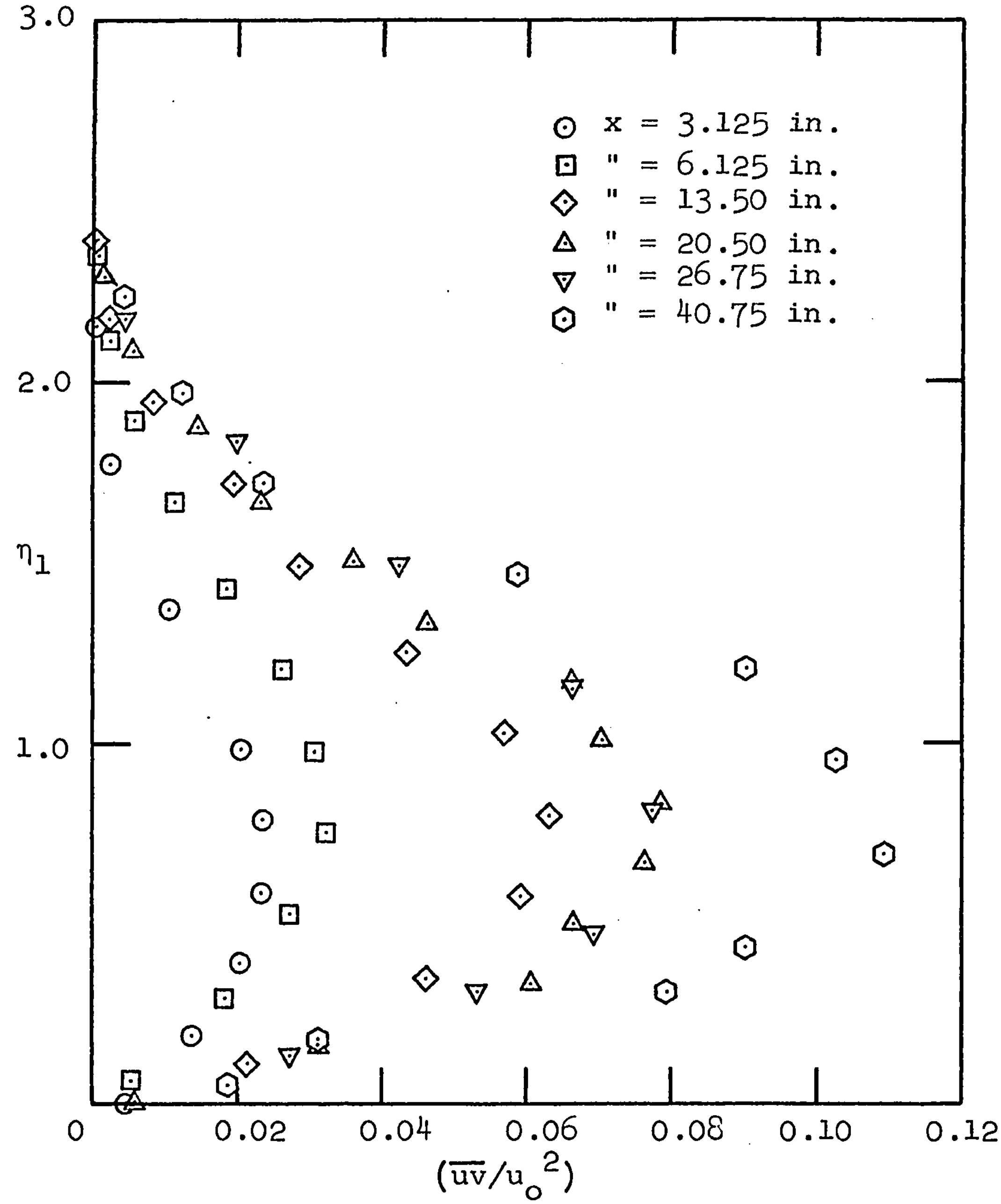

SHEAR STRESS DISTRIBUTIONS ON THE STREAMING SIDE OF THE ASYMMETRIC JET. $U_j/U_1 = 5.08$

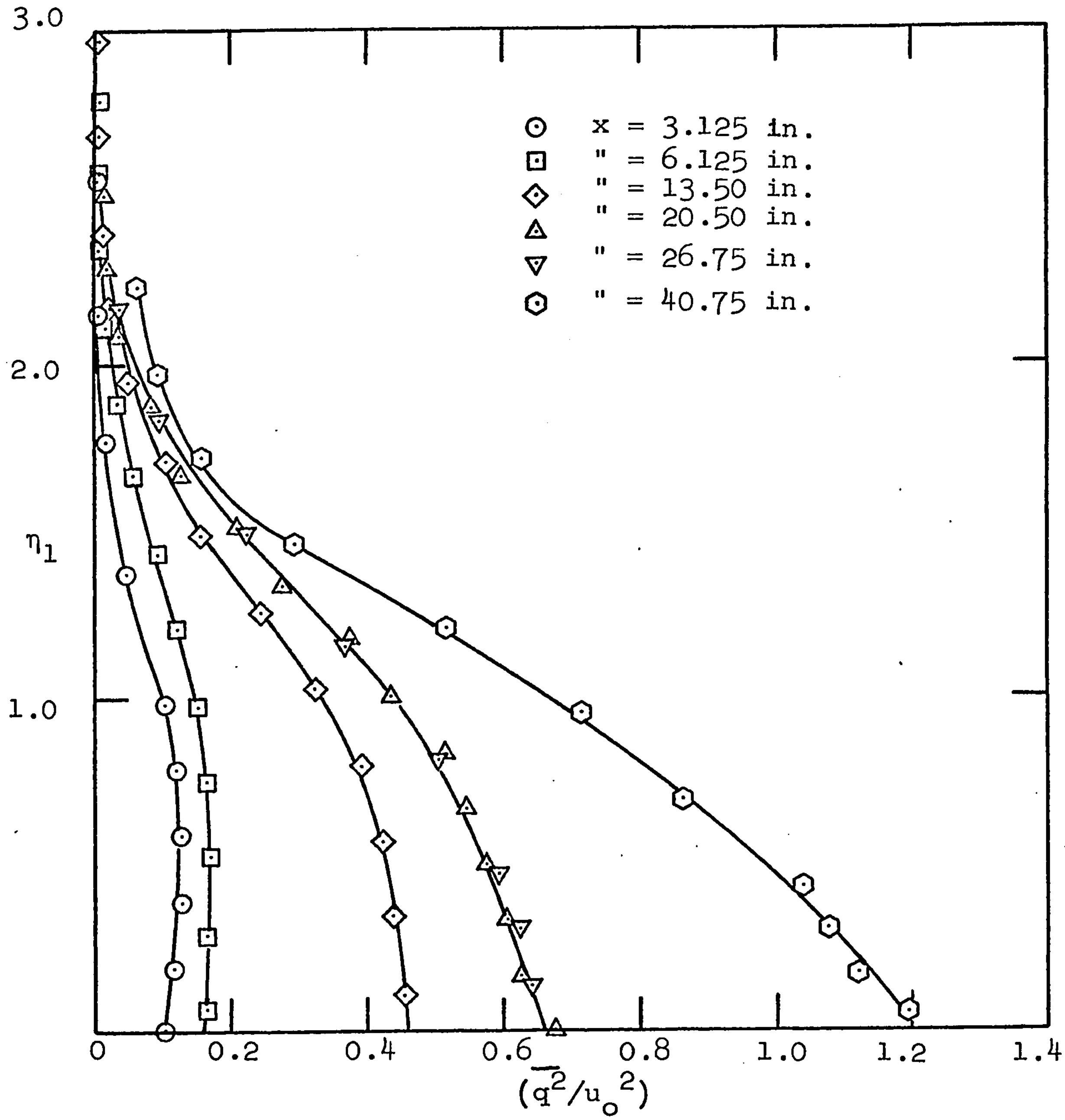

TURBULENT ENERGY DISTRIBUTION ON THE STREAMING SIDE OF THE ASYMMETRIC JET. $U_j/U_1 = 5.08$

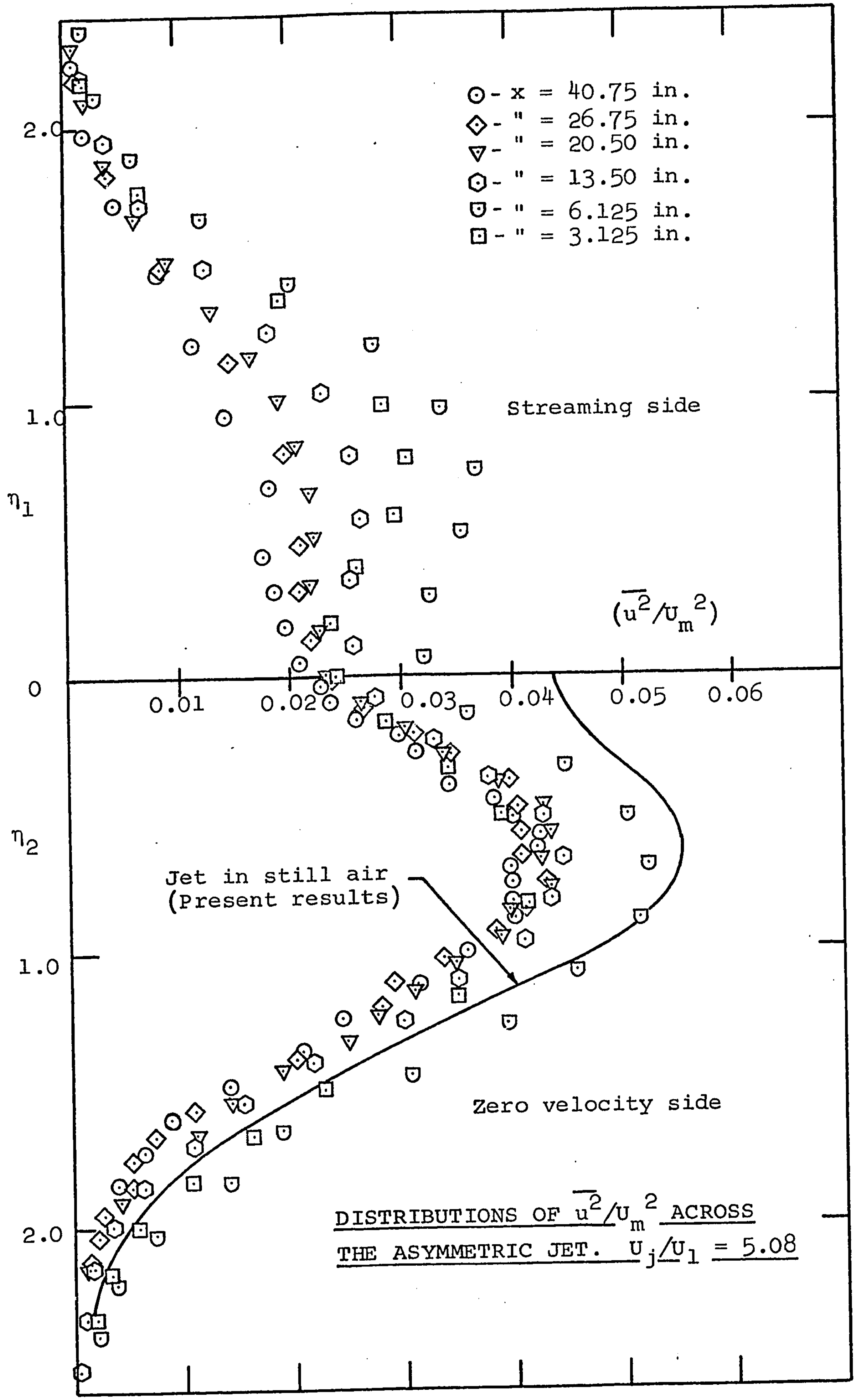

DISTRIBUTIONS OF $\overline{u^2}/U_m{}^2$ ACROSS THE ASYMMETRIC JET. $U_j/U_1 = 5.08$

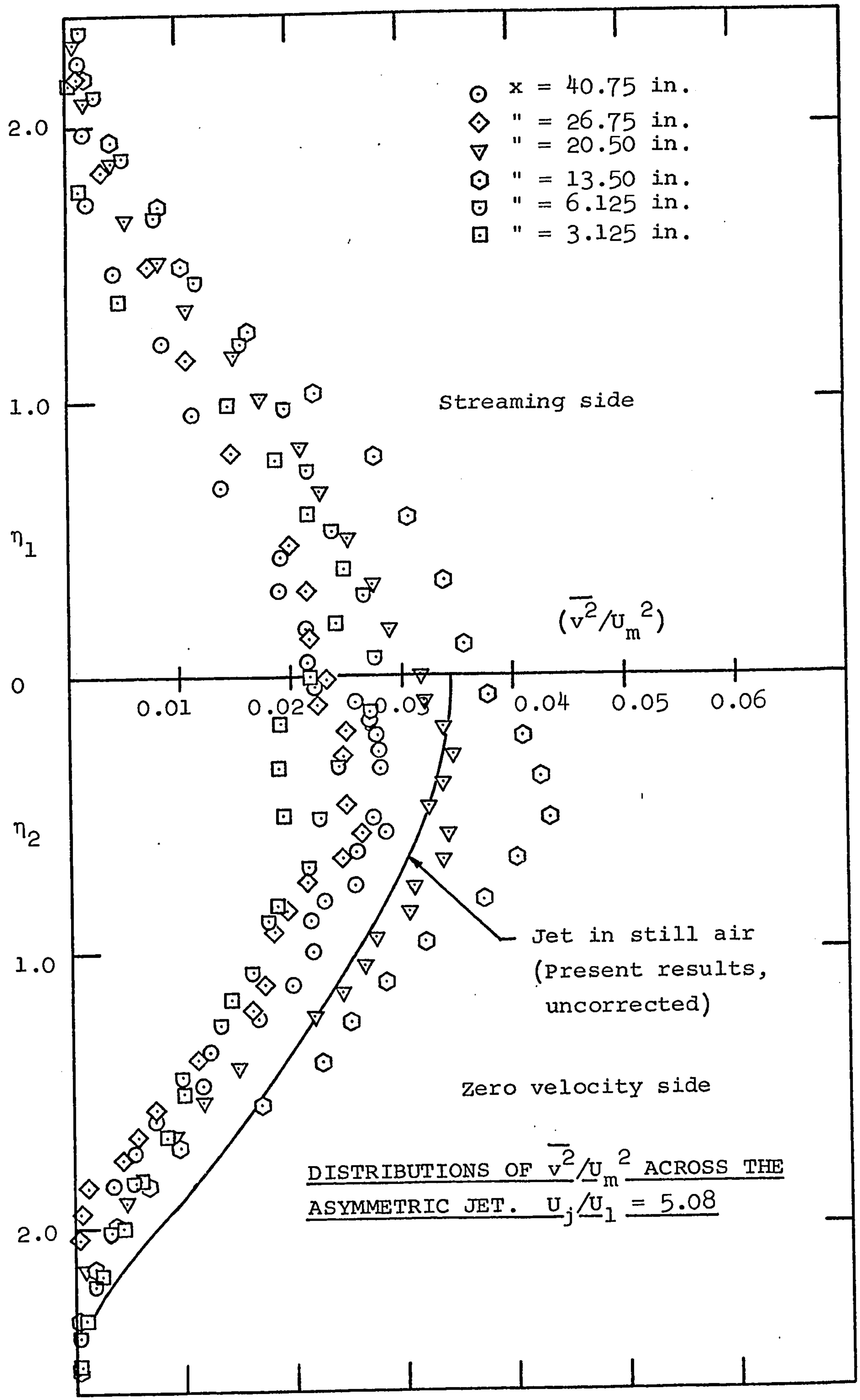

DISTRIBUTIONS OF $\overline{v^2}/U_m^{\ 2}$ ACROSS THE ASYMMETRIC JET. $U_j/U_1 = 5.08$

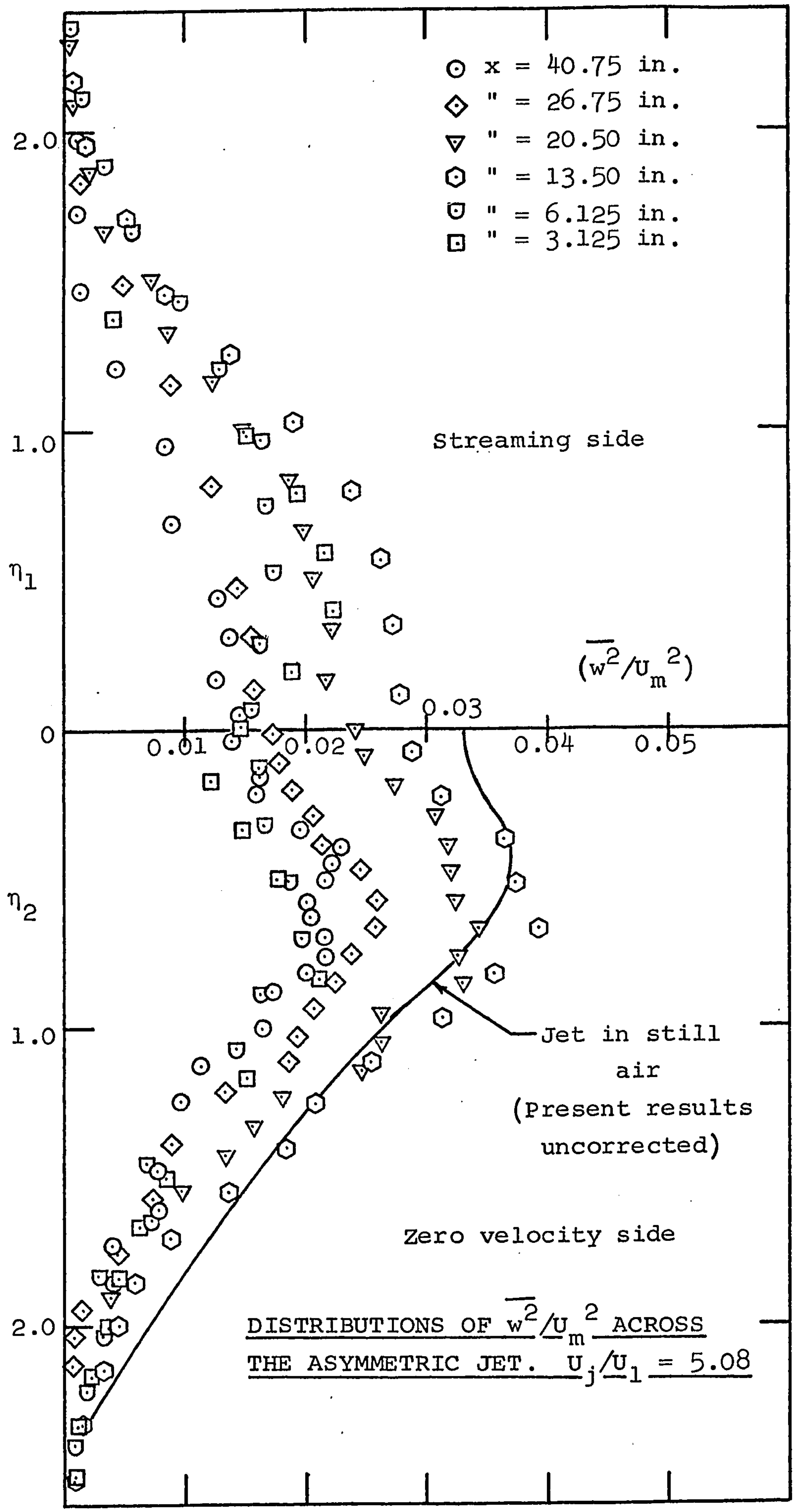

DISTRIBUTIONS OF $\overline{w^2}/U_m^2$ ACROSS THE ASYMMETRIC JET. $U_j/U_1 = 5.08$

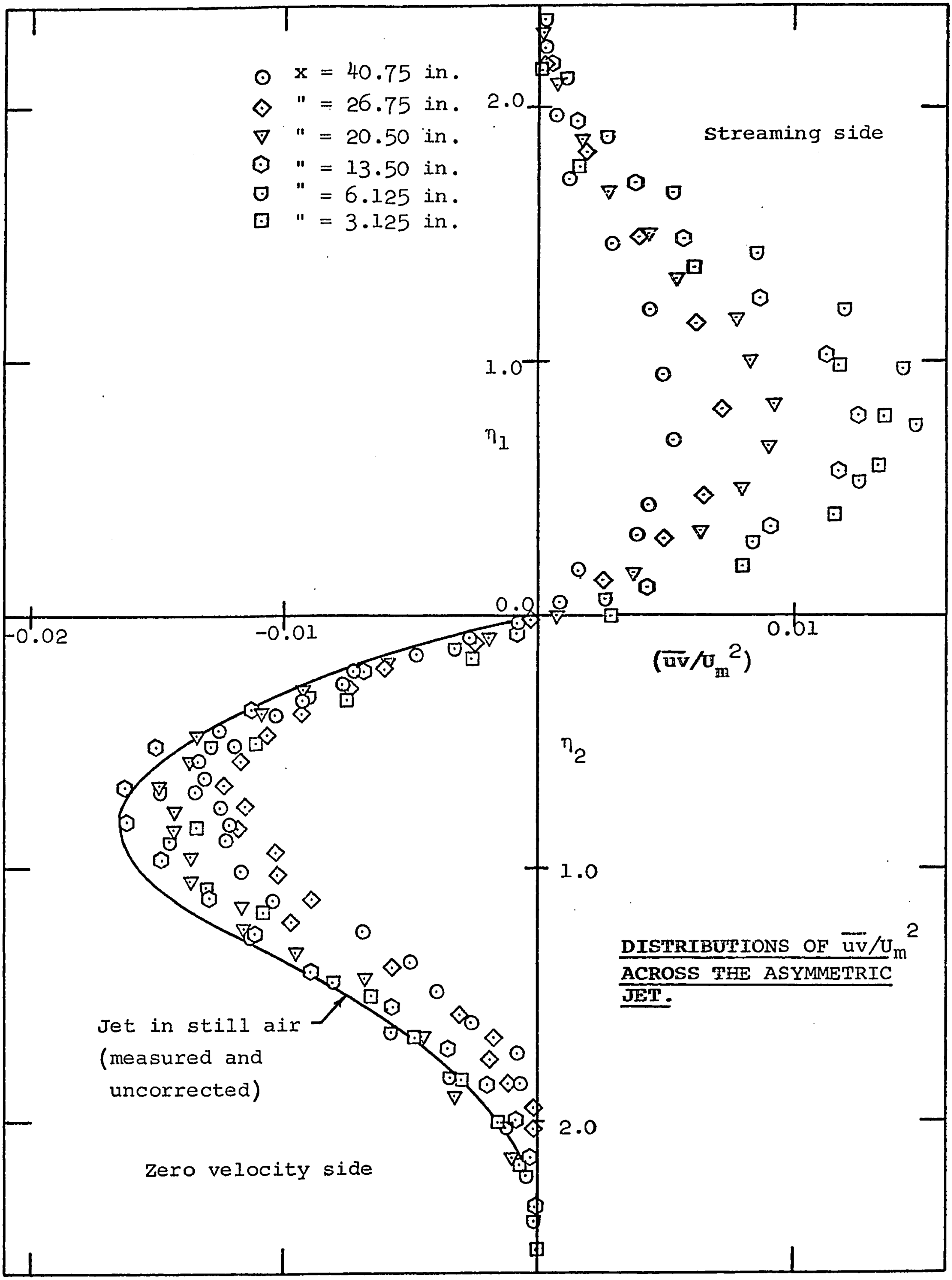

DISTRIBUTIONS OF $\overline{uv}/U_m^2$ ACROSS THE ASYMMETRIC JET.

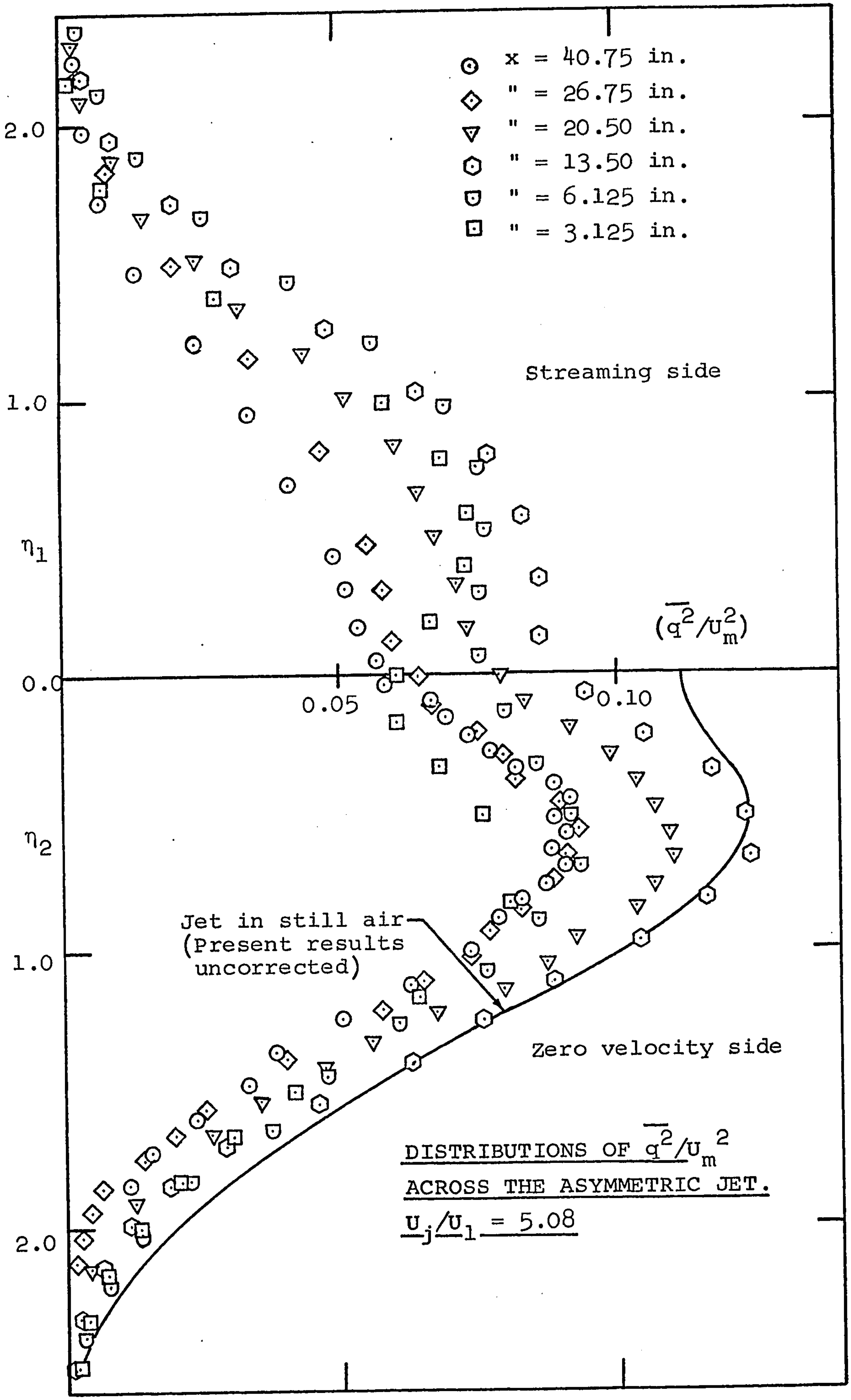

DISTRIBUTIONS OF $\overline{q^2}/U_m^2$ ACROSS THE ASYMMETRIC JET. $U_j/U_1 = 5.08$

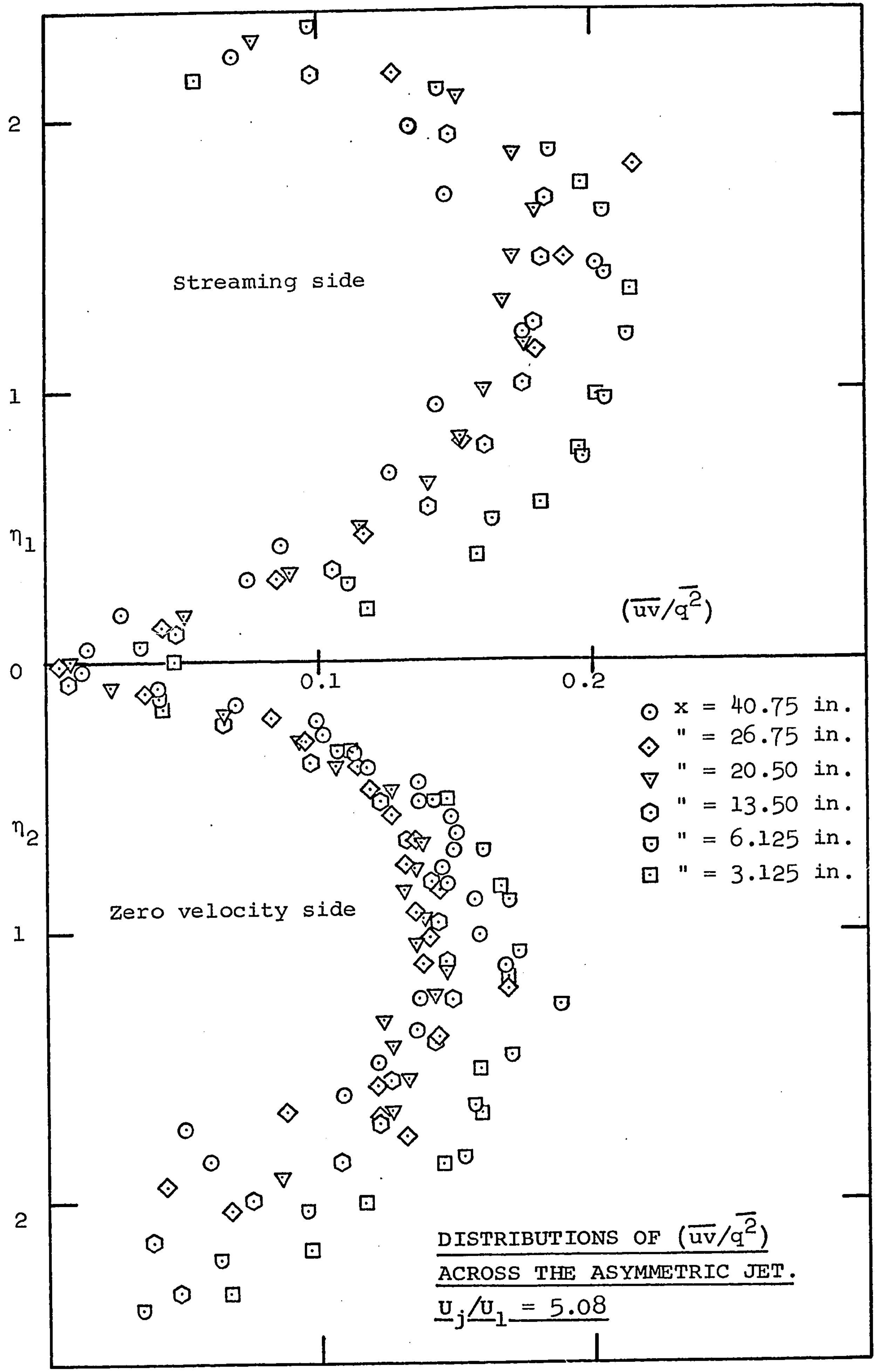

DISTRIBUTIONS OF $(\overline{uv}/\overline{q^2})$ ACROSS THE ASYMMETRIC JET. $U_j/U_1 = 5.08$

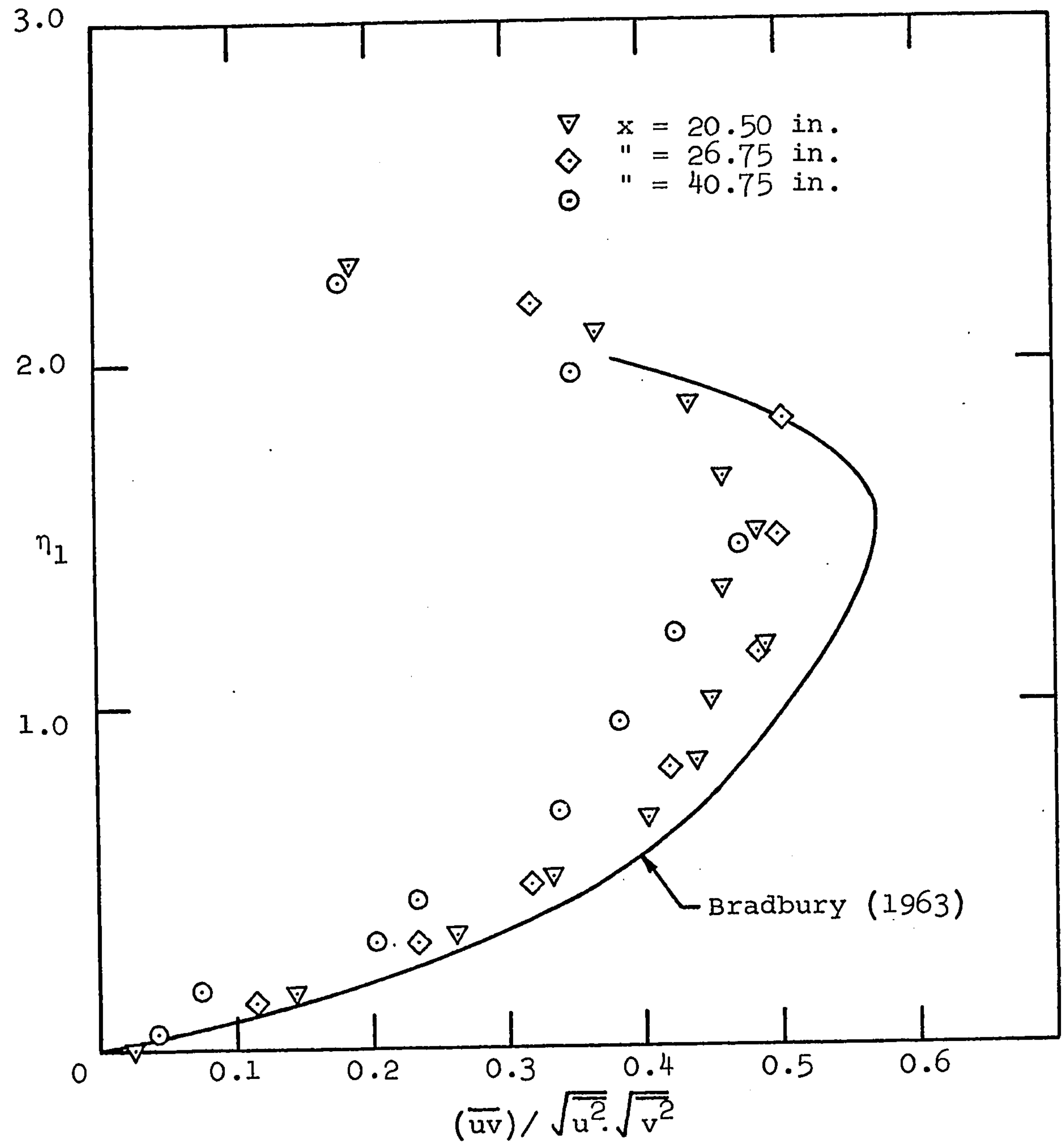

$R_{\overline{uv}}$ - CORRELATION ON THE STREAMING SIDE OF THE ASYMMETRIC JET. $U_j/U_1 = 5.08$

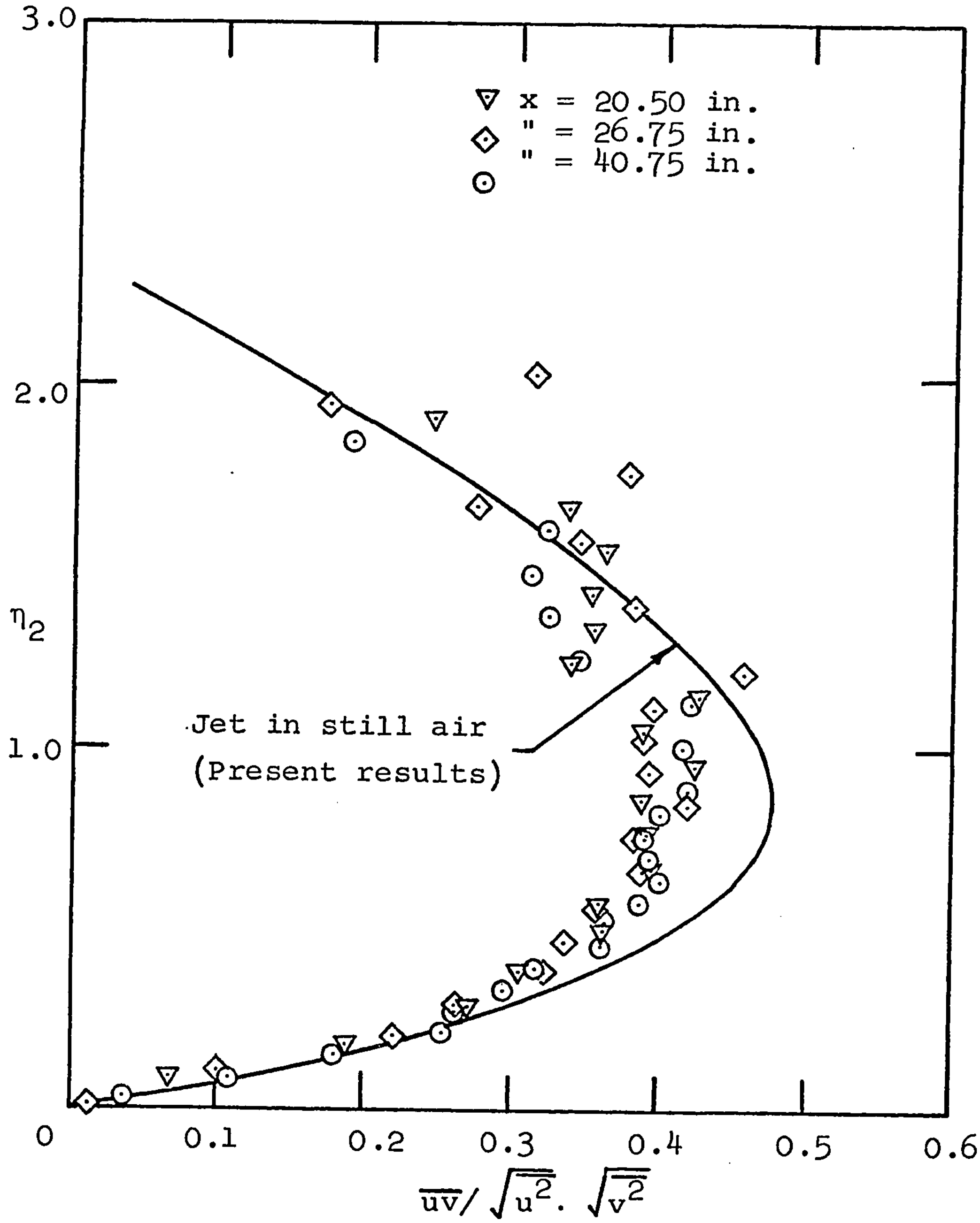

$R_{\overline{uv}}$ - CORRELATION ON THE STILL AIR SIDE OF THE ASYMMETRIC JET. $U_j/U_1 = 5.08$

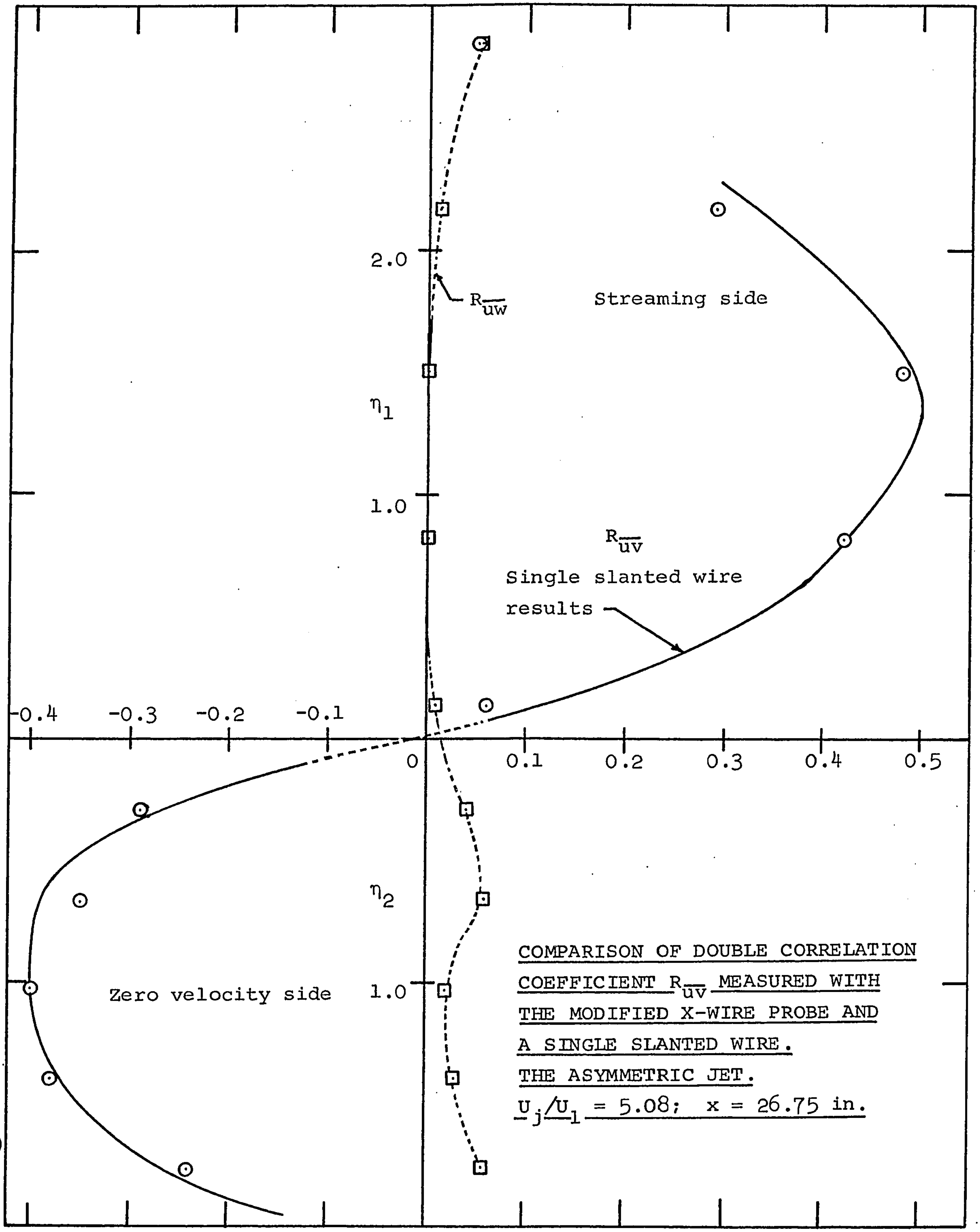

COMPARISON OF DOUBLE CORRELATION COEFFICIENT $R_{\overline{uv}}$ MEASURED WITH THE MODIFIED X-WIRE PROBE AND A SINGLE SLANTED WIRE.
THE ASYMMETRIC JET.
$U_j/U_1 = 5.08$; $x = 26.75$ in.

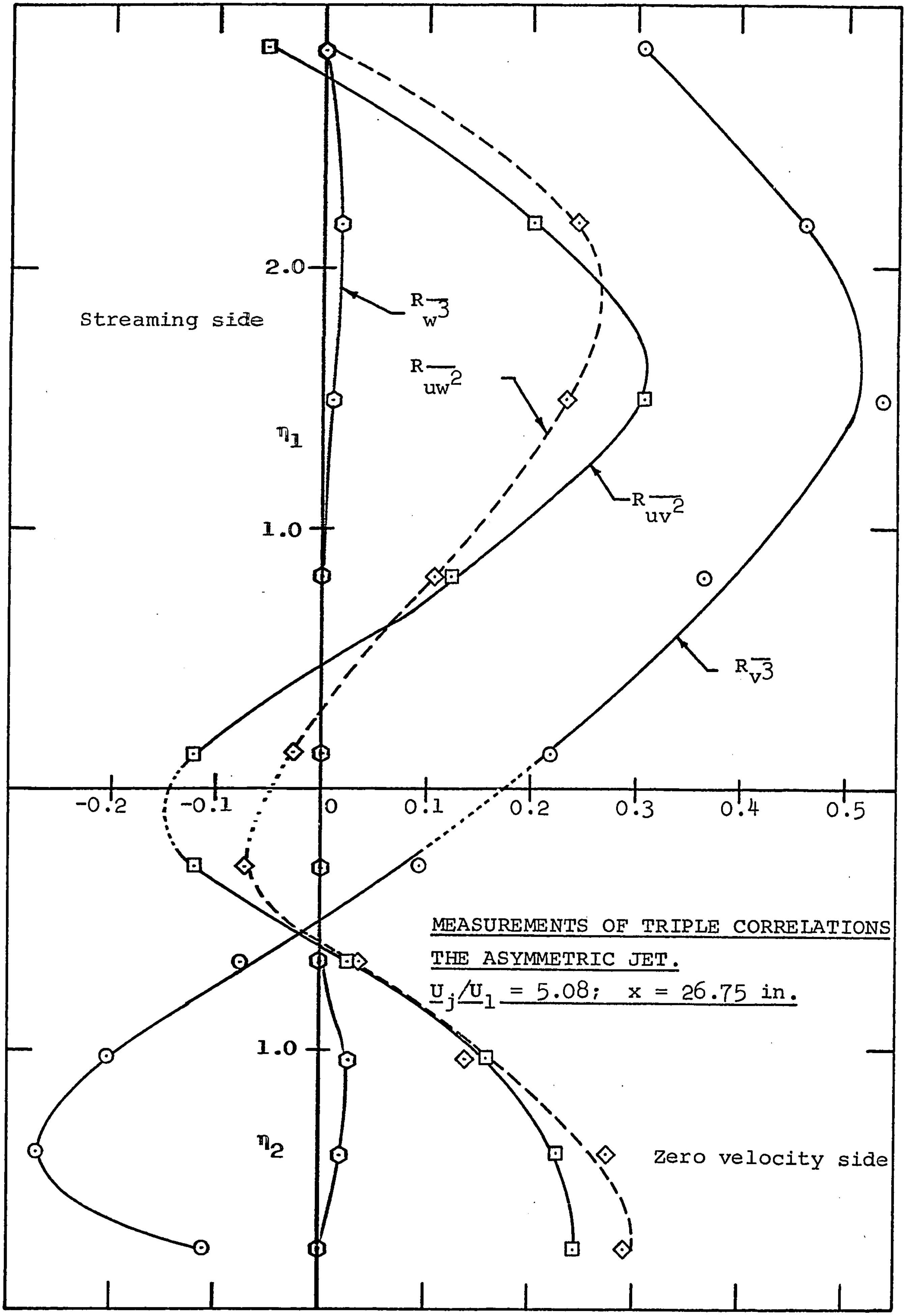

MEASUREMENTS OF TRIPLE CORRELATIONS THE ASYMMETRIC JET.

$U_j/U_1 = 5.08$; $x = 26.75$ in.

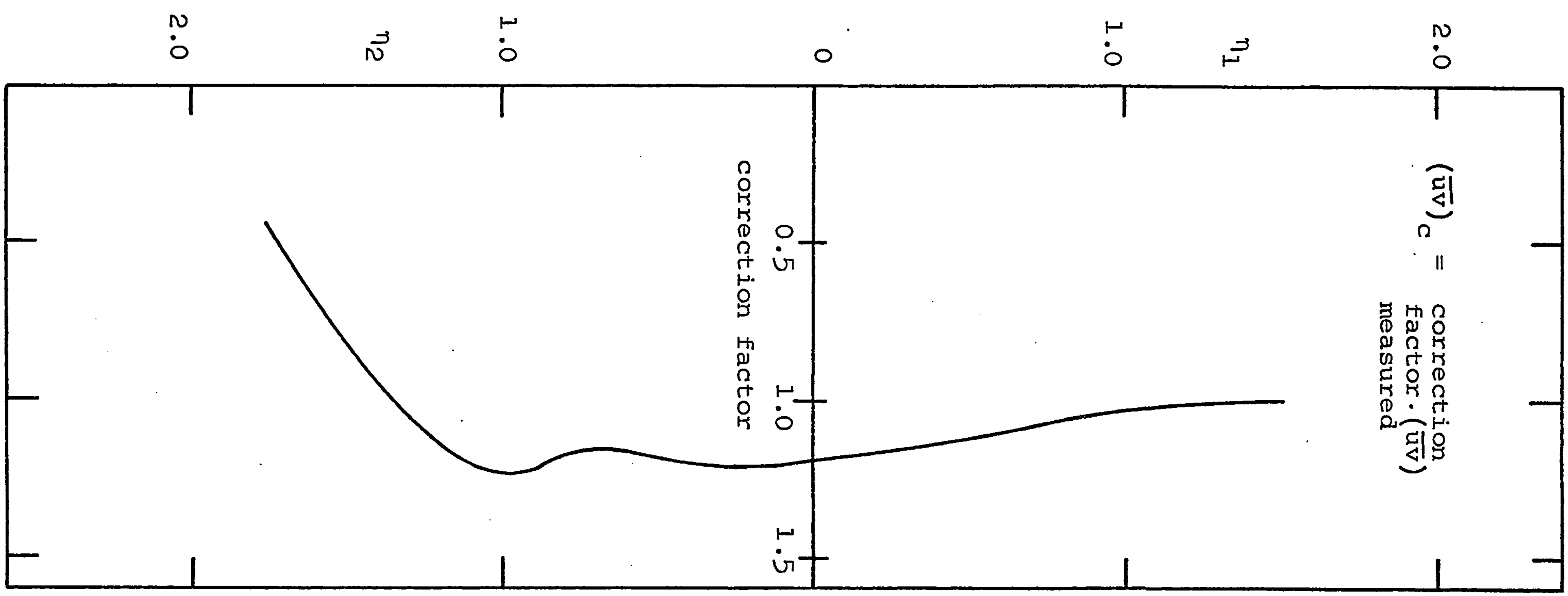

CORRECTION FACTOR FOR $\overline{uv}$ DUE TO HIGH INTENSITY AND THE LONGITUDINAL COOLING EFFECTS.
THE ASYMMETRIC JET. $U_j/U_1 = 5.08$; $x = 26.75$ in.

Fig. 49

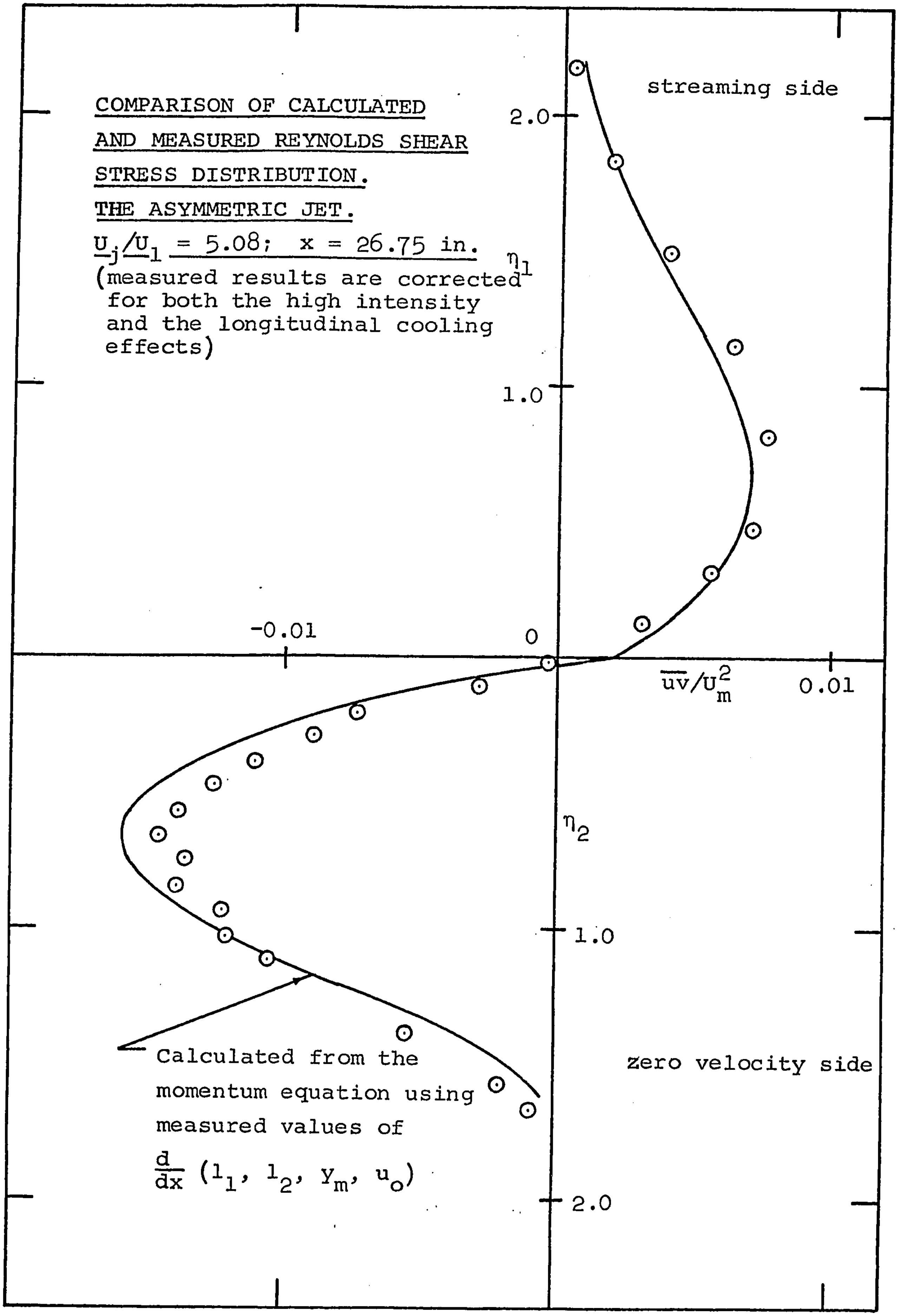
COMPARISON OF CALCULATED AND MEASURED REYNOLDS SHEAR STRESS DISTRIBUTION.
THE ASYMMETRIC JET.
$U_j/U_1 = 5.08$; $x = 26.75$ in.
(measured results are corrected for both the high intensity and the longitudinal cooling effects)
streaming side
zero velocity side
η_1
η_2
2.0
1.0
0
-0.01
0.01
1.0
2.0
$\overline{uv}/U_m^2$
Calculated from the momentum equation using measured values of $\frac{d}{dx}(l_1, l_2, y_m, u_o)$

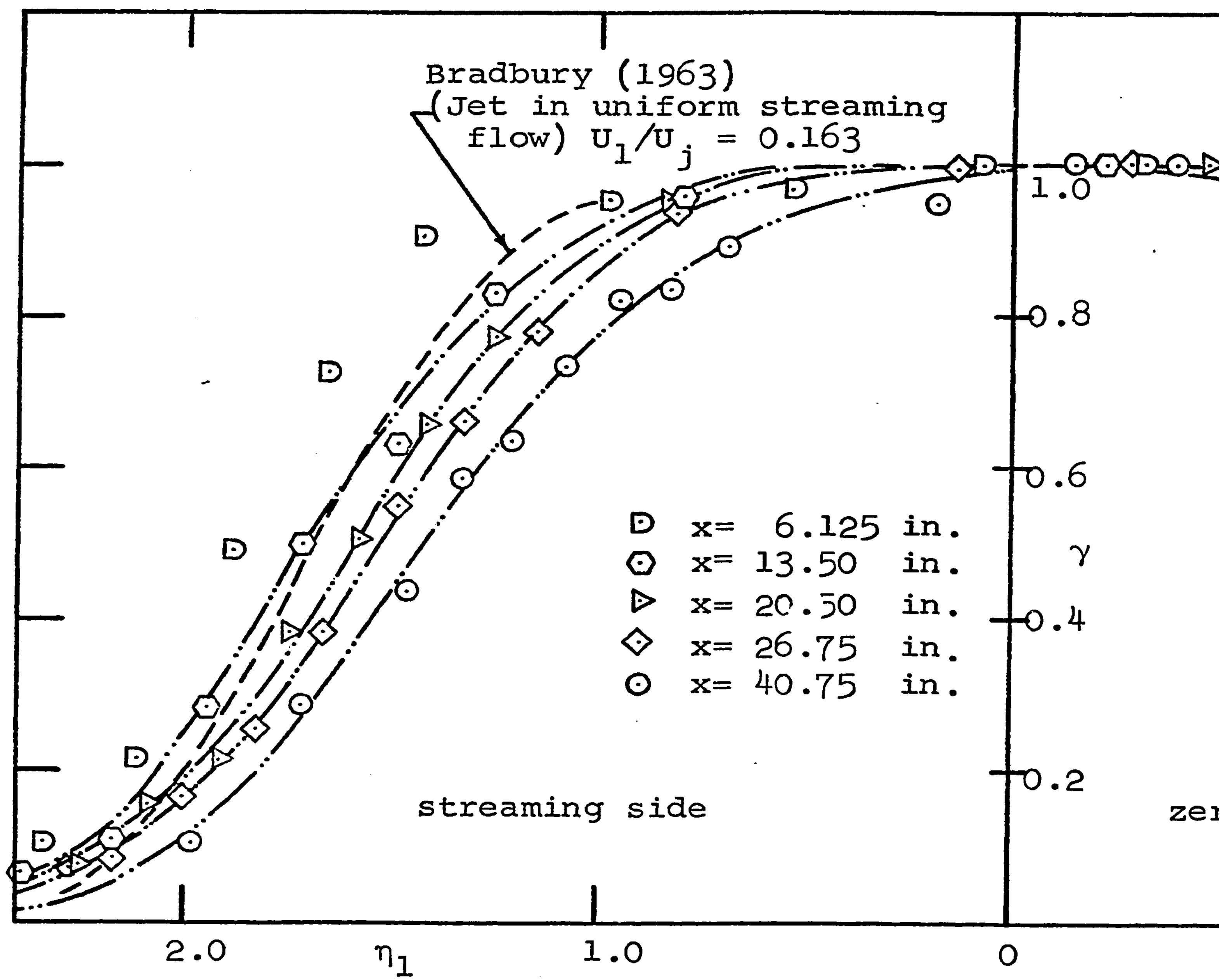

INTERMITTENCY DISTRIBUTIONS.

THE ASYMMETRIC JET. $U_j/U_1 = 5.08$

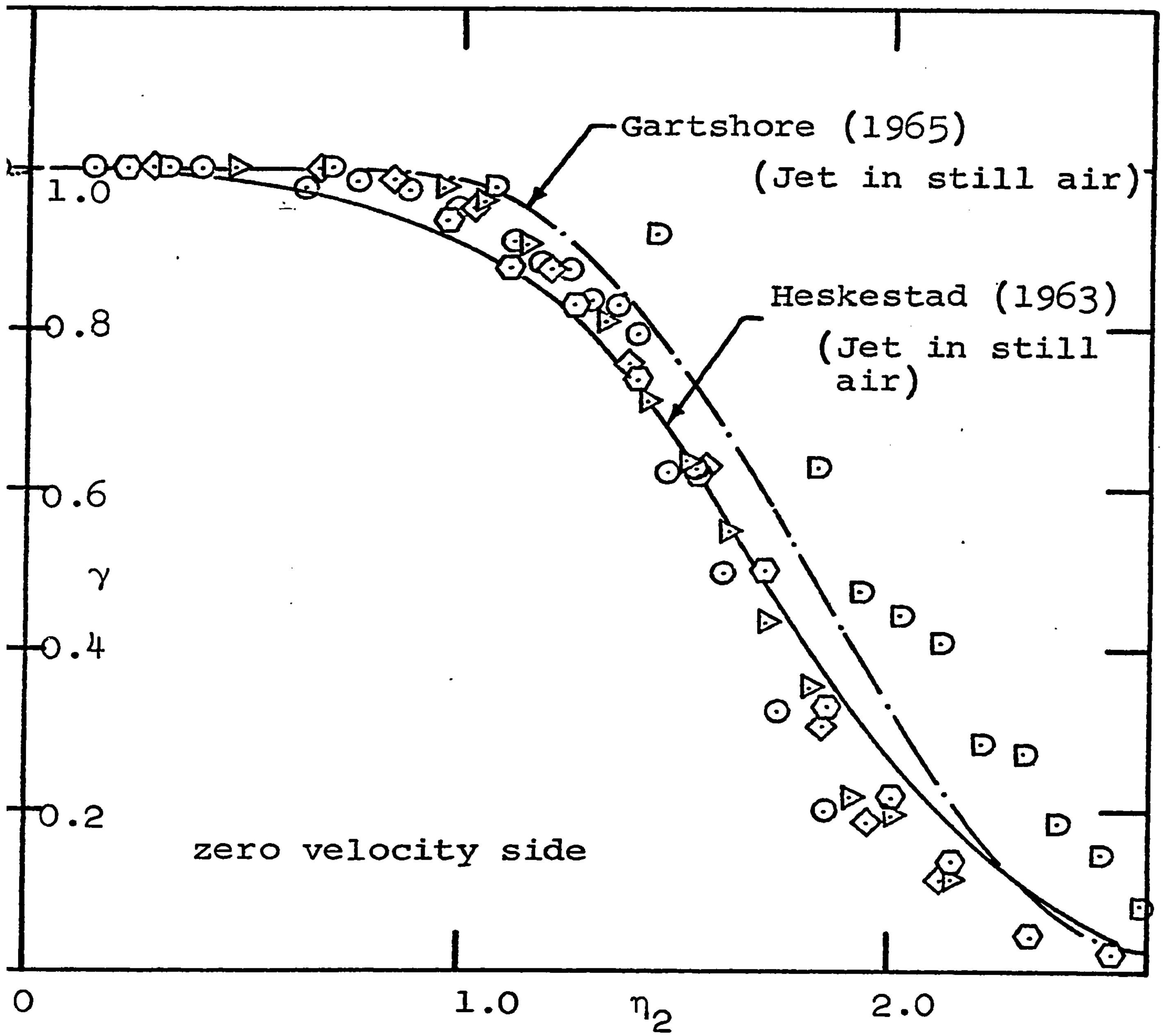

Gartshore (1965)
(Jet in still air)
Heskestad (1963)
(Jet in still air)
zero velocity side
1.0
0.8
0.6
0.4
0.2
γ
0
1.0
2.0
η2

Fig. 51

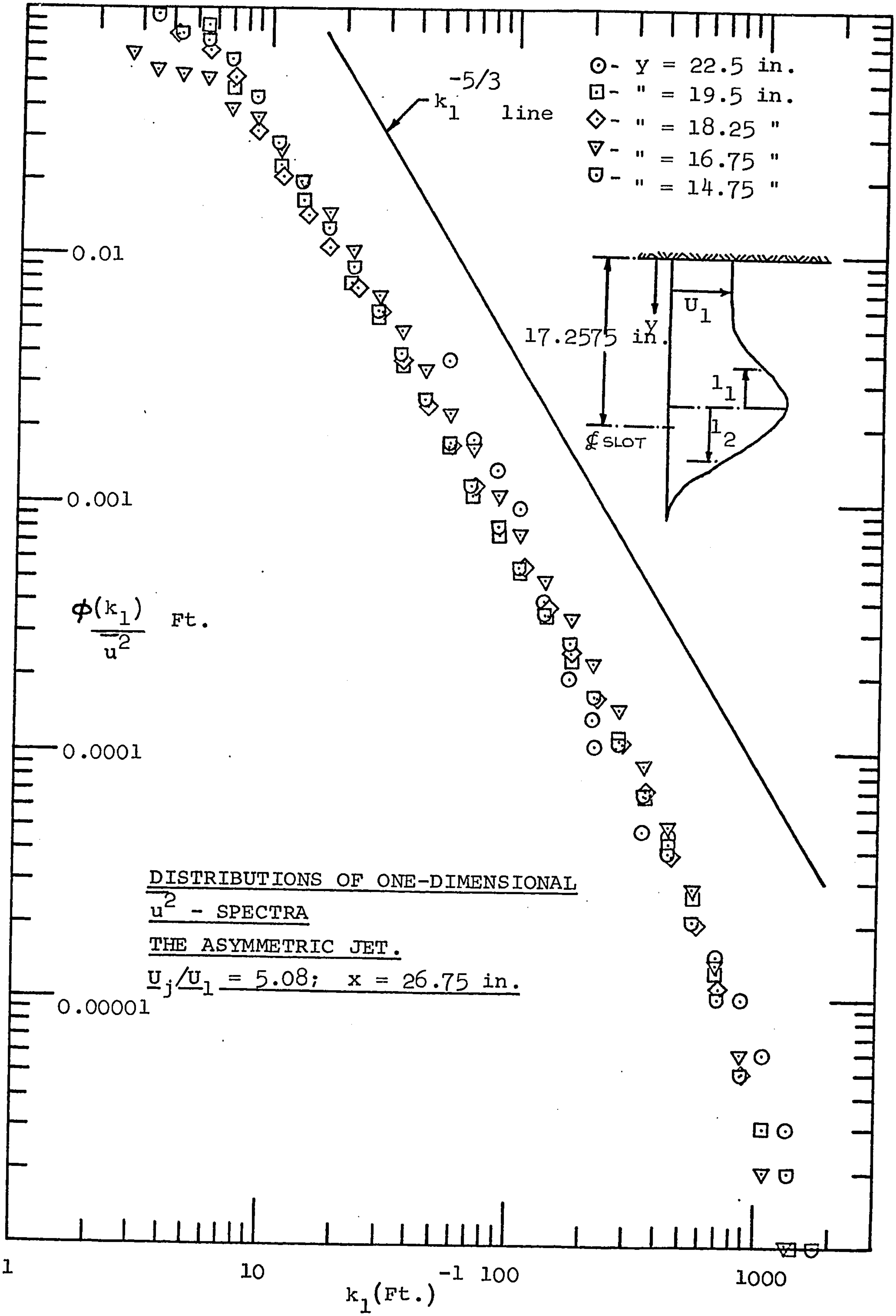

DISTRIBUTIONS OF ONE-DIMENSIONAL $\overline{u^2}$ - SPECTRA

THE ASYMMETRIC JET.

$U_j/U_1 = 5.08$; x = 26.75 in.

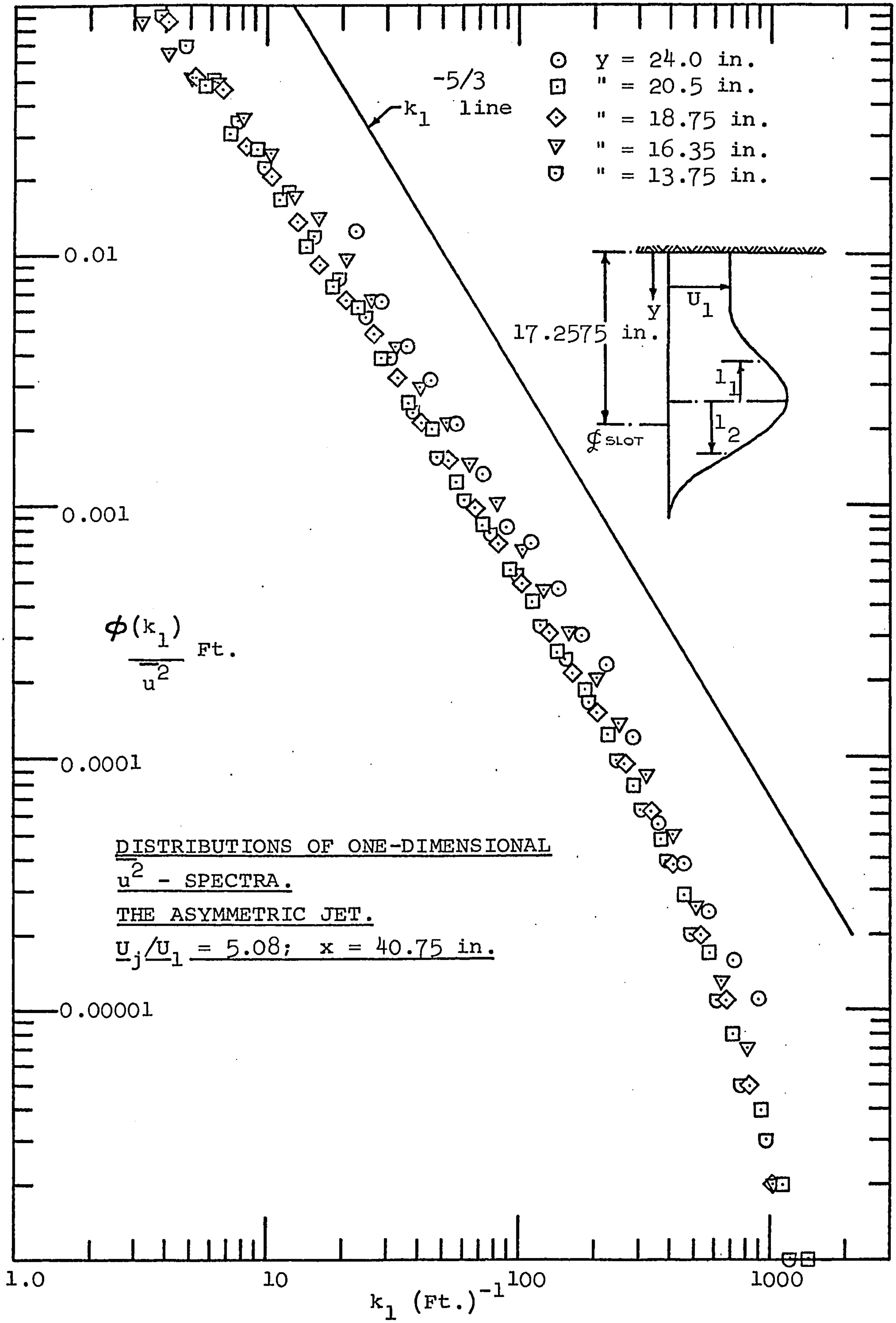

DISTRIBUTIONS OF ONE-DIMENSIONAL $\overline{u^2}$ - SPECTRA.

THE ASYMMETRIC JET.

$U_j/U_1 = 5.08$; $x = 40.75$ in.

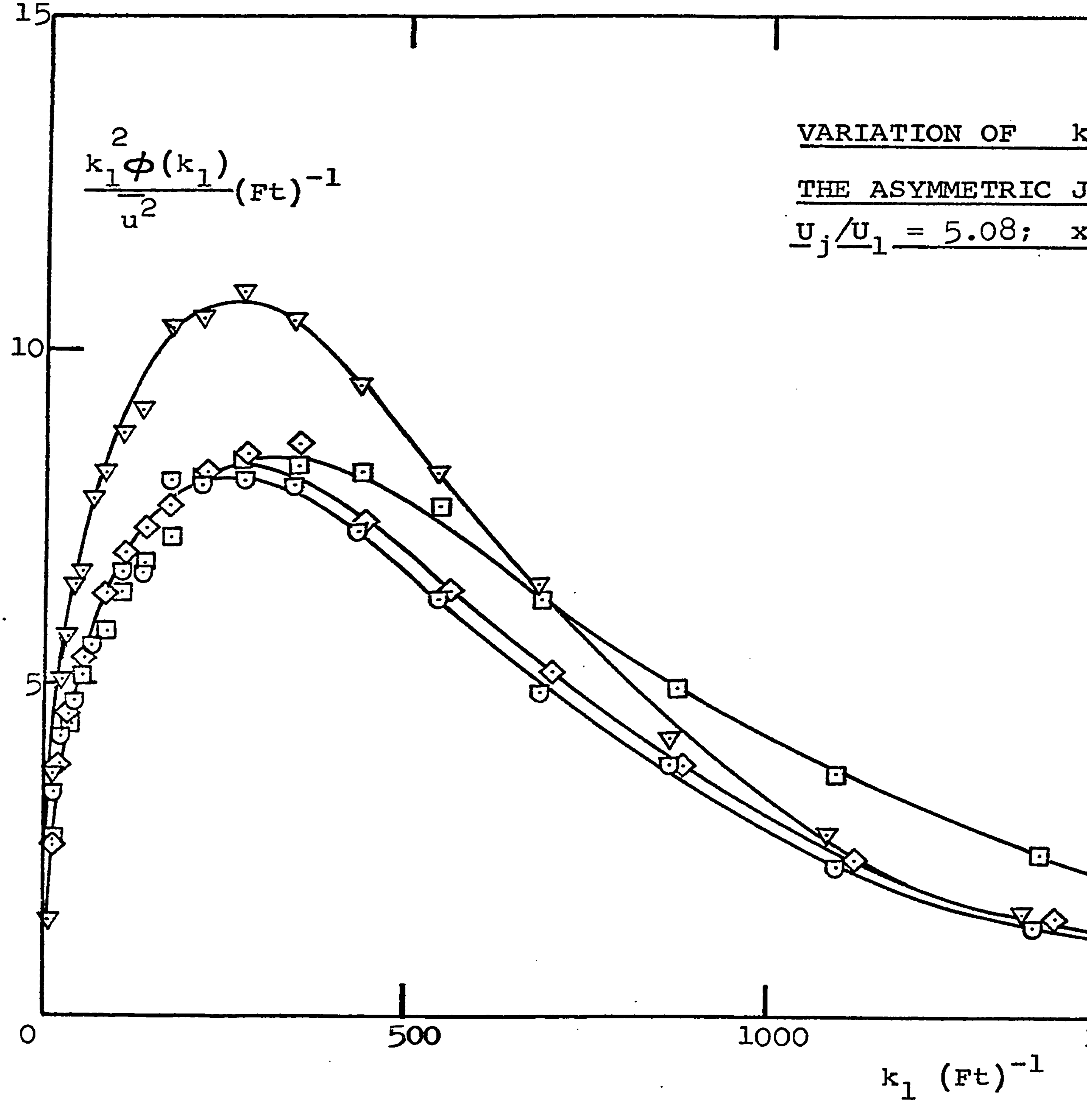

VARIATION OF k
THE ASYMMETRIC J
$U_j/U_1 = 5.08$; x
$\frac{k_1^2 \phi(k_1)}{\overline{u^2}} (Ft)^{-1}$
15
10
5
0
500
1000
$k_1 \ (Ft)^{-1}$

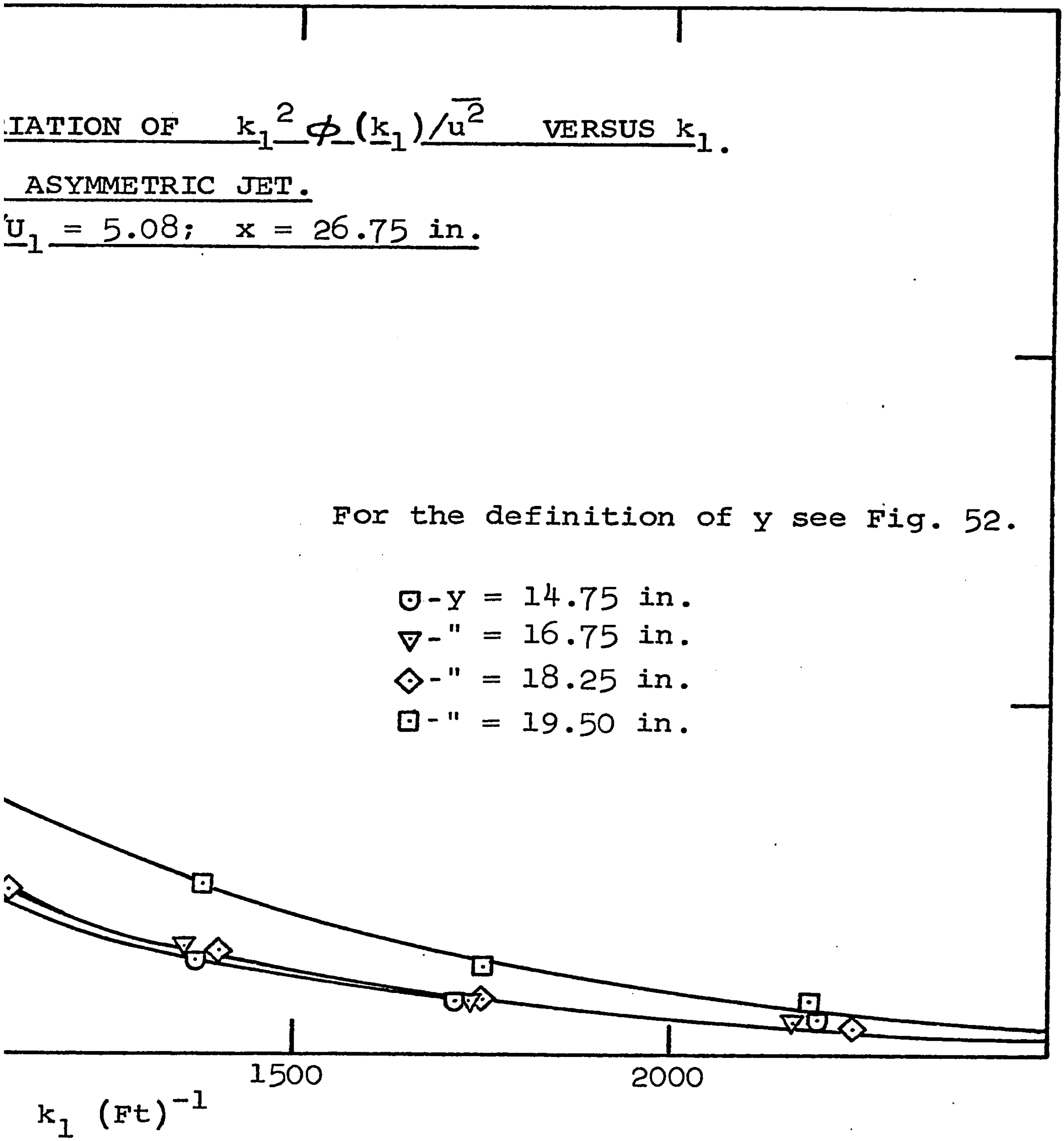
IATION OF $k_1^2 \phi(k_1)/\overline{u^2}$ VERSUS k_1.
ASYMMETRIC JET.
U_1 = 5.08; x = 26.75 in.
For the definition of y see Fig. 52.
- y = 14.75 in.
- " = 16.75 in.
- " = 18.25 in.
- " = 19.50 in.
1500
2000
k_1 (Ft)$^{-1}$

Fig. 54

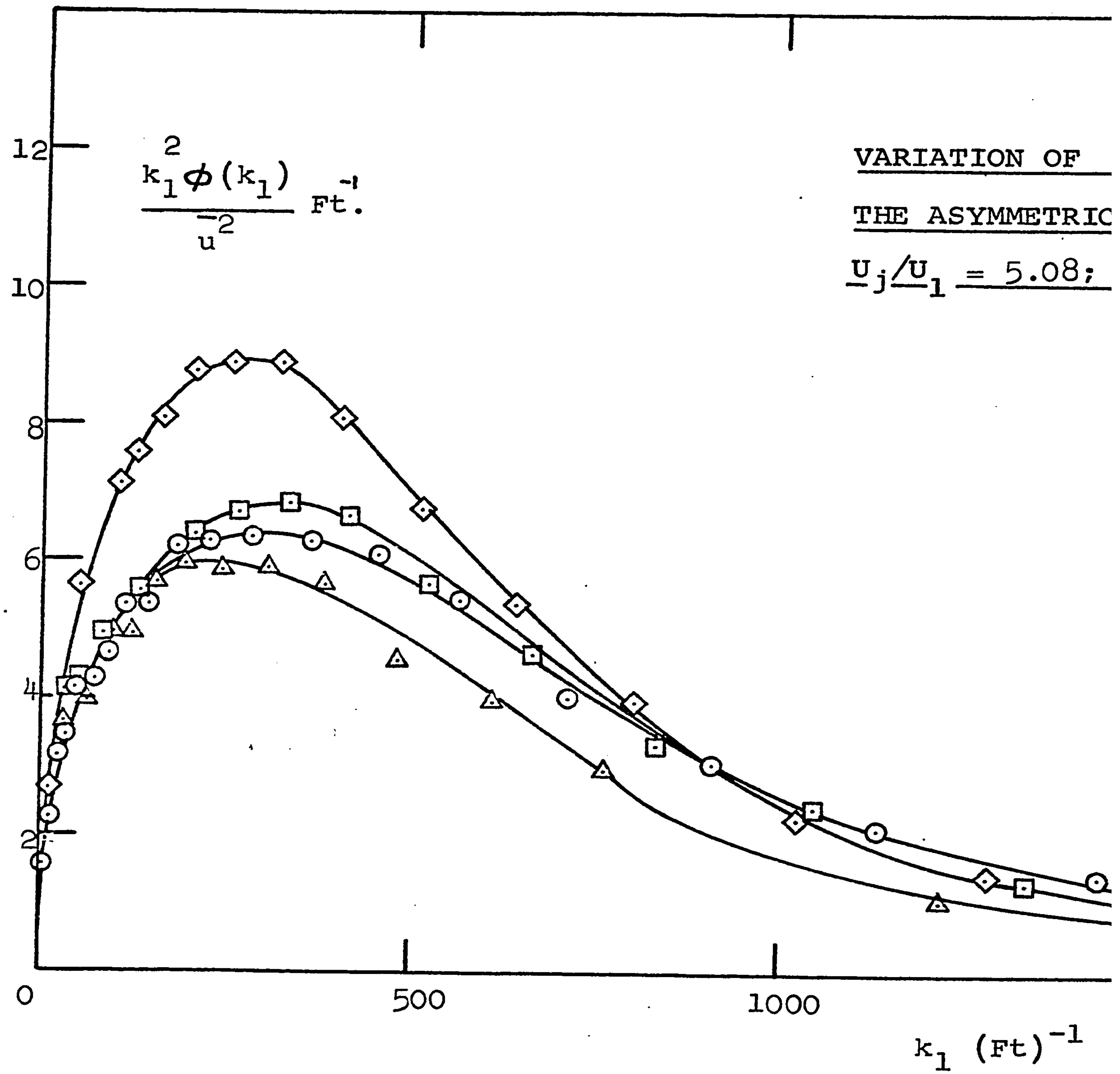

VARIATION OF
THE ASYMMETRIC
U_j/U_1 = 5.08;
$\frac{k_1^2 \phi(k_1)}{\overline{u}^2}$ Ft.$^{-1}$
12
10
8
6
4
2
0
500
1000
k_1 (Ft)$^{-1}$

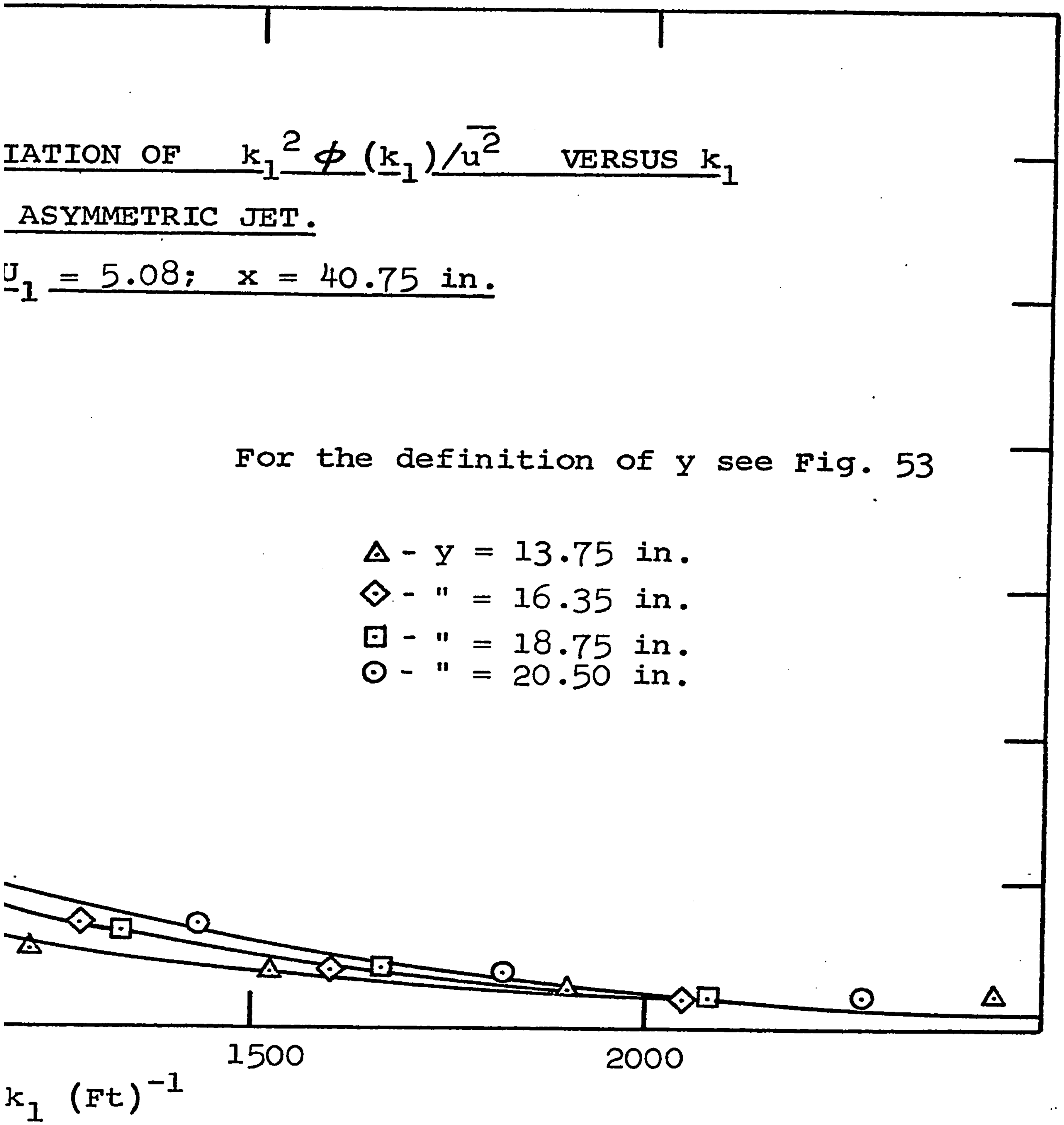
IATION OF $k_1^2 \phi(k_1)/\overline{u^2}$ VERSUS k_1
ASYMMETRIC JET.
U_1 = 5.08; x = 40.75 in.
For the definition of y see Fig. 53
△ - y = 13.75 in.
◇ - " = 16.35 in.
□ - " = 18.75 in.
⊙ - " = 20.50 in.
1500
2000
k_1 (Ft)$^{-1}$

Fig. 55

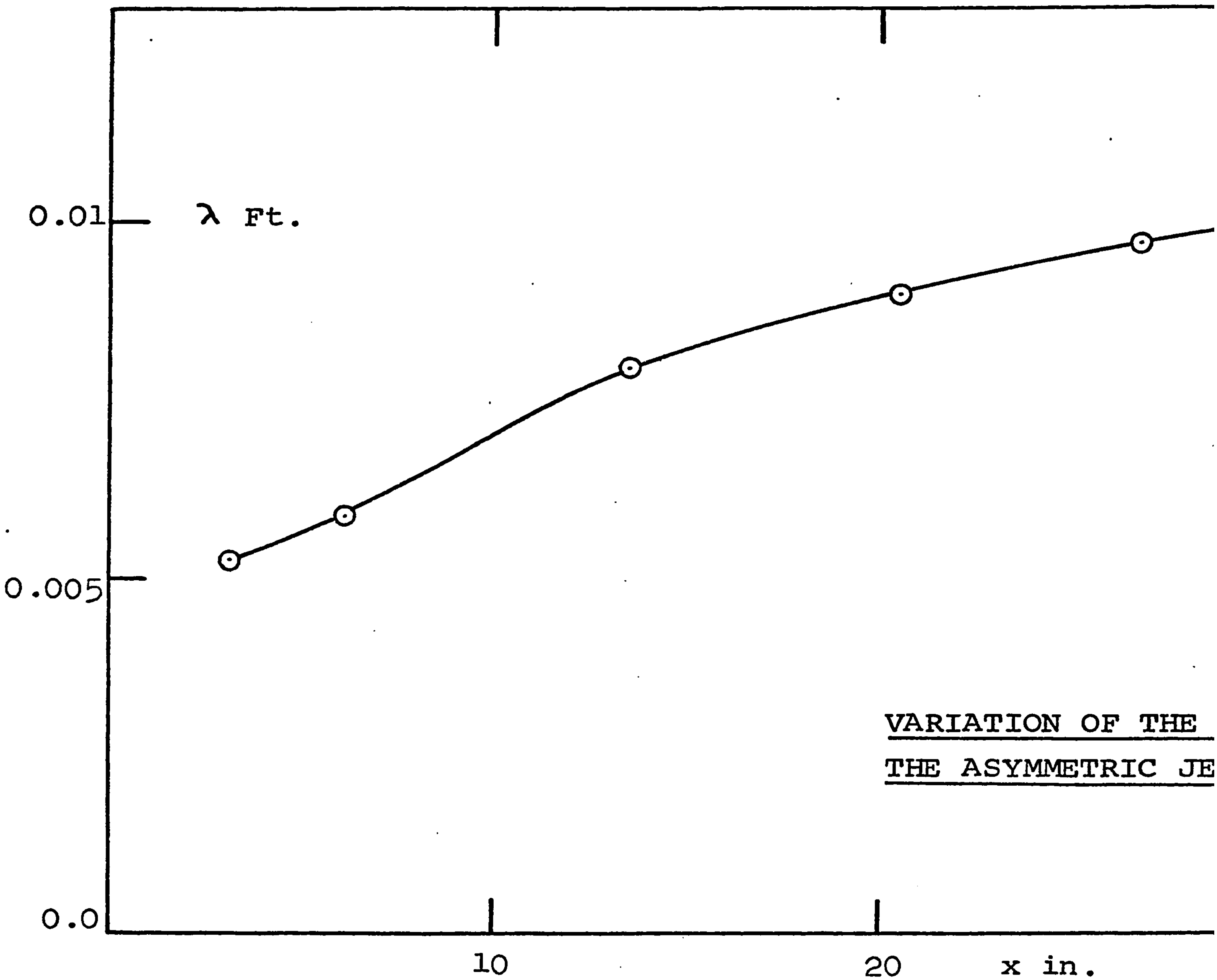

VARIATION OF THE
THE ASYMMETRIC JE

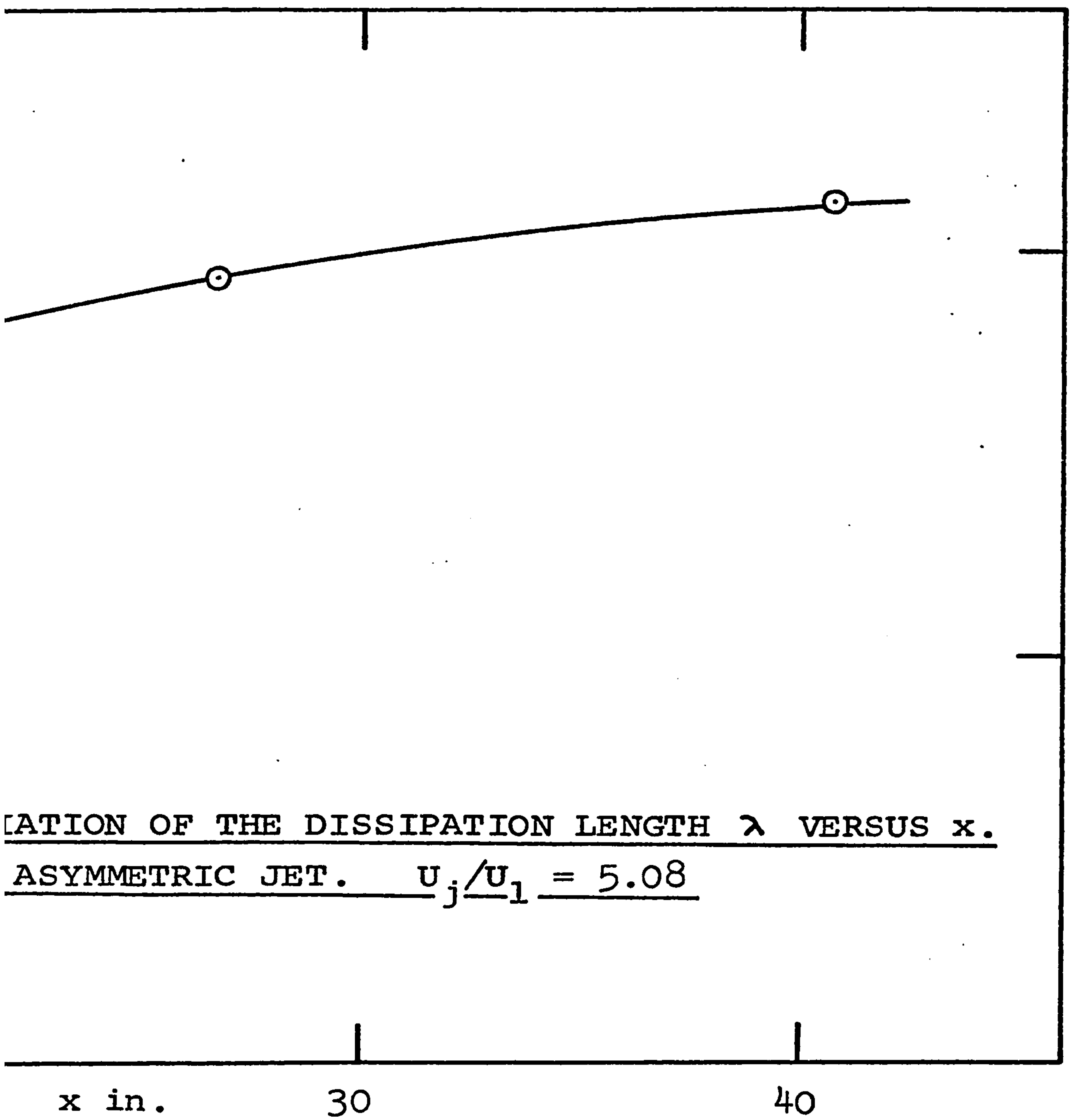

[V]ATION OF THE DISSIPATION LENGTH λ VERSUS x.
ASYMMETRIC JET. $U_j/U_1 = 5.08$

Fig. 56

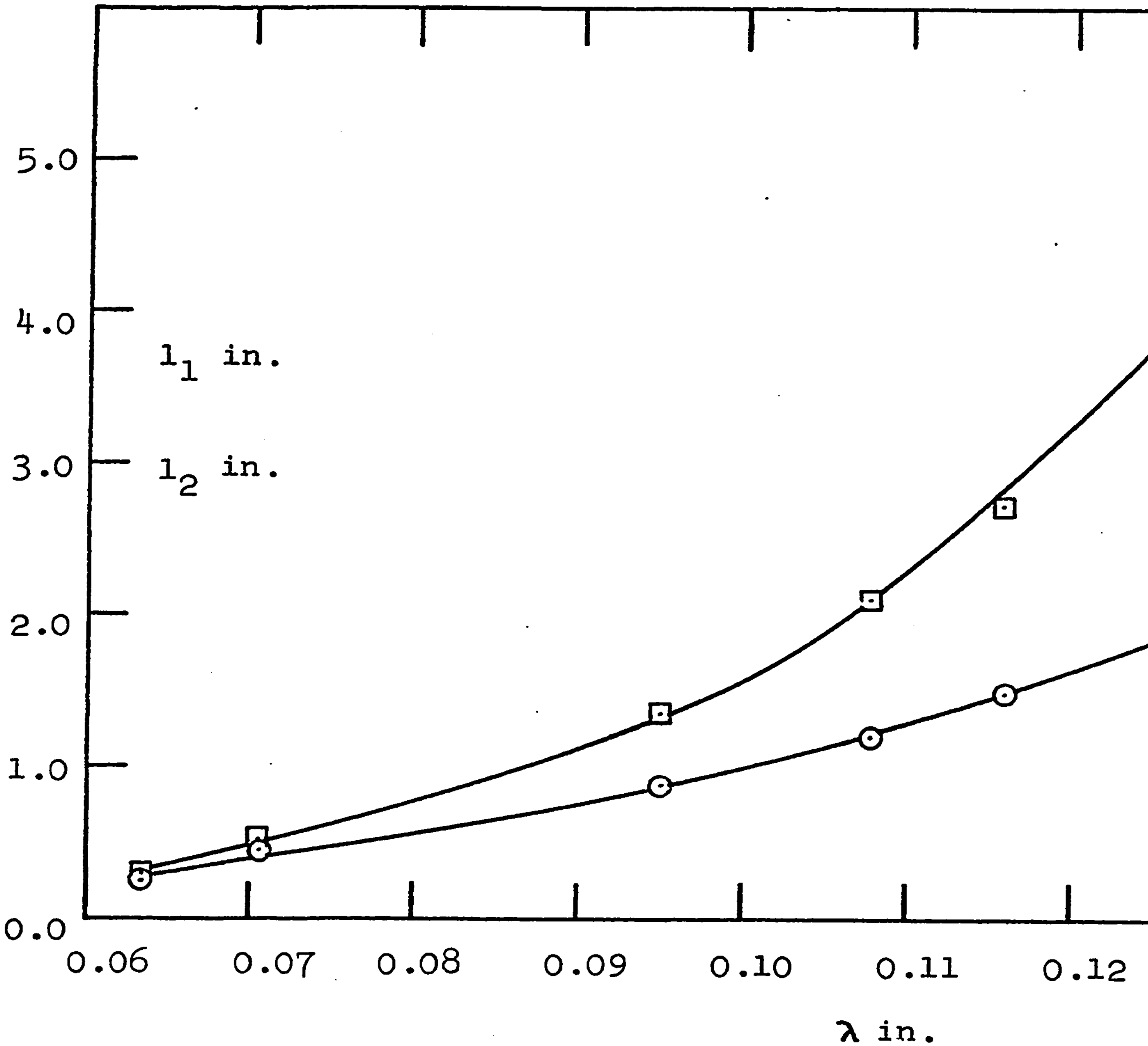

VARIATIONS OF MEAN FLOW LENGTH SCALES VERSUS λ
THE ASYMMETRIC JET. $U_j/U_1 = 5.08$

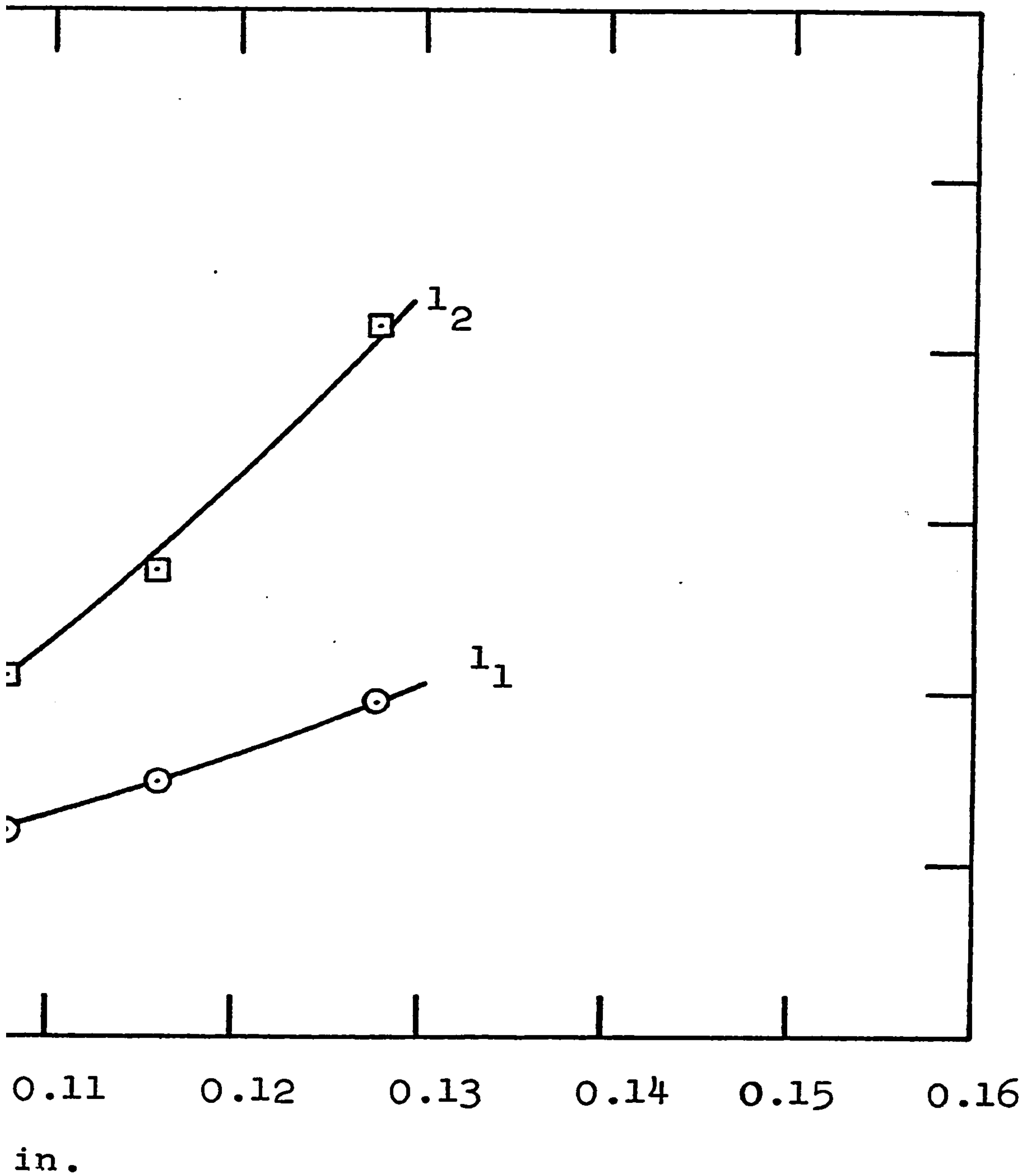

ALES VERSUS λ .
08

Fig. 57

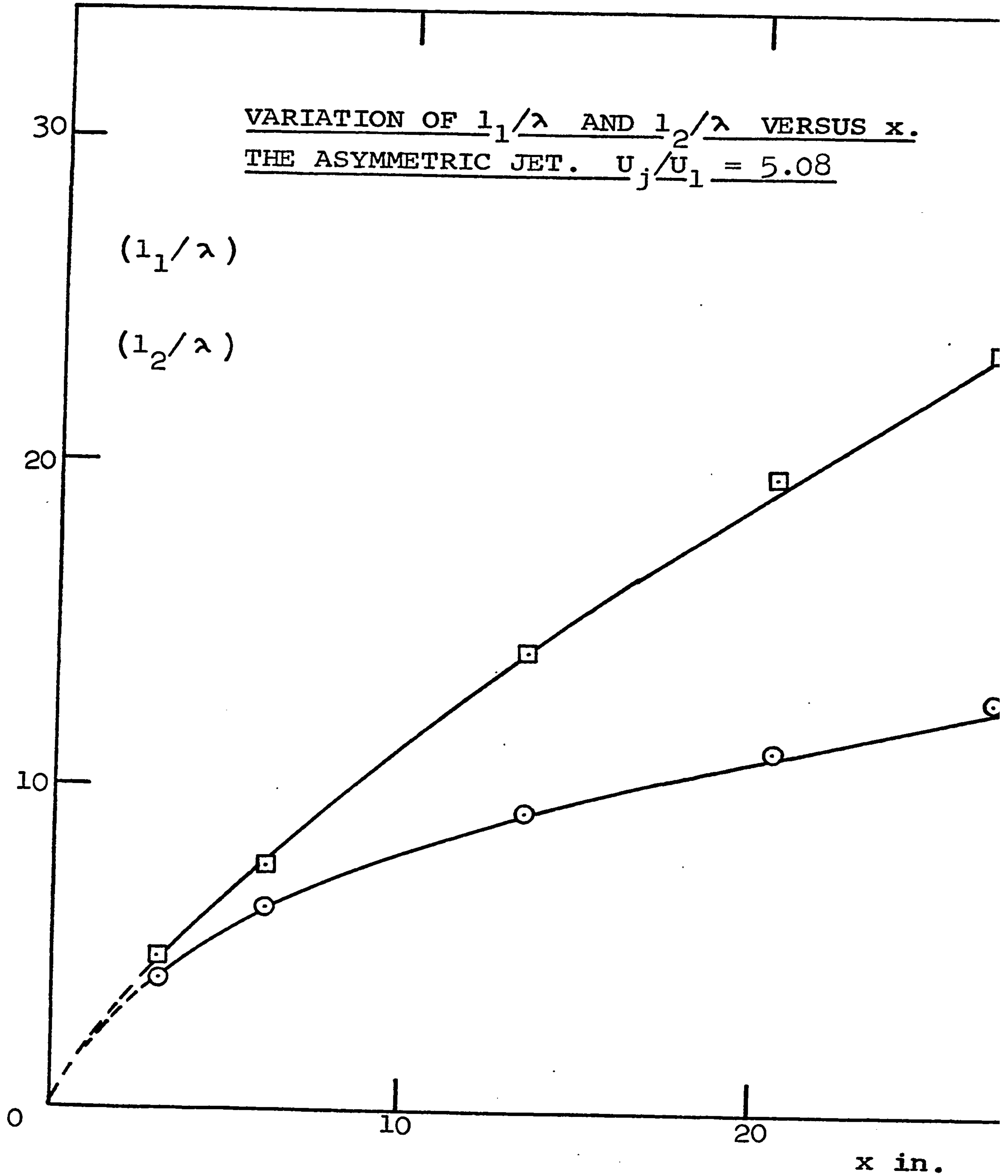
VARIATION OF l_1/λ AND l_2/λ VERSUS x.
THE ASYMMETRIC JET. $U_j/U_1 = 5.08$
(l_1/λ)
(l_2/λ)
30
20
10
0
10
20
x in.

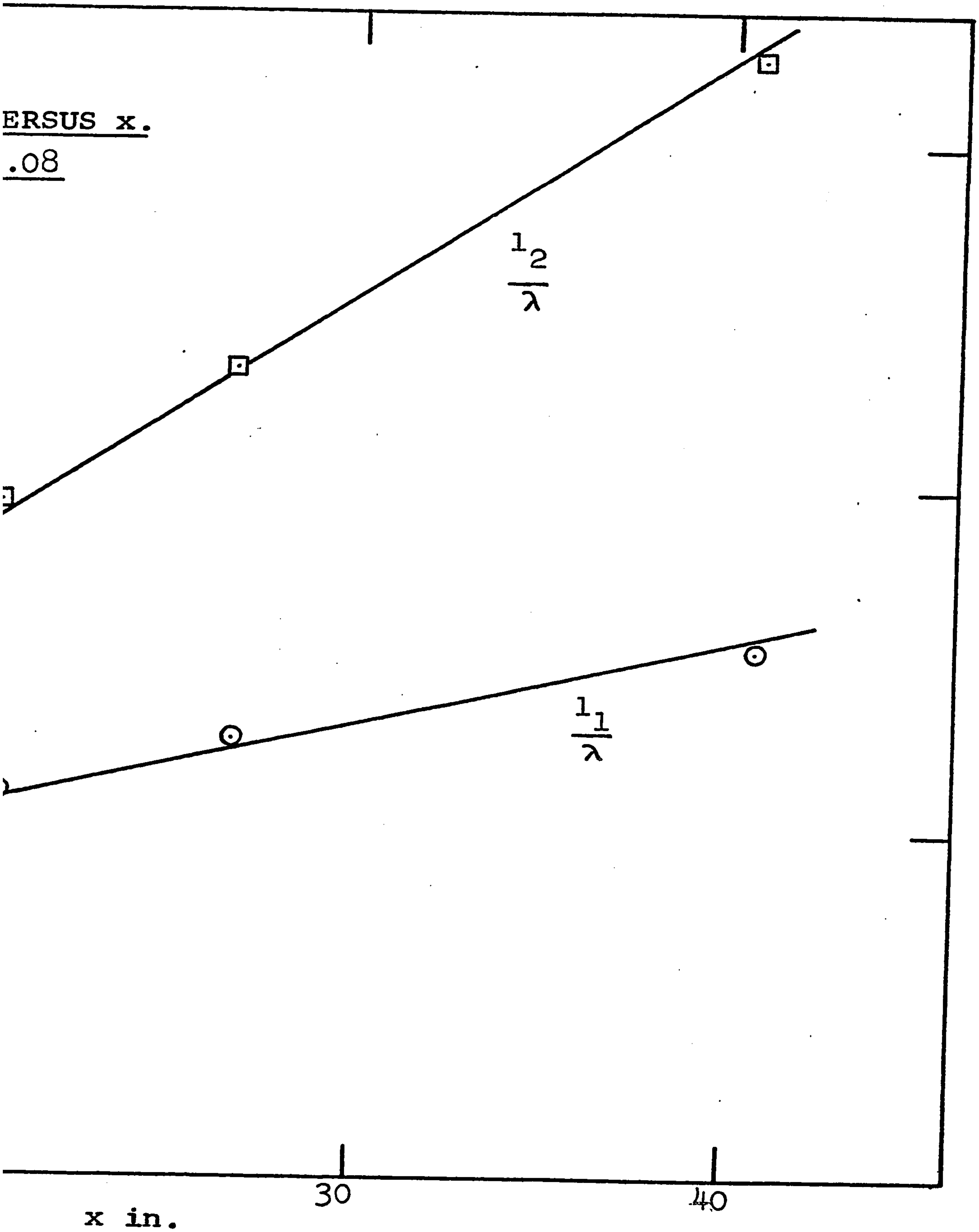

Fig. 58

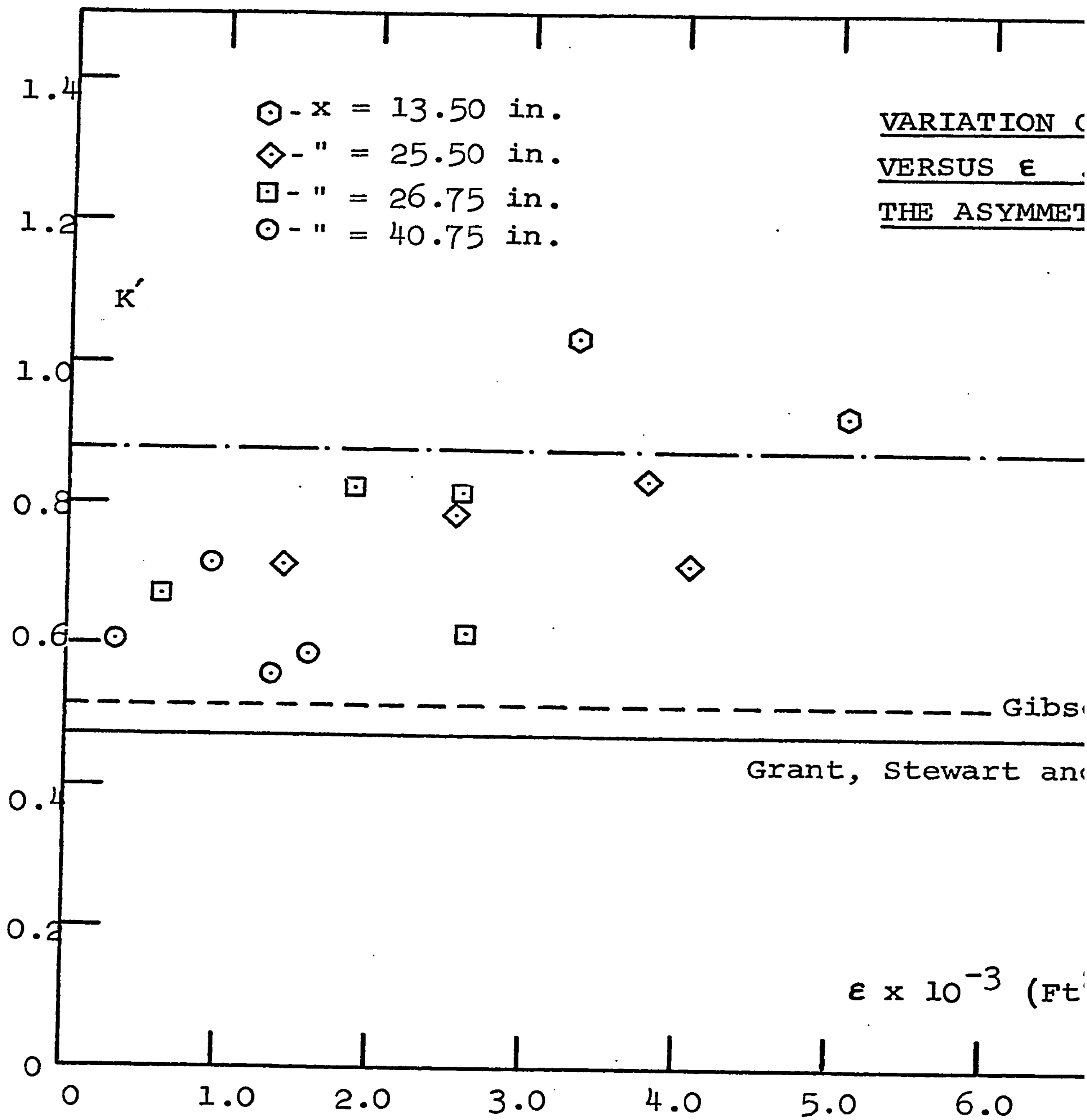

- x = 13.50 in.
- " = 25.50 in.
- " = 26.75 in.
- " = 40.75 in.
VARIATION
VERSUS ε
THE ASYMME
K'
Gibs
Grant, Stewart an
ε x 10^-3 (Ft
1.4
1.2
1.0
0.8
0.6
0.4
0.2
0
0
1.0
2.0
3.0
4.0
5.0
6.0

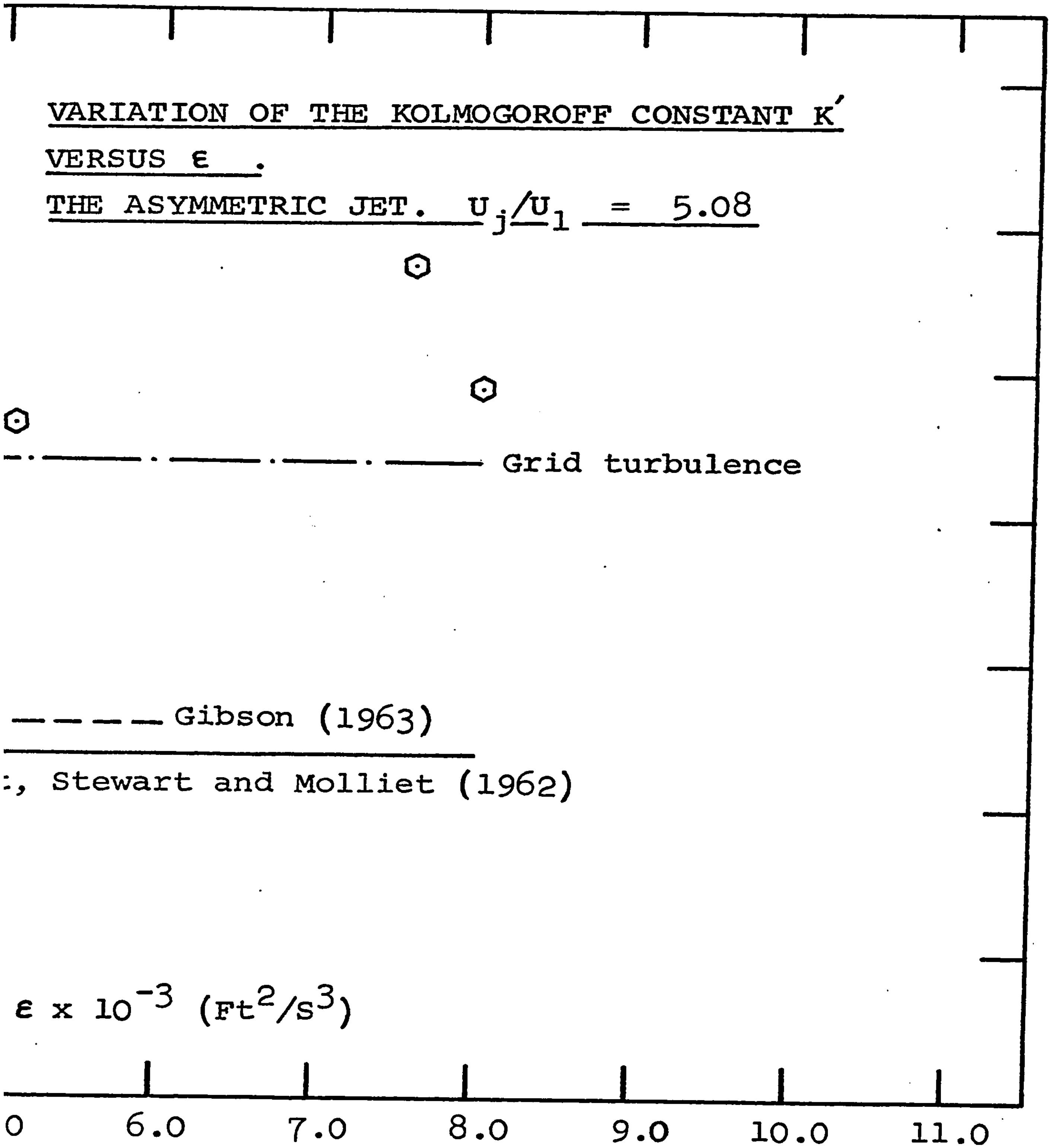
VARIATION OF THE KOLMOGOROFF CONSTANT K′
VERSUS ε .
THE ASYMMETRIC JET. U_j/U_1 = 5.08
Grid turbulence
Gibson (1963)
:, Stewart and Molliet (1962)
ε x 10^{-3} (Ft^2/s^3)
0
6.0
7.0
8.0
9.0
10.0
11.0

Fig. 59

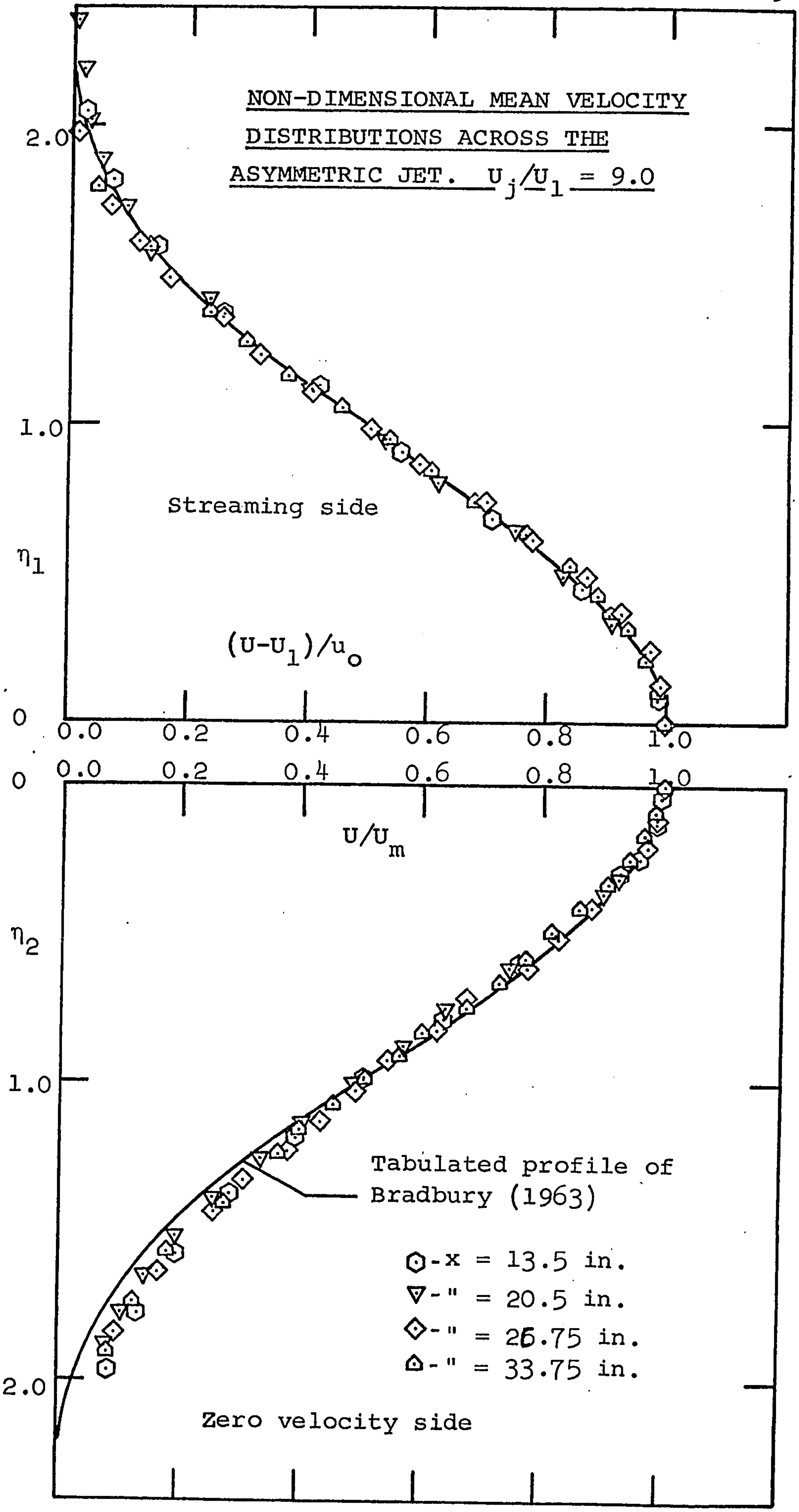
NON-DIMENSIONAL MEAN VELOCITY
DISTRIBUTIONS ACROSS THE
ASYMMETRIC JET. $U_j/U_1 = 9.0$
Streaming side
η_1
$(U-U_1)/u_o$
0.0 0.2 0.4 0.6 0.8 1.0
2.0
1.0
0
U/U_m
η_2
Tabulated profile of
Bradbury (1963)
⬡ - x = 13.5 in.
▽ - " = 20.5 in.
◇ - " = 26.75 in.
△ - " = 33.75 in.
Zero velocity side

Fig. 61

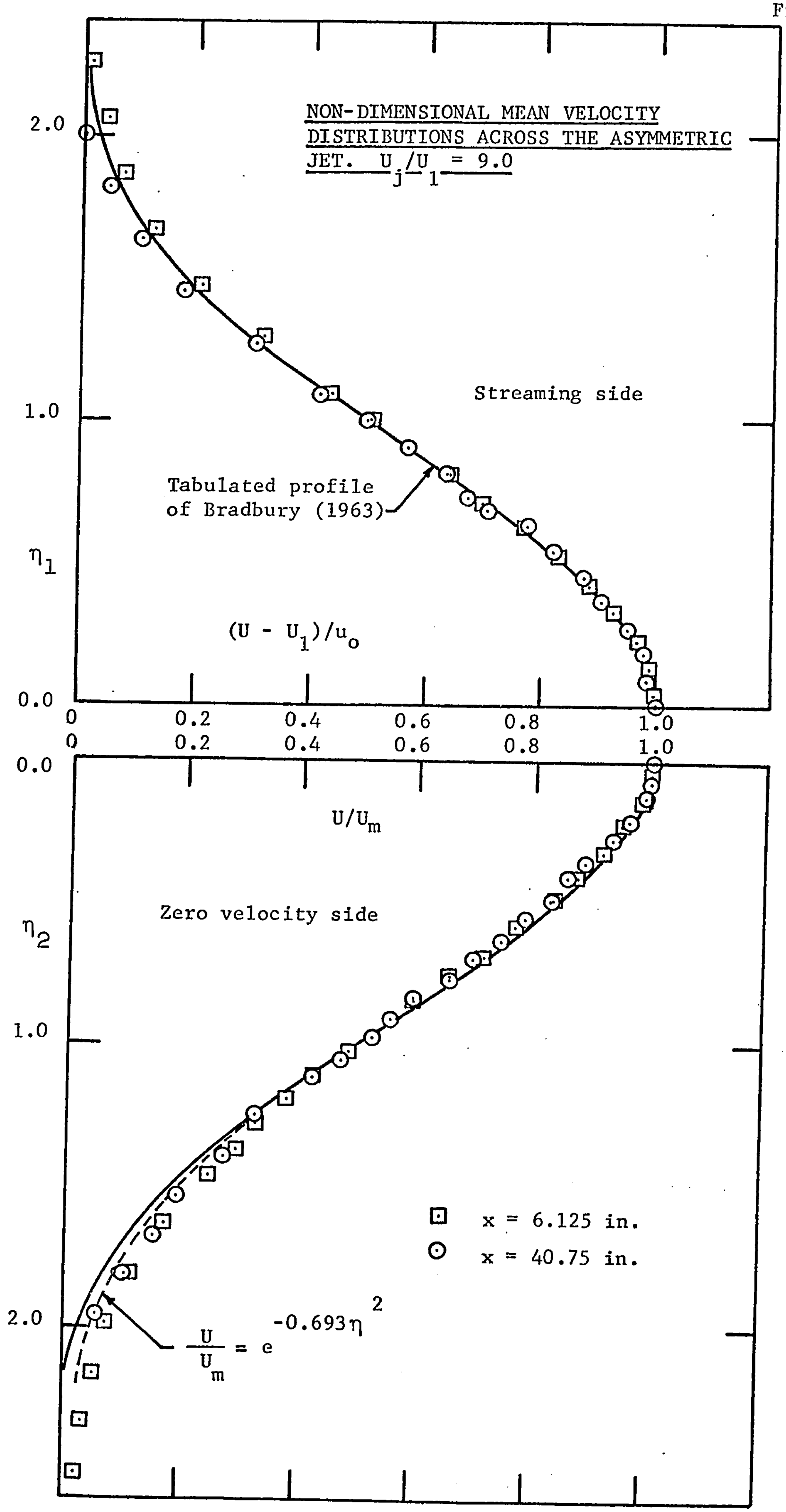
NON-DIMENSIONAL MEAN VELOCITY DISTRIBUTIONS ACROSS THE ASYMMETRIC JET. $U_j/U_1 = 9.0$
Streaming side
Tabulated profile of Bradbury (1963)
η_1
$(U - U_1)/u_o$
2.0
1.0
0.0
0
0.2
0.4
0.6
0.8
1.0
0
0.2
0.4
0.6
0.8
1.0
0.0
U/U_m
Zero velocity side
η_2
1.0
2.0
x = 6.125 in.
x = 40.75 in.
$\frac{U}{U_m} = e^{-0.693\eta^2}$

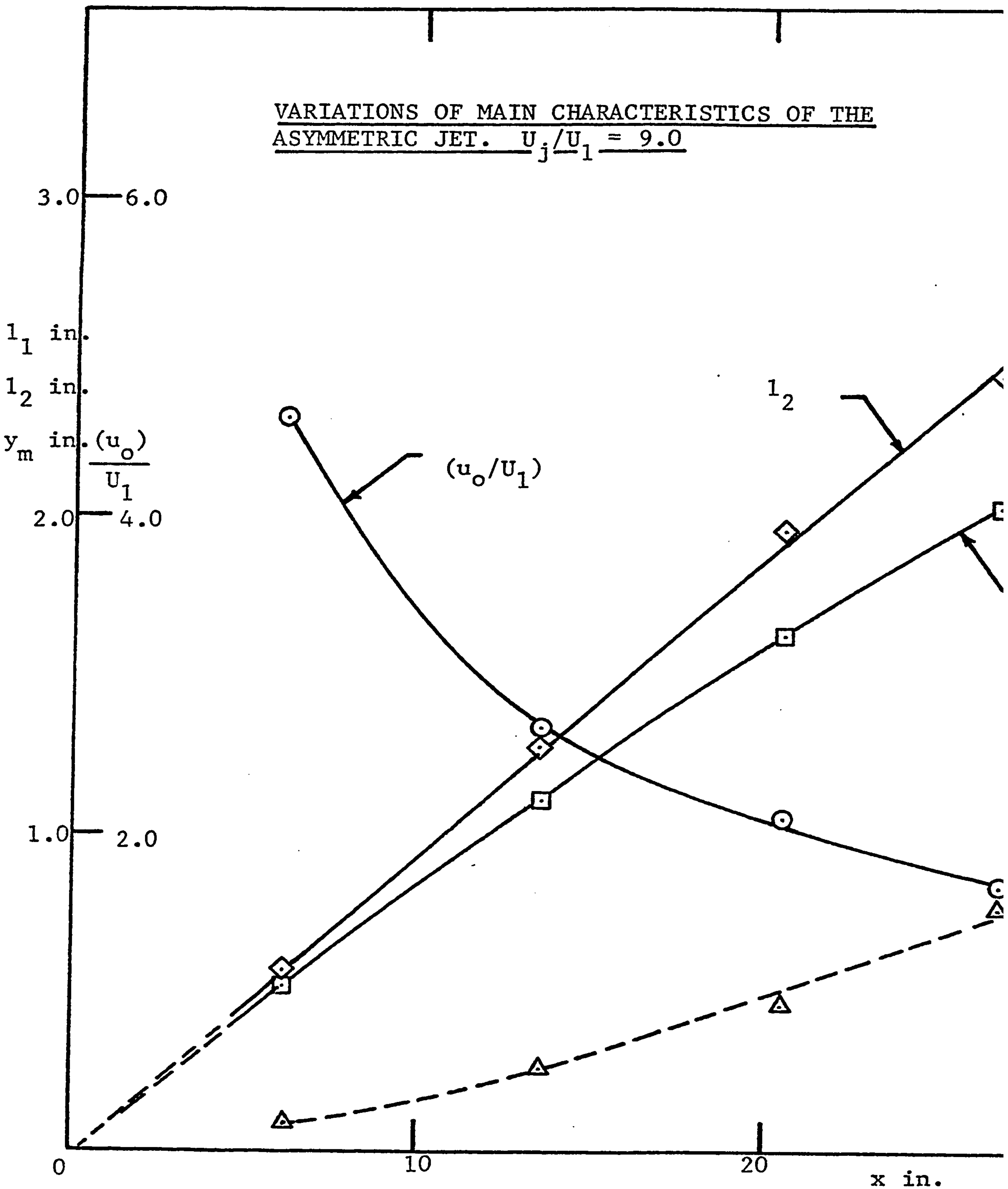
VARIATIONS OF MAIN CHARACTERISTICS OF THE ASYMMETRIC JET. $U_j/U_1 = 9.0$
3.0
6.0
l_1 in.
l_2 in.
y_m in.
$\frac{(u_o)}{U_1}$
2.0
4.0
1.0
2.0
l_2
(u_o/U_1)
0
10
20
x in.

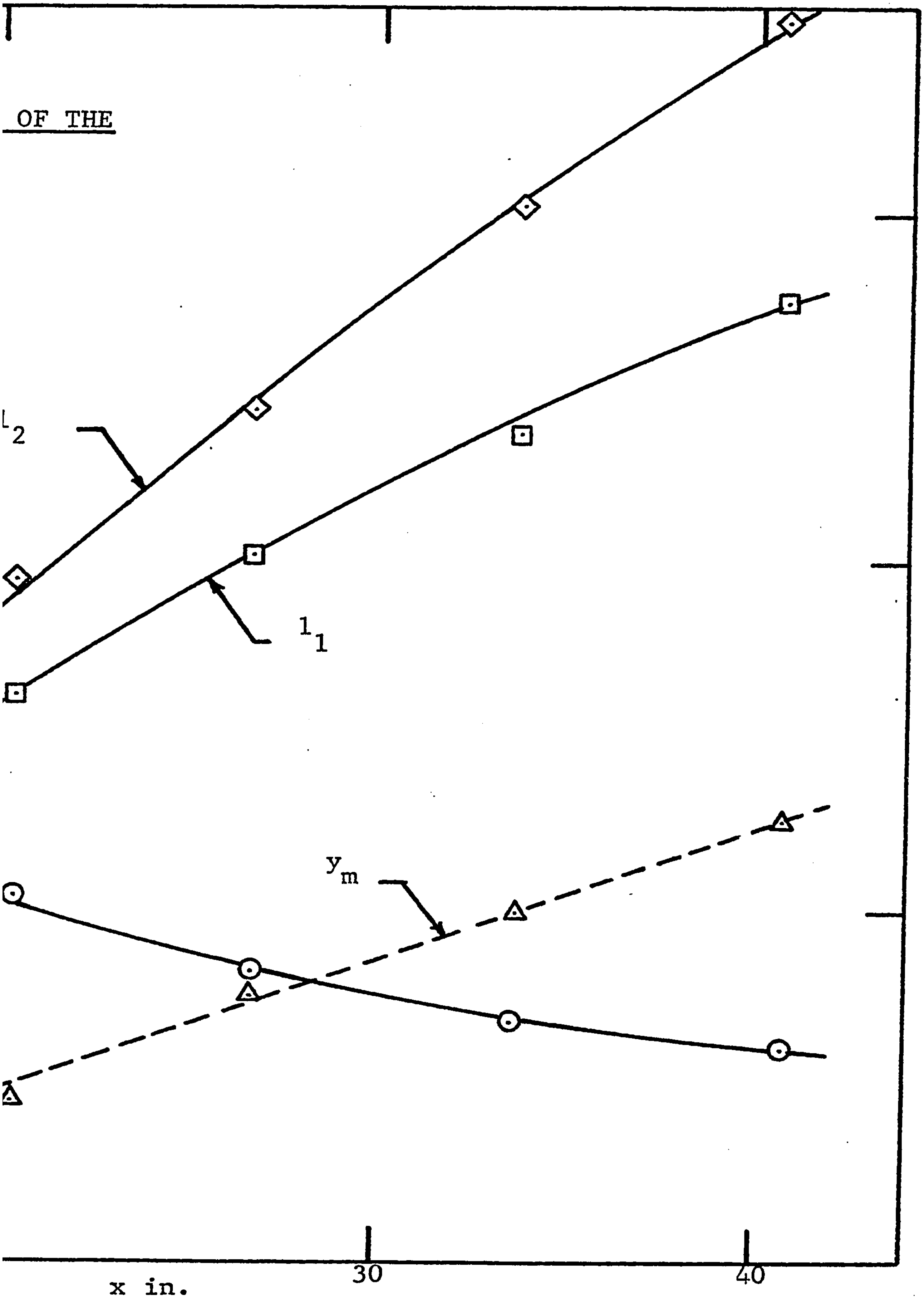

Fig. 62

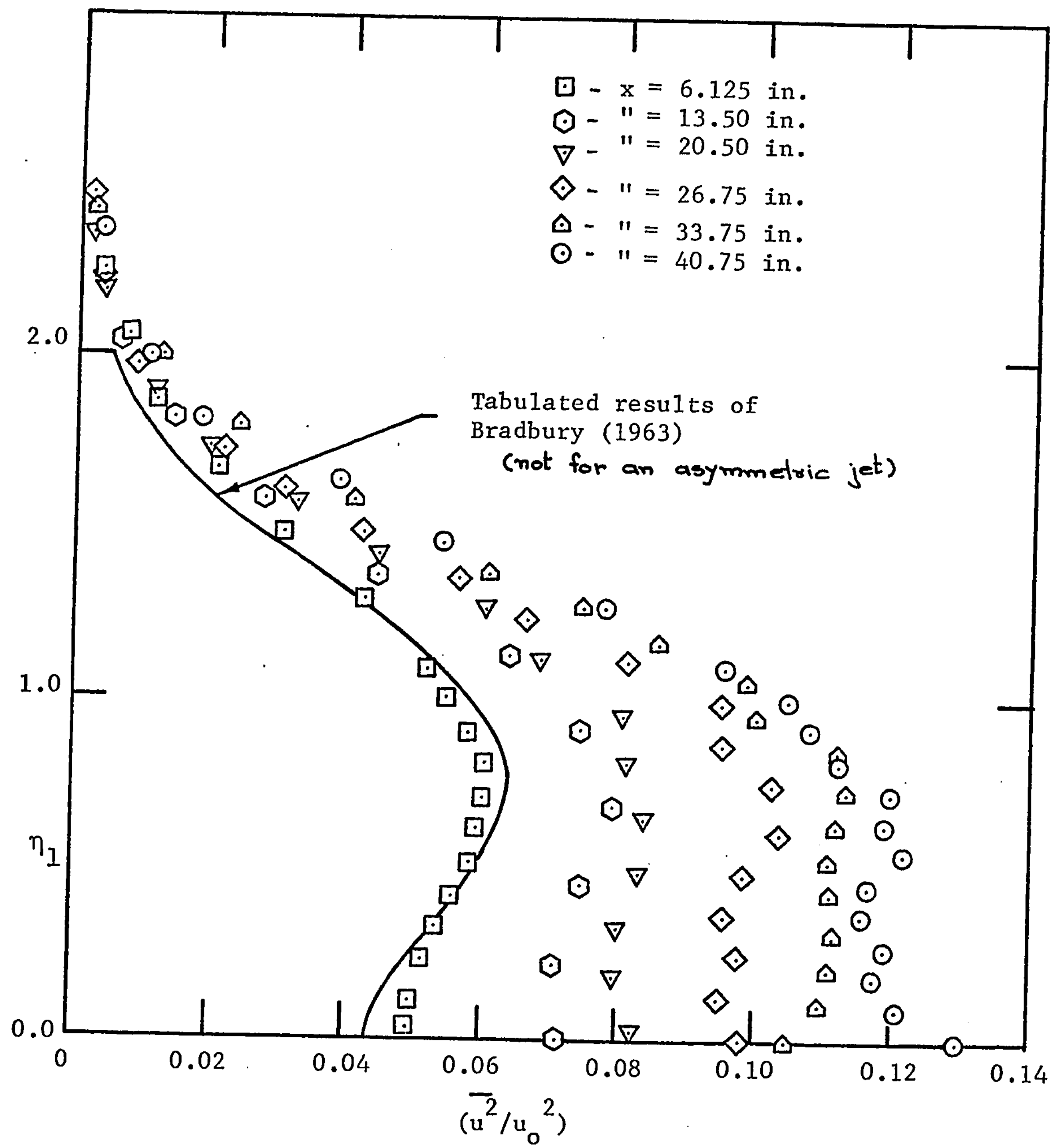

$\overline{u^2}/u_o^2$ - DISTRIBUTIONS ON THE STREAMING SIDE OF THE ASYMMETRIC JET. $U_j/U_1 = 9.0$

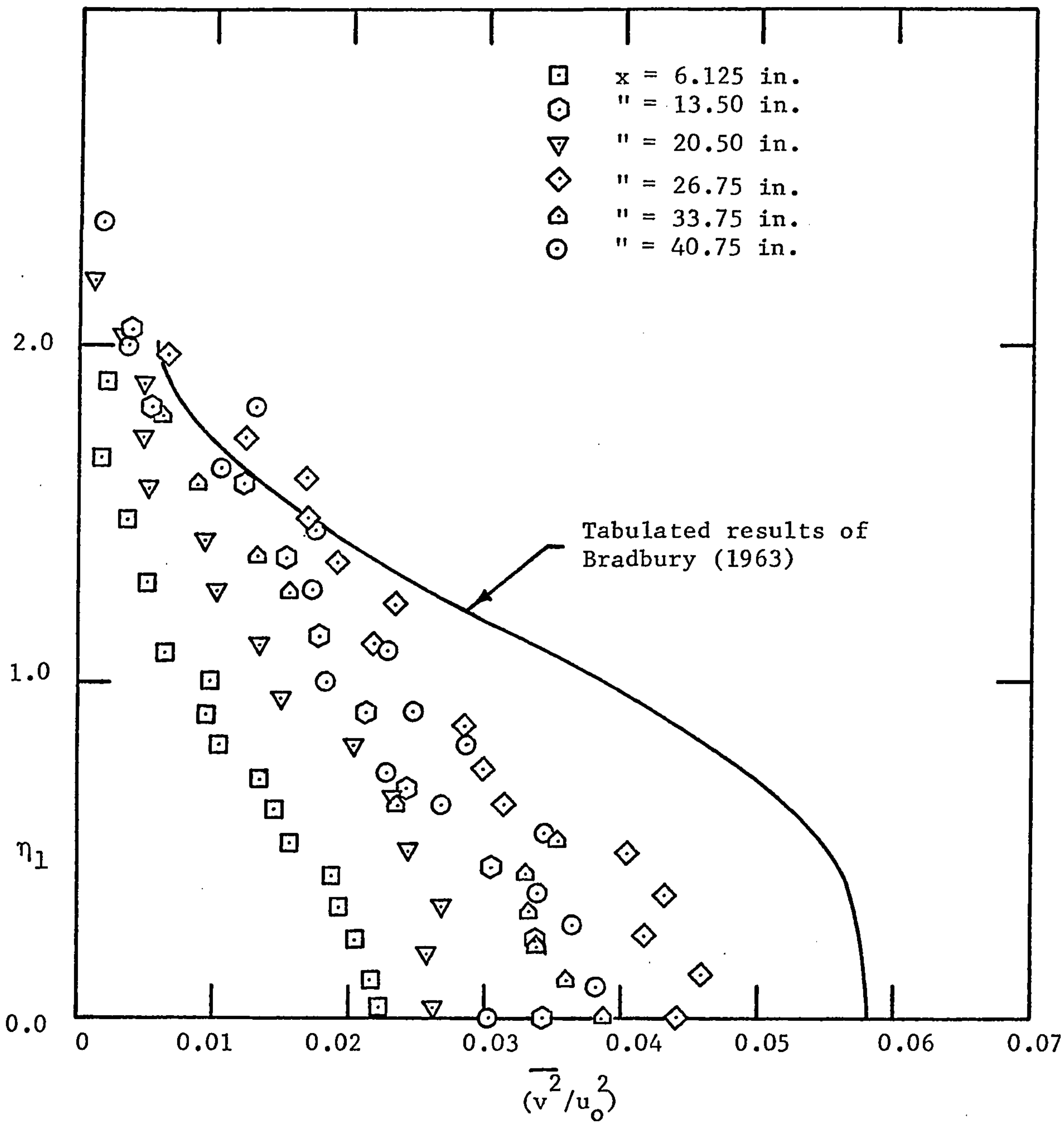

$\overline{v^2}/u_o^2$ - DISTRIBUTIONS ON THE STREAMING SIDE OF THE ASYMMETRIC JET. $U_j/U_1 = 9.0$

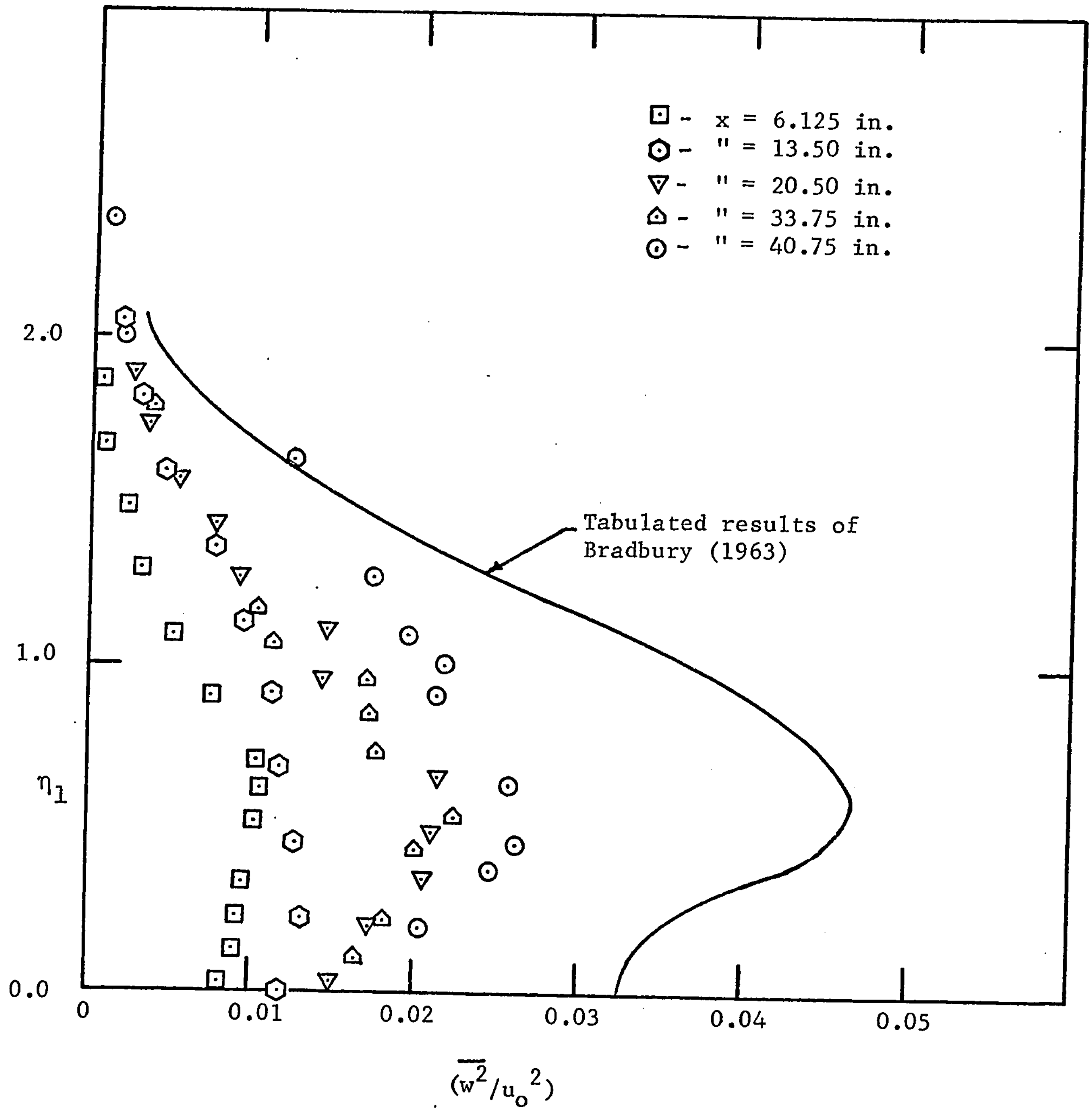

$\overline{w^2}/u_o^2$ - DISTRIBUTIONS ON THE STREAMING SIDE OF THE ASYMMETRIC JET. $U_j/U_1 = 9.0$

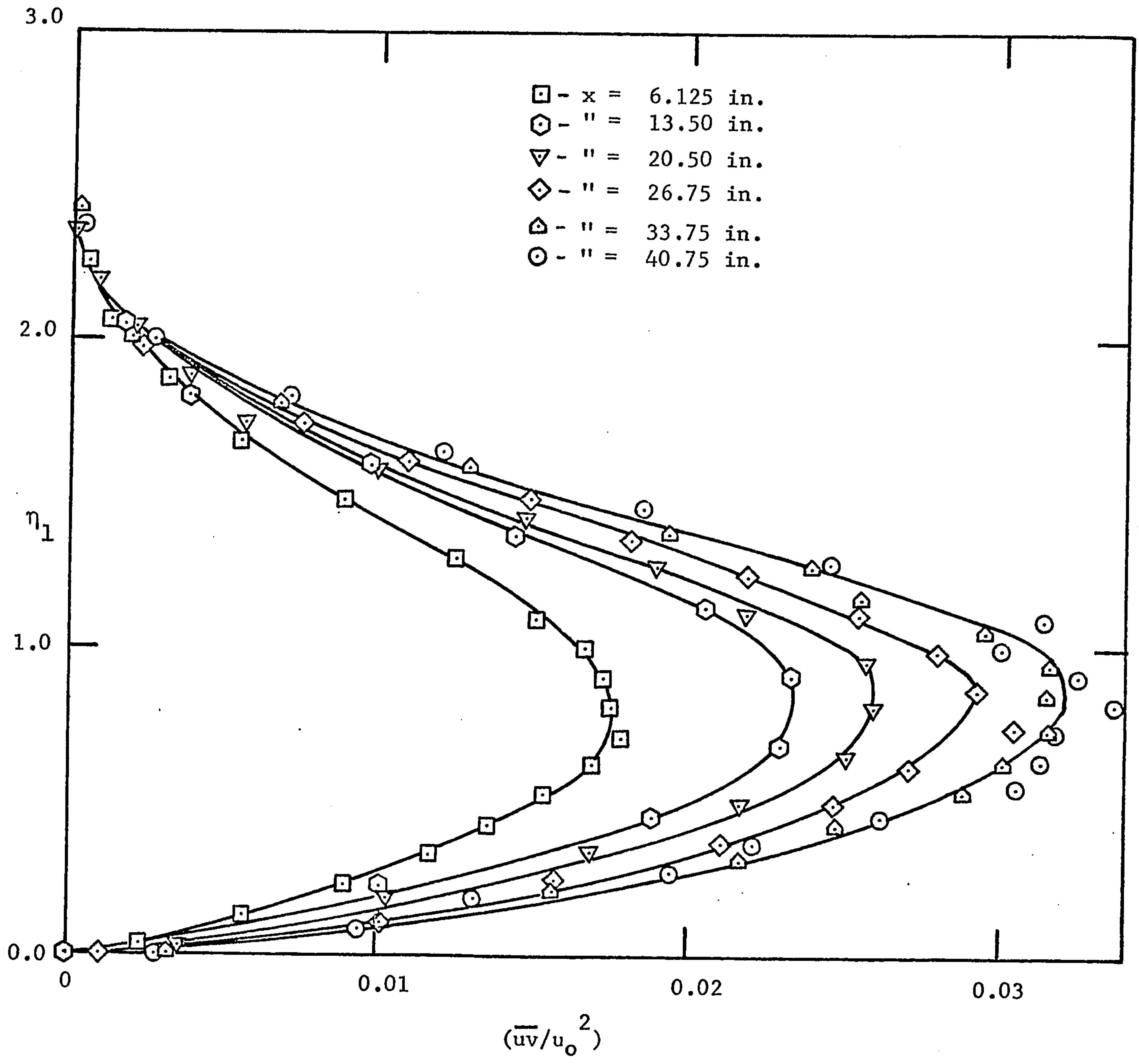

SHEAR STRESS DISTRIBUTIONS ON THE STREAMING SIDE OF THE ASYMMETRIC JET. $U_j/U_1 = 9.0$

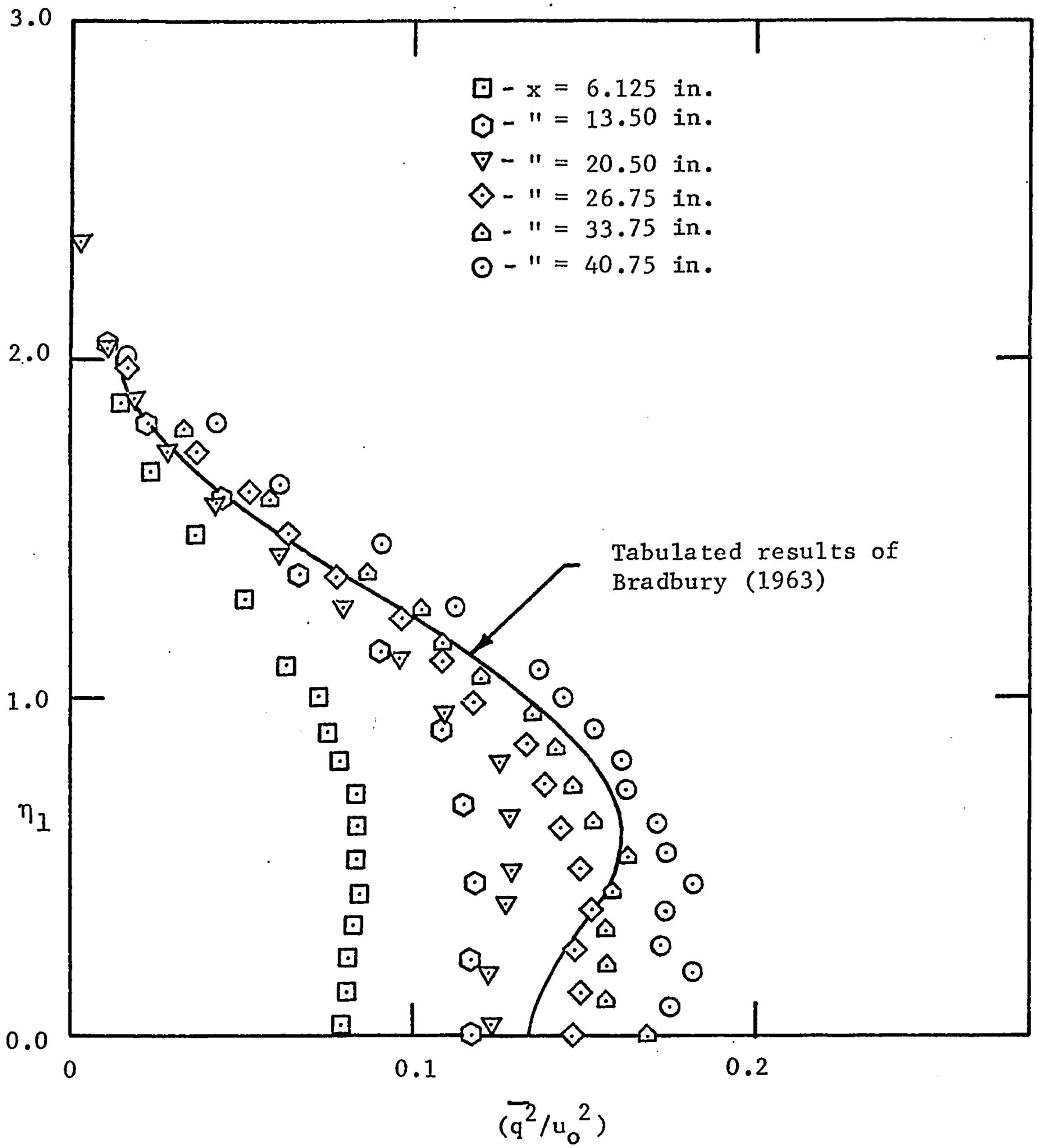

TURBULENT ENERGY DISTRIBUTIONS ON THE STREAMING SIDE OF THE ASYMMETRIC JET. $U_j/U_1 = 9.0$

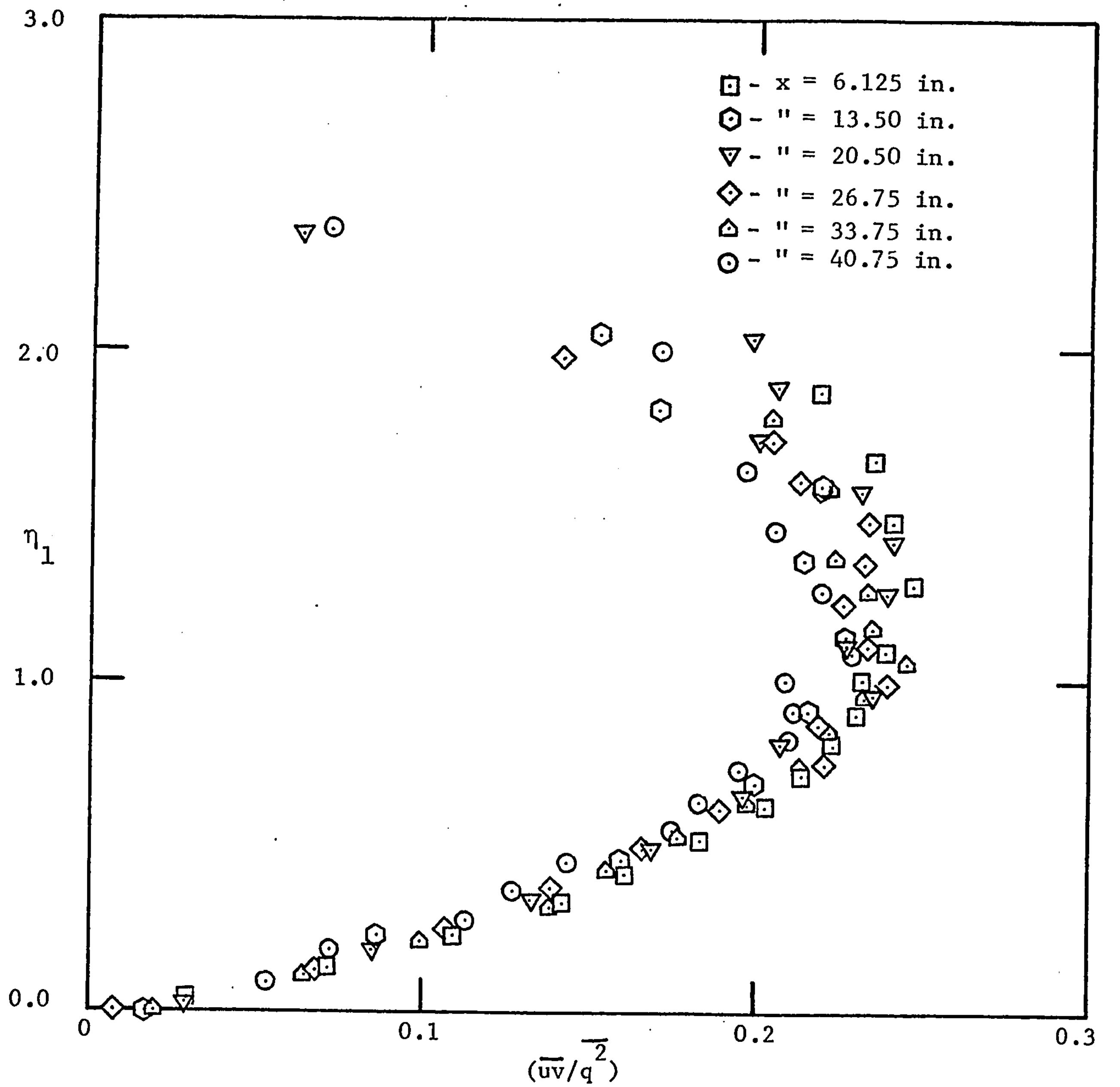

$\overline{uv}/\overline{q^2}$ - DISTRIBUTIONS ON THE STREAMING SIDE OF THE ASYMMETRIC JET. $U_j/U_1 = 9.0$

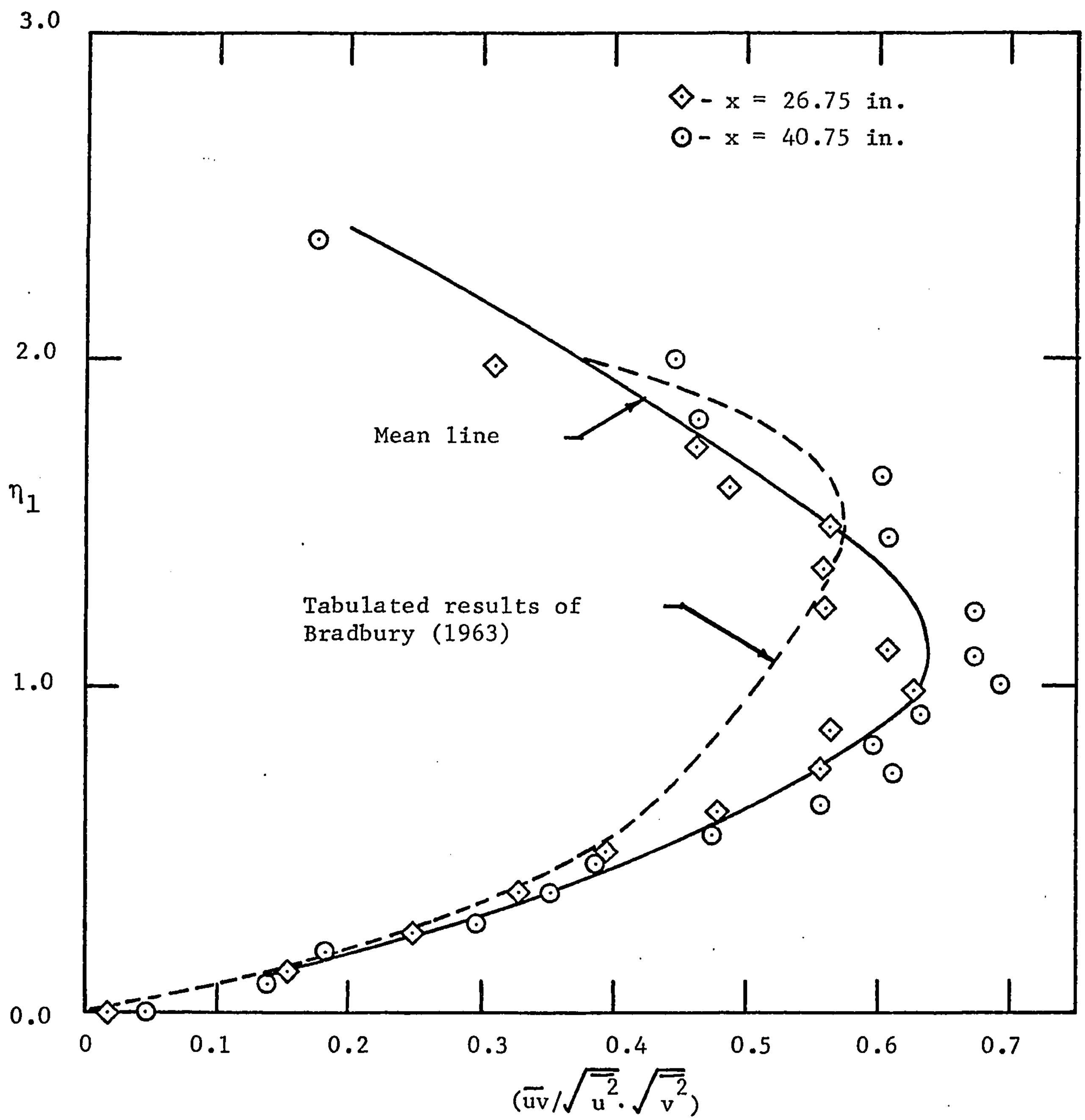

$R_{\overline{uv}}$ - CORRELATION ON THE STREAMING SIDE OF THE ASYMMETRIC JET. $U_j/U_1 = 9.0$

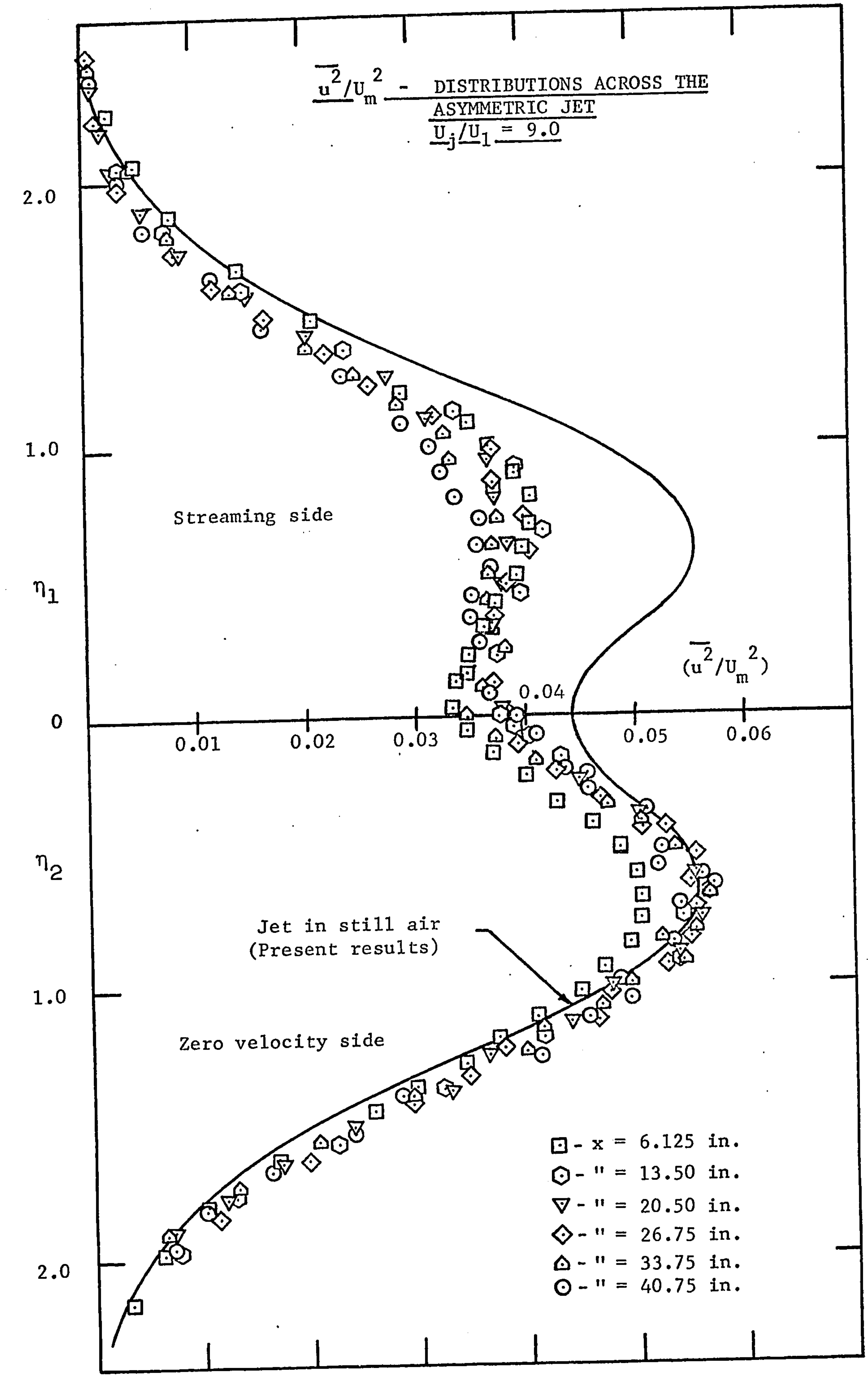
$\overline{u^2}/U_m^2$ - DISTRIBUTIONS ACROSS THE ASYMMETRIC JET
$U_j/U_1 = 9.0$
2.0
1.0
Streaming side
η_1
0
$(\overline{u^2}/U_m^2)$
0.01
0.02
0.03
0.04
0.05
0.06
η_2
Jet in still air
(Present results)
1.0
Zero velocity side
2.0
□ - x = 6.125 in.
⬡ - " = 13.50 in.
▽ - " = 20.50 in.
◇ - " = 26.75 in.
△ - " = 33.75 in.
⊙ - " = 40.75 in.

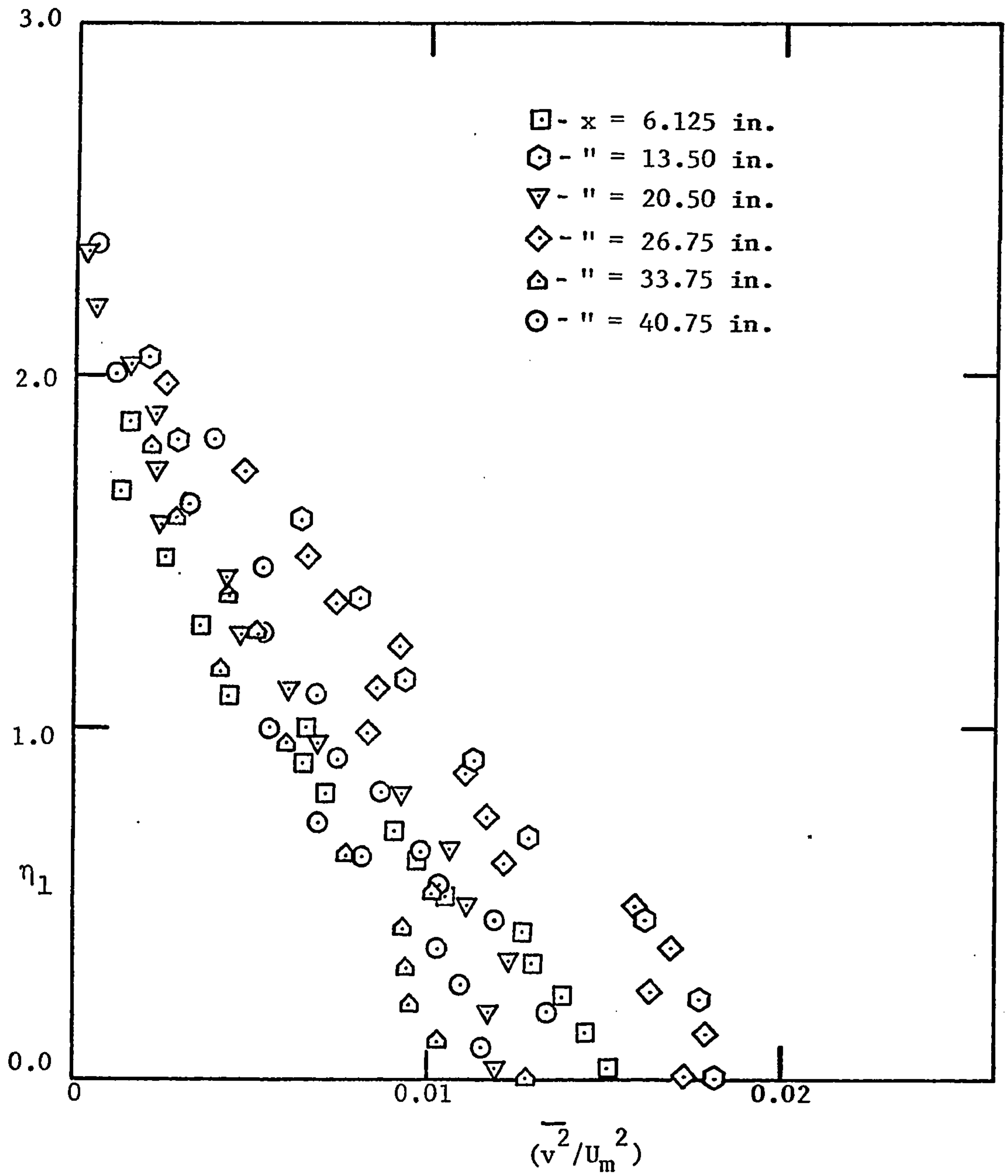

$\overline{v^2}/U_m^2$ - DISTRIBUTION ON THE STREAMING SIDE OF THE ASYMMETRIC JET. $U_j/U_1 = 9.0$

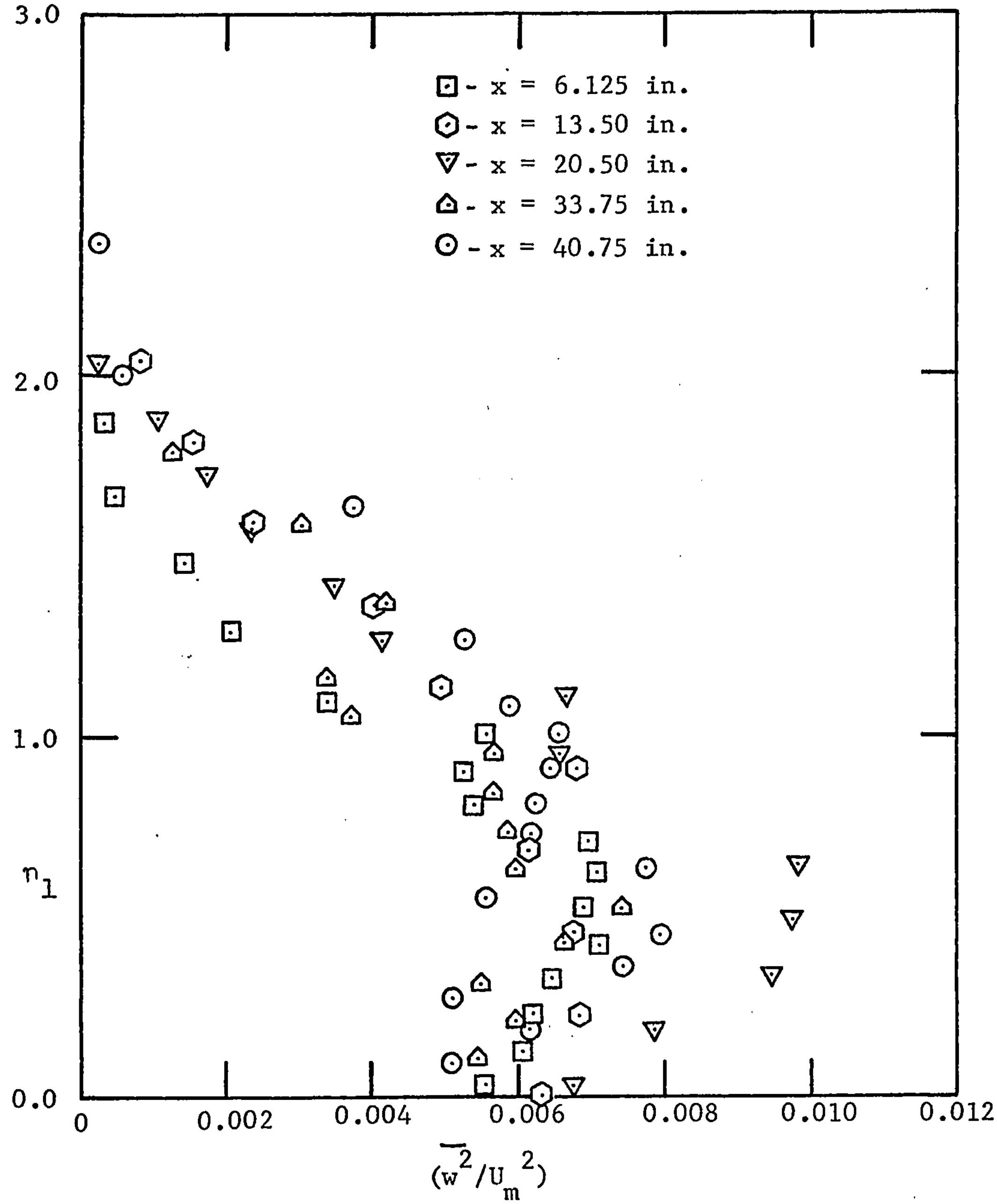

$\overline{w^2}/U_m^{\ 2}$ - DISTRIBUTIONS ON THE STREAMING SIDE OF THE ASYMMETRIC JET. $U_j/U_1 = 9.0$

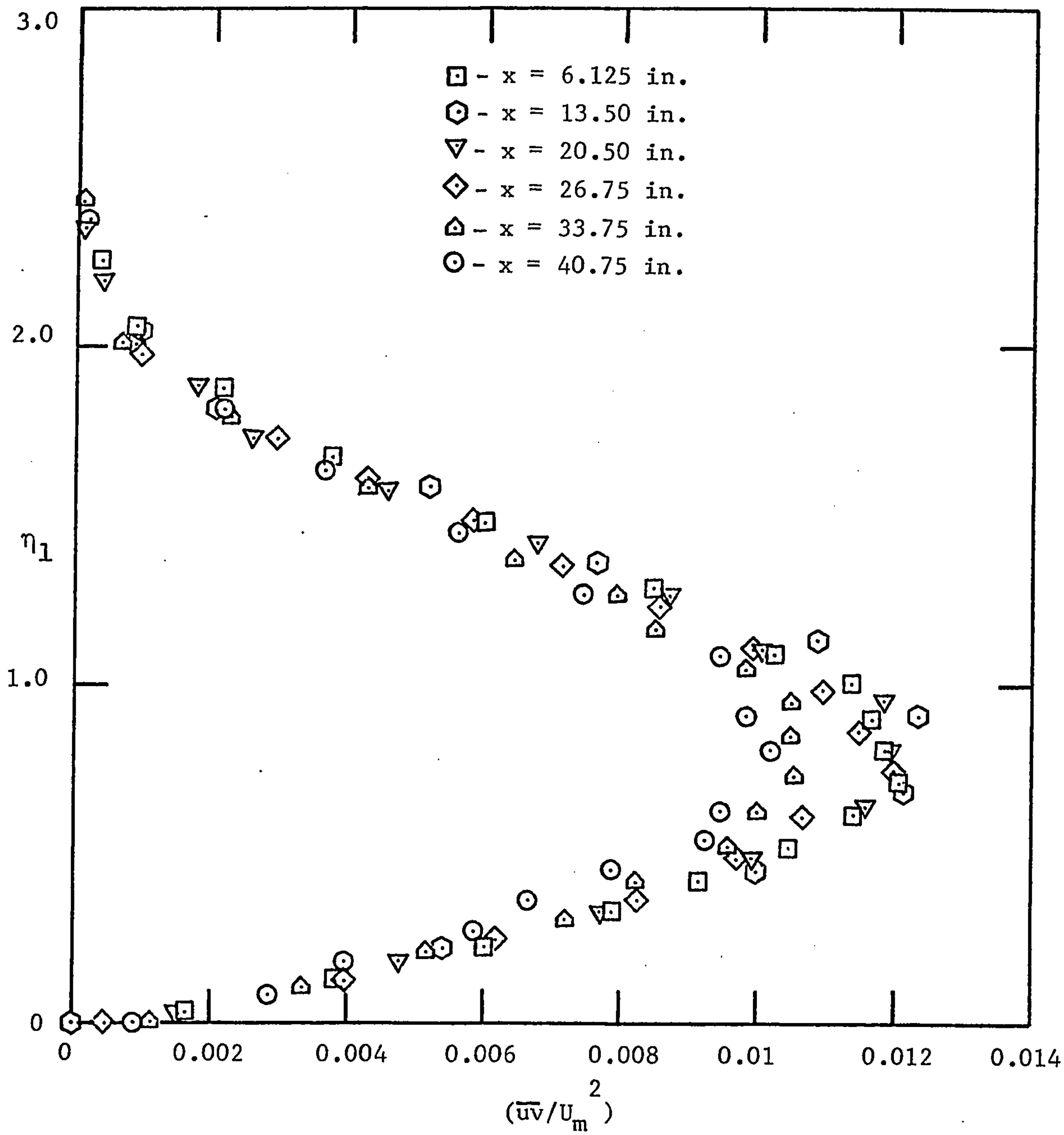

SHEAR STRESS DISTRIBUTIONS ON THE STREAMING SIDE OF THE ASYMMETRIC JET. $U_j/U_1 = 9.0$

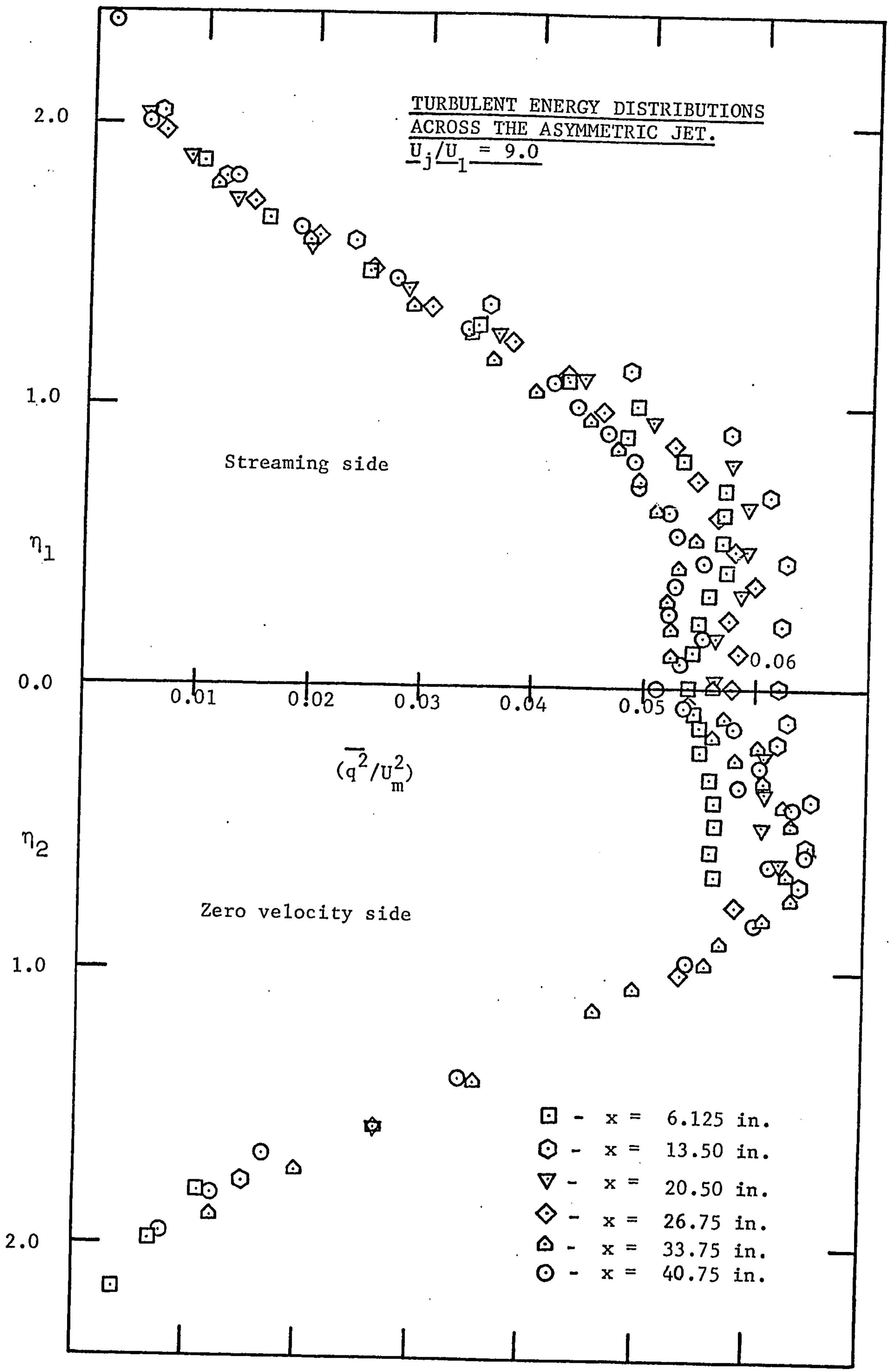

TURBULENT ENERGY DISTRIBUTIONS
ACROSS THE ASYMMETRIC JET.
$U_j/U_1 = 9.0$
2.0
1.0
0.0
1.0
2.0
η_1
η_2
Streaming side
Zero velocity side
0.01
0.02
0.03
0.04
0.05
0.06
$(\overline{q^2}/U_m^2)$
- x = 6.125 in.
- x = 13.50 in.
- x = 20.50 in.
- x = 26.75 in.
- x = 33.75 in.
- x = 40.75 in.

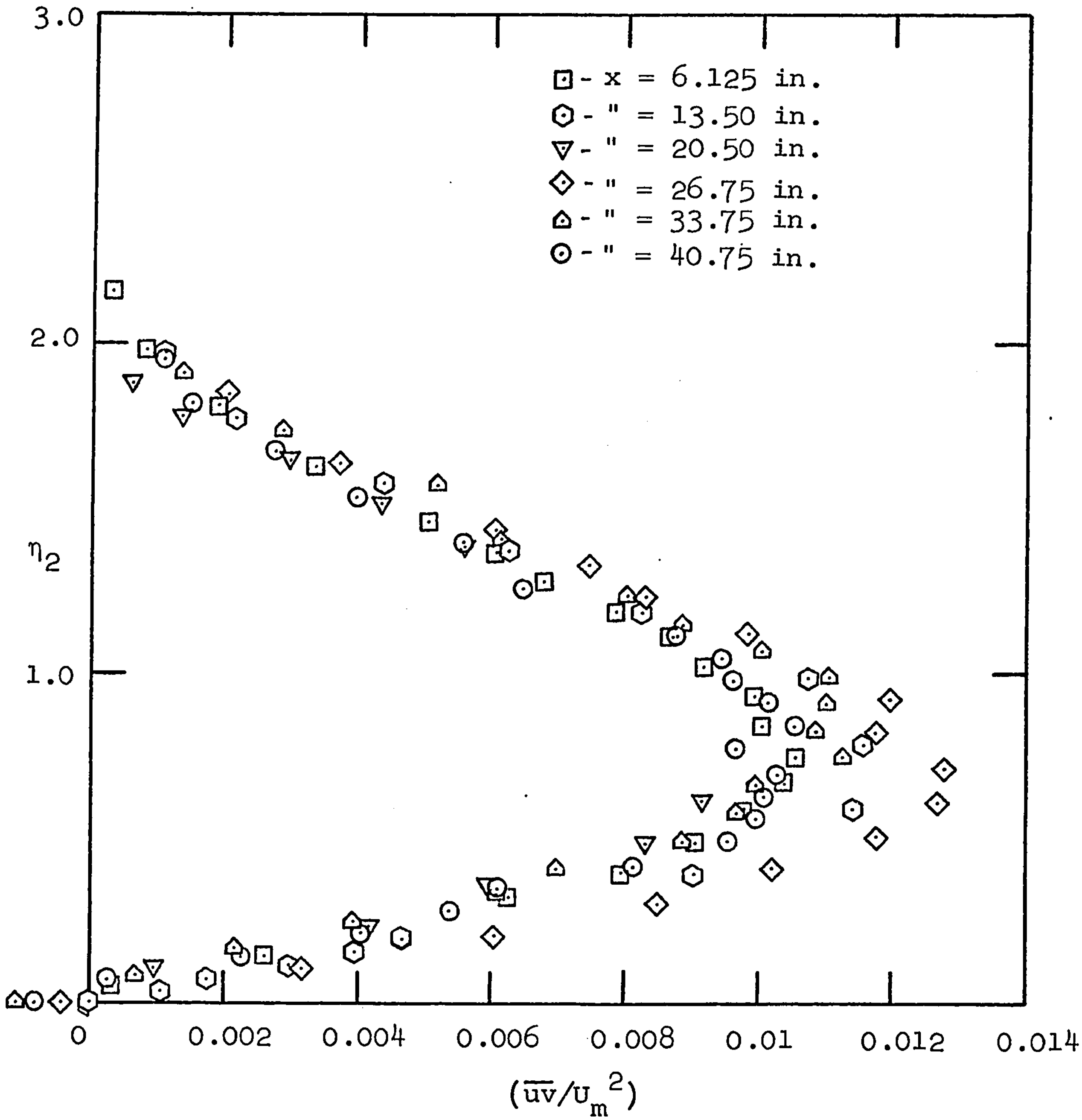

SHEAR STRESS DISTRIBUTIONS ON THE ZERO VELOCITY SIDE OF THE ASYMMETRIC JET. $U_j/U_1 = 9.0$

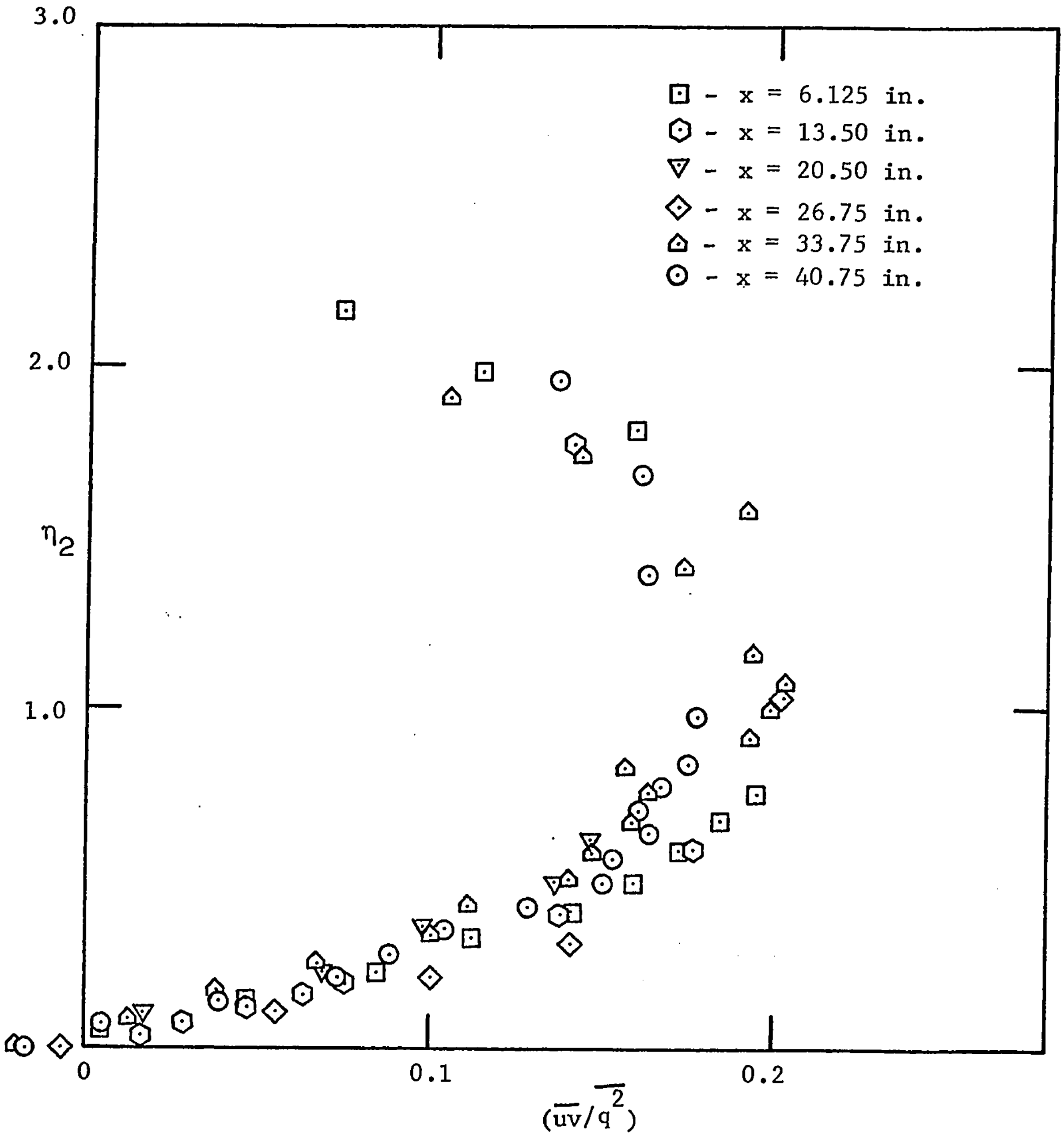

$\overline{uv}/\overline{q^2}$ - VARIATIONS ON THE ZERO VELOCITY SIDE OF THE ASYMMETRIC JET. $U_j/U_1 = 9.0$

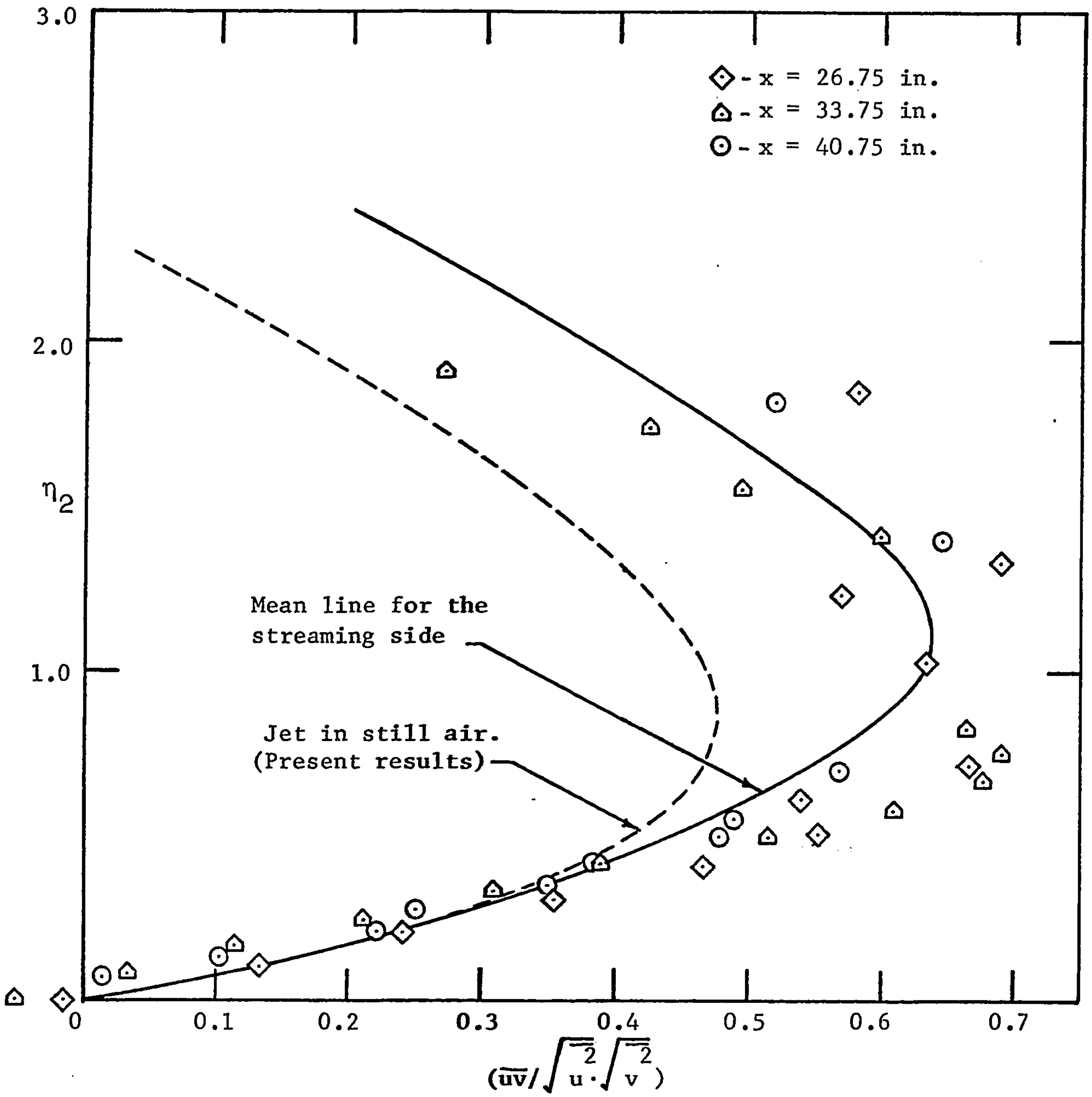

$R_{\overline{uv}}$ - CORRELATION ON THE ZERO VELOCITY SIDE OF THE ASYMMETRIC JET. $U_j/U_1 = 9.0$

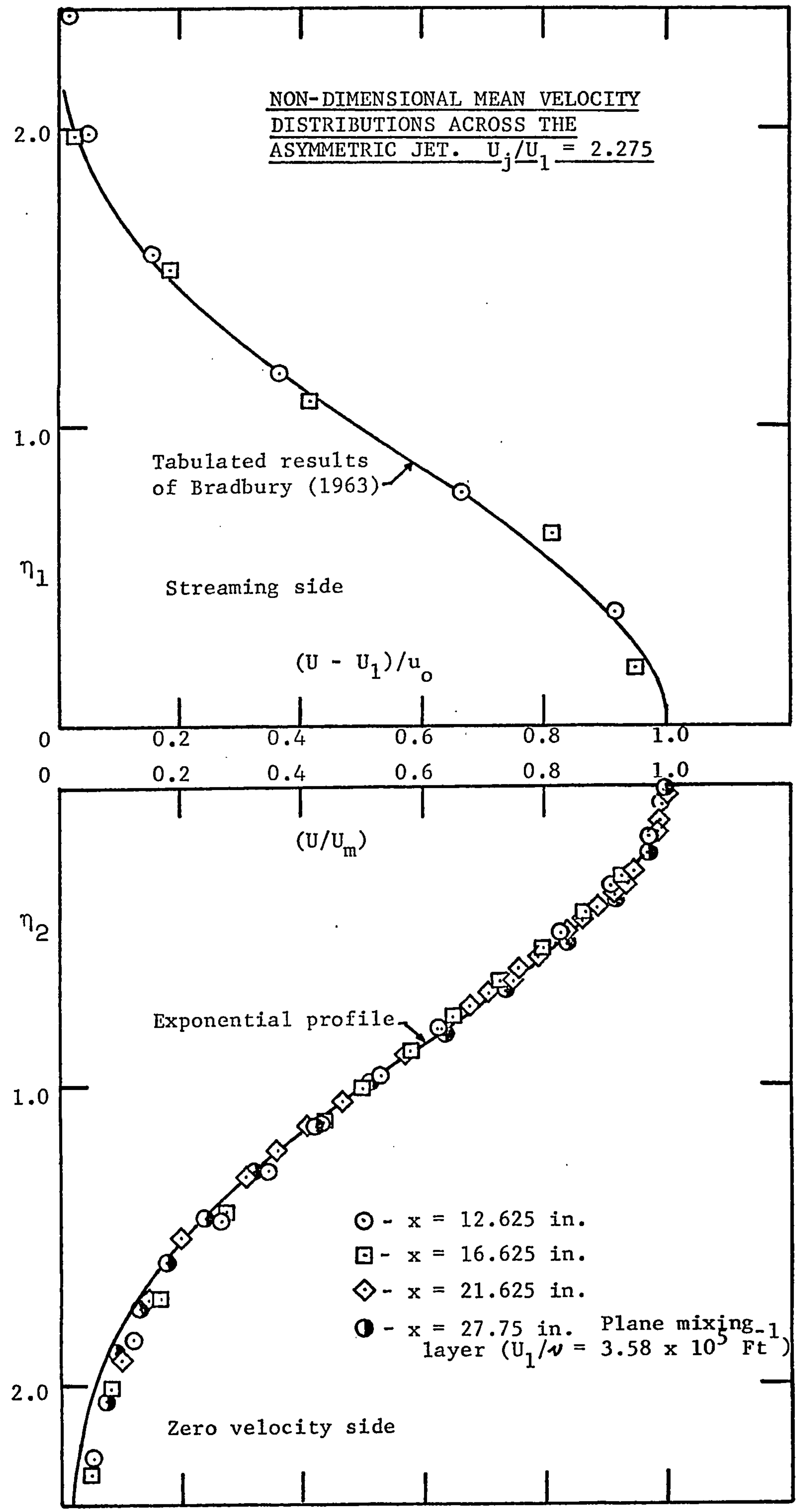
NON-DIMENSIONAL MEAN VELOCITY DISTRIBUTIONS ACROSS THE ASYMMETRIC JET. $U_j/U_1 = 2.275$
2.0
1.0
0
Tabulated results of Bradbury (1963)
η_1
Streaming side
$(U - U_1)/u_o$
0.2
0.4
0.6
0.8
1.0
0
0.2
0.4
0.6
0.8
1.0
(U/U_m)
η_2
Exponential profile
1.0
2.0
- x = 12.625 in.
- x = 16.625 in.
- x = 21.625 in.
- x = 27.75 in. Plane mixing layer ($U_1/\nu = 3.58 \times 10^5$ Ft^{-1})
Zero velocity side

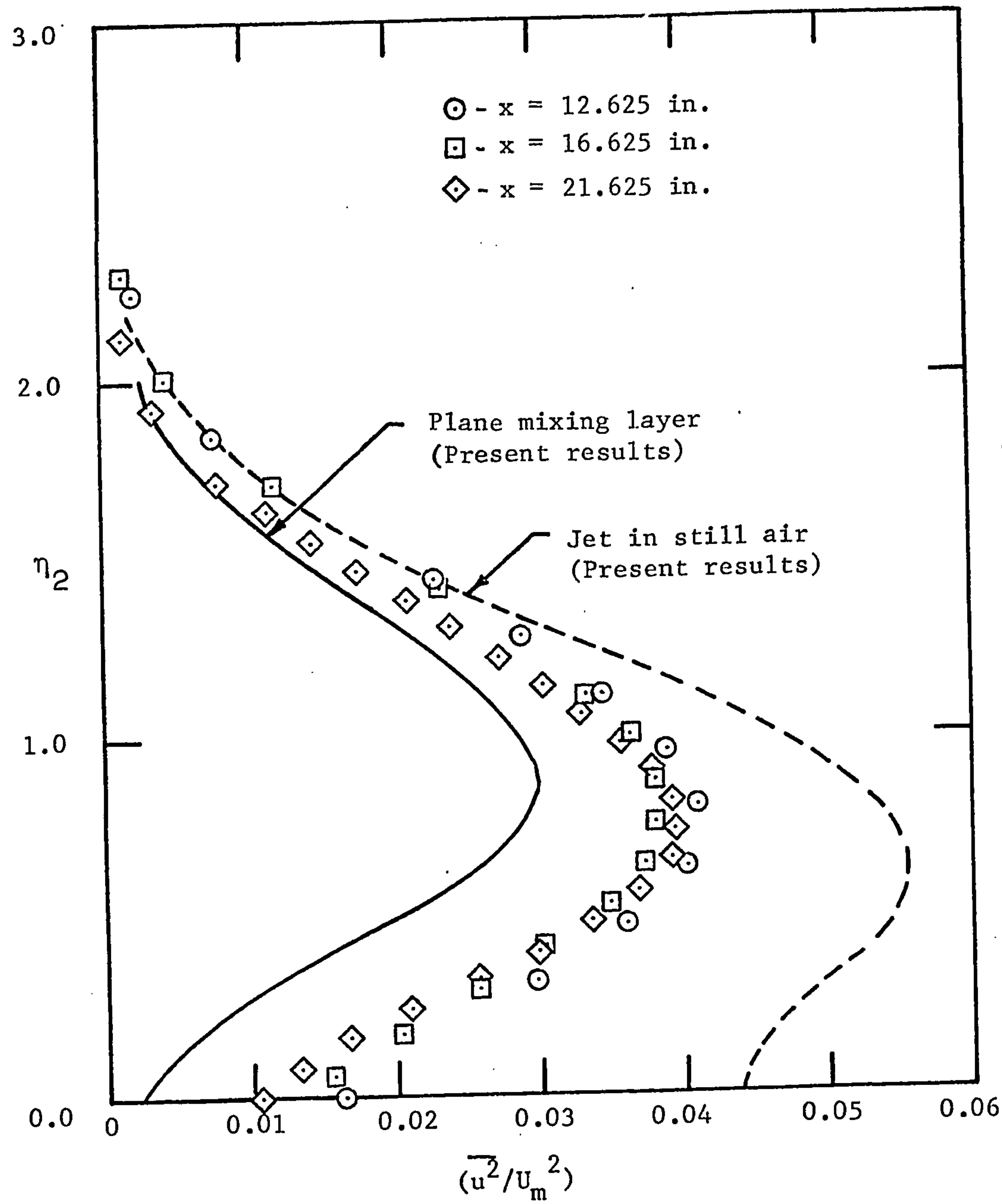

$\overline{u^2}/U_m^{\ 2}$ - DISTRIBUTIONS ON THE ZERO VELOCITY SIDE OF THE ASYMMETRIC JET. $U_j/U_1 = 2.275$

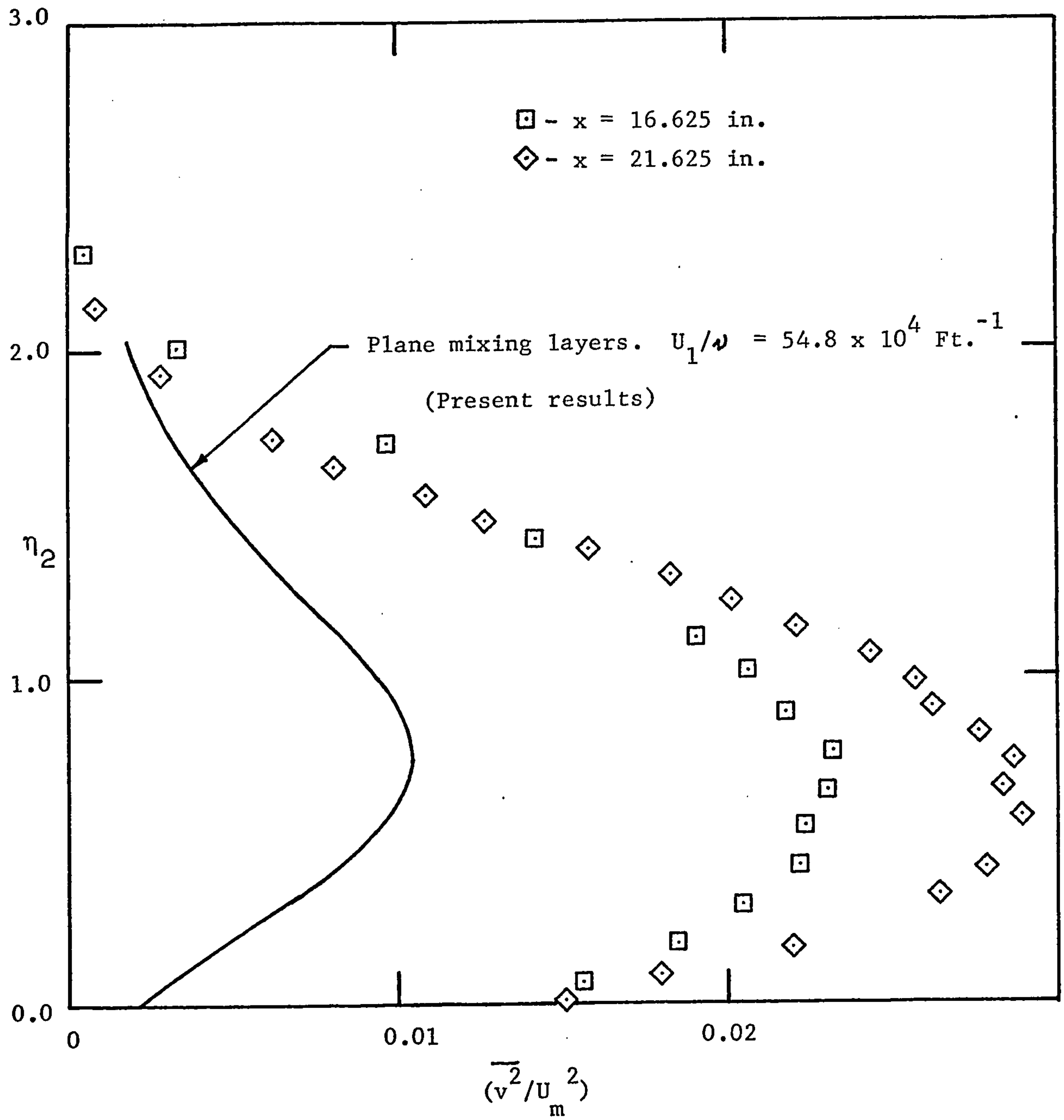

$\overline{v^2}/U_m^2$ - DISTRIBUTIONS ON THE ZERO VELOCITY SIDE OF THE ASYMMETRIC JET

$U_j/U_1 = 2.275$

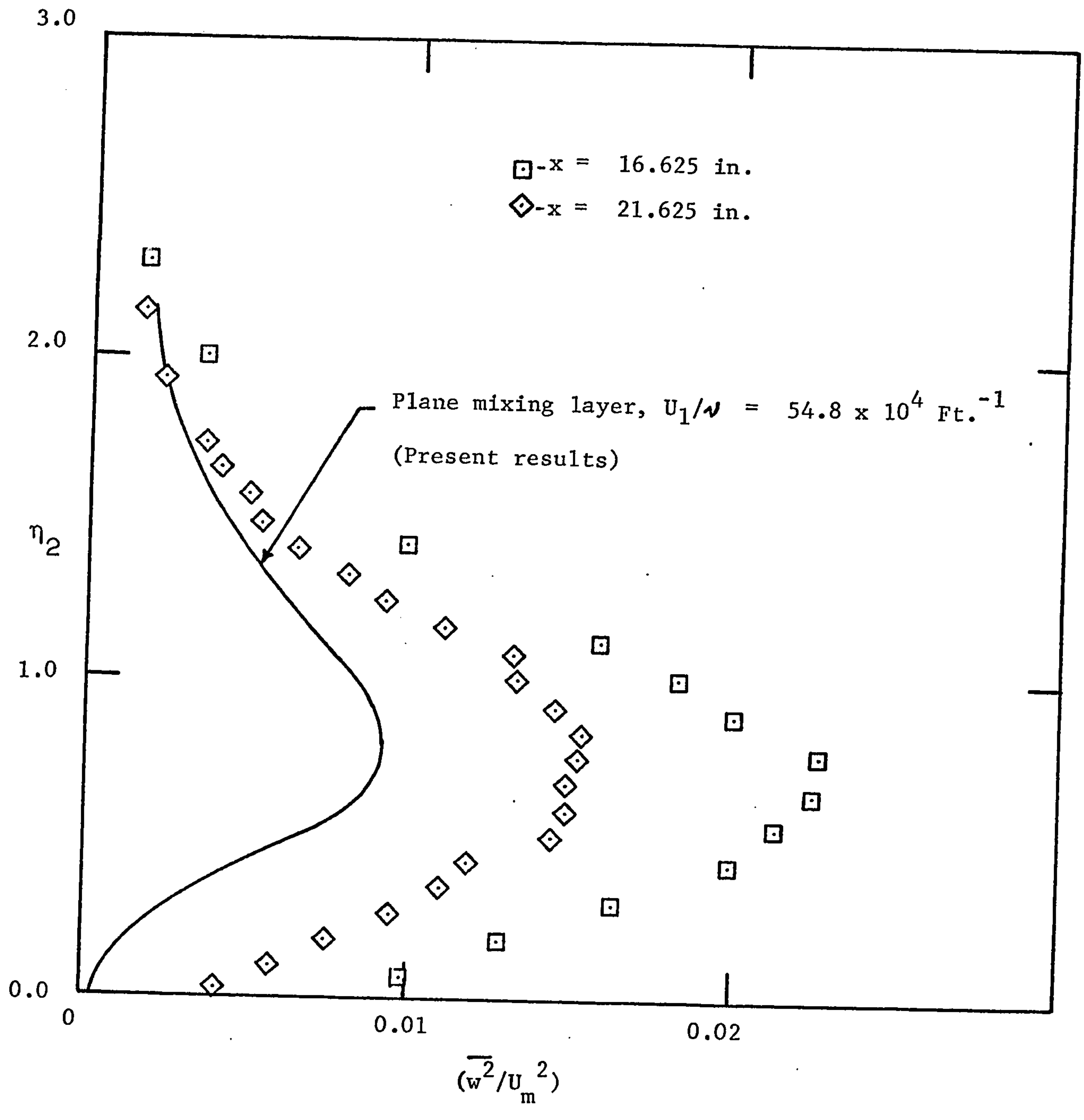

$\overline{w^2}/U_m^{\ 2}$ - DISTRIBUTIONS ON THE ZERO VELOCITY SIDE OF THE ASYMMETRIC JET. U_j/U_1 = 2.275

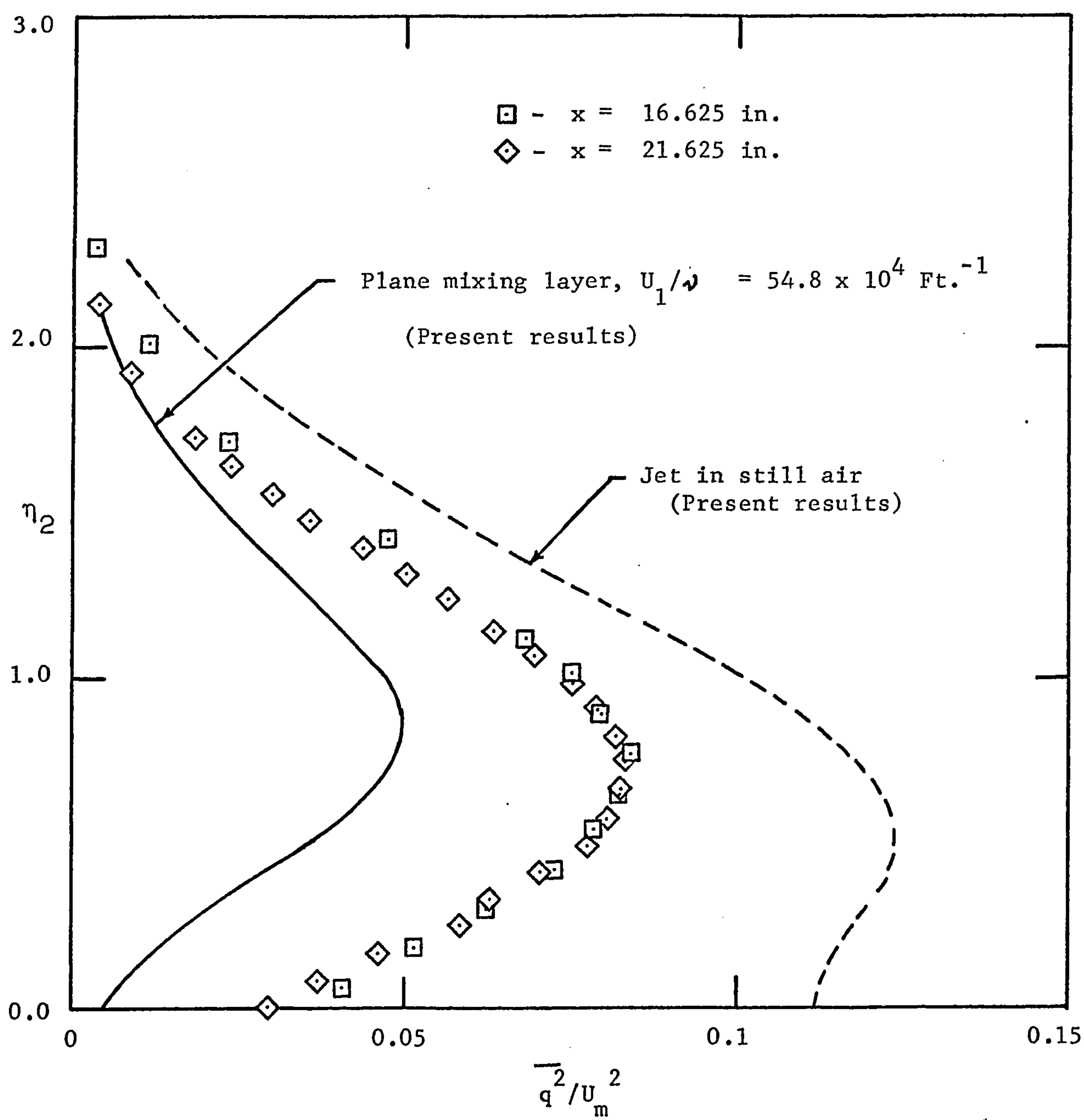

TURBULENT ENERGY DISTRIBUTION ON THE ZERO VELOCITY SIDE OF THE ASYMMETRIC JET. U_j/U_1 = 2.275

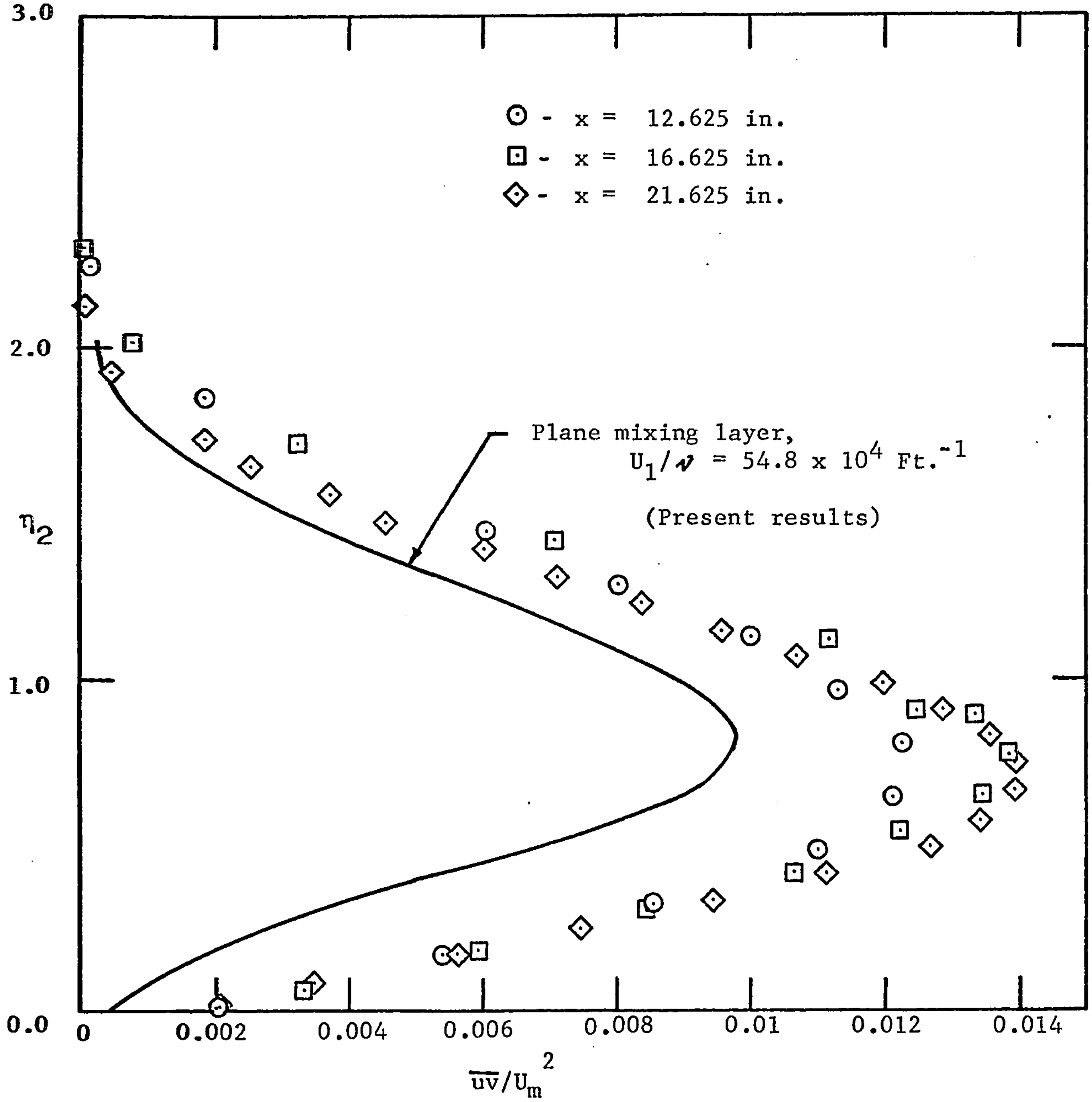

SHEAR STRESS DISTRIBUTIONS ON THE ZERO VELOCITY SIDE OF THE ASYMMETRIC JET. $U_j/U_1 = 2.275$

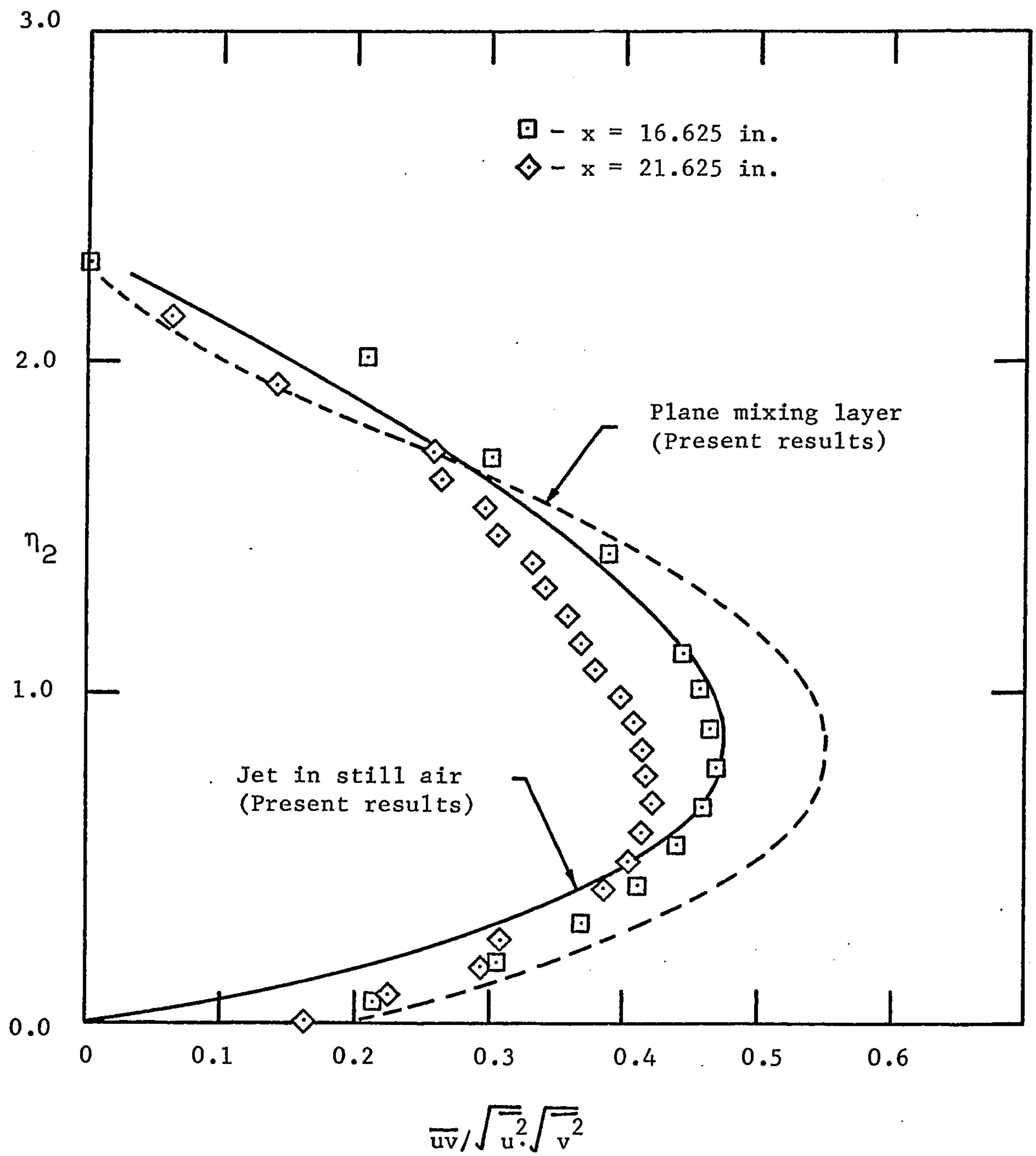

$R_{\overline{uv}}$ - CORRELATION ON THE ZERO VELOCITY SIDE OF THE ASYMMETRIC JET. $U_j/U_1 = 2.275$

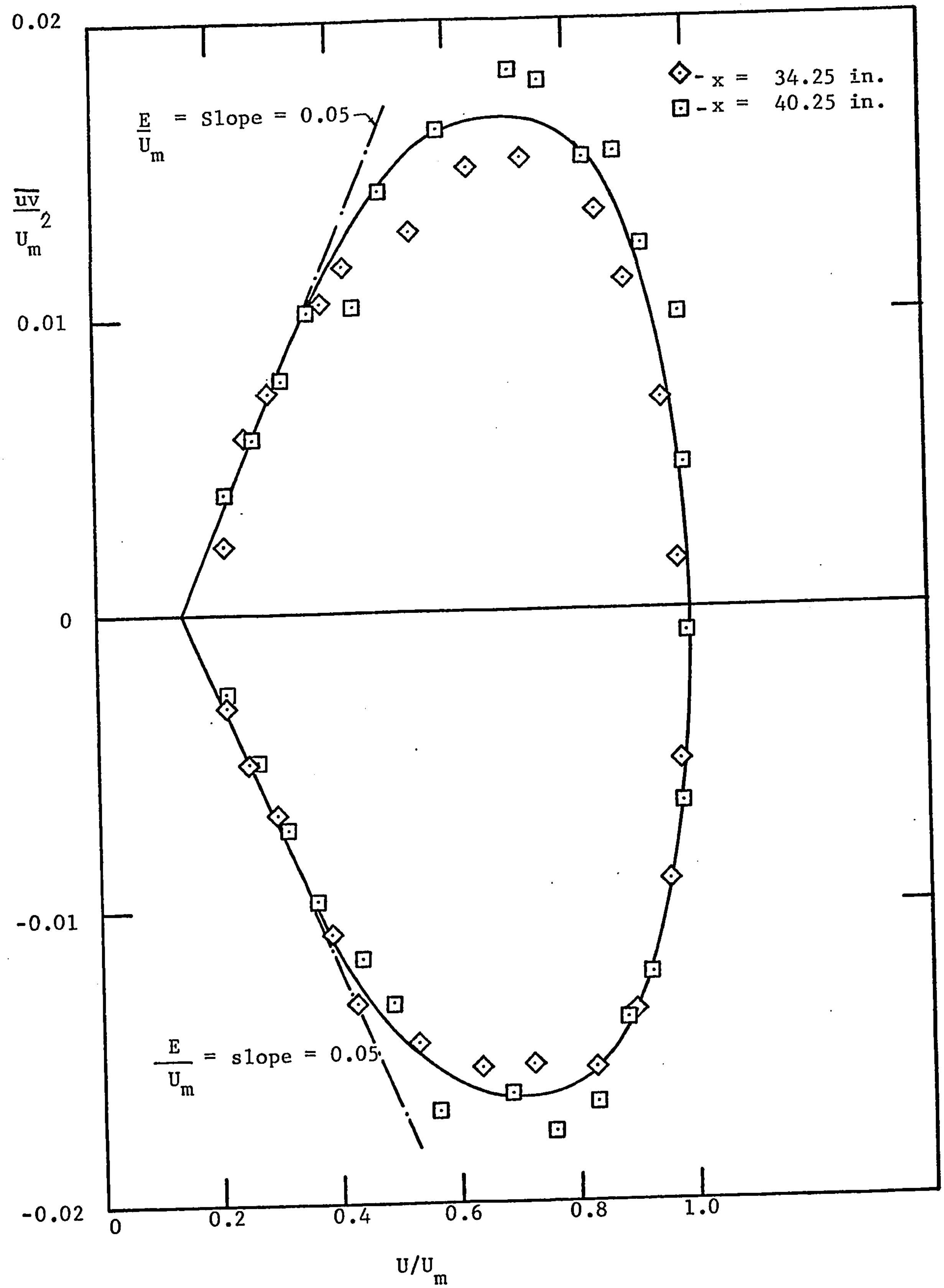

VARIATION OF $(\overline{uv}/U_m^2)$ VERSUS (U/U_m)

TWO-DIMENSIONAL JET IN STILL AIR. (Present results)

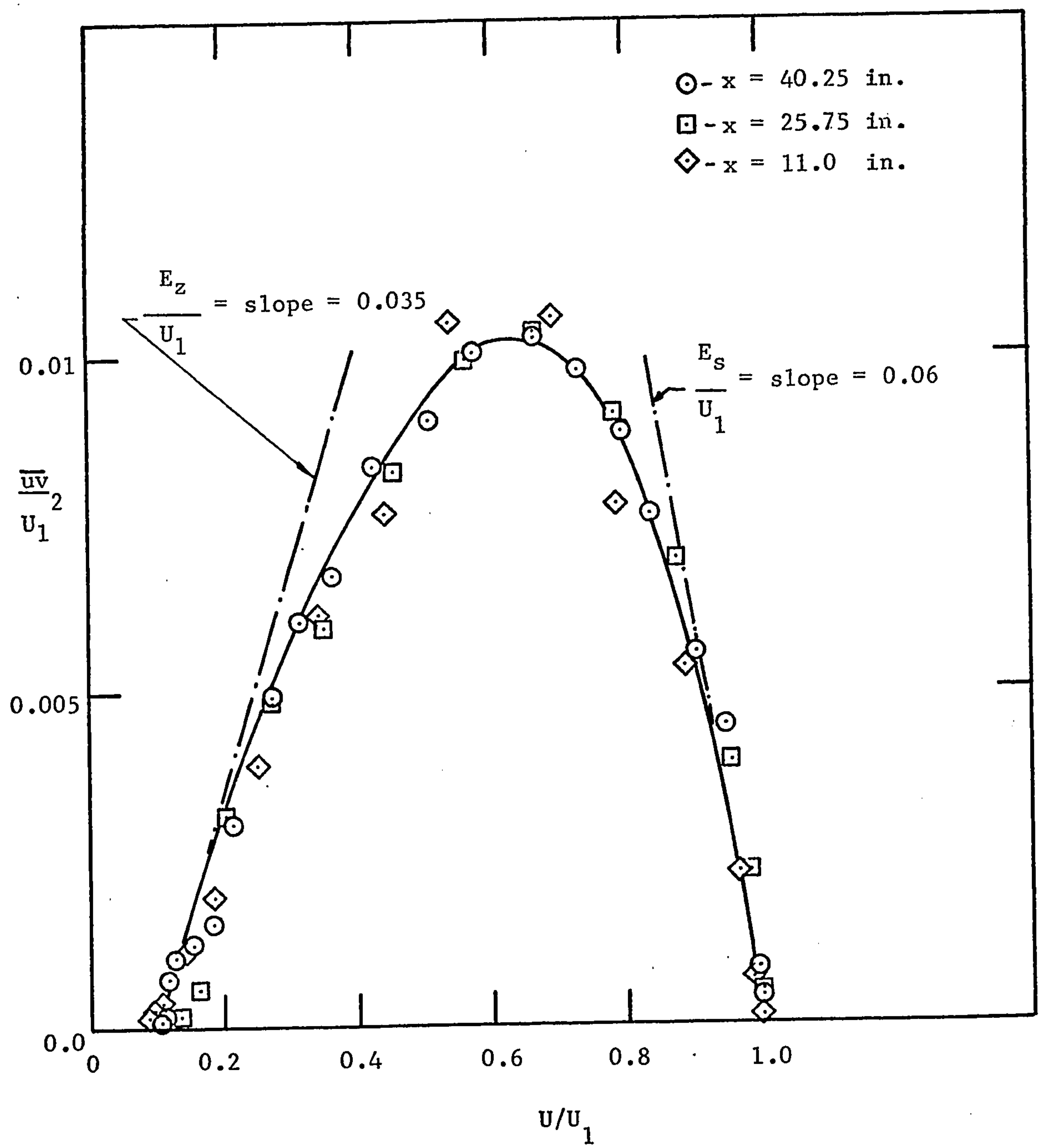

VARIATION OF $(\overline{uv}/U_1^{\ 2})$ VERSUS (U/U_1)

PLANE MIXING LAYER. U_1/ν = 54.8 x 10^4 Ft.$^{-1}$

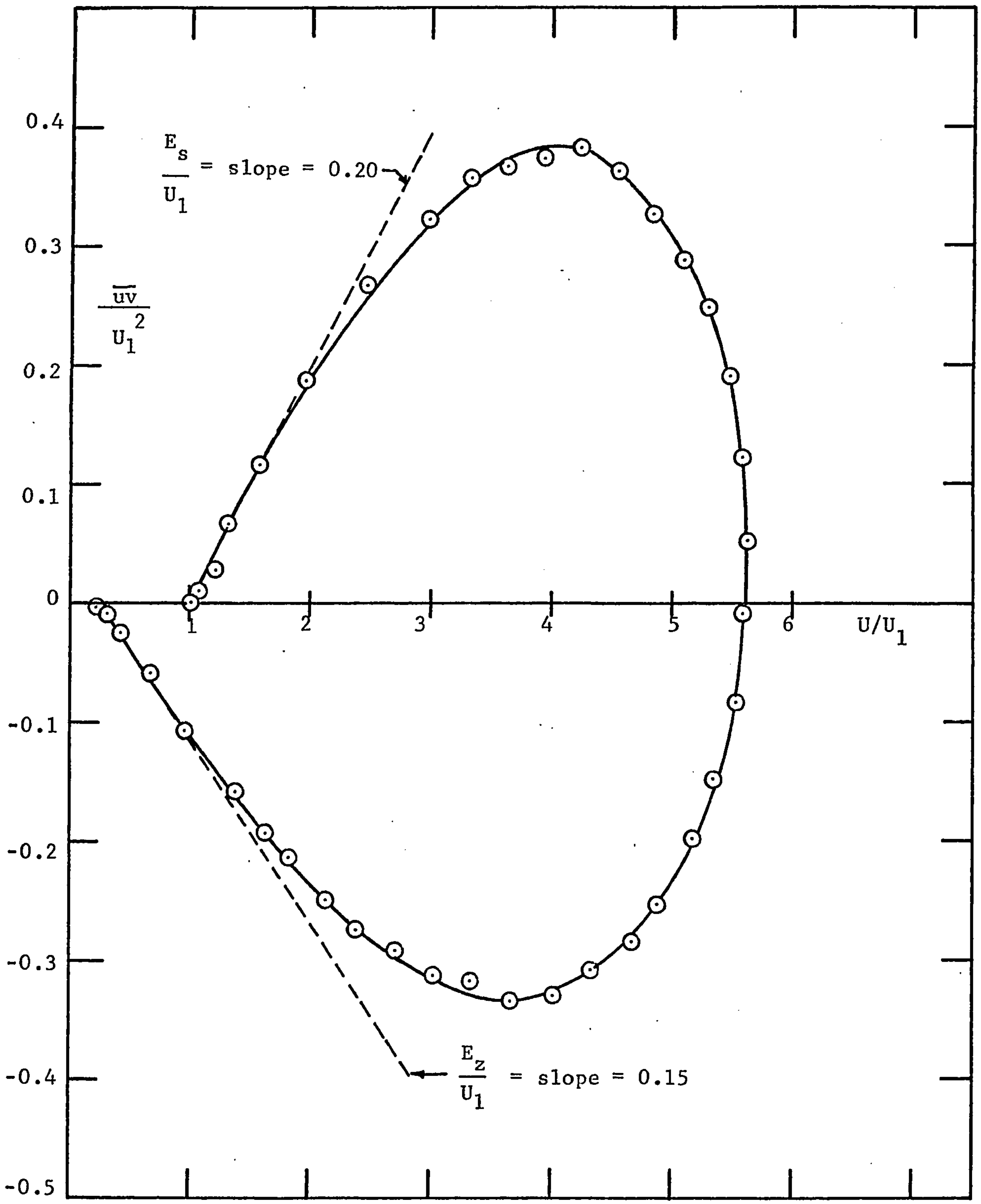

VARIATION OF $(\overline{uv}/U_1^2)$ VERSUS (U/U_1)

THE ASYMMETRIC JET. $U_j/U_1 = 9.0$; $x = 6.1$ in.

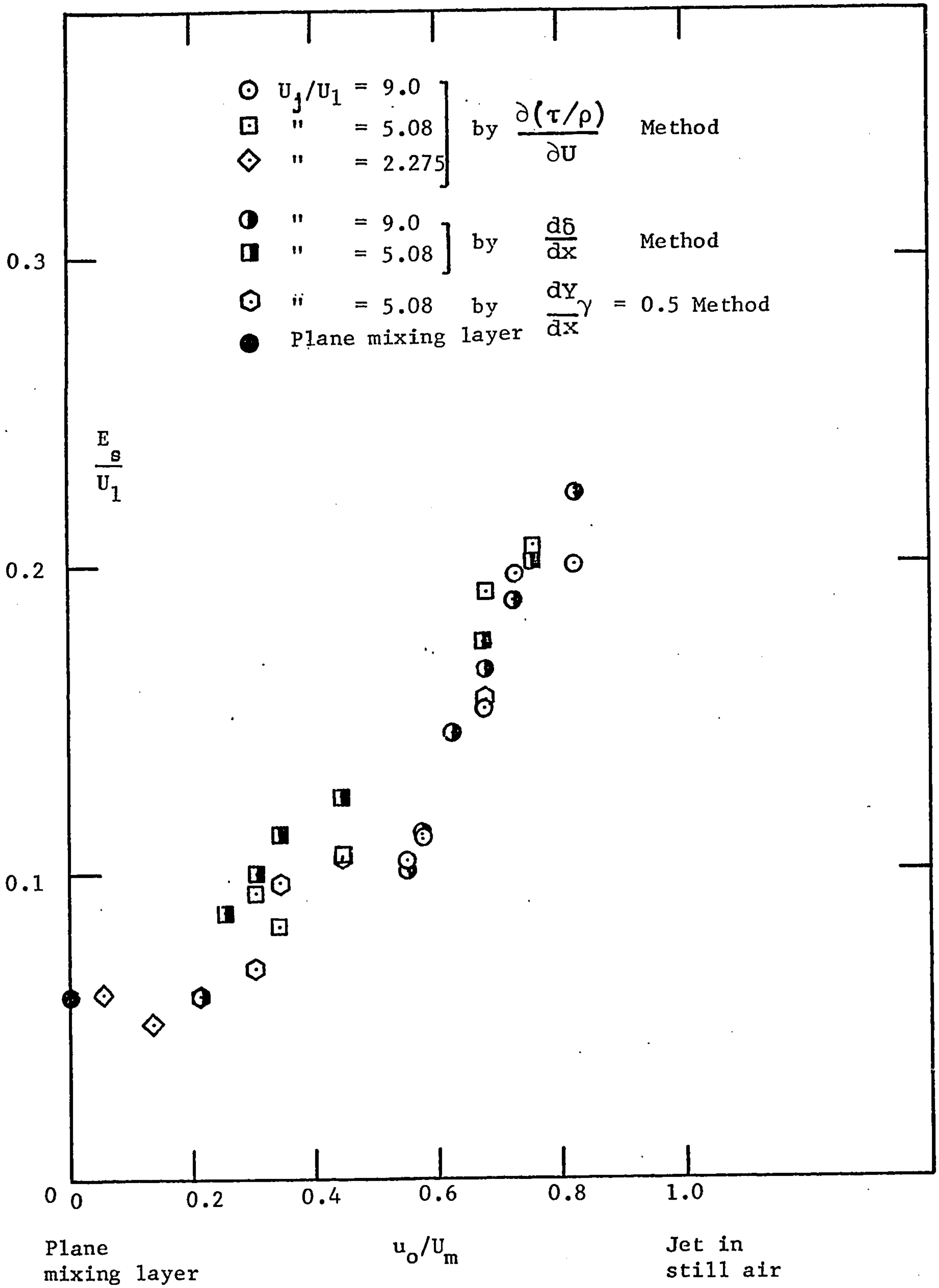

COMPARISON OF (E_s/U_1) OBTAINED BY VARIOUS METHODS

THE ASYMMETRIC JETS
(See section 8)

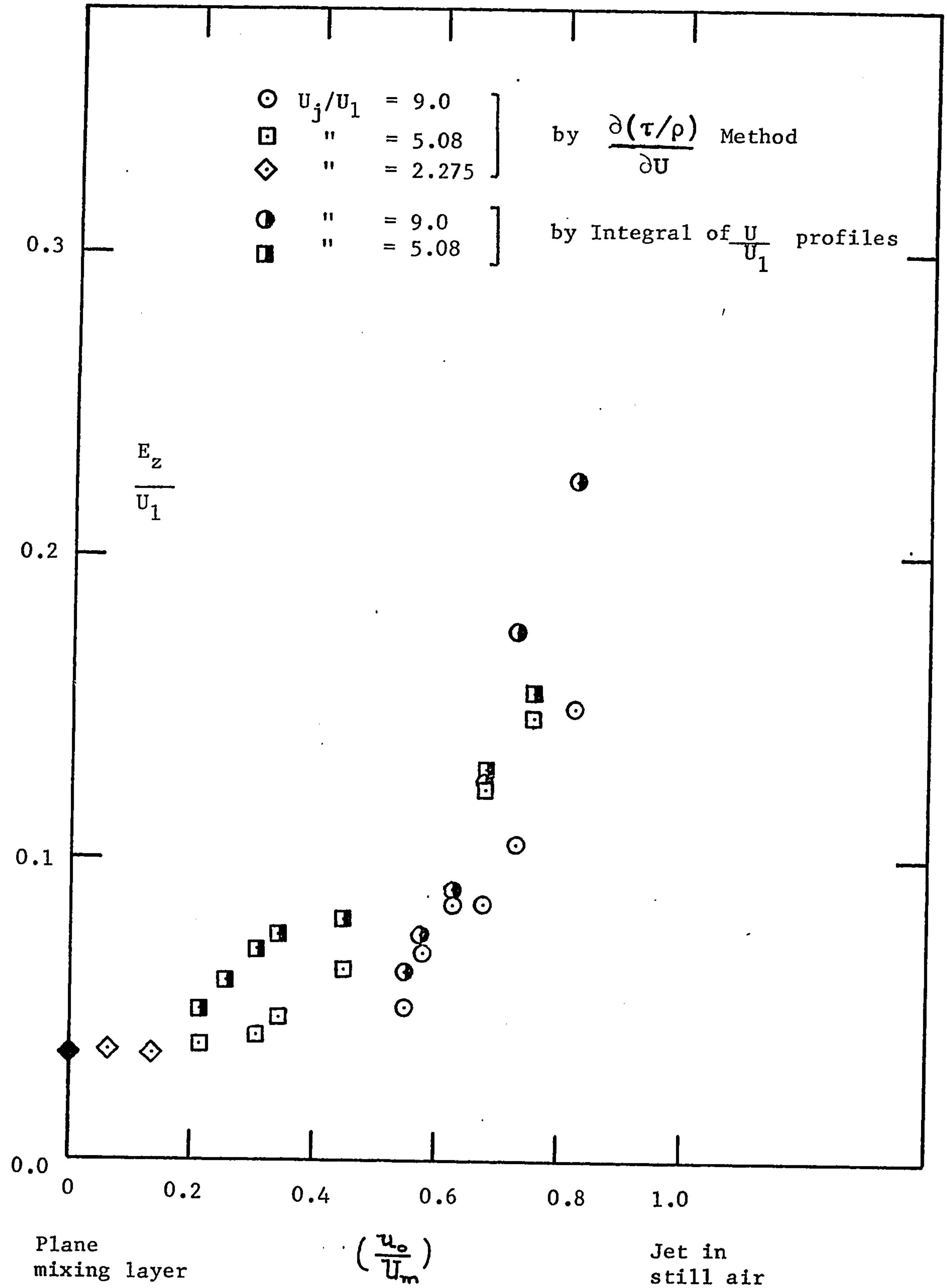

COMPARISON OF (E_z/U_1) OBTAINED BY VARIOUS METHODS

THE ASYMMETRIC JETS
(See section 8)

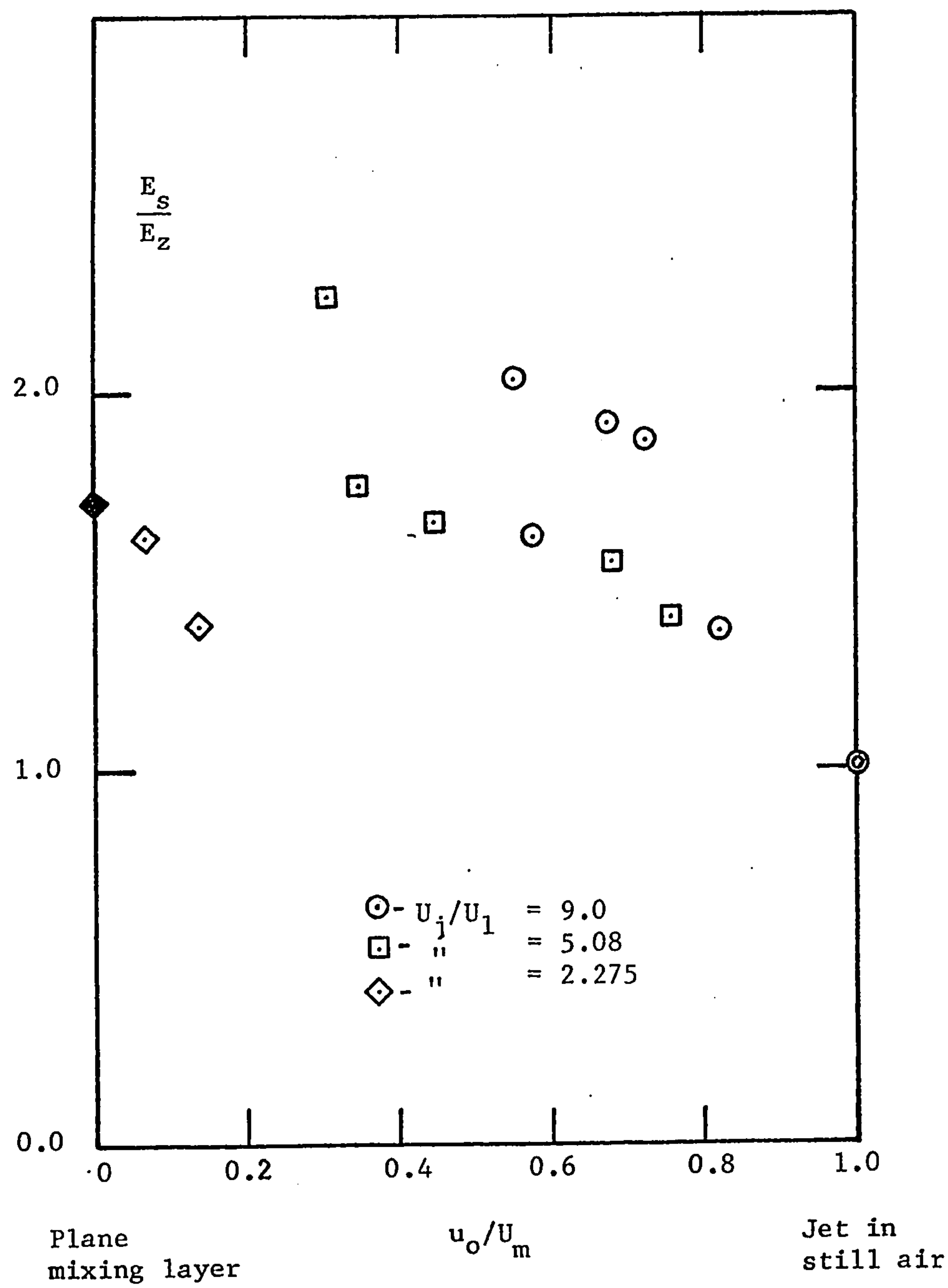

VARIATION OF (E_s/E_z) VERSUS (U_o/U_m): THE ASYMMETRIC JETS

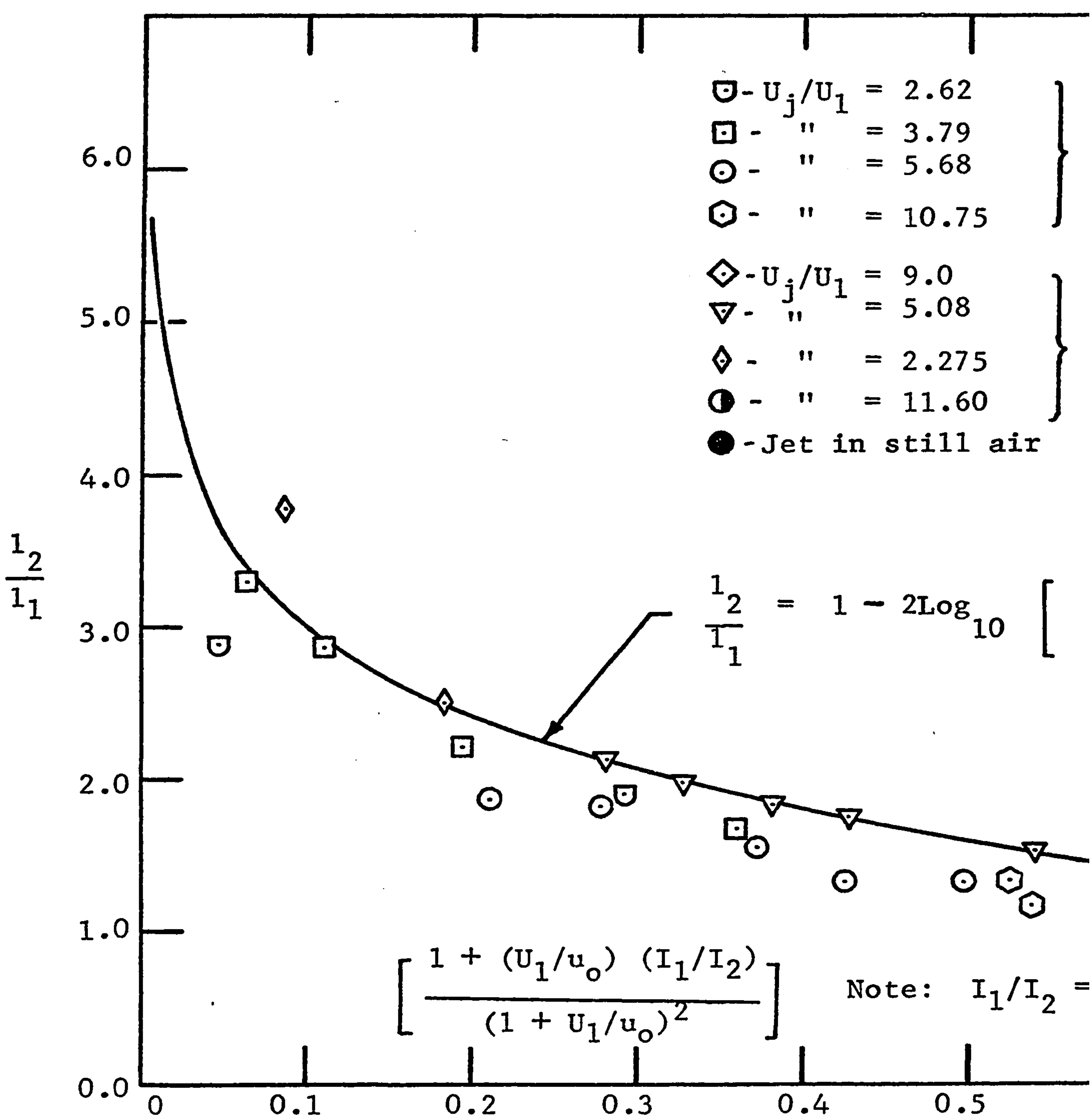

VARIATION OF THE RATIO (l_2/l_1) FOR THE ASYMMETRIC J

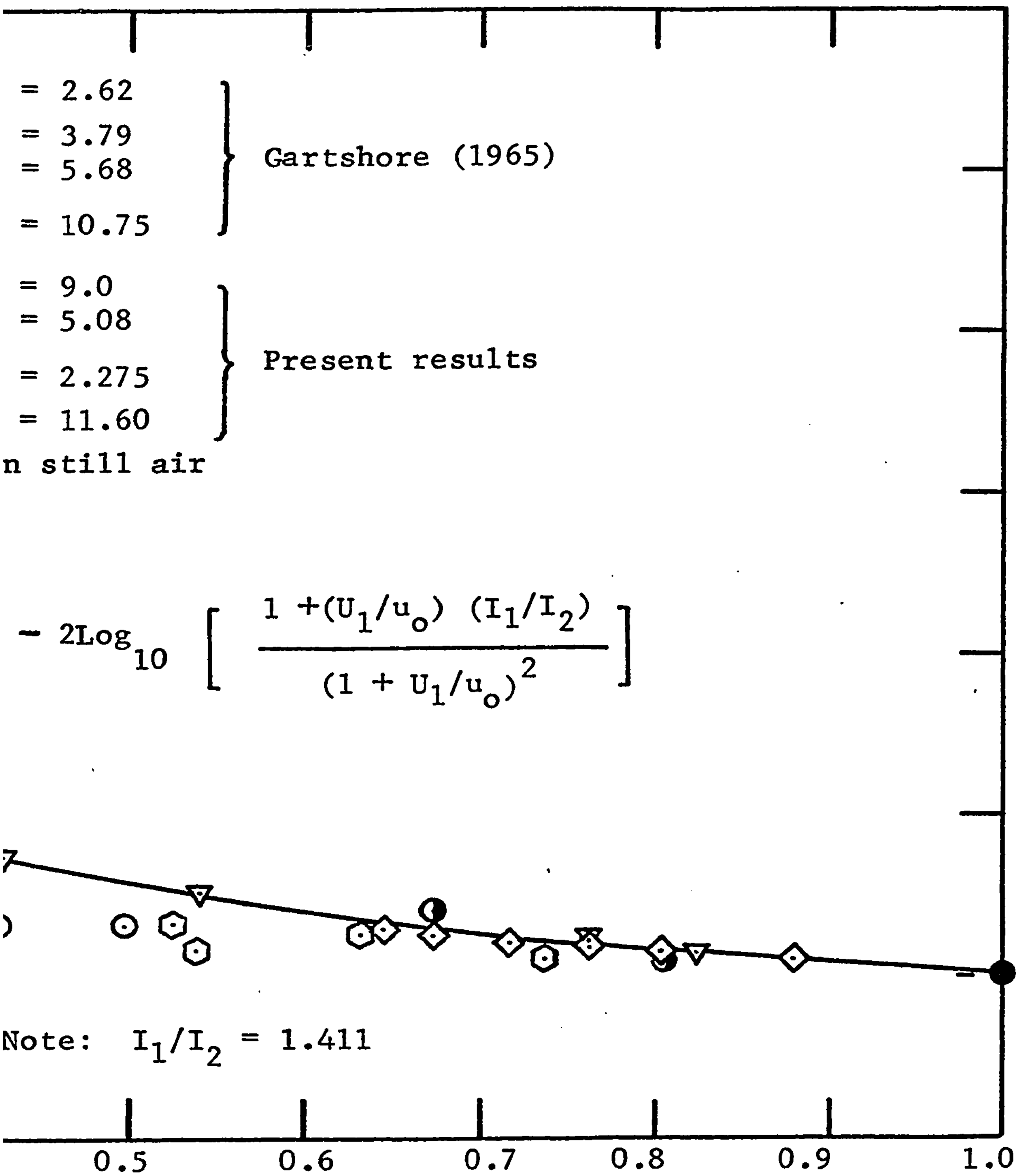

E ASYMMETRIC JETS.

Fig. 91

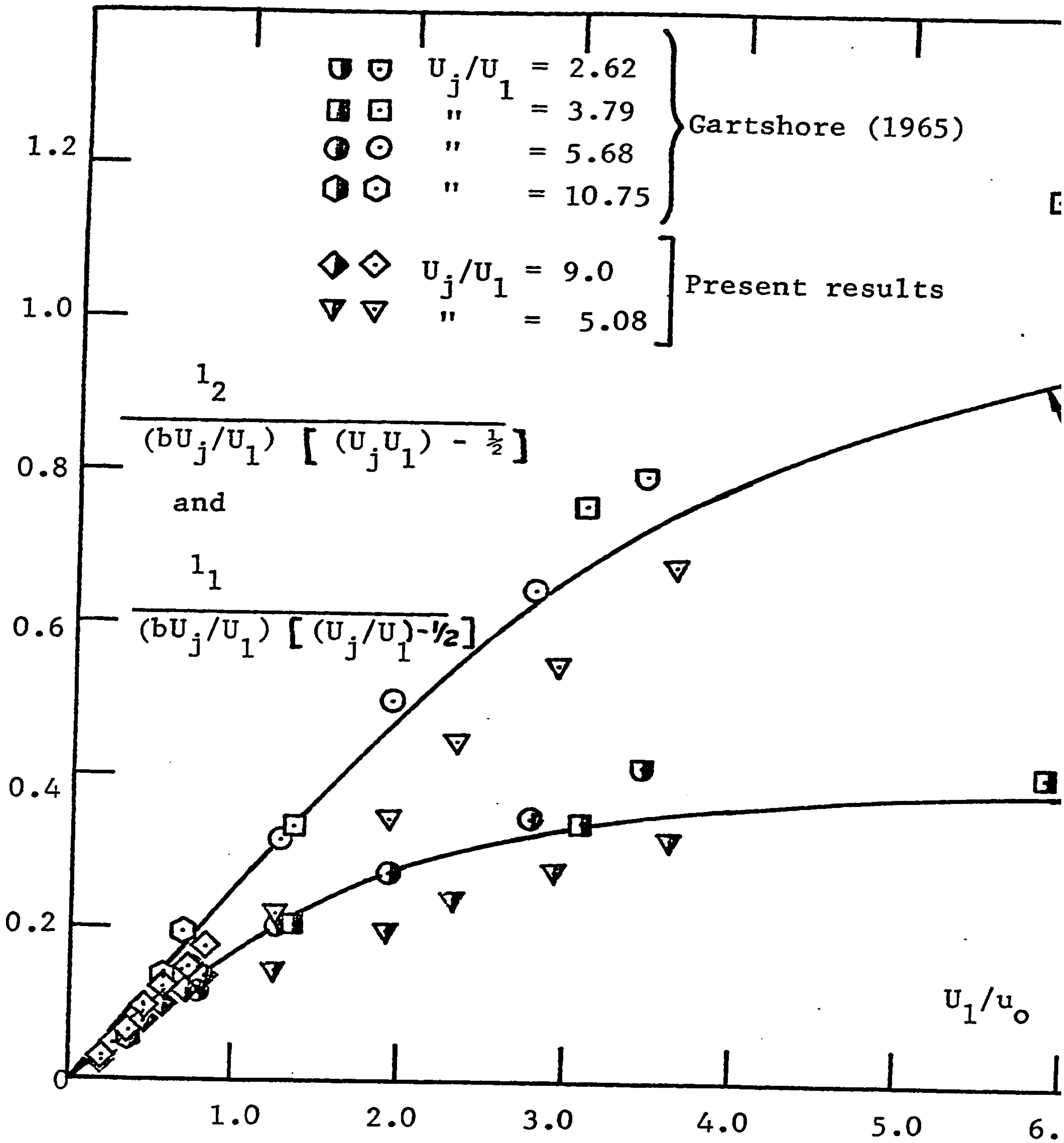

COMPARISON OF PREDICTED AND MEASURED VARIATIONS OF l_2 A

THE ASYMMETRIC JET.

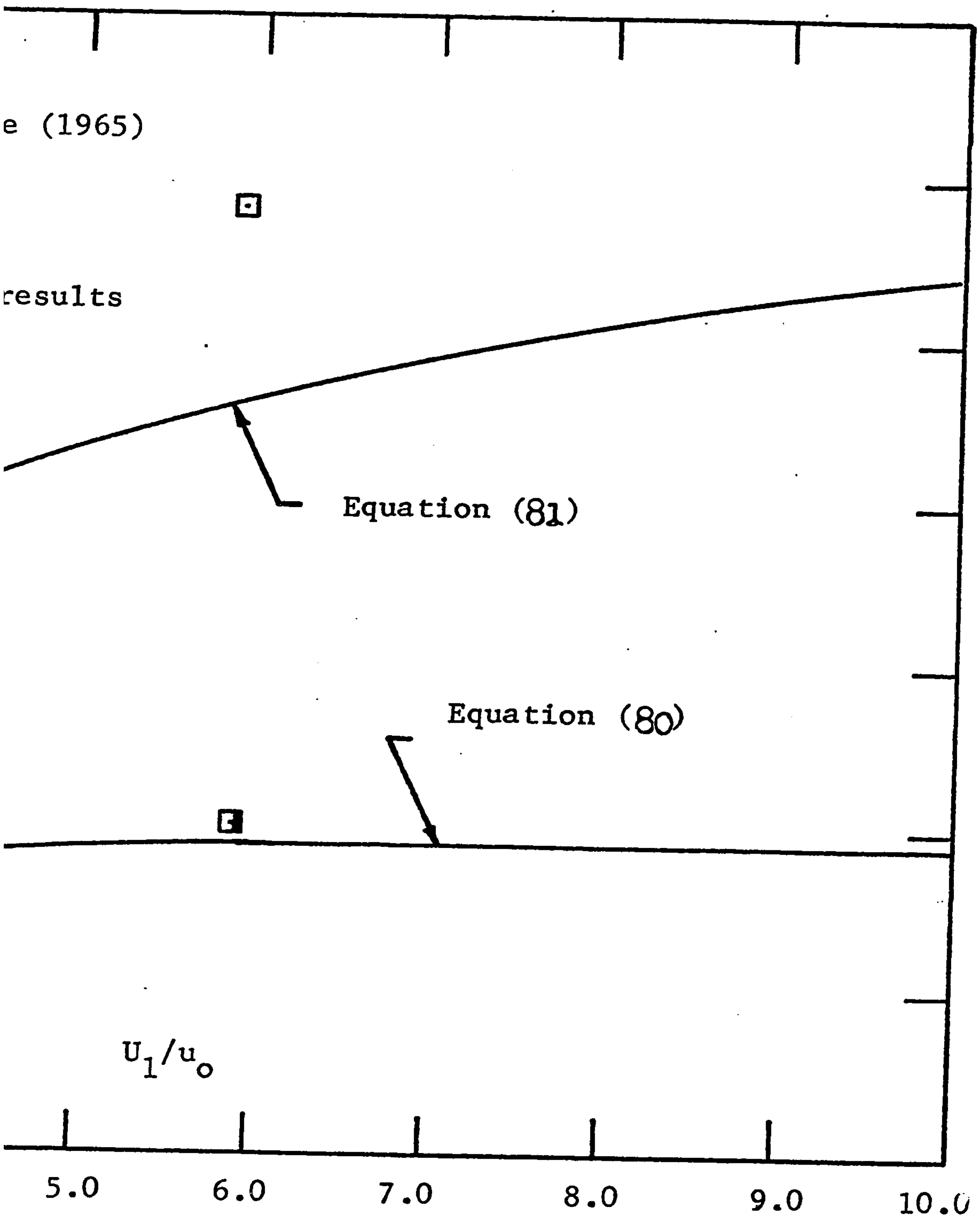

TIONS OF l_2 AND l_1

Fig. 92

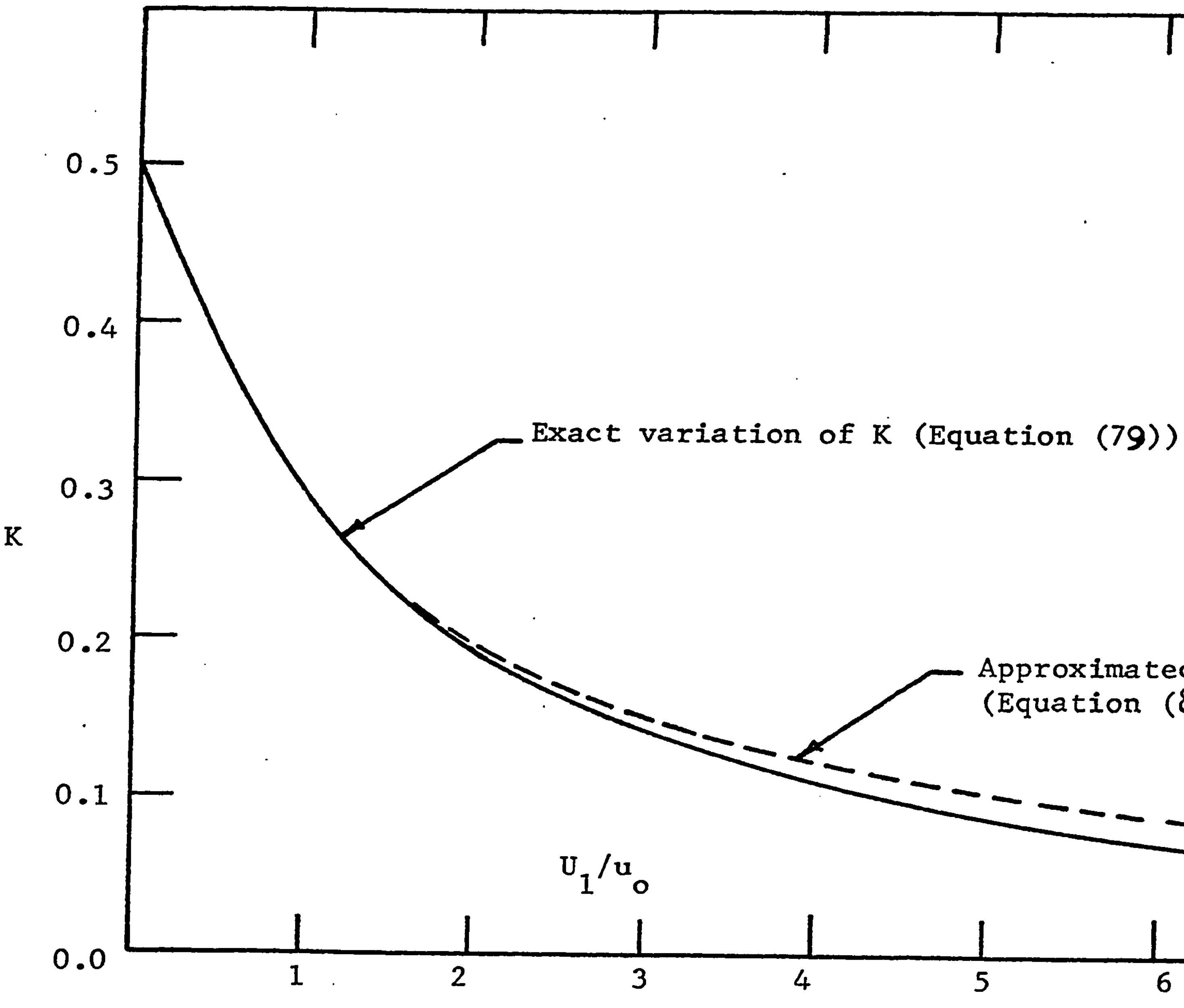

COMPARISON OF EXACT AND APPROXIMATED VARIATION OF K

THE ASYMMETRIC JETS

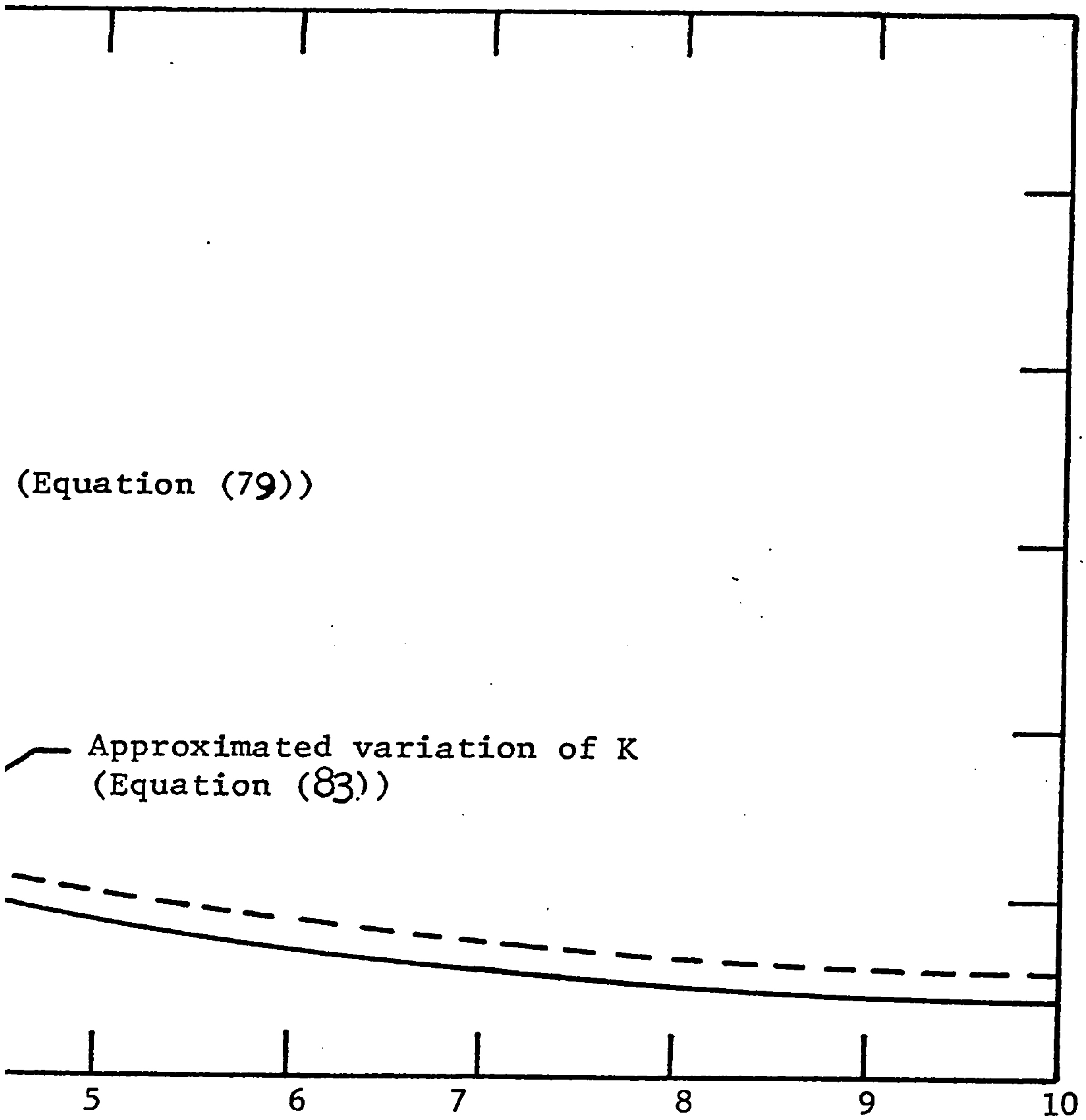

ARIATION OF K

Fig. 93

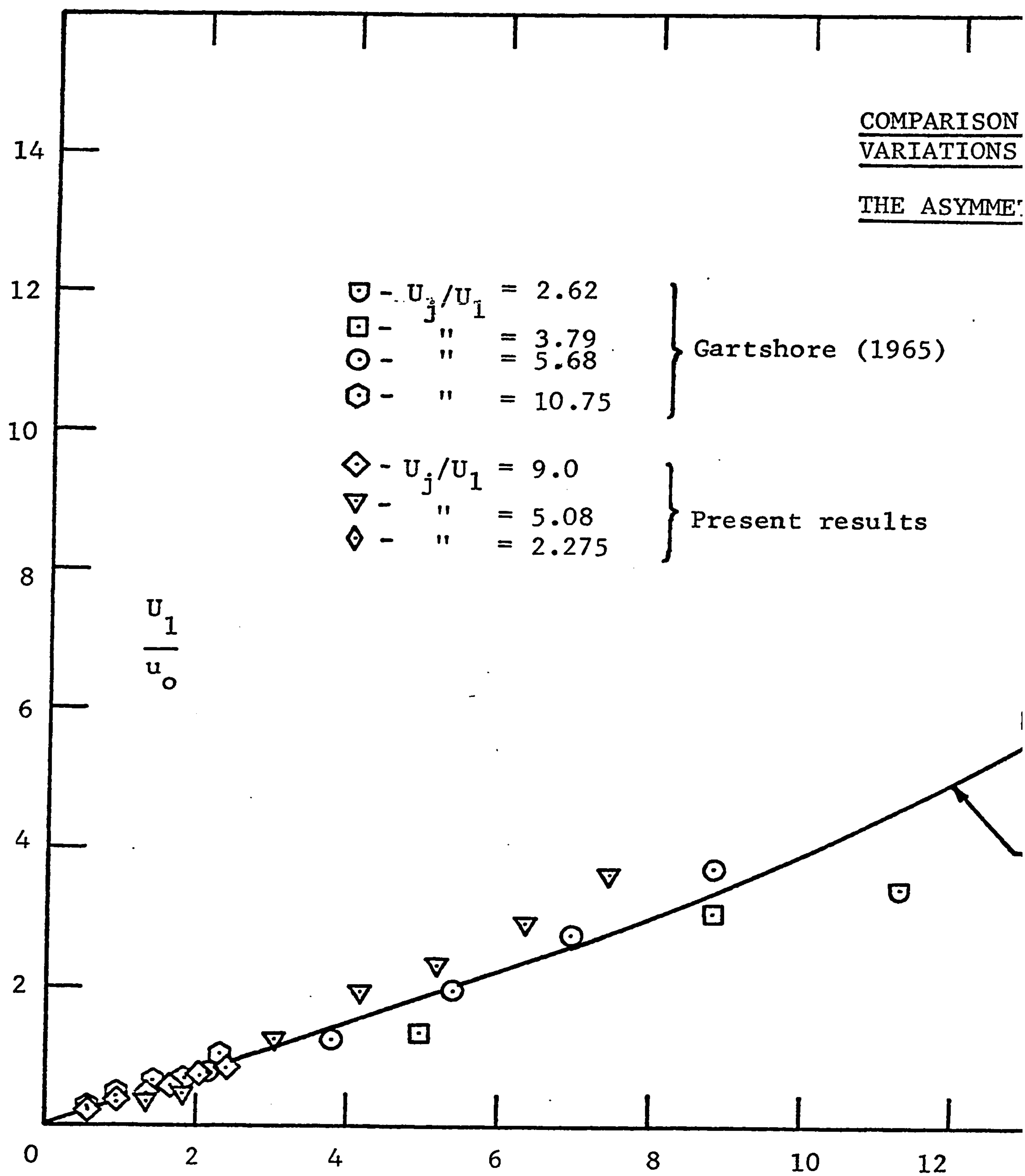

COMPARISON
VARIATIONS
THE ASYMME
U_j/U_1 = 2.62
" = 3.79
" = 5.68
" = 10.75
Gartshore (1965)
U_j/U_1 = 9.0
" = 5.08
" = 2.275
Present results
$\frac{U_1}{u_o}$
0
2
4
6
8
10
12
14

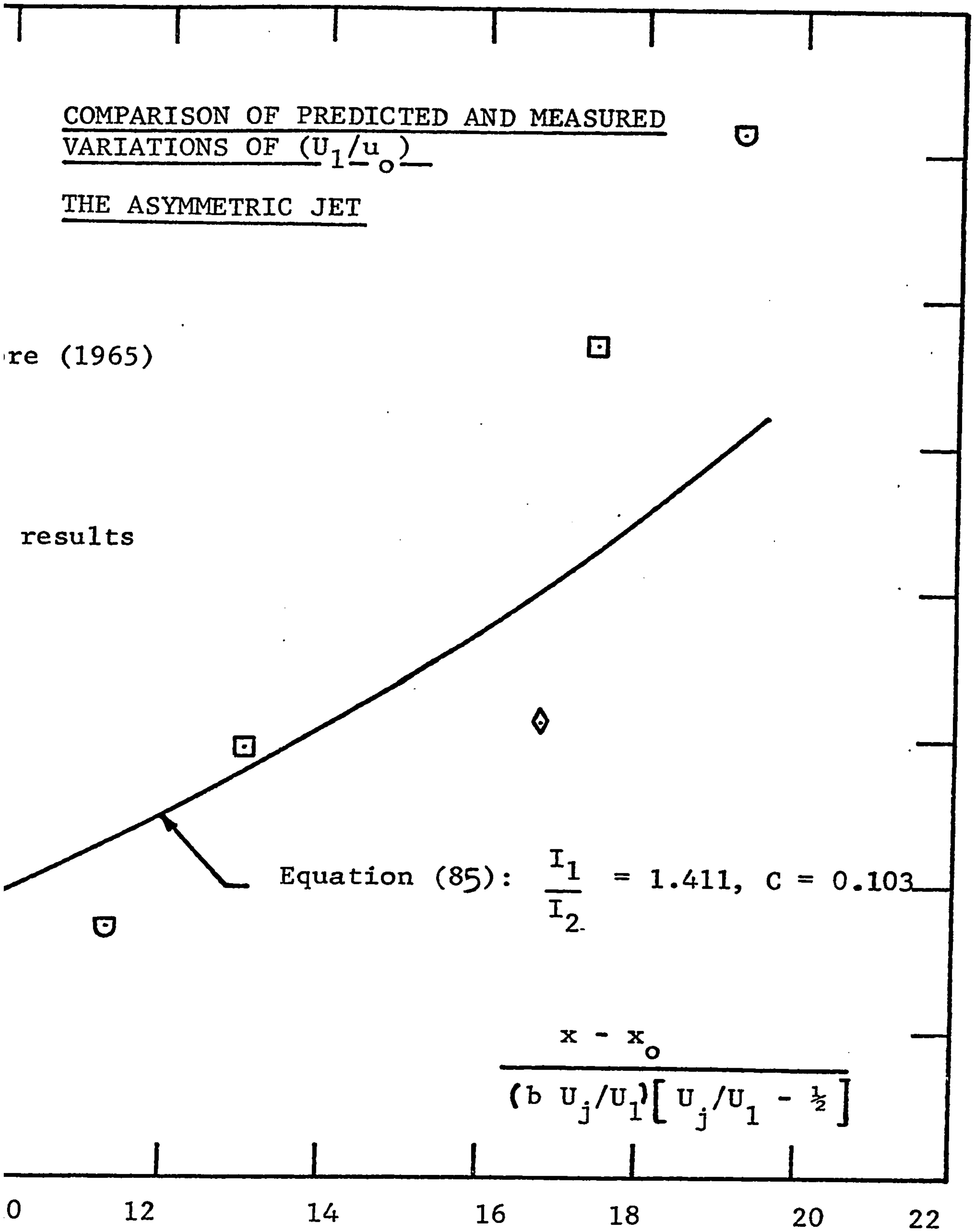

COMPARISON OF PREDICTED AND MEASURED VARIATIONS OF (U_1/u_o)
THE ASYMMETRIC JET
re (1965)
results
Equation (85): $\frac{I_1}{I_2} = 1.411$, $C = 0.103$
$\frac{x - x_o}{(b\, U_j/U_1)\left[U_j/U_1 - \frac{1}{2}\right]}$
0
12
14
16
18
20
22

Fig. 94

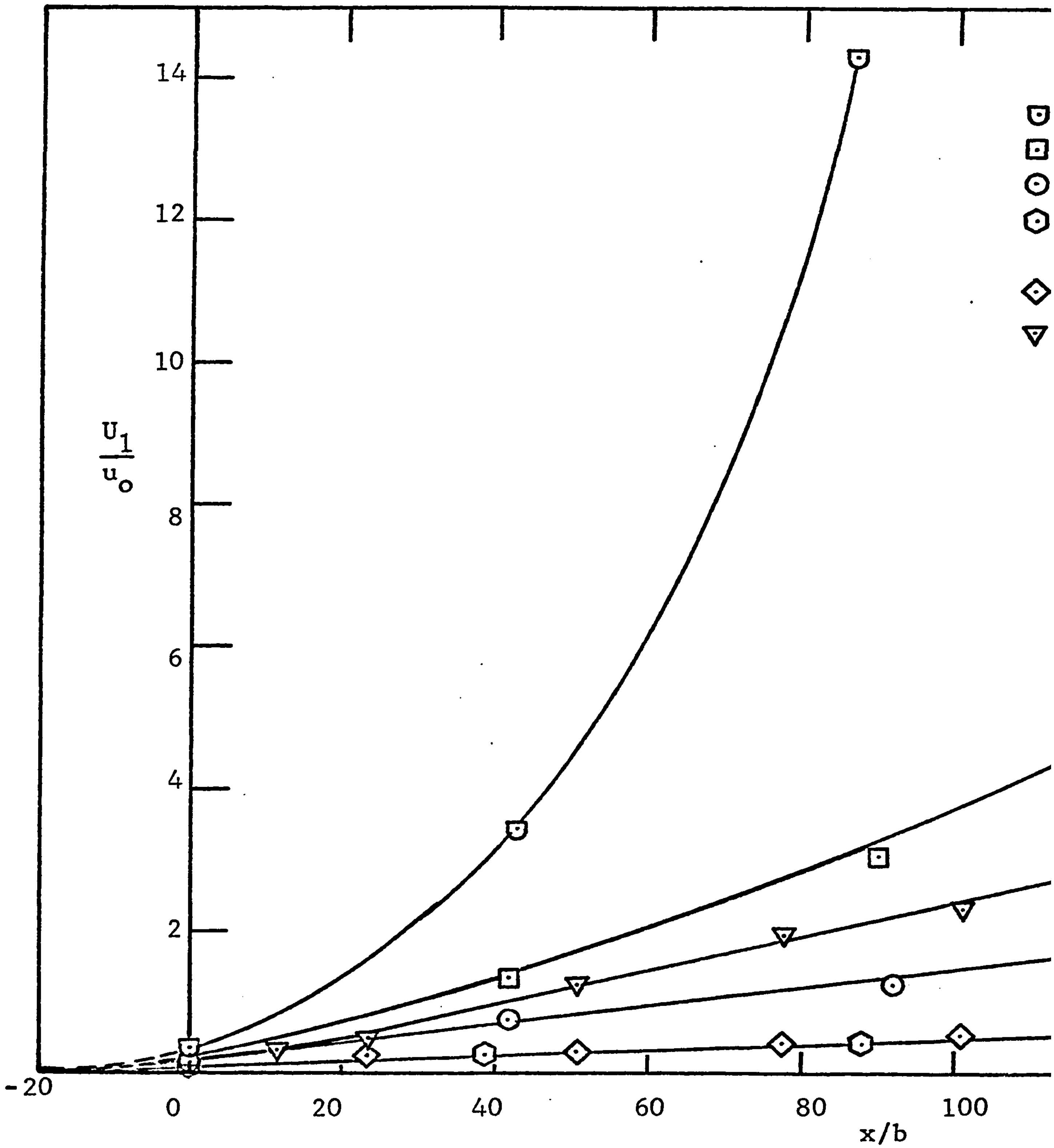

HYPOTHETICAL ORIGIN, x_o, FOR THE ASYMMETRIC JETS

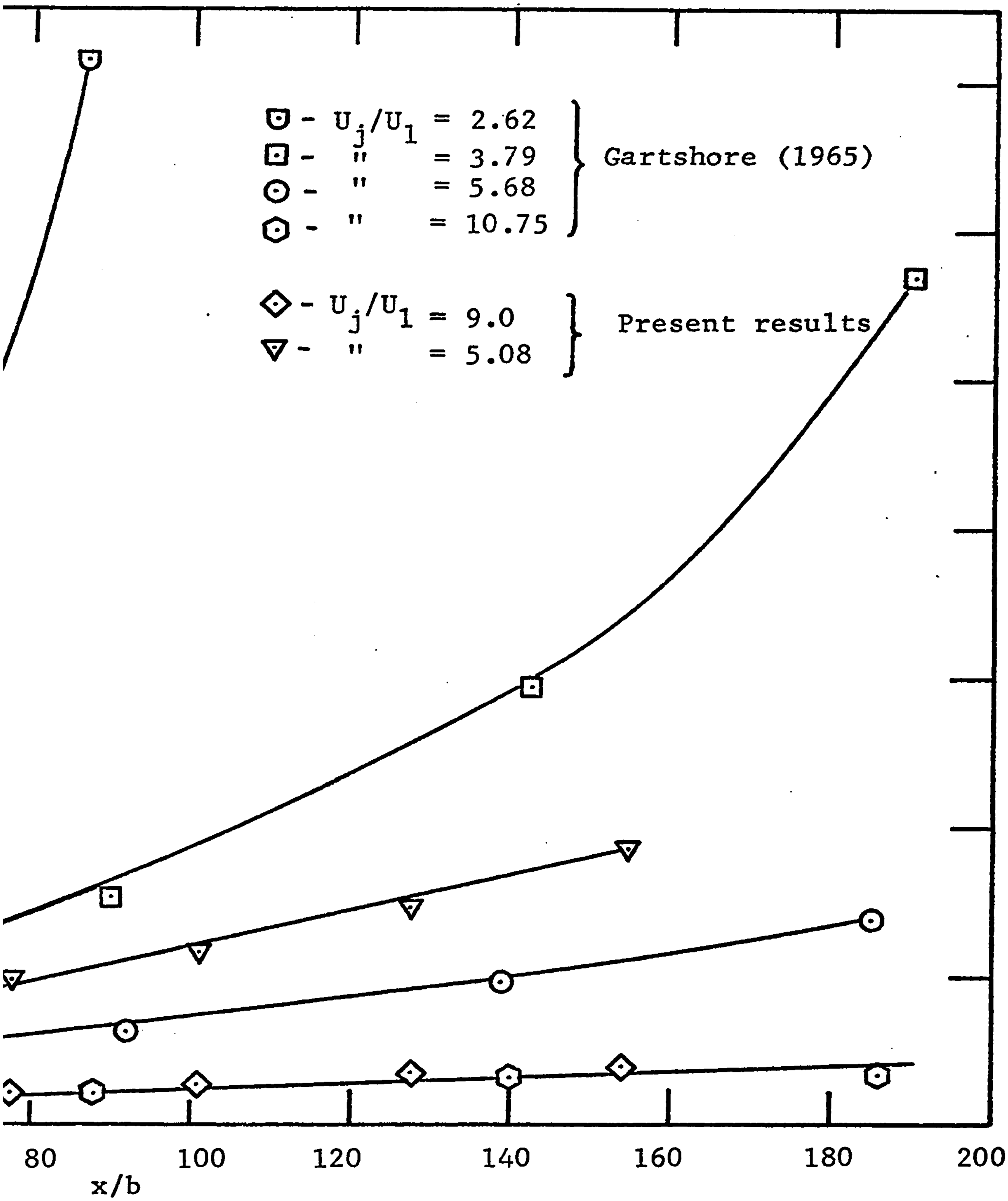

'RIC JETS

Fig. 95

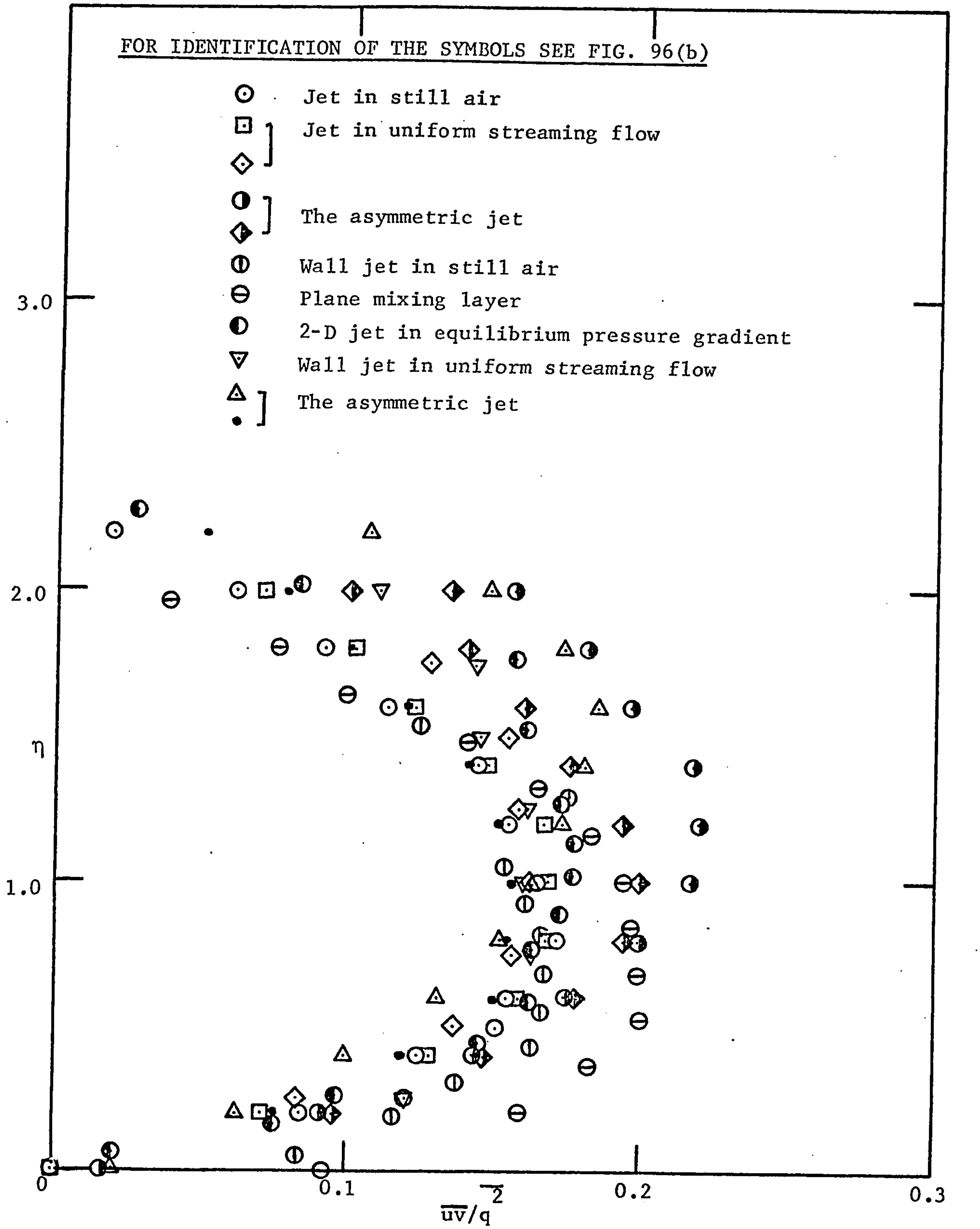

COMPARISON OF $(\overline{uv}/\overline{q^2})$ IN VARIOUS SHEAR FLOWS

IDENTIFICATION OF THE SYMBOLS FOR FIG. 96(a)

COMPARISON OF $(\overline{uv}/\overline{q^2})$ - DISTRIBUTIONS

IN VARIOUS FREE SHEAR FLOWS

(results are corrected for the longitudinal cooling effects)

⊙ - Jet in still air (Present results)

⊡ - Jet in uniform streaming flow (Bradbury (1963), 1.6 u_o/U_1 2)

⟐ - Jet in uniform streaming flow (Bradbury (1963), 0.2 u_o/U_1 0.23)

◑ - The asymmetric jet, $U_j/U_1 = 9.0$ (streaming side) (Present results)

⬗ - The asymmetric jet, $U_j/U_1 = 9.0$ (zero velocity side) (Present results)

⦶ - Wall jet in still air (Guitton (1970))

⊖ - Plane mixing layer (Present results)

◐ - 2-D jet in equilibrium pressure gradient (Fekete (1970), $u_o/U_1 = 0.57$)

▽ - Wall jet in uniform streaming flow (Kruka and Eskinazi (1964))

◬ - The asymmetric jet, $U_j/U_1 = 5.08$ (streaming side) (Present results)

● - The asymmetric jet, $U_j/U_1 = 5.08$ (zero velocity side) (Present results)

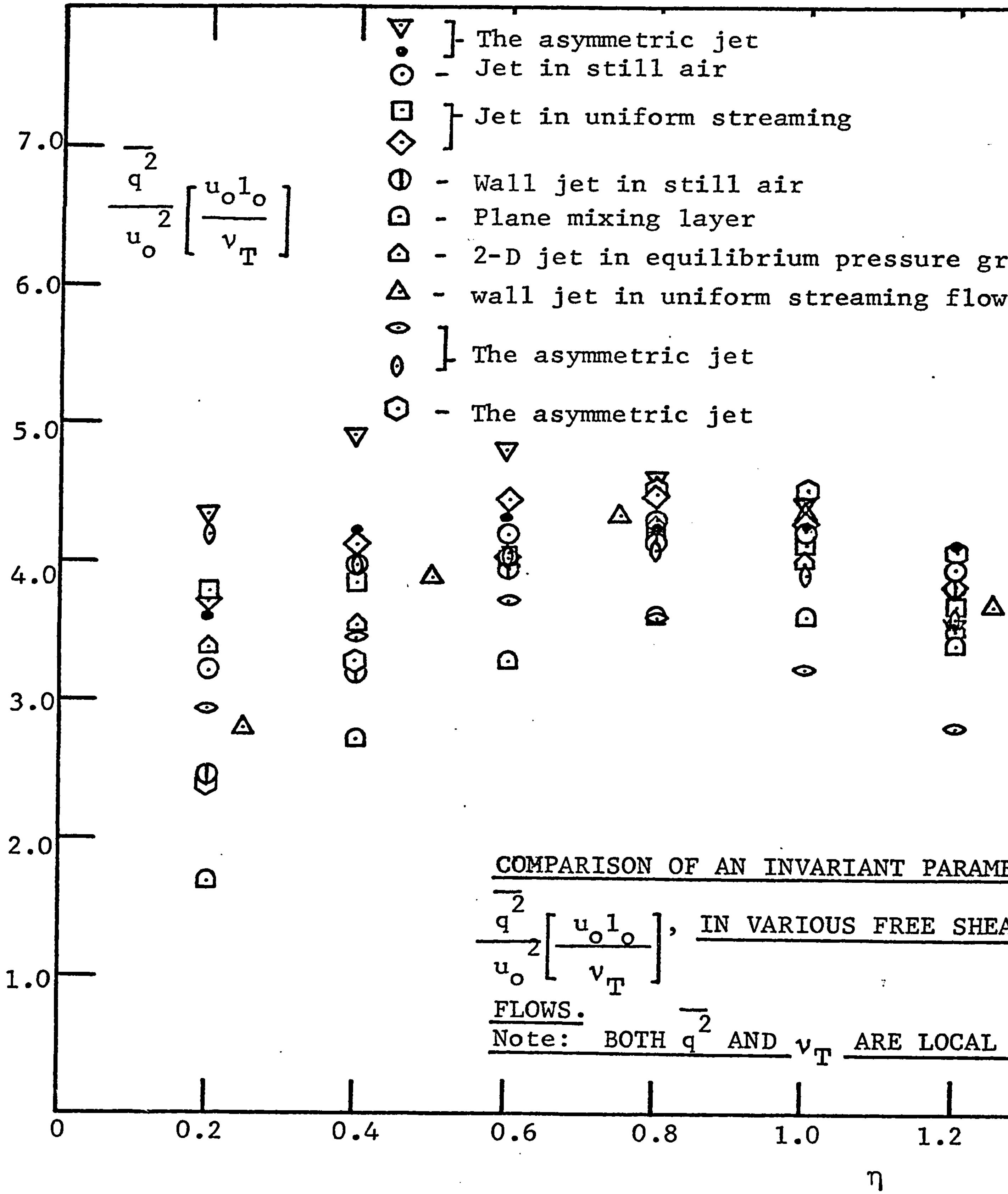

COMPARISON OF AN INVARIANT PARAME

$\frac{\overline{q^2}}{u_o^2}\left[\frac{u_o l_o}{\nu_T}\right]$, IN VARIOUS FREE SHEA

FLOWS.

Note: BOTH $\overline{q^2}$ AND ν_T ARE LOCAL

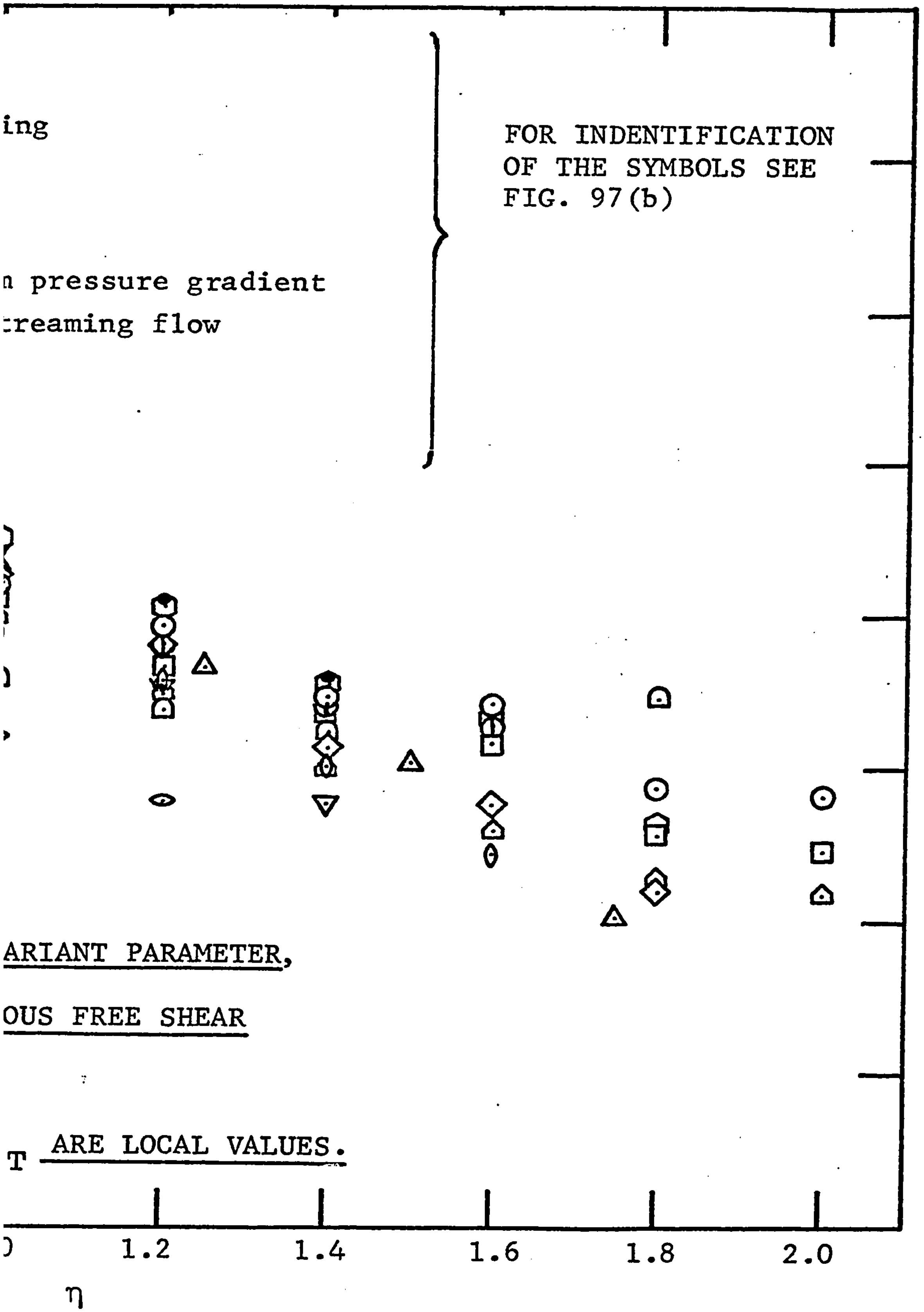
ing
n pressure gradient
treaming flow
FOR INDENTIFICATION
OF THE SYMBOLS SEE
FIG. 97(b)
ARIANT PARAMETER,
OUS FREE SHEAR
T ARE LOCAL VALUES.
1.2
1.4
1.6
1.8
2.0
η

Fig. 97 (a)

IDENTIFICATION OF THE SYMBOLS FOR FIG. 97(a)

COMPARISON OF AN INVARIANT PARAMETER,

$(\overline{q^2}/u_o^2)\ (u_o l_o/\nu_T)$, IN VARIOUS SHEAR FLOWS

(results are corrected for the longitudinal cooling effects)

▽ - The asymmetric jet, U_j/U_1 = 5.08 (streaming side) (Present results)

• - The asymmetric jet, U_j/U_1 = 5.08 (zero velocity side) (Present results)

⊙ - Jet in still air (Present results)

⊡ - U_1/U_j = 0.162 ⎤ Jet in uniform streaming flow (Bradbury (1963))
◇ - U_1/U_j = 0.58 ⎦

⦶ - Wall jet in still air (Guitton (1970))

⌂ - Plane mixing layer (Present results)

⌂ - 2-D Jet in equilibrium pressure gradient (Fekete (1970))

△ - Wall jet in uniform streaming flow (Kruka and Eskinazi (1964))

⊖ - Streaming side ⎤ The asymmetric jet, U_j/U_1 = 9.0 (Present results)
⦵ - Zero velocity side ⎦

⬡ - Zero velocity side. The asymmetric jet, U_j/U_1 = 2.275 (Present results)

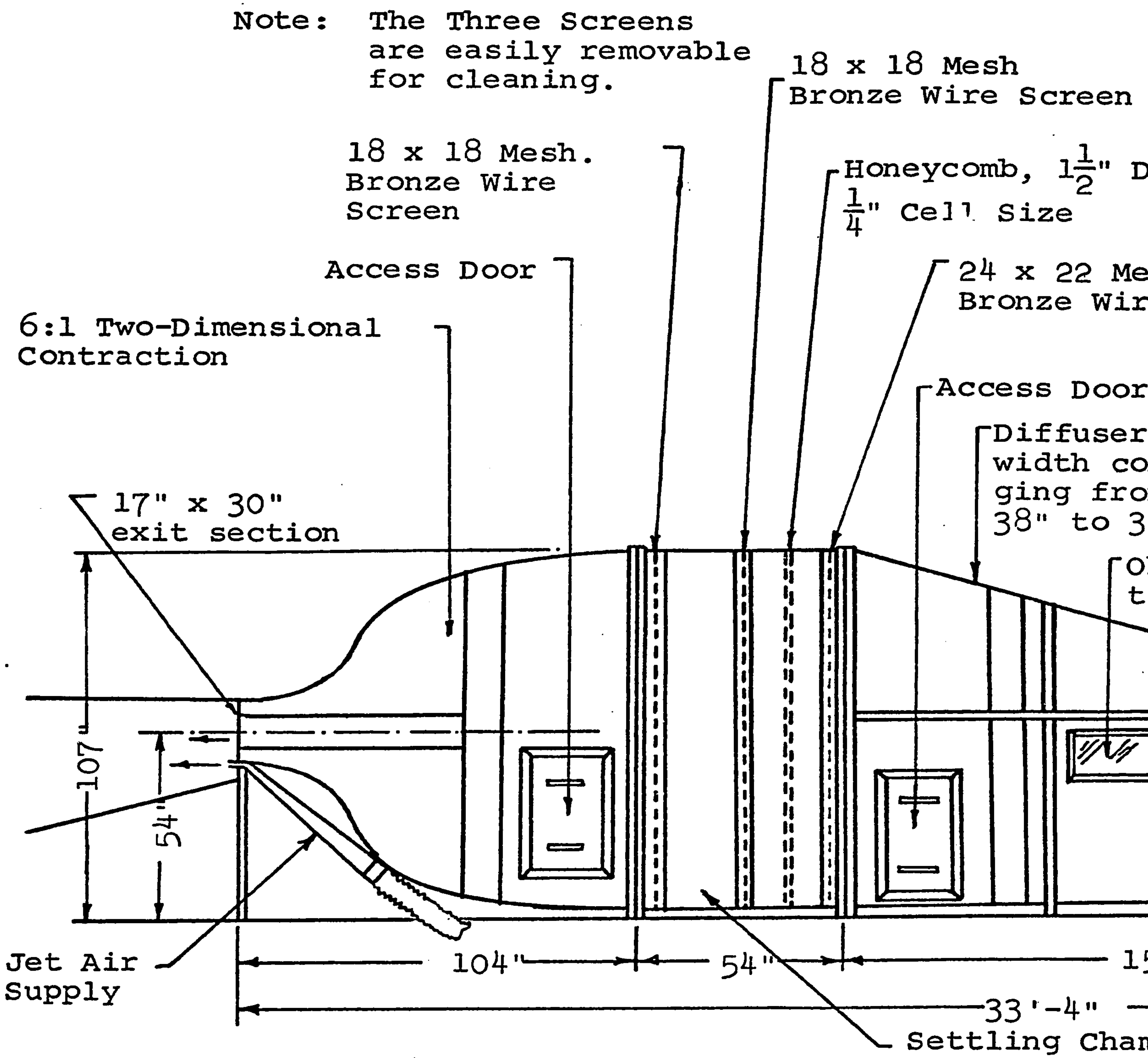

GENERAL LAYOUT OF BLOWER

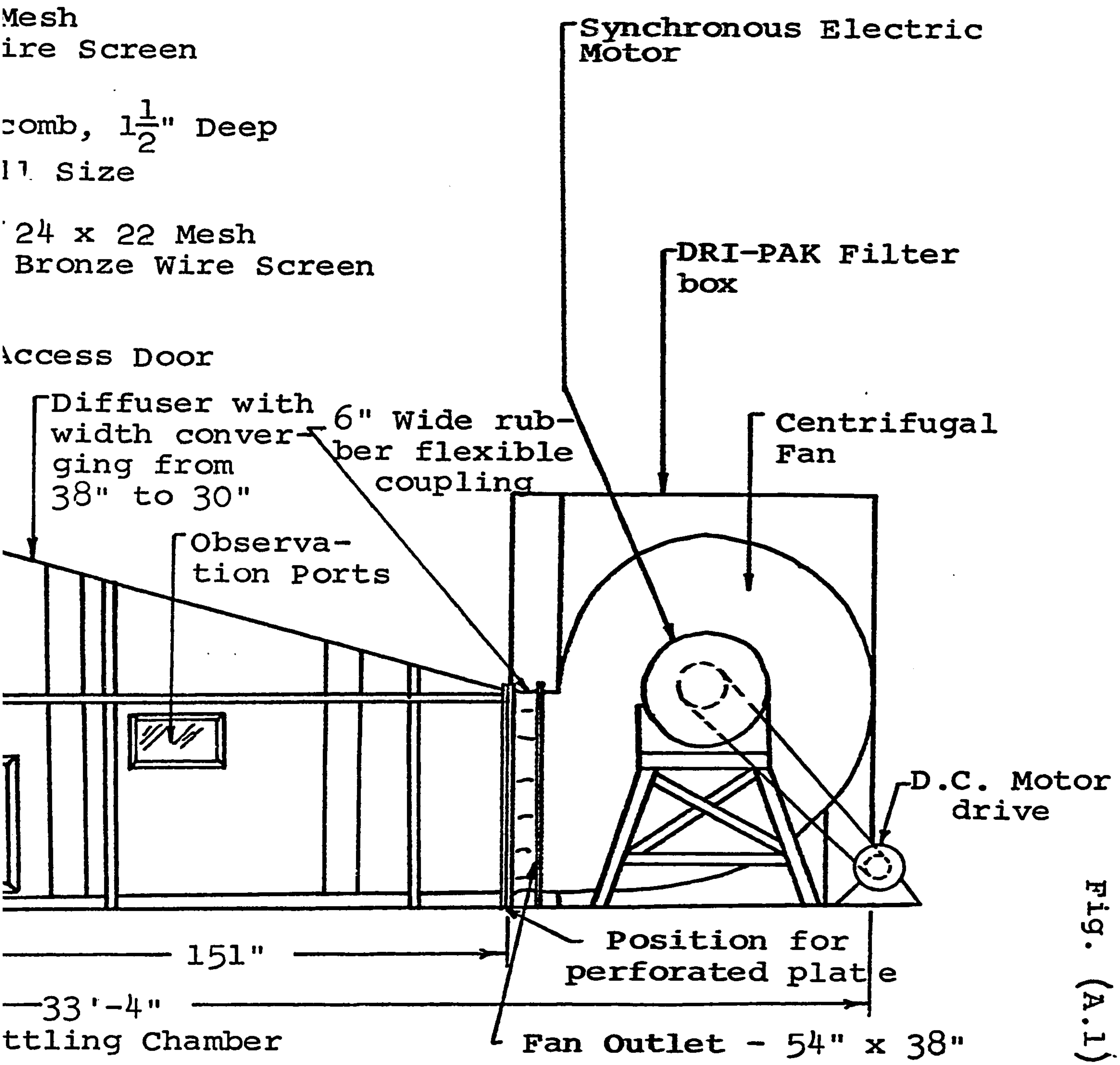

Fig. (A.1)

OF BLOWER CASCADE WIND-TUNNEL

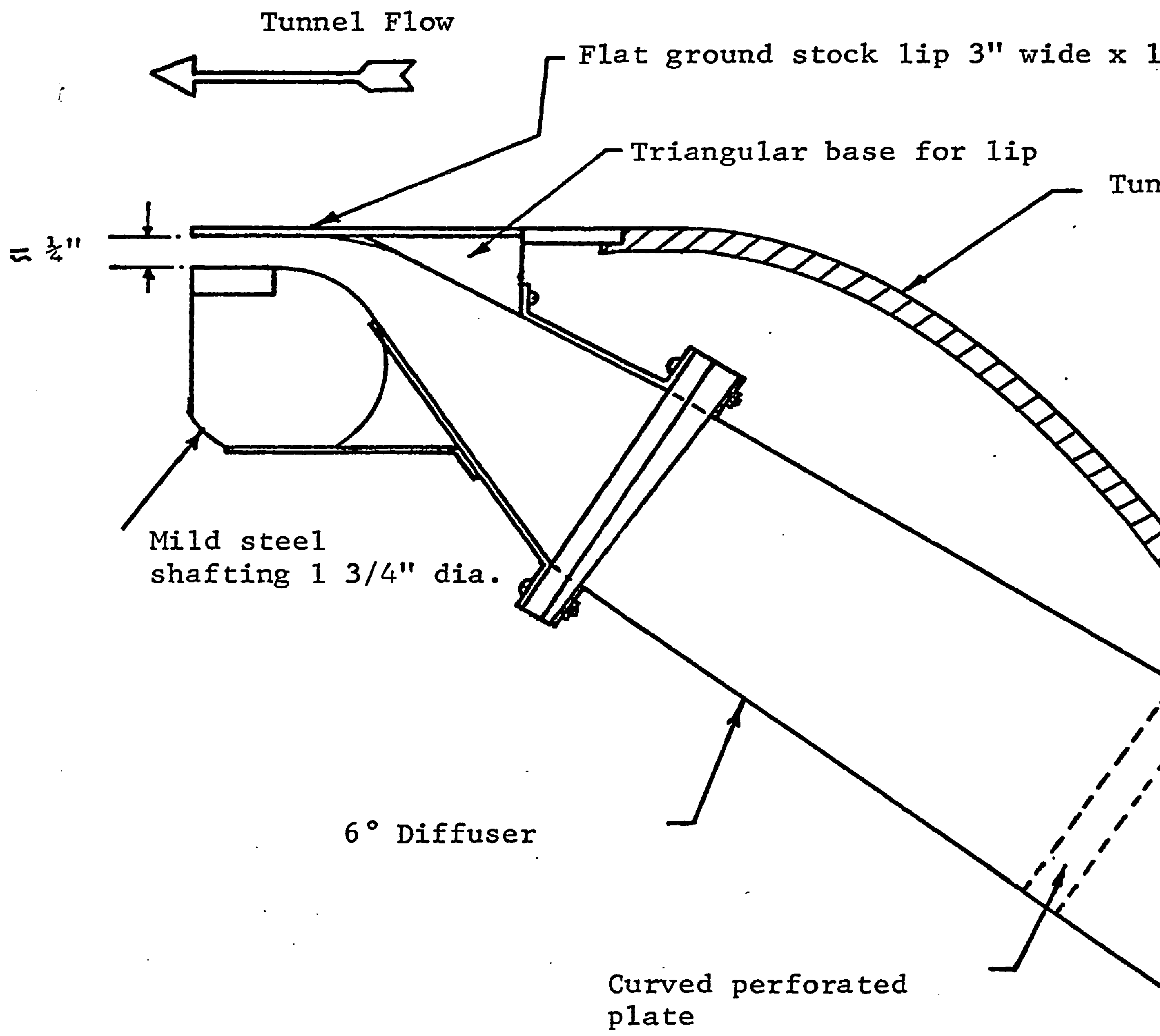

DETAILS OF SLOT ASSEMBLY

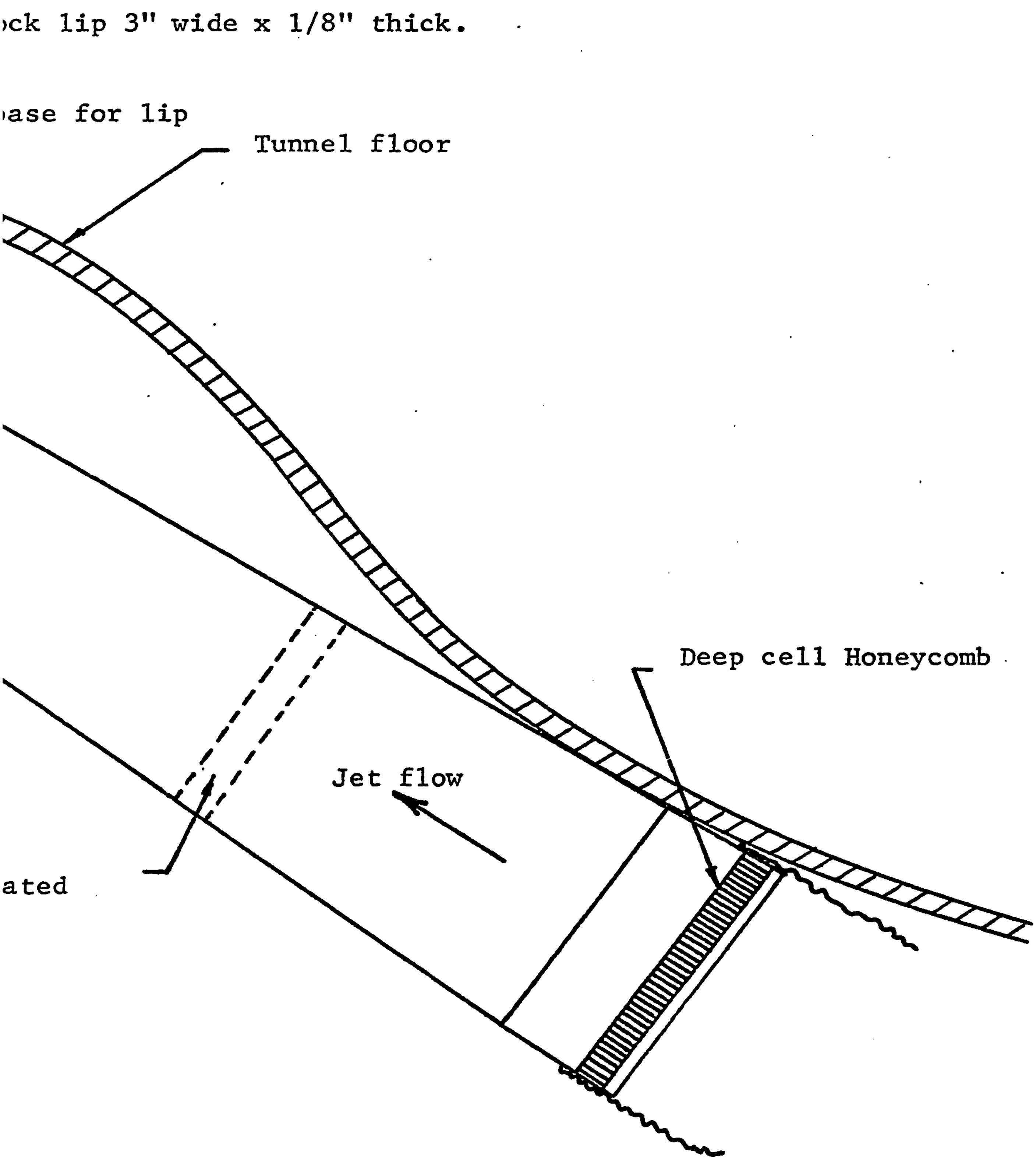
ock lip 3" wide x 1/8" thick.
ase for lip
Tunnel floor
Deep cell Honeycomb
Jet flow
ated

Fig. (A.2)

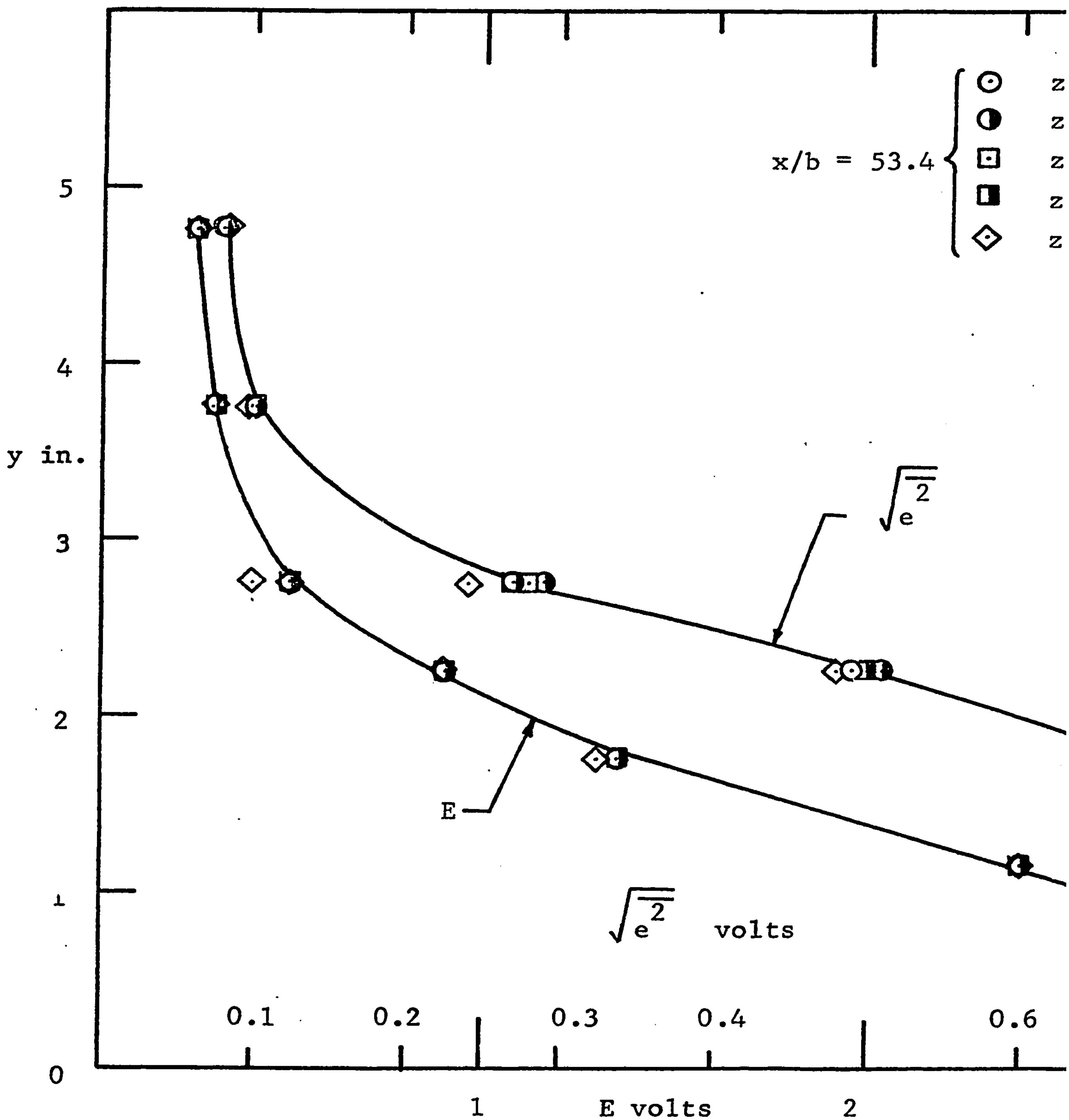

TWO-DIMENSIONALITY CHECK FOR A PLANE JET IN STILL AIR

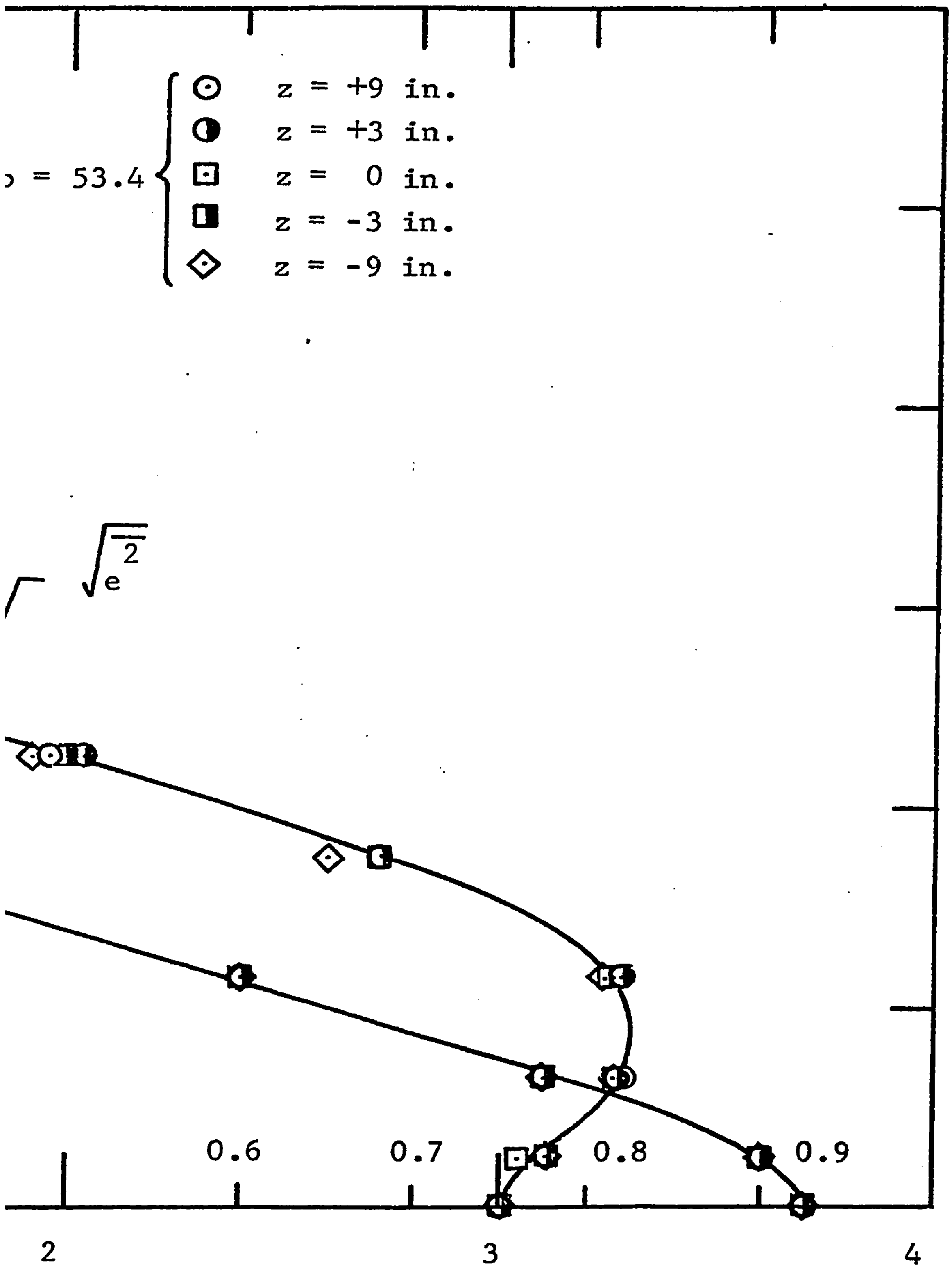

STILL AIR

Fig. (A.3)

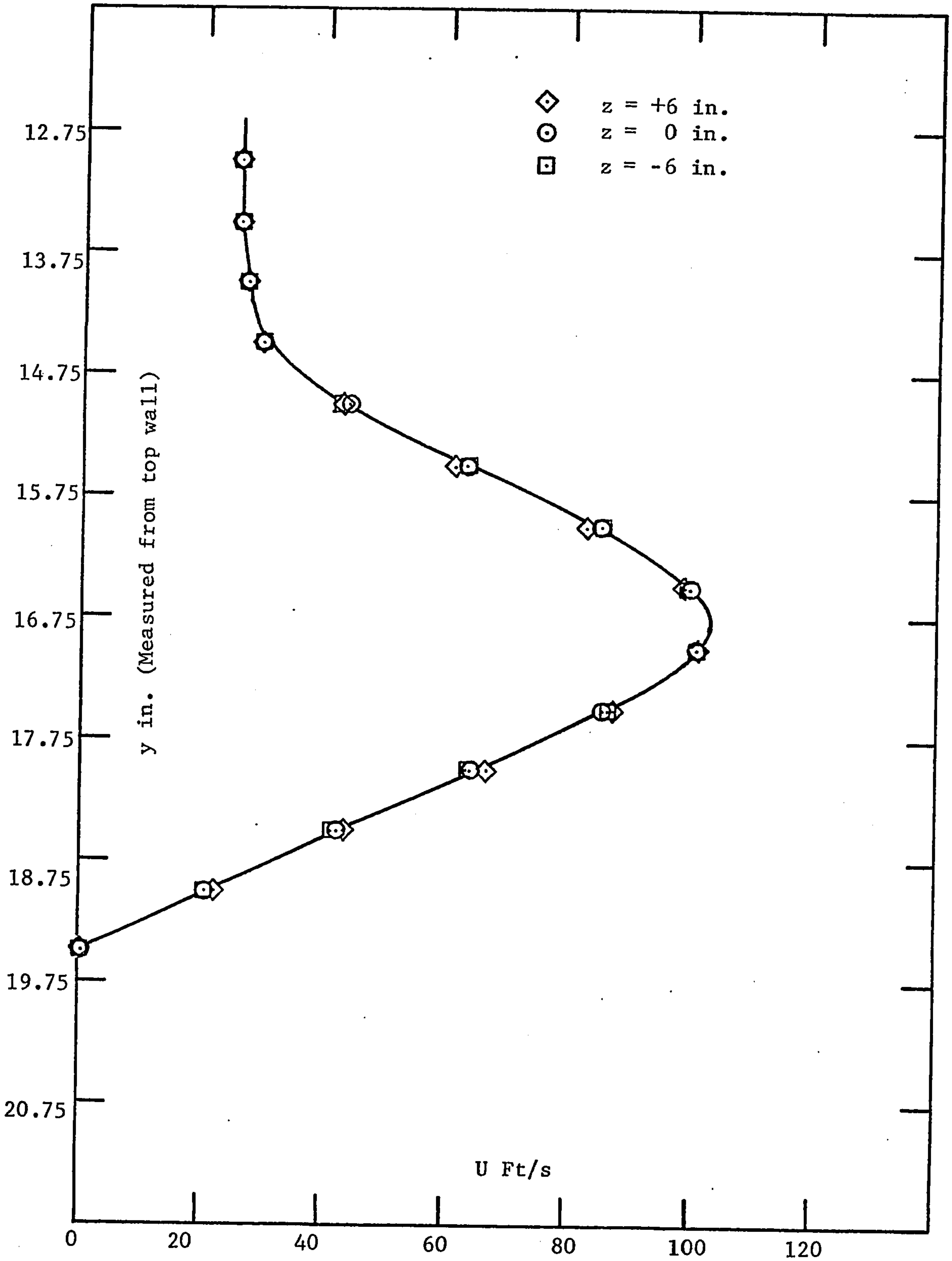

TWO-DIMENSIONALITY CHECK FOR THE ASYMMETRIC JET WITH A PITOT TUBE.
$x/b = 53.4$; $U_j/U_1 = 11.6$

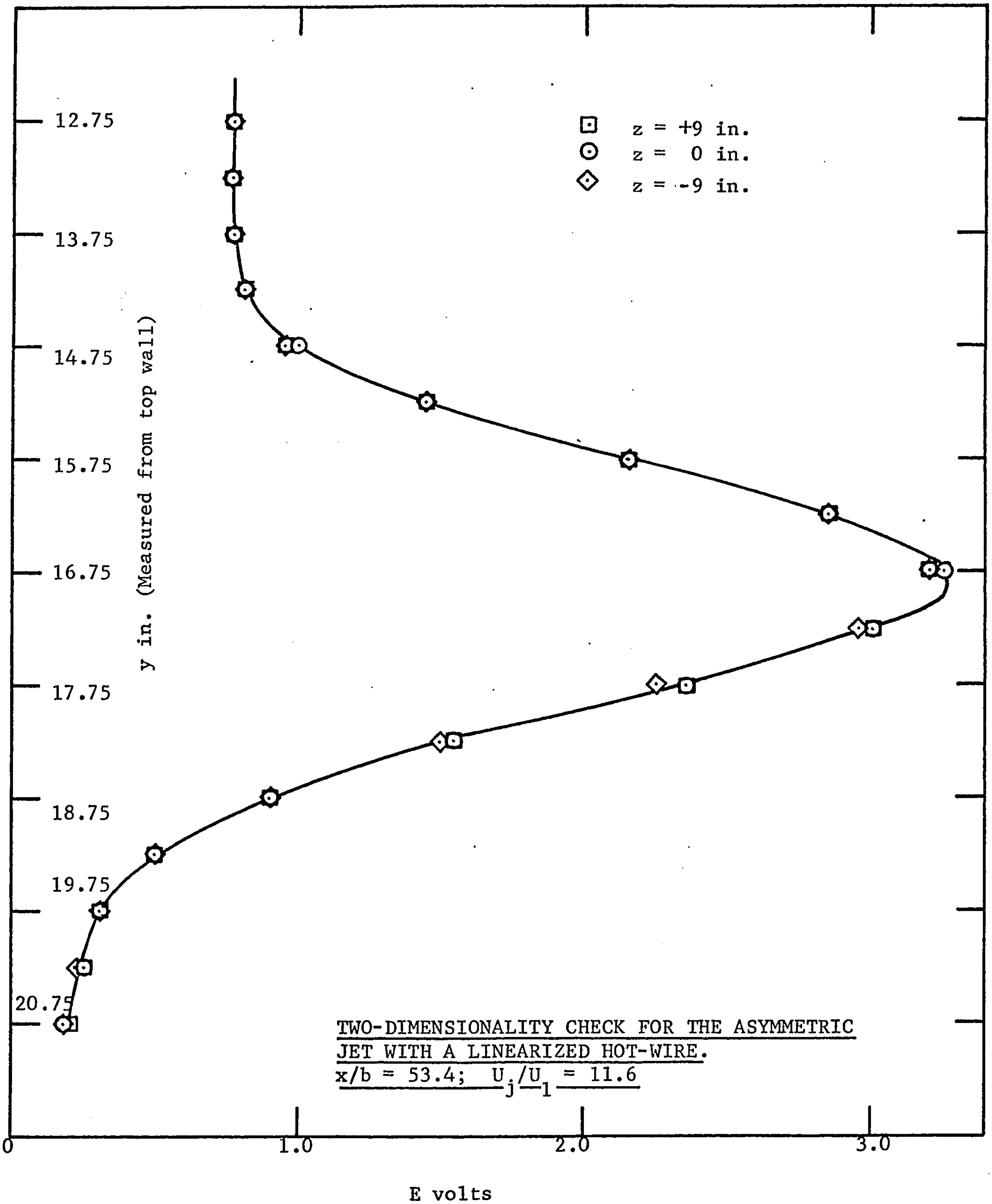

TWO-DIMENSIONALITY CHECK FOR THE ASYMMETRIC JET WITH A LINEARIZED HOT-WIRE.
$x/b = 53.4$; $U_j/U_1 = 11.6$

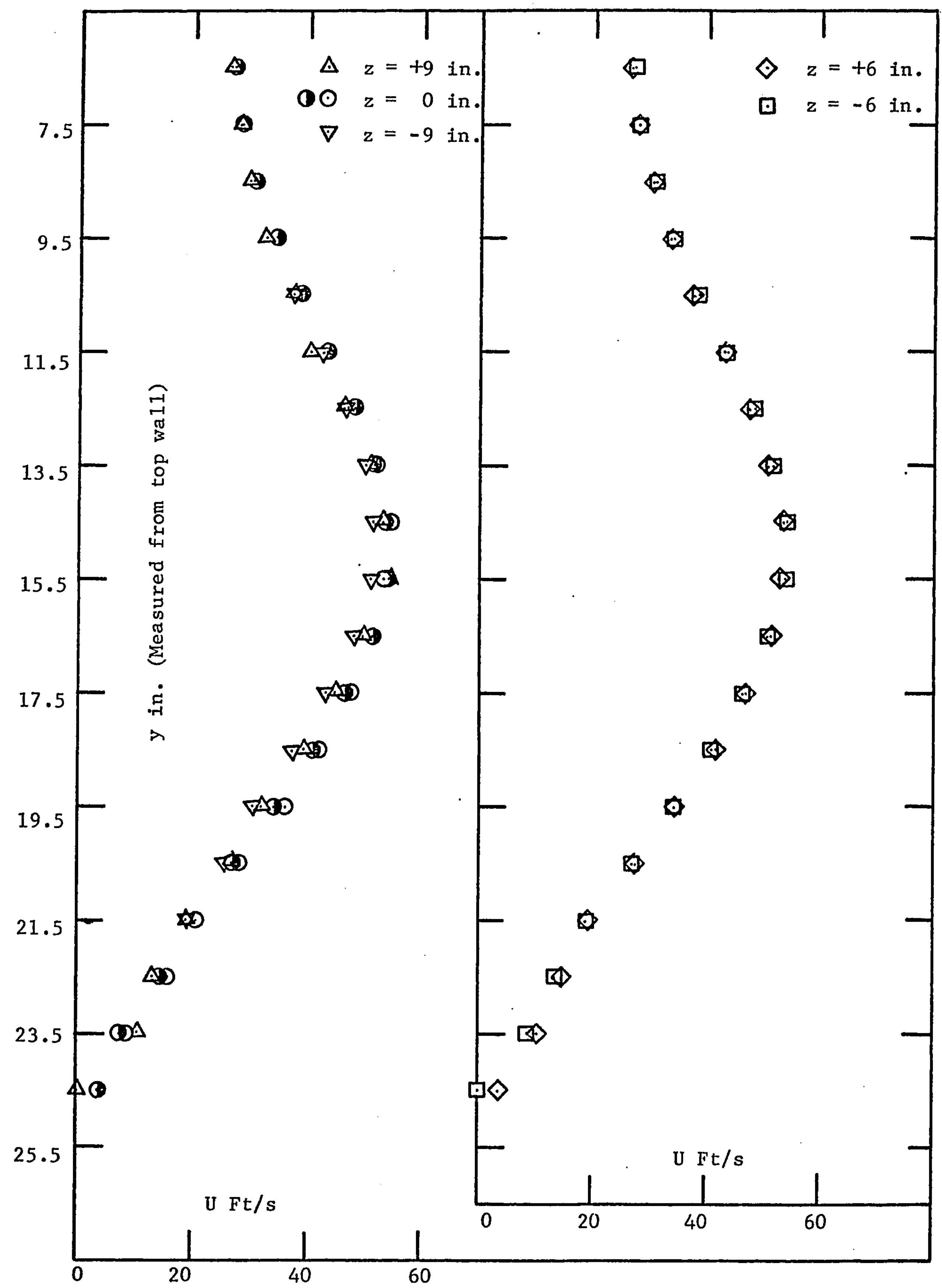

TWO-DIMENSIONALITY CHECK FOR THE ASYMMETRIC JET WITH A PITOT TUBE.
$x/b = 217$; $U_j/U_1 = 11.6$

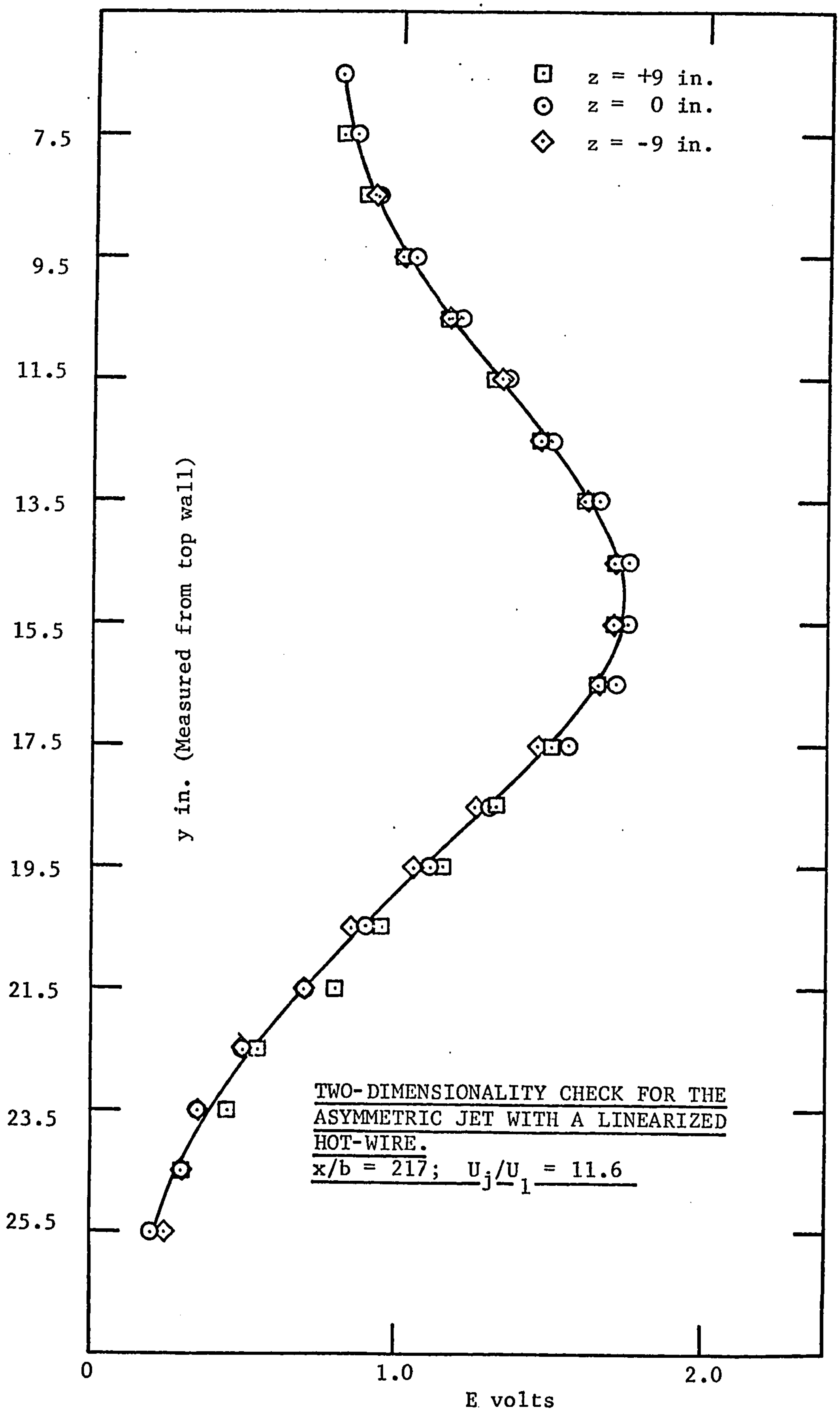

TWO-DIMENSIONALITY CHECK FOR THE ASYMMETRIC JET WITH A LINEARIZED HOT-WIRE.
$x/b = 217$; $U_j/U_1 = 11.6$

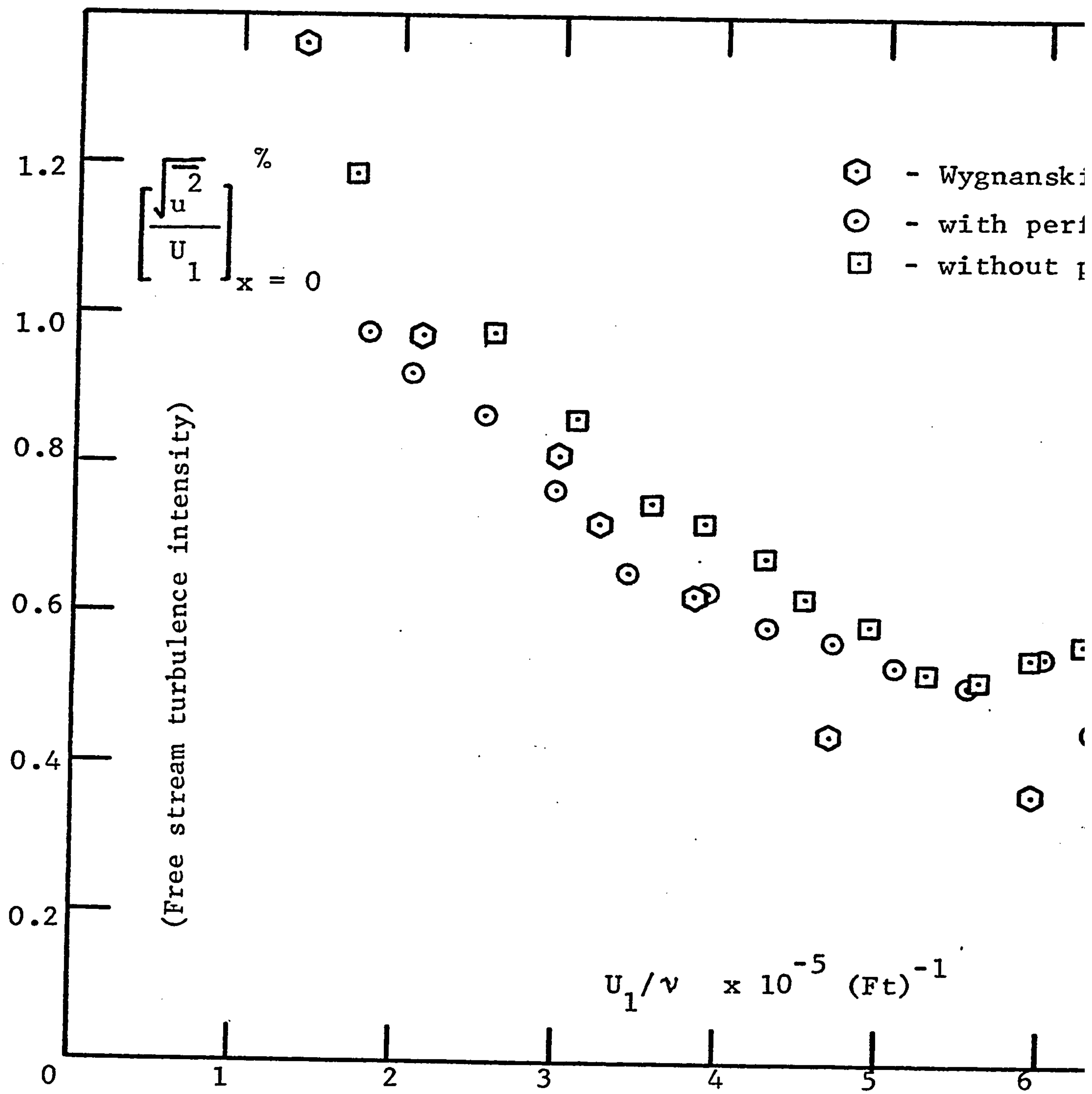

LONGITUDINAL TURBULENT INTENSITY ON TUNNEL CENTRE LINE

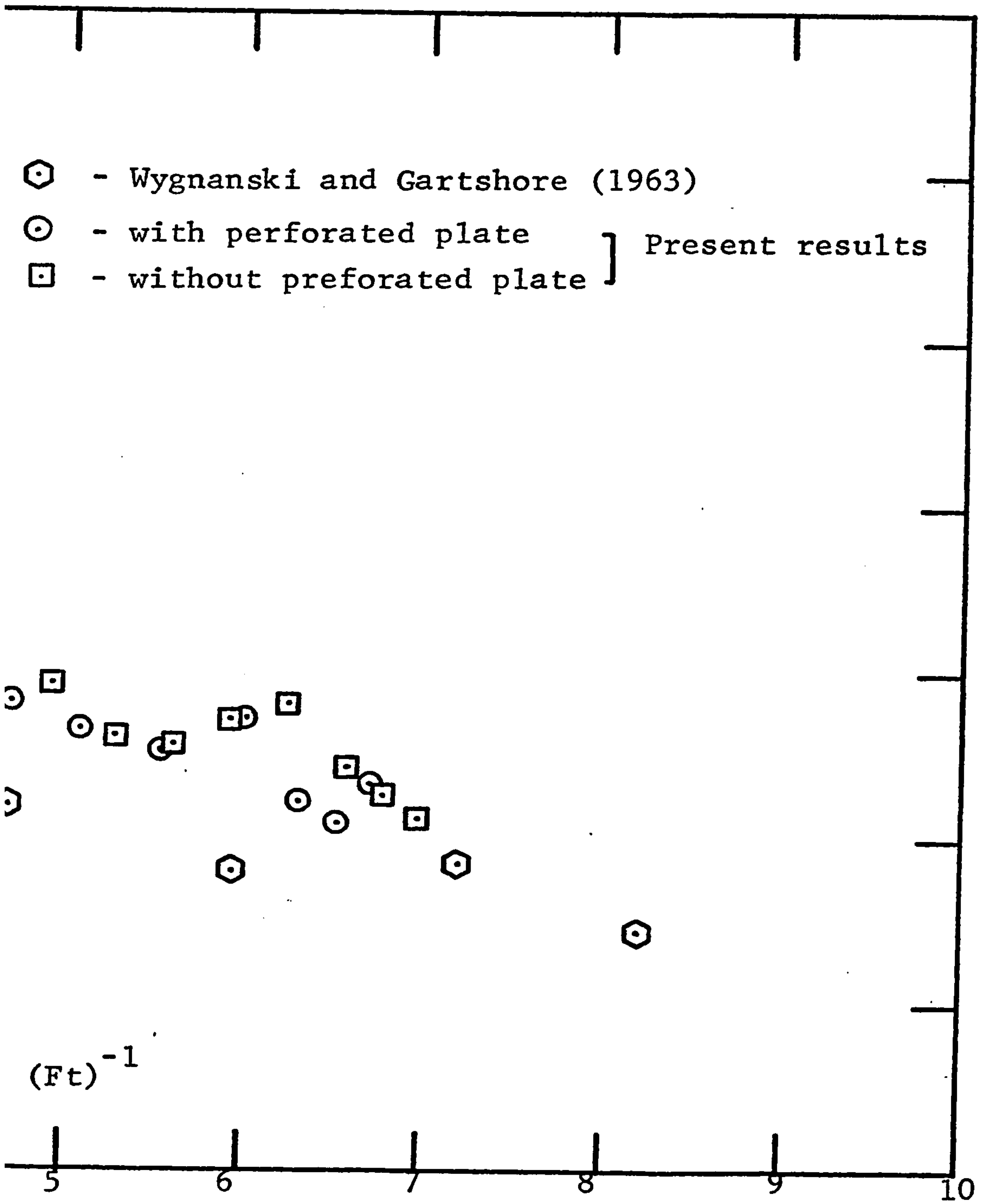

EL CENTRE LINE AT EXIT.

Fig. (B.1)

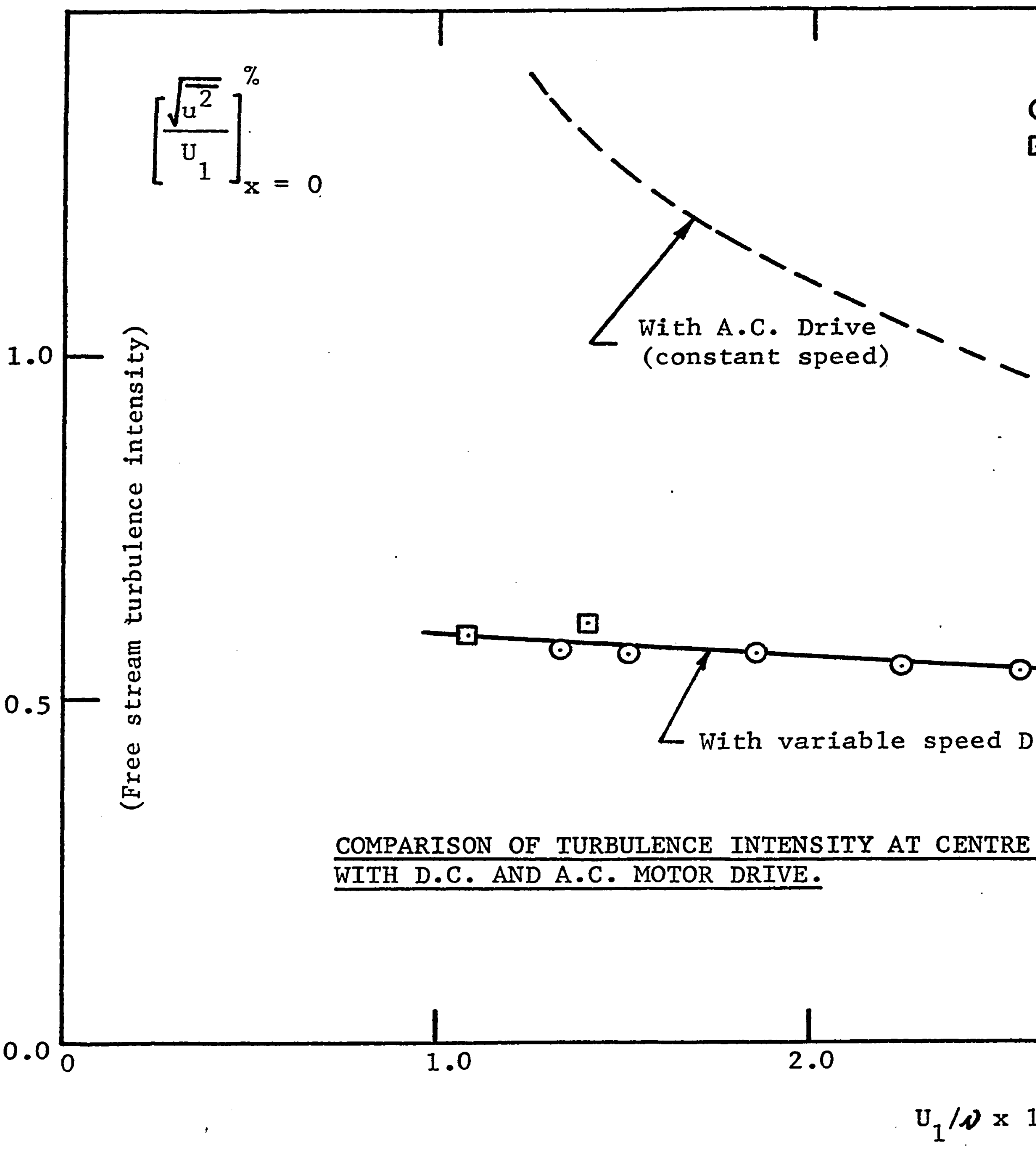

$\left[\frac{\sqrt{\overline{u^2}}}{U_1}\right]_{x=0}^{\%}$
(Free stream turbulence intensity)
1.0
0.5
0.0
0
1.0
2.0
With A.C. Drive
(constant speed)
With variable speed D
COMPARISON OF TURBULENCE INTENSITY AT CENTRE
WITH D.C. AND A.C. MOTOR DRIVE.
U_1/ν x 1

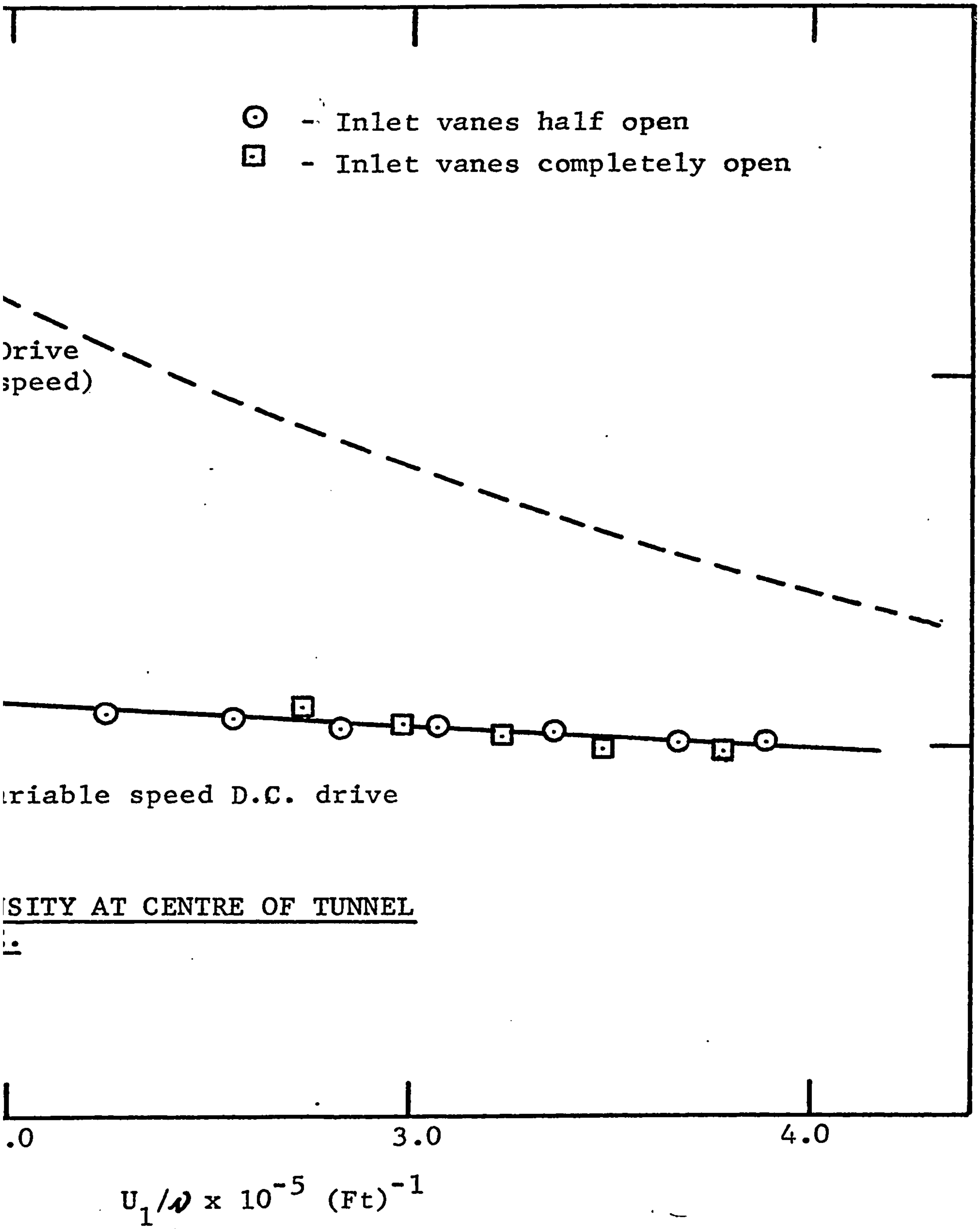

ISITY AT CENTRE OF TUNNEL

Fig. (B.2)

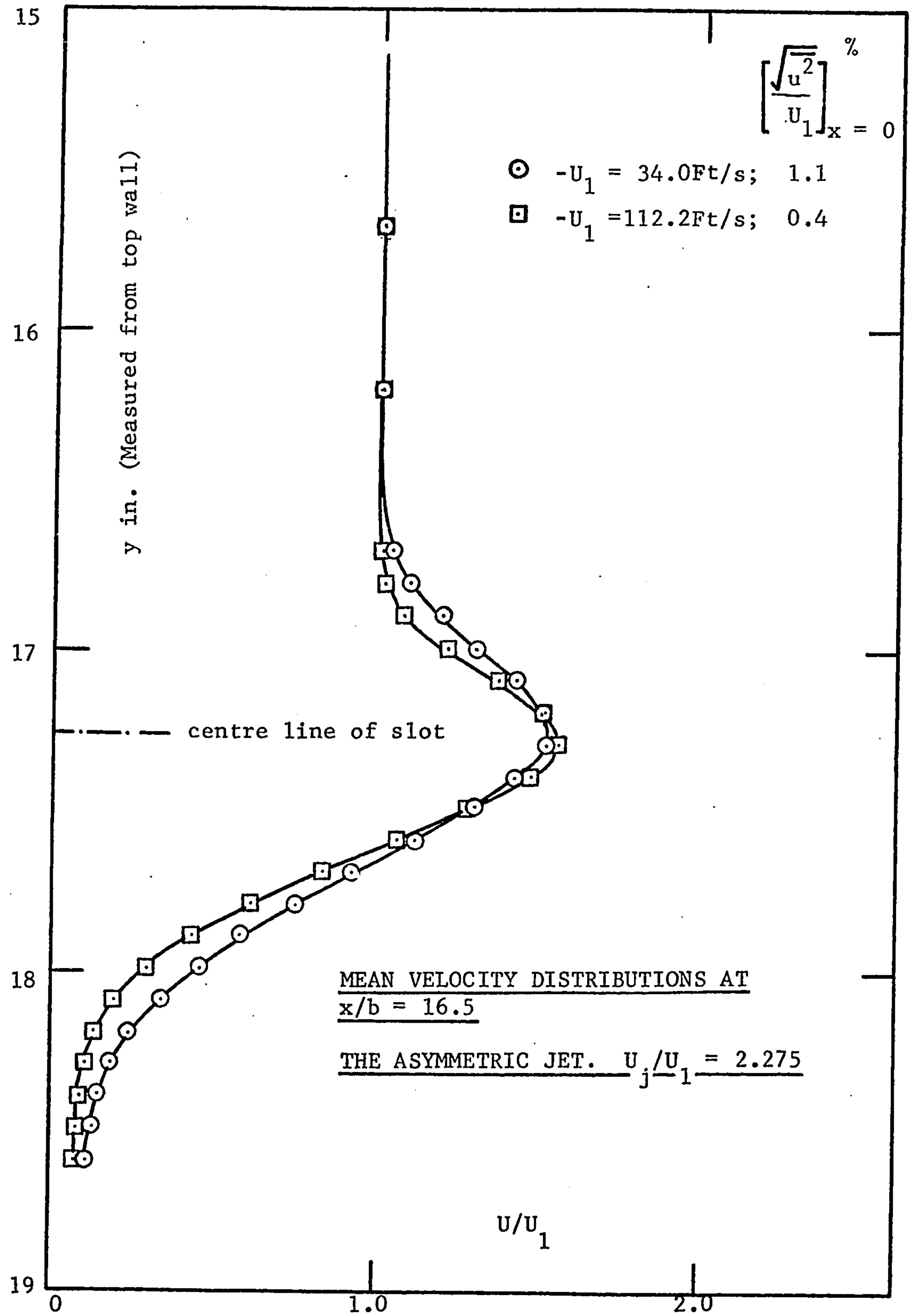

MEAN VELOCITY DISTRIBUTIONS AT x/b = 16.5

THE ASYMMETRIC JET. $U_j/U_1 = 2.275$

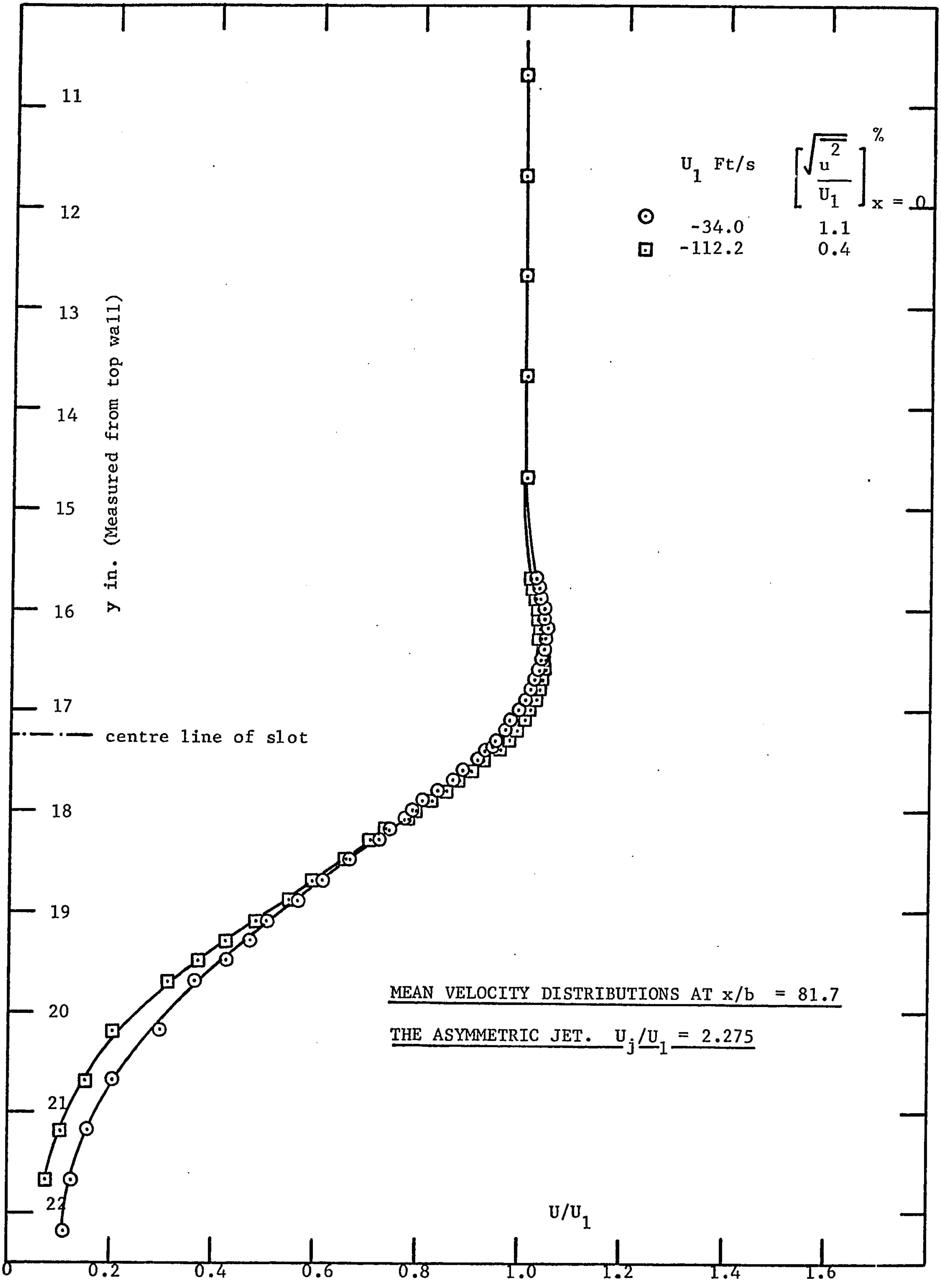

11
12
13
14
15
16
17
18
19
20
21
22
y in. (Measured from top wall)
centre line of slot
U1 Ft/s
[√(u²)/U1]x = 0 %
-34.0 1.1
-112.2 0.4
MEAN VELOCITY DISTRIBUTIONS AT x/b = 81.7
THE ASYMMETRIC JET. Uj/U1 = 2.275
U/U1
0
0.2
0.4
0.6
0.8
1.0
1.2
1.4
1.6

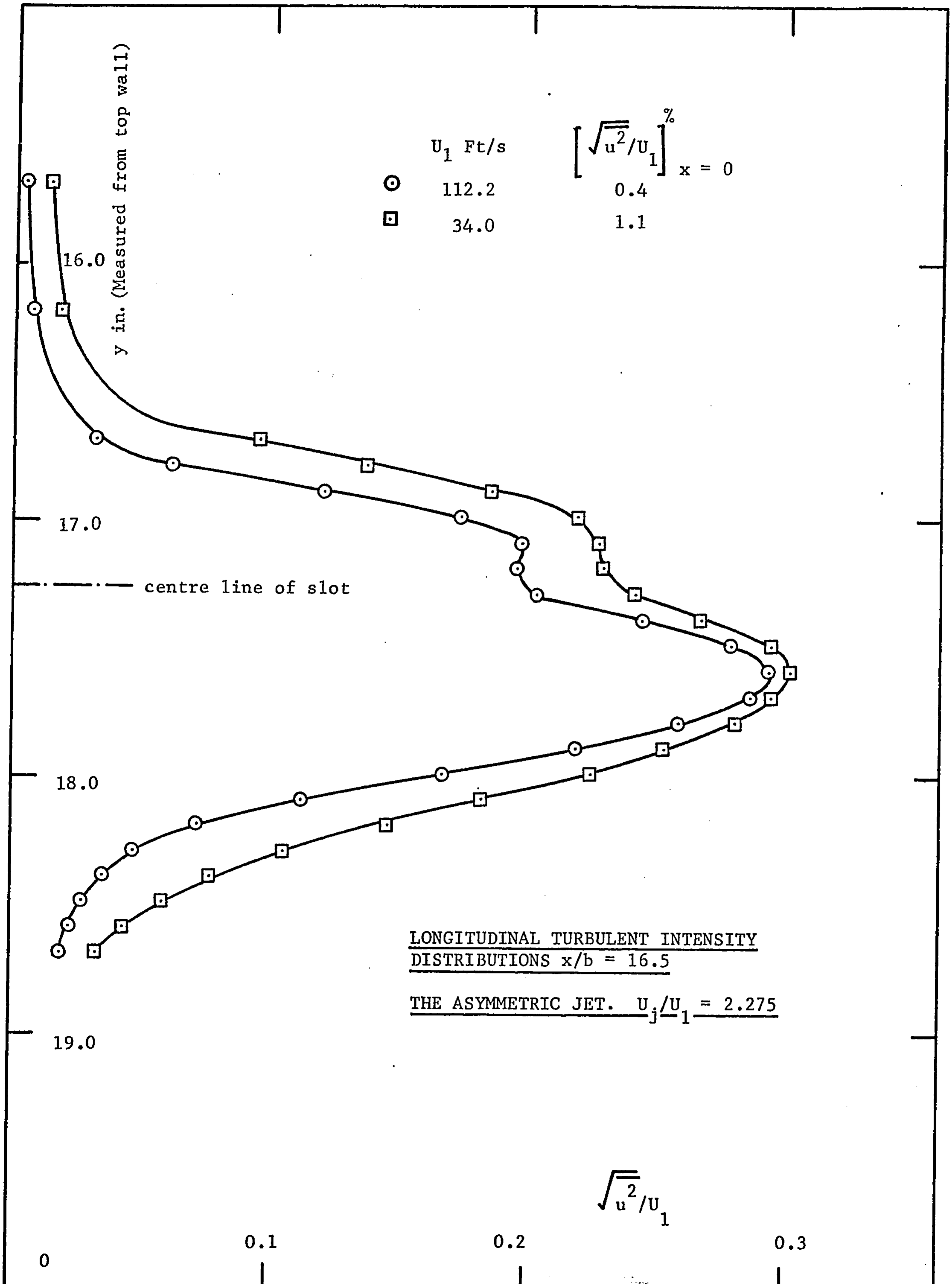
y in. (Measured from top wall)
U_1 Ft/s
$\left[\sqrt{\overline{u^2}}/U_1\right]^{\%}_{x=0}$
112.2
0.4
34.0
1.1
16.0
17.0
centre line of slot
18.0
19.0
LONGITUDINAL TURBULENT INTENSITY
DISTRIBUTIONS x/b = 16.5
THE ASYMMETRIC JET. $U_j/U_1 = 2.275$
$\sqrt{\overline{u^2}}/U_1$
0
0.1
0.2
0.3

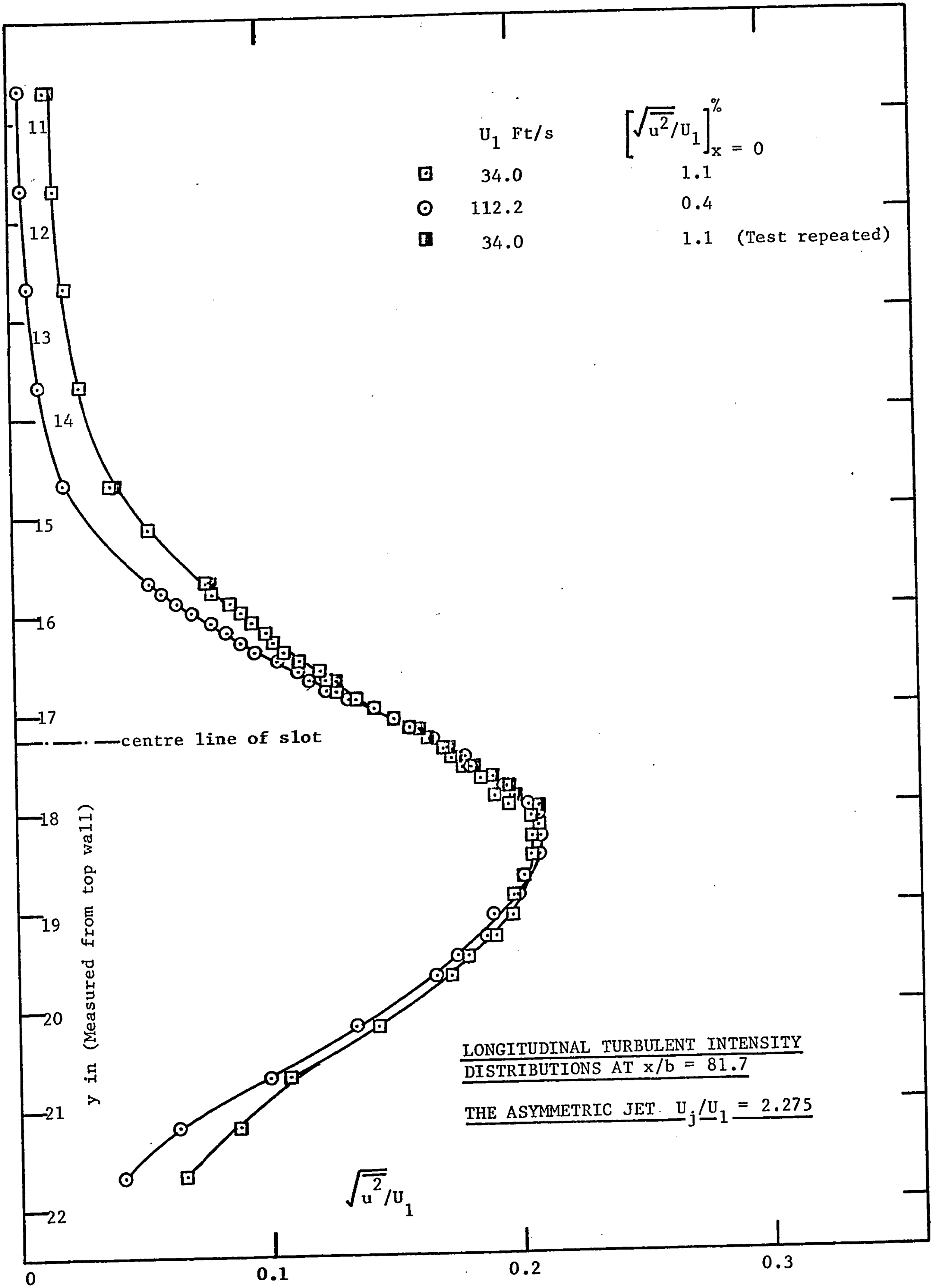

LONGITUDINAL TURBULENT INTENSITY DISTRIBUTIONS AT x/b = 81.7

THE ASYMMETRIC JET $U_j/U_1 = 2.275$

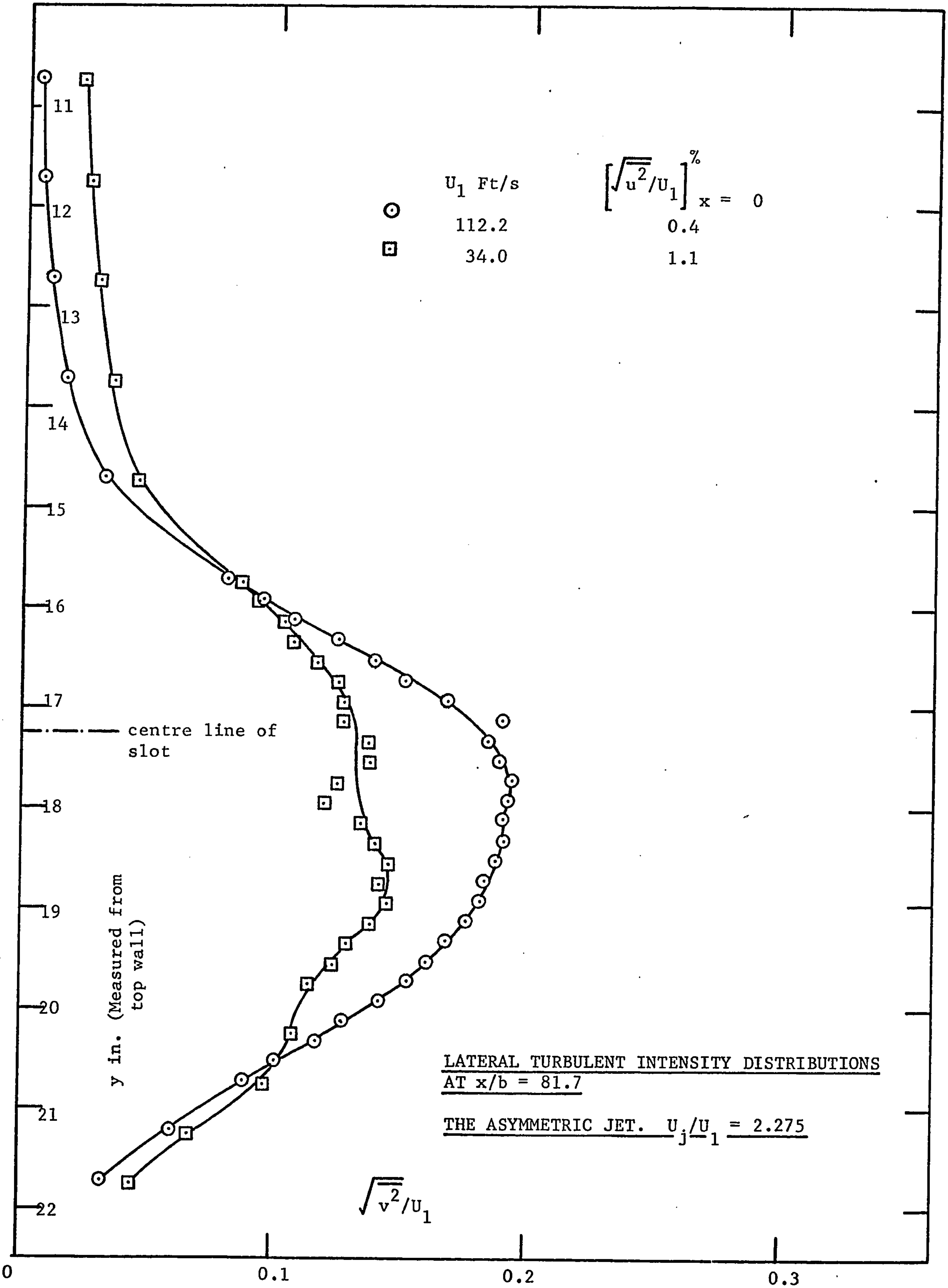

LATERAL TURBULENT INTENSITY DISTRIBUTIONS AT x/b = 81.7

THE ASYMMETRIC JET. $U_j/U_1 = 2.275$

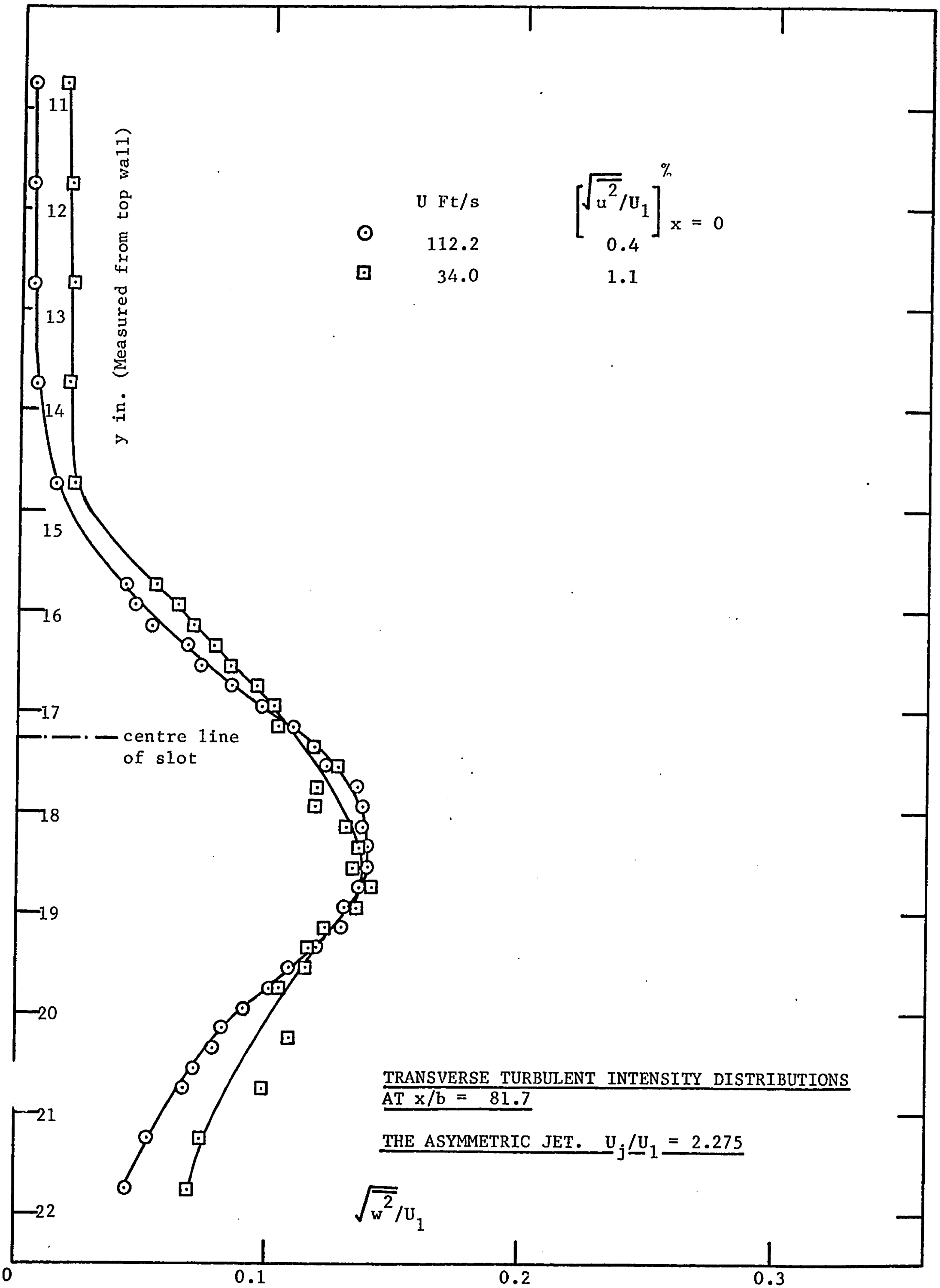

TRANSVERSE TURBULENT INTENSITY DISTRIBUTIONS AT $x/b = 81.7$

THE ASYMMETRIC JET. $U_j/U_1 = 2.275$

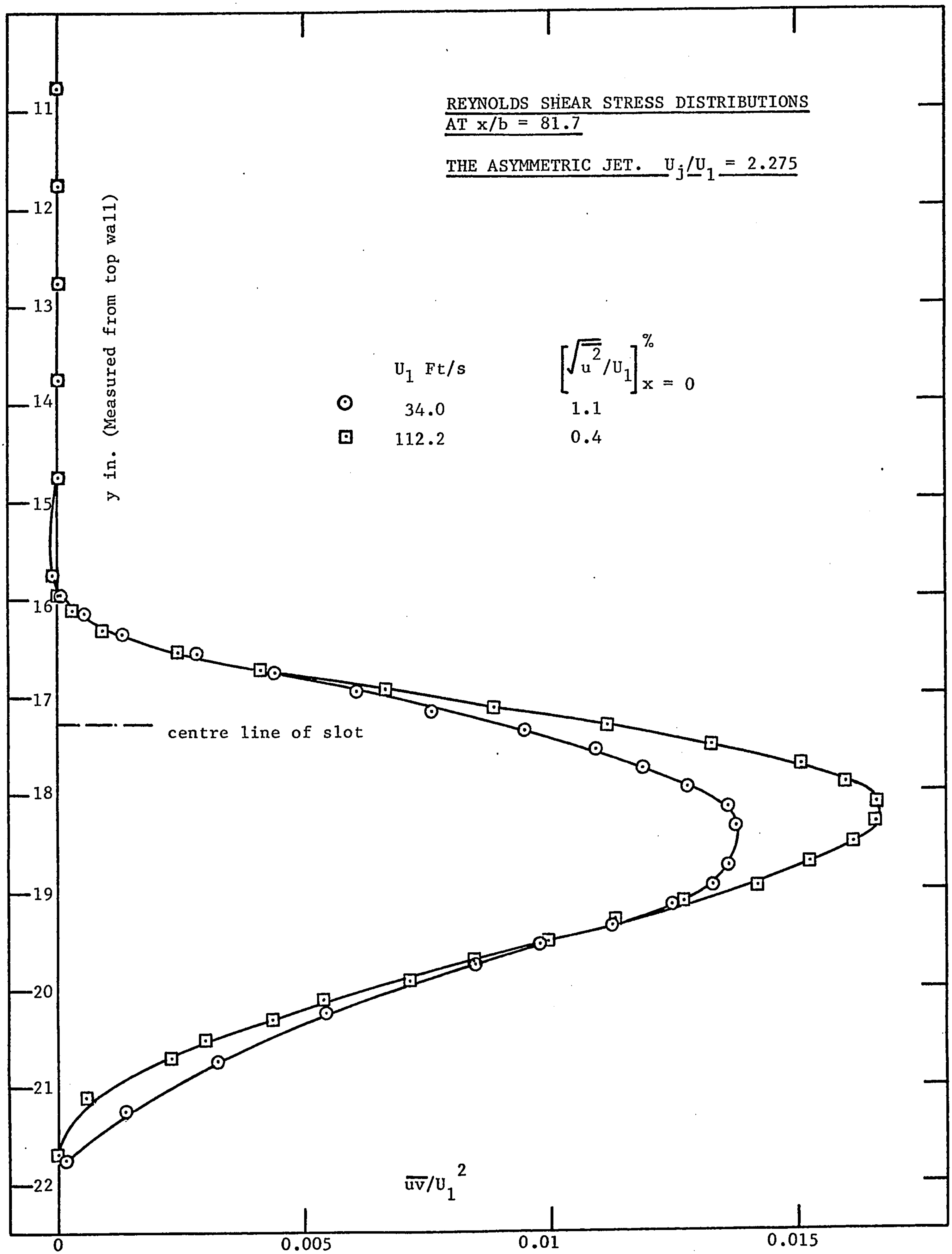
REYNOLDS SHEAR STRESS DISTRIBUTIONS
AT x/b = 81.7
THE ASYMMETRIC JET. U_j/U_1 = 2.275
U_1 Ft/s
$\left[\sqrt{\overline{u^2}}/U_1\right]^{\%}_{x=0}$
34.0
1.1
112.2
0.4
y in. (Measured from top wall)
centre line of slot
$\overline{uv}/U_1^2$
11
12
13
14
15
16
17
18
19
20
21
22
0
0.005
0.01
0.015

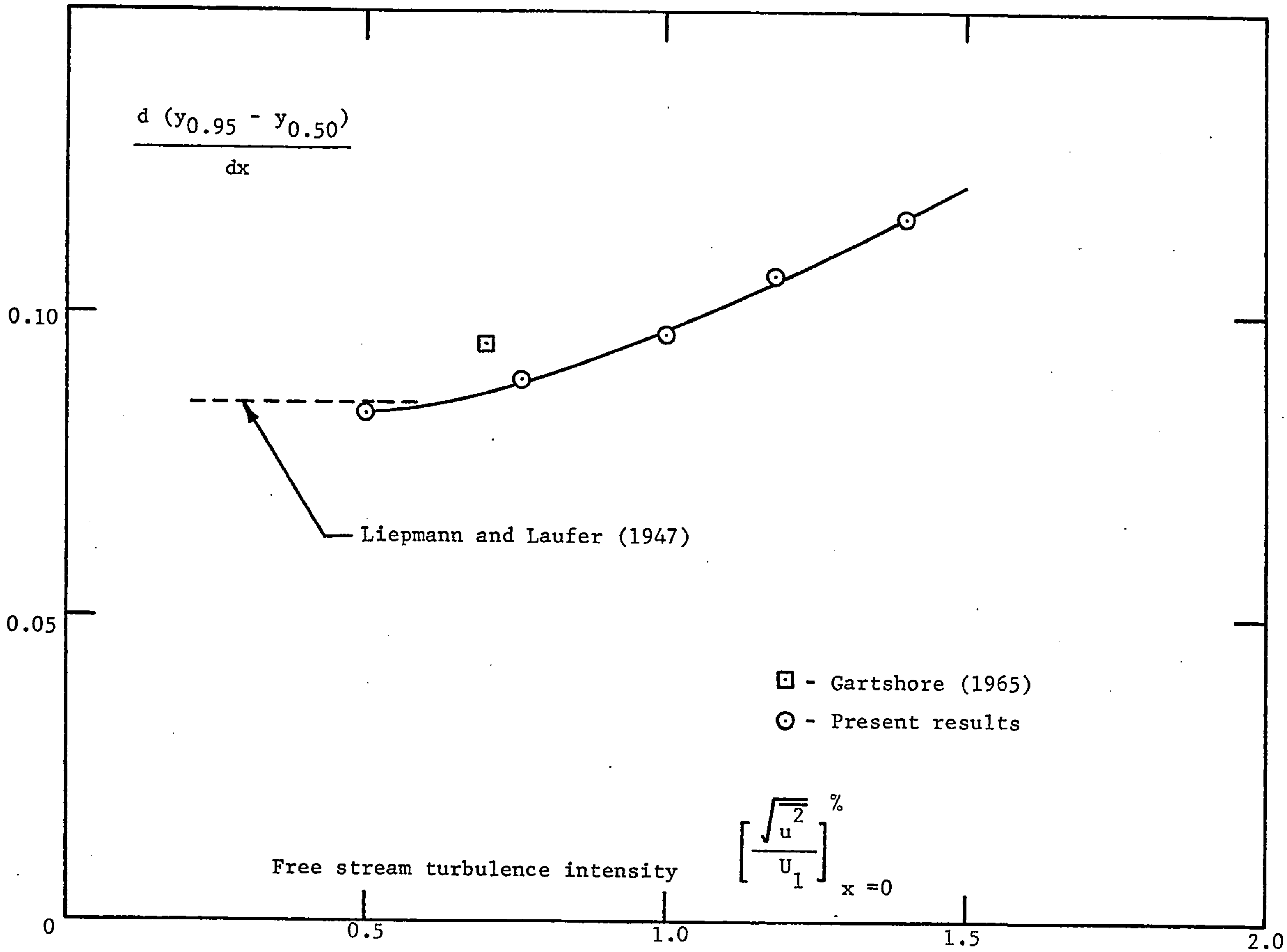

VARIATION OF RATE OF GROWTH WITH FREE STREAM TURBULENCE INTENSITY. THE PLANE MIXING LAYER.

Fig. (B.10)

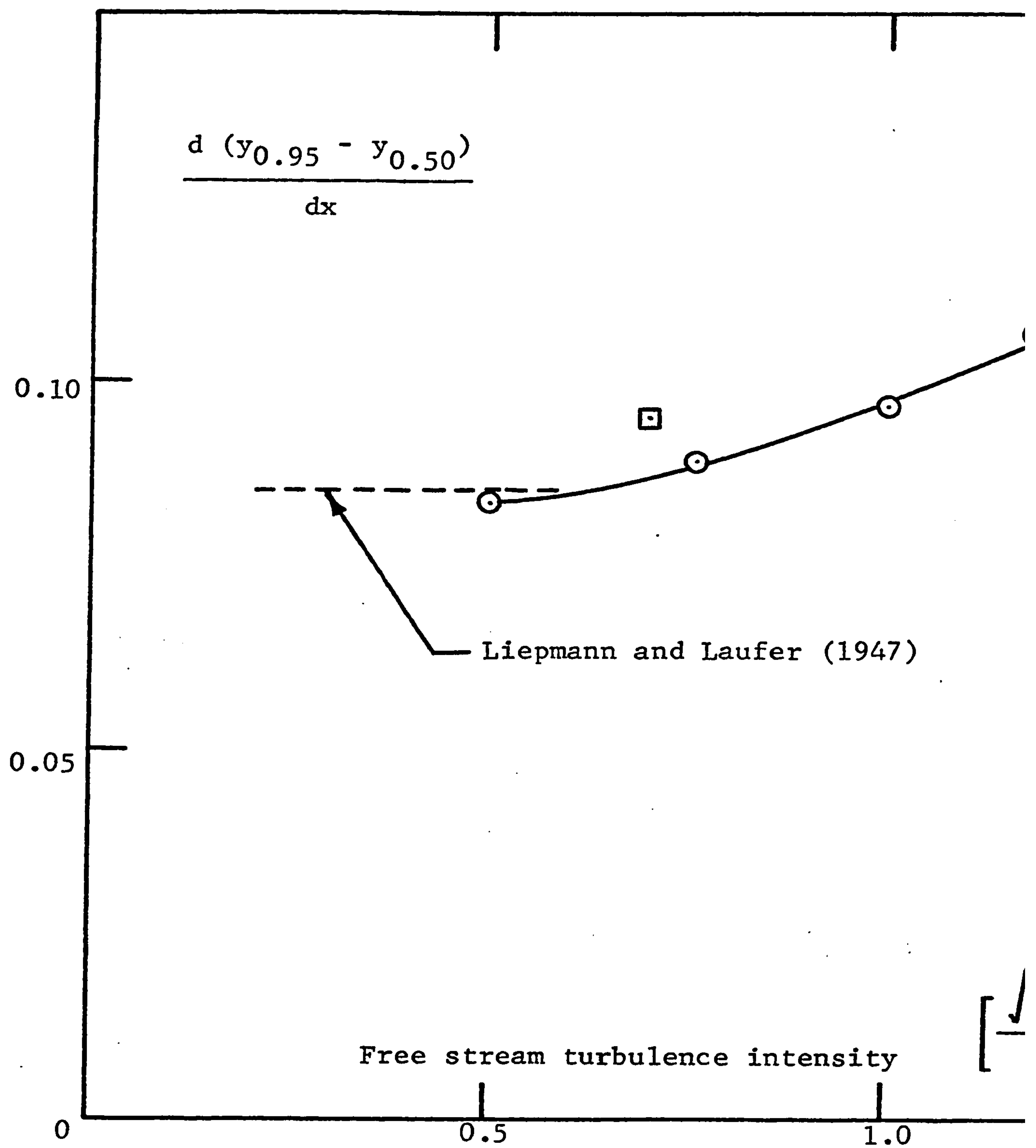

VARIATION OF RATE OF GROWTH WITH FREE STREAM TURBULENC
THE PLANE MIXING LAYER.

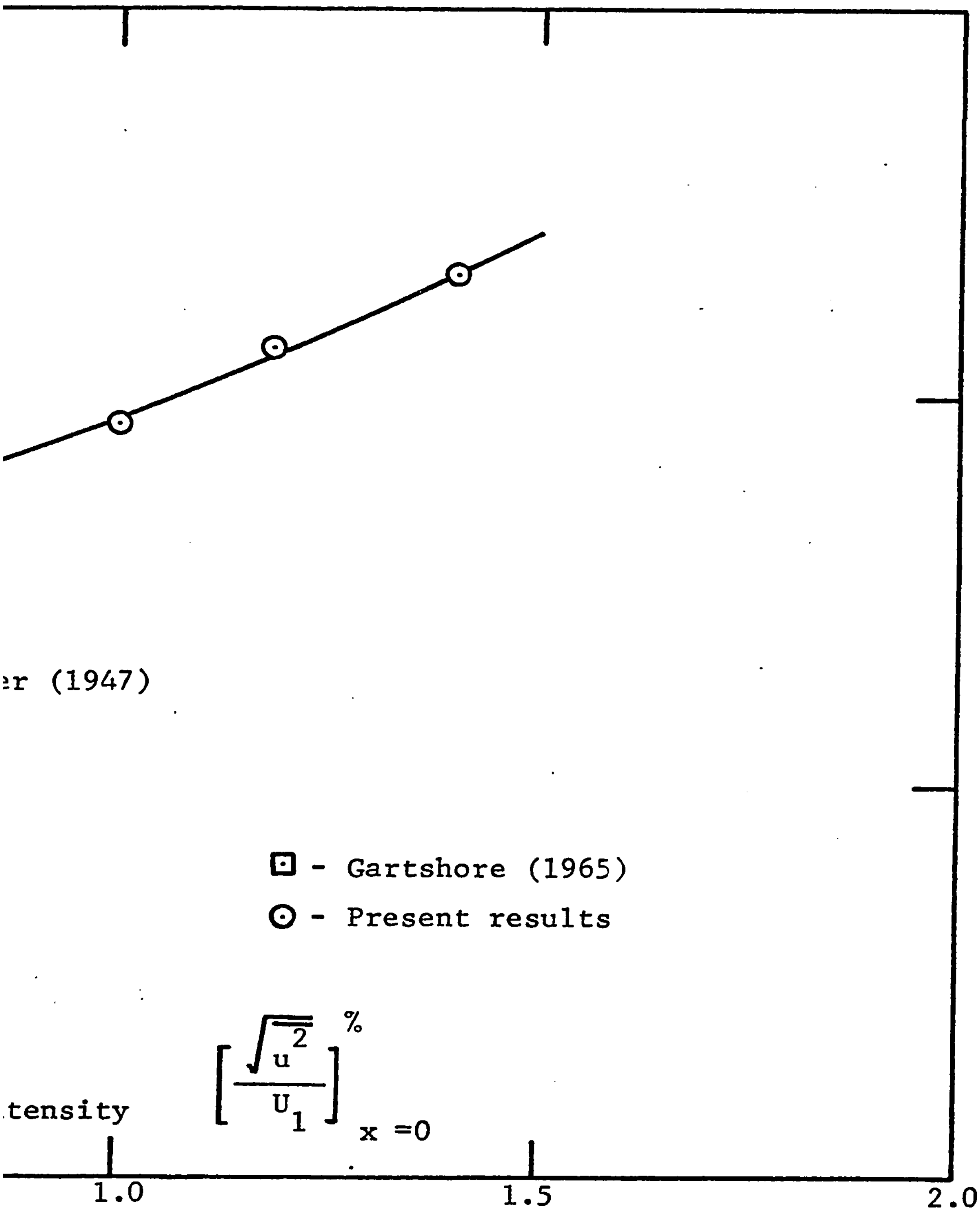

TREAM TURBULENCE INTENSITY.

Fig. (B.10)

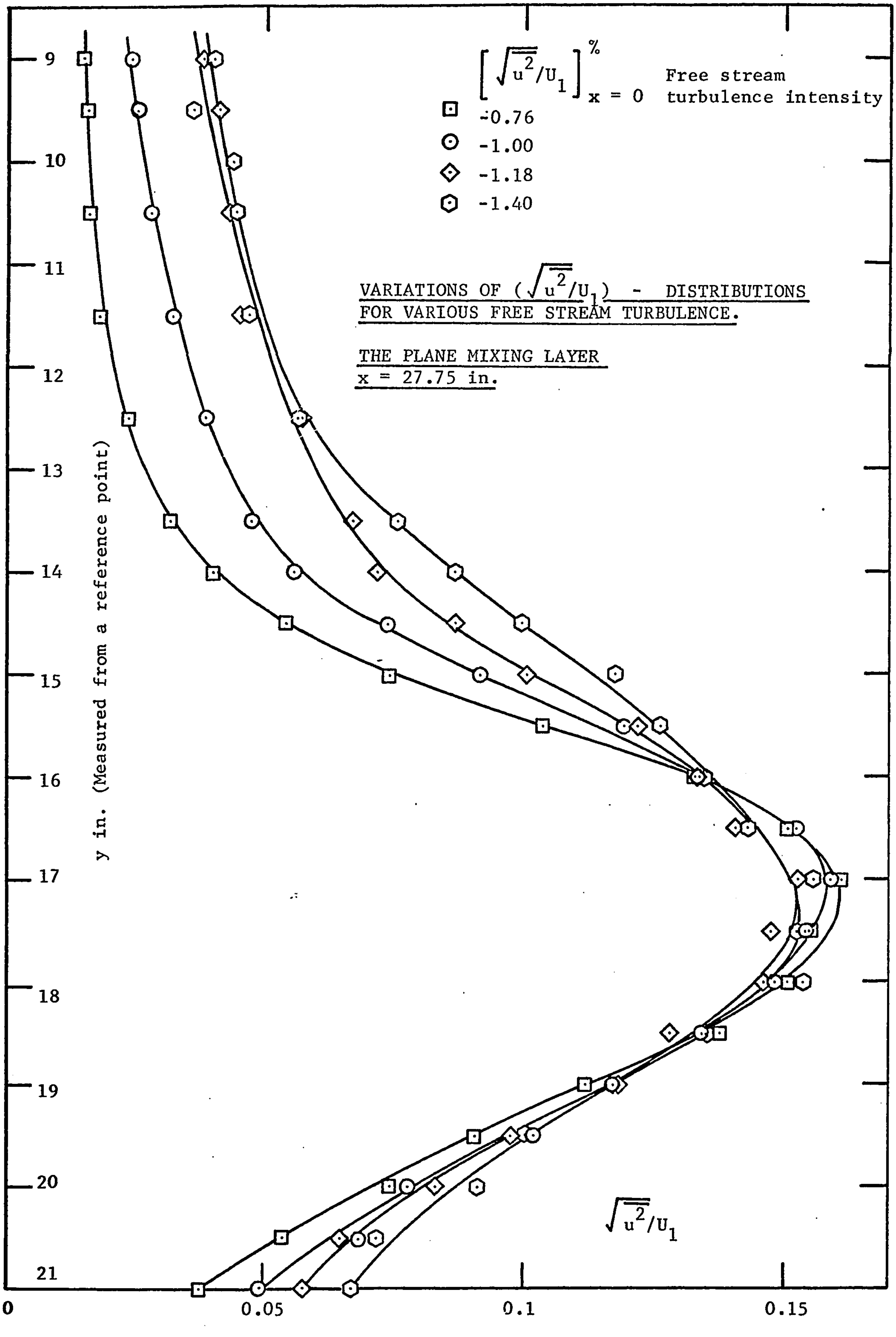

$\left[\sqrt{\overline{u^2}}/U_1\right]^{\%}_{x=0}$ Free stream turbulence intensity
-0.76
-1.00
-1.18
-1.40
VARIATIONS OF $(\sqrt{\overline{u^2}}/U_1)$ - DISTRIBUTIONS FOR VARIOUS FREE STREAM TURBULENCE.
THE PLANE MIXING LAYER
x = 27.75 in.
y in. (Measured from a reference point)
9
10
11
12
13
14
15
16
17
18
19
20
21
$\sqrt{\overline{u^2}}/U_1$
0
0.05
0.1
0.15

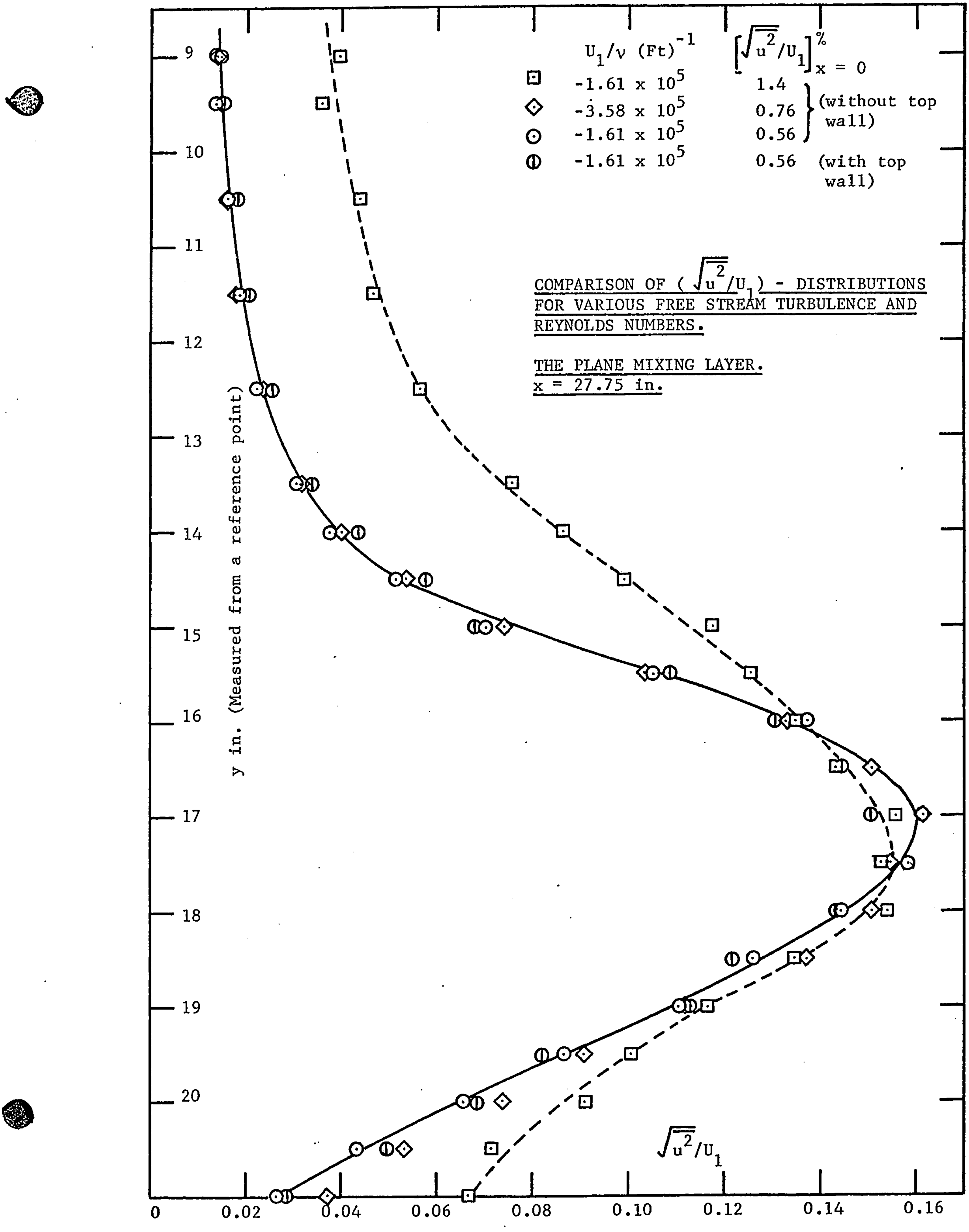

U_1/ν (Ft)$^{-1}$
$\left[\sqrt{\overline{u^2}}/U_1\right]^{\%}_{x=0}$
-1.61×10^5 1.4
-3.58×10^5 0.76
-1.61×10^5 0.56
(without top wall)
-1.61×10^5 0.56 (with top wall)
COMPARISON OF ($\sqrt{\overline{u^2}}/U_1$) - DISTRIBUTIONS FOR VARIOUS FREE STREAM TURBULENCE AND REYNOLDS NUMBERS.
THE PLANE MIXING LAYER.
x = 27.75 in.
y in. (Measured from a reference point)
$\sqrt{\overline{u^2}}/U_1$
9
10
11
12
13
14
15
16
17
18
19
20
0
0.02
0.04
0.06
0.08
0.10
0.12
0.14
0.16